'Through the looking glass': Diversity and its functional significance in marine benthic microbial eukaryotes

Arjun Verma

February 2018

Supervisor: Shauna Murray
Co-supervisor: Peter Ralph

CERTIFICATE OF ORIGINAL AUTHORSHIP

I certify that the work in this thesis has not previously been submitted for a degree nor has it been submitted as part of requirements for a degree except as part of the collaborative doctoral degree and/or fully acknowledged within the text.

I also certify that the thesis has been written by me. Any help that I have received in my research work and the preparation of the thesis itself has been acknowledged. In addition, I certify that all information sources and literature used are indicated in the thesis. This research is supported by an Australian Government Research Training Program Scholarship.

Production Note:
Signature of Student: Signature removed prior to publication.

Date: 23/01/2018

ACKNOWLEDGEMENTS

The woods are lovely, dark and deep,

But I have promises to keep,

And miles to go before I sleep,

And miles to go before I sleep.

-*Stopping by Woods on a Snowy Evening*, Robert Frost

I shall be telling this with a sigh

Somewhere ages and ages hence:

Two roads diverged in a wood, and I—

I took the one less travelled by,

And that has made all the difference.

-*The Road Not Taken*, Robert Frost

ORIGINAL PUBLICATIONS

Publications included in this thesis:

1. **Verma, A.**, Hoppenrath, M., Harwood, T., Brett, S., Rhodes, L., Murray, S., 2016, Molecular phylogeny, morphology and toxigenicity of *Ostreopsis* cf. *siamensis* (Dinophyceae) from temperate south-east Australia, Phycological Research 64(3), 146-59

2. **Verma, A.**, Hoppenrath, M., Dorantes-Aranda, J.J., Harwood, D.T. and Murray, S.A., 2016. Molecular and phylogenetic characterization of *Ostreopsis* (Dinophyceae) and the description of a new species, *Ostreopsis rhodesae* sp. nov., from a subtropical Australian lagoon. Harmful Algae, 60, 116-130.

3. **Verma, A.**, Kohli, G. S., Hoppenrath, M., Harwood, T., Kuzhiumparambil, U., Ralph, P. J., Murray, S. A., 2017 Systematics and diversity of the genus *Ostreopsis* in the East Australian Current region. In Proceedings of the 17th International Conference on Harmful Algae. International Society for the Study of Harmful Algae 2017.

TABLE OF CONTENTS

LIST OF FIGURES

Chloroplasts are elongated (arrows). C: Cell with different shape confirming the nucleus (n) position. Scale bars = 10 µm.

LIST OF TABLES

LIST OF SUPPLEMENTARY DATA

PREFACE

Lewis Carroll's 'Alice's Adventures in Wonderland*'* (1865) and 'Through the Looking-Glass and What Alice Found There*'* (1871) have fascinated readers for generations and have had a considerable impact on popular culture. Characters and references from these books have been used by scientists to explain the intricate phenomenon in microbial ecology, and particularly in marine microbial eukaryotes. Van Valen's 'Red Queen' hypothesis as a metaphor for an evolutionary 'arms race' and the 'Cheshire Cat' as a symbol of the complex phenomenon of sexual reproduction in *Emiliania huxleyi* are a few popular examples.

'*Through the looking glass*' depicts mirrors as a gateway to the wonderland and reflective of how mirrors are often illusionary. The book's finale centred around a game of chess where Alice finds herself as a pawn in the bigger game, highlights the importance of strategy to survive. The 'mirrors' and 'chess' from the storyline are symbolic of cryptic diversity and functional traits that exist in marine microbial eukaryotes, at a species, population, genetic and metabolic levels, enabling them to survive in the changing oceanic conditions. Cryptic diversity and strategic functional traits in *Ostreopsis* species are the fundamental questions that I have pursued in my dissertation and hence used the book title as a reference to symbolise the details of my aims and findings. The reference also highlights the enigmatic 'wonderland' of marine microbial eukaryotes that we witness through the lenses of a microscope (looking glass).

"There is a place like no other on earth. A land full of wonder, mystery and danger! Some say, to survive it, you need to be as mad as a hatter."

-Lewis Carroll, *Alice's Adventures in Wonderland*

THESIS ABSTRACT

Marine microbial eukaryotes are of immense ecological and evolutionary significance in marine ecosystems. Understanding their biodiversity and functional evolutionary traits are key to improving our understanding of marine ecosystem functioning. The East Australian Current (EAC) is a global climate change hotspot, and yet we lack in our understanding of its impact on phytoplankton distribution and dynamics. *Ostreopsis* species have been reported to cause severe blooms and produce palytoxin (PLTX) - like compounds all around the globe but we do not have basic information on the distribution and dynamics of *Ostreopsis* species in Australia.

In this dissertation, I established the first comprehensive report of *Ostreopsis* species from Australian waters and explored cryptic diversity and functional traits in this genus. Extensive sampling along a north-south gradient of 1800 km from sub-tropical to temperate waters yielded the identification of three species, including a novel pseudo-cryptic *Ostreopsis rhodesae* from the Great Barrier Reef, along with *Ostreopsis* cf. *ovata*. *Ostreopsis* cf. *siamensis* was identified at all locations and its eco-physiological traits and genetic population structure were investigated. The genetic diversity in the northern sub-tropical locations was greater compared to the more southern locations, reflecting a long-standing divergence and local radiations originating from the ancestral population and a potential southward range expansion, which may be related to the intensification of the EAC over the past century.

Intra- and inter-population variations in physiological traits were investigated to understand its range expansion and functional trade-offs. This is the first study to our knowledge to report growth rates, cell size, cellular toxic concentrations and photobiological parameters on fifty-three clones of a marine protist, in order to investigate intra-specific diversity in key functional traits. The toxin biosynthesis pathway in the three species was investigated using *de novo* transcriptomics and compared to *Coolia malayensis*. All essential domains needed to synthesize a PLTX-like carbon backbone were identified in the three *Ostreopsis* species and were also found in the non-PLTX producing *C. malayensis*. Putative molecules with potential polyketide-like backbone structures were reported in this investigation using non-targeted metabolomics,

suggesting a greater diversity of polyketide compounds amongst these species than previously anticipated.

Results from this dissertation add to the knowledge of species biodiversity, population structures, eco-physiological traits and toxin biosynthesis mechanisms in marine microbial eukaryotes, and *Ostreopsis* species in particular.

Chapter 1: General Introduction

1.1 Dinoflagellates: 'Through the looking glass'

Marine microbial eukaryotes (protists) are an extremely diverse polyphyletic group of organisms comprising lineages that differ widely in their evolutionary histories, ecological niches, growth, nutritional requirements and life strategies (Caron et al., 2009; Falkowski et al., 2004; Hackett et al., 2004; Keeling et al., 2014; Taylor, 1987) (Figure 1.1A). Understanding the range of biodiversity, its evolutionary drivers and the strategies with which populations and species evolve and maintain diversity is fundamental in understanding marine ecosystem functioning (Burki, 2014; Caron et al., 2012; Keeling et al., 2005; Massana et al., 2015). Amongst protists, dinoflagellates (class Dinophyceae) are of immense ecological and evolutionary significance (Hackett et al., 2004; Murray et al., 2016). Recent studies have revealed ~1/2 of protistan ribosomal DNA (rDNA) metabarcoding data richness to be represented by dinoflagellates across different size fractions, thereby displaying their extreme diversity, abundance and functional complexity in the world's oceans (De Vargas et al., 2015; Le Bescot et al., 2016). Their photosynthetic, heterotrophic, symbiotic, mixotrophic and parasitic lifestyles enables their adaptation to a wide variety of ecological niches. They possess significant variability in morphology, pigment composition and photosynthetic activity along with a broad spectrum of cell shapes and sizes (Schnepf and Elbrächter, 1992). Their occupation of such diverse niches can be witnessed in their fossil records that date back several hundred million years (Hackett et al., 2004; Schnepf and Elbrächter, 1992; Taylor, 1987).

Dinoflagellates are relatively inefficient in uptaking nutrients and exhibit slower growth rates compared to other protists such as chlorophytes, haptophytes and diatoms (Prince et al., 2008; Smayda and Reynolds, 2003). Despite being poor competitors within their ecosystems, they are known to produce complex secondary metabolites that can adversely affect interactions with their co-occurring phytoplankton and potential predators (Driscoll et al., 2016; Ives, 1987; John et al., 2015). These compounds display potent biological activities and appear to play distinct roles for the producing organisms (Murray et al., 2016; Yasumoto and Murata, 1993). Such toxic 'blooms', caused by sudden proliferation of certain dinoflagellate species, can also cause serious threats to public health and severe economic losses to fisheries and other coastal resources (Moestrup et al., 2009). Harmful algal blooms (HABs) have been occurring naturally throughout history but their

frequency, geographic range and intensity have increased in recent years (Hallegraeff, 1993; Hallegraeff, 2010; Smayda, 1990; Zingone and Oksfeldt Enevoldsen, 2000). The presence of HAB species is a significant challenge to the management of coastal resources and protection of public health, thereby making it essential to accurately assess the taxonomic identity of such species and examine the genes involved in toxin biosynthesis (Anderson et al., 2012).

Historically, the diversity of eukaryotic phytoplankton has been assessed by a comparison of morphological features, determined by using light or electron microscopy (Not et al., 2012; Stern et al., 2010). The approximately 2,400 recognized dinoflagellate species, of which about 80% are described from marine environments, include numerous morpho-types based on their tabulations, the arrangement of vesicles in the cell cortex and cellulosic thecal plates (Gómez, 2012; Smayda and Reynolds, 2003; Taylor et al., 2008; Taylor, 1987). Nuclear genetic markers, plastid genes and molecular data from metabolic pathways, along with morphological details have enabled the description of several distinct dinoflagellate orders; namely Gonyaulacales, Peridiniales, Gymnodiniales, Suessiales, Prorocentrales, Dinophysiales, Blastodiniales, Phytodiniales and Noctilucales (Guiry, 2012; Janouškovec et al., 2017; Not et al., 2012; Orr et al., 2012; Taylor et al., 2008; Taylor, 1987). Numerous genera make up these orders comprising species that occupy different ecological niches and have varying life histories (Figure 1.1B).

1.1.1 Contemporary issues in dinoflagellate studies

1.1.1.1 Cryptic species

Studies of dinoflagellate diversity and ecology, and more broadly that of phytoplankton microbial ecology and evolution, are driven by a number of major unresolved conceptual challenges, the foremost of which is the definition of a 'species' (Mann, 1999; Wood and Leatham, 1992). The species stands as 'a key concept, a basic unit and a common currency' for studies of diversity and ecology in the environment; yet, there is no consensus on its definition (Agapow et al., 2004; Not et al., 2012). Phytoplankton species are traditionally described according to their morphological features, but the recent combination of phylogenetic and morphological analyses have provided evidence for

4

cryptic or pseudo-cryptic species within a single morpho-species (Amato et al., 2007; Kremp et al., 2014; Le Bescot et al., 2016; Montresor et al., 2003). A well-investigated example is that of the symbiotic and free-living genus *Symbiodinium* (order Suessiales), that was divided into numerous ribotypes when analyzed with molecular tools (Coffroth and Santos, 2005; LaJeunesse, 2001; Sampayo et al., 2009). Another well-debated example is of the *Alexandrium tamarense* species (order Gonyaulacales) complex that was recently amended with the description of three new species (John et al., 2014).

In the last decade, an evaluation of dinoflagellate diversity in marine habitats using molecular approaches has highlighted massive undescribed diversity (De Vargas et al., 2015; Forster et al., 2016; Keeling et al., 2014; Le Bescot et al., 2016). Recent oceanic scale studies of phytoplankton have unraveled eight to ten times more unassigned operational taxonomic units (OTUs) than previously recognized morphological taxa for dinoflagellates (De Vargas et al., 2015). Such large-scale analyses of microbial eukaryotic diversity are not without error and require an accurate and curated taxonomic validation before novel biological insights can be extracted from such datasets. The lack of cultivability of numerous species, the difficulty in distinguishing them from similar species in the absence of clear morphological differences and knowledge of their sexual recombination, has meant that the confirmation of sequence identities deposited in databases using known 'voucher' specimens has been difficult (Del Campo et al., 2016; Del Campo et al., 2014; Guillou et al., 2013; Sampayo et al., 2009). Therefore, care must be taken in interpreting results from studies based purely on environmental metabarcoding.

Figure 1.1 A: The schematic of the major lineages in the eukaryotic tree of life as represented in Burki et al. (2014). B: Phylogenetic tree of dinoflagellates inferred from rDNA modified from Orr et al. (2012).
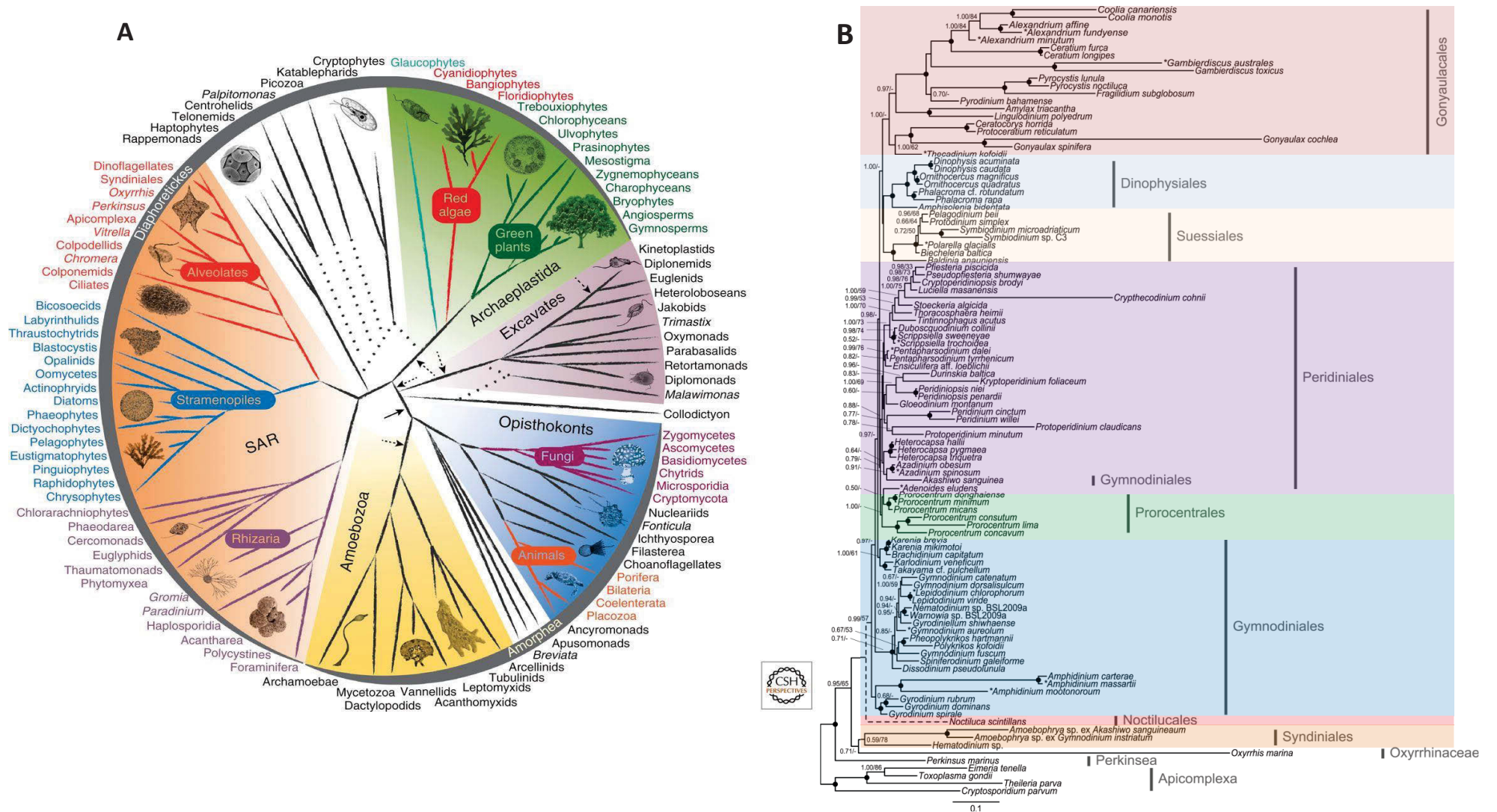
1.1.1.2 Population structure

Another long-standing debate amongst microbial ecologists concerns the hypothesis that 'everything occurs everywhere', postulating that phytoplankton populations are largely homogenous, as high dispersal capabilities and fast replication rates result in a continuous and cosmopolitan global distribution (Baas-Becking, 1934; De Wit and Bouvier, 2006; Finlay, 2002; O'Malley, 2007). The extensive dispersal capability, due to lack of barriers and oceanic currents, led to the assumption that planktonic populations are highly connected and should therefore exhibit extensive gene flow thereby preventing genetic isolation, fixation of genetic differences and allopatric speciation (Casabianca et al., 2011; Casteleyn et al., 2010; Nagai et al., 2007; Rengefors et al., 2015; Sjöqvist et al., 2015; Tahvanainen et al., 2012). As a consequence, microbial species were viewed as consisting of less genetically structured populations with lower levels of speciation compared to terrestrial animals and plants.

However, recent studies have highlighted that phytoplankton populations show immense spatial structuring and phylogeographic patterns that are reflective of historical, ecological and local conditions with communities occupying specialized niches to allow for their co-occurrence (Ellison et al., 2011; Knowlton, 1993; Rengefors et al., 2017) (Figure 1.2). Investigating the genetic 'seascape' provides a platform for understanding the connectivity and dispersal of planktonic and benthic organisms with the aid of population genetic data and micro-environmental profiles (Casabianca et al., 2011; Casteleyn et al., 2010; Sjöqvist et al., 2015). Increasing efforts have been made to link population genetic structure with large-scale ocean circulation patterns (Casteleyn et al., 2010; Lowe et al., 2012). Allopatric speciation, that may cause cryptic species divergence from one morpho-species, has been reported to occur in unicellular protists over large oceanic distances due to limited dispersal by geographic distance (Casabianca et al., 2011; Casteleyn et al., 2010). This has been highlighted by studies on cosmopolitan diatoms such as *Chaetoceros socialis* (Degerlund et al., 2012) and *Pseudo-nitzschia pungens* (Casteleyn et al., 2010). Genetic differentiation within species over small geographic scales have been reported for the diatom *Skeletonema marinoi* and also observed with *Alexandrium tamrense* along the Japanese coastline, *A. ostenfeldii* in the North Sea-Baltic

Sea and *A. minutum* in the Mediterranean Basin amongst dinoflagellates (Casabianca et al., 2011; Godhe et al., 2016; Nagai et al., 2007; Tahvanainen et al., 2012).
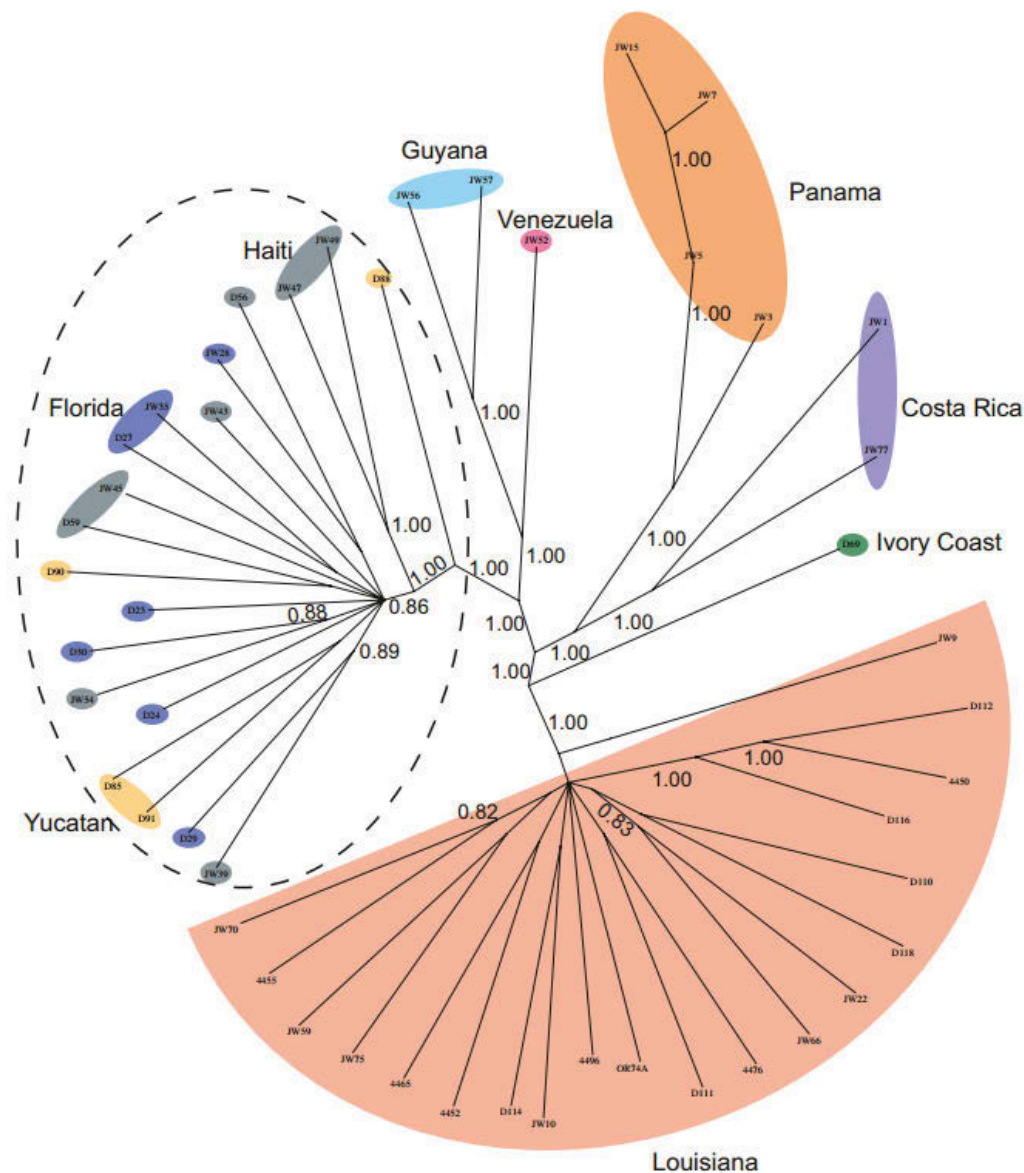
Figure 1.2 Unrooted Bayesian phylogeny showing cryptic population structure interred from 135,035 polymorphic sites in a fungal species *Neurospora crassa* as represented in Ellison et al. (2011).

Cryptic speciation can occur in sympatry, where specialization and separation in distinct ecological niches can promote speciation, as highlighted by studies on diatoms *Pseudo-nitzschia delicatissima* and *P. pseudodelicatissima* in the Gulf of Naples, as well as with the dinoflagellate genus *Symbiodinium* (Amato et al., 2007; Luo et al., 2017; Thornhill et al., 2014; Vanelslander et al., 2009). Such studies highlight the fact that phytoplankton need to be considered as consortiums of genetically structured 'meta-populations' with

low rates of dispersal, rather than single panmictic populations (Casteleyn et al., 2010; Godhe et al., 2013; Litchman and Klausmeier, 2008; Lynch and Walsh, 1998; Rengefors et al., 2017). Differences in eco-physiological processes are known to occur amongst sub-populations and communities that consist of similar species, thereby enabling their localization into distinct niches (Fenchel, 2005; Guiry, 2012; Nagai et al., 2007; Tahvanainen et al., 2012). However, such functional diversity and its ability to drive adaptive traits amongst morphologically indistinguishable members of the same species still remain poorly understood and unresolved.

1.1.1.3 Functional trait diversity

Phytoplankton niches consist of distinctive responses to fundamental physiological processes such as growth, and strategies for the acquisition of essential resources such as light, macro- and micro-nutrients, along with resistance to predation (Litchman et al., 2007; Margalef, 1978). The various niches and contrasting life histories of dinoflagellates make them complex study subjects for the investigation of eco-physiological traits (Hackett et al., 2004). Phenotypic variability at a population level may be related to distinctions in environmental conditions, leading to both phenotypically plastic responses, and genetic selection for specific traits that are beneficial under particular conditions (Hutchinson, 1961; Margalef, 1978; Petchey and Gaston, 2006; Smayda and Reynolds, 2003; Tilman, 1999; Tilman et al., 1997). However, recent studies have highlighted that variations in phenotypic traits may also be caused by random genetic variation caused by disruption of gene flow between populations, as demonstrated in recent studies of *Emiliania huxleyi* and the dinoflagellate species *Polarella glacialis* (Prada et al., 2008; Rengefors et al., 2015; Weithoff, 2003; Zhang et al., 2014). Eco-physiological traits in dinoflagellates have been measured in numerous laboratory and field studies over the past decades. Population level fitness and competitive ability have been computed using various mathematical models (Hulot et al., 2000; Litchman et al., 2007; Litchman et al., 2015; Petchey and Gaston, 2006; Smayda and Reynolds, 2003). However, the number of reports have increased recently due to the growing interest in phytoplankton community dynamics with anthropogenic nutrient loading, pollution and climate change (Barton et al., 2013; Collins et al., 2014; Edwards et al., 2011; Glibert, 2016; Litchman et al., 2015).

Blooming populations of algal species are an outcome of large-scale adaptive strategies, requiring strategic efforts from various 'individuals' making them subject of numerous functional trait based investigations (Driscoll et al., 2016; Glibert, 2016; Rengefors et al., 2017; Smayda, 1997; Thornton, 2002). These studies have improved our understanding of evolutionary and ecological determinants of diversity, ecosystem level processes and mechanisms such as resource use complementarity and facilitation (Driscoll et al., 2016; John et al., 2015; Kremp et al., 2012; Kremp et al., 2016; Petchey and Gaston, 2006). Investigating evolutionary mechanisms leading to diversification of major phenotypic traits such as cell size, photosynthetic optimization, growth rates or the production of secondary metabolites remains key to comprehending processes of phytoplankton adaptation, and also improve our understanding of the dynamics of future phytoplankton populations under changing climate regimes (John et al., 2015; Koester et al., 2010; Tillmann et al., 2009; Whittaker et al., 2012).

1.1.1.4 Secondary metabolites and biosynthetic pathways

Some dinoflagellates are known to produce and release a variety of potent bioactive secondary metabolites that aid in various ecological and metabolic processes such as immobilizing potential prey, osmoregulation, alleopathy and grazing deterrence (Driscoll et al., 2016; Hackett et al., 2004; John et al., 2015; Kellmann et al., 2010). Most of these metabolites described from dinoflagellates are polyketides in origin (Rein and Borrone, 1999; Shimizu, 1996; Snyder et al., 2003; Wright and Cembella, 1998). Polyketide biosynthesis is well studied in cyanobacteria and fungi, however very little is known about their biosynthesis and regulation from marine dinoflagellates (Kellmann et al., 2010; Rein and Borrone, 1999). These complex molecules are synthesized by sequential condensations of small carboxylic acid subunits into a growing acyl chain, similar to fatty acid synthesis (Hopwood, 1997; Jenke-Kodama et al., 2008; Khosla et al., 1999; Smith, 1994). The enzymes responsible for polyketide biosynthesis are large multi-domain enzyme complexes known as polyketide synthases (PKSs) that resemble fatty acid synthases (FASs), both in structure and function (Donadio et al., 1991; Hopwood, 1997; Hopwood and Sherman, 1990; Jenke-Kodama et al., 2008; Jenke-Kodama et al., 2005; Khosla et al., 1999; Shimizu, 1993). PKSs have been divided into three categories (Type I-III) depending on their domain organization; however, most polyketides studied in

dinoflagellates to date are synthesized by Type I modular PKSs and contain multiple modules on a single polypeptide (Eichholz et al., 2012; Khosla et al., 1999; Kohli et al., 2016; Shen, 2003).

The last decade has seen a rapid growth in molecular studies, especially with the use of *de novo* transcriptomic assemblies and phylogenetics, that has aided in our understanding of secondary metabolite biosynthesis and genome functionality amongst dinoflagellates (Bachvaroff and Place, 2008; Beauchemin et al., 2012; Eichholz et al., 2012; Kimura et al., 2015; Kohli et al., 2017; Kohli et al., 2015; López-Legentil et al., 2010; Meyer et al., 2015; Monroe and Van Dolah, 2008; Moustafa et al., 2010; Murray et al., 2012; Pawlowiez et al., 2014; Ryan et al., 2014; Salcedo et al., 2012). The genetic composition of dinoflagellates makes comparison of homologous genes with other microbial eukaryotes and bacteria very tedious, causing our understanding of genetic pathways in dinoflagellates to still quite rudementory (Kellmann et al., 2010; Kohli et al., 2016).

1.1.1.5 Dinoflagellate genomics

The genetic composition and nuclear structure of dinoflagellates are very unique (Keeling et al., 2014; Murray et al., 2016). Their nuclear chromosomes are permanently condensed except during replication and they express the most divergent histone proteins compared to other known microbial eukaryotes (Hackett et al., 2004; Marinov and Lynch, 2016). Their genomes are generally larger than most other eukaryotes, ranging from 1.5-250 pg DNA per haploid genome, which equates to approximately 1.85-112 x 10^9 base pairs (bps) (Hou and Lin, 2009; LaJeunesse et al., 2005; Murray et al., 2016). Their gene content is, however is much lower, ranging only from 38-87 x 10^3 protein coding genes (Hackett et al., 2004; Hou and Lin, 2009) (Figure 1.3).

The recently published *Symbiodinium minutum* genome showed that dinoflagellates have unusual gene arrangements such as the uni-directionally aligned genes throughout their genomes forming cluster-like gene arrangements (Lin et al., 2015; Shoguchi et al., 2013). Many of these genes are organized in multiple copies and/or as tandem repeats varying

between 30 copies, as in the case of protein kinase gene in *Lingulodinium polyedrum*, to approximately 100,000 copies similar to the common rRNA genes (Murray et al., 2011; Salois and Morse, 1997). Such genes usually have a low intron density and occasionally even lack introns, thereby being highly expressed (Bachvaroff and Place, 2008). However, certain genes seem to be more intron-rich, such as the ketoyl reductase (KR) domain in *Amphidinium carterae* that has 18 introns, thereby highlighting the diversity and complexity of genetic arrangements amongst dinoflagellates species (Bachvaroff and Place, 2008).
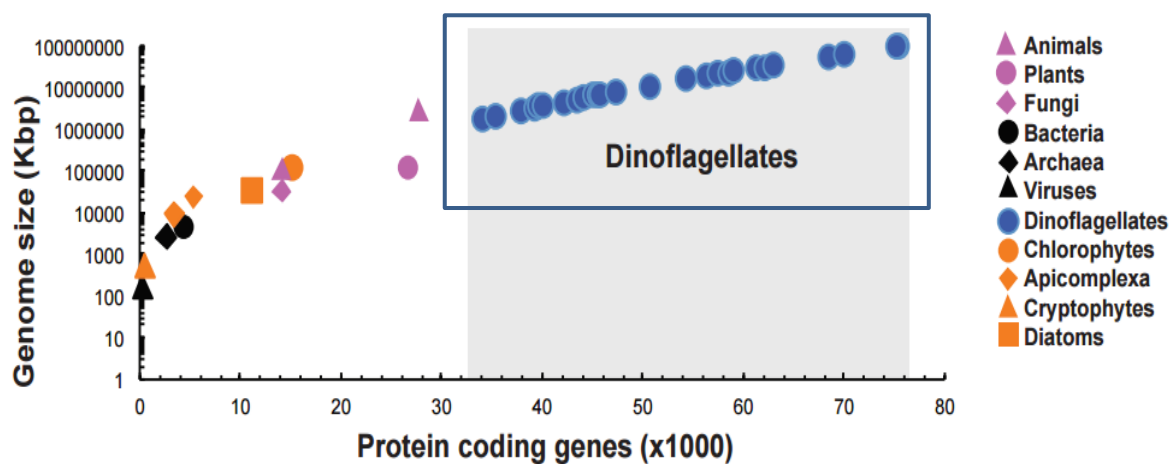
Figure 1.3 Number of protein coding genes compared to genome size (in log scale) of various organisms highlighting the large genome sizes of dinoflagellates as represented in Murray et al. (2016).

Several 'intron-less' genes have resulted from the incorporation of complementary DNA (cDNA) back into the dinoflagellate genome through a process of 'retro-mechanism'. This process generates translatable monocistronic messanger RNA (mRNA) from polycistronic transcripts by a *trans*-splicing process (Beauchemin et al., 2012; Slamovits and Keeling, 2008; Zhang and Lin, 2009). This involves splicing of a short RNA fragments from a small non-coding spliced leader to an acceptor site in the 5' untranslated region of an independent pre-mRNA transcript (Lidie and Van Dolah, 2007; Slamovits and Keeling, 2008; Zhang et al., 2013). This mechanism has been reported in most genetic studies of dinoflagellates, and along with horizontal gene transfer, has been postulated as the key reasons for their large genomes (Hou and Lin, 2009; Lin et al., 2008).

Dinoflagellate DNA is also known to contain 5-hydroxymethyluracil (5-meU) that substitutes 12-70% of thymidine, along with other modified nucleotide building blocks such as 5-methyl cytosine and N6-methyl adenine. These varying nucleotides are responsible for making dinoflagellate nuclear DNA extensively methylated. It has been suggested that 5-meU is associated with a restriction-modification system for discriminating between dinoflagellate and foreign DNA sequences (Davies and Jakobsen, 1988; Murray et al., 2016; Rae, 1976; Rae and Steele, 1978). Such features make transcription and gene regulation in dinoflagellates quite exceptional and whole genome sequencing and assemblies very tedious.

1.2 The East Australian Current region: a climate change hotspot

Our knowledge of phytoplankton communities from the southern hemisphere is not as comprehensive as those from the north, despite the southern hemisphere encompassing two-thirds of the global ocean surface (Ajani et al., 2016). In south-east Australia, the East Australian Current (EAC) runs from north to south, redistributing warm tropical waters from the Coral Sea into the temperate Tasman Sea. It also delivers a series of mesoscale eddies into the coastal waters which subsequently interact with upwellings to produce a range of highly energetic and complex coastal ecosystems (Ajani et al., 2016) (Figure 1.4). Observations from the past 60 years highlight the EAC's intensification, with a poleward extension of approximately 350 km, and a significant warming by 2.28°C/century (Ridgway, 2007; Ridgway and Hill, 2009; Suthers et al., 2011). This trend is expected to continue and is postulated to impact the coastal marine ecosystems, including phytoplankton diversity and distribution (Hallegraeff, 2010).

In recent years, nineteen harmful species have been described from south-east Australian waters with increasing reports of toxin producing species being linked to seafood poisoning events, mortalities in fish or other marine flora and fauna, and also direct human impacts through skin and aerosolic exposures (Ajani et al., 2016; Ajani et al., 2013b; Farrell et al., 2013; Kohli et al., 2014; Murray and Suthers, 1999). HABs are an emerging issue for south-east Australia (Ajani et al., 2016; Ajani et al., 2013b; Kohli et al., 2014). Recent studies have identified 45 potentially harmful taxa from operational

shellfish production and harvest sites along the New South Wales (NSW) coast, with recurrent presence of the epi-benthic toxic bloom forming *Ostreopsis* species in 26 of the studied 31 estuaries (Ajani et al., 2013a) (Figure 1.5). However, to date no comprehensive toxicological, morphological and molecular studies have been carried out on *Ostreopsis* species from this region.
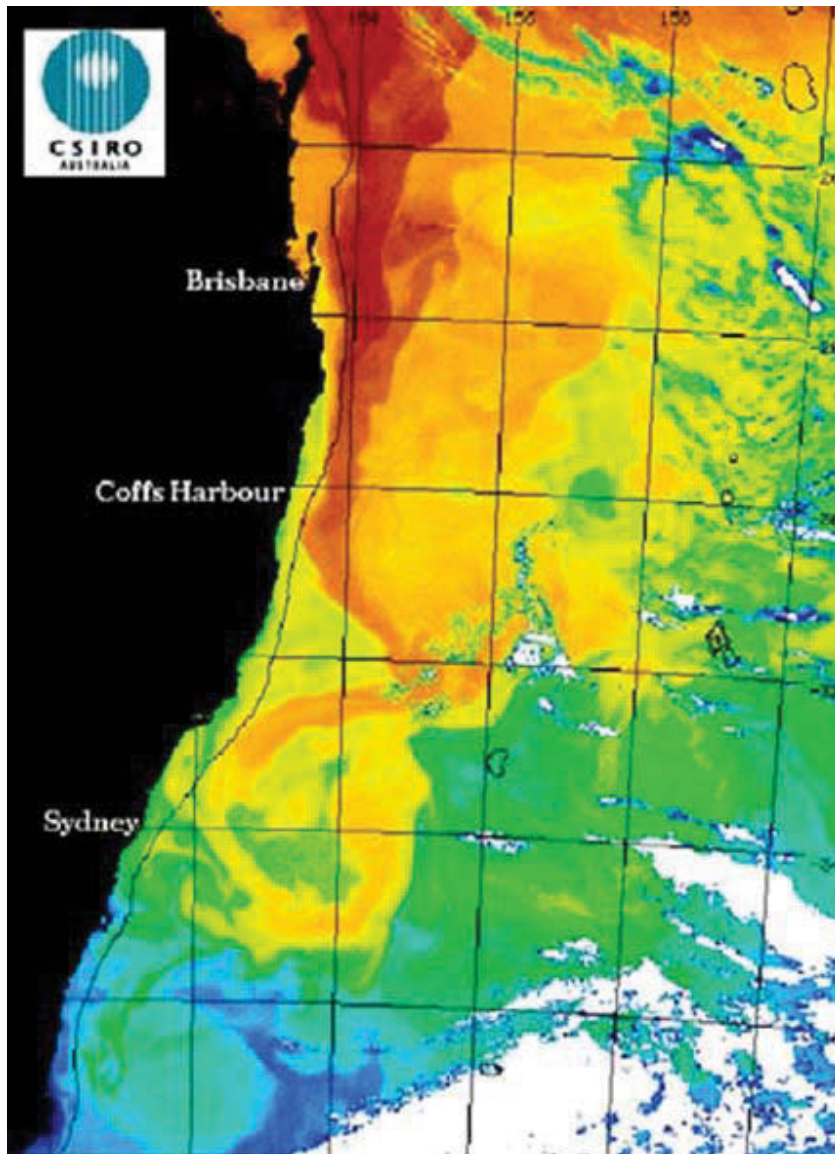
Figure 1.4 The warm EAC jet flows along the shelf-edge off eastern Australia as represented in Ridgway and Hill (2009).

Figure 1.5 Seasonal occurrence of *Ostreopsis* spp. in aquaculture plankton samples collected from shellfish producing estuaries along the New South Wales coastline between July 2005 and December 2013. Cell count represents cells identified microscopically in one litre of water sample.

1.3 Genus *Ostreopsis*

Species of genus *Ostreopsis* Schmidt (order Gonyaulacales) have been observed at shallow depths in diverse tropical and sub-tropical habitats binding epiphytically to coral rubble, macroalgae, seagrass and sand (Faust, 1995, 1999; Fukuyo, 1981; Morton and Faust, 1997; Norris et al., 1985; Schmidt, 1902). *Ostreopsis* species create rusty-brown mucous films colonizing the benthos and also the water column thereby creating harmful and toxic blooms (Faust et al., 1996; Rhodes, 2011; Shears and Ross, 2009). Many *Ostreopsis* species are known to produce extremely potent and complex molecules called palytoxin (PLTX) and/or its analogues (Ciminiello et al., 2008; Ciminiello et al., 2012b; Dell'Aversano et al., 2014; Usami et al., 1995). Blooms caused by *Ostreopsis* species have attracted significant attention over the last decade, particularly in temperate waters due to mass mortalities of benthic communities such as sea urchins (Faimali et al., 2012; Shears and Ross, 2009). Such events have caused damages to fisheries and ecosystems along the coastal areas of the Mediterranean basin, Japan and New Zealand, and have also presented a threat to human health due to respiratory disorders by inhalation of marine aerosols and skin irritations by seawater contact (Chang et al., 2000; Ciminiello et al., 2006; Ciminiello et al., 2008; Mangialajo et al., 2011; Monti et al., 2007; Sato et al., 2011; Shears and Ross, 2009). With the increasing threat of *Ostreopsis* blooms, and their negative impact on tourism and aquaculture, it is essential to understand the diversity of these bloom forming species, their genetic and phenotypic structures and the genetic pathways responsible for toxin biosynthesis.

1.3.1 Cryptic morphology

Genus *Ostreopsis* was established by Schmidt (1902) with the description of the type species, *Ostreopsis siamensis*. Distinguishing *Ostreopsis* species from each other based on morphology is very difficult, due to their similarity in size, shape and plate display, and also their co-existence in the environment (Hoppenrath et al., 2014; Penna et al., 2005). Almost all the described species have a thecal plate pattern that fits with the description of *O. siamensis*. The first records of *O. siamensis* described it as possessing a rounded epicone, but having an elongated and ventrally pointed hypocone (Figure 1.6). The study also mentioned the plates to be coarsely porous, which indicated relatively large sized pores, visible even with light microscopy (Schmidt, 1902).

Fukuyo (1981) displayed an undulated cingulum, also presented by Schmidt (1902), and reported pores of similar size scattered all over the thecal plates for *O. siamensis*. The apex was described to move dorsally and the cingulum as narrow and deep. The plate formula was described as Po, 3', 7'', 5''', 1'''' (Fukuyo, 1981). *Ostreopsis ovata* Fukuyo and *O. lentricularis* Fukuyo were also described in this study and were shown to have the same thecal plate configuration as *O. siamensis*. *O. lenticularis* was distinguished from *O. siamensis* by the lack of undulated cingulum along with two different pore sizes. *O. ovata* was described by its ovoidal, rather than clavate body shape and smaller size, making it distinguishable from the other two species (Fukuyo, 1981) (Figure 1.7).
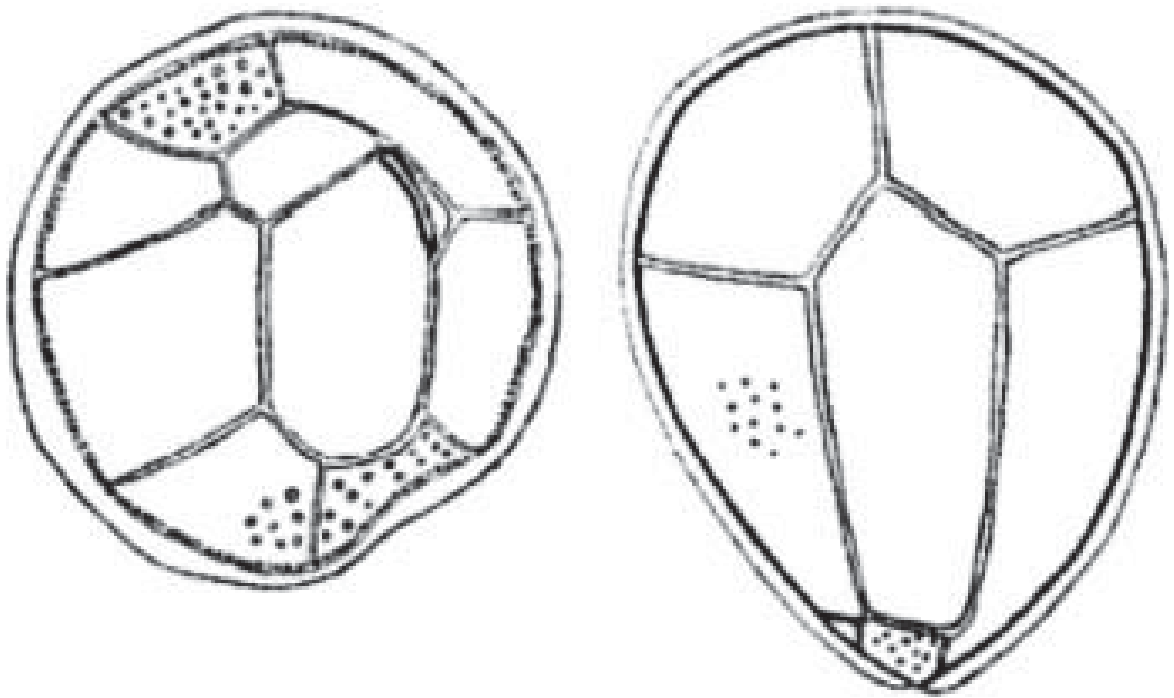
Figure 1.6 Original drawings of *Ostreopsis siamensis* as represented in Schmidt (1902). The epithecal view is presented on the left, the hypothecal view on the right (Parsons et al., 2010).

Three new species of *Ostreopsis* were described thereafter; *O. heptagona* Norris, Bomber and Balech, *O. mascarenensis* Quod and *O. labens* Faust and Morton with a more comprehensive thecal plate description for the genus (Po, 3', 7'', 6C, 6S?, Vp, Rp, 5''', 1p, 2'''') (Faust and Morton, 1995; Faust et al., 1996; Norris et al., 1985) (Figure 1.7). Faust et al. (1996) described *O. lentricularis* and *O. siamensis* differently from their first descriptions in Fukuyo (1981), stating that *O. siamensis* has a bigger cell size and had

two different thecal pore sizes, while *O. lentricularis* has only one pore size (Faust et al., 1996). However, lack of information about the undulation of the cingulum, led to uncertainty about the identity of Faust's specimens as *O. siamensis*.

Furthermore, three more novel *Ostreopsis* species with minor variations in their thecal plate sizes and shapes were described; *O. marinus* Faust, *O. belizeanus* Faust and *O. caribbeanus* Faust (Faust, 1999) (Figure 1.7). Over the last few decades, numerous reports of *Ostreopsis* specimens based solely on microscopy have led to contrasting descriptions of cell shapes and sizes leading to ambiguous species identification, thereby making the taxonomy of *Ostreopsis* species quite debatable (Aligizaki and Nikolaidis, 2006; Chang et al., 2000; Heimann et al., 2009; Holmes et al., 1988; Rhodes et al., 2000).

1.3.2 Phylogenetic studies

The nuclear internal transcribed spacer regions (ITS1 and ITS2) and 5.8 rRNA genes are widely used for phylogenetic characterization amongst cryptic dinoflagellate taxa (John et al., 2014; LaJeunesse, 2001; Litaker et al., 2009; Parsons et al., 2012; Rhodes, 2011). Extensive studies on *Ostreopsis* over the past decade have revealed numerous cryptic clades and sub-clades within this genus (Penna et al., 2005; Pin et al., 2001). Since there is no genetic data for the holotype specimen from which the original description was made, Penna et. al (2005) described the *O. siamensis* and *O. ovata* in their study as *O*. cf. *siamensis* and *O*. cf. *ovata* respectively, until accurate morphological and genetic data can be gathered from the type localities to define each species (Penna et al., 2005). Pin et al. (2001) reported genetic variation between the strains isolated from South China Sea and the Malacca Strait based on ITS-5.8S markers and also marked the distinction between *O. lentricularis* and *O*. cf. *ovata* based on phylogenetic analysis (Pin et al., 2001). An extensive study using partial nuclear LSU (D1/D2 domains), 5.8S and ITS rDNA regions on 82 strains from 26 localities around the globe found that *O. lentricularis* and *O. labens* to cluster together in a single clade (Penna et al., 2010). *O*. cf. *siamensis* and *O*. cf. *ovata* strains clustered in their own respective clades; however, genetic variations in *O*. cf. *ovata* populations were reported between the Atlantic/Mediterranean populations and the Indo/Pacific strains (Penna et al., 2010; Penna et al., 2012).
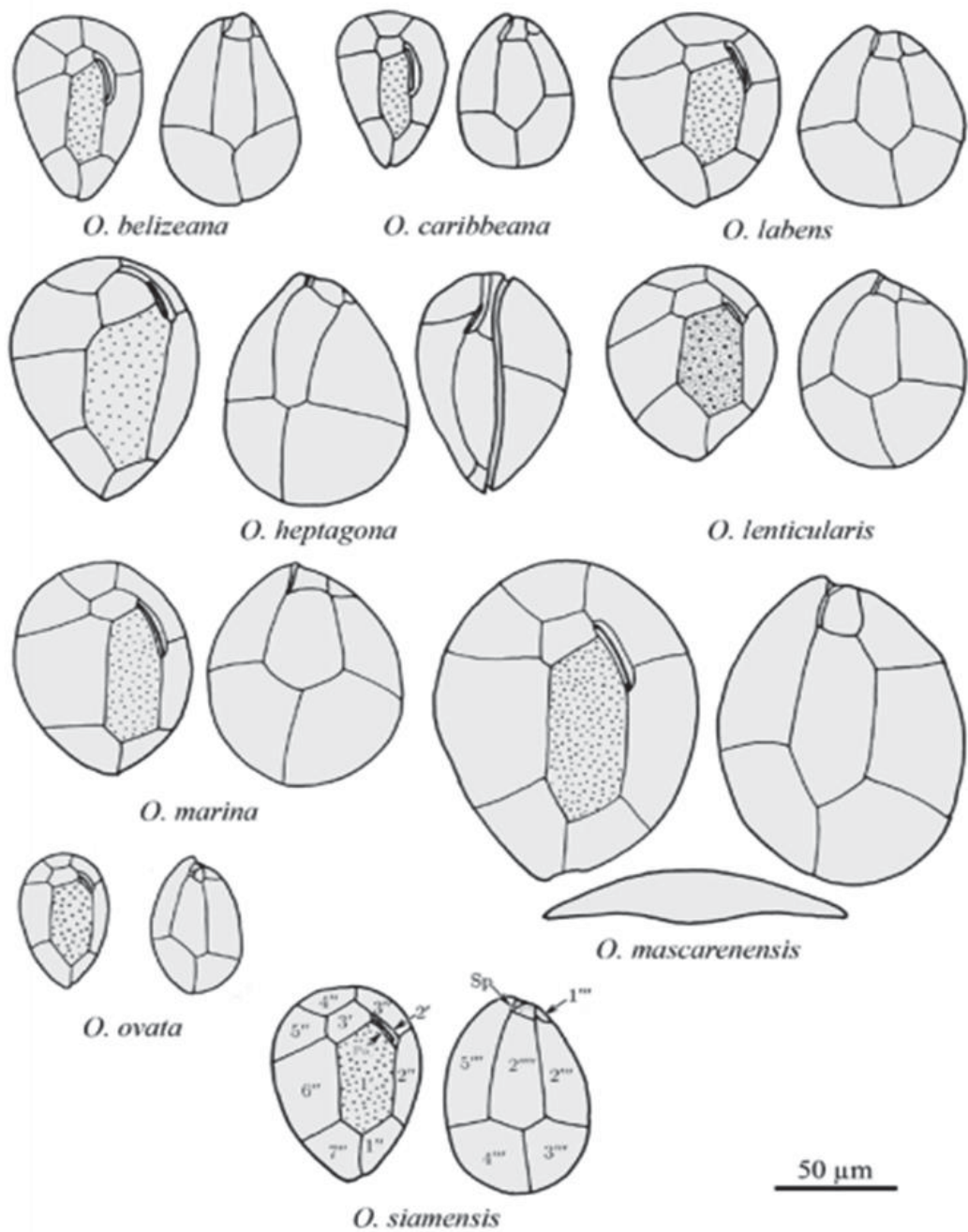
Figure 1.7 *Ostreopsis* species drawings of the plate patterns as represented in Hoppenrath et al. (2014).

A comprehensive phylogenetic study on *Ostreopsis* strains from Japan, using D8-D10 region of LSU rDNA markers, found the genus to comprise eight different clades/putative species. *Ostreopsis* clades 1-5 were reported for the first time, and an *Ostreopsis ovata* species complex was described comprising three cryptic morpho-species (Sato et al., 2011). Recently, a new clade *Ostreopsis* sp. 7 was described from the Gulf of Thailand along with a sub-clade in the *Ostreopsis ovata* species complex based on LSU and ITS

markers (Tawong et al., 2014). Despite an improvement in the detection of *Ostreopsis* species using molecular markers, the extent of cryptic species diversity in this genus remains unresolved, as there are no comprehensive reports about the population structures and reproductive incompatibility amongst the clades and sub-clades from this genus.

1.3.3 Biogeography

Early biogeographical studies found *Ostreopsis* species to be prevalent in sub-tropical coral reefs and lagoonal ecosystems from locations between 28°N and 20°S in the Pacific, Atlantic and the Indian Oceans (Faust, 1999; Faust et al., 1996; Fukuyo, 1981). However, recent reports of *Ostreopsis* blooms from temperate waters in the Mediterranean, Sea of Japan and the southern Pacific highlight a widespread distribution and varying eco-physiological traits amongst *Ostreopsis* species and populations (Parsons et al., 2012; Rhodes, 2011) (Figure 1.8). It was postulated that by developing 'resting cysts', the species can survive winter seasons in the surface sediments, enabling them to reappear in the summer (Pearce et al., 2001; Selina and Orlova, 2010). These cysts have also been linked with species dispersal through ocean currents, floating/drifting objects and/or through ballast waters of ships (Barnes, 2002; Bravo et al., 2012; Hallegraeff, 1993; Masó et al., 2003). Dormant resting cysts covered with mucilage have been reported for *O.* cf. *ovata* that were able to germinate even after six months of their formation, suggesting that the mucous might act as a protective coat for the cysts and aids in their subsequent germination (Barone, 2007; Bravo et al., 2012). Genetic variations based upon geographic origins have been investigated for *O.* cf. *ovata* over large oceanic scales that reported two separate clades, i.e. Atlantic/Mediterranean and the Indo/Pacific (Penna et al., 2010). It was postulated that the formation of the Isthmus of Panama in the mid-Pliocene epoch separated the *Ostreopsis* clades into two tropical-to-temperate geographical regions; i.e. the Atlantic that includes the Caribbean and Mediterranean Sea ribotypes, and the Indo/Pacific ribotype. These changes accompanied by temperature and salinity variations and oceanic circulation, suggest that ecological differentiation of *O.* cf. *ovata* had most likely occurred on both sides of the Isthmus of Panama, allowing geographical and subsequent genetic differentiation of the populations (Penna et al., 2010).
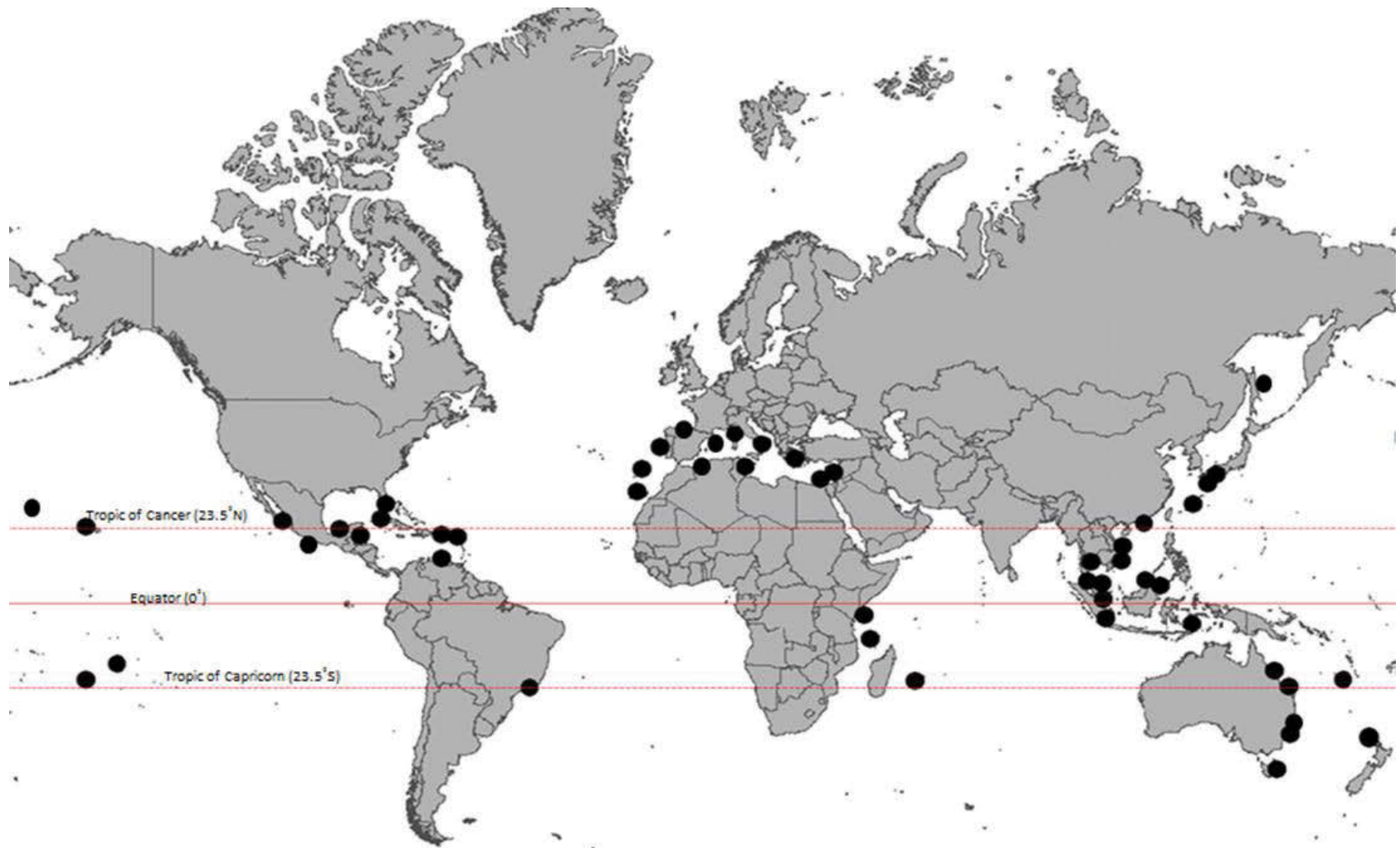
Figure 1.8 Global distribution of *Ostreopsis* species modified from Rhodes (2011). Black dots indicate locations of molecular and morphological reports.

However, geographic population structures over smaller distances remain to be resolved and no reports on the phylogeographic structures of any other *Ostreopsis* species have yet been documented. Such studies require a well-defined species concept, which has proven to be a challenging task for *Ostreopsis* species. Therefore, studies combining phylogeography with eco-physiological functional variability will aid in our understanding of factors controlling range expansion of *Ostreopsis* species.

1.3.4 Toxin producers: Palytoxin

1.3.4.1 Chemical structure and mode of action

PLTX ($C_{129}H_{223}N_3O_{54}$) are large complex molecules with one of the longest chains of continuous carbon atoms reported for any natural product (Moore and Bartolini, 1981; Uemura et al., 1981). These molecules are classified as polycyclic polyketides and are regarded as one of the most toxic substances known to date, with LD_{50} from 25–450 ng kg^{-1}, depending on the animal model and the administration route (Deeds and Schwartz, 2010; Kaul et al., 1974; Lenoir et al., 2004; Rhodes et al., 2002; Usami et al., 1995). PLTX have a long partially unsaturated aliphatic backbone with spaced cyclic ethers, hydroxyl groups, one primary amino and two amide functional groups in their structure (Moore and Bartolini, 1981; Uemura et al., 1981). These compounds have both hydrophilic and lipophilic regions containing 64 chiral centers. With such a high number of chiral centres and eight double bonds that are able to exhibit *cis-/trans-* isomerism, PLTX can have more than 10^{21} stereoisomers (Cha et al., 1982) (Figure 1.9). The molecular weight of putative PLTX was reported as 2,680 daltons (Da); however, the weight of PLTX analogues ranges from 2,500-2,707 Da depending on their structure (Ciminiello et al., 2010; Ciminiello et al., 2009; Ciminiello et al., 2008; Ciminiello et al., 2012b; Lenoir et al., 2006; Lenoir et al., 2004; Usami et al., 1995).

Their remarkable chemistry combined with high toxicity and global occurrences have led to multi-disciplinary approaches to investigate varying facets of these toxic molecules, ranging from the identification of novel putative analogues to their adverse impacts on mammalian cell systems (Deeds and Schwartz, 2010). PLTX molecules are known to block the sodium/potassium (Na^+/K^+)-ATPase channel, a trans-membrane protein that

transports three Na$^+$ ions out of the cell and two K$^+$ ions in, using ATP hydrolysis as the driving force (Habermann, 1989; Hirsh and Wu, 1997; Wu, 2009). The electrochemical gradient generated by the pump is essential for cellular homeostasis (Habermann, 1989; Hirsh and Wu, 1997; Wu, 2009). PLTX bind to the extracellular part of the pump thereby inhibiting the active transport of Na$^+$ and K$^+$ ions across the cell membrane by transforming the pump into a non-specific permanently open channel. Such membrane depolarization causes a massive amount of calcium ions to enter the cytosol causing nterference with several vital cellular functions and cell apoptosis (Habermann, 1989; Hirsh and Wu, 1997; Wu, 2009).
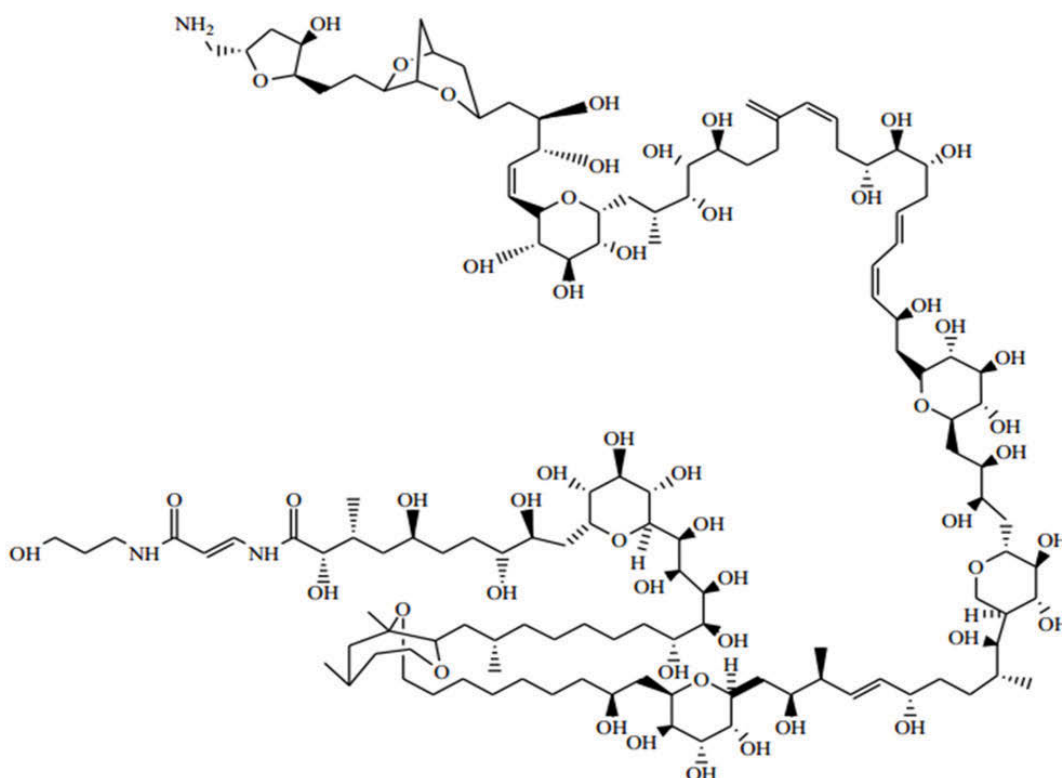
Figure 1.9 Structure of PLTX as represented in Ramos and Vasconcelos (2010)

1.3.4.2 Toxin analogues and variability

The first comprehensive study to report the chemical structure of toxins from *Ostreopsis siamensis* highlighted that the despite major constituent, Ostreocin-D, being responsible for 90% of the total toxicity, an additional 10 congeners were also produced by the strain (Ukena et al., 2001; Usami et al., 1995). In 2006, an outbreak of *O.* cf. *ovata* along the

Italian coastline led to description of a novel PLTX analogue, Ovatoxin-a (Ciminiello et al., 2008). The molecular structure ($C_{129}H_{223}N_3O_{52}$) and molecular weight (2,646 Da) was elucidated using high resolution (HR) LC-MS (Ciminiello et al., 2012a). The increasing number of *Ostreopsis* blooms and the extensive use of HR LC-MS analyses on both field and cultured samples have led to the discovery of numerous novel PLTX analogues (Ciminiello et al., 2010; Ciminiello et al., 2012b; Dell'Aversano et al., 2014; García-Altares et al., 2014; Ramos and Vasconcelos, 2010).

In Japan, Suzuki et al. (2012) identified novel analogues which were reported as isomers of ovatoxin -a, -b, -d and –e and named them ovatoxin-a AC, -b AC, -d AC and -e AC respectively (Suzuki et al., 2012). Mercado et al. (1994) reported Ostreotoxin (OXT)-1 and OXT-3 from *O. lentricularis* from the Caribbean and found them to cause fast contractions or twitches in frog sartorius muscles (Mercado et al., 1994). The study further highlighted OTX-3 to possess a novel sodium-channel activating activity that discriminated between nerve and skeletal muscle membranes, unlike PLTX and its other reported analogues (Meunier et al., 1997; Ramos and Vasconcelos, 2010). However, since the compounds were not structurally elucidated their involvement has not yet been proven with any toxic outbreaks.

Hwang et al. (2013) reported that an *O.* cf. *ovata* strain isolated from Korean waters produces a new cytotoxic compound, Ostreol A, which has not been described from other *Ostreopsis* species (Hwang et al., 2013; Kang et al., 2013). It was described as a non-PLTX compound possessing a polyhydroxy chain ending with a primary amino group and an amide bond, along with two tetrahydropyran rings in the chain (Hwang et al., 2013). Ostreol A was determined to have *in vitro* cytotoxicity against *Artemia salina* with an LD$_{50}$ of 0.9 µg/mL. The central portion of this compound is structurally common with amphidinols that are synthesized by *Amphidinium* spp., but the terminal ends of the molecule are characterized by the presence of an amide and a primary amine group, which differs from the conventional structure of amphidinols thereby indicating a new class of toxic compound being synthesized by *Ostreopsis* species (Hwang et al., 2013; Kobayashi and Kubota, 2007).

Significant inter-strain variation in toxin production has been reported from *O.* cf. *ovata* strains in the Mediterranean region, where the northern Adriatic samples present a higher toxin content than the strains isolated from the Ligurian and Tyrrhenian Seas, but the *O.* cf. *ovata* strains reported from south west Indian ocean have been identified as non-toxic (Bellocci et al., 2008; Guerrini et al., 2010; Rossi et al., 2010). In a recent study, it was shown that the Mediterranean and Atlantic *O.* cf. *siamensis* strains did not produce substantial amounts of PLTX-like compounds; in contrast to the reports of *O.* cf. *siamensis* from the New Zealand and the southern-Pacific region (Rhodes, 2011; Rhodes et al., 2010; Selwood et al., 2012).

1.3.4.3 Human health and ecological impact

Cases of human illness and death related to PLTX and/or its analogues have been reported through the consumption of contaminated crabs, serranid fish, parrotfish and smoked mackerel (Deeds and Schwartz, 2010; Onuma et al., 1999; Tubaro et al., 2011). Clupeotoxism, caused by consuming tropical clupeoids such as sardines, have been linked with PLTX and/or its analogues in Philippines, Japan, Madagascar, Hawaii, Vanuatu and Bangladesh (Deeds and Schwartz, 2010; Tubaro et al., 2011). *Ostreopsis* blooms in Greece and France were linked to shellfish contamination in the local areas and accumulation of low amounts of PLTX-like compounds has been found in mussels, scallops and Pacific oysters in New Zealand (Aligizaki et al., 2008; Amzil et al., 2012; Malagoli et al., 2008; Rhodes et al., 2002). In the Mediterranean Basin, blooms of *Ostreopsis* cf. *ovata* have caused threats to human health by causing skin and eye irritations and respiratory illnesses (rhinorrhea, pharyngeal pain, dry or mildly productive cough, nose irritation), due to exposure to toxic aerosols and lysed cells (Ciminiello et al., 2006; Durando et al., 2007; Mangialajo et al., 2008). In 2004, 74 cases of respiratory disorders were recorded with up to 200 people potentially affected, coinciding with an *O.* cf. *ovata* bloom.

Ostreopsis blooms adversely impact other benthic organisms by colonizing benthic substrates with mucous mats and potentially producing alleopathic compounds (Accoroni et al., 2016; Monti and Cecchin, 2012). Blooms of *O. siamensis* in northern New Zealand

have been linked to large scale mortalities in sea urchin (*Evechinus chloroticus*) populations whereas, *O*. cf. *ovata* blooms along the Northern Adriatic coast have been associated to increased seasonal mortalities of shellfish species *Patella coerulea* and *Mytilus galloprovincialis* as well as sea urchins (Accoroni et al., 2011; Shears and Ross, 2009).

1.4 Research objectives and thesis outline

Ostreopsis species have been well investigated along the Altantic/Mediterranean coast; however, a considerable knowledge gap exists in their species and population level diversity from the EAC region. Also, no integrated link between the phylogeographic distribution and eco-physiological functional variability in any *Ostreopsis* species as ever been established. As the threat of HABs increase, it is essential to investigate the toxin biosynthesis pathways, in order to develop better diagnostic and monitoring kits for fisheries and aquaculture industries. In this thesis, I have explored these knowledge gaps that link species, population and genetic level diversity back to the functional traits driving the physiology and diversity of *Ostreopsis* species in the EAC oceanic seascape. This thesis is presented as a series of chapters, each of which contributes to addressing a specific aim of this thesis. The chapters are written as stand-alone scientific manuscripts, and are linked and integrated into the existing scientific literature by a general introduction chapter (Chapter 1). The results from the four data chapters (Chapters 2-5) are summarized in a general discussion at the end (Chapter 6).

In Chapter 2, I established the first comprehensive toxicological, morphological and molecular study on an *Ostreopsis* species from Australian waters. A single strain was isolated and established from a shellfish estuary in south-east Australia and identified as *Ostreopsis* cf. *siamensis* using scanning electron microscopy and rDNA molecular markers. The toxicity and growth rates of the strain were compared at varying growth media concentrations. Toxicity was analysed using LC-MS/MS and mouse bioassays.

In Chapter 3, I explored the species biodiversity in the sub-tropical habitats of the north-east Australian coast. A new pseudo-cryptic species, *Ostreopsis rhodesae* sp. nov., was described in association with two other *Ostreopsis* species, *O.* cf. *ovata* and *O.* cf. *siamensis*, using rDNA molecular markers, scanning electron microscopy and compensatory base changes in helices of the ITS2 secondary structures. Fish gill cell line bioassay and LC-MS/MS were used to analyse the toxicity of the species.

In Chapter 4, I systematically sampled the coastline of NSW over a distance of 1,500 kms to establish 68 strains of *Ostreopsis* cf. *siamensis* and investigated their population genetic structure, eco-physiological variability and functional trade-offs. All strains that were established in this study were grown in the same laboratory conditions and their growth rates, cell volume, toxin content, light harvesting and utilizing parameters were measured. In this study, we integrated the physiological variability to phylogeography to highlight a standing genetic and phenotypic diversity in the northern sub-tropical populations in the EAC region.

In Chapter 5, I investigated the toxin biosynthesis pathways of *Ostreopsis* cf. *ovata*, *O.* cf. *siamensis* and *O. rhodesae* and compared it to a species of a closely related genus, *Coolia malayensis*. The study revealed numerous polyketide synthase (PKS) clades similar to previous dinoflagellate studies, but highlighted a novel non-ribosomal peptide synthase (NRPS)/PKS hybrid clade that is common to dinoflagellates. An untargeted metabolic approach was taken to investigate the various putative metabolites produced by the dinoflagellate species along with a targeted LC-MS/MS technique to screen for PLTX-like compounds. This study provides the first in-depth and multi-omics investigation on PLTX biosynthesis in *Ostreopsis* species.

In Chapter 6, I provide a synthesis of the key findings that have arisen from this research and discuss the contributions towards the larger discipline of marine microbial eukaryotes, concluding with suggestions for future directions in this field.

Chapter 2: Molecular phylogeny, morphology and toxigenicity of *Ostreopsis* cf. *siamensis* (Dinophyceae) from temperate south-east Australia

2.1 Abstract

Ostreopsis is a genus of dinoflagellates that includes species producing palytoxin and structurally related compounds. The distribution of *Ostreopsis* species in Australia is largely unknown, but they have been reported from north Queensland (18°S) to Tasmania (41–43°S). *Ostreopsis* spp. have been recurrently reported from estuaries around New South Wales, with persistent occurrences in Merimbula Lake inlet throughout the year. We isolated and characterized a strain of *Ostreopsis* cf. *siamensis* using light and scanning electron microscopy as well as molecular sequences of small subunit (SSU), large subunit (LSU) and ITS regions of ribosomal DNA. The strain grew significantly faster in low nutrient concentrations. Palytoxin-like compounds were produced by the strain, as determined by chemical analysis, and the LD_{50} of the cell extract by intraperitoneal injection in mice was 25.1 mg/kg. This is the first comprehensive molecular, morphological and toxicological study of an *Ostreopsis* species from Australian waters. Increasing reports of *Ostreopsis* from temperate waters suggest an empirical need to expand the knowledge of their diversity and distribution to aid aquaculture monitoring in Australian estuaries.

2.2 Introduction

Species of the marine epiphytic genus *Ostreopsis* Schmidt (1902) occur in tropical and sub-tropical waters attached to coral rubble, macroalgae, seagrass and sand. Nine *Ostreopsis* species have been described based on size and thecal plate patterns (Fukuyo 1981; Besada et al. 1982; Norris et al. 1985; Faust & Morton 1995; Faust et al. 1996; Faust 1999). *Ostreopsis* species have been recorded globally, and more frequently from temperate regions in recent years (Rhodes 2011). Many *Ostreopsis* species produce highly toxic, complex non-peptide marine compounds in the palytoxin (PLTX, $C_{129}H_{223}N_3O_{54}$) group of compounds and also PLTX analogues (including Ostreocin-D, ovatoxins a-g and isobaric palytoxin) (Usami et al. 1995; Ciminiello et al. 2008, 2012b; García-Altares et al. 2014).

PLTX and/or its analogues have been associated with human poisonings through the consumption of contaminated crabs (*Demania* sp. and *Lophozozymus* sp.), serranid fish (*Epinephelus* sp.), parrotfish (*Scarus ovifrons* Temminck & Schlegel) and smoked mackerel (*Decapterus macrosoma* Bleeker) (Alcala et al. 1988; Kodama et al. 1989; Taniyama et al. 2003; Tubaro et al. 2011). Clupeotoxism, caused by consuming tropical clupeoids such as sardines (*Herklotsichthys quadrimaculatus* Rüppell), has been suggested to be related to PLTX, however, this is not yet demonstrated (Onuma et al. 1999; Tubaro et al. 2011). In the Mediterranean Basin, blooms of *Ostreopsis* cf. *ovata* have been associated with human skin and eye irritations and respiratory illnesses, due to exposure to toxic aerosols and lysed cells (Durando et al. 2007; Tichadou et al. 2010; Ciminiello et al. 2014). *Ostreopsis* blooms in Greece and France have caused shellfish contamination in the Mediterranean (Aligizaki et al. 2008; Malagoli et al. 2008; Amzil et al. 2012). Accumulation of low amounts of PLTX-like compounds has been demonstrated in mussels (*Perna canaliculus* Gmelin), scallops (*Pecten novaezealandia* Reeve) and pacific oysters (*Crassostrea gigas* Thunberg) in New Zealand (Rhodes et al. 2002). Blooms of *Ostreopsis siamensis* Schmidt in northern New Zealand have been reported to coincide with large scale sea urchin mortalities (Shears & Ross 2009) highlighting the detrimental ecological impact of such blooms on benthic communities and the marine food web.

Distinguishing *Ostreopsis* species from one another in field samples based upon morphological differences is very difficult, due to their similarity in size, shape and thecal plate patterns, and also their co-existence in the environment (Penna et al. 2005). Almost all described *Ostreopsis* species are distinctly flattened, with a broadly oval to ovate shape, tapering ventrally in apical view. They all have thecal patterns that broadly fit with the description of the type species, *O. siamensis*, with the exception of *O. heptagona* Norris, Bomber et Balech that has a peculiar 1' heptagonal plate, which is not present in other species (David et al. 2013; Hoppenrath et al. 2014). Schmidt (1902) originally reported *O. siamensis* as possessing a rounded apical structure but having an elongated and ventrally pointed epitheca. The cells were reported as coarsely porous, with relatively large sized pores that were visible with light microscopy (Schmidt 1902). Fukuyo (1981) displayed an undulated cingulum, also presented by Schmidt (1902), and reported a single pore size scattered all over the thecal plates for *O. siamensis*. Fukuyo (1981) also proposed a new species, *O. lenticularis* Fukuyo with two pore sizes and no undulation in lateral view. Faust et al. (1996) reported larger sized cells with two kinds of pores for *O. siamensis*. However, lack of information about the undulation of the cingulum, led to uncertainty about the identity of Faust's specimens as *O. siamensis*. Some more recent reports of *O. siamensis* specimens have described cells of various sizes but these studies have lacked molecular genetic data (Table 2.1). The identities of the strains were therefore uncertain. Penna et al. (2005) described *Ostreopsis* cf. *siamensis* from the Italian coast and Catalan Sea with a single class of thecal pore sizes but no undulation in their morphology (Penna et al. 2005). David et al. (2013) reported *Ostreopsis* cf. *siamensis* from the Atlantic Iberian peninsula with two sizes of thecal pores with the smaller pore size class in the internal side of the theca as previously reported by Aligizaki and Nikolaidis (2006) from North Aegean Sea.

Identification of *Ostreopsis* species using molecular sequencing, in particular, ribosomal RNA (rDNA) genes and internal transcribed spacer regions (ITS), has enhanced the accuracy of detection and is increasingly being used with microscopy to resolve the cryptic variations amongst *Ostreopsis* species (Leaw et al. 2001; Penna et al. 2005; Penna et al. 2010; Sato et al. 2011; Tawong et al. 2014). Morphologically cryptic and pseudo-crytic species have been reported within clades of *Ostreopsis* as more isolates from

Atlantic, Mediterranean Sea and the Pacific regions are being sequenced (Sato et al. 2011; David et al. 2013; Penna et al. 2014).

In Australia, *O. siamensis* was first reported from tropical waters of Queensland (Heron Island, Lady Elliot Island and Hoffmans Rocks) based on morphological characteristics and the extraction of water-soluble toxins from isolated cultures similar to *O. siamensis* from Okinawa, Japan (Holmes et al. 1988). An intensive survey of toxic dinoflagellates around the Great Barrier Reef (18-20°S) reported high concentrations of *O. ovata, O. siamensis, O. lenticularis* and *O. heptagona* using light microscopy at Townsville, Magnetic and Orpheus Islands (18–20°S) (Heimann et al. 2009). *Ostreopsis siamensis* has also been reported as far south as the temperate lagoons of Tasmania (41–43°S) where sea surface temperatures can reach 9°C (Pearce et al. 2001). Monitoring of the New South Wales coast (28–37°S) between 2005 and 2009 revealed the recurrent presence of *Ostreopsis* species in 26 of 31 estuaries. However, cells were not identified to species level during this programme (Ajani et al. 2013).

No comprehensive toxicological, morphological and molecular studies have been carried out on *Ostreopsis* species in Australia. The aim of this study was to morphologically and genetically identify an *Ostreopsis* sp. and characterize the growth and morphometric features of the cultured strain. The strain was tested for the presence of PLTX-like compounds using liquid chromatography-mass spectrometry (LC-MS/MS) analysis and the acute toxicity of the sample extract was determined via mouse-bioassay.

2.3 Materials and methods
2.3.1 Site description

Merimbula Lake (36°53'S, 149°55'E) (Figure 2.1) is an open coastal lake with a permanently open entrance and an inlet channel forming a large marine delta that opens into the main basin with a deep center and deep navigational channels. Extensive seagrass meadows occupy over 50% of the lake bed, forming the fourth largest seagrass bed on the New South Wales South Coast. The beds consist mostly of strap weed (*Posidonia*

australis Hooker), eel grass (*Zostera capricorni* Ascherson) and paddleweed (*Halophila* spp.) (West et al. 1985; Williams et al. 2006).

Merimbula Lake is the fourth most productive estuary for the cultivation and sales of Sydney rock oysters (*Saccostrea glomerata* Gould) since 2010, along the coast of New South Wales (NSW Department of Primary Industries, 2013–14). Oyster farms are mainly in the southern part of the lake, which is shallower than the main basin. The inlet also provides for a wide variety of recreational fishing activities.

2.3.2 Sample collection and culture establishment

In May 2012, seagrass samples (*Zostera* sp.) were collected from approximately 1 m depth. At the time of sample collection, sea surface temperature was 17°C. Salinities in Merimbula Lake inlet commonly range from 30 to 35. Samples were placed in plastic bags containing local seawater and shaken vigorously to detach the epiphytic microalgal cells. The epiphytic suspension was then passed through a 100 μm mesh filter to remove larger fauna and debris (Kohli et al. 2014). Using a glass micropipette, a single *Ostreopsis* cell was isolated from this suspension under an inverted microscope and transferred to a drop of clean filtered seawater. The transfer was repeated five times until no nano- and pico- planktonic cells were observed in the vicinity of the cell under the inverted microscope. A non-axenic monoclonal culture was established in f/2 medium (Guillard 1975).

The strain was grown in 50 mL sterile tissue culture flasks (Becton Dickinson, Sydney, Australia) in both f/2 and f/10 media at 18°C and salinity of 35 under irradiance of 60-100 μmol photons m^{-2} s^{-1} and 12:12 hour light-dark cycle. It has now been deposited at the Cawthron Institute Culture Collection of Microalgae, New Zealand (CICCM: CAWD203).

Fortnightly water samples were collected from a depth of 50 cm and preserved with Lugol's iodine solution. Harmful phytoplankton cells were counted and identified using phase contrast light microscopy (Ajani et al. 2013). *Ostreopsis* cells were identified to genus level only for the monitoring program.
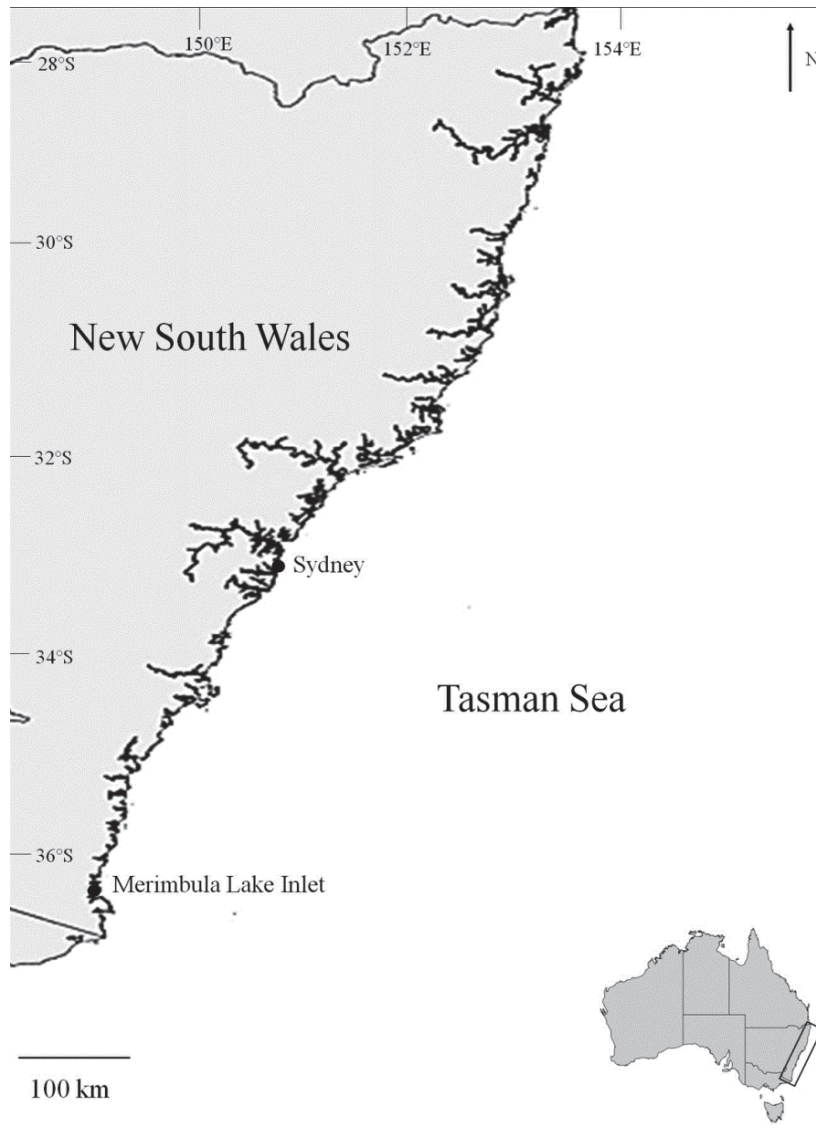
Figure 2.1 Map showing Merimbula lake inlet, south-east New South Wales, Australia.

2.3.3 Light microscopy

Living cells of interest were picked using a Leica DMIL inverted microscope (Leica Microsystems GmbH, Wetzlar, Germany), placed on an object slide and observed with a Leica DMRB (Leica Microsystems GmbH) equipped with differential interference

contrast and epifluorescence optics at 400 and 640 times magnification with oil immersion objectives. Digital photos were taken using a Leica DFC420C camera (Leica Microsystems GmbH).

2.3.4 Scanning electron microscopy (SEM)

For SEM, the culture was fixed with Lugol's solution for several weeks. Cells were treated with hydrogen peroxide (H_2O_2) for one day and then were placed on a 5 μm Millipore filter (Merck Millipore Darmstadt, Germany), rinsed in distilled water, and dehydrated in a series of increasing ethanol concentrations (30, 50, 70, 85, 90, 100 %), followed by chemical drying with hexamethyldisilazane at room temperature. When completely dry, the sample was mounted on a stub and sputter coated with gold-palladium (Bal-Tec SCD 050; BAL-TEC Präparations-gerätevertrieb, Wallof, Germany). Cells were observed using a Tescan VEGA3 microscope (Elekronen-Optik-Service GmbH, Dortmund, Germany) at 15 kV.

2.3.5 DNA extraction, PCR amplification and sequencing

DNA was extracted using FastDNA Spin kit for Soil (MP Biomedicals, Solon, USA), according to the manufacturer's protocol. The extracted DNA was visualised on 1% agarose gel and quantified using a Nanodrop ND-1000 (NanoDrop Technologies, Wilmington, USA). The near complete SSU rDNA, the D1/D3 and D8/D10 regions of the LSU rDNA, ITS and 5.8S rDNA gene regions (ITS1/5.8S/ITS2) were amplified and sequenced using primers as listed in supplementary data S1.

All PCR reactions were performed in 25 μL reaction volumes containing 12.5 μL 2× Immomix (Bioline, Sydney, Australia), 7.5 pmol of each primer, 1 μg μL^{-1} of BSA (Biolabs, Arundel, Australia), 1 μL of template DNA and PCR grade water to give the final volume. Thermocycling conditions consisted of an initial denaturing step of 95°C for 10 min, followed by 30 cycles of 95°C for 20 s, 30 s annealing (see supplementary data S1), 72°C for 1 min and a final extension of 72°C for 7 min. PCR products were purified with DNA Clean and Concentrator (Zymo Research, Irvine, USA) according to

the manufacturer's protocol. The PCR products were sequenced using a commercial service (Macrogen Inc., Seoul, Korea).

2.3.6 Sequence alignment and phylogenetic analysis

Analyses on SSU rDNA, ITS1/5.8S/ITS2, D1/D3 and D8/D10 region of LSU rDNA were conducted separately. The forward and reverse sequences were trimmed, aligned and visually refined using BioEdit v7.2.5 (Hall 1999). The obtained sequences were aligned with reference sequences retrieved from GenBank (see supplementary data S2). Multiple sequence alignments were performed using ClustalW v1.6 program as implemented in MEGA v6 (Tamura et al. 2013) and manual inspection. Phylogenetic analysis was performed using both a maximum likelihood (ML) and Bayesian inference (BI) approach.

ML trees were produced in MEGA v6 using Tamura 3 (T92) + G + I with 5 gamma categories substitution model for all sequence analyses. Substitution models were selected for each dataset based on lowest Bayesian Information criterion as a measure of the relative quality of the models. Nodal support of the ML tree was estimated via bootstrap algorithm with 1,000 replications. Bayesian analysis was performed using MrBayes v3.2.2 (Ronquist & Huelsenbeck 2003) as implemented in Geneious v6 (Kearse et al. 2012) using general time reversible (GTR) + gamma model for all analyses. Four independent Markov Chain Monte Carlo simulations were run simultaneously for 2,000,000 generations. Trees were sampled every 1,000 generations and 1,000 trees were discarded as burn- in.

2.3.7 Growth rate and cell size

To compare the strain growth rates in f/2 and f/10 batch cultures, 500 mL Erlenmeyer flasks containing 300 mL media were placed in an $18°C$ incubator under the photo illumination of 60–100 μmol photons $m^{-2}s^{-1}$ and 12:12 hour light-dark cycle. Triplicates were inoculated with exponentially growing cells (starting cell amount 60,000 cells) from respective stock cultures. Flasks within the incubator were randomly positioned during the experiment. Every two days, the flasks were gently shaken before collecting 3 mL of

culture volume to determine cell abundance in triplicates using a Sedgwick-Rafter chamber. The extracted culture volume was treated with 4 mM hydrochloric acid to dissolve mucous aggregates without disrupting *Ostreopsis* cells (Guerrini et al. 2010). Specific growth rates (μ) were calculated using the slope of natural log of cell number against culture day during exponential growth phase. Differences in growth rates between different media were tested using one-way analysis of variance (ANOVA) in SPSS v22.0 (IBM, Armonk, USA).

Cell dimensions were measured under 400 × magnifications and analysed using a calibrated scale in the eyepiece of an inverted microscope Eclipse TS100 (Nikon, Hilton, Australia). Cells in exponential growth phase were fixed in 1% Lugols to measure the depth = dorsoventral diameter (DV) and transdiameter width (W) using ImageJ v1.48 (Rasband 1997-2013).

2.3.8 Toxin analysis via LC-MS/MS and bioassays

Ostreopsis culture grown in f/10 medium was harvested in late stationary phase (Day 20) via centrifugation (50 mL; 2,300 *g*; 10 min; room temperature) and the cell pellet was freeze dried. Screening for PLTX-like compounds was conducted using a quantitative LC-MS/MS method at the Cawthron Institute, New Zealand as described in Selwood et al. (2012). This analytical approach monitors substructures generated by the oxidative cleavage, using periodic acid, of vicinal diol groups present in the intact toxins. Periodate oxidation of vicinal diols results in cleavage of carbon-carbon bonds via a cyclic transition state with formation of two aldehyde-containing fragments. It yields an amino aldehyde common to known palytoxins, ovatoxins and ostreocins, and an amide aldehyde that varies depending on the toxin type.

The cell pellet was resuspended in 4 mL of methanol-water (1:1 v/v) and then ultrasonicated for 20 min in a 59 kHz sonication bath (model 160HT, Soniclean Pty, Thebarton, Australia). The sample was centrifuged at 3,000 *g* for 5 min and 2 mL of supernatant was loaded onto the solid phase extraction cartridges for on-column periodic

acid oxidation. PLTX standards (5, 10, 20 and 50 ng mL^{-1}) were processed to generate a calibration curve. The limit of detection was determined to be 0.5 ng mL^{-1} for the PLTX amine fragment. The relative standard deviation of repeatability for LC-MS of oxidized PLTX standards were <10% and <8% for amino aldehyde and amide aldehyde, respectively, at 1 or 2 ng mL^{-1}, making this method suitable for monitoring trace levels of PLTX and/or its analogues (Selwood et al. 2012). Several additional multiple reaction monitoring transitions were also included to monitor oxidative cleavage fragments from other known PLTX-like compounds, such as bishomopalytoxin.

Mouse bioassays were conducted at AgResearch, Hamilton, New Zealand, using methanolic extract after removing all of the solvent from the cell pellet. The pellet was extracted using 5 mL methanol taken to dryness under nitrogen. This extract was then resuspended in 1% Tween 60 in saline and administered by intraperitoneal injection in Swiss albino mice (body weight 18-20 g) at various dose levels. LD$_{50}$ values were determined by the up and down method according to Organisation for economic Cooperation and Development Guideline 425 (OECD 2006). All mouse experiments were approved by the Ruakura Animal Ethics Committee.

Table 2.1 Geographic, morphological and molecular reports of *Ostreopsis siamensis*/ *Ostreopsis* cf. *siamensis*.

Site	DV (in µM)	W (in µM)	DV: W	Pores (in µM)	Ribotype	Reference
Koh Chang, Gulf of Thailand	90 F	–	NA	1 size	No	Schmidt 1901
Ryukyu Islands, Japan	60–100 F	45–90 F	NA	1 size	No	Fukuyo 1981
East China Sea, Mascareignes Archipelago, Caribbean Sea	108–123 F	76–86 F	1.42	0.5 and 0.1	No	Faust 1996
Northland, New Zealand	30–68 C 60–85 F	20–55 C 38–45 F	NA	0.08–0.1 0.18–0.38	No	Chang et al. 2000; Rhodes et al. 2000
North Aegean Sea, Greece	36–66 F	24–50 F	NA	0.23–0.29	No	Aligizaki & Nikolaidis 2006
Tyrrhenian Sea, Italy	50–75 C 63–90 F	38–62 C 34–56 F	NA	0.11–0.56	Yes	Penna et al. 2005
Peter the Great bay, Russia	63–78 F	36–54 F	1.3–1.9	0.14–0.32	No	Selina & Levchenko 2011
Cantabrian Sea, Bay of Biscay	51–67 C	33–56 C	NA	NA	Yes	Laza–Martínez et al. 2011
Galé, Portugal	55–75.5 F	27–56 F	1.1–2.1	0.07–0.13 0.15–0.39	Yes	David et al. 2013
San Sebastian, Spain	52–72 F	36–57 F	1.1–1.8	0.07–0.13 0.15–0.39	Yes	David et al. 2013
Heron Island, Australia	36–60 C 88–115 F	26–51 C 64–93 F	1–1.8 C 1.2–1.6 F	NA	No	Holmes et al. 1988
Isolabella, Italy	50–70 C	35–55 C	1.35	NA	Yes	Ciminiello et al. 2013
Merimbula, Australia	34–47 C	24.5–42 C	1.1–1.7	2 sizes	Yes	This Study

C–Cultured isolates; F–Field samples; NA–Data not available

2.4 Results

2.4.1 Morphology

The strongly antero-posteriorly flattened cells of the cultured *Ostreopsis* were drop/tear-shaped to nearly round (extremely wide) and ventrally tapering (Figure 2.2A, D, E). Smaller cells had a more symmetrical ovate shape (Figure 2.2C). Cells are 34–47 μm (41 ± 3 (SE), $n = 49$) long (in DV) and 24.5–42 μm (33 ± 4, $n = 49$) wide (in W), and varied from 1.1 –1.7 (1.3 ± 0.1, $n = 49$) in DV/W ratio. Cells are densely packed with golden-brown chloroplasts, except for the ventral area (Figure 2.2A–E). The nucleus is located dorsally (Figure 2.2A, D). Cells with one (Figure 2.2C) or two pusules (Figure 2.2D) are observed. The curved, long and narrow apical pore complex is located parallel to the left dorsal cell margin (Figure 2.2E). The cingulum is narrow and straight (not shown).

The plate formula is APC, 3', 7'', 6/7c, 6-7s, 5''', 2''''' (Figures 2.2F, G, 2.3, 2.4). Thecal plates are smooth with scattered pores of two size classes. The larger "pores" are shown to be depressions with few small pores inside, which are best visible on plate inside views (Figure 2.3D). Small pores are recorded only in low numbers, not evenly distributed on the plates and not recognizable in all cells (Figure 2.3D). The first apical plate (1') is long, hexagonal and located nearly in the center of the epitheca (Figures 2.2F, 2.3A). The third precingular (3'') and third apical (3') plates are in contact. The fifth precingular plate (5'') is hexagonal and not connected to the 1' plate (Figures 2.2F, 2.3A). The slightly curved and narrow apical pore plate with slit-like pore is about 7.2–8.4 μm long (Figure 2.3A, C). The plate margin connecting the third (3''') and fourth (4''') postcingular plates is nearly equal to the dorsoventral axis (Figures 2.2G, 2.3B).

Both plates are relatively large and not markedly different in size. Cingular plates are difficult to determine; six or seven plates are recognized (Figure 2.2F, G). In two cases it looked like the second and sixth plate respectively could split into two plates. More observations are needed for the cingular plates. Broken cells allowed the determination of the sulcal plates (Figure 2.4). Six or seven sulcal plates were observed (Figure 2.4), with seven plates including the split of the right anterior sulcal plate (sda) into two plates.

2.4.2 Phylogeny

ML and BI analyses conducted on SSU, LSU (D1/D3 and D8/D10) and ITS1/5.8S/ITS2 rDNA regions had the same topology and placed the Australian strain in a strongly supported clade with *Ostreopsis* cf. *siamensis* strains from Europe and New Zealand (only the ML trees are shown; BI = 1.00, ML = 100 for LSU rDNA and BI = 0.76, ML = 99 for ITS) (Figures 2.5, 2.6) (Accession numbers KT868526, KT868527 and KT868529). The ITS1/5.8S/ITS2 and D8/D10 LSU rDNA trees showed nine distinct clades and subsequent geographical sub-clades amongst the genus *Ostreopsis* as previously described in Sato et al. (2011) and Tawong et al. (2014) (Figures 2.5A, 2.6A).

The D1/D3 LSU rDNA sequences for *Ostreopsis* sp. 4 and *Ostreopsis* sp. 3 were not available in the GenBank but the topology of the phylogenetic tree was similar to that of the D8/D10 LSU rDNA analysis (Figure 2.5). No *Ostreopsis* cf. *siamensis* SSU rDNA sequences were available in the database (Figure 2.6). When aligned with the other *Ostreopsis* SSU rDNA sequences, *Ostreopsis* cf. *siamensis* showed 6.8% differences to *Ostreopsis* cf. *ovata* (Korea) and 6.5% differences to *Ostreopsis* cf. *ovata* (Malaysia) (see supplementary data S3).

2.4.3 Culturing and growth rates

Ostreopsis cf. *siamensis* grew successfully in f/10 and f/2 and displayed a typical growth curve (Figure 2.7). Aberrant cell shapes were observed in f/2 culture and the strain showed a growth rate of 0.24 ± 0.006 div day^{-1} (exponential phase between days 7–16) and a maximum yield of 23,700 cells mL^{-1}. The cell density remained high and relatively constant during the whole stationary phase. Cultures maintained in f/10 media grew faster, with a growth rate of 0.39 ± 0.01 (ANOVA, $p < 0.001$) (exponential phase between days 5–11). The cell density declined rapidly after reaching a maximum yield of 28,100 cells mL^{-1}.

2.4.4 Distribution and abundance

Routine monitoring of plankton samples from New South Wales shellfish growing areas during 2005–2015 detected *Ostreopsis* bloom-like episodes (upto 750–1,000 cells L^{-1}) at Merimbula Inlet, in October 2006, October 2010 and September and November 2013 (Figure 2.8). High abundances consistently occurred in the warmer months (October–December), but sparse cells were persistent in April–August (austral winter) (Figure 2.8).

2.4.5 Toxin analysis and toxicity

LC-MS/MS analysis of the oxidized cell extract showed presence of the amino aldehyde fragment, common to all known palytoxin, ovatoxin and ostreocin analogues. However, the PLTX amide fragment was not detected suggesting that another structurally related analogue gave rise to the amine fragment observed (Figure 2.9). The total amount of PLTX-like compounds was determined as 4.62 ng (total 26,700 cells) resulting in an estimate of 0.17 pg $cell^{-1}$.

The LD_{50} of *Ostreopsis* cf. *siamensis* extract by intraperitoneal injection in mice was 25.1 mg kg^{-1} (95% confidence interval of 14.0–33.2 mg kg^{-1}). The mice became hunched and lethargic soon after dosing, and remained so during the day of dosing. Loss of appetite and significant amount of weight loss was reported over the next 3 days. By the fifth day since dosing, the condition and appetite had improved, and they recovered over the remainder of the two-week observation period. The appearance and behaviour of mice was normal during this time, however, adhesions between the liver and diaphragm and between the liver and stomach were noted at necropsy indicating an irritant effect, but no other macroscopic changes were recorded. At a higher dose, the hind legs became paralysed and extended, and they died after 7.5 hours without any reported abnormalities in necropsy

.
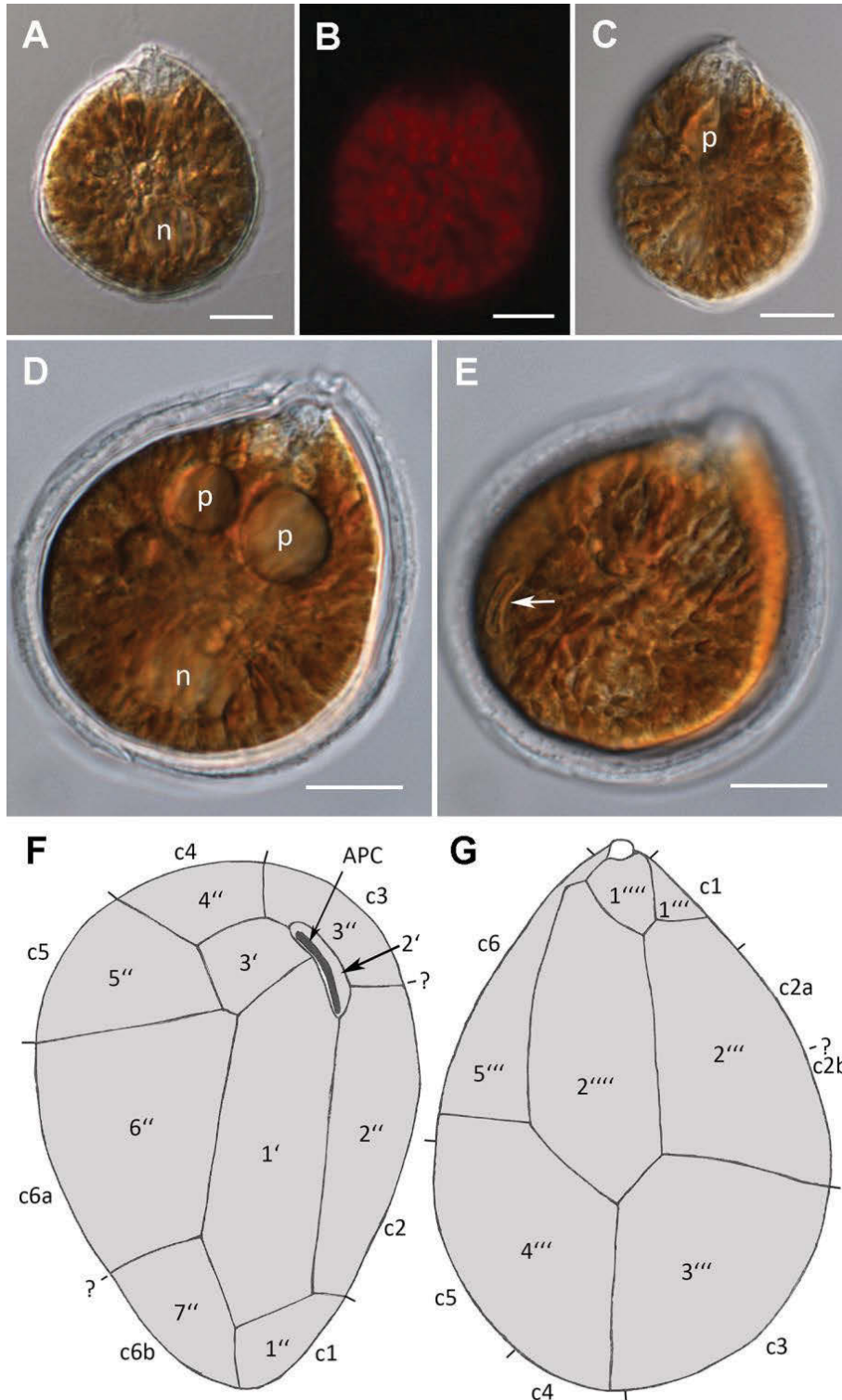
Figure 2.2 *Ostreopsis* cf. *siamensis* CAWD203 from Merimbula taken using light microscopy. A, C–E: Differential interference contrast showing the general morphology; and B: epifluorescence demonstrating the autofluorescence of the chloroplasts. A: Typical very wide cell, note the colourless ventral area and the dorsal nucleus (n). B: Chloroplast fluorescence of the cell shown in A. C: Smaller and narrower cell with one pusule (p) visible in the ventral cell half connected to the ventral area. D, E: Same cell in different focus. D: Note the nucleus (n) in the dorsal area and the two pusules (p). E: The apical pore complex (arrow) in the dorsal area. F, G: Line drawings illustrate the thecal plate pattern of the epitheca (F); and hypotheca (G) including cingular plates. The scale bars represent 10 μm. '?' represent verification of cingular plate borders.

44

Figure 2.3 Scanning electron micrographs (SEM) of *Ostreopsis* cf. *siamensis* CAWD203 from Merimbula. A: Epitheca; and B: Hypotheca. C: Inside view of the apical pore complex and surrounding plates. D: Plate detail showing two size classes of pores, small (arrowhead) and large (arrow) ones. Scale bars represent 10 μm in A, B; 5 μm in C, D.
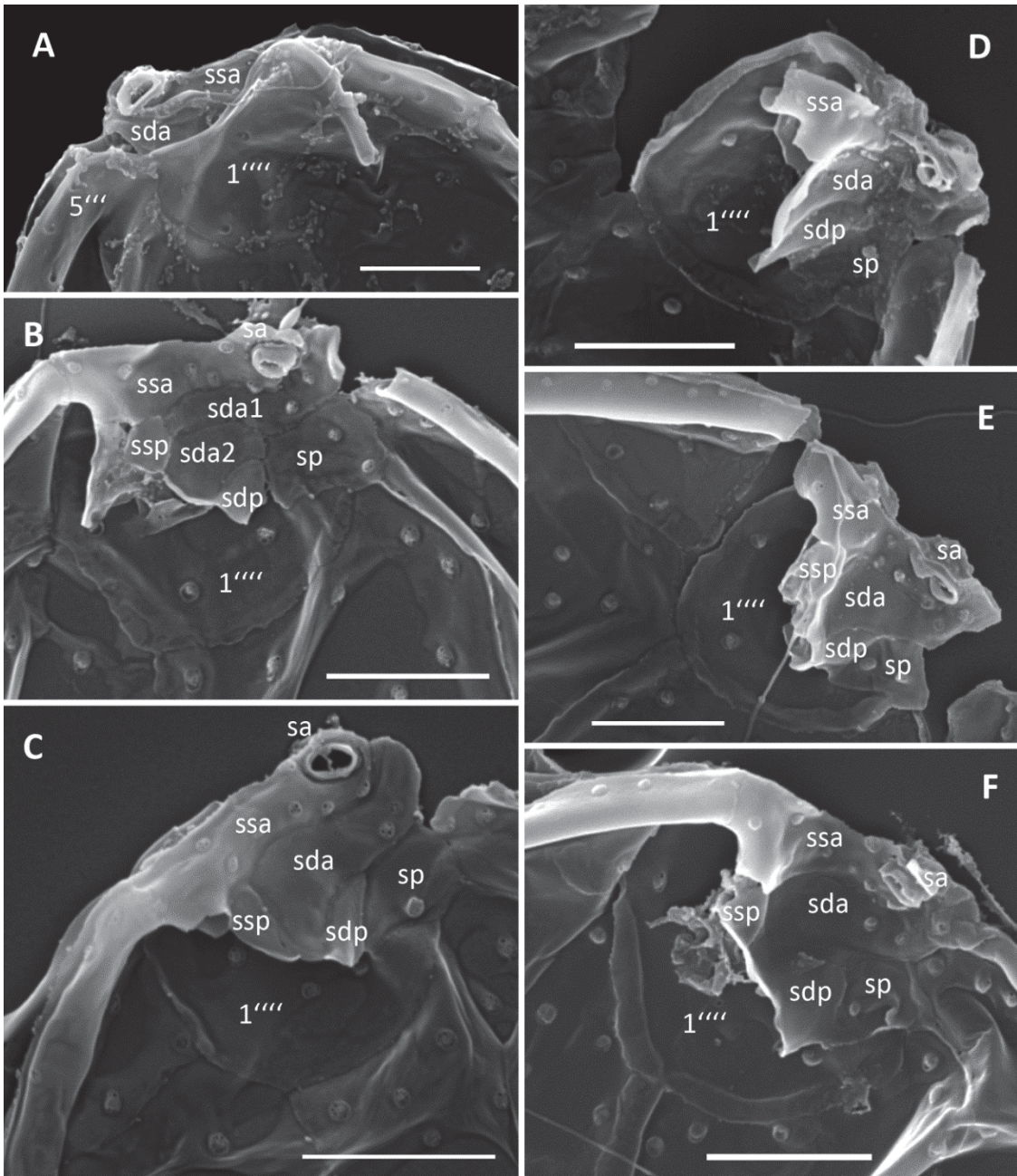
Figure 2.4 SEM of *Ostreopsis* cf. *siamensis* CAWD203 from Merimbula. Details of the sulcal area. A: Hypothecal view of the ventral area. B–F: Inside views of broken cells. sa = anterior sulcal plate, ssa = anterior left sulcal plate, ssp = posterior left sulcal plate, sda = anterior right sulcal plate, sdp = posterior right sulcal plate, sp = posterior sulcal plate, 1'''' = first antapical plate. Scale bars represent 5 μm.

2.5 Discussion

This is the first study to characterize the morphology, molecular phylogeny, toxigenicity and growth characteristics of an *Ostreopsis* species from Australian waters. The *Ostreopsis* strain isolated from Merimbula was identical in ITS/5.8S regions to strains identified as *Ostreopsis* cf. *siamensis* from the Atlantic/Mediterranean region and New Zealand, which was further confirmed with D1/D3 and D8/D10 regions of LSU rDNA.

In this study, we documented the smallest cell size ranges yet reported for the species. In comparison to published records of *Ostreopsis* cf. *siamensis,* this population has a straight cingulum path in lateral view as described by David et al. (2013) and Penna et al. (2005), in contrast to the original description by Schmidt (1902) and observations by Fukuyo (1981) and Rhodes et al. (2000). Aligizaki and Nikolaidis (2006) stated that cingulum is sometimes undulated in side view. Thecal plates have small pores and large depressions that have been recorded as large pores in the literature (Faust et al. 1996; Aligizaki & Nikolaidis 2006; David et al. 2013). Fukuyo (1981), Rhodes et al. (2000), Penna et al. (2005) and Laza-Martinez et al. (2011) described only one pore size class (large). In the Merimbula population, small pores were not evenly distributed on the plates and rare. They were not recognizable in all cells. That is different from the evenly distributed small pores reported for *Ostreopsis* species so far (e.g. Fukuyo 1981; Fast et al. 1996). The apical pore plate (Po) was found to be 7.2-8.4 µm, smaller than that reported by David et al. (2013) (10.3–11.9 µm) and by Aligizaki and Nikolaidis (2006) (~11 µm), but similar to that reported by Laza-Martinez et al. (2011) (7–9 µm). The third precingular plate of *Ostreopsis* cf. *siamensis* shown by Laza-Martinez et al. (2011, Figure 21) is different in size and location compared to our and previous studies. From published observations, the species has no clearly distinguishable morphological characterization (Table 2.1). Such morphological plasticity and/or ambiguities within the genus *Ostreopsis*, especially for *O. siamensis*, *O. ovata* and *O. lenticularis*, has led to repeated statements of the need to re-investigate the type localities of *Ostreopsis* species (Parsons et al. 2012; Hoppenrath et al. 2014).
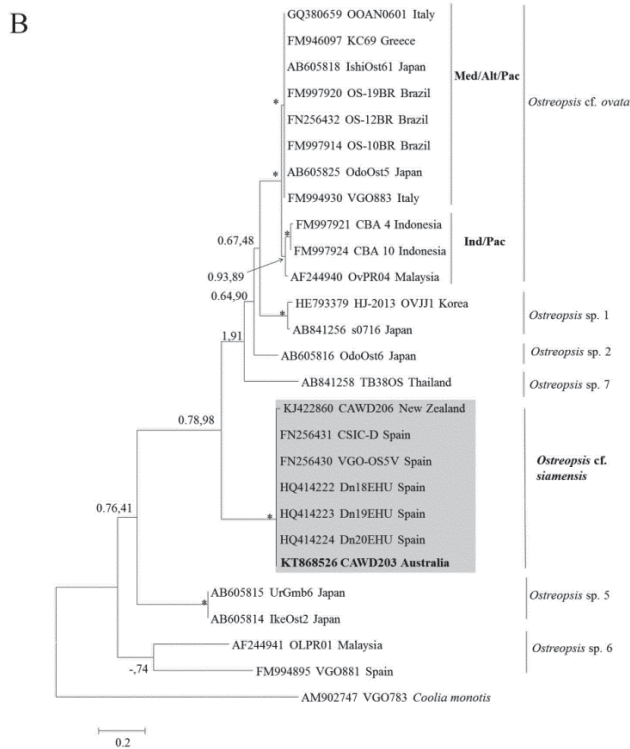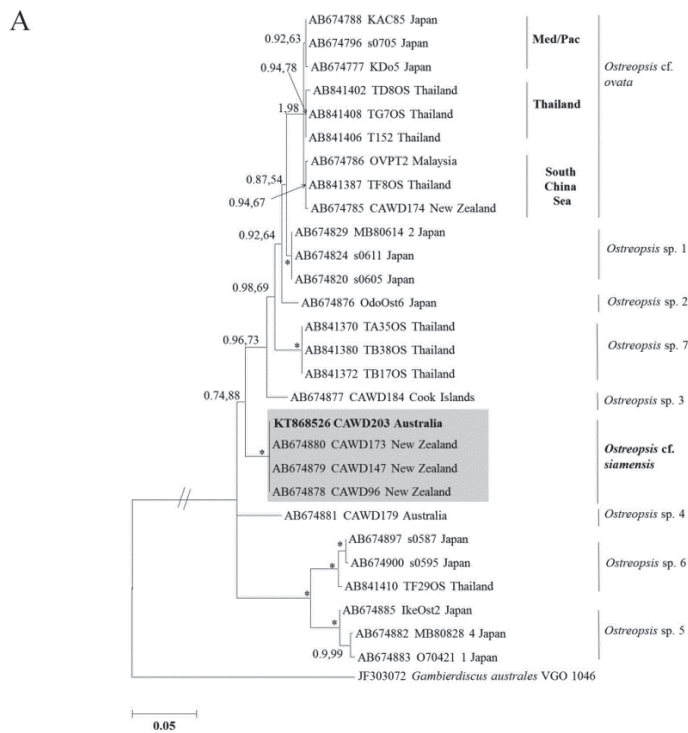
Figure 2.5 Maximum Likelihood (ML) phylogenetic trees of various *Ostreopsis* strains using A: D8/D10; and B: D1/D3 LSU rDNA regions. Merimbula strain CAWD203 shown in bold letters in *Ostreopsis* cf. *siamensis* clade shaded grey. External black vertical bars show each distinct *Ostreopsis* clade and internal vertical bars show each *Ostreopsis* sub-clade. Med, Atl, Pac and Ind represent Mediterranean Sea, Atlantic, Pacific and Indian Oceans sub-clades, respectively. South China Sea and Thailand are the *Ostreopsis* cf. *ovata* South China Sea and Gulf of Thailand sub-clades respectively. Numbers at nodes represent posterior probabilities from BI and bootstrap support values from ML based on 1,000 pseudo-replicates. Robust branches (BI=1.00 and ML=100) are indicated by asterisks.

A

```
                                    ┌─ KT868527 CAWD203 Australia
                                    ├─ AB674915 CAWD96; CAWD147; CAWD173 New Zealand
                                    ├─ FM244729 CNR-T5 Italy
                                    ├─ AJ301643 CNR-B4 Italy
                                    ├─ AJ312944 CSIC-D5 Spain
                                    ├─ AJ319871 IEO 1V Spain
                                    ├─ AJ491313 IEO-2V Spain
                                    ├─ AJ491332 IEO-3V Mediterranean Sea          Ostreopsis cf. siamensis
                                    ├─ AJ491333 CSIC-D1 spain
                                    ├─ AJ491335 CNR-B5 Italy
                                    ├─ AJ491334 CSIC-D7 spain
                                    ├─ JX987676 Dn91EHU Portugal
                                    ├─ JX987699 Dn201EHU France
                                    ├─ JX987692 Dn188EHU Spain
                                    ├─ JX987698 Dn199EHU Portugal
                                    ├─ JX987683 Dn144EHU Spain
                                    ├─ JX987682 143EHU Spain
                                    ├─ JX987681 142EHU Spain
                                    └─ JX987675 Dn86EHU Portugal
```

0.76,99

0.98,94 AF218455 OvPD06 Malaysia   Malacca
1,83   AF218456 OvPD07 Malaysia
0.97,94 FM244727 CBA 10 Indonesia   Celebes   Ostreopsis cf.ovata
1,93   FM244725CBA 6 Indonesia
         * AB674902 T60730 1 Japan   Med/Alt/Pac
         AB674906 KAC85 Italy
         * AB841242 T194 Thailand   Thailand
0.87,69 AB841247 T203 Thailand
0.53,-   AB674905 OVPT2 Malaysia   South China
         AB674904 CAWD174 cook Islands Sea
0.89,99
         HE793379 HJ-2013 OVJJ1 Korea
0.99,96 AB674910 s0617 Japan   Ostreopsis sp. 1
0.59,77 AB674909 MB61007 3 Japan
0.9,90   AB674908 T70828 5 Japan
         AB674913 OdoOst6 Japan   Ostreopsis sp. 2
0.67,70 AB674914 CAWD184 Cook Islands   Ostreopsis sp. 3
         -,98 FM244637 VGO881 Canary Islands   Ostreopsis sp. 4
         AB674916 CAWD179 Australia
         -,56 * AB841211 TA35OS Thailand   Ostreopsis sp. 7
         AB841218 TB30OS Thailand
1,83   AF218465 Ostreopsis lenticularis Malaysia   Ostreopsis sp. 6
         FM244728 VGO897 Malaysia
1,96   AB674921 OU11 Japan
1,97   AB674917 MB80828 4 Japan   Ostreopsis sp. 5
         AJ308524 Coolia monotis SZN 43
         AJ319578 Coolia monotis 2V

0.2

B

```
                    ┌─ KF359997 ORUS A2 Sea of Japan
                    ├─ KF359996 ORUS A1 Sea of Japan
                    ├─ KF359998 ORUS H1 Sea of Japan
                    ├─ KF359999 ORUS H2 Sea of Japan
               *    ├─ KF360000 ORUS K2 Sea of Japan    Unclassified Ostreopsis sp.
                    ├─ KF360004 ORUS J2 Sea of Japan
              *     ├─ KF360003 ORUS J1 Sea of Japan
                    ├─ KF360002 ORUS O2 Sea of Japan
                    └─ KF360001 ORUS O1 Sea of Japan
   0.64,68    HE793379 HJ-2013 Korea                    Ostreopsis sp. 1
              AF244939 OvPR04 Malaysia                  Ostreopsis cf. ovata
              KT868529 CAWD203 Australia                Ostreopsis cf. siamensis
         *    KJ362006 Alexandrium ostenfeldii K1354
              KF925334 Alexandrium andersonii CCMP2222
```

0.05

Figure 2.6 ML phylogenetic trees of various *Ostreopsis* strains using A: ITS1/5.8S/ITS2; and B: SSU rDNA regions. See the caption in Figure 2.5 for the detailed information.

49

Ostreopsis siamensis was initially described from the Gulf of Thailand (Schmidt 1902), however, no culture material from the type location was available till recently. Tawong et al. (2014) described the diversity and distribution of *Ostreopsis* spp. from the Gulf of Thailand and conducted sampling at Koh Chang, the type location for *O. siamensis*. Strains of *O. ovata* (Thailand sub-clade) were identified using molecular markers from this location that morphologically matched the description of *O. ovata* by Fukuyo (1981). This *O. ovata* sub-clade was most dominant in the Gulf of Thailand and present at all sampling sites, but no *Ostreopsis* cf. *siamensis* ribotype was reported (Tawong et al. 2014). Schmidt (1902) also reported the presence of large single sized pores for *O. siamensis* which was confirmed by Fukuyo (1981) from samples he obtained from Ryukyu Islands, Japan. Extensive sampling around the Japanese coast conducted in Sato et al. (2011) did not find any ribotype for *Ostreopsis* cf. *siamensis* from this region but described *O. ovata* complex with a cryptic new clade, *Ostreopsis* sp. 1. Conflicting descriptions of pore sizes and cingulum undulation have been reported for *Ostreopsis* species, and these reports have generally lacked genetic data (Fukuyo 1981; Faust & Morton 1995; Faust et al. 1996; Faust 1999; Chang et al. 2000; Rhodes et al. 2000; Aligizaki & Nikolaidis, 2006). David et al. (2013) differentiated between *Ostreopsis* cf. *siamensis* and *Ostreopsis* cf. *ovata* by the presence of single sized pores for *Ostreopsis* cf. *ovata* in contrast to *Ostreopsis* cf. *siamensis* but did not observe any differences between both species based on thecal plate structures. Such historical and recent evidence suggests Schmidt's original description of *O. siamensis* may be closer to our present understanding of *Ostreopsis* cf. *ovata* and *Ostreopsis* cf. *siamensis,* possibly representing a different species than previously described (Penna et al. 2005; Penna et al. 2012; David et al. 2013).

Molecular and morphological characterization of *Ostreopsis* cf. *siamensis* has been reported from the Atlantic-Iberian Peninsula, Mediterranean Sea, Aegean Sea and northern New Zealand with morphological reports from as north as Peter the Great bay in Russia (Penna et al. 2005; Aligizaki & Nikolaidis 2006; Shears & Ross 2009; Selina & Orlova 2010; Rhodes 2011; David et al. 2013; Rhodes et al. 2014). This suggests the species are common in temperate waters ($> 30^{\circ}$N and 30°S) than other *Ostreopsis* species. Although phylogeographical studies using ITS and LSU rDNA regions have unravelled

genetic diversity among geographically separated populations of *O. ovata* (Penna et al. 2005, 2010), no significant differences in *Ostreopsis* cf. *siamensis* populations were observed using these molecular markers (Figures 2.5A, B, 2.6A). The significant genetic differences among the different *O. ovata* sub-clades indicate that these might be considered separate species in the future (Penna et al. 2014) which might also be the case for *Ostreopsis* cf. *siamensis* (refer to Chapters 3 and 4).
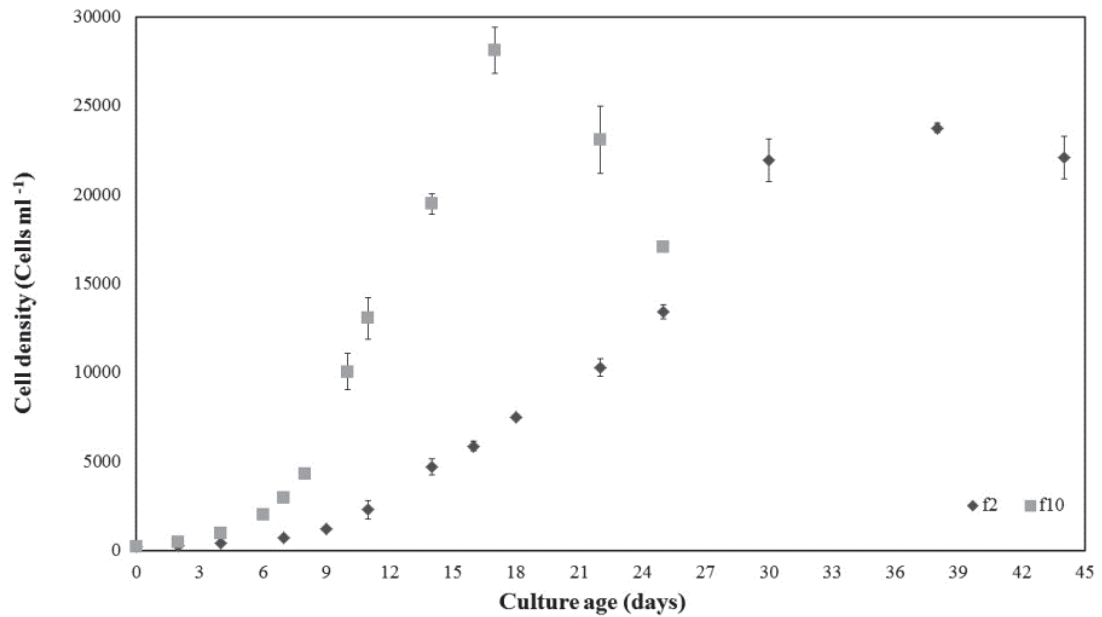
Figure 2.7 Growth pattern of *Ostreopsis* cf. *siamensis* from Merimbula in f/2 and f/10 batch cultures. Each point represents the mean ± SE of three experiments of three replicates.

At 18°C, which is close to the temperature at the site of isolation (17°C), *Ostreopsis* cf. *siamensis* grew more rapidly in lower nutrient conditions in our study (Figure 2.7), similar to *Ostreopsis* sp. 7 and its growth in IMK/2 medium as opposed to IMK medium (Tawong et al. 2015). *Ostreopsis* cf. *siamensis* isolate from Northland, New Zealand grown in 20% GP media at 25°C exhibited a growth rate of 0.3 div day[-1] (Rhodes et al. 2000). The growth rate for *Ostreopsis* cf. *siamensis* from Tasmania was reported to be higher (0.53 div day[-1]) in low nitrogen and phosphate containing K media at 20°C compared to nutrient rich GSe and f/2 media (Pearce et al. 2001) (see supplementary data S4). *Ostreopsis* cf. *siamensis* may grow faster in low nutrient conditions; however, strain-specific variability may occur, as documented in other dinoflagellate species (Doblin et al. 2000; Burkholder & Glibert 2006; Lartigue et al. 2009). Aberrant cell shapes were also reported from an *Ostreopsis* cf. *siamensis* culture from Tasmania grown in f/2 media (Pearce et al. 2001).

Similar morphological irregularities were also reported from *Ostreopsis* cf. *ovata* when grown in L-2 medium as opposed to L-2/2 (Nascimento et al. 2012).

	Jan	Feb	Mar	Apr	May	Jun	Jul	Aug	Sept	Oct	Nov	Dec
2005										x ▓	x	x
2006	x	x	▓	x	x					▓ ▓	x	
2007	▓ ▓			x			▓	x		▓	x	x
2008					x	x					▓ x	
2009		▓	▓		x	x	x x	▓	x		x	▓ ▓
2010	▓	x		x ▓	▓	x	x			▓ ▓		
2011		x				x						
2012					x	x x	x x	x	x	▓	x ▓	x
2013			x x				x		▓ ▓		▓ ▓	
2014			x ▓		▓	x	x ▓	x ▓	▓	x	x	
2015			▓ x		▓							

< 100 cells L⁻¹ (light grey)   > 100 cells L⁻¹ (dark grey)   Absent (white)   No sample X
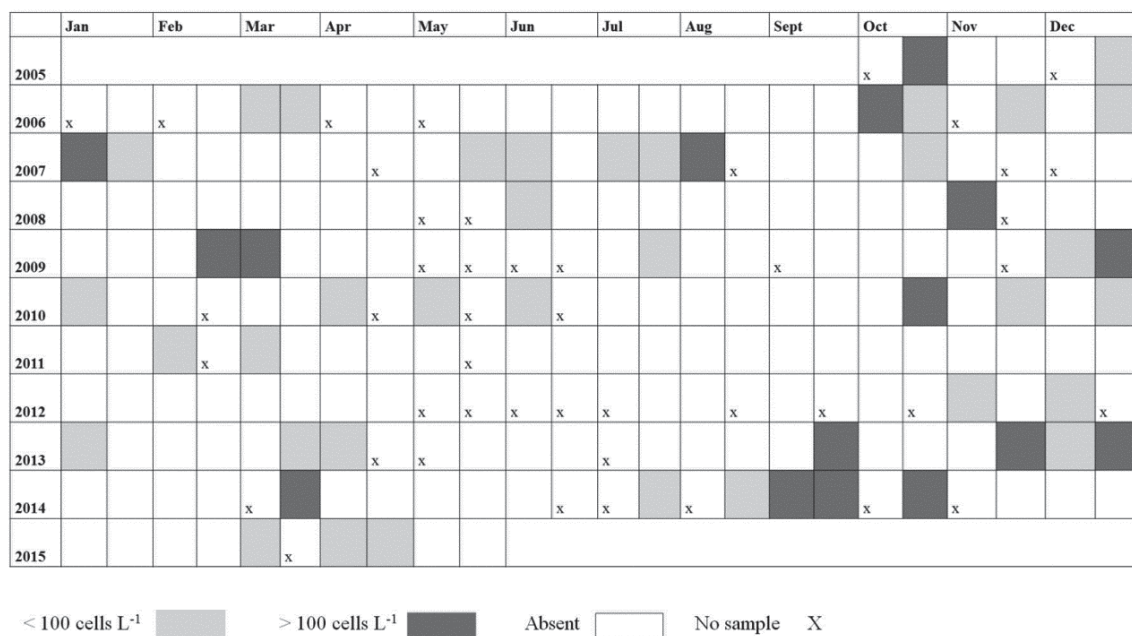
Figure 2.8 Seasonal occurrence of *Ostreopsis* spp. in aquaculture plankton samples collected from Merimbula Lake Inlet (two sites within the inlet) between October 2005 and May 2015, indicating year around presence with higher abundance in austral spring-summer.

The consistent presence of *Ostreopsis* spp. in routine plankton surveys from Merimbula Lake inlet between 2005–2015 suggest that species from this genus may be well established in the region (Figure 2.8), rather than being reintroduced every summer season from tropical Queensland via the East Australian Current (Hallegraeff 2010). However, there is a marked increase in the abundance of *Ostreopsis* spp. during warmer months (Figure 2.8). Similar observations have also been reported from New Zealand, as *Ostreopsis* cf. *siamensis* has been found regularly throughout the austral summer season (Rhodes 2011, 2014). Previous studies have presented the role of temperature in regulating *Ostreopsis* blooms (Mangialajo et al. 2008; Shears & Ross 2009); however, a positive correlation between temperature and *Ostreopsis* blooms has not yet been clearly shown (Accoroni et al. 2011). Sea surface temperature in Merimbula Inlet is 8–28°C highlighting a wide range of thermal tolerance for this species, similar to the reports from Peter the Great Bay in the Sea of Japan, in which *Ostreopsis* spp. cells have occurred on macrophytes at 7–22.2°C (Selina & Levchenko, 2011; Kohli et al. 2014). The resting stages of *Ostreopsis* cf. *siamensis* were reported to survive at 10°C in culture conditions

thereby suggesting a seeding mechanism for *Ostreopsis* cells to survive cooler temperatures and reinitiate in the summer (Pearce et al. 2001). The mucilage matrix produced by *Ostreopsis* species has been reported to work as a protective coating which may enable cysts to survive in them for more than 6 months after their formation and help the population to survive cooler temperatures (Bravo et al. 2012).

PLTX is highly toxic upon intraperitoneal (i.p.) administration in mice with reported LD_{50} values ranging between 0.15 and 0.72 µg kg^{-1} (EFSA 2009; Munday 2011). The symptoms displayed by mice upon exposure to high dose of cell extract exhibited similar symptoms to PLTX exposure suggesting that the extract may have contained small amounts of very toxic substances or larger amounts of substances of relatively low toxicity as highlighted by the high LD_{50} of 25 mg kg^{-1} i.p. in *Ostreopsis* cf. *siamensis* CAWD203 (Riobó et al. 2008; Munday 2011). Chemical analysis on CAWD203 exhibited only the common amine aldehyde fragment after periodate oxidation (Figure 2.9), similar to *Ostreopsis* cf. *siamensis* CAWD173 from Selwood et al. (2012), but no amide aldehyde fragment was obtained suggesting that some structurally related PLTX analogues were detected in the cell extract but PLTX itself was not contained in the sample. The total amount of PLTX equivalents obtained from the cell extract was comparable and in some cases, lower to other *Ostreopsis* cf. *siamensis* isolates from New Zealand (ranging 0.1–1.2 pg $cell^{-1}$) but was much higher compared to *Ostreopsis* cf. *siamensis* strains from the Mediterranean and Atlantic regions that only produced PLTX-like compounds at levels in the range 0.4–0.8 fg $cell^{-1}$ (Rhodes et al. 2013; Ciminiello et al. 2013) (see supplementary data S5). The cellular content of PLTX-like compounds in CAWD203 was also comparatively very low to that of some toxic *Ostreopsis* cf. *ovata* strains reported from previous studies (Guerrini et al. 2010; Suzuki et al. 2012).
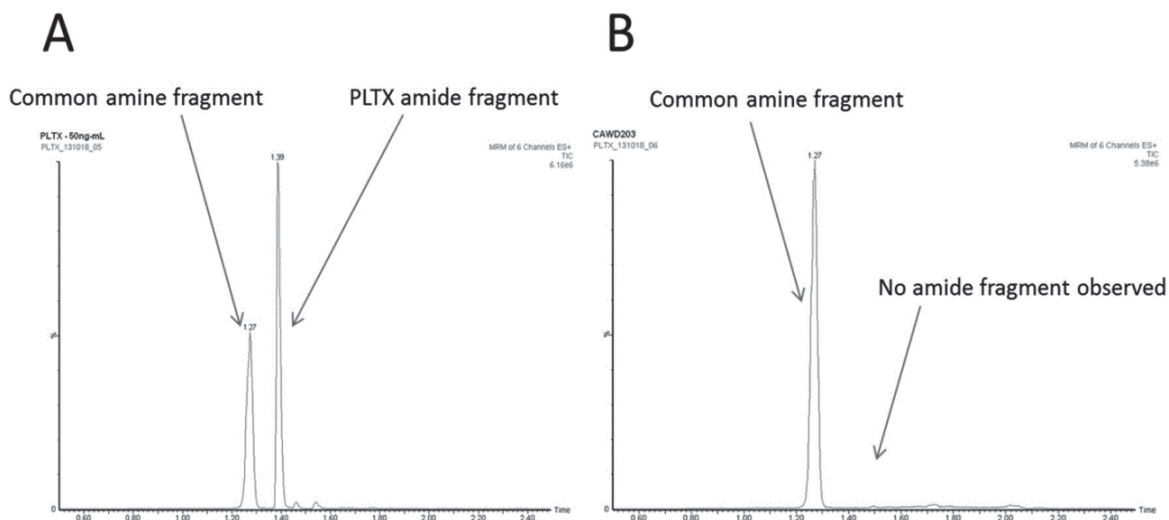
Figure 2.9 Extracted ion chromatograms from the solid phase extraction and on-column oxidation of A: Palytoxin (PLTX) standard (50 ng mL^{-1}); and B: *Ostreopsis* cf. *siamensis* CAWD203 from Merimbula, Australia.

Structural differences can have a great impact on the toxicity of the strain as highlighted by the mouse bioassay results where the LD$_{50}$ was a lot higher than LD$_{50}$ of palytoxin by i.p. in mice. Structural differences and varying amounts of PLTX-like compounds produced by *Ostreopsis* cf. *ovata* strains from Japan and Mediterranean regions have been identified by investigating the complete structures of such compounds, but have been relatively understudied amongst *Ostreopsis* cf. *siamensis* strains (Ciminiello et al. 2012a; Suzuki et al. 2012). Such distinctions may occur due to strain specific variability, as documented in *Ostreopsis* cf. *ovata* and other dinoflagellate strains, as well as different culturing conditions that might alter toxin composition in *Ostreopsis* cultures (Tillmann et al. 2009; Pezzolesi et al. 2012; Vanucci et al. 2012). Since *Ostreopsis* cf. *siamensis* CAWD203 was cultured in 5× diluted f/2 media, the nitrogen and phosphorus limitation in the media may have induced lower toxin production. However, this may be species-specific trait since high toxin contents have been reported in *Ostreopsis* cf. *ovata* in the same nutrient conditions (Guerrini et al. 2010; Vanucci et al. 2012). So far, information on effects of nutrient conditions on *Ostreopsis* cf. *siamensis* growth and toxin production are lacking and need to be further investigated.

Non PLTX-like cytotoxic compounds such as Ostreol-A have also been reported from *Ostreopsis* species highlighting a broad spectrum of toxins synthesized by species of this genus (Hwang et al. 2013). There is an increasing need to investigate the macrostructures of such complex biomolecules and the molecular mechanism involved in their synthesis. The genus *Ostreopsis* has been little studied from Australian waters despite recurrent occurrences from temperate shellfish growing estuaries (Ajani et al. 2013). Nine clades and sub-clades of *Ostreopsis* have been identified using molecular methods (Sato et al. 2011; Tawong et al. 2014). Increasing knowledge of species identity, distribution and toxigenicity of *Ostreopsis* spp. will enable more effective monitoring of harmful algal taxa in Australian waters.

2.6 Author Contributions

AV, SM designed research; SM isolated the strain; LR managed the strain at Cawthron institute; AV performed research and analysed and interpreted data; MH performed light and scanning electron microscopy; SB provided monitoring data; TH carried out LC-MS/MS at Cawthron institute. AV, SM wrote the paper with editorial input from all co-authors.

Chapter 3: Molecular and phylogenetic characterization of *Ostreopsis* (Dinophyceae) and the description of a new species, *Ostreopsis rhodesae* sp. nov., from a subtropical Australian lagoon

3.1 Abstract

Cryptic and pseudo-cryptic species are common amongst marine phytoplankton, and may cause misleading inferences of ecological and physiological data of plankton community studies. Deciphering the diversity and distribution of species of the benthic dinoflagellate *Ostreopsis* is one example, as there are many morphologically indistinct clades that differ greatly genetically and toxicologically from one another. In this study, a new species, *Ostreopsis rhodesae* from the southern Great Barrier Reef was described. While it initially appeared to be highly similar to several other *Ostreopsis* species, we found *O. rhodesae* can be distinguished based on the relative size of the second apical plate (2'), which is twice as long as the APC plate, and separates the third apical (3') from the third precingular (3'') plate. Phylogenetic trees based on the SSU, ITS/5.8S and D1-D2 and D8-D10 regions of the LSU rRNA were well supported, and showed a clear difference to other *Ostreopsis* clades. Compensatory base changes (CBCs) were identified in helices of the ITS2 between *O. rhodesae* and *O.* cf. *ovata* and *O.* cf. *siamensis*, which were also present in the same habitat. Fish gill cell lines were toxic to *O. rhodesae*, cell extracts but no palytoxin-like analogues were found in them. The findings highlight a case of pseudo-cryptic speciation, found in sympatry with closely related and morphologically similar species, but biologically and functionally distinct.

3.2 Introduction

Studies of the diversity, evolution and ecology of dinoflagellates in marine ecosystems are challenging. Some of the reasons for this are a lack of field data, under sampling at large spatial and temporal scales, low abundance of certain species and difficulties in establishing cultures (Heger et al., 2014; Keeling et al., 2014; Murray et al., 2012b, Sampayo et al., 2009). 'Cryptic' species also appear to be common, and further complicate the identification of dinoflagellate species when techniques such as light and scanning microscopy are used (Amato et al., 2007; Montresor et al., 2003; Murray et al., 2012a; Richlen et al., 2008). Recently, large scale oceanic and coastal diversity surveys using 'meta-barcoding' and other culture-independent molecular methods have shown that a significantly larger number of operational taxonomic units (OTUs) for dinoflagellate lineages exists, than there are morphologically recognized taxa (de Vargas et al., 2015; Le Bescot et al., 2015; Massana et al., 2015). Environmental sequencing techniques are not error-proof and require an accurate and curated taxonomic validation before novel biological insights can be made from the sequence dataset (Del Campo et al., 2013; Del Campo et al., 2016). Largely growing sequencing platforms and rapidly generated molecular data raises significant discussions on the choice of genetic markers and the divergence between 'units' of diversity before classifying them as ecologically and evolutionary distinct species (Del Campo et al, 2016; LaJeunesse, 2001; Sampayo et al., 2009; Stat et al., 2011).

Cryptic and pseudo-cryptic species are being discovered in many different dinoflagellate taxa at an interesting rate and are important for the precise representation of a phytoplankton community (Amato et al., 2007; Hoppenrath et al., 2014; Knowlton, 1993). Cryptic species are genetically different, but morphologically identical, whereas pseudo-cryptic species not only show genetic differences but also minor morphological variations after detailed examination (Lundholm et al., 2012). Such congeneric species can have different physiological responses despite similar morphologies (Hoppenrath et al., 2014; Orive et al., 2013). *Gambierdiscus toxicus* is an example of one such dinoflagellate taxon where detailed analyses suggested that it is not a single cosmopolitan species but a wide-ranging species complex with varying physiological traits which has aided in enhancing our knowledge of the tropical food borne disease ciguatera (Richlen

et al., 2008). Intragenomic rDNA polymorphisms, the existence of high copy numbers of rDNA cistrons and the presence of pseudogenes can make species delimitation problematic amongst dinoflagellates even with the use of DNA sequencing techniques (Alverson, 2008; Orive et al., 2013; Stat et al., 2011).

The presence of compensatory base pair changes (CBCs) in the 3' nuclear ribosomal transcribed spacer sequence region (second internal transcribed spacer region (ITS2)) has been extensively used for species delimitation purposes as their presence has been significantly correlated with mating incompatibility and reproductive isolation (Coleman, 2003, 2007, 2015; Coleman and Vacquier, 2002). DNA sequencing methods in combination with ITS2 secondary structure modelling have proven useful in resolving evolutionary relationships between diverse free living and symbiotic *Symbiodinium* lineages and also discovering novel clades (LaJeunesse, 2001; LaJeunesse et al., 2012; Pochon and Gates, 2010). It has also been used to delineate pseudo-cryptic species within toxin producing species complexes such as the *Alexandrium tamarense* species complex and the allopatric differentiation of *Coolia malayensis* and *C. monotis* (John et al., 2014; Leaw et al., 2010; Leaw et al., 2016).

The genus *Ostreopsis* Schmidt comprises several species that are similar in shape, size and thecal plate patterns and co-exist in tropical and temperate coastal habitats worldwide (Fukuyo, 1981; Parsons et al., 2012; Penna et al., 2005; Rhodes, 2011; Schmidt, 1902). All *Ostreopsis* species are flattened with an oval-ovate shape that tapers ventrally in the apical view. The plate patterns are largely identical and broadly fit the description of the type species, *Ostreopsis siamensis* Schmidt, except for *Ostreopsis heptagona* Norris, Bomber et Balech (David et al., 2013; Hoppenrath et al., 2014; Penna et al., 2005). Some, but not all, *Ostreopsis* species are known to produce palytoxin (PLTX) and/or its analogues and form harmful blooms which have been associated with human poisonings and accumulation in seafood (Ciminiello et al., 2012a; Ciminiello et al., 2006; Ciminiello et al., 2012b; Rhodes et al., 2002; Tubaro et al., 2011; Usami et al., 1995). Based on analyses of 28S and ITS/5.8S rDNA sequences, several clades of *Ostreopsis ovata* Fukuyo exist that are morphologically indistinguishable, comprising the *O. ovata* species complex (Sato et al., 2011; Tawong et al., 2014). Additionally, isolates of *Ostreopsis*

cf. *ovata* from the Mediterranean, NE Atlantic and the Brazilian coasts have exhibited genetic differences compared to the Indo-Pacific isolates based on their 28S D1/D2 rDNA and ITS/5.8S rDNA sequences (Penna et al., 2014; Penna et al., 2010; Penna et al., 2005; Pin et al., 2001; Sato et al., 2011; Tawong et al., 2014). The widespread geographic distribution of *Ostreopsis* populations provides vast opportunities for speciation events to occur which are highlighted by the sequence data comparisons of faster evolving genes, however, in order to compare between published findings and to establish accurate and more recent historical phylogenetic reconstruction of this genus, reporting sequences from different genes and the use of different molecular techniques is essential (LaJeunesse, 2001; Sampayo et al., 2009).

In Australia, what little is known about the diversity and ecology of *Ostreopsis* species has been derived from microscopic and morphological studies (Ajani et al., 2013; Heimann et al., 2009; Holmes et al., 1988; Pearce et al., 2001). It was only recently that an *Ostreopsis* cf. *siamensis* strain producing PLTX-like analogues was isolated and characterized, despite its frequent presence (Verma et al., 2016). In this study, fourteen isolates were cultured from the lagoon of Heron Island, from the southern Great Barrier Reef (GBR), and report the morphological and molecular phylogenetic characterization from 18S (SSU), partial regions of 28S (LSU) and ITS/5.8S rDNA sequences. The strains were tested for the production of PLTX-like analogues using liquid chromatography-mass spectrometry (LC-MS/MS) analysis and the toxicity of the sample extracts was determined using a fish gill cell line bioassay.

3.3 Materials and methods

3.3.1 Sample collection and culture establishment

Heron Reef (23°27′S, 151°55′E) is located in the southern Great Barrier Reef, approximately 85 km northeast of Gladstone, Queensland (Figure 3.1). This lagoonal platform reef is approximately 10 km in length and 4.5 km in width at its widest point, and the island itself, only 750 m by 240 m, is located at the western end of the reef (Rasheed et al., 2004; Webb et al., 1999). Seasonal water temperatures range from 19-

26°C, with occasional highs of 32°C. At the time of sample collection, sea surface temperature was 20°C.
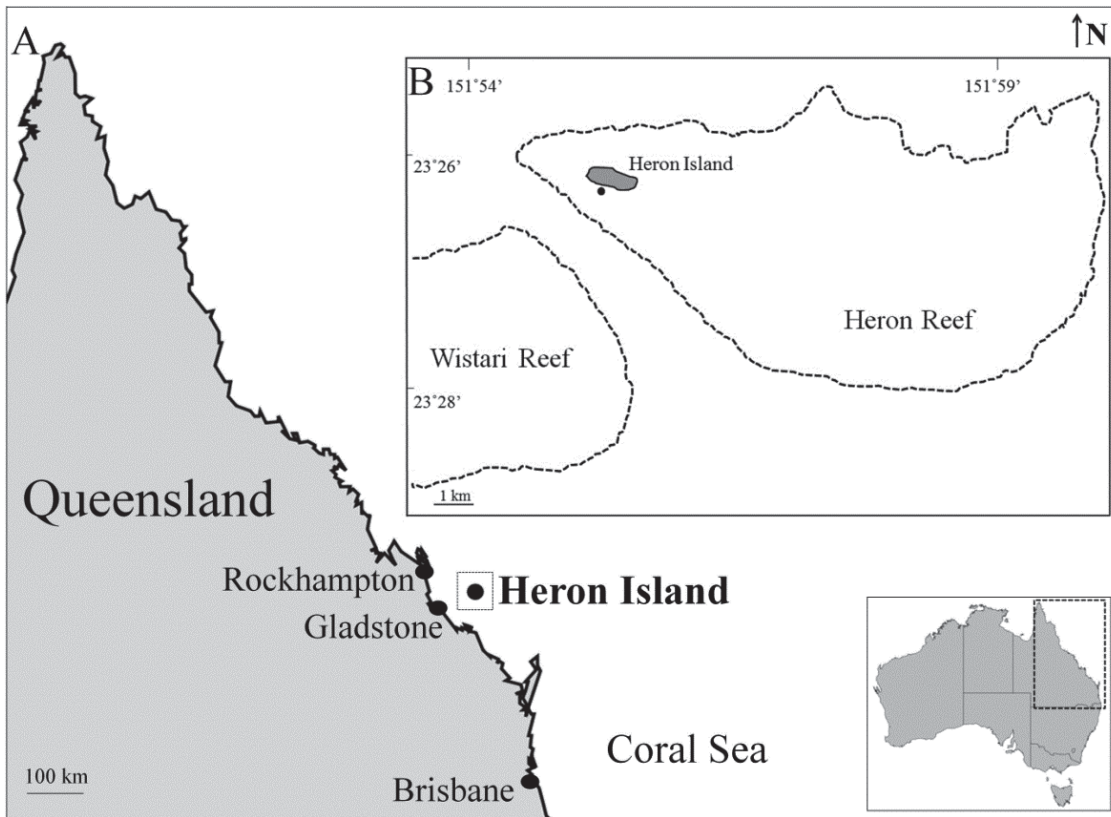
Figure 3.1 A: Map of the north-eastern coastline of Australia, showing Heron Island. B: Map of Heron reef lagoon, showing sampling site during June 2014 and February 2015 (shown as black dot).

Macroalgal samples (*Padina* and *Saragassum* spp.) were collected from a shallow area (less than 1.5 m) on the inner reef flat off Heron Island research station in June 2014 and February 2015. Samples were placed in plastic bags and bottles containing local seawater, and shaken vigorously to detach the epiphytic microalgal cells. The epiphytic suspension was passed through a 125 µm mesh filter to remove larger fauna and debris. Using a glass micropipette, single *Ostreopsis* cells were isolated using an inverted light microscope (Nikon Eclipse TS100) and transferred to a drop of clean filtered seawater. The transfer was repeated up to five times and fourteen non-axenic monoclonal cultures were established. The isolates were maintained in f/10 medium (Guillard 1975), at 25°C and salinity of 35 under the photo illumination of 80-100 µmol m^{-2}s^{-1} and 12:12 hour light-dark cycle in 24 multi-well culture plate (Corning Inc. Durham, USA) with 1 ml medium. After 4-6 weeks, they were transferred to 50 mL sterile tissue culture flasks (Becton

Dickinson, Sydney, Australia) and maintained in the same conditions. Cultures were subcultured in f/10 medium every 4 weeks thereafter.

3.3.2 Microscopy

Living cells of interest were picked using a Leica DMIL inverted microscope (Leica Microsystems GmbH, Wetzlar, Germany), placed on an object slide and observed with a Leica DMRB (Leica Microsystems GmbH, Wetzlar, Germany) equipped with differential interference contrast optics at 400 and 640 times magnification with oil immersion objectives. Digital photos were taken using a Leica DFC420C camera (Leica Microsystems GmbH, Wetzlar, Germany).

Cell dimensions of mid-log phase cultures were measured under 400× using a calibrated eyepiece of Eclipse TS100 inverted microscope with bright field optics (Nikon, Hilton, Australia). Cells were harvested from the culture medium phase 8-10 days after subculturing and fixed in 4% Lugol solution to measure the depth = dorsoventral diameter (DV) and transdiameter width (W) using ImageJ v1.48 (Rasband 1997-2013). Thirty cells for each strain were measured. The variations in DV and W were assessed through one-way analysis of variance (ANOVA) in SPSS v11.5 (IBM, Armonk, USA).

For SEM, the culture was fixed with Lugol solution and stored in the dark. Cells were placed on a 5 μm Millipore filter, rinsed in distilled water, and dehydrated in a series of increasing ethanol concentrations (30, 50, 70, 85, 90, 100%), followed by chemical drying with hexamethyldisilazane at room temperature for 20 mins and finally at 50°C in a drying oven for 5 mins. The sample/filter was mounted on a stub and sputter coated with gold-palladium (Bal-Tec SCD 050; BAL-TEC Präparations-gerätevertrieb, Wallof, Germany). Cells were observed using a Tescan VEGA3 microscope (Elekronen-Optik-Service GmbH, Dortmund, Germany) at 15 kV using the SE detector (Hoppenrath et al., 2014). The species description is based on light microscopic investigations of all 12 strains and a scanning electron microscopic study (theca description) of the type strain HER32.

3.3.3 DNA extraction and PCR amplification

DNA was extracted using a modified 3% CTAB buffer (100 mM Tris-HCl pH 8; 20mM EDTA pH 8; 1.4 M NaCl; 0.5% beta-mercaptoethanol) (Hoppenrath et al., 2009). In summary, ten ml of dense culture was centrifuged at 2,300 g for 10 mins at room temperature and the algal pellets were placed into 500 µL of buffer in the heat block at 68°C for 2 hours with several vigorous shakes during incubation. The aqueous layer was separated using 24:1 chloroform: isoamyl alcohol and precipitated in isopropanol and 3M sodium acetate (pH 5.2). The DNA pellet was washed with 70% ethanol and vacuum dried to remove any traces of ethanol. Sterile Milli-Q water was added to DNA pellets and the samples were stored at -20 °C prior to PCR reactions (Lang and Burger, 2009).

The extracted DNA was visualised on 1% agarose gel stained with GelRed (Gene Target Solutions, Dural, Australia) and quantified using a Nanodrop ND-1000 (NanoDrop Technologies, Wilmington, USA). The partial nuclear SSU rRNA gene, the D1/D2 and D8/D10 regions of the LSU rRNA gene, the internal transcribed spacer regions and 5.8S rRNA gene (ITS1/5.8S/ITS 2) were amplified and sequenced as described in Verma et al. (2016) (see supplementary data S1 for details). PCR products were purified with Sure Clean Plus (Bioline, Sydney, Australia), according to the supplied protocol from the manufacturer and sequenced using a commercial service (Macrogen Inc., Seoul, Korea).

3.3.4 Sequence analysis and phylogenetic reconstruction

Analyses on SSU, ITS1/5.8S/ITS2, D1-D2 and D8-D10 regions of LSU rDNA were conducted as described in Verma et al. (2016) (see supplementary data S2 for reference sequences retrieved from GenBank). In summary, multiple sequence alignments, post manual inspection, were performed using ClustalW v1.6 as implemented in MEGA v6 (Tamura et al., 2013). Substitution models were selected for each dataset based on lowest Bayesian information criterion (BiC). Phylogenetic analyses were performed using both maximum likelihood (ML) and Bayesian inference (BI) approaches. ML trees were produced in MEGA v6 using Tamura 3 (T92) +G +I with 5 gamma categories substitution model for all analyses with bootstrap of 1000 replications. Bayesian analyses was performed using MrBayes v3.2.2 (Ronquist and Huelsenbeck, 2003) as implemented in

Geneious v6 (Kearse et al. 2012) using general time reversible model (GTR) + gamma model for all analyses. Genetic distance (pairwise uncorrected p-distance) were estimated from the ITS/5.8S, D1/D2 and D8/D10 LSU and SSU rDNA sequences using the p-distance model and bootstrap procedure (1000 replicates) in MEGA v6 (Tamura et al., 2013). All positions containing gaps and missing data were eliminated for the analyses.

3.3.5 Modelling ITS2 secondary structure

The second internal transcribed spacer (ITS2) region was identified and delimited based on alignment with *O.* cf. *ovata* strain OvPD04 (GenBank accession number AF076217) from Leaw et al. (2001) and *O.* cf. *siamensis* strain CNR-B4 (Genbank accession number AJ301643) from Penna et al. (2005). After removing the 3' and 5' termini of the ribosomal 5.8S and 28S rRNA respectively, the annotated ITS2 sequences were aligned using ClustalW in MEGA v6 and manually adjusted. For homologous modelling, *Coolia monotis* strain SZN 43 (GenBank accession number AJ308524) was used as template. A total of 37 ITS2 secondary structures were analysed of which, 23 ITS2 sequences were sampled from GenBank and 14 were newly obtained from this study (see supplementary data S6). Incomplete ITS2 sequences were excluded from the analysis. RNA transcript folding of ITS2 for all *Ostreopsis* strains was predicted by the ITS2 Database V (http://its2.bioapps.biozentrum.uni-wuerzburg.de/), with ITS2 PAM50 matrix chosen and the percentage of transfer helices at 75% similarity selected (Ankenbrand et al., 2015). Structures were visualized using VARNA (Darty et al., 2009). The compensatory base changes (CBCs) and hemi-CBCs in the predicted secondary structure models were identified manually and with the aid of the software 4SALE (Schultz and Wolf, 2009; Seibel et al., 2006).

3.3.6 Toxin analysis via LC–MS/MS

All *Ostreopsis* cultures were harvested in late stationary phase by centrifugation (50 mL; 2,300 *g*; 10 mins; room temperature) and the cell pellets were freeze dried. PLTX and/or related structural analogues were screened using a quantitative LC-MS/MS method at the Cawthron Institute, New Zealand (Selwood et al. 2012). In summary, this analytical approach monitors substructures generated by the oxidative cleavage, using periodic acid,

of vicinal diol groups present in the intact toxins. It yields an amino aldehyde common to known palytoxins, ovatoxins and ostreocins, used for quantification, and an amide aldehyde that varies depending on the toxin type (Selwood et al., 2012; Verma et al., 2016).

3.3.7 Fish gill cell line assay for toxicity

The fish gill cell line RTgill-W1 was obtained from the American Type Culture Collection (CRL-2523). Primary cells were originally initiated from gill filaments of rainbow trout *Oncorhynchus mykiss* (Bols et al., 1994). Fish gill cells were cultured in 75-cm^2 culture treated flasks with Leibovitz medium (L1518, Sigma, Sydney, Australia) supplemented with 10% fetal bovine serum (v/v) (12003C, Sigma, Sydney, Australia) and an antibiotic-antimycotic solution (A5955, Sigma, Sydney, Australia) at 20°C in the dark. Confluent gill cells were detached with 0.25% trypsin-0.02% EDTA solution (59428C, Sigma, Sydney, Australia) for subculturing and seeding purposes (Dorantes-Aranda et al., 2011).

Pellets obtained from three *Ostreopsis* strains HER24 (*O.* cf. *siamensis*), HER27 (*O.* cf. *ovata*) and HER26 (*O. rhodesae*) at mid-exponential (day 8) and late stationary (day 21) growth phases were dissolved methanol (≥99.9%). Solvent volume was adjusted for each extract in order to achieve the same concentrations for all extracts. Pellets were resuspended in the solvents and sonicated for 5 mins to rupture the cells. Samples were centrifuged (3000 rpm; 10 mins) and the supernatant was transferred into new tubes and stored at -80°C until analysis. Gill cells were detached, counted and seeded at a concentration of 1.5×10^5 cells mL^{-1} in quadruplicate in Greiner Bio-One 96-well microplates (655180, Interpath Services Pty Ltd, Heidelberg West, Australia) 48 hours prior to the experiments (Dayeh et al., 2005; Dorantes-Aranda et al., 2011). Algal extracts were mixed with L-15/ex medium (Schirmer et al., 1997) to achieve final concentrations of 0.2, 1, 2, 4 and 8% for the exposure (equivalent to 80, 400, 800, 1600 and 3200 cells mL^{-1}, respectively). The methanol solvent final concentration for all treatments, including the control groups, was methanol/mQ, 4%. This solvent concentration had no effect on gill cell viability. Gill cells were exposed to the algal extracts and control treatments (only

L-15/ex with solvent) for 2 hours. After completion of the 2-hour exposure period, experimental solutions were discarded and gill cells were rinsed with phosphate buffer saline (PBS). Resazurin (Sigma, Sydney, Australia) in L-15-ex (5% v/v) was added to all wells and incubated for 2 hours in the dark to measure viability of gill cells (Dorantes-Aranda et al., 2015). Fluorescence of metabolised resazurin was measured with a microplate reader (FLUOstar OPTIMA, BMG Labtech, 413-3350), using excitation and emission filters of 540 and 590 nm, respectively. Statistical analysis for the fish gill cell assays was performed using the software Statistica v13 (StatSoft, Dell, Australia). Data were subjected to one-way ANOVA and *a posteriori* analysis was performed using the Tukey test for multiple comparisons. A significance level of 95% (α=0.05) was considered for all analysis.

3.4 Results

3.4.1 *Ostreopsis rhodesae* Verma, Hoppenrath et Murray sp. nov.

3.4.1.1 Morphological description

The strongly anterio-posteriorly flattened cells were ovate (drop/tear-shaped) and ventrally tapering (Figures 3.2A-C). Cells of the type strain (HER32) were 32-56 µm deep (44.2 ± 6.3 S.E., n = 30; DV diameter) and 23-42 µm (32.4 ± 5.3 S.E., n = 30) wide (W) and varied from 1.2–1.9 (mean = 1.4) in DV/W ratio (Table 3.1). The maximal size ranges of all investigated strains were 28.3-57.8 µm deep and 16.7-44.2 µm wide (Table 3.1). Cells were densely packed with elongated golden-brown chloroplasts (Figure 3.2B), except for the ventral area (Figures 3.2A-C). The oval nucleus was located dorsally (Figures 3.2B, C). Pusules were not recorded. No significant differences in DV diameter and width were identified between *O.* cf. *ovata*, *O.*cf. *siamensis* and *O. rhodesae* (Table 3.1).

The plate formula is APC 3' 7'' 6c 8?s 5'''' 2''''' (Figures 3.3-3.6). The narrow, slightly curved and elongated apical pore complex (APC) was located parallel to the left mid-lateral to dorsal cell margin (Figures 3.3A, D, 3.6A). The Po plate was about 9-11 μm long. The first apical plate (1') was long, hexagonal and most of it located left to the centre of the epitheca (Figures 3.3A, B, D). Extremely few cells had a heptagonal 1' plate contacting plate 5'' (Figure 3.3D, arrow). The characteristic second apical plate (2') was narrow and elongated, about twice as long as the Po plate (Figures 3.3A, D, 3.4, 3.6A). Plate 2' completely separates plate 3' from 3'' (Figures 3.4A, B). Its extension was very difficult to observe in complete cells (Figures 3A, 3.4C arrows). The third apical plate (3') was pentagonal, had a suture with plate 6'', and did not touch plate 3'' (Figures 3.3A-C, 3.4A). In the precingular series plate 1'' was the smallest and 6'' the largest (Figures 3.3A-D, 3.6A). All precingular plates were four-sided, except the second (2'') and sixth (6'') that were pentagonal (Figures 3.3A-D, 3.6A). Plate 5'' was not in contact with plate 1', with a few exceptions (Figures 3.3A-D).
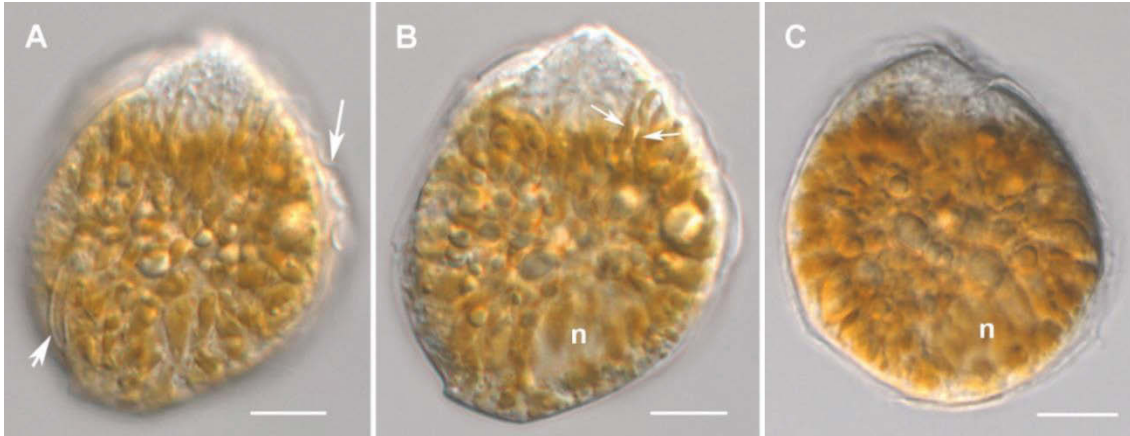
Figure 3.2 Light micrographs of *Ostreopsis rhodesae* sp. nov. HER32 showing the cell shape and general features. A, B: Same cell in different focal planes. Ovate cell ventrally tapering and ventral area devoid of chloroplasts. A: Note the APC (short arrow) and the transverse flagellum (long arrow). B: The nucleus (n) is located in the right dorsal area. Chloroplasts are elongated (arrows). C: Cell with different shape confirming the nucleus (n) position. Scale bars = 10 μm.

Table 3.1 Morphological characteristics (means and standard deviations, ranges) of *Ostreopsis* strains determined by light microscopy: dorso-ventral diameter (DV), trans-diameter (W) and DV/W ratio. All data were from cultured cells. * represents type strain.

S. No.	Species	Strain	DV (µm)	DV range (µm)	W (µm)	W range (µm)	DV/W
1	*Ostreopsis* cf. *ovata*	HER27	37.7 ± 4.3	30.2-48.3	28.7 ±3.7	21.9-37.5	1.3 (1.1-1.8)
2	*Ostreopsis* cf. *siamensis*	HER24	39.0 ± 4.0	32.3-46.9	30.1 ± 3.4	23.9-37.1	1.3 (1.2-1.4)
3	*Ostreopsis rhodesae*	HER3	39.7 ± 3.1	32.7-46.3	30.3 ± 4.2	22.1-39.6	1.3 (1.1-1.8)
4		HER6	42.3 ± 3.5	37-52.8	30.3 ± 3.3	22.4-38.4	1.4 (1.1-1.9)
5		HER7	41.4 ± 4.3	33.7-48.8	30.4 ± 5.3	19.9-37.6	1.4 (1.1-2.1)
6		HER15	42.3 ± 4.3	36.6-54.4	30.7 ±4.5	20.8-42.0	1.3 (1.1-1.9)
7		HER20	48 ± 3.8	40-57.8	36.8 ± 4.7	25.1-44.2	1.3 (1.1-1.9)
8		HER21	38.6 ± 3.1	32.1-45.7	28.7 ± 4.3	16.7-39.1	1.4 (1.1-2.1)
9		HER25	39.1 ± 3.7	32.1-45.7	27.9 ± 3.8	19.8-37.5	1.4 (1.2-1.9)
10		HER26	44.8 ± 4	37-52.8	32 ± 4.3	22.5-41.4	1.4 (1.2-1.8)
11		HER28	37.3 ± 3.3	28.9-43.1	28.2 ± 3.8	21.3-34.1	1.3 (1.1-1.7)
12		HER30	40.4 ± 6.2	32.7-55.4	27.7 ± 5.7	17.9-39.3	1.5 (1.2-1.9)
13		HER32*	44.2 ± 6.3	31.9-55.9	32.4 ± 5.3	22.9-42.3	1.4 (1.2-1.9)
14		HER301	37.1 ± 4.4	28.3-46	26.9 ± 4.6	19.5-36.8	1.4 (1.1-1.9)
		Mean	41.3 ± 5.3	28.3-57.8	30.2 ± 5.1	16.7- 44.2	1.4 (1.1-2.1)

The cingulum was narrow, deep, and slightly undulated (Figures 3.3C, 3.5A) and cingular plates were difficult to determine, nearly only in broken cells (not shown). Six cingular plates were observed (Figures 3.6A, B). The postcingular plate series consisted of a very small first (1''') plate, a medium sized fifth (5''') plate and three large plates (2''', 3''', 4''') with pentagonal 2''' and four-sided 3''' and 4''' (Figures 3.3E, F, 3.6B). The two antapical plates were of unequal size, 1'''' relatively small and 2'''' being asymmetrical pentagonal, and relatively wide with nearly parallel sides (sutures with 2''' and 5''') (Figures 3.3E, F, 3.6B).
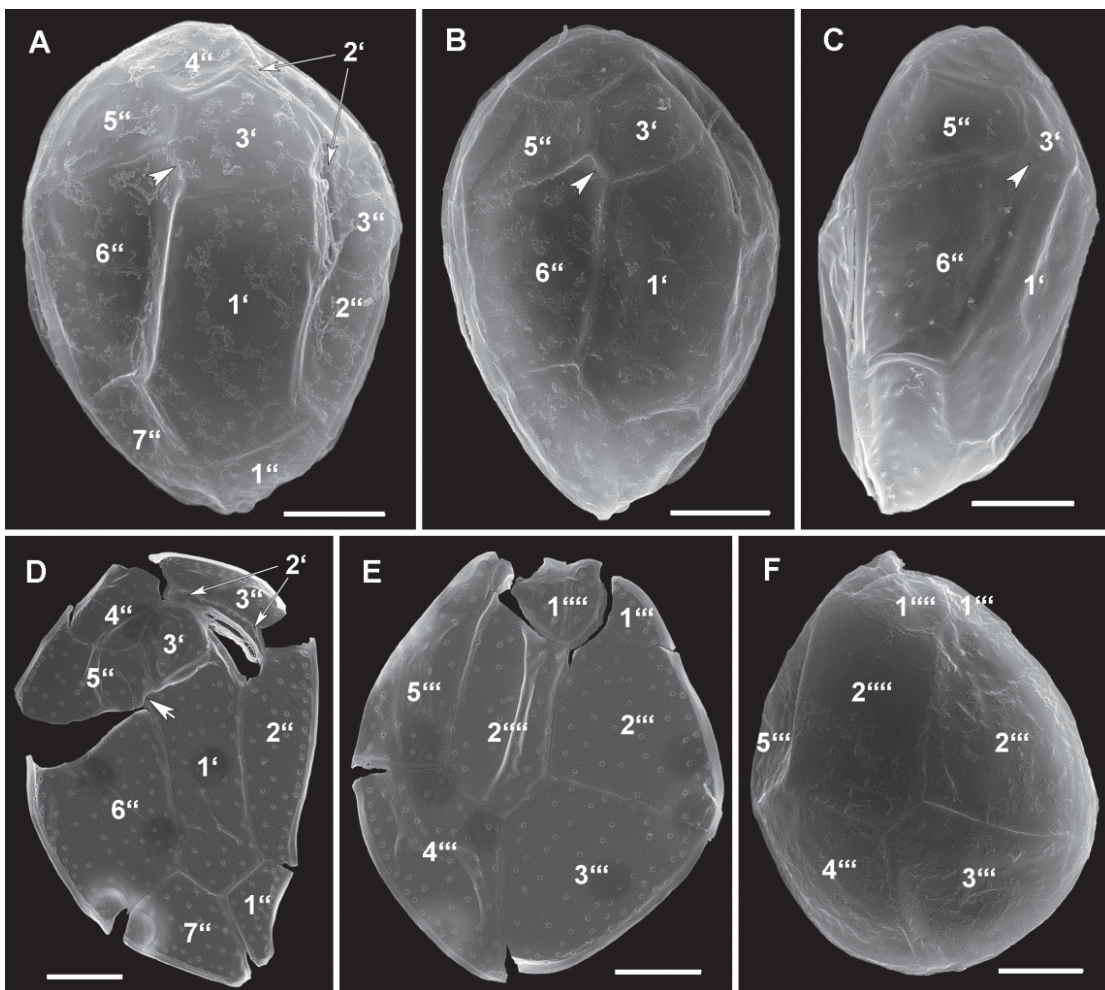
Figure 3.3 Scanning electron micrographs of *Ostreopsis rhodesae* sp. nov. HER32 showing the general thecal tabulation. A, B: Epitheca in apical view. Note the suture between plates 3' and 6'' (arrowhead). C: Epitheca in right lateral view. Note the suture between plates 3' and 6'' (arrowhead). D: Epitheca in apical view with heptagonal 1' plate, with suture between plates 1' and 5'' (arrow). E, F: Hypotheca in antapical view. Scale bars = 10 μm.

The hidden sulcal construction was not completely visible (in broken cells) and it consisted of at least 8 plates (Figures 3.5B-F, sa not visible). Thecal plates were smooth with scattered large pores with an internal sieve-like structure of small pores (Figures 3.3D, E, 3.5G-J). Nearly all pores were of the same size class (Figures 3.3D, E). Only in a very few cases, best recognizable in thecal plate inside views, single smaller and simple pores were observed (Figures 3.5I, J).
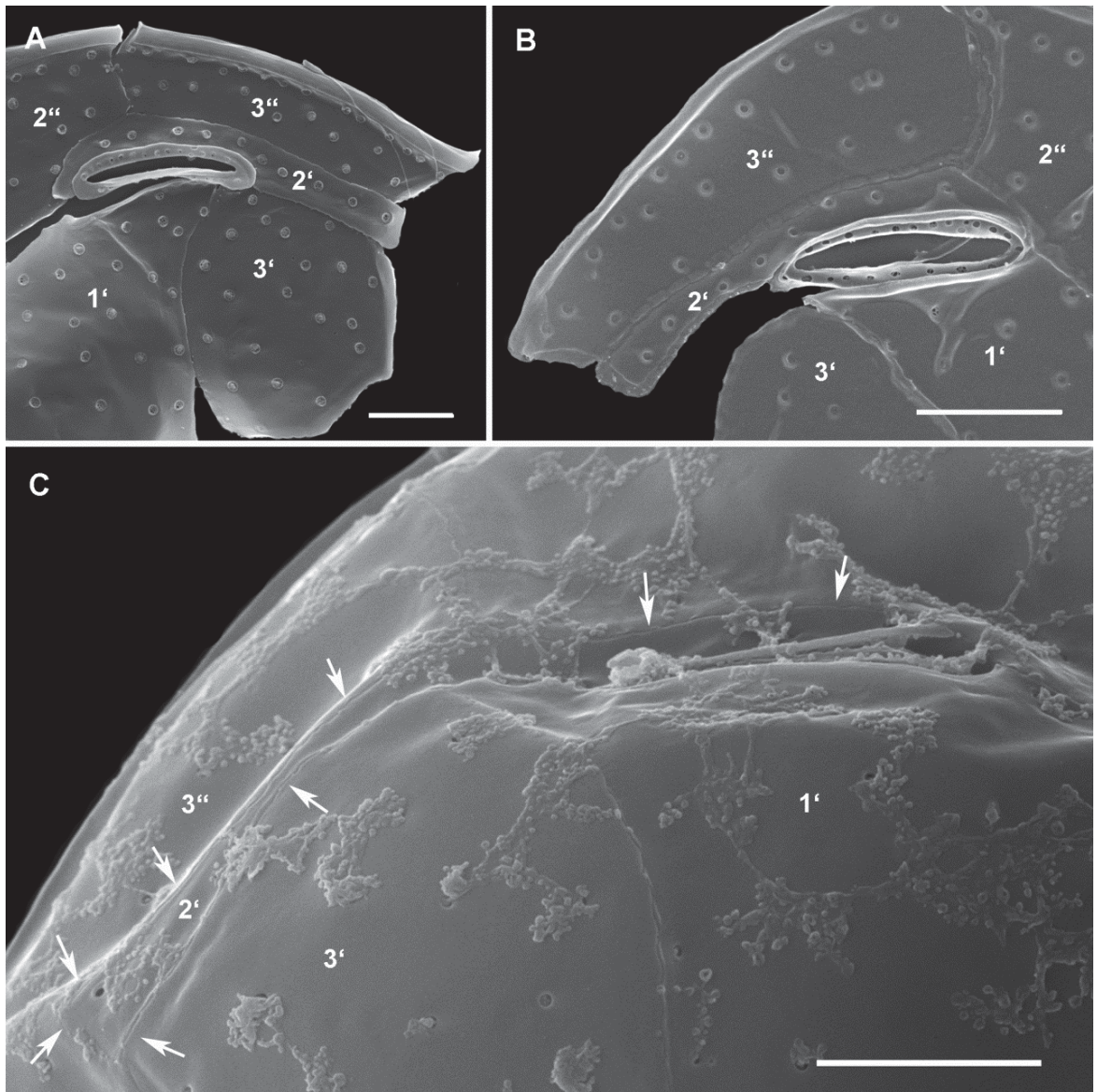
Figure 3.4 Scanning electron micrographs of *Ostreopsis rhodesae* sp. nov. HER32 showing details of the second apical plate (2'). A: Inside view of a broken theca. B: Outside view of a broken theca. C: Outside view of an intact cell. Note the 2' plate margins (arrows). Scale bars = 5 μm.

3.4.1.2 Holotype

Figure 3.3A was obtained from strain HER32. SEM-stub (designation CEDiT2016H56) deposited at Senckenberg am Meer, German Centre for Marine Biodiversity Research, Centre of Excellence for Dinophyte Taxonomy, Germany.
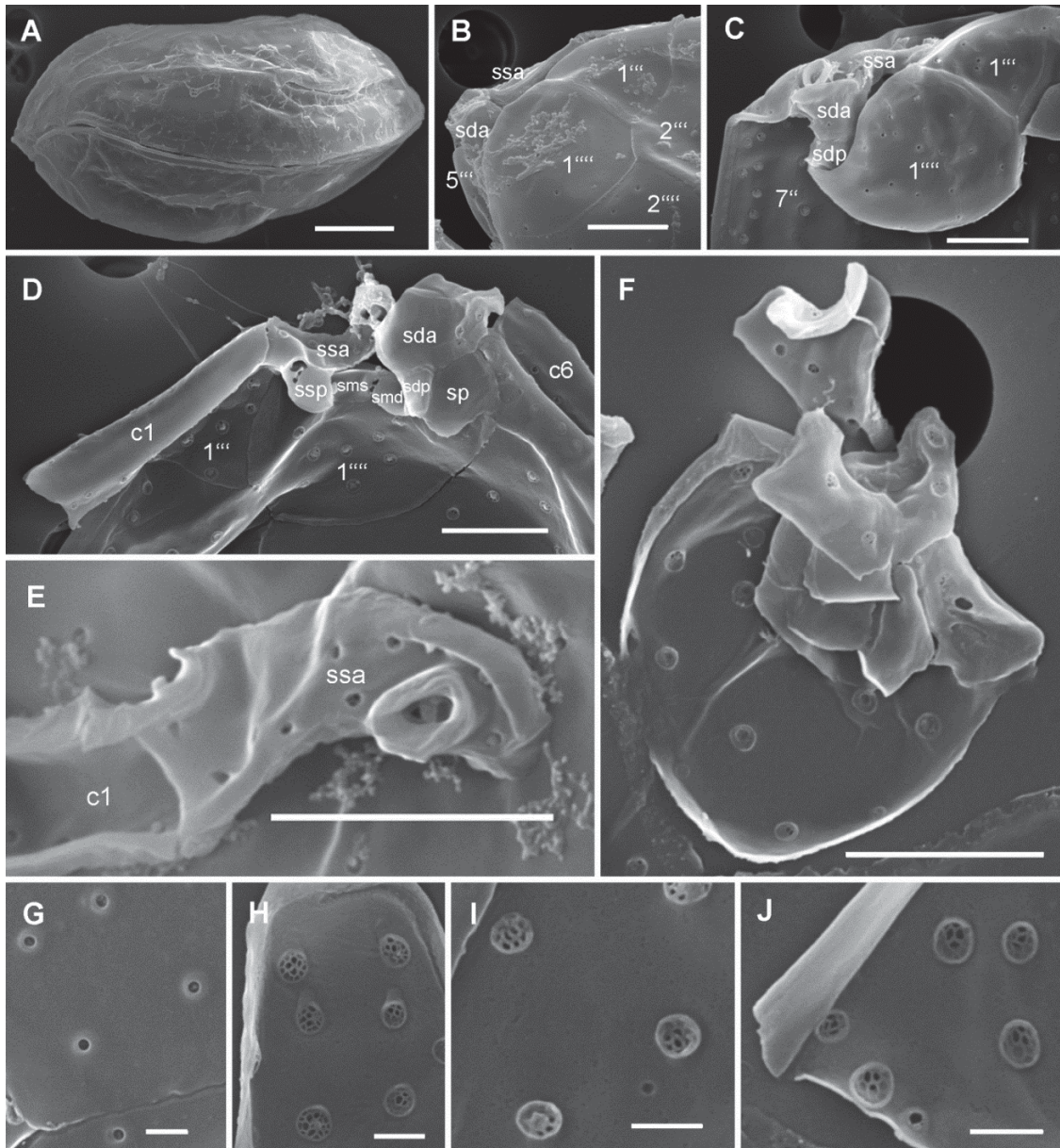
Figure 3.5 Scanning electron micrographs of *Ostreopsis rhodesae* sp. nov. HER32. A: Cell in left lateral view showing the undulated cingulum path. B-F: Sulcal details. B: Ventral hypotheca, outside view. C: Ventral hypotheca, outside view of a broken cell. D: Ventral part of a broken cell. E: Isolated ssa plate in connection with the first cingular plate. F: Sulcal plates separated from the theca, inside view. G-J: Thecal pores. G: Thecal plate detail, outside view. H-J: Details of the inside of thecal pores showing the sieve-like structure. Note the simple small pores in I and J. Scale bars A: 10 μm, C-F: 5 μm, G-J: 1 μm.
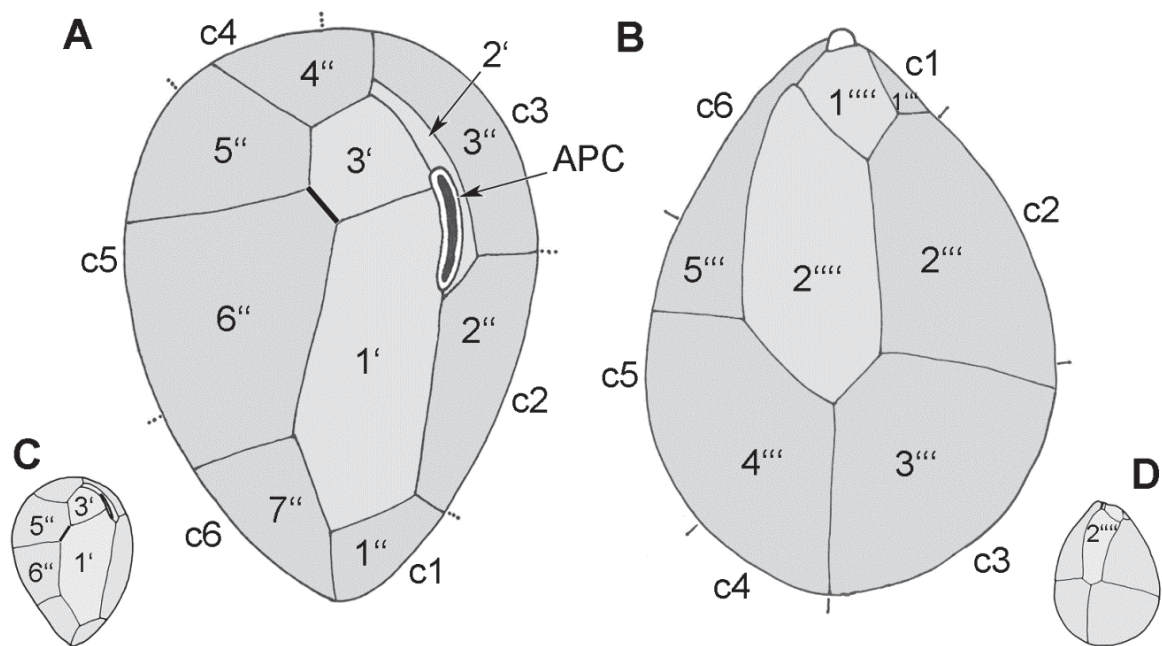
Figure 3.6 Line drawings showing thecal plate patters. A, B: *Ostreopsis rhodesae* **sp. nov. A: Epitheca; and B: Hypotheca. C, D:** *Ostreopsis heptagona* **(from Hoppenrath et al., 2014). C: Epitheca; and D: Hypotheca.**

3.4.1.3 Isotype

Lugol-fixed subsample of strain HER32 (designation CEDiT2016I57) deposited at the Senckenberg am Meer, German Centre for Marine Biodiversity Research, Centre of Excellence for Dinophyte Taxonomy, Germany.

3.4.1.4 Type locality

Heron Reef Lagoon, 23°27′ S, 151°55′ E, southern Great Barrier Reef, Coral Sea, Australia.

3.4.1.5 Etymology

The species is named in honour of Dr. Lesley Rhodes, whose pioneering research has significantly contributed to the general understanding of the impact of toxic dinoflagellates and harmful algal blooms worldwide.

3.4.1.6 Accession numbers

ITS1/5.8S/ITS2 sequences (n=12): KX0558769-80; SSU sequences (n=12): KX055855-66; and LSU (D1-D2 and D8-D10) sequences (n=12): KX055841-52.

3.4.2 Molecular analyses and phylogeny

ML and BI analyses performed on fourteen *Ostreopsis* strains with additional reference sequences from Genbank identified nine strongly supported clades (*O.* cf. *ovata*, *O.* cf. *siamensis* and *Ostreopsis* spp. 1–7). Twelve strains of *Ostreopsis rhodesae* clustered together and formed a novel fully supported monophyletic clade (BI = 1.00; ML = 100) shown by ITS/5.8S and D8/D10 LSU regions of rDNA (Accession numbers: KX0558769-80 and KX055841-52) (Figure 3.7). This was further confirmed with D1/D2 LSU and partial 18S rDNA regions (Accession numbers: KX055841-52) (Figure 3.8). This clade formed the sister clade to *O.*cf. *siamensis* with high nodal support in all phylogenetic analyses (Figures 3.7, 3.8).

The strain HER24 was placed in the *O.*cf. *siamensis* clade along with strains from the Mediterranean and South Pacific regions and showed identical sequences for all analysed rDNA regions (Accession numbers: KX055868, KX055882 and KX055854) (Figures 3.7, 3.8). The molecular phylogenetic trees revealed the separation of *O.* cf. *ovata* clade into various geographic sub-clades of which HER27 belonged with the South China Sea sub-clade (Accession numbers KX055867, KX055881 and KX055853) comprising strains isolated from Malaysia, Thailand and New Zealand (Figures 3.7, 3.8).

Uncorrected genetic distance values were calculated from the ITS/5.8S, D1/D2 and D8/D10 LSU rDNA and 18S rDNA datasets. The genetic distance values within *O. rhodesae* based on the LSU rDNA sequences were higher than ITS/5.8S and 18S sequences (Table 3.2). Furthermore, the genetic distance values based on the data from the rDNA regions between *O. rhodesae* and *O.* cf. *ovata* were larger than those between *O. rhodesae and O.* cf. *siamensis* and were comparable to the distance values between *O.* cf. *ovata* and *O.* cf. *siamensis* (Table 3.2).

Table 3.2 Distance values (pairwise uncorrected *p*-distances) based on the ITS/5.8S, D1/D2, D8/D10 LSU and 18S rDNA sequences respectively within *Ostroepsis rhodesae* strains and between *Ostreopsis* cf. *siamensis* HER24 and *Ostreopsis* cf. *ovata* HER27 from Heron Island (based on Clustal W alignment). Standard error estimate(s) are shown in brackets and were obtained by a bootstrap procedure (1000 replicates).

	Ostreopsis rhodesae	*Ostreopsis* cf. *siamensis* HER 24	*Ostreopsis* cf. *ovata* HER27
Ostreopsis rhodesae	0		
	0.0126 (0.003)		
	0.0033 (0.001)		
	0		
Ostreopsis cf. *siamensis* HER 24	0.2783 (0.0247)	n/a	
	0.1627 (0.162)	n/a	
	0.033 (0.006)	n/a	
	0.0795 (0.0068)	n/a	
Ostreopsis cf. *ovata* HER27	0.3172 (0.0256)	0.3398 (0.0264)	n/a
	0.5426 (0.0217)	0.5495 (0.022)	n/a
	0.0452 (0.0067)	0.0448 (0.0066)	n/a
	0.5493 (0.0176)	0.5912 (0.0194)	n/a

3.4.3 ITS2 secondary structure

Only the *Ostreopsis* species discovered at Heron Island in this investigation were included in the molecular analyses. A total of 37 strains from *O*.cf. *siamensis*, *O*. cf. *ovata* and *O. rhodesae* were used for the analysis (14 sequences obtained from this study, 23 obtained from GenBank, see supplementary data S6). The ITS2 region of the *Ostreopsis* species was 88-91 base pairs (bp): 90 bp for *O. rhodesae*, 91 bp for *O*. cf. *siamensis* and 88-91 bp for *O*. cf. *ovata*. The ITS2 transcripts for the analysed *Ostreopsis* species have two helices. Although there were exceptions, the structure of the helices typically consisted of a base-paired stem capped by an apical loop of unpaired nucleotides (Fig 3.9, see supplementary data S6). The universal Helices III and IV are missing. No CBCs and Hemi-CBCs were detected within *O*. cf. *siamensis* strains from Med/Pac clade and the South Pacific (13 sequences). Also, the ITS2 transcripts for all *O. rhodesae* strains were identical and no CBCs were detected (12 sequences).

Helix I was conserved amongst all *O*. cf. *ovata* sub-clades but varied from *O*. cf. *siamensis* and *O*. *rhodesae* (Figure 3.9). Sequence variability was observed within Helix II amongst *O*. cf. *ovata* strains (12 sequences) belonging to different sub-clades that led to different number of pairings in the branches, especially in South China Sea and Thailand sub-clades (see supplementary data S6). Single Hemi-CBC was detected in Celebes Sea sub-clade (Helix II U-G ↔ C-G) whereas; three HCBCs were detected in *O*. cf. *ovata* Med/Pac subclade when compared with other *O*. cf. *ovata* sub clades (Helix II U-A ↔U-G; G-U ↔G-C; U-G ↔U-A), including the motif of pyrimidine-pyrimidine mismatch (U-G ↔ U-U) in helix II (see supplementary data S6). CBCs and Hemi CBCs were detected between *O*. cf. *siamensis*, *O*. cf. *ovata* and *O*. *rhodesae* strains including the motif of pyrimidine-pyrimidine mismatch (U-G ↔ U-U) in helix I between *O*. cf. *ovata* and *O*. *rhodesae* (Table 3.3 and Figure 3.9).

Table 3.3 List of Compensatory base changes (CBCs) and hemi-CBCs between *Ostreopsis rhodesae*, *Ostreopsis* cf. *ovata* strain HER27 and *Ostreopsis* cf. *siamensis* strain HER24.

Species	*Ostreopsis* cf. *ovata* HER27	*Ostreopsis* cf. *siamensis* HER24	*Ostreopsis rhodesae* HER26
Ostreopsis cf. *ovata* **HER 27**	X	1 CBC (Helix I G-C↔U-A) 1 HCBC (Helix II G-C↔G-U	
Ostreopsis cf. **siamensis HER24**	1 CBC (Helix II U-A↔G-C) 1 HCBC (Helix I G-U↔G-C)	X	
Ostreopsis rhodesae **HER26**	2 HCBCs (Helix I G-U↔A-U, Helix II G-U↔A-U); 2 CBCs (Helix I C-G↔U-A, Helix II G-U↔U-C)	3 HCBCs (Helix I G-U↔A-U, Helix II G-C↔U-C, Helix II G-U↔A-U); 1 CBC (Helix II G-C↔U-A)	X

3.4.4 Toxin presence

LC-MS/MS analysis of the oxidized cell extract from *O.*cf. *ovata* HER27 showed the presence of both the amino aldehyde fragment, common to all known PLTX, ovatoxin and ostreocin analogues, as well as the amide aldehyde fragment, thereby confirming the presence of PLTX-like analogues in the extract. The total amount of PLTX-like analogues found were 11.8 ng (total 6,400 cells) resulting in an estimate of 1.8 pg cell^{-1}. No PLTX-like analogues were detected from cellular isolates of *O. rhodesae* strains and *O.* cf. *siamensis*.

3.4.5 Fish gill cell assays

Fish gill cells were sensitive to *Ostreopsis* extracts, especially those from *O. rhodesae* and *O.* cf. *ovata*, which caused ≥98.5% decrease of gill cell viability. Extracts from *O.* cf. *siamensis* decreased gill cell viability by no more than 69%; the extract prepared from the stationary growth phase was significantly less toxic than that from the exponential phase (p≤0.009), particularly at the two highest extract concentrations (4 and 8%). The same pattern was observed for the *O. rhodesae* extract, with the extract from the stationary growth phase being less toxic than the extract from exponential phase. This extract was the most toxic among all extracts, causing a decrease of ≥97% in gill cell viability from concentrations of 4%, whereas the extract from the stationary growth phase caused ≤34% decrease in gill cell viability.

The opposite pattern was observed for the *O.* cf. *ovata* HER27 extract in which the stationary growth phase was significantly more toxic than the extract from the exponential growth phase at all concentrations (p≤0.025). Gill cell viability decreased gradually with increasing extract concentration, decreasing by 26% and 99.6% in gill cell viability at 0.2% and 8% of the algal extract (stationary growth phase), respectively (Figure 3.10).

3.5 Discussion

3.5.1 Morphological comparison among *Ostreopsis* species

Ostreopsis rhodesae sp. nov. has a tabulation pattern typical for the genus (Hoppenrath et al., 2014) and although it is genetically different from other *Ostreopsis* species, it appears highly similar to *O.* cf. *siamensis* and *O.* cf. *ovata* based on light microscopy (Table 3.1). The species distinction for *O. rhodesae* was determined through rDNA phylogenetic analyses, presence of CBCs in the ITS2 region and thorough SEM investigations.

The elongated second apical plate (2') is twice as long as the APC plate and it separates the third apical (3') from the third precingular (3'') plate (Figure 3.6A). All *Ostreopsis* species have a 2' plate about the length of the APC, and plates 3' and 3'' are in contact, except for *O. heptagona* Norris, Bomber et Balech (Faust et al., 1996; Hoppenrath et al., 2014; Norris et al., 1985). The 2' plate is a characteristic feature for *O. rhodesae* and *O. heptagona* (Figures 3.6A, C). The irregular heptagonal first apical plate (1') having an additional suture with the fifth precingular plate (Figure 3.6C) is special for *O. heptagona* (Faust et al., 1996; Norris et al., 1985). In contrast, *O. rhodesae* typically has a hexagonal 1' plate that is not in contact with plate 5'' (Figure 3.6A) but plates 3' and 6'' touch each other in a suture (Figures 3.3A-C arrowheads). Only extremely few cells were observed with a heptagonal plate 1' (Figure 3.3D). Aberrant specimens with a heptagonal 1' plate were also recorded in culture for *O. ovata* (Besada et al., 1982) and *O.* cf. *ovata* (Penna et al., 2010). In these rare cases, the shape of the 1' plate is ambiguous for species identification. *Ostreopsis rhodesae* can additionally be clearly distinguished from *O. heptagona* by the shape of the second antapical plate (2'''') that has normal width as described for most *Ostreopsis* species and nearly parallel lateral plate sides (Figure 3.6B), in contrast to a relatively narrow plate that widens ventrally (Figure 3.6D) (1p plate in Norris et al., 1985). Many small protuberances, each with a pore, were described as thecal ornamentation in the original description of *O. heptagona* (Norris et al., 1985), but Faust et al. (1996) recorded a smooth surface.

O. heptagona belongs to the largest species of the genus with a cell depth of 80-122 μm (Faust et al., 1996; Norris et al., 1985) in contrast to the small *O. rhodesae* with a depth range of 32-56 μm. The combination of morphological characters (hexagonal 1' plate, elongated 2' plate, shape of plate 2'''', and cell size) distinguish *O. rhodesae* from all described *Ostreopsis* species and warrants its description as new species.Interestingly, Parsons et al. (2012) provided an epithecal image of a species he identified as *O.* cf. *ovata* that shows an elongated 2' plate disconnecting plates 3' and 3'' as in *O. rhodesae,* and additionally with a heptagonal 1' plate as characteristic for *O. heptagona*. The size of the scale bar has not been provided. Hence, in the absence of further information no clear identification could be made. The corresponding specimen from the same strain in Penna et al. (2010) had a hexagonal 1' plate and an elongated 2' plate that was not twice the length of the APC, but also separated plates 3' from 3'' (not clearly visible). That makes it more similar to *O. rhodesae* and the cell was 57.5 µm deep, fitting into the species size range. Besada et al. (1982, Figure 4) published an epitheca of *O. ovata* showing an elongated 2' plate that seems to separate plates 3' and 3'' like the specimen in Penna et al. (2010).

3.5.2 Phylogeny and biogeography of genus *Ostreopsis*

The phylogenetic analyses in our study revealed the discovery of a novel species *O. rhodesae* that diverged from other clades with full nodal support and was found to be sister group to *O.* cf. *siamensis*. *Ostreopsis* cf. *siamensis* and *O.* cf. *ovata* were also reported from the same environmental sample. Previously, Holmes et al. (1988) has reported *O. siamensis* from Heron Island, Lady Elliot Island and Hoffmans Rocks based on morphological characteristics. A survey of toxic dinoflagellates from Townsville, Magnetic and Orpheus Islands reported high concentrations of *O. ovata, O. siamensis, O. lenticularis* and *O. heptagona,* without accompanying data to verify their identities (Heimann et al., 2009). Here, the first molecular description of *Ostreopsis* species from the Australian GBR is reported.

O. cf. *siamensis* ribotype has previously been reported from temperate locations around the globe (Rhodes, 2011). This study has provided the first report of this ribotype from sub-tropical waters, suggestive of a more cosmopolitan distribution than previously described. Recently, *O.* cf. *siamensis* has been reported from a shellfish estuary in southern New South Wales and its seasonal occurrence in New Zealand suggests its transportation from tropical/sub-tropical waters via the East Australian current and the Tasman front (Murray et al., 2014; Rhodes, 2011). The genetic homogeneity of *O.* cf. *ovata* found in the Coral Sea with populations in Malaysia, Cook Islands and Japanese waters might be due to the connectivity of the Equatorial counter currents with the EAC in the southern hemisphere and the Kuroshio current in the north (Sato et al., 2011).

The genetic distances based on ITS regions between *O. rhodesae* and *O.* cf. *siamensis* were comparable to the distance between *O.* cf. *siamensis* and *O.* cf. *ovata*, which suggests that the genetic differentiation between *O. rhodesae* and other *Ostreopsis* species/clades are at the species level (Table 3.2) as suggested in Litaker et al., (2007). Low levels of intragenetic variations amongst *O. rhodesae* strains in the LSU rDNA regions were observed, however ITS regions in *O. rhodesae* were relatively homogenous (Table 3.2). Sato et al. (2011) suggested that the evolutionary divergence of the ITS region reflects the genomic heterogeneity in a cladal population and is reflective of its potential to adapt to changing environments, making *O.* cf. *ovata* clades to be more ecologically versatile compared to the genetically homogeneous *O. rhodesae* and *O.* cf. *siamensis*.
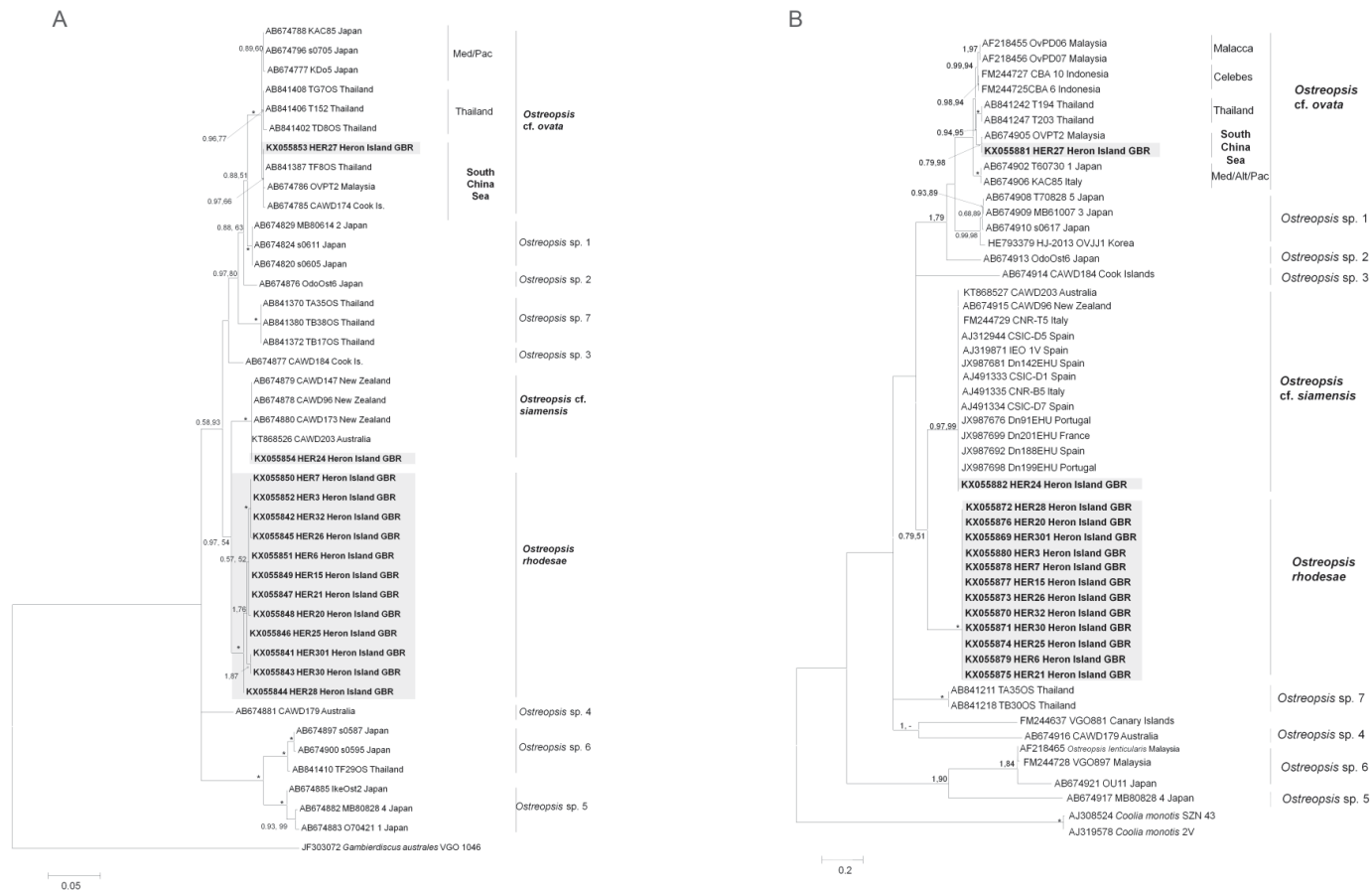
Figure 3.7 Maximum Likelihood (ML) phylogenetic trees of various *Ostreopsis* strains using primer sets for A: ITS1-5.8S-ITS2; and B: D8-D10 LSU rDNA regions. External Black vertical bars show each distinct *Ostreopsis* clade and internal vertical bars show each *Ostreopsis* subclade. Med, Atl, Pac and Ind are the *Ostreopsis* cf. *ovata* Mediterranean Sea, Atlantic, Pacific and Indian Oceans subclades respectively. Malacca, Celebes, South China Sea and Thailand are the *Ostreopsis* cf. *ovata* Malacca strait, Celebes Sea, South China Sea and Gulf of Thailand sub clades respectively. Numbers at nodes represent posterior probabilities from Bayesian Inferences (BI) and bootstrap support values from Maximum Likelihood (ML) based on 1000 pseudo-replicates. * represents 1, 100 support values for BI and ML respectively.

A

FM997920 OS-19BR Brazil
FN256432 OS-12BR Brazil
FM997914 OS-10BR Brazil
AB605825 OdoOst5 Japan
FM994930 VGO883 Italy
AB605818 IshiOst61 Japan

Med/Alt/Pac

Ostreopsis cf. *ovata*

FM997921 CBA_4 Indonesia
FM997924 CBA_10 Indonesia
KX055853 HER27 Heron Island GBR
AF244940 OvPR04 Malaysia

Ind/Pac

1.94
1.65
0.82, 60

AB841256 s0716 Japan — *Ostreopsis* sp. 1
0.66, 55
AB841258 TB38OS Thailand — *Ostreopsis* sp. 7
0.99, 98
AB605816 OdoOst6 Japan — *Ostreopsis* sp. 2

HQ414222 Dn18EHU Spain
HQ414224 Dn20EHU Spain
FN256430 VGO-OS5V Spain
FN256431 CSIC-D Spain
HQ414223 Dn19EHU Spain
KT868526 CAWD203 Australia
KJ422860 CAWD206 New Zealand
KX055854 HER24 Heron Island GBR

Ostreopsis cf. *siamensis*

1, 98

KX055841 HER301 Heron Island GBR
KX055843 HER30 Heron Island GBR
KX055842 HER32 Heron Island GBR
KX055851 HER6 Heron Island GBR
KX055852 HER3 Heron Island GBR
KX055846 HER25 Heron Island GBR
KX055844 HER28 Heron Island GBR
KX055845 HER26 Heron Island GBR
KX055847 HER21 Heron Island GBR
KX055849 HER15 Heron Island GBR
KX055850 HER7 Heron Island GBR
KX055848 HER20 Heron Island GBR

Ostreopsis rhodesae

1.86
1.90
1.98
1, 98
-, 65

AB605815 UrGmb6 Japan — *Ostreopsis* sp. 5
AB605814 IkeOst2 Japan
AF244941 OLPR01 Malaysia — *Ostreopsis* sp. 6

FM994895 VGO881 Spain
AM902747 *Coolia monotis* VGO783

0.1

B

KF359996 ORUS A1 Sea of Japan
KF359997 ORUS A2 Sea of Japan
KF359998 ORUS H1 Sea of Japan
KF359999 ORUS H2 Sea of Japan
KF360000 ORUS K2 Sea of Japan
KF360001 ORUS O1 Sea of Japan
KF360002 ORUS O2 Sea of Japan
KF360004 ORUS J2 Sea of Japan
KF360003 ORUS J1 Sea of Japan

Unclassified *Ostreopsis* sp.

1.93

HE793379 HJ-2013 Korea — *Ostreopsis* sp. 1

KX055867 HER27 Heron Island GBR
AF244939 OvPR04 Malaysia

Ostreopsis cf. *ovata*

0.72, 97

KX055868 HER24 Heron Island GBR
KT868529 CAWD203 Australia

Ostreopsis cf. *siamensis*

0.63, 50

KX055859 HER26 Heron Island GBR
KX055860 HER25 Heron Island GBR
KX055857 HER30 Heron Island GBR
KX055856 HER32 Heron Island GBR
KX055865 HER6 Heron Island GBR
KX055858 HER28 Heron Island GBR
KX055855 HER301 Heron Island GBR
KX055861 HER21 Heron Island GBR
KX055862 HER20 Heron Island GBR
KX055864 HER7 Heron Island GBR
KX055866 HER3 Heron Island GBR
KX055863 HER15 Heron Island GBR

Ostreopsis rhodesae

1, 95

FR847217 *Coolia monotis* CMJJ1
EF492487 *Coolia monotis* CCMP1345
HQ897279 *Coolia malayensis* NQAIF35

0.02

Figure 3.8 ML phylogenetic trees of various *Ostreopsis* strains using primer sets for A: D1-D3 LSU rDNA; and B: SSU rDNA regions. See the caption in Figure 3.7 for the detailed information.

In this study, the ITS2 region of *Ostreopsis* species was found to be the shortest amongst dinoflagellates at 87-92 bp, as previously reported in Leaw et al. (2001) and Ramos et al. (2015). The ITS2 secondary structure does not conform to the conventional eukaryotic four domain structure, which has been observed in other genera of the order Gonyaulacales such as *Coolia, Alexandrium*, *Gambierdiscus* and *Fukuyoa* (John et al., 2014; Laza-Martínez et al., 2015; Leaw et al., 2016; Ramos et al., 2015; Schultz et al., 2005). ITS2 structure variants deviating from the eukaryote core structure are known in several organisms including alga, plant, fungi, and animals suggesting that several organisms, including *Ostreopsis*, may have species or organism specific solutions for ITS2 processing such as *Isopora*/*Acropora* scleractinian corals and the ciliate genus *Spirostomum* (Coleman, 2007; Coleman and van Oppen, 2008; Shazib et al., 2016).

Within dinoflagellate genera, non-coding internal transcribed spacers (i.e. ITS1 and ITS2) have a fast-evolutionary rate, and the short ITS2 length of *Ostreopsis* may be a result of such rapid evolution as seen in the case of *Symbiodinium* clades and sub-clades (LaJeunesse et al., 2012; Ramos et al., 2015). Long periods of evolution or mutations may be responsible for such diversity in *Ostreopsis*. Three HCBCs were detected in the Mediterranean/Altantic *O*. cf. *ovata* sub clade as compared to other *O*. cf. *ovata* sub-clades from the Indian/Pacific Ocean regions. Although there is no rule about the presence of hemi-CBCs and species delineation, previous studies have separated biological species when two hemi-CBCs have been reported as in the case of *Pseudo-nitzschia* (Amato et al., 2007; Teng et al., 2015). Geographic isolation, phylogenetic divergence as reported in previous studies and the presence of HCBCs suggest that *O*. cf. *ovata* Med/Atl sub-clade represents a separate taxonomic unit and requires further investigation (Penna et al., 2014; Penna et al., 2010).

Figure 3.9 Predicted ITS2 secondary structure of *Ostreopsis* strains. A: *O*streopsis cf. *ovata* HER27; B: *O*streopsis cf. *siamensis* HER24; and C: *Ostreopsis rhodesae* HER26.

3.5.3 Toxicity

No PLTX-like analogues were detected from *O*. cf. *siamensis* HER24 and *O. rhodesae* strains, however the fish gill cells used in the bioassay were sensitive to their cellular extracts (Figure 3.10 A, B). Previously, non-PLTX derivatives produced by *Ostreopsis* species, such as Ostreol-A, have shown to be cytotoxic towards brime-shrimp (Hwang et al., 2013). Since the oxidative cleavage method does not identify these compounds, it is possible that the production of such non-PLTX-like compounds by *O. rhodesae* strains might be responsible for the toxic effect and were not detected (Selwood et al., 2012). Crude methanolic extracts from ichthyotoxic microalgae have shown to be highly toxic towards the fish gill cell line RTgill-W1. These effects have been associated with the production of fatty acids and reactive oxygen species (ROS) in microalgae, causing the release of free radicals that are toxic to the fish gill cells (Dorantes-Aranda et al., 2015). Usup et al. (2008) found *Ostreopsis* species to produce eicosapentaenoic (EPA, 20:5ω3) and docosahexaenoic (DHA, 22:6ω3) acids, which have been proven to be cytotoxic towards the fish gill cells RTgill-W1 (Mardones et al., 2015; Mooney et al., 2011). The toxic effect of *O. rhodesae* and *O*. cf. *siamensis* can be possibly explained by the production of such lipid molecules that were extracted in the methanol extracts of these species.

Using the oxidative cleavage method, both the amine and amide aldehyde fragments were detected in *O*. cf. *ovata* HER27 and the peak area ratio was almost identical to the PLTX standard (Selwood et al., 2012). No intact PLTX molecules were detected, suggesting structural modifications in the central portion of the molecule which might yield different analogues in the cellular extract. The strain showed higher toxicity in the stationary phase compared to the exponential growth phase due to the accumulation of PLTX-like compounds (Guerrini et al., 2010) (Figure 3.10C). While the complete structure of these molecules remains to be elucidated, the cellular content of PLTX-like analogues was lower compared to the toxic *O*. cf. *ovata* strains reported in previous studies from Mediterranean and Japanese waters (Dell'Aversano et al., 2014; Guerrini et al., 2010; Suzuki et al., 2012).

Figure 3.10 Effect of crude extracts from A: *Ostreopsis* **cf.** *siamensis* **HER24; B:** *Ostreopsis rhodesae* **HER26; and C:** *Ostreopsis* **cf.** *ovata* **HER27 on viability of fish gill cells RTgill-W1. Plots are average from quadruplicate wells and bars represent their standard deviation. Symbols (*) indicate significant differences (at p≤0.05) when comparing the effect of extracts from exponential and stationary growth phase at each extract concentration. Arrows and negative values show the decrease in gill cell viability.**
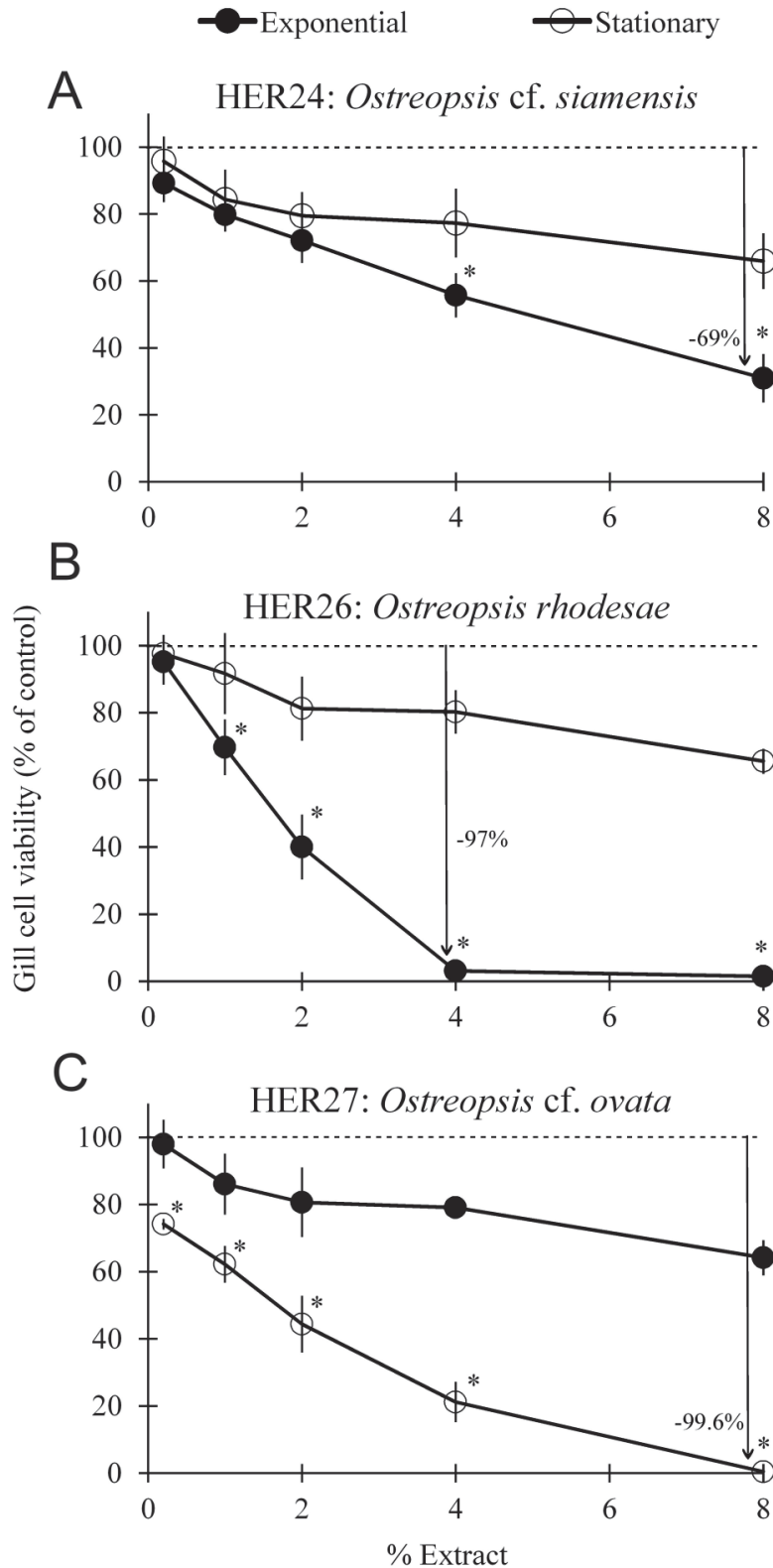
In conclusion, a new pseudo-cryptic species, *Ostreopsis rhodesae,* is described based on a combination of morphological features and unique sequences of rRNA gene regions with the presence of CBCs present in the ITS2 secondary structure. This species was not found to produce PLTX-like analogues but showed toxicity towards fish gill cell lines. This species is morphologically similar to other toxic species of *Ostreopsis* which demonstrates that highly similar species of *Ostreopsis* with differing physiological or toxicological features may co-occur in a given habitat.

3.6 Author contributions

AV, SM designed research; AV isolated strains, performed research, analysed and interpreted data; MH performed light and scanning electron microscopy; TH carried out LC-MS/MS at Cawthron institute; JJ performed fish gill assay at University of Tasmania; AV, SM wrote the paper with editorial input from all co-authors.

Chapter 4: Functional significance of phylogeographic structure in a toxic marine protist (*Ostreopsis*, Dinophyceae) along a 1500 km of north-south gradient in the East Australian Current

4.1 Abstract

Recent research is increasingly indicating that marine microbial eukaryotes consist of consortia of genetically structured 'meta-populations' with large phenotypic diversity of functional traits. These factors may drive their ecological success, enabling them to buffer against changing environmental conditions. Despite this new information, many studies of marine protist evolution and physiology continue to use single or small numbers of strains to analyse traits, under the assumption that this would be representative of the species. In the south-east Australian coastal region, the warming of the East Australian Current (EAC) over the past decades has made it a global 'hotspot' of climate variation. *Ostreopsis* 'cf.' *siamensis* is a cosmopolitan epi-benthic species found globally in sub-tropical and temperate waters and can cause harmful blooms by producing highly toxic palytoxin-like compounds. The aim of the current study is to determine the genetic diversity, functional and niche divergence in *O*. cf. *siamensis* along a 1500 km gradient along the EAC. The study revealed widespread distribution of *O*. cf. *siamensis* along coastline from which 68 isolates, sampled from eight locations spanning across five bioregions, were established. The highest genetic and phenotypically variability, in growth rates, toxin production and profiles, cell volume and photophysiological responses, within populations was observed in the northern sub-tropical sites suggesting that southerly populations may have colonised their habitats more recently in geological time due to the southward extension and intensification of the EAC. Locally-adapted phenotypic trait variations demonstrate the importance of investigating multiple isolates of a species to characterize the range of a particular trait and highlight the importance of integrating genetic, physiological and ecological data to investigate the phylogeographic structure in coastal oceanographic studies of phytoplankton.

4.2 Introduction

Microbial eukaryotes are an essential component of marine ecosystems, driving productivity and biogeochemical cycles (Falkowski et al., 1998). Despite this, our understanding of the processes driving their genotypic and phenotypic diversity remain poorly understood (Falkowski et al., 2004; Lowe et al., 2012). Phytoplankton populations were originally thought to be largely homogenous, as high dispersal capabilities (e.g., lack of geographical barriers) and fast replication rates were thought to result in a continuous and cosmopolitan distribution with little or no allopatric speciation (De Wit and Bouvier, 2006; Logares et al., 2007; Sjöqvist et al., 2015). However, recent studies have highlighted that phytoplankton populations do show spatial structuring, and that phylogeographic patterns may be more reflective of historical (e.g., dispersal limitation), ecological (e.g., divergence resulting from local selection) and local conditions (trait-based niches) that drive the fundamental physiological processes altering population structures (Godhe et al., 2013; Litchman and Klausmeier, 2008). This would suggest that phytoplankton should be considered as consortiums of genetically structured 'meta-populations' with low rates of dispersal (isolation by physical and/or ecological barriers), rather than single panmictic populations (Annenkova et al., 2015; Ellison et al., 2011; Foissner, 2006; Masseret et al., 2009; Nagai et al., 2007; Tahvanainen et al., 2012).

The ecological success of phytoplankton populations living in shifting environments is driven by phenotypic diversity of functional traits that drives adaptation by allowing for the selection of strains (Chevin et al., 2013). Phenotypic variability can buffer the immediate detrimental effects of environmental fluctuations, while standing genetic variation influences the longer-term selection on populations (Kearney et al., 2010; Kremp et al., 2012). Investigating the evolutionary mechanisms of diversification of phenotypic traits such as cell size, photosynthetic optimization, growth rates or the production of secondary metabolites remain key to our understanding of the processes of phytoplankton adaptation, and also inform us of the dynamics of future phytoplankton populations under changing climatic regimes (John et al., 2015; Koester et al., 2010; Tillmann et al., 2009; Whittaker et al., 2012).

In the south-east Australian coastal region, the East Australian Current (EAC) runs north to south, redistributing warm tropical waters from the Coral Sea into the temperate Tasman Sea. The increase in ocean temperature at mid-latitudes of up to 2.0 °C over the past decades is related to a southern range extension of the EAC, and has made it a global 'hotspot' of climate variation (Ridgway, 2007; Suthers et al., 2011). Such ecological variations may result in phytoplankton population shifts, depending on their genotypic diversity, with more diverse populations expected to buffer changing environmental conditions more efficiently than their genetically uniform counterparts (Bell and Collins, 2008; Kremp et al., 2016).

Ostreopsis 'cf.' *siamensis* is a cosmopolitan epi-benthic species, among the genus *Ostreopsis*, found globally in sub-tropical and temperate waters (Penna et al., 2005; Rhodes, 2011; Verma et al., 2016a). *O.* cf. *siamensis* can cause harmful blooms by producing highly toxic palytoxin-like compounds (PLTX, $C_{129}H_{223}N_3O_{54}$) and are known to cause large-scale sea mortalities of benthic organisms (Hoppenrath et al., 2014; Penna et al., 2005; Shears and Ross, 2009). In the EAC region, strains of *O.* cf. *siamensis* are found in temperate estuaries and sub-tropical coral reefs (Heimann et al., 2009; Holmes et al., 1988; Pearce et al., 2001; Verma et al., 2016a; Verma et al., 2016b). The aim of the current study is to determine; (i) the genetic diversity in *O.* cf. *siamensis* along a 1500 km gradient from sub-tropical to temperate coastal regions of the EAC, and (ii) determine the functional and phenotypic niche divergence of growth rates, cell volume, strategies for moderating light harvesting and utilization as well as PLTX production amongst the clonal isolates.

4.3 Materials and methods

4.3.1 Site descriptions, sample collection and strain establishment

The approx. 1500 km coastline of New South Wales (NSW) has around 950 water bodies with seagrasses and macroalgal communities in the intertidal regions. The coastline spans over five bioregions that are defined using biological (marine flora and fauna) and physical information (oceanographic features) ranging from warm sub-tropical waters in the north to cool temperate waters in the south (Ajani et al., 2013).

Macroalgal and seagrass samples were collected from eight shallow intertidal locations spanning the five bioregions along the NSW coast as listed in Table 4.1 between April-July 2014 (Figure 4.1). Samples were immediately brought back to University of Technology Sydney and shaken vigorously to detach the epiphytic microalgal cells. The epiphytic suspension was passed through a 125 µm mesh filter to remove larger fauna and debris. *Ostreopsis* cells were identified microscopically and non-axenic monoclonal isolates were established according to single cell isolation protocol as described in Verma et al. (2016b).
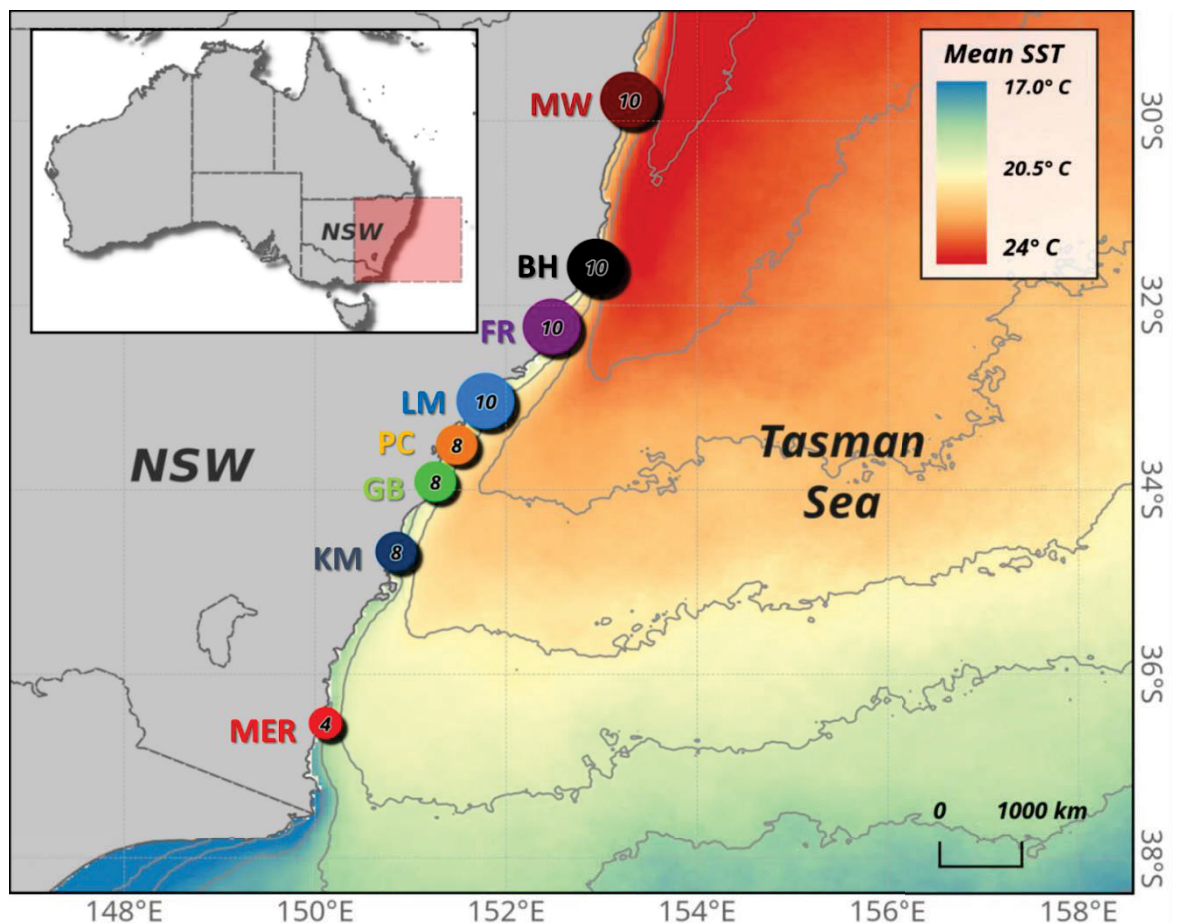
Figure 4.1 Map of the south-eastern coastline of Australia showing sampling locations in this study. Macroalgal samples were collected during April-July 2014. MW, BH, FR, LM, PC, GB, KM and MER represent sampling sites, i.e. Minnie Waters, Bonny Hills, Wallis Lake in Forster, Lake Macquarie, Patonga Creek, Gordons Bay, Kiama and Merimbula Lake Inlet respectively. Numbers in the circles represent the number of clonal isolates that were established from the sampling site. Isothermal lines represent the mean sea surface temperature (SST) from 2012-2017 varying north to south from 24-17°C by a gradient of 1°C.

All isolates were grown in f/10 medium (Guillard, 1975) at 18 ± 1°C and salinity of 35 under an irradiance of 60 ± 15 µmol photons m^{-2} s^{-1} (TLD 18W/54 fluorescent tubes, Philips, colour temperature 10,000 K) set to a 12h:12h light: dark cycle in 24 multi-well culture plate (Corning Inc. Durham, USA) with 1 mL medium. After 3-4 weeks, the clonal isolates were transferred to 50 mL sterile tissue culture flasks (Becton Dickinson, Sydney, Australia) and maintained in semi-continuous batch mode and diluted to maintain exponential growth as described in Hennige et al. (2009). Cultures were transferred to new flasks after 6-8 weeks to avoid cells sticking to the vessel wall and accumulation of bacterial populations.

4.3.2 DNA extraction, PCR and sequencing

DNA was extracted from cell pellets harvested via centrifugation (50 mL; 2300 g; 5 mins; room temperature) using a modified 3% CTAB extraction buffer (100 mM Tris-HCl pH 8; 20 mM EDTA pH 8; 1.4 M NaCl; 0.5% beta-mercaptoethanol) as described in Verma et al. (2016a). All PCR reactions were performed in 25 µL reaction volumes containing 12.5 µL 2× Immomix (Bioline, Sydney, Australia), 7.5 pmol of each primer (Table 4.2), 1 µg $µL^{-1}$ of BSA (Biolabs, Arundel, Australia), 1 µL of template DNA and PCR grade water to give the final volume. Thermocycling conditions consisted of an initial denaturing step of 95°C for 10 min, followed by 35 cycles of 95°C for 20 s, 30 s annealing (Table 4.2), 72°C for 1.5 min and a final extension of 72°C for 7 mins. PCR products were purified with Sure Clean Plus (Bioline, Sydney, Australia), according to the supplied protocol from the manufacturer and sequenced using a commercial service (Macrogen Inc., Seoul, Korea).

Table 4.1 Details of the sampling sites and macroalgal samples used for establishing monoclonal cultures of *Ostreopsis* cf. *siamensis* in this study

Site	Zone	Latitude; Longitude	Bioregion	Macroalgal species	Date of sample collection	Temp (˚C)	Salinity (psu)	No. of initial isolates	No. of isolates with successful DNA extraction	No. of isolates used for physiological assesments
Minnie Waters	North	29.77°S 153.29°E	Tweed-Moreton	*Hormosira banksii*	16 July 2014	18	35	10	10	9
Bonny Hills	North	31.58°S 152.82°E	Tweed-Moreton	*Hormosira banksii*	16 July 2014	18.5	34	12	10	10
Wallis Lake, Forster	Central	32.23°S 152.48°E	Manning shelf	*Zostera* sp.	17 July 2014	19	34	14	10	9
Lake Macquarie	Central	33.09°S 151.88° E	Hawkesbury shelf	*Ecklonia* sp.	29 June 2014	17	34	10	10	7
Patonga Creek	Central	33.51°S 151.28° E	Hawkesbury shelf	*Sargassum* sp.; *Phyllospora* sp.	31 May 2014	18	35	13	8	5
Gordons Bay	South	33.91°S 151.26°	Hawkesbury shelf	*Sargassum* sp.	1 April 2014	18	34	11	8	7
Kiama	South	34.67°S 150.85°E	Batemans shelf	*Phyllospora* sp.; *Sargassum* sp.	27 July 2014	18	34	8	8	3
Merimbula Lake Inlet	South	36.53°S 149.54°E	Twofold shelf	*Zostera* sp.	7 April 2014	19	28	7	4	3

4.3.3 Phylogenetic analyses

Bayesian inference (BI) and maximum likelihood (ML) analyses on individual alignments of ITS/5.8S, D1-D3 and D8-D10 rDNA LSU regions were performed in MEGA v6 (Tamura et al., 2013) and Geneious v6 (Kearse et al., 2012). The forward and reverse sequences were trimmed, aligned and visually refined using BioEdit v7.2.5 (Hall, 1999). Multiple sequence alignments were performed using ClustalW v1.6 (Thompson et al., 2002) as implemented in MEGA v6 with the closely related *Ostreopsis* cf. *ovata* HER27 (ITS/5.8S GenBank accession number: KX055853; LSU GenBank accession number: KX055881) and *Ostreopsis rhodesae* strains HER6 (ITS/5.8S GenBank accession number: KX055851; LSU GenBank accession number: KX055879) and HER20 (ITS/5.8S GenBank accession number: KX055848; LSU GenBank accession number: KX055876) used as outgroups. Substitution models were selected for each dataset based on lowest Bayesian information criterion (BiC) as a measure of the relative quality of the models. ML trees were produced using Tamura-Nei (T92) with 5 gamma categories substitution model for all sequence analyses. Nodal support of the ML tree was estimated via bootstrap algorithm with 1000 replications. Bayesian analysis was performed using MrBayes v3.2.2 (Ronquist and Huelsenbeck, 2003) as implemented in Geneious v6 using general time reversible model (GTR) + gamma model for all sequence analyses. Four independent Markov Chain Monte Carlo (MCMC) simulations were run simultaneously for 2,000,000 generations. Trees were sampled every 1,000 generations and 1,000 trees were discarded as burn- in.

Concatenated sequences from the ITS/5.8S, D1-D3 and D8-D10 rDNA LSU regions for each strain were prepared by removing poorly aligned positions using GBLOCKS set at default settings (Castresana, 2000). ML and BI analyses were performed on the concatenated sequences as described above. Molecular diversity indexes (pairwise uncorrected *p*-distance) were estimated from individual sequence datasets as well as concatenated sequences between and within sites using the *p*-distance model and bootstrap procedure (1000 replicates) in MEGA v6. All positions containing gaps and missing data were eliminated for the analyses. Mean number pair wise differences, nucleotide diversity (π), no. of polymorphic sites (S) and haplotype diversity (H_d) for each site were calculated on the concatenated sequences using Arlequin v 3.5.2.2 (Excoffier

and Lischer, 2010). A statistical parsimony network (Templeton et al., 1992) was obtained based with TCS v1.18 software (Clement et al., 2000).

Table 4.2 Primers used for phylogenetic analyses in this study and the annealing temperature (T_a) used for the PCR reactions.

Primer Name	Primer sequence	Target region	Direction	T_a ($^{\circ}$C)
D1R[a]	5'-ACC CGC TGA ATT TAA GCA TA-3'	D1-D3	Forward	56
D3B[b]	5'-TCG GAG GGA ACC AGC TAC TA-3'	D1-D3	Reverse	56
FD8/D8[c]	5'-GGA TTG GCT CTG AGG GTT GGG-3'	D8-D10	Forward	62
RB/D10[c]	5'-GAT AGG AAG AGC CGA CAT CGA-3'	D8-D10	Reverse	62
GLD8_421F[d]	5'-ACA GCC AAG GGA ACG GGC TT-3'	D8-D10	Forward	62
GLD8_677R[d]	5'-TGT GCC GCC CCA GCC AAA CT-3'	D8-D10	Reverse	62
ITS A[e]	5'-GTA ACA AGG THT CCG TAG GT-3'	ITS/5.8S	Forward	56
ITS B[e]	5'-AKA TGC TTA ART TCA GCR GG-3'	ITS/5.8S	Reverse	56

[a] Scholin et al. (1994); [b] Nunn et al. (1996); [c] Chinain et al. (1999); [d] Nishimura et al. (2013); [e] LaJeunesse (2001)

4.3.4 Growth rates estimates

Growth rates (μ) were determined during exponential growth using minimum fluorescence from Fast Repetition Rate Fluorometry (FRRf) and obtained from at least three sequential dilutions as described in Suggett et al. (2015). Samples were also periodically verified from independent measurements of cell counts using Sedgerick rafter chamber (Hennige et al., 2009; Suggett et al., 2015). Each culture was grown for over one year in the culturing conditions described in section 4.3.1 prior to estimating growth rates.

4.3.5 Cell volume analysis

Cell dimensions of cultures in mid-exponential phase were measured under 200× using a calibrated eyepiece of inverted microscope (Eclipse TS100, Nikon, Hilton, Australia) with bright field optics. Cells were harvested from the culture medium, 8-10 days of sub-culturing, and concentrated through gravity filtration. Samples were fixed in 1% Lugol solution to measure the dorso-ventral diameter (DV), trans-diameter width (W) and anterior-posterior diameter (AP) using ImageJ v1.48 (Abràmoff et al., 2004). Twenty

cells for each clonal isolate were measured. Calculations of cell volume were performed with the assumption of ellipsoid shape using the following equation (Sun and Liu, 2003):

$$V = \pi/6 \; DV * W * AP$$

4.3.6 PLTX toxin determination

All cultures were harvested in late-stationary phase (Day 19-21) by centrifugation (50 mL; 2,300 g; 10 mins; room temperature) and the cell pellets were freeze-dried. PLTX and related structural analogues were screened using a quantitative LC-MS/MS method at the Cawthron Institute, New Zealand. In summary, The LC-MS/MS analytical approach monitored the sub-structures generated by the oxidative cleavage of vicinal diol groups, present in the intact toxins, using periodic acid. Periodate oxidation results in the cleavage of carbon-carbon bonds via a cyclic transition state with formation of two aldehyde containing fragments. A commercially available PLTX standard was used to generate a calibration curve and to allow unambiguous identification of the oxidation products. This yields an amino-aldehyde common to known palytoxins, ovatoxins and ostreocins, and an amide-aldehyde that varies depending on the toxin type (Selwood et al., 2012).

4.3.7 FRRf - Dark-acclimated photophysiology

All samples were transiently acclimated to low light (c. 5 μmol photons m^{-2} s^{-1}) for at least 20 mins to relax non-photochemical quenching (NPQ), yet simultaneously minimise the potential for chlororespiration (Hill and Ralph, 2008; Kromkamp and Forster, 2003). Three mL culture samples were loaded into borosilicate test-tubes, and measured with a FastOcean FRR fluorometer attached to a FastAct base unit (Chelsea Technologies Group, West Molesey, Surrey, UK). The optical head housing the test tube was temperature-controlled (at growth temperature) via continuous flushing via from a heater–cooler circulator (SC100; Thermo Fisher Scientific Inc., Waltham, MA, USA).

The FRRf was set to deliver a single-turnover induction protocol of 100 flashlets of 1.1 µs at 2.8-µs intervals (Hill et al., 2014; Robinson et al., 2014). Measurements were taken from the average of 40 consecutive sequences, spaced 150 ms intervals apart. The measured fluorescence transient from each acquisition was subsequently fitted to the KPF model (Kolber et al., 1998) using FastPRO software v1.5.2 (Chelsea Technologies Group) to extract the minimum (F_0, F') and maximum (F_m, F_m') PSII fluorescence yields (instrument units) and PSII functional absorption cross-section (σ, σ'; nm^2), for dark (unprimed) and actinic light (primed) conditions. Values for the PSII photochemical efficiency (ϕ_{PSII}, ϕ_{PSII}'; dimensionless) were subsequently derived as $[F_m - F_0]/F_m$ or $[F_m' - F']/F_m'$. Baseline fluorescence was subtracted from all fluorescence measurements, using filtrates of each sample obtained from 0.2 µm syringe filter.

4.3.8 FRRf – Photosynthetic-Irradiance (PE) Response

Photosynthesis-Irradiance (PE) response for all strains was assessed by performing fluorescence light curves (FLCs) in triplicate. A cluster of white LEDs housed within the FRRf optical head were programmed to deliver 20 s steps of increasing irradiance (0, 10, 28, 47, 66, 85, 104, 123, 160, 251, 330, 402, 550, 756, 905 and 1208 µmol photons m^{-2} s^{-1}). Due to the relatively short length of each light step, we refer to this protocol as a 'rapid light curve' (RLC).

For each actinic light step, the electron transport rate through PSII (ETR$_{PSII}$) was measured according to the sigma algorithm proposed by Kolber and Falkowski (1993):

$$\text{ETR}_{PSII} = E \cdot \sigma_{PSII}' \cdot (1/[F_v/F_m]) \cdot [\text{RCII}] \cdot (1\text{-}C)$$

where E is the irradiance (µmol photons m^{-2} s^{-1}), σ_{PSII}' is the functional absorption cross-section of PSII under actinic light (nm^2 quanta^{-1}), and [RCII] is the concentration of PSII reaction centres (mol RCII m^{-3}). The inclusion of the factor $1/[F_v/F_m]$ (where $F_v/F_m = [F_m - F_0]/F_m$) accounts for the non-radiative loss of energy associated with σ_{PSII}' (Kolber et al., 1998; Oxborough et al., 2012; Suggett et al., 2009) and C represents the fraction of RCII in the closed state, estimated as here as $1\text{-}qP$ ($qP = (F'\text{-}F_0')/(F_m'\text{-}F_0')$).

For this study, [RCII] was estimated according to the algorithm developed by Oxborough et al. (2012):

$$[\text{RCII}] = \frac{K_R}{E_{LED}} \times \frac{F_o}{\sigma_{PSII}}$$

where K_R represents an instrument-specific constant (photons m^{-3} s^{-1}) and E_{LED} is the intensity of the fluorometers measuring beam (photons m^{-2} s^{-1}). Photosynthesis-Irradiance (PE) curves were then fitted to the hyperbolic tangent function described by Platt et al. (1981) using the Solver function in Microsoft Excel, from which the maximum photosynthetic rate (ETR$_{max}$), the light saturation parameter (E$_k$) and the light utilisation efficiency (α) were derived as suggested in Jassby and Platt (1976).

To compare the transient influence of photochemical quenching (1-C) versus non-photochemical quenching (NPQ) in governing photosynthetic efficiency across strains, we followed the procedure of Suggett et al. (2015) and calculate non-photochemical quenching as normalised F_v'F_m' (=[F_v'F_m'] / [F_v/F_m]), which is thereafter referred to as 1-Q throughout the text. Whilst the RLC is a powerful tool to probe photosynthetic response (Ralph et al. 2009), its short length (20 s) provides limited time for the generation of NPQ mechanisms; thus, in this study, values of 1-Q derived from RLCs are most useful to identify strains capable of rapid upregulation of non-photochemical energy dissipation (Lavaud et al., 2007).

4.3.9 Pigments and Photosynthetic Unit (PSU) Size

Fifteen mL of culture samples were withdrawn and filtered on GF/F filters and immediately re-suspended in 3 mL of acetone (90%, v/v), and stored at 4°C to allow for pigment extraction. After the extraction period (24-36 hr) samples were centrifuged at 1000 g for 10 mins, the absorbance of extracts was measured at 665 and 750 nm (UV/VIS, JASCO 7800, Tokyo, Japan) and the concentration of chlorophyll-a was determined according to the following equation (Pezzolesi et al., 2014; Ritchie, 2006):

Chlorophyll-a (µg L^{-1}) = 11.4062 * [$A_{665} - A_{750}$] * v * 10^3/ (c$_o$ * V)

where A_{665} = the blank corrected absorbance at 665 nm, A_{750} = the blank corrected absorbance at 750 nm, v = volume of acetone solution used for the extraction (mL), c_o = cell path length (cm), V = volume of filtered sample (mL). The concentration of Chlorophyll-a was then used to calculated the photosynthetic unit (PSU) (mol Chl-a m^{-3} (mol RCII m^{-3})$^{-1}$) according to Oxborough et al. (2012).

4.3.10 Statistical analysis

One-way Analysis of variance (ANOVA) and Tukey's HSD post-hoc tests were applied to determine significant differences across clonal isolates from each site for growth rates, total cellular biovolumes, F_v/F_m, PSII functional absorption cross-section (σ), maximum photosynthetic rate (ETR$_{max}$), the light saturation parameter (E$_k$) and the light utilisation efficiency (α). These analyses were conducted in SPSS (Coakes and Steed, 2009). When data were not normally distributed, the non-parametric Kruskal–Wallis test was applied. The relative standard deviation of repeatability for LC-MS/MS of oxidized PLTX standards were <10% and <8% for amino aldehyde and amide aldehyde, respectively (Selwood et al., 2012).

To identify photobiological functional groupings amongst strains based on components moderating light harvesting and utilization, cluster analysis and multi-dimensional scaling (MDS) were performed with σ, F_v/F_m, [RCII cell^{-1}], [1 − C] and 1-Q using PRIMER-E v6.1 (PRIMER-E Ltd, Ivybridge, Devon, UK). Values of fluorescence ratios (F_v/F_m, [1 − C] and [1-Q]) were arcsine transformed to stabilize the variance for MDS analysis.

Photophysiological parameters (σ, F_v/F_m, [RCII cell^{-1}], [1 − C] and 1-Q) along with growth rate, cell volume and PLTX amounts in 53 O. cf. *siamensis* strains were compared by MDS and principal component analysis (PCA) in PRIMER-E v6.1. Variables were standardised prior to analysis to account for order of magnitude differences in value ranges. The correlation matrix was used for a two-dimensional PCA, and the principal components were displayed as an ordination plot.

4.4 Results

4.4.1 Sampling and species identification

Sampling carried out in April-July 2014 obtained *O.* cf. *siamensis* isolates from each sampling site. Cells were initially identified using a light microscope, based on their tear drop shaped morphology and cell size. A total of 85 clonal isolates were obtained, from which 68 were used for phylogenetic analyses (Table 4.1 and supplementary data S8A). The monophyly of *O.* cf. *siamensis* was strongly supported by phylogenetic analyses using both ML and BI methods, for all three molecular markers (supplementary data S7).

4.4.2 Phylogeographic structures and genetic diversity

Phylogenetic analysis of the concatenated data from the three molecular markers was broadly congruent with the analyses based on individual genes, yielding two distinct sub-clades (Figure 4.2) and a total of 23 haplotypes (8 in sub-clade 2 and 15 in sub-clade 1) (Figure 4.3). Only isolates from the northern most sites, Minnie Water (MW1, MW2, MW3, MW7, MW8, MW9 and MW10) and Bonny Hills (BH1 and BH3) clusted together to form sub-clade 2. The remaining isolates from the sampled sites clustered in sub-clade 1. Unique haplotypes were identified at all sites using statistical parsimony network analysis (Figure 4.3). All sites shared a common haplotype (haplotype 1), however a greater number of haplotypes were identified from the northern sites (Figure 4.2, 4.3). Eight haplotypes were found at Minnie Water (MW), four at Bonny Hills (BH), Wallis Lake, Forster (FR) and Gordons Bay (GB), three in Lake Macquarie (LM) and Patonga Creek (PC) and only two in Kiama (KM) and Merimbula (MER) samples respectively (Figure 4.3, Table 4.5). Uncorrected *p*-distances based on concatenated sequences showed higher values of molecular diversity indices within the northern locations (MW, BH, and FR) compared to the central and southern sites (Table 4.3, Table 4.4). Genetic distances between MW samples and other locations were considerably higher compared to the differences between other locations (Table 4.4). Mean number of pairwise differences, number of polymorphic sites and haptotype diversity (H_d) were also greater in strains isolated from MW, BH and FR compared to other locations (Table 4.5). Molecular diversity indices obtained from D8-D10 LSU rDNA and ITS regions were lower compared to those obtained from D1-D3 rDNA LSU region (Table 4.3).
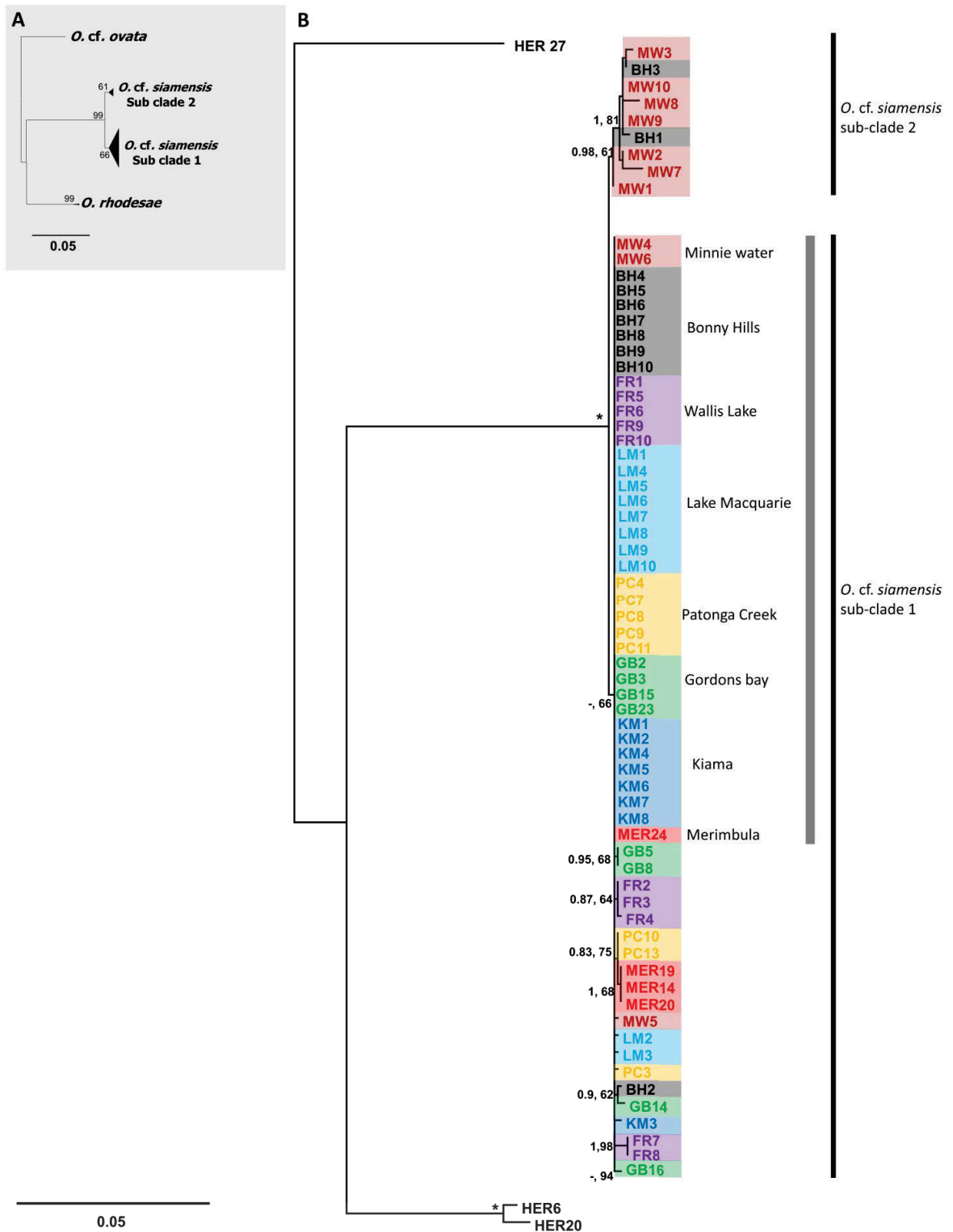
Figure 4.2 A: Maximum likelihood (ML) phylogenetic tree based on ITS-5.8S/D1-D3 and D8-D10 LSU rDNA concatenated sequences representing the two sub-clades of *O*streopsis cf. *siamensis*. B: Phylogram representing the various haplotypes within the two sub-clades. The internal grey line represents haplotype 1 common to all locations. Numbers at nodes represent posterior probabilities from Bayesian Inferences (BI) and bootstrap support values from ML based on 1000 pseudo-replicates. Only bootstrap values > 50% are shown. * represents 1, 100 support values for BI and ML respectively. Colour codes represent origin of strains as represented in Figure 4.1.

Table 4.3 Molecular diversity indexes (uncorrected *p*-distances) in the ITS1-5.8S-ITS2, D1-D3, D8-D10 rDNA and concatenated sequences within sampling locations. Standard error estimate(s) are shown in brackets and were obtained by a bootstrap procedure (1000 replicates).

	ITS	D1-D3 LSU	D8-D10 LSU	Concatenated
MW	0.006 (0.003)	0.01 (0.002)	0.002 (0.001)	0.005 (0.001)
BH	0.003 (0.002)	0.009 (0.002)	0 (0.000)	0.003 (0.001)
FR	0.007 (0.003)	0.001 (0.000)	0.001 (0.001)	0.002 (0.001)
LM	0 (0.000)	0.001 (0.000)	0.001 (0.001)	0 (0.000)
PC	0.001 (0.001)	0.001 (0.000)	0.001 (0.001)	0.001 (0.001)
GB	0.003 (0.002)	0.002 (0.001)	0.001 (0.001)	0.001 (0.001)
KM	0 (0.000)	0.002 (0.001)	0.001 (0.001)	0 (0.000)
MER	0 (0.000)	0.083 (0.007)	0.002 (0.001)	0.001 (0.001)
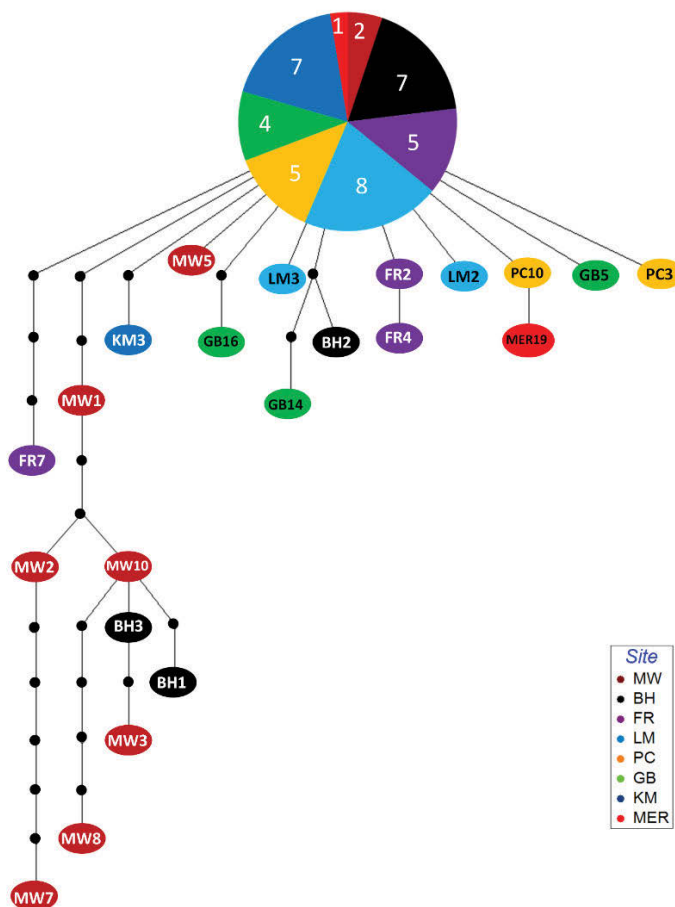
Figure 4.3 Haplotype network based on 68 concatenated sequences using statistical parsimony. Mutation steps are shown in black dots. Colour codes represent origin of strain as represented in Figure 4.1. Strain codes are representatives of haplotypes as described in Table 4.5. Numbers in the pie chart represent the number of isolates from each location that belong to haplotype 1.

Table 4.4 Molecular diversity indexes (uncorrected *p*-distances) in the ITS1-5.8S-ITS2, D1-D3, D8-D10 rDNA and concatenated sequences between sampling locations. Standard error estimate(s) are shown in brackets and were obtained by a bootstrap procedure (1000 replicates).

Origin	MW	BH	FR	LM	PC	GB	KM	MER
MW								
BH	0.005 (0.003)							
	0.011 (0.003)							
	0.001 (0.000)							
	0.005 (0.001)							
FR	0.009 (0.003)	0.005 (0.002)						
	0.011 (0.003)	0.005 (0.001)						
	0.002 (0.001)	0.001 (0.003)						
	0.006 (0.001)	0.002 (0.001)						
LM	0.005 (0.003)	0.002 (0.001)	0.004 (0.002)					
	0.011 (0.003)	0.005 (0.001)	0.001 (0.000)					
	0.002 (0.001)	0 (0.000)	0.001 (0.001)					
	0.005 (0.001)	0.002 (0.000)	0.001 (0.000)					
PC	0.006 (0.003)	0.002 (0.001)	0.004 (0.002)	0.001 (0.000)				
	0.011 (0.003)	0.005 (0.001)	0.001 (0.000)	0.001 (0.000)				
	0.002 (0.001)	0 (0.000)	0.001 (0.001)	0.001 (0.000)				
	0.005 (0.001)	0.002 (0.001)	0.001 (0.000)	0 (0.000)				
GB	0.007 (0.003)	0.003 (0.002)	0.005 (0.002)	0.002 (0.001)	0.002 (0.001)			
	0.011 (0.003)	0.006 (0.001)	0.001 (0.000)	0.001 (0.000)	0.001 (0.000)			
	0.002 (0.001)	0(0.000)	0.001 (0.001)	0.001 (0.000)	0.001 (0.001)			
	0.005 (0.001)	0.002 (0.001)	0.002 (0.001)	0.001 (0.000)	0.001 (0.000)			
KM	0.005 (0.003)	0.002 (0.001)	0.004 (0.002)	0 (0.000)	0.001 (0.000)	0.002 (0.001)		
	0.011 (0.003)	0.006 (0.001)	0.001 (0.001)	0.001 (0.001)	0.001 (0.001)	0.002 (0.001)		
	0.001 (0.001)	0 (0.000)	0.001 (0.001)	0.001 (0.000)	0.001 (0.001)	0.001 (0.000)		
	0.005 (0.001)	0.002 (0.000)	0.001 (0.000)	0 (0.000)	0.001 (0.000)	0.001 (0.000)		
MER	0.005 (0.003)	0.002 (0.001)	0.004 (0.002)	0 (0.000)	0.001 (0.000)	0.002 (0.001)	0 (0.000)	
	0.052 (0.004)	0.046 (0.004)	0.042 (0.003)	0.042 (0.003)	0.042 (0.003)	0.042 (0.004)	0.043 (0.004)	
	0.004 (0.002)	0.003 (0.002)	0.003 (0.002)	0.003 (0.002)	0.002 (0.002)	0.003 (0.002)	0.003 (0.002)	
	0.006 (0.002)	0.003 (0.001)	0.002 (0.001)	0.001 (0.001)	0.001 (0.001)	0.002 (0.001)	0.001 (0.001)	

Table 4.5 Haplotype diversity of *Ostreopsis* cf. *siamensis* isolates based upon location of origin as obtained from Arlequin. Standard error estimate(s) are shown in brackets and were obtained by a bootstrap procedure (1000 replicates). Strain codes are representatives of the various haplotypes. Number in the bracket represents the number of isolates that belong to the representative haplotype. [1]represent the strain codes and the number of isolates from each location that belong to haplotype 1.

Origin	Sample size	Mean number pair wise differences	Nucleotide diversity (Average over loci (π))	No. of polymorphic sites (S)	Haplotype diversity (H_d)	No. of haplotypes
MW	10	6.08 (3.17)	0.005 (0.003)	20	0.9556 (0.0594)	8 [MW1, MW2, MW3, MW4(2)[1], MW5, MW7, MW8, MW10(2)]
BH	10	3.04 (1.73)	0.002 (0.001)	9	0.5333 (0.1801)	4 [BH1, BH2, BH3, BH10(7)[1]]
FR	10	2.09 (1.27)	0.0017 (0.0012)	6	0.7333 (0.1199)	4 [FR1(5)[1], FR2(2), FR4, FR7(2)]
LM	10	0.4 (0.4)	0.000338 (0.000385)	2	0.3778 (0.1813)	3 [LM2, LM3, LM5(8)[1]]
PC	8	0.678 (0.57)	0.000574 (0.000553)	2	0.6071 (0.1640)	3 [PC3, PC7(5)[1], PC10(2)]
GB	8	1.6785 (1.095)	0.00142	6	0.75 (0.1391)	4 [GB2(4)[1], GB5(2), GB14, GB16]
KM	8	0.5 (0.47)	0.000423 (0.000455)	2	0.25 (0.18)	2 [KM3, KM8(7)[1]]
MER	4	1 (0.829)	0.000846 (0.000838)	2	0.5 (0.2652)	2 [MER19(3), MER24(1)[1]]
Total	68	2.841528 (1.5159)	0.0024 (0.0014)	40	0.6712 (0.0663)	23

4.4.3 Trait variability among isolates

4.4.3.1 Growth rates and cell volume

Fifty-three strains were used for physiological data analyses (Table 4.1). Large inter-strain variability in growth rates, cell volumes and cellular toxin contents was identified amongst all isolates (Figure 4.4). Mean growth rates (μ) varied from 0.12-0.27 day $^{-1}$. The range of growth rates was particularly high amongst isolates from MW (0.13-0.27 day $^{-1}$), FR (0.13-0.24 day $^{-1}$) and GB (0.12-0.23 day $^{-1}$) (Figure 4.4A and supplementary data S8B). Significant differences in growth rate were found within strains isolated from MW and GB (ANOVA, F= 4.093, 3.213 respectively; $P < 0.05$) (see supplementary data S9). Cell volumes varied significantly between isolates (ANOVA, $P < 0.001$), ranging from 9,200-27,500 μm^3, with the exceptions of strains isolated from KM and MER (ANOVA, $P > 0.05$) (Figure 4.4B, supplementary data S8B and S9).

4.4.3.2 Toxin production

LC-MS/MS analysis of the oxidized cellular extracts yielded the common PLTX amino-aldehyde fragment, used for quantification, and an amide-aldehyde fragment which was identified in various isolates (Figure 4.5A), thereby confirming the presence of PLTX-like compounds in those strains. The PLTX amide fragment was not detected in several isolates (Figure 4.5B). Other structurally-related analogues could potentially be produced by these clones, which require further structural elucidation. Non-PLTX producing isolates were identified in every location, with the exception of BH and LM (Figs 4.4C, 4.5D). Strains MW1 and MW10 displayed a unique profile, where only the amide-aldehyde fragment was observed (Figure 4.5C and supplementary data S8A). Cellular PLTX contents varied amongst strains isolated from the same locations with the highest toxin concentrations measured in isolates from MW and GB (1.48 pg cell $^{-1}$ from MW2 and 1.57 pg cell $^{-1}$ from MW3 and GB2) (Figure 4.4C). Toxin content in the isolates from the southern locations KM and MER were lower in contrast to the isolates from the northern and central sampling sites, with the most toxin profile variability amongst the isolates from MW (Figure 4.4C, 4.5 and supplementary data S8B).
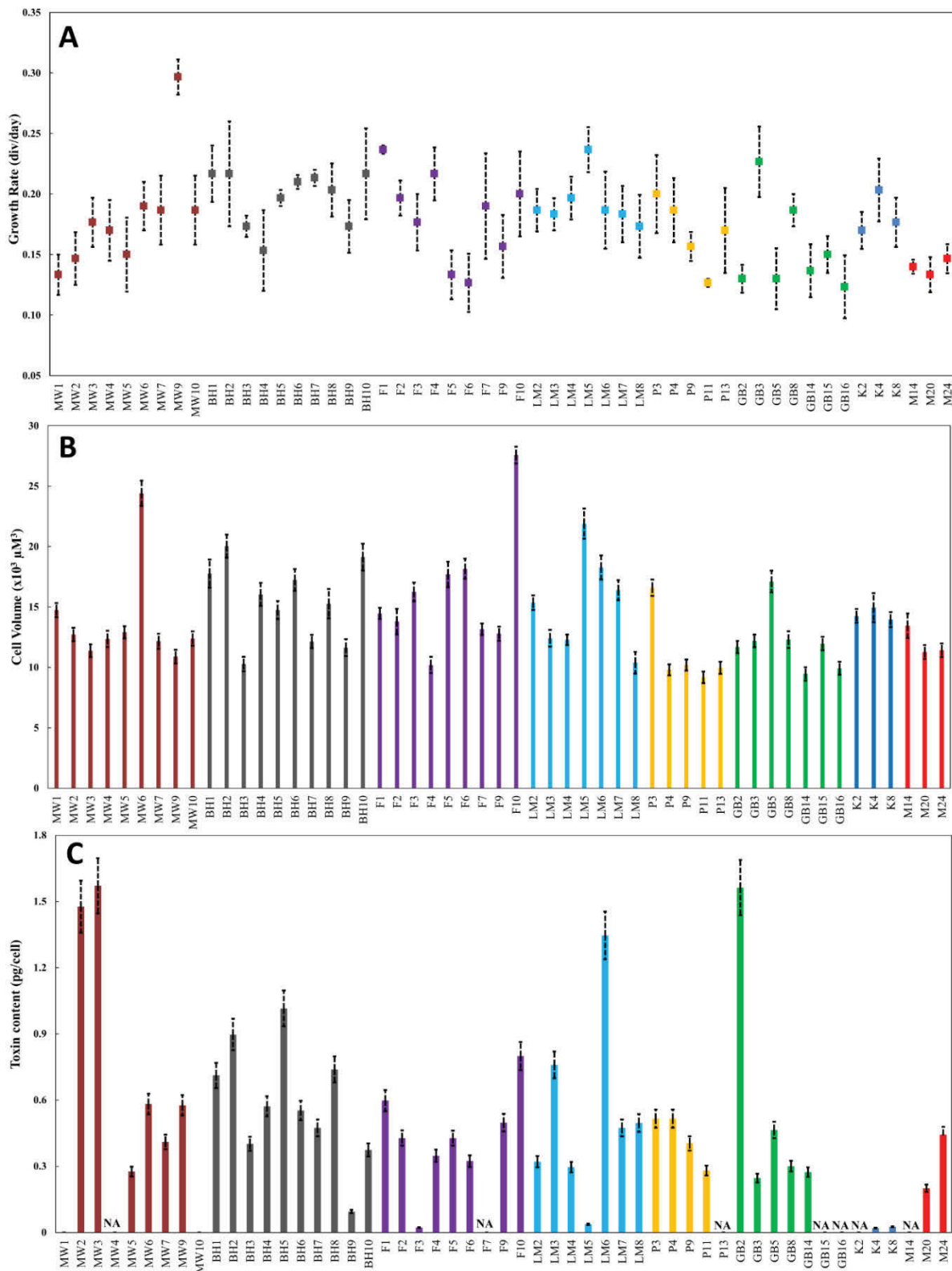
Figure 4.4 Phenotypic variation of 53 *Ostreopsis* cf. *siamensis* strains (represented on the x axes). Colour codes represent origin of strain as represented in Figure 4.1. A: Mean growth rates. Error bars represent standard error of three replicate measurements. B: Cell volume. Error bars represent standard error of twenty measurements. C: Cellular toxin content. Error bars represent 8-10% relative standard deviation of repeatability for LC-MS measurements. NA represents toxin amount below the limit of detection.
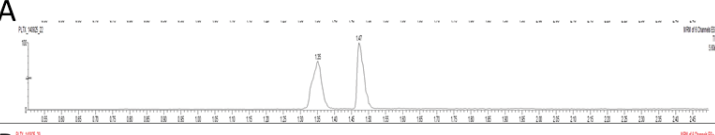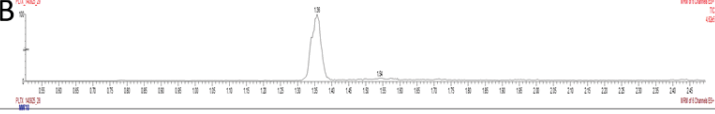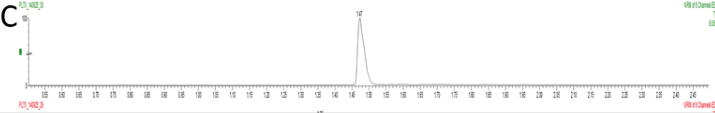
Toxin profiles	Strains
A	MW2, MW3, BH3, BH4, FR1, FR2, FR4, FR9, FR10, LM2, LM3, LM4, LM6, LM7, LM8, PC3, GB2, MER24
B	MW5, MW6, MW7, MW9, BH1, BH2, BH5, BH6, BH7, BH8, BH9, BH10, FR3, FR5, FR6. LM5, PC4, PC9, PC11, GB3, GB5, GB8, GB14, KM6, KM8, MER20
C	MW1, MW10
D NA	MW4, FR7, PC13, GB15, GB16, KM2, MER14

Figure 4.5 Toxin profile variation amongst *Ostreopsis* cf. *siamensis* strains in this study. A: Both amino and amide aldehyde fragments observed; B: only amino aldehyde fragment observed; C: Only amide aldehyde fragment observed; and D: No fragments observed (Below the limit of detection).

4.4.3.3 Photobiological parameters

After being kept in the same light conditions for over a year, *Ostreopsis* cf. *siamensis* isolates exhibited considerable variability amongst photophysiological parameters which govern dark acclimated and irradiance responses. F_v/F_m (dimensionless) varied from 0.42-0.59 (average: 0.5). This is within the range expected from dinoflagellate cultures under steady state growth (Suggett et al., 2015). σ typically varied from 3.08-3.97 nm^2 (average: 3.5 nm^2), however it did not display any immediate correlated trend with F_v/F_m. Chlorophyll concentrations varied from 30-100 pg $cell^{-1}$ amongst *Ostreopsis* isolates (average: 60 pg $cell^{-1}$) which are similar to chlorophyll concentrations reported from other *Ostreopsis* strains (Pezzolesi et al., 2014). The PSU size amongst the *Ostreopsis* isolates varied from 500-1800 mol chl (mol $RCII)^{-1}$ with no strong correlation amongst the isolates based on their geographic origin (Figure 4.6D and supplementary data 8C).

To avoid any errors caused by clumping of cells when exposed to high light (E_{LED}), maximum photosynthetic rate (ETR_{max}) and the light utilisation efficiency (α) were normalised to cellular concentration. ETR_{max} ranged from 0.8-11 μmol e^- $cell^{-1}$ with high variability amongst isolates from MW, BH and FR (Figure 4.6A). A similar trend in variability was observed with α, with values ranging from 4×10^{-3}- 5.5×10^{-2} μmol $cell^{-1}$,

and high variability amongst the isolates from the northern locations (Figure 4.6B). The derived light saturation parameter (E_k) varied from 90-240 µmol photons m^{-2} s^{-1} amongst isolates, even after being grown under 60-80 µmol photons m^{-2} s^{-1} for one year suggesting that the cultures were maintained at sub-optimal light, but the isolates retained their ancestral photosynthetic properties (Figure 4.6C). Significant variation in E_k were observed amongst isolates from the same geographic origin suggesting various light utilization and harvesting strategies being implemented by clones within the same latitudinal populations (sees supplementary data S8D and S9).
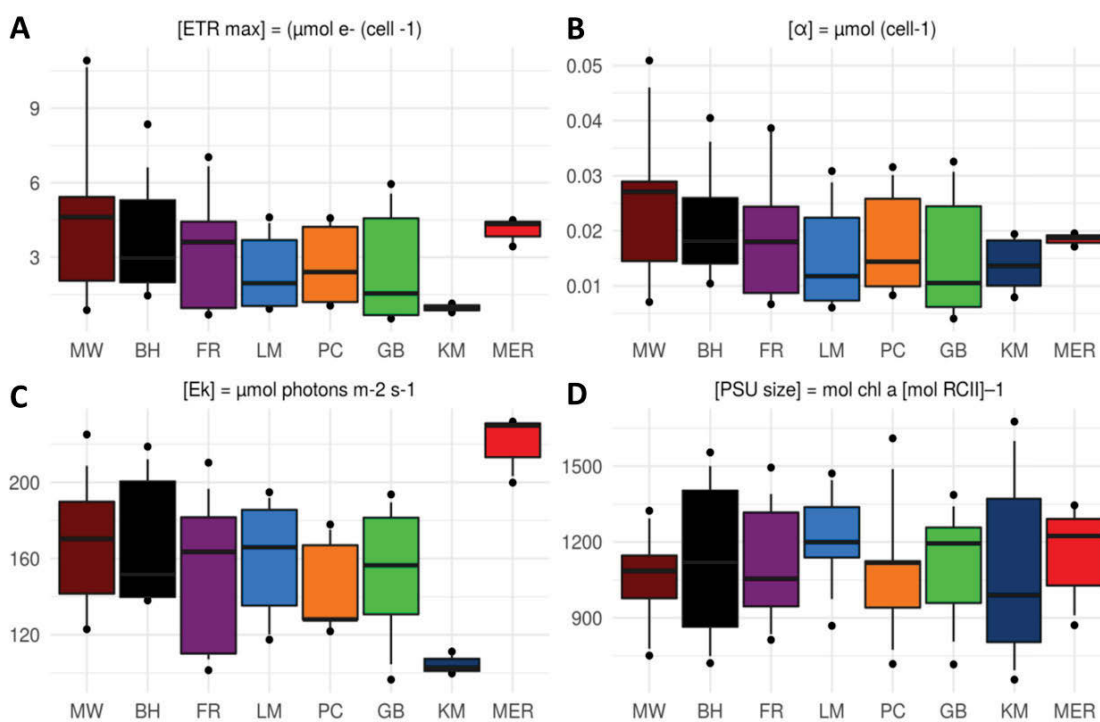
Figure 4.6 Whisker plots of A: maximum photosynthetic rate (ETR$_{max}$); B: light utilisation efficiency (α); C: light saturation parameter (E_k); and D: PSU size amongst *Ostreopsis* cf. *siamensis* isolates based upon sampling sites. Whiskers above and below the boxes indicate the 90/10 percentiles, dots the respective 95/5 percentiles.

The multi-dimensional scaling test based on photoacclimation (F$_v$F$_m$, σ, RCII cell^{-1}), light utilization (photochemical (1-C) and non-photochemical quenching (1-Q) is presented in supplementary data S10. Light utilization parameters were selected at 400 PAR representing a saturating level for all strains, and generally the highest signal-to-noise ratio across the samples. The graph shows relationship between similarities in the item–item matrix and the location of each strain in low-dimensional space. The variability amongst functional groups is seen to be driven by RCII concentration and σ light

harvesting parameters. This highlights that *O*. cf. *siamensis* can employ several distinct adaptive strategies to optimise their photosynthetic capacity relative to metabolic demand and microenvironments. This includes a) modifying the size of the PSII antenna complex serving the core reaction centre (σ-type strategy) and/or b) increasing the number of PSII units (n-strategy) (Hennige et al., 2009).
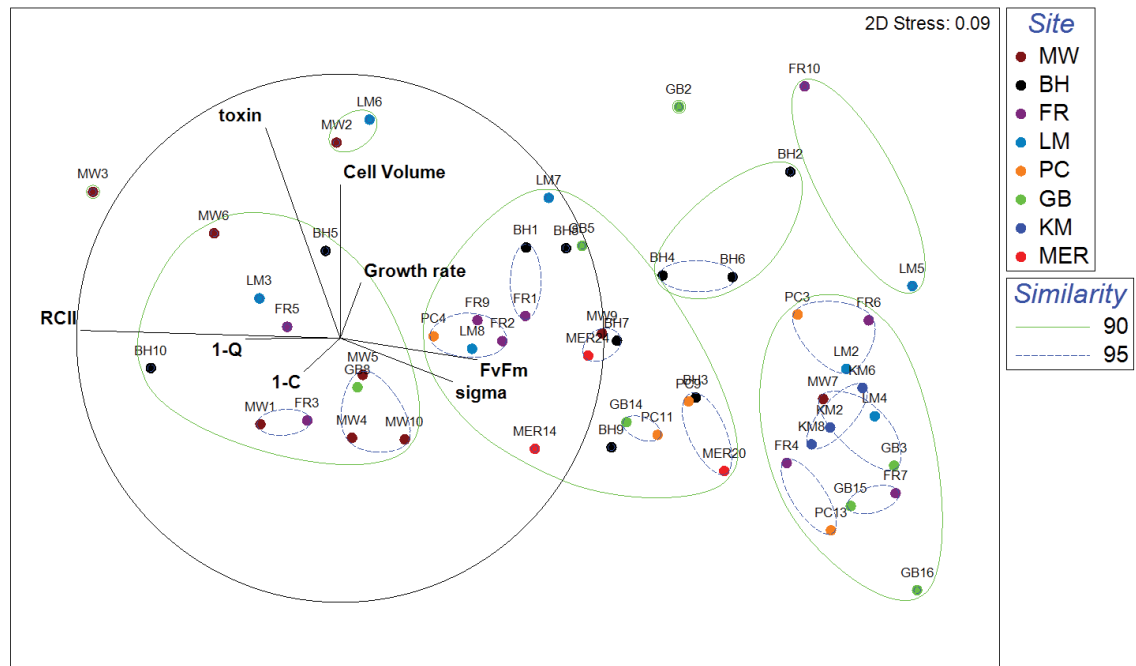
Figure 4.7 Functional groupings based on phenotypic variability in *Ostreopsis* cf. *siamensis* clones. Light harvesting (*Fv/Fm*, σ, Cellular RCII concentration ([RCII])) and light utilization ([1-C] and [1-Q]) along with cell volume, toxin amounts and growth rates were measured across all strains. Cluster analysis and multi-dimensional scaling (MDS) were performed on the average of each variable per strain; similarity is shown at 90 and 95% level and vectors driving the clustering are shown in black.

The multidimensional scaling plot of 53 *O*. cf. *siamensis* strains based on light harvesting and utilization parameters, growth rates, cell volume and toxin amounts in represented in Figure 4.7. The ordination plot with respect to two principal component axes (PC I and PC II) based on PCA analysis of eight aforementioned eco-physiological traits is shown in supplementary data S11A. PC I and II account for 76% and 12% of the total variation, respectively (see supplementary data 11B and C). Phenotypic differences based on location were not evident because of the high overlap between the strains similar to the pattern observed in Figure 4.7. Axis 1 has strong positive loadings for RCII and strong negative loading for σ. This highlights the varying light harvesting adaptive strategies in the strains. Axis 2 has strong positive loadings for cell volume and PLTX-like compounds

produced by the strains with negative loadings for phytophysiological variables. This is reflective of a potential trade-off of photobiological fitness to invest in producing the energetically costly PLTX-like toxin compounds.

4.5 Discussion

4.5.1 Population divergence

In our study, phylogenetic analysis on the concatenated sequences of three nuclear molecular markers, ITS-5.8S and two regions from the large ribosomal subunit (LSU), i.e. D1-D3 and D8-D10, displayed the presence of numerous polymorphic loci amongst *O*. cf. *siamensis* isolates, thereby separating the populations into two sub-clades (Figure 4.2 and table 4.5). Isolates from Minnie Water, Bonny Hills and Wallis Lake exhibited a large number of polymorphic sites in their sequences compared to isolates collected from other locations along the coastline (Tables 4.3, 4.4 and 4.5).

On large oceanic scales, genetic differentiation has been linked to distance or historical legacies, leading to spatial genetic structure as reported in the case of the *Pseudo nitzschia punges* and genus *Oxyrrhis* (Casteleyn et al., 2010; Lowe et al., 2012). Such models have also been used to highlight differentiation on smaller scales as reported by Nagai et al. (2007) for *Alexandrium tamarense* along the Japanese coastline. However, at a finer regional scale, complex oceanographic circulation can lead to patterns that are not well explained by distance as observed with *P. pungens* in the North Sea, where an unstructured population was reported over a distance of a few hundred kilometres (Casteleyn et al., 2010; Evans et al., 2005; Godhe et al., 2013). Recent studies have linked local hydrological connectivity to populations structures at fine geographic scales as shown for *Skeletenoma marinoi* and *Alexandrium ostenfeldii* in the North Sea-Baltic Sea region, highlighting a clear salinity gradient impeding the gene flow and causing local adaptation (Godhe et al., 2013; Sjöqvist et al., 2015; Tahvanainen et al., 2012).

The ribosomal genealogy shows that *O*. cf. *siamensis* populations consist of a tight assemblage of haplotypes that are separated by a small number of mutations. The centre of the network is haplotype 1 that is abundant and geographically widespread giving rise to a large number of related and rare haplotypes especially in the northern sub-tropical locations of the EAC coastal regions (Figure 4.3). The observed differentiation suggests long-standing divergence in the Minnie Water and Bonny Hills populations, with signals of local radiations of haplotypes that could have originated from the ancestral population. However, such a pattern is not clear in other populations further south. One possible explanation for this pattern of diversity is that the southerly populations may have colonised their habitats more recently in geological time. A further possibility requiring investigation is that this colonisation has occurred due to the southward extension and intensification of the EAC. This southward EAC extension has been responsible for the range expansions in species of invertebrates, zooplankton, coastal estuarine fish and other harmful algal species along the south-east coastline of Australia (Johnson et al., 2011; Last et al., 2011; Ling et al., 2009; McLeod et al., 2012).

Concatenated alignments of several genes aid in resolving the phylogeny in cases where single gene phylogenies provide insufficient resolution to distinguish sub-clades. The greater number of nucleotide sites that can be reliably aligned in the analyses can lead to a more strongly supported topology (Murray et al., 2005; Orr et al., 2012). In our study, we notice a larger number of polymorphic sites in the LSU D1-D3 region compared to ITS-5.8S and D8-D10 rDNA LSU region (Table 4.3, 4.4). LSU rRNA gene sequences have been demonstrated to contain phylogenetic information that have been used for phylogeographic surveys for several microbial eukaryotic genera such as *Pseudo-nitzschia*, *Alexandrium*, *Dinophysis* and *Skeletonema* (Auwera and Wachter, 1998; Godhe et al., 2006). Sato et al. (2011) reported the use of D1-D3 rDNA markers for phylogeographic surveys for its high mutation rates in *Ostreopsis* leading to the identification of various *Ostreopsis* ribotypes along the Japanese coast. Penna et al. (2010) used ITS and LSU rDNA regions to separate the population of *O*. cf. *ovata* between the Mediterranean and the Atlantic. The small ribosomal subunit (SSU) marker has been used extensively for biodiversity studies but has shown to lack sufficient

polymorphic resolution and population level variability for intraspecific division (Aurahs et al., 2009; Rynearson and Armbrust, 2004).

4.5.2 Phenotypic variability

The nature and extent of intra- and inter- population clonal variations are important concepts for population dynamics of marine microbial eukaryotes (Alpermann et al., 2010; Kremp et al., 2012; Tillmann et al., 2009). In our study, we have reported a multitude of co-existing phenotypic characteristics in a subset of *Ostreopsis* isolates from each geographic population along the EAC, suggestive of a broad capacity to acclimate to a wide range of environmental conditions in highly variable habitats. Variability amongst phenotypic traits was independent of the clustering of strains into two distinct sub-clades but appears to be greater in northern geographic populations, similar to the trend observed with our genetic data, suggestive of a more diverse and adaptive population in the sub-tropical regions of the EAC.

4.5.2.1 Growth rates and cell volume

Growth rates are a significant variable in population ecology, as it integrates various biochemical processes to yield a single 'output' and reflects the ability of individuals to adapt to the changing environments (Alpermann et al., 2010; Tillmann et al., 2009). However, it depends on a wide range of interplays between intrinsic (genetic/epigenetic) and environmental factors. All clonal isolates used in our study were acclimated under identical growth conditions in a constant environment for more than a year prior to experimentation, yet the growth rates varied from 0.12-0.27 day $^{-1}$. Such variation is quite large compared to previous inter-strain and/or inter-cladal dinoflagellate studies (Figure 4.4A) (Kremp et al., 2012; Kremp et al., 2016; Suggett et al., 2015; Tillmann et al., 2009).

Cell size is often considered a 'master trait' to predict light harvesting and utilization as well as nutrient acquisition in microalgae (Harvey et al., 2015; Suggett et al., 2015; Wu et al., 2014). Variability in growth rates due to cell volume are known to be driven by metabolic processes of gain (eg. nutrient uptake and assimilation, carbon fixation) and

114

loss (eg. respiration) (Litchman and Klausmeier, 2008; Litchman et al., 2007). Cell volumes reported in our study varied from 9,200-27,500 μm^3 (Figure 4.4B). Significant variations in cell volumes between large and small-sized isolates were reported from each sampling site, with the exception of the southern locations. Previous studies have also reported variability in cell volumes amongst *Ostreopsis* cf. *ovata* strains but not to such an extent (Guerrini et al., 2010; Pezzolesi et al., 2014).

Size-scaling relationships from other microbial eukaryotic studies have suggested that small cells are unlikely to prevail in blooming conditions because of constraints on nutrient uptake and reduced biosynthetic abilities, whereas large cells are limited by the conversion of nutrients into biomass due to size-related constraints levied on intracellular resource transportation (Ward et al., 2017). The resulting trade-off between these opposing size-driven limiting processes is likely to explain the varying sizes amongst *Ostreopsis* clones from different locations (Marañón, 2015). Such range of growth rates and cell volumes reflects the adaptation of populations, especially in the northern sampling sites, to frequently changing environmental variables leading to such balancing selection of phenotypic diversity suggestive of a more persistent dominance and niche colonisation (Alpermann et al., 2010; Tillmann et al., 2009). The traditional model of estimating growth rates in phytoplankton suggests that the growth rate decreases with increase in cell size (Eppley and Sloan, 1966). However, in our study no clear correlation of physiological parameters could be established with cell volume. For the clonal populations under study, the stages of population development and cell cycle are not known, but future studies on these phenotypic traits can benefit from incorporating such information in the experimental design.

4.5.2.2 Toxin content and composition

In this study, fifty-three isolates of the same HAB species, collected within a 1500 km distance, showed a very wide variation in toxin production. While many isolates produced PLTX analogues at concentrations similar to that reported previously for *Ostreopsis* species, some strains were apparently non-toxic, and others produced a potentially unique toxin analogue, with more variability amongst isolates from the northern sampling sites

(Figures 4.4C and 4.5) (Rhodes et al., 2017; Verma et al., 2016a; Verma et al., 2016b). Such high variability amongst isolates from the same location, as well as from different locations, has rarely been observed before in a HAB species (Bachvaroff et al., 2009; Kremp et al., 2016; Tillmann et al., 2009). In general, it was considered that within most toxin-producing HAB species, the vast majority of strains produce a given toxin, with rare exceptions. Variation in cellular toxin content and composition within local populations has been reported with paralytic shellfish toxins (PSTs) in *Alexandrium* spp., PLTX and its analogues in *Ostreopsis* cf. *ovata* and karlotoxins (KmTxs) in *Karlodinium veneficum* (Alpermann et al., 2010; Bachvaroff et al., 2009; Kremp et al., 2016; Tillmann et al., 2009; Uchida et al., 2013). However, in most cases, only a few strains were examined, or strains were isolated from widely different geographic regions.

John et al. (2015) has suggested that diversity in the production of secondary metabolites within a population of a HAB species might allow for intraspecific facilitation, particularly as a defence mechanism against grazers (John et al., 2015). Recent studies have reported *Ostreopsis* species as easily edible prey by heterotrophic dinoflagellates and grazers owing to their slow swimming speed (Du Yoo et al., 2015). Also, induction of harmful effects on the behaviour and survival of grazers when exposed to *Ostreopsis* species has been demonstrated (Neves et al., 2017). This suggests that PLTX-like compounds could potentially be produced as a grazer defence trait, as a trade-off for low motility of this species and/or also at the expense of photobiological fitness as the cost of producing such energetically costly molecules (Figure 4.7 and supplementary data S11).

Such traits can be induced, but the changes may be too slow to provide protection from immediate predation pressure. Rapid selection of highly toxic strains from a pool of individuals with varying defence capabilities might be a more effective mechanism for populations to cope with different grazing regimes (Driscoll et al., 2016; Selander et al., 2006). Within structurally diverse populations of closely related individuals, cooperative traits can be favoured as being for the 'public good' and enable the success of the entire population (Hamilton, 1964). This principle of facilitation has been shown in populations of various organisms such as antibiotic-resistant bacterial strains and toxigenic cyanobacterial species (John et al., 2015; Lee et al., 2010; Van Gremberghe et al., 2009).

Fitness of highly toxic individuals will be higher during periods of high grazing pressure, whereas low- or non-toxic clonal lineages might benefit during periods when grazing is low (John et al., 2015; Kremp et al., 2016).

4.5.2.3 Photophysiological strategies

In this study, we have used FRRf to demonstrate the interplay of various factors that govern electron transport rate in microalgae and highlight several photo-acclimation strategies (Falkowski and Raven, 2013; Hennige et al., 2009; Oxborough et al., 2012; Suggett et al., 2015; Suggett et al., 2009). We demonstrate the evidence for both σ and n-type photoacclimatory strategies amongst *O.* cf. *siamensis* isolates from same as well as different locations suggestive of a localised, short term 'niche' driven adaptability of photobiological functional traits (see supplementary data S10 and S11). More functional 'eco-types' were observed from northern locations compared to the southern sampling sites (Figure 4.7 and supplementary data S10).

Predominance of n-type strategy has been suggested to be a 'generalist' strategy for microalgae which are subject to varying light intensities, where modifying reaction centre concentrations (RCII) over antennae size (σ) is beneficial under conditions that are likely to cause photoinhibition, such as high irradiance (Hennige et al., 2009). Under more stable light regimes, σ strategy maybe incorporated to reduce the energetic cost. The ability to employ either n-type or σ strategy can be dictated by nutrients, where low nitrogen availability is more conducive to σ type strategy as it is less energetically costly (Six et al., 2008). In coastal environments where the nutrient concentrations are relatively higher to open ocean, *O.* cf. *siamensis* can afford to use a higher cost n-type acclimation of photosystem contents to exploit a wider range of light.

We also see the ability to upregulate NPQ rapidly (within the timeframe of a RLC) in a select few strains (see supplementary data S10). This suggests that some strains may be able to better cope with rapid fluctuations of light on short-time scales, such as the passage of clouds, coastal turbulence or even wave-flickers and wave-lensing. NPQ in microalgae

has been linked to production of photoprotective pigments to regulate excess light. It has been previously determined that photoprotective compounds (e.g., carotenoids) increase during exposure to high PAR and ultraviolet radiation (Patil et al., 2017). *Ostreopsis* species are known produce extracellular polysaccharide secretions that have been linked with their bloom formation capabilities and providing mechanical resistance to dynamic wave motion (Honsell et al., 2013; Sechet et al., 2012). Such secretions might be driven by the upregulation of NPQ in certain individuals within a population which might lead to the production of mucilage blooms.

Such eco-physiological strategies might highlight an advantage for *Ostreopsis* in the colonization of different surfaces and could also explain its rapid proliferation under varying environmental conditions. The presence of different light harvesting strategies highlight a greater potential for *O*. cf. *siamensis* to cope with highly dynamic light regimes and thereby colonise new areas successfully which might aid in its range expansion towards the southern regions of the EAC.

4.6 Conclusion and significance

The study revealed high genetic and phenotypically variability within *O*. cf. *siamensis* populations over a 1500 km north-south gradient along the EAC. The northern-most sites showed the highest genotypic diversity, as well as the greatest phenotypic diversity in growth rates, toxin production and profiles, cell volume and photophysiological responses. The latitudinal gradient in variability supports the hypothesis that genetic diversity is linked to increased diversity in phenotypic responses in marine microbial eukaryotic populations. As phenotypic diversity is crucial in buffering population responses to environmental variation, understanding its role along a marine temperature gradient will enable improved predictions of species responses to the warming EAC.

Our results demonstrate the importance of investigating multiple isolates of a species to characterize the range of a particular phenotypic trait, given the very high variability that may be encompassed within population standing stocks. Finally, these results highlight

the importance of integrating genetic, physiological and ecological data for investigating the phylogeographic structure in coastal oceanographic studies of phytoplankton in response to changing oceanic climate conditions.

4.7 Author contributions

AV, SM designed research; AV isolated strains; performed research, analysed and interpreted data. AV, DH conducted photophysiological measurements and statistical analysis; TH carried out LC-MS/MS at Cawthron institute; DS and PR contributed to physiological data interpretation; AV, SM wrote the paper with editorial input from all co-authors.

Chapter 5: Transcriptomic and metabolomic insights into polyketide toxin production in species of *Ostreopsis* (Dinophyceae)

5.1 Abstract

Dinoflagellates play vital ecological roles in marine and freshwater ecosystems and are known for their ability to produce complex secondary metabolites that have toxic impacts on co-occurring phytoplankton, fisheries and humans. Species of the genus *Ostreopsis* are associated with the production of highly toxic polyketide palytoxin molecules (PLTX, $C_{129}H_{223}N_3O_{54}$) and its analogues that are associated with benthic blooms, human skin and eye irritations, and poisonings through the consumption of contaminated fish and shellfish. In this study, we described, assembled and functionally annotated the *de novo* transcriptomes of three *Ostreopsis* species; *O*. cf. *ovata*, *O*. cf. *siamensis* and *O. rhodesae* and compared them to a close phylogenetic relative and non-PLTX producer, *Coolia malayensis*. Additionally, a non-targeted metabolomic screening was performed using ultra performance liquid chromatography to investigate the key metabolites produced by these species. We report for the first time, type I single-domain and multi-domain polyketide synthases (PKS) along with hybrid non-ribosomal peptide synthase (NRPS)/PKS hybrids from *Ostreopsis* and *Coolia* species, including a potentially novel dinoflagellate specific NRPS/PKS hybrid clade. The genetic differentiation of PKS and fatty acid synthase pathways in *Ostreopsis* species was also reported to facilitate approaches of investigating toxin biosynthesis pathways in dinoflagellates. We report the putative identification of numerous compounds from these species, suggesting a vast diversity of previously undescribed molecules that may be of ecological and medical significance.

5.2 Introduction

Dinoflagellates (Alveolates) play vital ecological roles in marine and freshwater ecosystems despite being comparatively poor competitors in such environments (John et al., 2015; Murray et al., 2016). One potential reason for their ecological success is their ability to produce complex secondary metabolites that impact their interactions with potential predators and co-occurring phytoplankton (allelopathy) (Anderson et al., 2012; Hallegraeff, 1993; John et al., 2015; Kohli et al., 2016). Majority of these compounds display potent biological activities as well as enable specialist functions for the producing organisms such as immobilising potential prey (mixotrophy), osmoregulation and grazing deterrence and can also cause serious threats to public health and severe economic losses to fisheries and other coastal resources (Murray et al., 2016; Yasumoto and Murata, 1993). Most known dinoflagellate 'toxins' are broadly classified into three main categories according to their chemical structures; (a) polycyclic polyketides (e.g. brevetoxins, ciguatoxins, maitotoxins, yessotoxins), (b) macrolides (e.g. amphidinolides, pectenotoxins, spirolides), and (c) linear polyketides (e.g. dinophysistoxins, okadaic acid) (Hopwood, 1997; Kalaitzis et al., 2010).

The biosynthesis of these toxic compounds involves enzymes that are classified as polyketide synthases (PKSs) and non-ribosomal peptide synthases (NRPS) (Kellmann et al., 2010; Rein and Borrone, 1999). These enzymes produce linear precursors by successive condensation reactions similar to fatty acid biosynthesis, which extend a growing carbon chain through the addition of coenzyme A thioester derivatives of carboxylic acids for PKSs, or amino acids for NRPSs (Hopwood, 1997; Kellmann et al., 2010; Khosla et al., 1999; Rein and Borrone, 1999; Shimizu, 2003). PKSs can be classified into three groups according to structural and functional elements (domain organisation). Type I PKS enzymes are large multifunctional proteins comprising either one large protein used in a cyclic fashion for chain elongation (iterative), or organized into modules where each component is only used once during assembly (modular). Type II PKS comprise different domains that are organized as individual proteins, forming complexes for polyketide synthesis. Type III PKSs, typically associated with chalcone (CHS) and stillbene (STS) synthases in higher plants, are similar to Type II but smaller in size (Hopwood, 1997; Khosla et al., 1999).

The minimal catalytic domains required for PKS biosynthesis include a β-ketosynthase domain (KS), an acyltransferase (AT) and an acyl carrier protein (ACP). Ketoreductase (KR), dehydratase (DH) and enoylreductase (ER) domains are used for modifications along the elongating chain, and finally, a thioesterase domain (TE) releases the full-length molecule from the PKS complex (Hopwood, 1997; Khosla et al., 1999; Pawlowiez et al., 2014). Similarly, a minimal NRPS provides an adenylation domain (A), which specifically activates an amino acid, a peptidyl carrier protein (PCP) and a condensation domain (C) that creates a peptide bond between two PCP-bound amino acids (Kellmann et al., 2010).

In the last decade, numerous Type I modular PKS genes have been identified through *de novo* transcriptomic analyses of harmful algal bloom (HAB)-forming dinoflagellate species such as *Karenia* spp., *Heterocapsa* spp., *Amphidinium* spp., *Gambierdiscus* spp., *Alexandrium* spp., *Karlodinium veneficum*, *Lingulodinium polyedrum* and *Azadinium spinosum* (Bachvaroff and Place, 2008; Beauchemin et al., 2012; Eichholz et al., 2012; Kimura et al., 2015; Kohli et al., 2017; Kohli et al., 2015; López-Legentil et al., 2010; Meyer et al., 2015; Monroe and Van Dolah, 2008; Moustafa et al., 2010; Murray et al., 2012a; Pawlowiez et al., 2014; Ryan et al., 2014; Salcedo et al., 2012). Sequencing of mature mRNA transcripts containing the spliced leader (SL) sequence and poly A tails, coupled with phylogenetic analyses has enabled the discrimination of dinoflagellate sequences from contaminating bacterial sequences which are present in non-axenic cultures (Lidie and Van Dolah, 2007; Monroe and Van Dolah, 2008; Zhang et al., 2007). Interestingly, in most studies, each full-length PKS transcript only encoded one catalytic domain, in line with the observation of monocistronic transcription (Murray et al., 2012b; Murray et al., 2016). However, their homology to type I PKSs was intriguing, as the mono-functional organisation of catalytic domains is a typical type II PKS feature. These findings suggest the presence of a novel structure of PKSs in dinoflagellates, involving unique mono-functional type I PKS units (Eichholz et al., 2012).

Species of the genus *Ostreopsis* are associated with the production of the highly toxic polycyclic polyketide compounds, palytoxin (PLTX, $C_{129}H_{223}N_3O_{54}$) and its analogues (including Ostreocin-D, ovatoxins a-k and isobaric palytoxin) (Ciminiello et al., 2012a;

Ciminiello et al., 2012b; Dell'Aversano et al., 2014; Tartaglione et al., 2016; Van Dolah et al., 2013). PLTX and/or its analogues have been associated with human poisonings through the consumption of contaminated fish and shellfish and have been linked to incidents of clupeotoxism (Amzil et al., 2012; Rhodes et al., 2002; Tubaro et al., 2011). *O*. cf. *ovata* blooms have been associated with human skin and eye irritations and respiratory illnesses, due to exposure to toxic aerosols (Ciminiello et al., 2014). *Ostreopsis* blooms adversely impact other benthic organisms by colonizing benthic substrates with mucous mats and potentially producing alleopathic compounds (Accoroni et al., 2016; Monti and Cecchin, 2012). Blooms of *O. siamensis* in northern New Zealand have been linked to large scale mortalities in sea urchin populations whereas, *O*. cf. *ovata* blooms along the Northern Adriatic coast have also been associated to increased seasonal mortalities of sea urchins as well as shellfish species (Accoroni et al., 2011; Shears and Ross, 2009).

To investigate the putative genes underlying the biosynthesis of PLTX-like compounds and other potential complex polyketides produced by *Ostreopsis* species, we describe, assemble and functionally annotate the *de novo* transcriptomes of three *Ostreopsis* species from the East Australian current (EAC) region; *O*. cf. *ovata*, *O*. cf. *siamensis* and *O. rhodesae* in this study. A close phylogenetic relative to *Ostreopsis* and non-PLTX producer, *Coolia malayensis* was used as a comparison for this investigation. Furthermore, we performed a 'non-targeted' high-throughput screening of key metabolites produced by these species using ultra performance liquid chromatography (UPLC). By putatively identifying KS domains involved in polyketide biosynthesis, we aim to elucidate the unique biology of toxic *Ostreopsis* species and provide the first comparative transcriptomic and metabolomic analyses of *Ostreopsis* and *Coolia* species.

5.3 Materials and methods

5.3.1 Cultures

Clonal cultures of *Ostreopsis* cf. *ovata* HER27, *O. rhodesae* HER26, *O*. cf. *siamensis* BH1 and *Coolia malayensis* MAB were established as described in chapters 3 and 4 (section 3.3.1 and 4.3.1). *Ostreopsis* cf. *ovata* HER27 and *O. rhodesae* HER26 were

isolated from Heron Island, Great Barrier Reef (Verma et al., 2016a). *O.* cf. *siamensis* BH1 was isolated from Bonny Hills, New South Wales and *C. malayensis* MAB was isolated from Malabar beach, Sydney, New South Wales. Cultures were maintained either at 25 ± 1°C (*O.* cf. *ovata* and *O. rhodesae*) or 18 ± 1°C (*O.* cf. *siamensis* and *C. malayensis*), representative of the sea surface temperature at the time of sample collection, in 5x diluted f/2 media under cool white fluorescent light at an intensity of 60-80 μmol photons m^{-2} s^{-1} and a 12:12 hrs light: dark cycle (Verma et al., 2016b).

5.3.2 PLTX analysis via LC-MS/MS

PLTX-like compounds were screened from cell pellets using the methodology described in Selwood et al. (2012). Please refer to section 4.3.6 for more details.

5.3.3 RNA isolation and sequencing

Triplicate 1 L cultures of each species were sampled at mid-late exponential growth phase (days 11-12) for RNA extractions simultaneously. Cell pellets were obtained via filtration through 5 μm filters (Millipore) and washed with 1x PBS to remove bacterial contaminants. RNA extraction was performed using 60˚C hot Trireagent (Ambion) according to the protocol described in Meyer et al. (2015) and purified using RNeasy Mini Kit (Qiagen). Any residual DNA was removed via the TURBO DNA-free™ Kit (Life Technologies) and RNA was stored at -80°C until further analyses. The RNA purity, quantity and integrity were assessed using a Nanodrop ND-1000 (Thermo Scientific, Woltham, MA) and 2100 Bioanalyser (Agilent Technologies, Santa Clara, CA). The libraries were prepared using TruSeq RNA Sample prep kit v2 following the manufacturer's instructions and sequencing was performed using NextSeq500 (Illumina, San Diego, CA) generating 75 base pair (bp) paired end reads. For sequencing, all 4 libraries were multiplexed in one lane along with two other samples.

5.3.4 Transcriptome Assemblies and Annotation

Raw reads were quality filtered and assembled into contigs using CLC Genomics Workbench Version 7.0 (CLC bio, Cambridge, MA) using default software settings.

During the assembly, scaffolding was performed and the assembly was also validated using read mapping. Any contigs less than 300 bp of length and/or containing gaps of more than 100 bp were discarded from the analyses.BLASTx analyses were performed at an e-value cut-off of 10^{-3} against the non-redundant (nr) database of GenBank. BLAST2GO v3.1.3 and Kyoto Encyclopedia of Gene and Genomes (KEGG) analyses were performed for mapping and annotation using default program settings. InterProScan analysis was carried out in BLAST2GO using; BlasProDom, FPrintScan, HMM-PIR, HMM-Pfam, HMM-Smart, HMM-Tigr, Profile-Scan, HAMAP, Pattern-Scan, Super-Family, Signal-PHMM, TM-HMM, HMM-Panther, Gene3D, Phobius and Coils, to further improve our annotation of the dinoflagellate transcriptomes (Conesa et al., 2005). For analyzing the completeness of the transcriptomes, the Core Eukaryotic Genes Mapping approach (CEGMA) tool was used as implemented in CYVERSE Discovery Environment using default settings (Parra et al., 2007).

NRPS/PKS and FAS genes were identified with HMMER through in-house HMM databases containing sequences identified from previous dinoflagellate transcriptomic reports for each enzyme investigated in this study (Finn et al., 2011). Pfam (Finn et al., 2013) and conserved domain database (CDD) (Marchler-Bauer et al., 2016) were used for identification of conserved amino acid residues and functional prediction of NRPS/PKS and FAS genes. Transit peptides targeted towards the chloroplast were detected using ChloroP (Emanuelsson et al., 1999).

MAFFT v7.017 (Katoh et al., 2002) was used for sequence alignment within Geneious v 7.1.7 (Kearse et al., 2012) using default settings. Alignments were manually inspected and trimmed to ensure similar length of the coding regions. Phylogenetic analysis was carried out in RAxML v7.0 using GAMMA and LG models with 1,000 bootstraps (Stamatakis, 2006).

5.3.5 Non-targeted metabolomics using UPLC

A non-targeted metabolic approach to screen putative metabolites from the four dinoflagellate species was performed along with the RNA extractions. All triplicate 1 L algal cultures were harvested by filtration and freeze dried. The pellets were extracted twice with 5 mL methanol–water (1:1 v/v), centrifuged at 3000 g for 5 min and finally extracted in 100% methanol. All supernatants were pooled and stored at -80°C until further analyses. One µL of metabolite extract was injected on an Agilent Zorbax Eclipse XDB-C18 (50 mm X 2.1 mm ID, 1.8 µm particle size) column coupled to a Thermo Scientific Q Exactive Plus Hybrid Quadrupole- Orbitrap Mass Spectrometer. A gradient from solvent A (Water, 30 mM acetic acid) to solvent B (95 % acetonitrile, 30 mM acetic acid) was used to achieve separation. The elution gradients were 10−50% B over 11 min, 50−80% B over 5 min, 80−100% B in 1 min and held for 3 min and re-equilibrated for 3 mins. Flow rate was set at 400 µL min^{-1} for the duration of the run, the column was held at 50 °C, and samples were held at 5 °C. Column eluate was infused into a Thermo Scientific Q Exactive Plus fitted with an electrospray source. Data was collected in full scan mode from 400 to 2750 m/z at a resolution of 120,000 in positive ion mode.

Raw data from the spectral analyses was processed using Progenesis QI software (Waters Corporation, Newcastle, UK) to screen for differences in the dinoflagellate metabolite profiles. The spectral data were aligned to a quality control sample, adduct ions were deconvoluted and ion abundance above the threshold level performed to obtain an ion-intensity map, including m/z and retention time. These ion maps were then aligned in the retention-time direction. From the aligned runs, an aggregate run representing the compounds in all samples was used for peak picking. An output table with paired m/z retention times and raw and normalized peak intensities for individual samples was generated. The putative identification of the ions was attempted by database searches against their accurate masses using publicly available databases including ChemSpider and Marine Natural Product Database (Lei and Zhou, 2002). These metabolic features were exported to Mass Profiler Professional (MPP) for statistical analysis and data visualisation. Statistical evaluation was performed using univariate and multivariate analyses. p-value computation was done asymptotically with cut-off value of $p<0.05$ being considered statistically significant. The difference in expressed putative metabolites

between *Coolia malayensis* and *Ostreopsis* spp. was investigated with one-way analysis of variance (ANOVA) and using Tukey HSD post-hoc test, which resulted in a matrix table representing differentially expressed entities. Principal component analysis (PCA) was performed to detect similarity between the samples, discriminated by the major trends in the data.

5.4 Results

5.4.1 Targeted screening of PLTX-like compounds

The analyses of the oxidized cellular extracts showed the occurrence of both the amino and amide-aldehyde fragments from *Ostreopsis* cf. *ovata* HER27 yielding 1.8 pg cell^{-1} PLTX-like compounds from the cellular extract (Verma et al., 2016a). No PLTX-like compounds were detected from cellular extracts of *O. rhodesae* HER26 and *Coolia malayensis* MAB. Only the amino-aldehyde fragment was observed in *Ostreopsis* cf. *siamensis* extract suggesting the presence of a structurally related PLTX-like compounds being produced by this strain (Selwood et al., 2012; Verma et al., 2016b). 0.71 pg cell^{-1} PLTX-like compounds were detected from this extract (see Chapter 4 for details).

5.4.2 *De novo* assembly and annotation

A total of 75-87 million reads were extracted from each RNA-Seq library (Table 5.1). After removing redundancies, 67,000-91,000 contigs were assembled of which, 68,759 (Mean length: 1,002 bp; GC content: 63.6%), 67,786 (Mean length: 854 bp; GC content: 63.3%), 71,151 (Mean length: 955 bp; GC content: 63.8%) and 57,063 (Mean length: 1,279 bp; GC content: 59.3%) contigs were greater than 300 bp amongst *O.* cf. *ovata*, *O.* cf. *siamensis, O. rhodesae* and *C. malayensis* libraries respectively (Table 5.1). 81-85% of 458 highly conserved proteins were included in the transcriptomes of these species when analyzed using the core eukaryotic genes mapping approach (CEGMA) (Table 5.1). This is comparable to other dinoflagellate transcriptomes investigated to date (Kohli et al., 2017; Kohli et al., 2015; Meyer et al., 2015; Ryan et al., 2014), indicating a comprehensive coverage of the transcriptome. Transcriptomes of the four dinoflagellate species encoded 67-80% of the essential enzymes, required for C3 carbon cycle, oxidative

phosphorylation, pentose phosphate pathway, glycolysis, tricaroxalic acid cycle, purine and pyrimidine nucleotide synthesis as well as essential amino acid synthesis, which are comparable to other dinoflagellate species (Kohli et al., 2017) (see supplementary data S12A-D).

Using BLASTx analyses (e-value cut-off 10^{-3}), 25-33% of contigs were found to have annotated matches in GenBank *nr* database (Figure 5.1). Forty-fifty percent of the contigs lacked similarity to any sequence in the database (Figure 5.1). This is in line with previous findings in dinoflagellates and might be an indication of novel and complex genomic features in dinoflagellates (Keeling et al., 2014; Kohli et al., 2016). Amongst the annotated matches, the low representation of dinoflagellates in the top-hit species of BLASTx matches likely reflects the limited number of genes deposited in the NCBI *nr* database, despite a growing number of transcriptomic studies conducted on these organisms (Kimura et al., 2015; Pawlowiez et al., 2014).

Of the transcripts with positive BLAST hits and annotations with Gene ontology (GO) terms, a similar distribution of transcripts involved in keystone molecular and metabolic functions were observed for the four species. Protein binding, cytoskeleton proteins, ion channels and ATP binding domains were the most abundant protein domains identified in each of these libraries (see supplementary data S13). These domains play vital roles in maintaining essential functions in the organisms, such as signalling pathways, gene expression, cellular organization, and homeostasis of ions and small molecules. These findings are similar to other published datasets amongst dinoflagellate species (Meyer et al., 2015; Ryan et al., 2014).
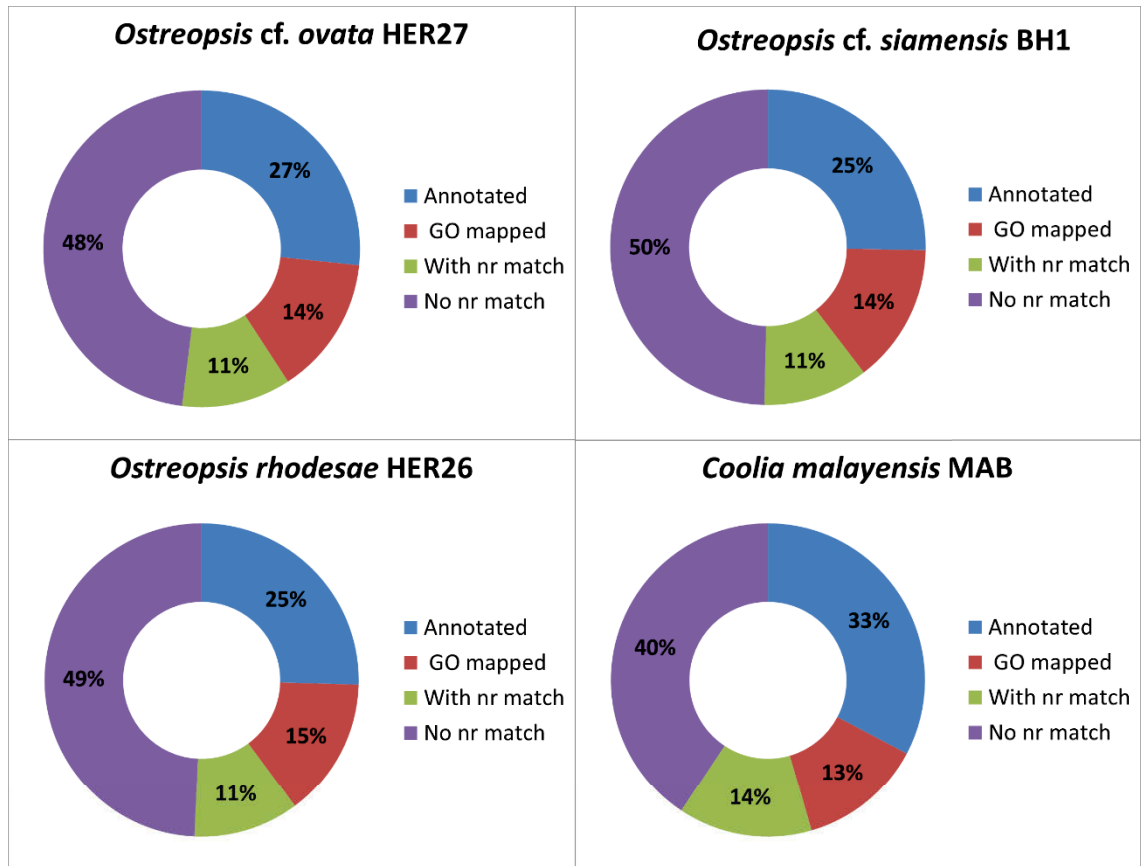
Figure 5.1 BLASTx analysis using BLAST2GO (e-value cut off 10⁻³) for *Ostreopsis* cf. ovata HER27, *Ostreopsis* cf. *siamensis* BH1, *Ostreopsis rhodesae* HER26 and *Coolia malayensis* MAB.

In dinoflagellates, the presence of a dinoflagellate-specific splice leader (SL) sequence at the 5' end provides means to distinguish full-length mature dinoflagellate transcripts from transcripts derived from bacteria (Lidie and Van Dolah, 2007; Zhang et al., 2007). Our gene catalogue consisted of a large collection of full-length transcripts (SL at 5' end and poly A tail at 3' end). The Dino-SL sequence was found at the end of 1,462, 1,410, 1,662 and 1,118 contigs in *O*. cf. *ovata*, *O*. cf. *siamensis*, *O. rhodesae* and *C. malayensis* libraries respectively and both the spliced leader and the poly-A tail were identified in 864, 609, 697, 514 contigs in the aforementioned dinoflagellate EST libraries (Table 5.1).

Table 5.1 Transcriptome assembly statistics including the total number of polyketide synthase associated domains found for the three *Ostreopsis* species and *Coolia malayensis* used in this study.

	Ostreopsis cf. *ovata* HER27	*Ostreopsis* cf. *siamensis* BH1	*Ostreopsis rhodesae* HER26	*Coolia malayensis* MAB
Total reads	87,542,370	75,911,647	87,665,817	85,733,553
Total Contigs (>300 bp) (GC content)	87,382 (68,759) (63.6)	88,929 (67,786) (63.3)	91,824 (71,151) (63.8)	67,053 (57,063) (59.3)
Average length	1002	854	955	1279
SL-polyA	864	609	697	514
SL only	1462	1410	1662	1118
CEGMA analysis	85.5%	82.7%	81%	85.5%
KS domains full/partial (GC content)	77/21 (62.5/67.2)	61/53 (61.8/65.3)	67/25 (62/67.7)	76/17 (58.4/60.3)
KR domains full/partial (GC content)	8/13 (62/64.6)	5/12 (59.9/67.3)	7/10 (61.3/65.5)	6/8 (55.9/61)
Multi domains (GC content)	23 (66.7)	10 (61.4)	27 (65.5)	23 (61.2)
PKS-NRPS hybrids (GC content)	2 (68.4)	3 (58.6)	1 (67.2)	4 (61.4)

5.4.3 Polyketide biosynthesis

The three *Ostreopsis* species and *Coolia malayensis* investigated in this study yielded numerous and diverse types of PKS domains. Five hundred and fifty-eight domains, including full and partial KS, KR and multi domains, were putatively identified from the four transcriptomic libraries (see supplementary data S14, S15, S16). Ninety-eight (77 full, 21 partial), 115 (62 full, 53 partial), 93 (68 full, 25 partial) and 93 (76 full and 17 partial) KS domains were identified from *Ostreopsis* cf. *ovata*, *O.* cf. *siamensis*, *O. rhodesae* and *C. malayensis* respectively (Table 5.1). The centrally conserved ExExGYLG motif at the N-terminal region of single KS domains was found in 15, 13, 13 and 18 transcripts in *Ostreopsis* cf. *ovata*, *O.* cf. *siamensis*, *O. rhodesae* and *C. malayensis*

respectively. Other variants (DYLG, HYLG, YYLG, GLLG, AYLG and ALLG) were also observed in other sequences at the same position showing the diversified nature of the N-terminus of KS domains.

Twenty-one (8 full, 13 partial), 17 (5 full, 12 partial), 17 (7 full, 10 partial) and 14 (6 full, 8 partial) KR domains were identified from *Ostreopsis* cf *ovata*, *O*. cf. *siamensis*, *O. rhodesae* and *C. malayensis*, respectively. In addition to single encoding KS and KR domains, a total of 88 multi-domain PKS sequences were obtained (Tables 5.1, 5.2) of which 25 (including 2 NRPS/PKS hybrids), 12 (including 2 NRPS/PKS hybrids), 27 (including 1 NRPS/PKS hybrids) and 24 (including 4 NRPS/PKS hybrids) were obtained from *Ostreopsis* cf *ovata*, *O*. cf. *siamensis*, *O. rhodesae* and *C. malayensis*, respectively (Tables 5.1, 5.2).

The phylogenetic analyses using maximum likelihood yielded insights into relationships of PKS sequences from the three *Ostreopsis* spp. and *C. malayensis* compared with additional PKS sequences (Figure 5.2). Type II PKS sequences grouped consistently as out-group taxa with 100% bootstrap support (BT). The transcripts in the current study grouped strongly alongside Type I PKS sequences, consisting of apicomplexans, two fungal (reducing and non-reducing KS domains) clades, an animal FAS clade, several prokaryotic type I KS clades along with haptophytes, chlorophytes and other dinoflagellates (Figure 5.2). Within the Type I 'protistan' clade, the dinoflagellate clade encoding single (iterative) KS domains formed three sub-clades (i, ii, and iii), as reported previously (Eichholz et al., 2012; Monroe and Van Dolah, 2008). Clade i and iii consisted of KS domains with all their active site residues intact (Cys-His-His), which are essential for their functionality. KS domains in clade ii did not have one or more active site residues intact (Eichholz et al., 2012).

Contigs comprising multiple (modular) KS domains formed six separate clades (A-F) (Figure 5.2). Clades A, B and C are closely related to the previously described modular type I PKSs found in apicomplexans, chlorophytes and haptophytes. Clades D-F branch separately and comprise previously reported contigs from *Karenia brevis*, *Symbiodinium*

minutum and *Gambierdiscus* spp. along with *Coolia* and *Ostreopsis* spp. Three modular clades comprising NRPS/PKS hybrids were identified, consisting of the bur-A like NRPS/PKSs from bacteria and other recently discovered hybrids from dinoflagellate, along with two novel NRPS/PKS hybrid clades consisting of transcripts reported from this study (Table 5.2). The reported A domain in NRPS proteins are responsible for recruiting amino acids into the final product was determined in all four species.

The maximum likelihood phylogeny based on KR contigs broadly followed the same pattern as the KS domain phylogeny with the iterative KR domains forming one single large clade along with three modular clades. Three NRPS/PKS hybrid clades were again determined with bur-A bacterial clade along with two novel dinoflagellate specific clades (Figure 5.3).

Table 5.2 List of PKS-NRPS found in the four transcriptomes. ACP- Acyl carrier protein; TE-Thioestrase; NRPS(a)- The adenylation domain of non-ribosomal peptide synthetases (NRPS); ER-Enoylreductase; KS- Ketosynthase; KR-ketoreductase; AT-Acyl transferase; DH- dehydratase; NRPS(p)- partial NRPS domain

Species	Contig	Encoding sequence	Length (in bp)	GC content (%)
***Coolia malayensis* MAB**	2223	NRPS(a)-ACP-KS-KR-DH-ER-ACP	2740	62.7
	12141	TE-NRPS(a)-ACP-KS-AT-TE-KR-ACP	2787	60.2
	22683	KR-ACP-KS-ACP-NRPS(p)	1176	60
	43946	NRPS(a)-KR	974	60.3
***Ostreopsis* cf. *ovata* HER27**	10200	TE-NRPS(a)-ACP-KS-AT-TE-KR(p)-ACP	2789	67.7
	17054	NRPS(a)-ACP-KS	1266	69.9
***Ostreopsis* cf. *siamensis* BH1**	6810	NRPS(a)-KS-DH-KR-ACP-KS-AT-KR-ACP-TE	7226	58.6
	13158	NRPS(a)-ACP-KS-DH-KR-ACP-KS-AT-DH	3338	58.6
***Ostreopsis rhodesae* HER26**	804	TE-NRPS(a)-ACP-KS-AT-TE-KR-ACP	2799	67.2
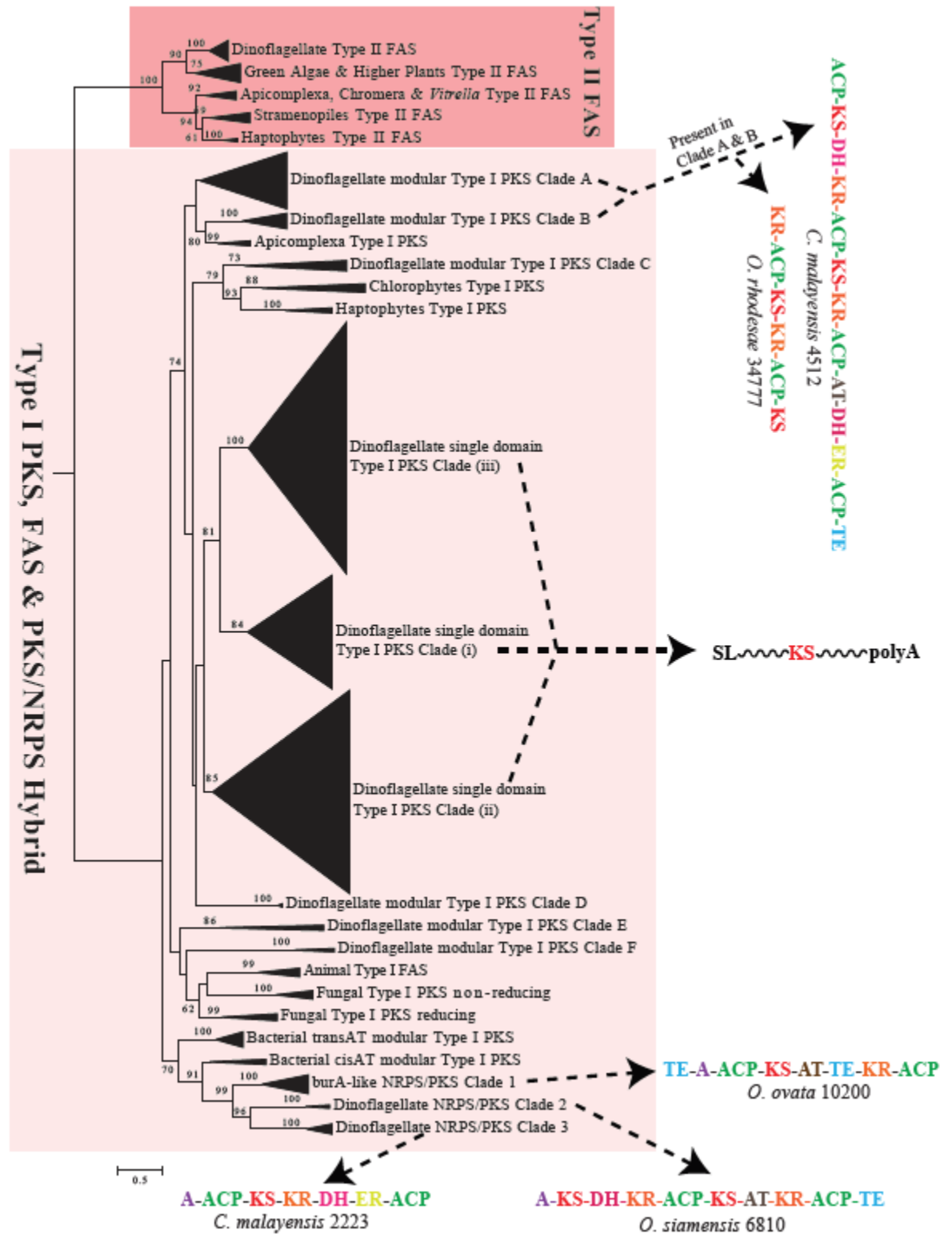
Figure 5.2 Phylogenetic analysis of ketoacyl synthase (KS) domains from prokaryotic and eukaryotic type I & II polyketide synthases (PKS) and fatty acid synthases. Consensus schematic representation of the multi-KS and NRPS/PKS hybrid domains are displayed on the right. AT: acyl transferase, A: Non-Ribosomal Peptide Synthase, KS: ketosynthase, DH: dehydratase, KR: ketoreductase, TE: thioesterase, ACP: acyl carrier protein, ER: enoyl reductase; SL: 5' splice leader; Poly-A: 3' poly A tail.

135
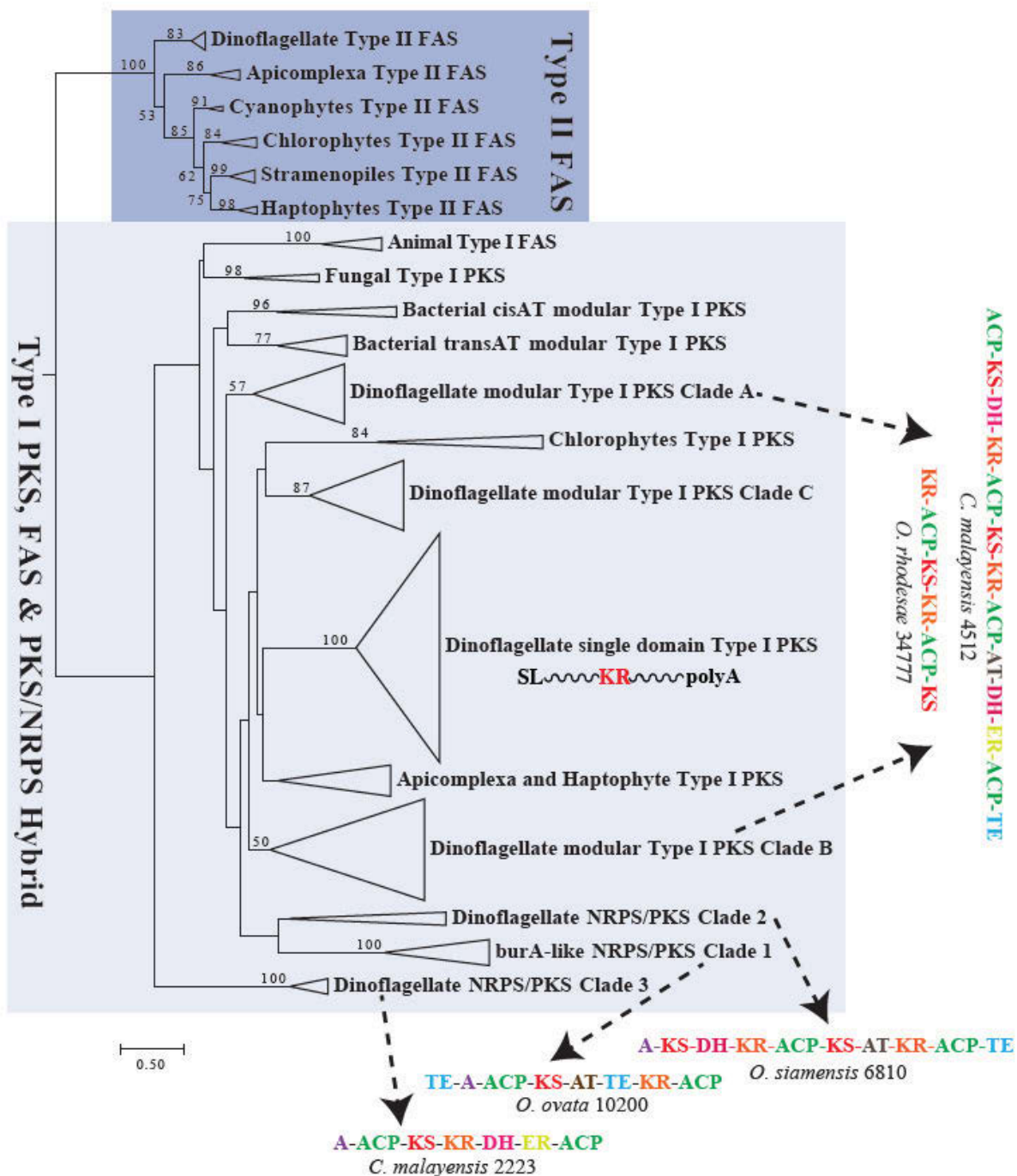
Figure 5.3 Phylogenetic analysis of ketoacyl reductase (KR) domains from prokaryotic and eukaryotic type I & II polyketide synthases (PKS) and fatty acid synthases. Consensus schematic representation of the multi-KS and NRPS/PKS hybrid domains are displayed similar to Figure 5.2.

5.4.4 Fatty acid synthesis

The genes involved in fatty acid synthesis and encoding for 3-ketoacyl ACP synthase I, II and III, ACP s-malonyl-transacylase, trans3-ketoacyl ACP reductase, 3-hydroxyacyl-ACP dehydratase, and enoyl-ACP reductase were identified in the transcriptomes of each

of the four species (Table 5.3). Each transcript in the *Ostreopsis* and *Coolia* species encoded an individual FAS domain, typical of type II FASs, as observed in other dinoflagellates and protists. The conserved amino acid sites were identified in 70% of the sequences, whereas transit peptides targeted towards the chloroplast were found in 60% of the contigs encoding for type II FAS enzymes (Table 5.3).

Table 5.3 List of FAS encoding transcripts from the four transcriptomes

Enzyme name	Contig	Conserved amino acid intact	ChloroP signal
3-ketoacyl ACP synthase I	coolia_mab_contig_17793	N	N
	ost_ovt_her27_contig_6552	N	Y
	ost_siam_bh1_contig_2667	N	Y
	ost_sp8_her26_contig_2705	N	N
3-ketoacyl ACP synthase II	coolia_mab_contig_6469	Y	Y
	ost_ovt_her27_contig_20050	Y	Y
	ost_siam_bh1_contig_36603	Y	N
	ost_sp8_her26_contig_34372	Y	N
3-ketoacyl ACP synthase III	coolia_mab_contig_11446	Y	N
	coolia_mab_contig_37122	Y	N
	ost_ovt_her27_contig_8188	Y	Y
	ost_ovt_her27_contig_12561	Y	N
	ost_siam_bh1_contig_6465	Y	Y
	ost_siam_bh1_contig_16921	Y	N
	ost_sp8_her26_contig_16208	Y	Y
	ost_sp8_her26_contig_39770	Y	N
AT-FabD	coolia_mab_contig_20410	Y	Y
	ost_ovt_her27_contig_12909	Y	Y
	ost_siam_bh1_contig_7984	Y	Y
	ost_sp8_her26_contig_2776	Y	Y
FabG	coolia_mab_contig_9840	Y	Y
	ost_ovt_her27_contig_18319	Y	Y
	ost_siam_bh1_contig_26250	Y	Y
	ost_sp8_her26_contig_5826	Y	Y
DH-FabZ	coolia_mab_contig_11121	Y	Y
	ost_ovt_her27_contig_983	Y	N
	ost_siam_bh1_contig_2059	Y	N
	ost_sp8_her26_contig_7804	N	Y
ER-FabI	coolia_mab_contig_23870	N	N
	ost_ovt_her27_contig_6043	N	Y
	ost_siam_bh1_contig_2862	N	Y
	ost_sp8_her26_contig_9766	N	Y

To understand the evolutionary history of these genes, a concatenated phylogeny of 5 type II FAS enzymes (KASIII-FabH, AT-FabD, DH-FabZ, ER ER-FabI, KR- FabG) was carried out (Figure 5.4). *Chromera velia* was used as an outgroup, and dinoflagellates formed a distinct well-supported monophyletic clade. Within the dinoflagellate clade, the evolution of these genes broadly follows the trend of dinoflagellate evolution with the different dinoflagellate orders forming monophyletic clades as described previously using ribosomal marker sequences (Kohli et al., 2017; Orr et al., 2012). Within the Gonyaulacales clade comprising of *Gambierdiscus* and *Alexandrium* spp. contigs, the three *Ostreopsis* species clustered together, with *C. malayensis* forming a sister clade as these genera are closely related (Figure 5.4).
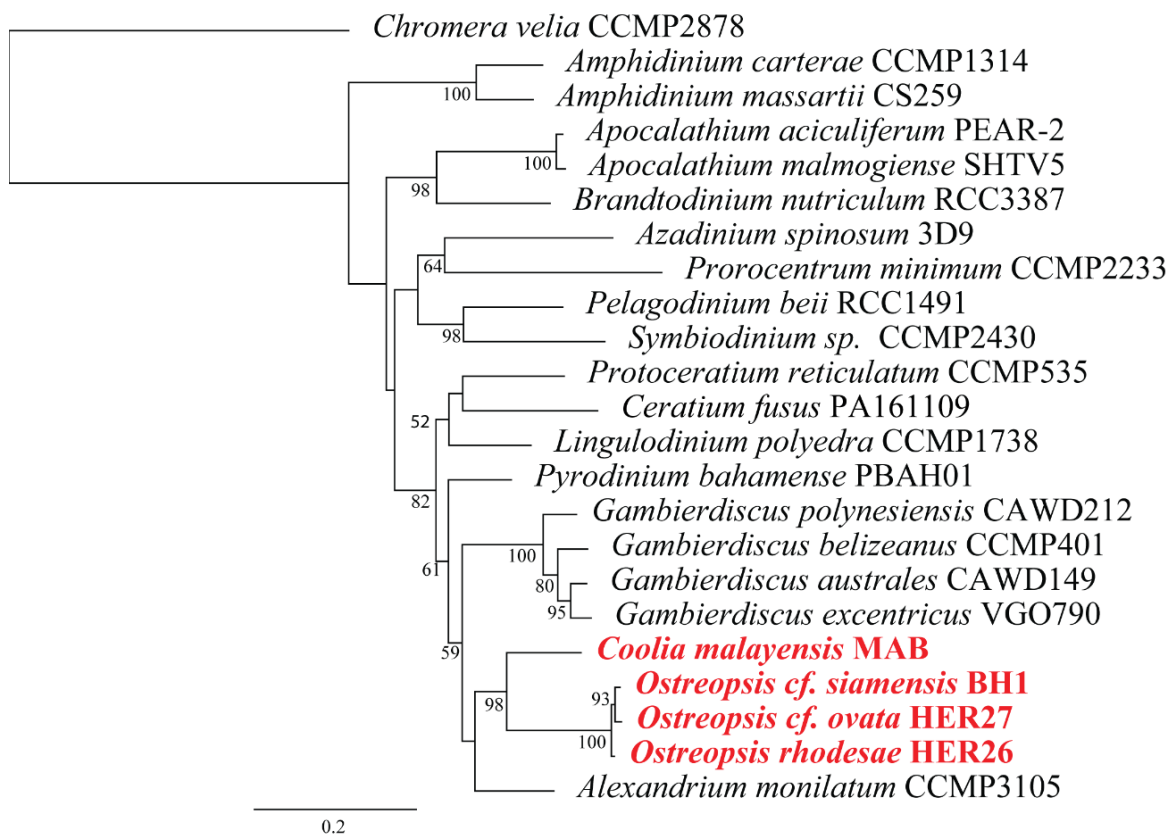
Figure 5.4 Concatenated phylogeny of five enzymes involved in type II fatty acid synthesis (3-ketoacyl ACP synthase III, s-malonyltransacylase, trans3-ketoacyl ACP reductase, 3-hydroxyacyl-ACP dehydratase and enoyl-ACP reductase) from 22 dinoflagellates and one other alveolate *Chromera velia* which was used as an outgroup. Phylogeny was inferred using RAxML, GAMMA model of rate heterogeneity and 1,000 bootstraps.

5.4.5 Putative metabolomic profiles of dinoflagellate species

A non-targeted profiling strategy was employed to analyze and tentatively identify key metabolites produced by the three *Ostreopsis* species in comparison to *C. malayensis*. Differential analysis on 1350 entities with their corresponding peak areas and retention times between 500-2400 *m/z* broadly followed the evolutionary trend amongst the four dinoflagellate species, with the *Ostreopsis* profiles clustering together and distinctly from *C. malayensis* (Figure 5.5). A total of 676 entities were significantly different between *C. malayensis* and the three *Ostreopsis* species. Of these, 444, 344 and 364 chemical entities were significantly different between *Ostreopsis* cf. *ovata*, *O.* cf *siamensis* and *O. rhodesae* respectively (Figure 5.6). One hundred and forty-four chemical entities were unique to *O.* cf. *ovata*, whereas 54 and 80 were unique to *O.* cf. *siamensis* and *O. rhodesae*, respectively. Fifty molecules were putatively annotated highlighting a massive diversity of compounds being produced by these species (see supplementary data S17).
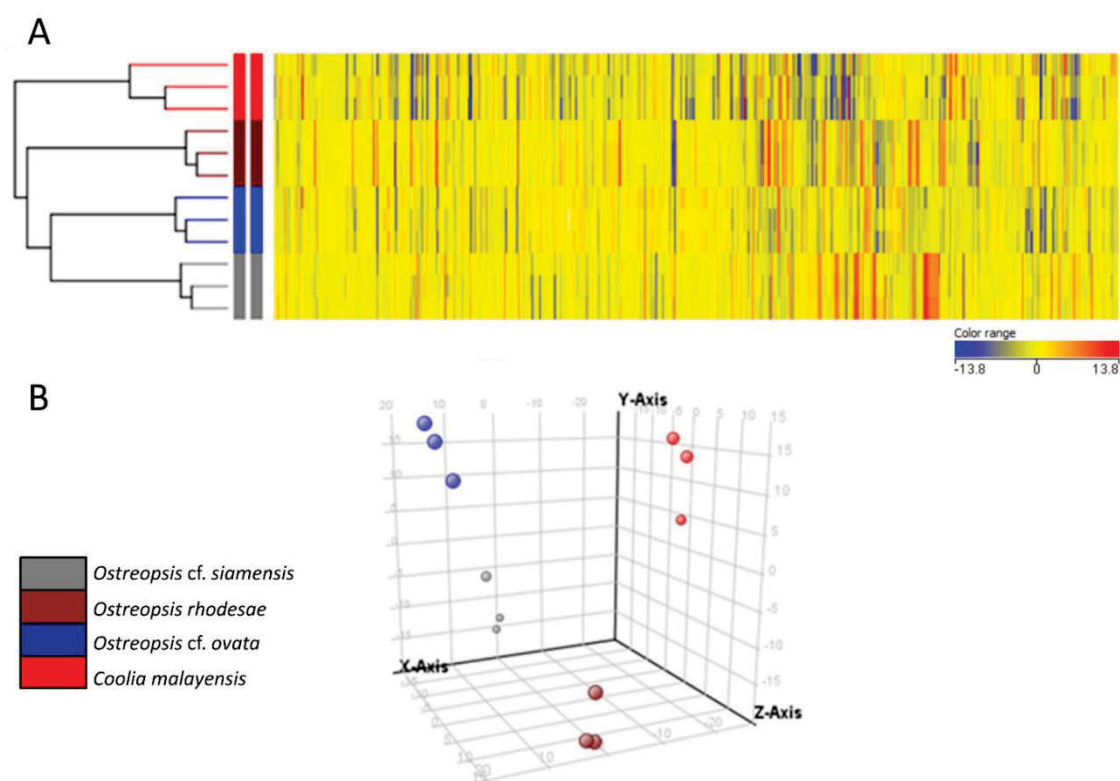
Figure 5.5 Non-targeted metabolomics on *Ostreopsis* and *Coolia* spp. A: Heat map of differential analysis of the four metabolomic profiles between 500-2400 *m/z* ratios. B: 3-D principal component plot of the four dinoflagellate metabolomic profiles.

5.5 Discussion

The primary focus of this study was to putatively identify the genes coding for the highly conserved KS domains in *Ostreopsis* species that are potentially involved in the biosynthesis of PLTX-like compounds. All polyketide biosynthetic enzyme domains needed to synthesize the PLTX-like carbon backbone were identified in all three *Ostreopsis* species and were also found in the non-PLTX producing *Coolia malayensis* suggesting that the diversity of KS domains did not have a clear relation to the species phylogeny or the chemical structure of the compounds. To date, no gene cluster amongst dinoflagellates has been definitively linked to the synthesis of a polyketide molecule due to their large and complex genomes and the inability to create genetic transformants in the lab (Keeling et al., 2014; Kohli et al., 2016).

Entity List 1 : C. malayensis vs O. rhodesae 364 entities

Entity List 2 : C. malayensis vs O. siamensis 344 entities

Entity List 3 : C. malayensis vs O. ovata 444 entities

41

80

54

51

192

57

144
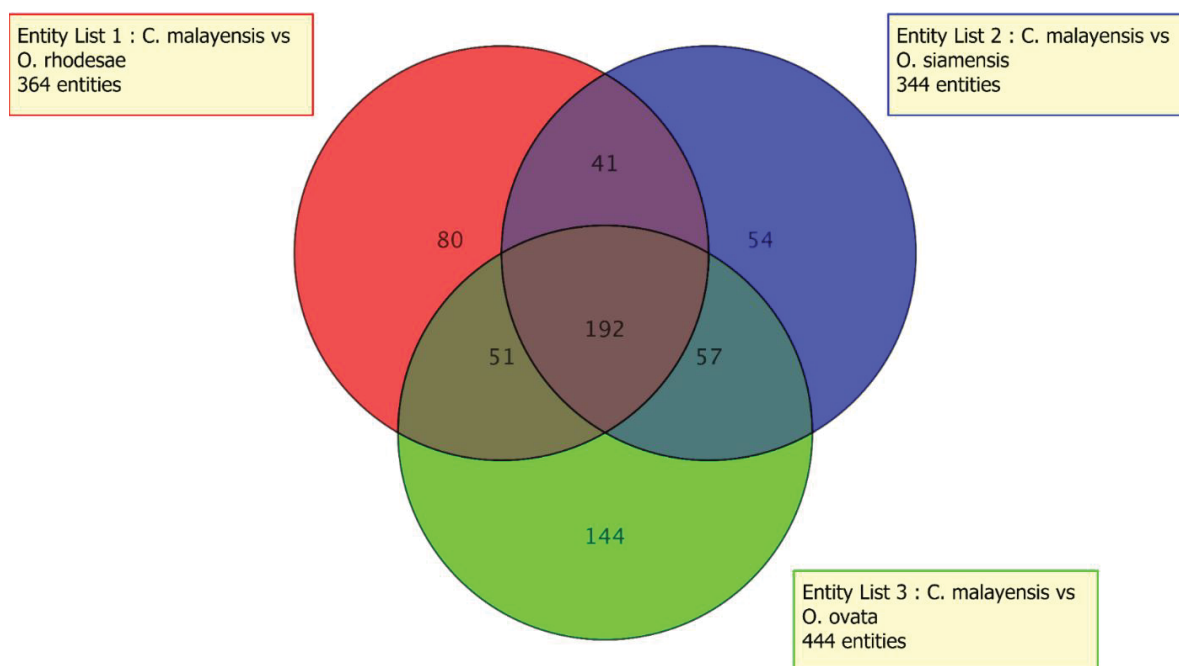
Figure 5.6 Venn diagram displaying shared metabolites detected in the non-targeted metabolic analyses of *Ostreopsis* species. The numbers represent the total entities that are significantly different between *Coolia malayensis* and the respective *Ostreopsis* species.

5.5.1 Polyketide biosynthesis

In dinoflagellates, the lack of correlation with the species phylogeny and the large intraspecific diversity in KS domains, suggests that multiple gene duplication events, domain shuffling and losses have occurred. This highlights that relaxed selection pressures have acted on the evolution of these secondary metabolite genes that may have been acquired or lost based on the functionality they provided to the organism (Kohli et al., 2016). Genes involved in secondary metabolite biosynthesis tend to be located in sub telomeric regions, which may contribute to their rapid evolution and novel functionality in PKS biosynthesis (Beedessee et al., 2015). We report a relatively high abundance of KS domains from our transcriptomic libraries compared to the average number of KS domains that have identified from previous dinoflagellate libraries uploaded on the Marine Microbial Eukaryote Sequencing Project (MMETSP) database (Keeling et al., 2014; Kohli et al., 2016).

Eichholz et al. (2012) speculated that the N-terminus is related to the mono-functional nature of KS domains and may play a role in structural rearrangements, substrate docking, or protein-protein interactions. Recent studies have highlighted the potential role of these regions as "linkers" and their interactions with linker regions at the C-termini of PKS multi-enzymes (Beedessee et al., 2015; Meyer et al., 2015). A low degree of conservation was noted within the N-terminal ExExGYLG signature sequence of the KS domains. Variations of the GYLG motif (DYLG, HYLG, YYLG, GLLG, AYLG and ALLG) have also been reported from other dinoflagellate libraries (Eichholz et al., 2012; Meyer et al., 2015; Monroe and Van Dolah, 2008; Pawlowiez et al., 2014). The absence or alteration of the conserved N terminal motif in the KS transcripts could explain the alternations/diversification in polyketide synthesis or the possibility that these copies might have diverged to play a role in other pathways via gene duplication (Eichholz et al., 2012; Pawlowiez et al., 2014).

The phylogenetic trees based on KS and KR domains show that the 'protistan' KS and KR domains form a monophyletic group comprising dinoflagellate, chlorophyte, haptophyte and apicomplexan KS and KR domains, respectively (Figures 5.2, 5.3). Our

KS phylogenetic tree reports similar evolutionary trends compared to previous studies, such as the three iterative dinoflagellate sub-clades amongst the 'protistan' clade and numerous modular KS domains, with the addition of novel dinoflagellate NRPS/PKS hybrid clades closely related to bacterial type I PKS clade (Figure 5.2). NRPS/PKS hybrids were first reported in dinoflagellates from *Karenia brevis*, with close relation to cyanobacterial genes, postulating horizontal gene transfer which has since then been linked to the introduction of toxin biosynthesis gene clusters into dinoflagellate species from toxigenic bacterium/cyanobacterium (López-Legentil et al., 2010; Stüken et al., 2011; Wang et al., 2014).

Contigs belonging to bur-A like NRPS/PKS hybrid clade (Figure 5.2) have been reported from a broad range of dinoflagellates suggesting their acquisition in the hosts prior to dinoflagellate diversification (Bachvaroff et al., 2015). The order and composition of hybrid domains reported in our study are comparable to the bacterial domains suggesting that both versions of the protein may catalyse similar reactions (Bachvaroff et al., 2015). The bacterial bur-A adds 3 carbons derived from methionine to malonyl-CoA. The major partner of bur-A is bur-F in bacterial domains which might suggest the novel NRPS/PKS clade in our study to be the candidate partner for the dinoflagellate bur-A domains. Previous studies on dinoflagellate NRPS/PKS hybrids have suggested the trisynthesis of glutamine, proline and isoleucine resulting in the formation of putative cyanobacterial-like peptolides, which might suggest the functional significance of these domains in the synthesis of polyketide molecules (Kellmann et al., 2010; López-Legentil et al., 2010).

Previous studies on dinophysistoxins (DTX)-5a/5b, that are produced by *Dinophysis* spp., have postulated that the process of incorporation of an intact glycine molecule as a replacement for an acetate unit in the side chains of DTX-5a/5b could potentially involve the role of an NRPS/PKS hybrid (Kellmann et al., 2010). Such hybrid domains would generally incorporate the NRPS domains at the start or terminal of the modular enzyme, similar to those identified in our study. Ostreol-A, a non-PLTX compound was recently described from *Ostreopsis* cf. *ovata* isolated form Korean waters. Its structural elucidation highlighted a polyhydroxy chain ending with a primary amino group and an amide bond, along with two tetrahydropyran rings in the chain (Hwang et al., 2013). The

142

central portion of this compound is structurally common with amphidinols that are synthesized by *Amphidinium* spp., but the terminal ends are characterized by the presence of an amide and a primary amine group, which differ from the conventional structure of amphidinols (Hwang et al., 2013; Kobayashi and Kubota, 2007). Such domains could be added on the carbon backbone of the molecule by NRPS/PKS hybrids. Hence, we postulate that the incorporation of amide and amino groups at the terminal ends of PLTX-like compounds and/or other complex non-PLTX molecules could be the potential functional significance of these NRPS/PKS hybrid domains.

5.5.2 Fatty acid biosynthesis

Fatty acid biosynthesis is essential for cell survival and is found ubiquitously across all groups of organisms (Jenke-Kodama et al., 2005). These molecules are vital to cellular membrane composition and also serve as secondary messengers thereby contributing to a variety of biological functions (Jenke-Kodama and Dittmann, 2009; Jenke-Kodama et al., 2005). Like PKSs, FASs are divided into two types; Type I FASs are found in the cytosol of fungi and metazoans as homodimers of polypeptides with eight distinct catalytic domains. Type II FASs are found in bacteria, chlorophytes and plant chloroplasts and are composed of a series of structurally dissociated enzymes (Jenke-Kodama et al., 2005; Van Dolah et al., 2013). FAS are similar to PKSs in both structure and function, and have been subject to considerable debate in the past due to their common evolutionary history in microbial eukaryotes (Jenke-Kodama and Dittmann, 2009; Jenke-Kodama et al., 2005; Monroe and Van Dolah, 2008; Snyder et al., 2005; Van Dolah et al., 2013).

Previous studies of dinoflagellates reported cytosolic FASs from the heterotrophic *Crypthecodinium cohnii*, which possessed a dimeric structure consistent with a Type I FAS structure (Sonnenborn and Kunau, 1982; Zhu et al., 2002). Recent studies in *Karenia brevis* found cytosolic incorporation of ^{3}H acetate into fatty acids, with little incorporation within the isolated chloroplasts. Along with the absence of Type II FAS contigs in the investigated transcriptome, it was suggested that *K. brevis* might possess a Type I FAS system or involve the role of PKS-like domains for fatty acid synthesis (Van Dolah et al., 2013). Kohli et al. (2016) reported type II FAS genes resembling plants to

be found in dinoflagellates and other protists after a detailed investigation of 213 strains and 152 genera from the Marine Microbial Eukaryote Transcriptome Sequencing Project database.

Similar genes encoding for type II FAS were reported from *Ostreopsis* and *Coolia* species (Figure 5.4). The detection of transit peptides targeted towards the chloroplast validates the nuclear encoding of the FAS domains and hence confirming their identity as type II FAS. This suggest that type II FAS genes were transferred from the plastid to the genome during the evolutionary history of the organisms thereby allowing for selection processes to act on genes based on their functional advantage to the host (Murray et al., 2015; Murray et al., 2016). Such mechanisms would restrict the accumulation of deleterious mutations and also provides protection from reactive oxygen species generated during the process of photosynthesis (Kohli et al., 2016). As fatty acid synthesis is essential for survival, these genes were likely retained by protists in the nucleus due to strong selective pressure. Within the dinoflagellate clade, their evolution broadly follows the trend of dinoflagellate evolution also highlights the conserved nature of these domains (Figure 5.4).

5.5.3 Metabolomic insights

The large numbers of KS domains in dinoflagellates have been linked to the production of numerous undetected or uncharacterised polyketide molecules (Kohli et al., 2016). The application of metabolomics to toxin biosynthesis in harmful algal species is somewhat limited. In our study, we have used a non-targeted metabolomics approach to investigate the tentative diversity of metabolites in the three *Ostreopsis* species and compared it to *Coolia malayensis*. We analyzed the metabolomics data in two ways. First, we considered the pattern of shared metabolites to examine the similarities (or differences) between the different species. These comparisons do not require identification of unknown compounds; rather all detected intracellular and extracellular metabolites were compared simultaneously (Klueter et al., 2015; Longnecker et al., 2015; Nielsen and Larsen, 2015). Next, the list of *m/z* values was prepared to obtain putative compound identifications. Figure 5.5 highlights the variability in the metabolomic profiles of the four investigated

dinoflagellate species. While each dinoflagellate profile is distinct, the pattern broadly follows the trend of dinoflagellate evolution as described using ribosomal markers, with *Coolia malayensis* clustering as an outgroup to the *Ostreopsis* species. However, it should be noted that the trends of gene evolution and metabolomic profiles are not always a direct relationship, but a complex result of multiple gene expression and a phenotypic output of numerous encoded enzymes. It is therefore inherently difficult to interpret the patterns of metabolites, and particularly to infer something about gene functions based on metabolite profiling (Smedsgaard and Nielsen, 2005).

The annotated chemical formulae of the molecules in this study indicate a potential long carbon backbone structure with the incorporation of nitrogen containing domains. Such strctures could potentially be synthesized by polyketide synthase genes, with NRPS/PKS hybrids incorporating the amino acid domains into the structure. Previously, numerous analogues of PLTX have been detected from *Ostreopsis* spp. and Cooliatoxin has been presented from *Coolia* spp. (Ciminiello et al., 2012b; Ciminiello et al., 2012c; Holmes et al., 1995; Usami et al., 1995; Wakeman et al., 2015). This is the first study using a non-targeted metabolomic approach to putatively annotate metabolites with potential polyketide-like strucutures from these species (see supplementary data S17). However, linking specific genes to specific molecules and biochemical pathways remains to be established. The definitive identification of a compound requires at least two independent assessments of the metabolite compared to an authentic standard. Unlike the targeted method, this technique is only semi-quantitative and relative abundances cannot be converted into molar quantities (Hoffmann et al., 2014). Thus, a definitive identification will require additional verification before we can hypothesize the role of these compounds within the metabolism of *Ostreopsis* and *Coolia* species. Once we have confirmed the identity of these compounds, we can develop an appropriate quantitative assay and conduct laboratory experiments to address hypotheses about the significance of these compounds in dinoflagellate chemical ecology.

Potent biomolecular activity can always be considered a rare event in evolution considering that such activity is based on very specific interactions between molecules. In the screening hypothesis model (Firn and Jones, 2003), it is suggested that organisms may have selected specific evolutionary traits to increase the probability of developing a compound, with potent biomolecular activity, that enhances the generation and retention of chemical diversity and concurrently reduce the fitness costs (Jenke-Kodama and Dittmann, 2009). This would predict that organisms that produce and screen a larger variety of chemical compounds, as demonstrated in our study, have an increased likelihood of enhanced fitness, as the chance of producing a rare chemical with a useful biological activity will be increased (Firn and Jones, 2003; Jenke-Kodama and Dittmann, 2009; Jenke-Kodama et al., 2008).

5.6 Conclusion and significance

Our current knowledge of the biosynthetic machinery responsible for dinoflagellate polyketide toxin biosynthesis is rudimentary. *Ostreopsis* species are known to produce polyketide toxins, and we therefore paid special attention to the enzymes involved in polyketide biosynthesis. In order to gain insight into the molecular basis of PLTX biosynthesis, cDNA libraries of 3 *Ostreopsis* species were constructed and compared to a close relative and a non-PLTX producer, *C. malayensis*. In this study, we report for the first time type I single-domain, multi-domain and hybrid NRPS/PKSs from *Ostreopsis* and *Coolia* species. We also report the putative identification of several polyketide-like entities from these species suggesting a vast diversity of previously undescribed molecules that are synthesized by them.

To date, no gene clusters associated with the biosynthesis of polyether ladder compounds have been elucidated from dinoflagellates. Polyketide synthases (PKS) and non-ribosomal peptide synthases (NRPS) are involved in the synthesis of a broad range of structurally diverse natural compounds, many of which are of medical importance and remain to be fully annotated and described.

5.7 Author contributions

AV, SM designed research; AV isolated strains, performed research, analysed and interpreted data; AV and GSK performed transcriptomics and phylogenetic analysis; AV and UK performed non-targeted metabolomics and interpreted the data; PR provided critical feedback on data analysis and manuscript writing; AV, SM wrote the paper with editorial input from all co-authors.

Chapter 6: Discussion

6.1 Overview

The view on marine microbial eukaryotic biodiversity and functional evolutionary traits has changed substantially during the past few decades (Caron et al., 2017). Protistan populations and traits were traditionally considered to be largely homogenous and molecular biology studies of these species have lagged behind compared to other organisms (Fenchel and Finlay, 2004; Keeling et al., 2014). However, in the past few decades, a large amount of DNA sequence information from protistan 'marker' genes, transcriptomes, genomes, meta-transcriptomes and even meta-genomes have become available (Caron et al., 2017; Cuvelier et al., 2010; de Vargas et al., 2015; Keeling et al., 2014; Le Bescot et al., 2016; Lin et al., 2015). Analyses of these data have altered our understanding of microbial eukaryotic diversity, phylogeny, evolution and physiology (Caron et al., 2017).

The changing climatic conditions and growing frequencies of toxic blooms have increased the scientific interest in toxin producing dinoflagellates (Anderson et al., 2012; Hackett et al., 2004). In order to investigate the causes and consequences of harmful algal blooms, it is necessary to precisely determine the identities of culprit species and their population level strategies (Driscoll et al., 2016; Murray et al., 2016; Rengefors et al., 2017). The EAC is a global climate change hotspot and yet our understanding of its impact on phytoplankton distribution and dynamics is limited (Hallegraeff, 2010; Ridgway, 2007). Species of genus *Ostreopsis* have been reported from tropical and temperate waters across the globe and are known to cause severe blooms and produce highly toxic palytoxin-like compouds (Rhodes, 2011). In Australia, we do not yet have basic information on the distribution, diversity and dynamics of these species. In this dissertation, I established the first comprehensive description of *Ostreopsis* species from Australian waters and explored cryptic diversity and functional traits in this genus, which is readily prevalent along the sub-tropical and temperate regions of the EAC. Results from this dissertation will add to our broader understanding of microbial eukaryotic ecology and to the standing knowledge of species biodiversity, population structures, eco-physiological traits and toxin biosynthesis pathways in *Ostreopsis* species.

6.2 Significance and future of findings

In Chapter 2, the investigation of a single strain was undertaken to establish the first molecular, morphological and toxicological study of an *Ostreopsis* species from the Australian EAC region. The strain was isolated during an expedition to Merimbula Lake inlet in 2012 (Kohli et al., 2014). The strain, initially identified as *Ostreopsis* sp., was established and grown in both f/2 and f/10 media to evaluate growth rates and observe cell shapes (Guillard, 1975). Cells maintained their 'normal' morphology in f/10 media and henceforth, all cultures in this dissertation were cultivated in f/10 media. Deformed cells, as found growing in f/2 media, have led to inconsistent evaluations of cell size in morphological studies, which is particularly problematic given the minor morphological differences observed between species of *Ostreopsis* (David et al., 2013; Hoppenrath et al., 2014). The culturing conditions play a vital role in the cellular morphometrics of dinoflagellate isolates as aberrant morphologies have been described from enriched nutrient media in various growth comparison studies (Nascimento et al., 2012). High concentration of nutrients and non-limiting light conditions, typical of standard culturing conditions, can result in an upregulation of light harvesting peridinin- chl *a* protein (PCP) complexes, chl *a* chl *c2* peridinin-protein complexes (acpPC), xanthophyll content and lipid molecules in the cells. Such molecules have been shown to accumulate in the cytoplasm and affect the carbon to volume relationships for the culture and may potentially affect cellular morphologies (Escalera et al., 2014; Falkowski and LaRoche, 1991; Iglesias-Prieto and Trench, 1997). Therefore, it is important to evaluate physiological parameters of the study organisms in its culturing condition as conducted in Chapter 4.

The strain identity was established as *Ostreopsis* cf. *siamensis* based on four ribosomal molecular markers, ITS-5.8S, D1-D3 and D8-D10 LSU rDNA and the 18S rDNA regions (SSU) (Verma et al., 2016b). SSU is commonly used for investigating protistan biodiversity, but the sequence data for *O.* cf. *siamensis*, a cosmopolitan benthic species, had never been reported (Forster et al., 2016; Le Bescot et al., 2016). The lack of annotated sequence data on public databases can lead to inaccurate species identifications, which is problematic considering the potential of this species to form harmful algal

blooms. Therefore, it is important that curated taxonomic studies of such specimens be conducted using multiple 'barcode' genes.

The lack of genetic data from the type location and contrasting morphological accounts for *Ostreopsis* species continue to present issues in the taxonomic studies of this genus. A systematic description of morphological features along with concatenated gene sequence alignments of functional genes amongst *Ostreopsis* species can improve in understanding the phylogenetic trends and diversity within this genus. Chapter 5 presents the transcriptomic dataset of three *Ostreopsis* species. Investigating more species using transcriptomics will provide a large catalogue of functional genes, which will aid in better resolving trends of evolution in this genus. Fatty acid synthase (FAS) genes, as described in Chapter 5, is one such example since their conserved nature and similar evolutionary trend to ribosomal markers could suggest their use in the future as a potential functional marker. The increased use of transcriptomics to understand dinoflagellate genetics can unravel other prospective functional markers for this purpose (Keeling et al., 2014).

In Chapter 3, a species level biodiversity study at Heron Island, Great Barrier Reef was undertaken. Previous morphological reports of *Ostreopsis* species from this region and the northern origin of the EAC made it a suitable candidate location to begin this investigation (Heimann et al., 2009). A novel pseudo-cryptic species, *Ostreopsis rhodesae* was described after the genetic investigation of 14 isolates, along with the first molecular report of *Ostreopsis* cf. *ovata* from Australian waters. *O. rhodesae* was found to be closely related to *O.* cf. *siamensis*, also isolated in this study, but after thorough microscopic investigations, distinguishing morphological features were observed in the new species (Verma et al., 2016a).

In this study, the secondary structure of ITS2 region was used for species delineation. This region in *Ostreopsis* species was found to be the shortest amongst all reported dinoflagellates as it did not conform to the conventional eukaryotic four domain structure This suggests the potential of rapid evolutionary divergence amongst *Ostreopsis* species highlighted by the various geographic sub-clades and cryptic clades within this genus

(Penna et al., 2005; Sato et al., 2011). ITS2 secondary structures have been very useful in improving phylogenetic estimation and species delineation amongst cryptic phytoplankton taxa (Amato et al., 2007; Coleman, 2007; John et al., 2014; Leaw et al., 2016). Only the secondary structures of the three species isolated from the Great Barrier Reef were reported in this study. Further studies on the ITS2 secondary structures from other *Ostreopsis* species and sub-clades will aid in our understanding of species divergence within this genus. The short length of ITS2 and the variable secondary structures amongst *Ostreopsis* species suggest epigenetic modifications to the transcript, which need to be further investigated as it would provide novel insights into the genetic processes amongst dinoflagellates. ITS2 is also a popular meta-barcoding marker and the short length of this region amongst *Ostreopsis* species should be taken into consideration while using this marker in biodiversity and monitoring studies.

We also reported toxic effects of cellular extracts towards fish gill cell lines. These results, to our knowledge, report the first toxic effect of *Ostreopsis* species on fish gill cell lines, suggesting that *Ostreopsis* species should also be considered to possess ichthyotoxic effects. Previous studies have suggested that lipid and/or polyketide molecules may cause such effects (Dorantes-Aranda et al., 2015). A large variety of molecules with potential polyketide backbone structures are synthesized by *Ostreopsis* species as highlighted in Chapter 5. Structural elucidation of these molecules could highlight the compounds responsible for such effects and aid in further understanding the impact of polyketides on the chemical ecology of the producing organism.

The confirmed molecular reports of *Ostreopsis* species from the sub-tropical Great Barrier Reef in Chapter 3 and temperate New South Wales in Chapter 2 suggest a wide range of functional traits in these species that would enable such a range expansion. Spatial distribution and functional traits of *Ostreopsis* species were further investigated in Chapter 4. This study marks the first investigation of population level based genetic and phenotypic diversity in protists in the EAC region.

A systematic sampling methodology encompassing 1500 km along the NSW coastline, across eight different sampling locations and five coastal bioregions, discovered *O.* cf. *siamensis* at all sites. Eighty-five clonal cultures were established, of which 68 were used for phylogenetic analyses and 53 for physiological assessments. The concatenated phylogenies, based on three ribosomal markers, highlighted two sub-clades and numerous haplotypes along the NSW coastline. The genetic diversity in the northern sub-tropical locations was greater compared to the more southern locations. This trend reflects the long-standing divergence and local radiations of haplotypes originating from the ancestral population and a potential southward range expansion, which may be related to the intensification of the EAC. It is interesting to note that genetic diversity within *Ostreopsis* specimens was found to decrease along the EAC gradient. Three species were reported in Chapter 3 from GBR, the most northerly site examined in this study, followed by only one species further south. Further investigation using microsatellites or amplified fragment length polymorphisms can aid in better resolution of population structure along the EAC. It should be noted that most sampling for this project was done during April – July (Austral Winter). Further sampling at various timepoints in the year would yield the seasonal distribution of these species and would improve our understanding of their habitats and southward distribution. It will also open avenues to unravel more *Ostreopsis* species from the EAC region.

The study also demonstrated intra- and inter-population variation in physiological traits amongst isolates under the same culturing conditions. This is the first study to our knowledge that reports growth rates, cell size, cellular toxic concentrations and photobiological parameters on such many clones for a marine protist. All strains established in this study were grown in the same culturing conditions. Phenotypic diversity is crucial in buffering responses to environmental variation. Hence understanding its role along a marine temperature gradient such as the EAC will enable improved predictions of species responses to the warming of the current in the future. Our results demonstrate the importance of investigating multiple isolates of a species to characterize the range of a phenotypic trait, given that very high variability may be encompassed within the standing stocks of phytoplankton populations. The study also used *O.* cf. *siamensis* as a model to investigate photo-physiological traits amongst epi-

benthic dinoflagellates and reported many 'functional' groups amongst the investigated isolates. Different light harvesting strategies were reported from these strains suggesting that their ability to quickly adapt to varying light intensities can aid in range expansion and colonization of various substrates (Hennige et al., 2009). The photobiology of benthic microalgae is not very well documented. A detailed investigation of light harvesting and utilization parameters would improve our understanding of the photobiological blue print of such organisms and add to the current standing knowledge of photosynthesis in aquatic ecosystems.

The aim of our investigation was to comprehend standing phenotypic and genetic variability amongst isolates and therefore, all isolates were investigated under a single culturing condition. Phenotypic plasticity could be investigated in future in order to aid in our understanding of clonal response to short-term environmental change (Thomas et al., 2016). It should also be considered that algal-bacterial interactions play a vital role in the physiology of algal cultures (Amaro et al., 2005; Bolch et al., 2017). Establishing and interpreting experimental data from large number of axenic clones would present considerable challenges, but could be undertaken with a few selected strains in order to test preliminary theories.

The varying profiles of PLTX- like compounds amongst *Ostreopsis* clones reported in Chapters 3 and 4 and their toxic impact as highlighted in Chapters 2 and 3, led to the investigation of biosynthesis of PLTX- like compounds from *Ostreopsis* species. The transcriptomic profiles of *O.* cf. *siamensis*; *O. rhodesae* and *O.* cf. *ovata* were reported and compared to the closely related *Coolia malayensis* in Chapter 5. All polyketide domains needed to synthesize a PLTX-like carbon backbone were identified in all three *Ostreopsis* species and were also found in the non-PLTX producing *C. malayensis* suggesting that the diversity of polyketide domains did not have a clear relation to the species phylogeny or the chemical structure of those compounds. This study marks the first transcriptomic investigation of *Ostreopsis* species. To date, no gene cluster amongst dinoflagellates have been definitively linked to the synthesis of a polyketide molecule due to their large and complex genomes, and our inability to genetically transform them (Kohli et al., 2016; Murray et al., 2016). Many compounds with putative polyketide like

structures were reported in this investigation using non-targeted metabolomics, suggesting a greater diversity of polyketide-like compounds amongst these species than previously anticipated. Detailed structural annotation of the compounds is essential before their ecological, metabolic and evolutionary roles can be deciphered. These results broaden the scope of bioprospecting and exploring therapeutic and industrial value of such compounds. However, the lack of axenic cultures, complicated and unconventional genetic features and the difficulty in constructing and screening mutants amongst dinoflagellates will make such goals quite challenging (Murray et al., 2016).

The results obtained in this dissertation establish the grounds for numerous eco-evolutionary experiments and open avenues for using novel molecular and physiological techniques to answer fundamental questions in microbial ecology. While previously, studies based on single strains were used for hypothesis driven experiments, we are now able to screen multiple strains to investigate phenotype-genotype interactions and population driven physiological responses.

The use of high throughput sequencing in *de novo* molecular biology studies, such as the using transcriptomics on numerous strains/species or partial genome sequencing will aid in investigating divergence amongst populations/species by examining single nucleotide polymorphisms across entire transcriptomes/draft genomes (Ellison et al., 2011; Le Gac et al., 2016). These approaches can benefit with the use of single cell genomics/transcriptomics in exploring functional traits amongst specimens without inducing any culturing bias. This will benefit our understanding of eco-evolutionary drivers of population structures, especially for organisms that are difficult to culture in the laboratory (Liu et al., 2017). Transcriptomic/genomic data from more species will help in improving the resolution of evolutionary distances and our understanding of dinoflagellate evolution (Janouškovec et al., 2017).

6.3 Thesis conclusion

The central aim of this thesis was to use *Ostreopsis* as a model organism to investigate species, population and functional diversity amongst dinoflagellates, particularly in the EAC region. Dinoflagellates continue to remain enigmatic, due to their diverse ecological strategies and complex genetic features. Results from this thesis will benefit our understanding of phytoplankton diversity and physiology along the EAC. These results will also aid in establishing the key metabolites and genes that cause the toxic effects in blooming populations. This study has broadened our understanding of the eco-evolutionary processes driving diversity and function amongst phytoplankton.

Bibliography

Abràmoff, M.D., Magalhães, P.J., Ram, S.J., 2004. Image processing with ImageJ. Biophotonics International 11(7), 36-42.

Accoroni, S., Romagnoli, T., Colombo, F., Pennesi, C., Di Camillo, C.G., Marini, M., Battocchi, C., Ciminiello, P., Dell'Aversano, C., Dello Iacovo, E., 2011. *Ostreopsis cf. ovata* bloom in the northern Adriatic Sea during summer 2009: Ecology, molecular characterization and toxin profile. Marine Pollution Bulletin 62(11), 2512-2519.

Accoroni, S., Romagnoli, T., Pichierri, S., Totti, C., 2016. Effects of the bloom of harmful benthic dinoflagellate Ostreopsis cf. ovata on the microphytobenthos community in the northern Adriatic Sea. Harmful Algae 55, 179-190.

Agapow, P.-M., Bininda-Emonds, O.R., Crandall, K.A., Gittleman, J.L., Mace, G.M., Marshall, J.C., Purvis, A., 2004. The impact of species concept on biodiversity studies. The quarterly review of biology 79(2), 161-179.

Ajani, P., Brett, S., Krogh, M., Scanes, P., Webster, G., Armand, L., 2013. The risk of harmful algal blooms (HABs) in the oyster-growing estuaries of New South Wales, Australia. Environmental Monitoring and Assessment 185(6), 5295-5316.

Ajani, P., Hallegraeff, G., Allen, D., Coughlan, A., Richardson, A., Armand, L., Ingleton, T., Murray, S., 2016. Establishing baselines: a review of eighty years of phytoplankton diversity and biomass in south-eastern Australia. Oceanography and Marine Biology: an annual review. 54, 387-412

Ajani, P., Murray, S., Hallegraeff, G., Lundholm, N., Gillings, M., Brett, S., Armand, L., 2013b. The diatom genus *Pseudo-nitschia* (Bacillariophyceae) in New South Wales, Australia: morphotaxonomy, molecular phylogeny, toxicity, and distribution. Journal of Phycology 49(4), 765-785.

Alcala, A. C., Alcala, L. C., Garth, J. S., Yasumura, D. and Yasumoto, T. 1988. Human fatality due to ingestion of the crab *Demania reynaudii* that contained a palytoxin-like toxin. Toxicon 26, 105-7.

Aligizaki, K. and Nikolaidis, G. 2006. The presence of the potentially toxic genera *Ostreopsis* and *Coolia* (Dinophyceae) in the North Aegean Sea, Greece. Harmful Algae 5, 717-30.

Aligizaki, K., Katikou, P., Nikolaidis, G. and Panou, A. 2008. First episode of shellfish contamination by palytoxin-like compounds from *Ostreopsis* species (Aegean Sea, Greece). Toxicon 51, 418-27.

Alpermann, T.J., Tillmann, U., Beszteri, B., Cembella, A.D., John, U., 2010. Phenotypic variation and genotypic diversity in a planktonic population of the toxigenic marine dinoflagellate *Alexandrium tamarense*. Journal of Phycology 46(1), 18-32.

Alverson, A.J., 2008. Molecular systematics and the diatom species. Protist 159(3), 339-353.

Amaro, A.M., Fuentes, M.S., Ogalde, S.R., Venegas, J.A., Suarez-Isla, B.A., 2005. Identification and Characterization of Potentially Algal-lytic Marine Bacteria Strongly Associated with the Toxic Dinoflagellate *Alexandrium catenella*. Journal of Eukaryotic Microbiology 52(3), 191-200.

Amato, A., Kooistra, W.H., Ghiron, J.H.L., Mann, D.G., Pröschold, T., Montresor, M., 2007. Reproductive isolation among sympatric cryptic species in marine diatoms. Protist 158(2), 193-207.

Amzil, Z., Sibat, M., Chomerat, N., Grossel, H., Marco-Miralles, F., Lemee, R., Nezan, E., Sechet, V., 2012. Ovatoxin-a and palytoxin accumulation in seafood in relation to *Ostreopsis* cf. *ovata* blooms on the French Mediterranean coast. Marine Drugs 10(2), 477-496.

Anderson, D.M., Alpermann, T.J., Cembella, A.D., Collos, Y., Masseret, E., Montresor, M., 2012. The globally distributed genus *Alexandrium*: multifaceted roles in marine ecosystems and impacts on human health. Harmful Algae 14, 10-35.

Anderson, D.M., Cembella, A.D., Hallegraeff, G.M., 2012. Progress in understanding harmful algal blooms: paradigm shifts and new technologies for research, monitoring, and management. Annual Review of Marine Science 4, 143-176.

Ankenbrand, M.J., Keller, A., Wolf, M., Schultz, J., Förster, F., 2015. ITS2 database V: Twice as much. Molecular Biology and Evolution 32(11), 3030-3032.

Annenkova, N.V., Hansen, G., Moestrup, Ø., Rengefors, K., 2015. Recent radiation in a marine and freshwater dinoflagellate species flock. The ISME journal 9(8), 1821-1834.

Aurahs, R., Grimm, G.W., Hemleben, V., Hemleben, C., Kucera, M., 2009. Geographical distribution of cryptic genetic types in the planktonic foraminifer *Globigerinoides ruber*. Molecular Ecology 18(8), 1692-1706.

Auwera, G.V.D., Wachter, R.D., 1998. Structure of the large subunit rDNA from a diatom, and comparison between small and large subunit ribosomal RNA for studying stramenopile evolution. Journal of Eukaryotic Microbiology 45(5), 521-527.

Baas-Becking, L.G.M., 1934. Geobiologie; of inleiding tot de milieukunde.

Bachvaroff, T. R., Williams, E., Jagus, R, Place, A. R. 2015. A noncryptic noncanonical multi-module PKS/NRPS found in dinoflagellates. The 16th International Conference on Harmful Algae. Wellington, New Zealand.101-104

Bachvaroff, T.R., Adolf, J.E., Place, A.R., 2009. Strain variation in *Karlodinium veneficum* (Dinophyceae): toxin profiles, pigments, and growth characteristics. Journal of Phycology 45(1), 137-153.

Bachvaroff, T.R., Place, A.R., 2008. From stop to start: tandem gene arrangement, copy number and trans-splicing sites in the dinoflagellate Amphidinium carterae. PLoS One 3(8), e2929.

Barnes, D.K., 2002. Biodiversity: invasions by marine life on plastic debris. Nature 416(6883), 808-809.

Barone, R., 2007. Behavioural trait of *Ostreopsis ovata* (Dinophyceae) in Mediterranean rock pools: the spider's strategy. Harmful Algae News.

Barton, A.D., Finkel, Z.V., Ward, B.A., Johns, D.G., Follows, M.J., 2013. On the roles of cell size and trophic strategy in North Atlantic diatom and dinoflagellate communities. Limnology and Oceanography 58(1), 254-266.

Beauchemin, M., Roy, S., Daoust, P., Dagenais-Bellefeuille, S., Bertomeu, T., Letourneau, L., Lang, B.F., Morse, D., 2012. Dinoflagellate tandem array gene transcripts are highly conserved and not polycistronic. Proceedings of the National Academy of Sciences 109(39), 15793-15798.

Beedessee, G., Hisata, K., Roy, M.C., Satoh, N., Shoguchi, E., 2015. Multifunctional polyketide synthase genes identified by genomic survey of the symbiotic dinoflagellate, *Symbiodinium minutum*. BMC Genomics 16(1), 941.

Bell, G., Collins, S., 2008. Adaptation, extinction and global change. Evolutionary Applications 1(1), 3-16.

Bellocci, M., Ronzitti, G., Milandri, A., Melchiorre, N., Grillo, C., Poletti, R., Yasumoto, T., Rossini, G.P., 2008. A cytolytic assay for the measurement of palytoxin based on a cultured monolayer cell line. Analytical Biochemistry 374(1), 48-55.

Besada, E., Loeblich, L., Loeblich Iii, A., 1982. Observations on tropical, benthic dinoflagellates from ciguatera-endemic areas: *Coolia*, *Gambierdiscus*, and *Ostreopsis*. Bulletin of Marine Science 32(3), 723-735.

Bolch, C.J., Bejoy, T.A., Green, D.H., 2017. Bacterial Associates Modify Growth Dynamics of the Dinoflagellate *Gymnodinium catenatum*. Frontiers in Microbiology 8, 670.

Bols, N., Barlian, A., Chirino-Trejo, M., Caldwell, S., Goegan, P., Lee, L., 1994. Development of a cell line from primary cultures of rainbow trout, *Oncorhynchus mykiss* (Walbaum), gills. Journal of Fish Diseases 17(6), 601-611.

Bravo, I., Vila, M., Casabianca, S., Rodriguez, F., Rial, P., Riobó, P. and Penna, A. 2012. Life cycle stages of the benthic palytoxin-producing dinoflagellate *Ostreopsis* cf. *ovata* (Dinophyceae). Harmful Algae 18: 24-34.

Burkholder, J. and Glibert, P. 2006. Intraspecific variability: an important consideration in forming generalisations about toxigenic algal species. African Journal of Marine Science 28, 177-180.

Burki, F., 2014. The eukaryotic tree of life from a global phylogenomic perspective. Cold Spring Harbor Perspectives in Biology 6(5), a016147.

Caron, D.A., Alexander, H., Allen, A.E., Archibald, J.M., Armbrust, E.V., Bachy, C., Bell, C.J., Bharti, A., Dyhrman, S.T., Guida, S.M., 2017. Probing the evolution, ecology and physiology of marine protists using transcriptomics. Nature Reviews Microbiology 15, 6–20

Caron, D.A., Countway, P.D., Jones, A.C., Kim, D.Y., Schnetzer, A., 2012. Marine protistan diversity. Annual review of Marine Science 4, 467-493.

Caron, D.A., Worden, A.Z., Countway, P.D., Demir, E., Heidelberg, K.B., 2009. Protists are microbes too: a perspective. The ISME Journal 3(1), 4-12.

Casabianca, S., Penna, A., Pecchioli, E., Jordi, A., Basterretxea, G., Vernesi, C., 2011. Population genetic structure and connectivity of the harmful dinoflagellate *Alexandrium minutum* in the Mediterranean Sea. Proceedings of the Royal Society of London B: Biological Sciences, rspb20110708.

Casteleyn, G., Leliaert, F., Backeljau, T., Debeer, A.-E., Kotaki, Y., Rhodes, L., Lundholm, N., Sabbe, K., Vyverman, W., 2010. Limits to gene flow in a cosmopolitan marine planktonic diatom. Proceedings of the National Academy of Sciences 107(29), 12952-12957.

Castresana, J., 2000. Selection of conserved blocks from multiple alignments for their use in phylogenetic analysis. Molecular Biology and Evolution 17(4), 540-552.

Cha, J., Christ, W., Finan, J., Fujioka, H., Kishi, Y., Klein, L., Ko, S., Leder, J., McWhorter, W., Pfaff, K., 1982. Stereochemistry of palytoxin. Part 4. Complete structure. Journal of the American Chemical Society 104(25), 7369-7371.

Chang, F., Shimizu, Y., Hay, B., Stewart, R., Mackay, G., Tasker, R., 2000. Three recently recorded Ostreopsis spp.(Dinophyceae) in New Zealand: temporal and regional distribution in the upper North Island from 1995 to 1997. New Zealand Journal of Marine and Freshwater Research 34(1), 29-39.

Chevin, L.M., Collins, S., Lefèvre, F., 2013. Phenotypic plasticity and evolutionary demographic responses to climate change: taking theory out to the field. Functional Ecology 27(4), 967-979.

Chinain, M., Faust, M.A., Pauillac, S., 1999. Morphology and molecular analyses of three toxic species of *Gambierdiscus* (Dinophyceae): *G. pacificus*, sp. nov., *G. australes*, sp. nov., and *G. polynesiensis*, sp. nov. Journal of Phycology 35(6), 1282-1296.

Ciminiello, P., Dell'Aversano, C., Dello Iacovo, E., Fattorusso, E., Forino, M., Grauso, L., Tartaglione, L., Florio, C., Lorenzon, P., De Bortoli, M., 2009. Stereostructure and biological activity of 42-hydroxy-palytoxin: a new palytoxin analogue from Hawaiian *Palythoa* subspecies. Chemical Research in Toxicology 22(11), 1851-1859.

Ciminiello, P., Dell'Aversano, C., Dello Iacovo, E., Fattorusso, E., Forino, M., Grauso, L., Tartaglione, L., Guerrini, F., Pezzolesi, L., Pistocchi, R., Vanucci, S., 2012a. Isolation and Structure Elucidation of Ovatoxin-a, the Major Toxin Produced by *Ostreopsis ovata*. Journal of the American Chemical Society 134(3), 1869-1875.

Ciminiello, P., Dell'Aversano, C., Fattorusso, E., Forino, M., Tartaglione, L., Grillo, C., Melchiorre, N., 2008. Putative palytoxin and its new analogue, ovatoxin-a, in *Ostreopsis ovata* collected along the Ligurian coasts during the 2006 toxic outbreak. Journal of the American Society for Mass Spectrometry 19(1), 111-120.

Ciminiello, P., Dell'aversano, C., Iacovo, E. D. et al. 2013. Investigation of toxin profile of Mediterranean and Atlantic strains of *Ostreopsis* cf. *siamensis* (Dinophyceae) by liquid chromatography–high resolution mass spectrometry. Harmful Algae 23, 19-27.

Ciminiello, P., Dell'Aversano, C., Iacovo, E.D., Fattorusso, E., Forino, M., Tartaglione, L., Battocchi, C., Crinelli, R., Carloni, E., Magnani, M., 2012b. Unique toxin profile of a Mediterranean *Ostreopsis cf. ovata* strain: HR LC-MS n characterization of ovatoxin-f, a new palytoxin congener. Chemical Research in Toxicology 25(6), 1243-1252.

Ciminiello, P., Dell'Aversano, C., Iacovo, E.D., Fattorusso, E., Forino, M., Tartaglione, L., Benedettini, G., Onorari, M., Serena, F., Battocchi, C., 2014. First finding of *Ostreopsis* cf. *ovata* toxins in marine aerosols. Environmental Science & Technology 48(6), 3532-3540.

Ciminiello, P., Dell'Aversano, C., Fattorusso, E., Forino, M., Magno, G.S., Tartaglione, L., Grillo, C., Melchiorre, N., 2006. The Genoa 2005 Outbreak. Determination of Putative Palytoxin in Mediterranean *Ostreopsis ovata* by a New Liquid Chromatography Tandem Mass Spectrometry Method. Analytical chemistry 78(17), 6153-6159.

Ciminiello, P., Dell'Aversano, C., Iacovo, E.D., Fattorusso, E., Forino, M., Grauso, L., Tartaglione, L., Guerrini, F., Pistocchi, R., 2010. Complex palytoxin like profile of *Ostreopsis ovata*. Identification of four new ovatoxins by high resolution liquid chromatography/mass spectrometry. Rapid Communications in Mass Spectrometry 24(18), 2735-2744.

Clement, M., Posada, D., Crandall, K.A., 2000. TCS: a computer program to estimate gene genealogies. Molecular Ecology 9(10), 1657-1659.

Coakes, S.J., Steed, L., 2009. SPSS: Analysis without anguish using SPSS version 14.0 for Windows. John Wiley & Sons, Inc.

Coffroth, M.A., Santos, S.R., 2005. Genetic diversity of symbiotic dinoflagellates in the genus *Symbiodinium*. Protist 156(1), 19-34.

Coleman, A.W., 2003. ITS2 is a double-edged tool for eukaryote evolutionary comparisons. TRENDS in Genetics 19(7), 370-375.

Coleman, A.W., 2007. Pan-eukaryote ITS2 homologies revealed by RNA secondary structure. Nucleic Acids Research 35(10), 3322-3329.

Coleman, A.W., 2015. Nuclear rRNA transcript processing versus internal transcribed spacer secondary structure. Trends in Genetics 31(3), 157-163.

Coleman, A.W., Vacquier, V.D., 2002. Exploring the phylogenetic utility of ITS sequences for animals: a test case for abalone (Haliotis). Journal of Molecular Evolution 54(2), 246-257.

Coleman, A.W., van Oppen, M.J., 2008. Secondary structure of the rRNA ITS2 region reveals key evolutionary patterns in acroporid corals. Journal of Molecular Evolution 67(4), 389-396.

Collins, S., Rost, B., Rynearson, T.A., 2014. Evolutionary potential of marine phytoplankton under ocean acidification. Evolutionary Applications 7(1), 140-155.

Conesa, A., Götz, S., García-Gómez, J.M., Terol, J., Talón, M., Robles, M., 2005. Blast2GO: a universal tool for annotation, visualization and analysis in functional genomics research. Bioinformatics 21(18), 3674-3676.

Cuvelier, M.L., Allen, A.E., Monier, A., McCrow, J.P., Messié, M., Tringe, S.G., Woyke, T., Welsh, R.M., Ishoey, T., Lee, J.-H., 2010. Targeted metagenomics and ecology of globally important uncultured eukaryotic phytoplankton. Proceedings of the National Academy of Sciences 107(33), 14679-14684.

Darty, K., Denise, A., Ponty, Y., 2009. VARNA: Interactive drawing and editing of the RNA secondary structure. Bioinformatics 25(15), 1974-1975.

David, H., Laza-Martínez, A., Miguel, I. and Orive, E. 2013. *Ostreopsis* cf. *siamensis* and *Ostreopsis* cf. *ovata* from the Atlantic Iberian Peninsula: morphological and phylogenetic characterization. Harmful Algae 30, 44-55.

Davies, W., Jakobsen, K., 1988. Characterization of DNA from the Dinoflagellate *Woloszynskia bostoniensis*. Journal of Eukaryotic Microbiology 35(3), 418-422.

Dayeh, S.A., Butler, D.P., Celik-Butler, Z., 2005. Micromachined infrared bolometers on flexible polyimide substrates. Sensors and Actuators A: Physical 118(1), 49-56.

De Vargas, C., Audic, S., Henry, N., Decelle, J., Mahé, F., Logares, R., Lara, E., Berney, C., Le Bescot, N., Probert, I., 2015. Eukaryotic plankton diversity in the sunlit ocean. Science 348(6237), 1261605.

De Wit, R., Bouvier, T., 2006. 'Everything is everywhere, but, the environment selects'; what did Baas Becking and Beijerinck really say? Environmental Microbiology 8(4), 755-758.

Deeds, J.R., Schwartz, M.D., 2010. Human risk associated with palytoxin exposure. Toxicon 56(2), 150-162.

Degerlund, M., Huseby, S., Zingone, A., Sarno, D., Landfald, B., 2012. Functional diversity in cryptic species of *Chaetoceros socialis* Lauder (Bacillariophyceae). Journal of Plankton Research 34(5), 416-431.

Del Campo, J., Balagué, V., Forn, I., Lekunberri, I., Massana, R., 2013. Culturing bias in marine heterotrophic flagellates analyzed through seawater enrichment incubations. Microbial ecology 66(3), 489-499.

Del Campo, J., Guillou, L., Hehenberger, E., Logares, R., López-García, P., Massana, R., 2016. Ecological and evolutionary significance of novel protist lineages. European Journal of Protistology 55, 4-11.

Del Campo, J., Sieracki, M.E., Molestina, R., Keeling, P., Massana, R., Ruiz-Trillo, I., 2014. The others: our biased perspective of eukaryotic genomes. Trends in Ecology & Evolution 29(5), 252-259.

Dell'Aversano, C., Ciminiello, P., Iacovo, E.D., Tartaglione, L., Forino, M., Casabianca, S., Penna, A., 2014. *Ostreopsis* cf. *ovata* from the Mediterranean area. Variability in toxin profiles and structural elucidation of unknowns through LC-HRMSn, *In* MacKenzie, A.L. (Ed.) 2015. Proceedings of the 16th International Conference on Harmful Algae. International Society for the Study of Harmful Algae and Intergovernmental Oceanographic Commission of UNESCO, 40-40.

Dell'Aversano, C., Tartaglione, L., Iacovo, E.D., Forino, M., Casabianca, S., Penna, A., Ciminiello, P., 2015. *Ostreopsis* cf. *ovata* from the Mediterranean area. Variability in toxin profiles and structural elucidation of unknowns through LC-HRMSn, *In* MacKenzie, A.L. (Ed.) 2015. Proceedings of the 16th International Conference on Harmful Algae. International Society for the Study of Harmful Algae and Intergovernmental Oceanographic Commission of UNESCO, 70-73

Doblin, M. A., Blackburn, S. I. and Hallegraeff, G. M. 2000. Intraspecific variation in the selenium requirement of different geographic strains of the toxic dinoflagellate *Gymnodinium catenatum*. Journal of Plankton Research 22, 421-432.

Donadio, S., Staver, M.J., McAlpine, J.B., Swanson, S.J., Katz, L., 1991. Modular organization of genes required for complex polyketide biosynthesis. Science 252(5006), 675-679.

Dorantes-Aranda, J.J., Seger, A., Mardones, J.I., Nichols, P.D., Hallegraeff, G.M., 2015. Progress in understanding algal bloom-mediated fish kills: the role of superoxide radicals, phycotoxins and fatty acids. PloS one 10(7), e0133549.

Dorantes-Aranda, J.J., Waite, T.D., Godrant, A., Rose, A.L., Tovar, C.D., Woods, G.M., Hallegraeff, G.M., 2011. Novel application of a fish gill cell line assay to assess ichthyotoxicity of harmful marine microalgae. Harmful Algae 10(4), 366-373.

Driscoll, W.W., Hackett, J.D., Ferrière, R., 2016. Eco-evolutionary feedbacks between private and public goods: evidence from toxic algal blooms. Ecology Letters 19(1), 81-97.

Du Yoo, Y., Jeong, H.J., Lee, S.Y., Yoon, E.Y., Kang, N.S., Lim, A.S., Lee, K.H., Jang, S.H., Park, J.Y., Kim, H.S., 2015. Feeding by heterotrophic protists on the toxic dinoflagellate *Ostreopsis* cf. *ovata*. Harmful Algae 49, 1-9.

Durando, P., Ansaldi, F., Oreste, P., Moscatelli, P., Marensi, L., Grillo, C., Gasparini, R., Icardi, G. and Collaborative Group for the Ligurian Syndromic Algal Surveillance, 2007. Ostreopsis ovata and human health: epidemiological and clinical features of respiratory syndrome outbreaks from a two-year syndromic surveillance, 2005–06, in north-west Italy. Euro Surveill, 12(6), p. E070607.

Edwards, K.F., Klausmeier, C.A., Litchman, E., 2011. Evidence for a three way trade off between nitrogen and phosphorus competitive abilities and cell size in phytoplankton. Ecology 92(11), 2085-2095.

Eichholz, K., Beszteri, B., John, U., 2012. Putative monofunctional type I polyketide synthase units: a dinoflagellate-specific feature? PloS One 7(11), e48624.

Ellison, C.E., Hall, C., Kowbel, D., Welch, J., Brem, R.B., Glass, N., Taylor, J.W., 2011. Population genomics and local adaptation in wild isolates of a model microbial eukaryote. Proceedings of the National Academy of Sciences 108(7), 2831-2836.

Emanuelsson, O., Nielsen, H., Heijne, G.V., 1999. ChloroP, a neural network-based method for predicting chloroplast transit peptides and their cleavage sites. Protein Science 8(5), 978-984.

Eppley, R.W., Sloan, P.R., 1966. Growth rates of marine phytoplankton: correlation with light absorption by cell chlorophyll a. Physiologia Plantarum 19(1), 47-59.

Escalera, L., Benvenuto, G., Scalco, E., Zingone, A. and Montresor, M., 2014. Ultrastructural features of the benthic dinoflagellate *Ostreopsis* cf. *ovata* (Dinophyceae). Protist 165(3), 260-274.

Evans, K.M., Kühn, S.F., Hayes, P.K., 2005. High levels of genetic diversity and low levels of genetic differciation in North Sea *Pseudo-nitzschia pungens* (Bacillariophyceae) populations. Journal of Phycology 41(3), 506-514.

Excoffier, L., Lischer, H.E., 2010. Arlequin suite ver 3.5: a new series of programs to perform population genetics analyses under Linux and Windows. Molecular ecology resources 10(3), 564-567.

Faimali, M., Giussani, V., Piazza, V., Garaventa, F., Corrà, C., Asnaghi, V., Privitera, D., Gallus, L., Cattaneo-Vietti, R., Mangialajo, L., 2012. Toxic effects of harmful benthic dinoflagellate *Ostreopsis ovata* on invertebrate and vertebrate marine organisms. Marine Environmental Research 76, 97-107.

Falkowski, P.G. and LaRoche, J., 1991. Acclimation to spectral irradiance in algae. Journal of Phycology 27(1), 8-14

Falkowski, P.G., Barber, R.T., Smetacek, V., 1998. Biogeochemical controls and feedbacks on ocean primary production. Science 281(5374), 200-206.

Falkowski, P.G., Katz, M.E., Knoll, A.H., Quigg, A., Raven, J.A., Schofield, O., Taylor, F., 2004. The evolution of modern eukaryotic phytoplankton. Science 305(5682), 354-360.

Falkowski, P.G., Raven, J.A., 2013. Aquatic photosynthesis. Princeton University Press.

Farrell, H., Brett, S., Ajani, P., Murray, S., 2013. Distribution of the genus *Alexandrium* (Halim) and paralytic shellfish toxins along the coastline of New South Wales, Australia. Marine Pollution Bulletin 72(1), 133-145.

Faust, M.A., 1995. Observation of sand dwelling toxic dinoflagellates (Dinophyceae) from widely differing sites, including two new species. Journal of Phycology 31(6), 996-1003.

Faust, M.A., 1999. Three new *Ostreopsis* species (Dinophyceae): *O. marinus* sp. nov., *O. belizeanus* sp. nov., and *O. caribbeanus* sp. nov. Phycologia 38(2), 92-99.

Faust, M.A., Morton, S.L., 1995. Morphology and ecology of the marine dinoflagellate *Ostreopsis Labens* Sp. Nov. (Dinophyceae). Journal of Phycology 31(3), 456-463.

Faust, M.A., Morton, S.L., Quod, J.P., 1996. Further SEM study of Marine dinoflagellates: the genus *Ostreopsis* (Dinophyceae) Journal of Phycology 32(6), 1053-1065.

Fenchel, T., 2005. Cosmopolitan microbes and their 'cryptic'species. Aquatic Microbial Ecology 41(1), 49-54.

Fenchel, T., Finlay, B.J., 2004. The ubiquity of small species: patterns of local and global diversity. Bioscience 54(8), 777-784.

Finlay, B.J., 2002. Global dispersal of free-living microbial eukaryote species. Science 296(5570), 1061-1063.

Finn, R.D., Bateman, A., Clements, J., Coggill, P., Eberhardt, R.Y., Eddy, S.R., Heger, A., Hetherington, K., Holm, L., Mistry, J., 2013. Pfam: the protein families database. Nucleic Acids Research, gkt1223.

Finn, R.D., Clements, J., Eddy, S.R., 2011. HMMER web server: interactive sequence similarity searching. Nucleic Acids Research, gkr367.

Firn, R.D., Jones, C.G., 2003. Natural products–a simple model to explain chemical diversity. Natural Product Reports 20(4), 382-391.

Foissner, W., 2006. Biogeography and dispersal of micro-organisms: a review emphasizing protists. Acta Protozoologica 45(2), 111-136.

Forster, D., Dunthorn, M., Mahé, F., Dolan, J.R., Audic, S., Bass, D., Bittner, L., Boutte, C., Christen, R., Claverie, J.-M., 2016. Benthic protists: the under-charted majority. FEMS Microbiology Ecology 92(8), fiw120.

Fukuyo, Y., 1981. Taxonomical study on benthic dinoflagellates collected in coral reefs [French Polynesia, Japan]. Bulletin of the Japanese Society of Scientific Fisheries 47(8), 967-978.

García-Altares, M., Tartaglione, L., Dell'Aversano, C., Carnicer, O., de la Iglesia, P., Forino, M., Diogène, J., Ciminiello, P., 2014. The novel ovatoxin-g and isobaric palytoxin (so far referred to as putative palytoxin) from *Ostreopsis* cf. *ovata* (NW Mediterranean Sea): structural insights by LC-high resolution MSn. Analytical and Bioanalytical Chemistry, 1-14.

Glibert, P.M., 2016. Margalef revisited: A new phytoplankton mandala incorporating twelve dimensions, including nutritional physiology. Harmful Algae 55, 25-30.

Godhe, A., Egardt, J., Kleinhans, D., Sundqvist, L., Hordoir, R., Jonsson, P.R., 2013. Seascape analysis reveals regional gene flow patterns among populations of a marine planktonic diatom. Proceedings of the Royal Society of London B: Biological Sciences 280(1773), 20131599.

Godhe, A., McQuoid, M.R., Karunasagar, I., Karunasagar, I., Rehnstam Holm, A.S., 2006. Comparison of three common molecular tools for distinguishing among geographically

separated clones of the diatom *Skeletonema marinoi* Sarno et Zingone (Bacillariophyceae). Journal of Phycology 42(2), 280-291.

Godhe, A., Sjöqvist, C., Sildever, S., Sefbom, J., Harðardóttir, S., Bertos Fortis, M., Bunse, C., Gross, S., Johansson, E., Jonsson, P.R., 2016. Physical barriers and environmental gradients cause spatial and temporal genetic differentiation of an extensive algal bloom. Journal of Biogeography. 43, 1130–1142

Gómez, F., 2012. A quantitative review of the lifestyle, habitat and trophic diversity of dinoflagellates (Dinoflagellata, Alveolata). Systematics and Biodiversity 10(3), 267-275.

Guerrini, F., Pezzolesi, L., Feller, A., Riccardi, M., Ciminiello, P., Dell'Aversano, C., Tartaglione, L., Iacovo, E.D., Fattorusso, E., Forino, M., 2010. Comparative growth and toxin profile of cultured *Ostreopsis ovata* from the Tyrrhenian and Adriatic Seas. Toxicon 55(2), 211-220.

Guillard, R. R. 1975. Culture of phytoplankton for feeding marine invertebrates. *In* Smith, W. L. and Chanley, M. H. (Eds) *Culture of marine invertebrate animals* Springer, US pp. 29-60.

Guillou, L., Bachar, D., Audic, S., Bass, D., Berney, C., Bittner, L., Boutte, C., Burgaud, G., de Vargas, C., Decelle, J., del Campo, J., Dolan, J.R., Dunthorn, M., Edvardsen, B., Holzmann, M., Kooistra, W.H.C.F., Lara, E., Le Bescot, N., Logares, R., Mahé, F., Massana, R., Montresor, M., Morard, R., Not, F., Pawlowski, J., Probert, I., Sauvadet, A.-L., Siano, R., Stoeck, T., Vaulot, D., Zimmermann, P., Christen, R., 2013. The Protist Ribosomal Reference database (PR2): a catalog of unicellular eukaryote Small Sub-Unit rRNA sequences with curated taxonomy. Nucleic Acids Research 41(D1), D597-D604.

Guiry, M.D., 2012. How many species of algae are there? Journal of Phycology 48(5), 1057-1063.

Habermann, E., 1989. Palytoxin acts through Na^+, K^+-ATPase. Toxicon 27(11), 1171-1187.

Hackett, J.D., Anderson, D.M., Erdner, D.L., Bhattacharya, D., 2004. Dinoflagellates: a remarkable evolutionary experiment. American Journal of Botany 91(10), 1523-1534.

Hall, T.A., 1999. BioEdit: a user-friendly biological sequence alignment editor and analysis program for Windows 95/98/NT, Nucleic acids symposium series, 95-98.

Hallegraeff, G.M., 1993. A review of harmful algal blooms and their apparent global increase. Phycologia 32(2), 79-99.

Hallegraeff, G.M., 2010. Ocean climate change, phytoplankton community responses, and harmful algal blooms: a formidable predictive challenge. Journal of Phycology 46(2), 220-235.

Hamilton, W.D., 1964. The genetical evolution of social behaviour. II. Journal of Theoretical Biology 7(1), 17-52.

Harvey, E.L., Menden-Deuer, S., Rynearson, T.A., 2015. Persistent Intra-Specific Variation in Genetic and Behavioral Traits in the Raphidophyte, *Heterosigma akashiwo*. Frontiers in Microbiology 6.

Heger, T.J., Edgcomb, V.P., Kim, E., Lukeš, J., Leander, B.S., Yubuki, N., 2014. A resurgence in field research is essential to better understand the diversity, ecology, and evolution of microbial eukaryotes. Journal of Eukaryotic Microbiology 61(2) 214-223.

Heimann, K., Sparrow, L. and Blair, D. 2009. Interim report on the continuing development of the toxic dinoflagellates atlas. In Marine and Tropical Sciences Research Facility (Ed) June Interim Report (Part 1), Reef and Rainforest Research Center, Cairns, 1-25

Hennige, S., Suggett, D.J., Warner, M.E., McDougall, K., Smith, D.J., 2009. Photobiology of *Symbiodinium* revisited: bio-physical and bio-optical signatures. Coral Reefs 28(1), 179-195.

Hill, R., Ralph, P.J., 2008. Dark-induced reduction of the plastoquinone pool in zooxanthellae of scleractinian corals and implications for measurements of chlorophyll a fluorescence. Symbiosis 46(1):45-56

Hill, R., Szabó, M., ur Rehman, A., Vass, I., Ralph, P.J., Larkum, A.W., 2014. Inhibition of photosynthetic CO2 fixation in the coral Pocillopora damicornis and its relationship to thermal bleaching. Journal of Experimental Biology 217(12), 2150-2162.

Hirsh, J.K., Wu, C.H., 1997. Palytoxin-induced single-channel currents from the sodium pump synthesized by in vitro expression. Toxicon 35(2), 169-176.

Hoffmann, T., Krug, D., Hüttel, S. and Müller, R., 2014. Improving natural products identification through targeted LC-MS/MS in an untargeted secondary metabolomics workflow. Analytical Chemistry, 86(21), 10780-10788.

Holmes, M., Gillespie, N. and Lewis, R. 1988. Toxicity and morphology of *Ostreopsis* cf. *siamensis* cultured from a ciguatera endemic region of Queensland, Australia. In Choat, J. H., Barnes, D., Borowitzka, M. A. et al. (Eds) Proceedings 6th International Coral Reef Symposium. 6th International Coral Reef Symposium Executive Committee, Townsville, 49–54.

Holmes, M.J., Lewis, R.J., Jones, A., Hoy, A.W.W., 1995. Cooliatoxin, the first toxin from *Coolia monotis* (Dinophyceae). Natural Toxins 3(5), 355-362.

Honsell, G., Bonifacio, A., De Bortoli, M., Penna, A., Battocchi, C., Ciminiello, P., Dell'Aversano, C., Fattorusso, E., Sosa, S., Yasumoto, T., 2013. New insights on cytological and metabolic features of *Ostreopsis* cf. *ovata* Fukuyo (Dinophyceae): A multidisciplinary approach. PLoS One 8(2), e57291.

Hoppenrath, M., Bachvaroff, T.R., Handy, S.M., Delwiche, C.F., Leander, B.S., 2009. Molecular phylogeny of ocelloid-bearing dinoflagellates (Warnowiaceae) as inferred from SSU and LSU rDNA sequences. BMC evolutionary biology 9(1), 116-130

Hoppenrath, M., Murray, S. A., Chomérat, N. and Horiguchi, T. 2014. Marine benthic dinoflagellates-unveiling their worldwide biodiversity, Kleine Senckenberg-Reihe, Frankfurt am Main, 116-126

Hopwood, D.A., 1997. Genetic contributions to understanding polyketide synthases. Chemical Reviews 97(7), 2465-2498.

Hopwood, D.A., Sherman, D.H., 1990. Molecular genetics of polyketides and its comparison to fatty acid biosynthesis. Annual Review of Genetics 24(1), 37-62.

Hou, Y., Lin, S., 2009. Distinct gene number-genome size relationships for eukaryotes and non-eukaryotes: gene content estimation for dinoflagellate genomes. PLoS One 4(9), e6978.

Hulot, F.D., Lacroix, G., Lescher-Moutoue, F., Loreau, M., 2000. Functional diversity governs ecosystem response to nutrient enrichment. Nature 405(6784), 340-344.

Hutchinson, G.E., 1961. The paradox of the plankton. The American Naturalist 95(882), 137-145.

Hwang, B.S., Yoon, E.Y., Kim, H.S., Yih, W., Park, J.Y., Jeong, H.J., Rho, J.-R., 2013. Ostreol A: A new cytotoxic compound isolated from the epiphytic dinoflagellate *Ostreopsis* cf. *ovata* from the coastal waters of Jeju Island, Korea. Bioorganic & Medicinal Chemistry Letters 23(10), 3023-3027.

Iglesias-Prieto, R., Trench, R., 1997. Acclimation and adaptation to irradiance in symbiotic dinoflagellates. Response of chlorophyll–protein complexes to different photon-flux densities. Marine Biology 130(1), 23-33.

Ives, J.D., 1987. Possible mechanisms underlying copepod grazing responses to levels of toxicity in red tide dinoflagellates. Journal of Experimental Marine Biology and Ecology 112(2), 131-144.

Janouškovec, J., Gavelis, G.S., Burki, F., Dinh, D., Bachvaroff, T.R., Gornik, S.G., Bright, K.J., Imanian, B., Strom, S.L., Delwiche, C.F., 2017. Major transitions in dinoflagellate evolution unveiled by phylotranscriptomics. Proceedings of the National Academy of Sciences 114(2), 171-180.

Jassby, A.D., Platt, T., 1976. Mathematical formulation of the relationship between photosynthesis and light for phytoplankton. Limnology and Oceanography 21(4), 540-547.

Jenke-Kodama, H., Dittmann, E., 2009. Evolution of metabolic diversity: insights from microbial polyketide synthases. Phytochemistry 70(15), 1858-1866.

Jenke-Kodama, H., Müller, R., Dittmann, E., 2008. Evolutionary mechanisms underlying secondary metabolite diversity. Natural Compounds as Drugs Volume I, 119-140.

Jenke-Kodama, H., Sandmann, A., Müller, R., Dittmann, E., 2005. Evolutionary implications of bacterial polyketide synthases. Molecular Biology and Evolution 22(10), 2027-2039.

John, U., Litaker, R.W., Montresor, M., Murray, S., Brosnahan, M.L., Anderson, D.M., 2014. Formal revision of the *Alexandrium tamarense* species complex (Dinophyceae) taxonomy: the introduction of five species with emphasis on molecular-based (rDNA) classification. Protist 165(6), 779-804.

John, U., Tillmann, U., Hülskötter, J., Alpermann, T.J., Wohlrab, S., Van de Waal, D.B., 2015. Intraspecific facilitation by allelochemical mediated grazing protection within a toxigenic dinoflagellate population. Proceedings of the Royal Society of London B: Biological Sciences 282(1798), 20141268.

Johnson, C.R., Banks, S.C., Barrett, N.S., Cazassus, F., Dunstan, P.K., Edgar, G.J., Frusher, S.D., Gardner, C., Haddon, M., Helidoniotis, F., 2011. Climate change cascades: Shifts in oceanography, species' ranges and subtidal marine community dynamics in eastern Tasmania. Journal of Experimental Marine Biology and Ecology 400(1), 17-32.

Kalaitzis, J.A., Chau, R., Kohli, G.S., Murray, S.A., Neilan, B.A., 2010. Biosynthesis of toxic naturally-occurring seafood contaminants. Toxicon 56(2), 244-258.

Kang, N.S., Jeong, H.J., Lee, S.Y., Lim, A.S., Lee, M.J., Kim, H.S., Yih, W., 2013. Morphology and molecular characterization of the epiphytic benthic dinoflagellate *Ostreopsis* cf. *ovata* in the temperate waters off Jeju Island, Korea. Harmful Algae 27, 98-112.

Katoh, K., Misawa, K., Kuma, K.., Miyata, T., 2002. MAFFT: a novel method for rapid multiple sequence alignment based on fast Fourier transform. Nucleic Acids Research 30(14), 3059-3066.

Kaul, P., Farmer, M., Ciereszko, L., 1974. Pharmacology of palytoxin: The most potent marine toxin known, Proceeding of Western Pharmacological Society 17, 294-301.

Kearney, M., Simpson, S.J., Raubenheimer, D., Helmuth, B., 2010. Modelling the ecological niche from functional traits. Philosophical Transactions of the Royal Society of London B: Biological Sciences 365(1557), 3469-3483.

Kearse, M., Moir, R., Wilson, A., Stones-Havas, S., Cheung, M., Sturrock, S., Buxton, S., Cooper, A., Markowitz, S., Duran, C., 2012. Geneious Basic: an integrated and extendable desktop software platform for the organization and analysis of sequence data. Bioinformatics 28(12), 1647-1649.

Keeling, P.J., Burger, G., Durnford, D.G., Lang, B.F., Lee, R.W., Pearlman, R.E., Roger, A.J., Gray, M.W., 2005. The tree of eukaryotes. Trends in Ecology & Evolution 20(12), 670-676.

Keeling, P.J., Burki, F., Wilcox, H.M., Allam, B., Allen, E.E., Amaral-Zettler, L.A., Armbrust, E.V., Archibald, J.M., Bharti, A.K., Bell, C.J., Beszteri, B., Bidle, K.D., Cameron, C.T., Campbell, L., Caron, D.A., Cattolico, R.A., Collier, J.L., Coyne, K., Davy, S.K., Deschamps, P., Dyhrman, S.T., Edvardsen, B., Gates, R.D., Gobler, C.J., Greenwood, S.J., Guida, S.M., Jacobi, J.L., Jakobsen, K.S., James, E.R., Jenkins, B., John, U., Johnson, M.D., Juhl, A.R., Kamp, A., Katz, L.A., Kiene, R., Kudryavtsev, A., Leander, B.S., Lin, S., Lovejoy, C., Lynn, D., Marchetti, A., McManus, G., Nedelcu, A.M., Menden-Deuer, S., Miceli, C., Mock, T., Montresor, M., Moran, M.A., Murray, S., Nadathur, G., Nagai, S., Ngam, P.B., Palenik, B., Pawlowski, J., Petroni, G., Piganeau, G., Posewitz, M.C., Rengefors, K., Romano, G., Rumpho, M.E., Rynearson, T., Schilling, K.B., Schroeder, D.C., Simpson, A.G.B., Slamovits, C.H., Smith, D.R., Smith, G.J., Smith, S.R., Sosik, H.M., Stief, P., Theriot, E., Twary, S.N., Umale, P.E., Vaulot, D., Wawrik, B., Wheeler, G.L., Wilson, W.H., Xu, Y., Zingone, A., Worden, A.Z., 2014. The Marine Microbial Eukaryote Transcriptome Sequencing Project (MMETSP): Illuminating the Functional Diversity of Eukaryotic Life in the Oceans through Transcriptome Sequencing. PLoS Biology 12(6), e1001889.

Kellmann, R., Orr, R.J., Svendsen, H.M., Jakobsen, K.S., 2010. Biosynthesis and molecular genetics of polyketides in marine dinoflagellates. Marine Drugs 8(4), 1011-1048.

Kellmann, R., Stuken, A., Orr, R.J., Svendsen, H.M., Jakobsen, K.S., 2010. Biosynthesis and molecular genetics of polyketides in marine dinoflagellates. Marine Drugs 8(4), 1011-1048.

Khosla, C., Gokhale, R.S., Jacobsen, J.R. and Cane, D.E., 1999. Tolerance and specificity of polyketide synthases. Annual Review of Biochemistry, 68(1), 219-253.

Kimura, K., Okuda, S., Nakayama, K., Shikata, T., Takahashi, F., Yamaguchi, H., Skamoto, S., Yamaguchi, M., Tomaru, Y., 2015. RNA Sequencing Revealed Numerous Polyketide Synthase Genes in the Harmful Dinoflagellate *Karenia mikimotoi*. PloS One 10(11), e0142731.

Klueter, A., Crandall, J.B., Archer, F.I., Teece, M.A., Coffroth, M.A., 2015. Taxonomic and environmental variation of metabolite profiles in marine dinoflagellates of the genus *Symbiodinium*. Metabolites 5(1), 74-99.

Knowlton, N., 1993. Sibling Species in the Sea. Annual Review of Ecology and Systematics 24, 189-216.

Kobayashi, J.i., Kubota, T., 2007. Bioactive Macrolides and Polyketides from Marine Dinoflagellates of the Genus *Amphidinium*. Journal of Natural Products 70(3), 451-460.

Kodama, A. M., Hokama, Y., Yasumoto, T., Fukui, M., Jo Manea, S. and Sutherland, N. 1989. Clinical and laboratory findings implicating palytoxin as cause of ciguatera poisoning due to *Decapterus macrosoma* (mackerel). Toxicon 27: 1051-3.

Koester, J.A., Swalwell, J.E., Von Dassow, P., Armbrust, E.V., 2010. Genome size differentiates co-occurring populations of the planktonic diatom *Ditylum brightwellii* (Bacillariophyta). BMC Evolutionary Biology 10(1), 1.

Kohli, G. S., Murray, S. A., Neilan, B. A. et al. 2014. High abundance of the potentially maitotoxic dinoflagellate *Gambierdiscus carpenteri* in temperate waters of New South Wales, Australia. Harmful Algae 39, 134-45.

Kohli, G.S., Campbell, K., John, U., Smith, K.F., Fraga, S., Rhodes, L.L., Murray, S.A., 2017. Role of Modular Polyketide Synthases in the Production of Polyether Ladder Compounds in Ciguatoxin-producing *Gambierdiscus polynesiensis* and *G. excentricus* (Dinophyceae). Journal of Eukaryotic Microbiology. doi:10.1111/jeu.12405

Kohli, G.S., John, U., Figueroa, R.I., Rhodes, L.L., Harwood, D.T., Groth, M., Bolch, C.J., Murray, S.A., 2015. Polyketide synthesis genes associated with toxin production in two species of *Gambierdiscus* (Dinophyceae). BMC Genomics 16(1), 410.

Kohli, G.S., John, U., Van Dolah, F.M., Murray, S.A., 2016. Evolutionary distinctiveness of fatty acid and polyketide synthesis in eukaryotes. ISME Journal 10(8), 1877-1890.

Kohli, G.S., Murray, S.A., Neilan, B.A., Rhodes, L.L., Harwood, D.T., Smith, K.F., Meyer, L., Capper, A., Brett, S., Hallegraeff, G.M., 2014. High abundance of the potentially maitotoxic dinoflagellate *Gambierdiscus carpenteri* in temperate waters of New South Wales, Australia. Harmful Algae 39, 134-145.

Kolber, Z., Falkowski, P.G., 1993. Use of active fluorescence to estimate phytoplankton photosynthesis *in situ*. Limnology and Oceanography 38(8), 1646-1665.

Kolber, Z.S., Prášil, O., Falkowski, P.G., 1998. Measurements of variable chlorophyll fluorescence using fast repetition rate techniques: defining methodology and experimental protocols. Biochimica et Biophysica Acta (BBA)-Bioenergetics 1367(1), 88-106.

Kremp, A., Godhe, A., Egardt, J., Dupont, S., Suikkanen, S., Casabianca, S., Penna, A., 2012. Intraspecific variability in the response of bloom forming marine microalgae to changed climate conditions. Ecology and Evolution 2(6), 1195-1207.

Kremp, A., Oja, J., LeTortorec, A.H., Hakanen, P., Tahvanainen, P., Tuimala, J., Suikkanen, S., 2016. Diverse seed banks favour adaptation of microalgal populations to future climate conditions. Environmental Microbiology. 18(2), 679–691

Kremp, A., Tahvanainen, P., Litaker, W., Krock, B., Suikkanen, S., Leaw, C.P., Tomas, C., 2014. Phylogenetic relationships, morphological variation, and toxin patterns in the *Alexandrium ostenfeldii* (Dinophyceae) complex: implications for species boundaries and identities. Journal of Phycology 50(1), 81-100.

Kromkamp, J.C., Forster, R.M., 2003. The use of variable fluorescence measurements in aquatic ecosystems: differences between multiple and single turnover measuring protocols and suggested terminology. European Journal of Phycology 38(2), 103-112.

LaJeunesse, T.C., 2001. Investigating the biodiversity, ecology, and phylogeny of endosymbiotic dinoflagellates in the genus *Symbiodinium* using the ITS region: in search of a "species" level marker. Journal of Phycology 37(5), 866-880.

LaJeunesse, T.C., Lambert, G., Andersen, R.A., Coffroth, M.A., Galbraith, D.W., 2005. *Symbiodinium* (Pyrrhophyta) genome sizes (DNA content) are smallest among dinoflagellates Journal of Phycology 41(4), 880-886.

LaJeunesse, T.C., Parkinson, J.E., Reimer, J.D., 2012. A genetics-based description of *Symbiodinium minutum* sp. nov. and *S. psygmophilum* sp. nov. (Dinophyceae), two dinoflagellates symbiotic with cnidaria. Journal of Phycology 48(6), 1380-1391.

Lang, B.F. and Burger, G., 2007. Purification of mitochondrial and plastid DNA. Nature Protocols 2(3), 652-660.

Lartigue, J., Jester, E. L. E., Dickey, R. W. and Villareal, T. A. 2009. Nitrogen source effects on the growth and toxicity of two strains of the ciguatera-causing dinoflagellate *Gambierdiscus toxicus*. Harmful Algae 8, 781-791.

Last, P.R., White, W.T., Gledhill, D.C., Hobday, A.J., Brown, R., Edgar, G.J., Pecl, G., 2011. Long-term shifts in abundance and distribution of a temperate fish fauna: a response to climate change and fishing practices. Global Ecology and Biogeography 20(1), 58-72.

Lavaud, J., Strzepek, R.F., Kroth, P.G., 2007. Photoprotection capacity differs among diatoms: possible consequences on the spatial distribution of diatoms related to fluctuations in the underwater light climate. Limnology and Oceanography 52(3), 1188-1194.

Laza-Martínez, A., David, H., Riobó, P., Miguel, I., Orive, E., 2016. Characterization of a Strain of *Fukuyoa paulensis* (Dinophyceae) from the Western Mediterranean Sea. Journal of Eukaryotic Microbiology 63(4), 481-497.

Laza-Martinez, A., Orive, E. and Miguel, I. 2011. Morphological and genetic characterization of benthic dinoflagellates of the genera *Coolia*, *Ostreopsis* and *Prorocentrum* from the south-eastern Bay of Biscay. European Journal of Phycology 46, 45-65.

Le Bescot, N., Mahé, F., Audic, S., Dimier, C., Garet, M.J., Poulain, J., Wincker, P., Vargas, C., Siano, R., 2015. Global patterns of pelagic dinoflagellate diversity across protist size classes unveiled by metabarcoding. Environmental Microbiology. 18, 609–626

Le Gac, M., Metegnier, G., Chomérat, N., Malestroit, P., Quéré, J., Bouchez, O., Siano, R., Destombe, C., Guillou, L., Chapelle, A., 2016. Evolutionary processes and cellular functions underlying divergence in *Alexandrium minutum*. Molecular Ecology 25(20), 5129-5143.

Leaw, C. P., Lim, P. T., Ahmad, A. and Usup, G. 2001. Genetic diversity of *Ostreopsis ovata* (Dinophyceae) from Malaysia. Marine Biotechnology 3, 246-55.

Leaw, C.P., Lim, P.T., Cheng, K.W., Ng, B.K., Usup, G., 2010. Morphology and molecular characterization of a new species of thecate benthic dinoflagellate, *Coolia malayensis* sp. nov. (Dinophyceae). Journal of Phycology 46(1), 162-171.

Leaw, C.P., Tan, T.H., Lim, H.C., Teng, S.T., Yong, H.L., Smith, K.F., Rhodes, L., Wolf, M., Holland, W.C., Vandersea, M.W., 2016. New scenario for speciation in the benthic dinoflagellate genus *Coolia* (Dinophyceae). Harmful Algae 55, 137-149.

Lee, H.H., Molla, M.N., Cantor, C.R., Collins, J.J., 2010. Bacterial charity work leads to population-wide resistance. Nature 467(7311), 82-85.

Lei, J., Zhou, J., 2002. A marine natural product database. Journal of chemical information and computer sciences 42(3), 742-748.

Lenoir, S., Ten-Hage, L., Turquet, J., Quod, J., Hennion, M., 2006. Characterisation of new analogues of palytoxin isolated from an *Ostreopsis mascarenensis* bloom in the south-western Indian Ocean. African Journal of Marine Science 28(2), 389-391.

Lenoir, S., Ten-Hage, L., Turquet, J., Quod, J.P., Bernard, C., Hennion, M.C., 2004. First evidence of palytoxin analogues from an *Ostreopsis mascarenensis* (Dinophyceae) benthic bloom in South western Indian ocean Journal of Phycology 40(6), 1042-1051.

Lidie, K.B., Van Dolah, F.M., 2007. Spliced leader RNA-mediated trans-splicing in a dinoflagellate, *Karenia brevis*. Journal of Eukaryotic Microbiology 54(5), 427-435.

Lin, S., Cheng, S., Song, B., Zhong, X., Lin, X., Li, W., Li, L., Zhang, Y., Zhang, H., Ji, Z., 2015. The *Symbiodinium kawagutii* genome illuminates dinoflagellate gene expression and coral symbiosis. Science 350(6261), 691-694.

Lin, S., Zhang, H., Gray, M.W., 2008. RNA editing in dinoflagellates and its implications for the evolutionary history of the editing machinery. RNA and DNA editing: molecular mechanisms and their integration into biological systems, 280-309.

Ling, S., Johnson, C., Ridgway, K., Hobday, A., Haddon, M., 2009. Climate-driven range extension of a sea urchin: inferring future trends by analysis of recent population dynamics. Global Change Biology 15(3), 719-731.

Litaker, R.W., Vandersea, M.W., Faust, M.A., Kibler, S.R., Chinain, M., Holmes, M.J., Holland, W.C., Tester, P.A., 2009. Taxonomy of *Gambierdiscus* including four new species, *Gambierdiscus caribaeus*, *Gambierdiscus carolinianus*, *Gambierdiscus carpenteri* and *Gambierdiscus ruetzleri* (Gonyaulacales, Dinophyceae). Phycologia 48(5), 344-390.

Litchman, E., Klausmeier, C.A., 2008. Trait-based community ecology of phytoplankton. Annual Review of Ecology, Evolution, and Systematics 39, 615-639.

Litchman, E., Klausmeier, C.A., Schofield, O.M., Falkowski, P.G., 2007. The role of functional traits and trade-offs in structuring phytoplankton communities: scaling from cellular to ecosystem level. Ecology Letters 10(12), 1170-1181.

Litchman, E., Tezanos Pinto, P., Edwards, K.F., Klausmeier, C.A., Kremer, C.T., Thomas, M.K., 2015. Global biogeochemical impacts of phytoplankton: a trait-based perspective. Journal of Ecology 103(6), 1384-1396.

Liu, Z., Hu, S.K., Campbell, V., Tatters, A.O., Heidelberg, K.B., Caron, D.A., 2017. Single-cell transcriptomics of small microbial eukaryotes: limitations and potential. The ISME Journal. 11 1282–1285

Logares, R., Rengefors, K., Kremp, A., Shalchian-Tabrizi, K., Boltovskoy, A., Tengs, T., Shurtleff, A., Klaveness, D., 2007. Phenotypically different microalgal morphospecies with identical ribosomal DNA: a case of rapid adaptive evolution? Microbial Ecology 53(4), 549-561.

Longnecker, K., Soule, M.C.K., Kujawinski, E.B., 2015. Dissolved organic matter produced by *Thalassiosira pseudonana*. Marine Chemistry 168, 114-123.

López-Legentil, S., Song, B., DeTure, M., Baden, D.G., 2010. Characterization and localization of a hybrid non-ribosomal peptide synthetase and polyketide synthase gene from the toxic dinoflagellate *Karenia brevis*. Marine biotechnology 12(1), 32-41.

Lowe, C.D., Martin, L.E., Montagnes, D.J., Watts, P.C., 2012. A legacy of contrasting spatial genetic structure on either side of the Atlantic–Mediterranean transition zone in a marine protist. Proceedings of the National Academy of Sciences 109(51), 20998-21003.

Lundholm, N., Bates, S.S., Baugh, K.A., Bill, B.D., Connell, L.B., Léger, C., Trainer, V.L., 2012. Crytptic and pseudo-cryptic diversity in diatoms- with descriptions of *Pseudo-nitzchia hasleana* sp. nov. and *P. fryxelliana* sp. nov. Journal of Phycology 48(2), 436-454.

Luo, Z., Yang, W., Leaw, C.P., Pospelova, V., Bilien, G., Liow, G.R., Lim, P.T., Gu, H., 2017. Cryptic diversity within the harmful dinoflagellate *Akashiwo sanguinea* in coastal Chinese waters is related to differentiated ecological niches. Harmful Algae 66, 88-96.

Lynch, M., Walsh, B., 1998. Genetics and analysis of quantitative traits. Sinauer Sunderland, MA.

Malagoli, D., Casarini, L., Ottaviani, E., 2008. Effects of the marine toxins okadaic acid and palytoxin on mussel phagocytosis. Fish & Shellfish Immunology 24(2), 180-186.

Mangialajo, L., Bertolotto, R., Cattaneo-Vietti, R., Chiantore, M., Grillo, C., Lemee, R., Melchiorre, N., Moretto, P., Povero, P., Ruggieri, N., 2008. The toxic benthic dinoflagellate *Ostreopsis ovata*: Quantification of proliferation along the coastline of Genoa, Italy. Marine Pollution Bulletin 56(6), 1209-1214.

Mangialajo, L., Ganzin, N., Accoroni, S., Asnaghi, V., Blanfuné, A., Cabrini, M., Cattaneo-Vietti, R., Chavanon, F., Chiantore, M., Cohu, S., 2011. Trends in *Ostreopsis* proliferation along the Northern Mediterranean coasts. Toxicon 57(3), 408-420.

Mann, D.G., 1999. The species concept in diatoms. Phycologia 38(6), 437-495.

Marañón, E., 2015. Cell size as a key determinant of phytoplankton metabolism and community structure. Annual Review of Marine Science 7, 241-264.

Marchler-Bauer, A., Bo, Y., Han, L., He, J., Lanczycki, C.J., Lu, S., Chitsaz, F., Derbyshire, M.K., Geer, R.C., Gonzales, N.R., 2016. CDD/SPARCLE: functional classification of proteins via subfamily domain architectures. Nucleic Acids Research, gkw1129.

Mardones, J.I., Dorantes-Aranda, J.J., Nichols, P.D., Hallegraeff, G.M., 2015. Fish gill damage by the dinoflagellate *Alexandrium catenella* from Chilean fjords: Synergistic action of ROS and PUFA. Harmful Algae 49, 40-49.

Margalef, R., 1978. Life-forms of phytoplankton as survival alternatives in an unstable environment. Oceanologica acta 1(4), 493-509.

Marinov, G.K., Lynch, M., 2016. Diversity and Divergence of Dinoflagellate Histone Proteins. G3: Genes, Genomes, Genetics 6(2), 397-422.

Masó, M., Garcés, E., Pagès, F., Camp, J., 2003. Drifting plastic debris as a potential vector for dispersing Harmful Algal Bloom (HAB) species. Scientia Marina 67(1), 107-111.

Massana, R., Gobet, A., Audic, S., Bass, D., Bittner, L., Boutte, C., Chambouvet, A., Christen, R., Claverie, J.M., Decelle, J., 2015. Marine protist diversity in European coastal waters and sediments as revealed by high-throughput sequencing. Environmental Microbiology 17(10), 4035-4049.

Masseret, E., Grzebyk, D., Nagai, S., Genovesi, B., Lasserre, B., Laabir, M., Collos, Y., Vaquer, A., Berrebi, P., 2009. Unexpected genetic diversity among and within populations of

the toxic dinoflagellate Alexandrium catenella as revealed by nuclear microsatellite markers. Applied and Environmental Microbiology 75(7), 2037-2045.

McLeod, D.J., Hallegraeff, G.M., Hosie, G.W., Richardson, A.J., 2012. Climate-driven range expansion of the red-tide dinoflagellate *Noctiluca scintillans* into the Southern Ocean. Journal of Plankton Research 34(4), 332-337.

Mercado, J.A., Rivera-Rentas, A.L., Gonzalez, I., Tosteson, T.R., Molgo, J. and Escalona de Motta, G., 1994. Neuro-and myo-toxicity of extracts from the benthic dinoflagellate *Ostreopsis* lenticularis is sensitive to µ-conotoxin. In Soc. Neurosci. Abstracts 20, 718

Meunier, F.A., Mercado, J.A., Molgó, J., Tosteson, T.R., Escalona de Motta, G., 1997. Selective depolarization of the muscle membrane in frog nerve-muscle preparations by a chromatographically purified extract of the dinoflagellate *Ostreopsis lenticularis*. British Journal of Pharmacology 121(6), 1224-1230.

Meyer, J.M., Rödelsperger, C., Eichholz, K., Tillmann, U., Cembella, A., McGaughran, A., 2015. Transcriptomic characterisation and genomic glimps into the toxigenic dinoflagellate *Azadinium spinosum*, with emphasis on polykeitde synthase genes. BMC Genomics 16, 27

Moestrup, Ø.; Akselmann, R.; Fraga, S.; Hoppenrath, M.; Iwataki, M.; Komárek, J.; Larsen, J.; Lundholm, N.; Zingone, A. (Eds) (2009 onwards). IOC-UNESCO Taxonomic Reference List of Harmful Micro Algae. Accessed at http://www.marinespecies.org/hab on 2017-06-20

Monroe, E.A., Van Dolah, F.M., 2008. The toxic dinoflagellate *Karenia brevis* encodes novel type I-like polyketide synthases containing discrete catalytic domains. Protist 159(3), 471-482.

Monti, M., Cecchin, E., 2012. Comparative Growth of Three Strains of *Ostreopsis ovata* at Different Light Intensities with Focus on Inter-Specific Allelopathic Interactions. Cryptogamie Algologie 33(2), 113-119.

Monti, M., Minocci, M., Beran, A., Iveša, L., 2007. First record of *Ostreopsis cfr. ovata* on macroalgae in the Northern Adriatic Sea. Marine Pollution Bulletin 54(5), 598-601.

Montresor, M., Sgrosso, S., Procaccini, G., Kooistra, W.H., 2003. Intraspecific diversity in *Scrippsiella trochoidea* (Dinopbyceae): evidence for cryptic species. Phycologia 42(1), 56-70.

Mooney, B.D., Dorantes-Aranda, J.J., Place, A.R., Hallegraeff, G.M., 2011. Ichthyotoxicity of gymnodinioid dinoflagellates: PUFA and superoxide effects in sheepshead minnow larvae and rainbow trout gill cells. Marine Ecology Progress Series 426, 213-224.

Moore, R.E., Bartolini, G., 1981. Structure of palytoxin. Journal of the American Chemical Society 103(9), 2491-2494.

Morton, S.L., Faust, M.A., 1997. Survey of toxic epiphytic dinoflagellates from the Belizean barrier reef ecosystem. Bulletin of Marine Science 61(3), 899-906.

Moustafa, A., Evans, A.N., Kulis, D.M., Hackett, J.D., Erdner, D.L., Anderson, D.M., Bhattacharya, D., 2010. Transcriptome profiling of a toxic dinoflagellate reveals a gene-rich protist and a potential impact on gene expression due to bacterial presence. PloS One 5(3), e9688.

Munday, R. 2011. Palytoxin toxicology: animal studies. Toxicon 57, 470-7.

Murray, S., Jørgensen, M.F., Ho, S.Y., Patterson, D.J., Jermiin, L.S., 2005. Improving the analysis of dinoflagellate phylogeny based on rDNA. Protist 156(3), 269-286.

Murray, S., Momigliano, P., Heimann, K., Blair, D., 2014. Molecular phylogenetics and morphology of *Gambierdiscus yasumotoi* from tropical eastern Australia. Harmful Algae 39, 242-252.

Murray, S., Suthers, I.M., 1999. Population ecology of *Noctiluca scintillans* Macartney, a red-tide-forming dinoflagellate. Marine and Freshwater Research 50(3), 243-252.

Murray, S.A., Diwan, R., Orr, R.J., Kohli, G.S., John, U., 2015. Gene duplication, loss and selection in the evolution of saxitoxin biosynthesis in alveolates. Molecular Phylogenetics and Evolution 92, 165-180.

Murray, S.A., Garby, T., Hoppenrath, M. and Neilan, B.A., 2012. Genetic diversity, morphological uniformity and polyketide production in dinoflagellates (*Amphidinium*, Dinoflagellata). PLoS One, 7(6), e38253.

Murray, S.A., Garby, T., Hoppenrath, M., Neilan, B.A., 2012a. Genetic diversity, morphological uniformity and polyketide production in dinoflagellates (*Amphidinium*, Dinoflagellata). PloS one 7(6), e38253.

Murray, S.A., Patterson, D.J., Thessen, A.E., 2012b. Transcriptomics and microbial eukaryote diversity: a way forward. Trends in Ecology & Evolution 27(12), 651-652.

Murray, S.A., Suggett, D.J., Doblin, M.A., Kohli, G.S., Seymour, J.R., Fabris, M., Ralph, P.J., 2016. Unravelling the functional genetics of dinoflagellates: a review of approaches and opportunities. Perspectives in Phycology 3(1), 37-52.

Murray, S.A., Wiese, M., Stüken, A., Brett, S., Kellmann, R., Hallegraeff, G., Neilan, B.A., 2011. SxtA-based quantitative molecular assay to identify saxitoxin-producing harmful algal blooms in marine waters. Applied and Environmental Microbiology 77(19), 7050-7057.

Nagai, S., Lian, C., Yamaguchi, S., Hamaguchi, M., Matsuyama, Y., Itakura, S., Shimada, H., Kaga, S., Yamauchi, H., Sonda, Y., 2007. Microsatellite markers reveal population genetic structure of the toxin dinoflagellate *Alexandrium tamarense* (Dinophyceae) in Japanese coastal waters. Journal of Phycology 43(1), 43-54.

Nascimento, S.M., Corrêa, E.V., Menezes, M., Varela, D., Paredes, J., Morris, S., 2012. Growth and toxin profile of *Ostreopsis* cf. *ovata* (Dinophyta) from Rio de Janeiro, Brazil. Harmful Algae 13, 1-9.

Neves, R.A., Fernandes, T., dos Santos, L.N., Nascimento, S.M., 2017. Toxicity of benthic dinoflagellates on grazing, behavior and survival of the brine shrimp *Artemia salina*. PloS One 12(4), e0175168.

Nielsen, K.F., Larsen, T.O., 2015. The importance of mass spectrometric dereplication in fungal secondary metabolite analysis. Frontiers in Microbiology 6, 71.

Nishimura, T., Sato, S., Tawong, W., Sakanari, H., Uehara, K., Shah, M.M.R., Suda, S., Yasumoto, T., Taira, Y., Yamaguchi, H., 2013. Genetic diversity and distribution of the ciguatera-causing dinoflagellate *Gambierdiscus* spp.(Dinophyceae) in coastal areas of Japan. PloS one 8(4), e60882.

Norris, D.R., Bomber, J.W. and Balech, E. 1985. Benthic dinoflagellates associated with ciguatera from Florida Keys I. *Ostreopsis heptagona* sp. nov. *In* Anderson, D. M., White, A. W. and Baden, D. G. (Eds) *Toxic Dinoflagellates*. Elsevier Scientific, New York, pp. 39-44.

Not, F., Siano, R., Kooistra, W.H., Simon, N., Vaulot, D., Probert, I., 2012. Diversity and ecology of eukaryotic marine phytoplankton. Advances in Botanical Research 64, 1-53.

Nunn, G., Theisen, B., Christensen, B., Arctander, P., 1996. Simplicity-correlated size growth of the nuclear 28S ribosomal RNA D3 expansion segment in the crustacean order Isopoda. Journal of Molecular Evolution 42(2), 211-223.

OECD 2006. OECD Guideline for Testing of Chemicals 425. Acute Oral Toxicity – Up-and-Down-Procedure (UDP). Organisation for Economic Co-operation and Development, Paris. http://213.253.134.43/oecd/pdfs/browseit/9742501e.pdf

O'Malley, M.A., 2007. The nineteenth century roots of' everything is everywhere'. Nature Reviews Microbiology 5(8), 647-651.

Onuma, Y., Satake, M., Ukena, T., Roux, J., Chanteau, S., Rasolofonirina, N., Ratsimaloto, M., Naoki, H., Yasumoto, T., 1999. Identification of putative palytoxin as the cause of clupeotoxism. Toxicon 37(1), 55-65.

Orive, E., Pérez Aicua, L., David, H., García-Etxebarria, K., Laza-Martínez, A., Seoane, S., Miguel, I., 2013. The genus *Pseudo-nitzschia* (Bacillariophyceae) in a temperate estuary with description of two new species: *Pseudo-nitzschia plurisecta* sp. nov. and *Pseudo-nitzschia abrensis* sp. nov. Journal of Phycology 49(6), 1192-1206.

Orr, R.J., Murray, S.A., Stüken, A., Rhodes, L., Jakobsen, K.S., 2012. When naked became armored: an eight-gene phylogeny reveals monophyletic origin of theca in dinoflagellates. PloS One 7(11), e50004.

Oxborough, K., Moore, C.M., Suggett, D.J., Lawson, T., Chan, H.G., Geider, R.J., 2012. Direct estimation of functional PSII reaction center concentration and PSII electron flux on a volume basis: a new approach to the analysis of Fast Repetition Rate fluorometry (FRRf) data. Limnology and Oceanography: Methods 10(3), 142-154.

Parra, G., Bradnam, K., Korf, I., 2007. CEGMA: a pipeline to accurately annotate core genes in eukaryotic genomes. Bioinformatics 23(9), 1061-1067.

Parsons, M.L., Aligizaki, K., Bottein, M.-Y.D., Fraga, S., Morton, S.L., Penna, A., Rhodes, L., 2012. *Gambierdiscus* and *Ostreopsis*: Reassessment of the state of knowledge of their taxonomy, geography, ecophysiology, and toxicology. Harmful Algae 14, 107-129.

Patil, J., Rodrigues, R., Paul, P., Sathish, K., Rafi, M., Anil, A., 2017. Benthic dinoflagellate blooms in tropical intertidal rock pools: elucidation of photoprotection mechanisms. Marine Biology 164(4), 89.

Pawlowiez, R., Morey, J., Darius, H., Chinain, M., Van Dolah, F., 2014. Transcriptome sequencing reveals single domain Type I-like polyketide synthases in the toxic dinoflagellate *Gambierdiscus polynesiensis*. Harmful Algae 36, 29-37.

Pearce, I., Marshall, J. and Hallegraeff, G. 2001. Toxic epiphytic dinoflagellates from east coast Tasmania. In Hallegraeff, G., Blackburn, S., Bolch, C., Lewis, R. (Eds) Proceedings of the 9th International Conference on Harmful Algal Blooms. International Society for the Study of Harmful Algae and Intergovernmental Oceanographic Commission of UNESCO, 54-57.

Penna, A., Battocchi, C., Capellacci, S., Fraga, S., Aligizaki, K., Lemée, R., Vernesi, C., 2014. Mitochondrial, but not rDNA, genes fail to discriminate dinoflagellate species in the genus *Ostreopsis*. Harmful Algae 40, 40-50.

Penna, A., Fraga, S., Battocchi, C. et al. 2012. Genetic diversity of the genus *Ostreopsis* Schmidt: phylogeographical considerations and molecular methodology applications for field detection in the Mediterranean Sea. Cryptogamie Algologie 33, 153-63.

Penna, A., Fraga, S., Battocchi, C., Casabianca, S., Giacobbe, M.G., Riobó, P., Vernesi, C., 2010. A phylogeographical study of the toxic benthic dinoflagellate genus *Ostreopsis* Schmidt. Journal of Biogeography 37(5), 830-841.

Penna, A., Fraga, S., Battocchi, C., Casabianca, S., Perini, F., Capellacci, S., Casabianca, A., Riobó, P., Giacobbe, M.G., Totti, C., 2012. Genetic diversity of the genus *Ostreopsis* Schmidt: phylogeographical considerations and molecular methodology applications for field detection in the Mediterranean Sea. Cryptogamie, Algologie 33(2), 153-163.

Penna, A., Vila, M., Fraga, S., Giacobbe, M.G., Andreoni, F., Riobó, P., Vernesi, C., 2005. Characterization of *Ostreopsis* and *Coolia* (Dinophceae) isolates in the western Mediterranean Sea based on Morphology, toxicity and Internal Transcrined spacer 5.8S rDNA sequences. Journal of Phycology 41(1), 212-225.

Petchey, O.L., Gaston, K.J., 2006. Functional diversity: back to basics and looking forward. Ecology Letters 9(6), 741-758.

Pezzolesi, L., Guerrini, F., Ciminiello, P. et al. 2012. Influence of temperature and salinity on *Ostreopsis* cf. *ovata* growth and evaluation of toxin content through HR LC-MS and biological assays. Water Research 46, 82-92.

Pezzolesi, L., Pistocchi, R., Fratangeli, F., Dell'Aversano, C., Iacovo, E.D., Tartaglione, L., 2014. Growth dynamics in relation to the production of the main cellular components in the toxic dinoflagellate *Ostreopsis* cf. *ovata*. Harmful Algae 36, 1-10.

Pin, L.C., Teen, L.P., Ahmad, A., Usup, G., 2001. Genetic diversity of *Ostreopsis ovata* (Dinophyceae) from Malaysia. Marine Biotechnology 3(3), 246-255.

Platt, T., Gallegos, C., Harrison, W., 1981. Photoinhibition of photosynthesis in natural assemblages of marine phytoplankton.

Pochon, X. and Gates, R.D., 2010. A new *Symbiodinium* clade (Dinophyceae) from soritid foraminifera in Hawai'i. Molecular Phylogenetics and Evolution 56(1), 492-497.

Prada, C., Schizas, N.V., Yoshioka, P.M., 2008. Phenotypic plasticity or speciation? A case from a clonal marine organism. BMC Evolutionary Biology 8(1), 47.

Prince, E.K., Myers, T.L., Kubanek, J., 2008. Effects of harmful algal blooms on competitors: allelopathic mechanisms of the red tide dinoflagellate *Karenia brevis*. Limnology and Oceanography 53(2), 531-541.

Rae, P., 1976. Hydroxymethyluracil in eukaryote DNA: a natural feature of the pyrrophyta (dinoflagellates). Science 194(4269), 1062-1064.

Rae, P.M., Steele, R.E., 1978. Modified bases in the DNAs of unicellular eukaryotes: an examination of distributions and possible roles, with emphasis on hydroxymethyluracil in dinoflagellates. Biosystems 10(1), 37-53.

Ramos, V., Salvi, D., Machado, J.P., Vale, M., Azevedo, J., Vasconcelos, V., 2015. Culture-Independent Study of the Late-Stage of a Bloom of the Toxic Dinoflagellate *Ostreopsis* cf. *ovata*: Preliminary Findings Suggest Genetic Differences at the Sub-Species Level and Allow ITS2 Structure Characterization. Toxins 7(7), 2514-2533.

Ramos, V., Vasconcelos, V., 2010. Palytoxin and analogs: biological and ecological effects. Marine Drugs 8(7), 2021-2037.

Rasband, W. S. 1997–2013. Image J, U.S. National Institutes of Health, Bethesda, Maryland, USA, http://imagej.nih.gov/ij/.

Rasheed, M., Wild, C., Franke, U., Huettel, M., 2004. Benthic photosynthesis and oxygen consumption in permeable carbonate sediments at Heron Island, Great Barrier Reef, Australia. Estuarine, Coastal and Shelf Science 59(1), 139-150.

Rein, K.S., Borrone, J., 1999. Polyketides from dinoflagellates: origins, pharmacology and biosynthesis. Comparative Biochemistry and Physiology Part B: Biochemistry and Molecular Biology 124(2), 117-131.

Rengefors, K., Kremp, A., Reusch, T.B., Wood, M., 2017. Genetic diversity and evolution in eukaryotic phytoplankton: revelations from population genetic studies. Journal of Plankton Research 39(2), 165-179

Rengefors, K., Logares, R., Laybourn Parry, J., Gast, R.J., 2015. Evidence of concurrent local adaptation and high phenotypic plasticity in a polar microeukaryote. Environmental Microbiology 17(5), 1510-1519.

Rhodes, L., 2011. World-wide occurrence of the toxic dinoflagellate genus *Ostreopsis* Schmidt. Toxicon 57(3), 400-407.

Rhodes, L., Adamson, J., Suzuki, T., Briggs, L., Garthwaite, I., 2000. Toxic marine epiphytic dinoflagellates, *Ostreopsis siamensis* and *Coolia monotis* (Dinophyceae), in New Zealand. New Zealand Journal of Marine and Freshwater Research 34(2), 371-383.

Rhodes, L., Smith, K., Munday, R., Briggs, L., Selwwod, A., Adamson, J. and Holland, P. 2013. *Ostreopsis* isolates from the Pacific region. *In* Pagou, P. and Hallegraeff, G. (Eds) *Proceedings of the 14th International Conference on Harmful Algae*. International Society for the Study of Harmful Algae and Intergovernmental Oceanographic Commission of UNESCO, pp. 36-38

Rhodes, L., Smith, K., Papiol, G. G., Adamson, J., Harwood, T. and Munday, R. 2014. Epiphytic dinoflagellates in sub-tropical New Zealand, in particular the genus *Coolia* Meunier. Harmful Algae 34, 36-41.

Rhodes, L., Towers, N., Briggs, L., Munday, R., Adamson, J., 2002. Uptake of palytoxin-like compounds by shellfish fed *Ostreopsis siamensis* (Dinophyceae). New Zealand Journal of Marine and Freshwater Research 36(3), 631-636.

Rhodes, L.L., Smith, K.F., Verma, A., Murray, S., Harwood, D.T., Trnski, T., 2017. The dinoflagellate genera *Gambierdiscus* and *Ostreopsis* from subtropical Raoul Island and North Meyer Island, Kermadec Islands. New Zealand Journal of Marine and Freshwater Research, 1-15.

Richlen, M.L., Morton, S.L., Barber, P.H., Lobel, P.S., 2008. Phylogeography, morphological variation and taxonomy of the toxic dinoflagellate *Gambierdiscus toxicus* (Dinophyceae). Harmful Algae 7(5), 614-629.

Ridgway, K., 2007. Long-term trend and decadal variability of the southward penetration of the East Australian Current. Geophysical Research Letters 34(13).

Ridgway, K., Hill, K., 2009. The East Australian Current. A marine climate change impacts and adaptation report card for Australia 5(09).

Riobó, P., Paz, B., Franco, J. M., Vázquez, J. A., Murado, M. A. and Cacho, E. 2008 Mouse bioassay for palytoxin. Specific symptoms and dose–response against dose–death time relationships. Food and Chemical Toxicology 46, 2639–2647.

Ritchie, R.J., 2006. Consistent sets of spectrophotometric chlorophyll equations for acetone, methanol and ethanol solvents. Photosynthesis research 89(1), 27-41.

Robinson, C., Suggett, D., Cherukuru, N., Ralph, P., Doblin, M., 2014. Performance of Fast Repetition Rate fluorometry based estimates of primary productivity in coastal waters. Journal of Marine Systems 139, 299-310.

Ronquist, F., Huelsenbeck, J.P., 2003. MrBayes 3: Bayesian phylogenetic inference under mixed models. Bioinformatics 19(12), 1572-1574.

Rossi, R., Castellano, V., Scalco, E., Serpe, L., Zingone, A., Soprano, V., 2010. New palytoxin-like molecules in Mediterranean *Ostreopsis* cf. *ovata* (dinoflagellates) and in *Palythoa tuberculosa* detected by liquid chromatography-electrospray ionization time-of-flight mass spectrometry. Toxicon 56(8), 1381-1387.

Ryan, D., Pepper, A., Campbell, L., 2014. De novo assembly and characterization of the transcriptome of the toxic dinoflagellate *Karenia brevis*. BMC Genomics 15, 888.

Rynearson, T.A., Virginia Armbrust, E., 2004. Genetic differentiation among populations of the planktonic marine diatom *Ditylum brightwellii* (Bacillariophyceae). Journal of Phycology 40(1), 34-43.

Salcedo, T., Upadhyay, R.J., Nagasaki, K., Bhattacharya, D., 2012. Dozens of toxin-related genes are expressed in a nontoxic strain of the dinoflagellate *Heterocapsa circularisquama*. Molecular Biology and Evolution 29 (6), 1503-1506

Salois, P., Morse, D., 1997. Characterization and molecular phylogeny of Protein kinase cDNA from the dinoflagellate *Gonyaulax* (Dinophceae). Journal of Phycology 33(6), 1063-1072.

Sampayo, E., Dove, S., LaJeunesse, T., 2009. Cohesive molecular genetic data delineate species diversity in the dinoflagellate genus *Symbiodinium*. Molecular Ecology 18(3), 500-519.

Sato, S., Nishimura, T., Uehara, K., Sakanari, H., Tawong, W., Hariganeya, N., Smith, K., Rhodes, L., Yasumoto, T., Taira, Y., Suda, S., Yamaguchi, H., Adachi, M., 2011. Phylogeography of *Ostreopsis* along west Pacific coast, with special reference to a novel clade from Japan. PloS One 6(12), e27983.

Schirmer, K., Chan, A., Greenberg, B., Dixon, D., Bols, N., 1997. Methodology for demonstrating and measuring the photocytotoxicity of fluoranthene to fish cells in culture. Toxicology in vitro 11(1), 107-119.

Schmidt, J., 1902. Flora of Koh Chang. Contribution to the knowledge of the vegetation in the Gulf of Siam. Part IV. Peridiniales. J. Botanique 23, 212-218.

Schnepf, E., Elbrächter, M., 1992. Nutritional strategies in dinoflagellates: a review with emphasis on cell biological aspects. European Journal of Protistology 28(1), 3-24.

Scholin, C.A., Herzog, M., Sogin, M., Anderson, D.M., 1994. Identification of group- and strain-specific genetic markers for globally distributed *Alexandrium* (Dinophyceae). II. Sequence analysis of a fragment of the LSU rRNA gene. Journal of Phycology 30(6), 999-1011.

Schultz, J., Maisel, S., Gerlach, D., Müller, T., Wolf, M., 2005. A common core of secondary structure of the internal transcribed spacer 2 (ITS2) throughout the Eukaryota. RNA 11(4), 361-364.

Schultz, J., Wolf, M., 2009. ITS2 sequence–structure analysis in phylogenetics: a how-to manual for molecular systematics. Molecular Phylogenetics and Evolution 52(2), 520-523.

Sechet, V., Sibat, M., Chomérat, N., Nézan, E., Grossel, H., Lehebel-Peron, J.-B., Jauffrais, T., Ganzin, N., Marco-Miralles, F., Lemée, R., 2012. *Ostreopsis* cf. *ovata* in the French Mediterranean coast: molecular characterisation and toxin profile. Cryptogamie, Algologie 33(2), 89-98.

Seibel, P.N., Müller, T., Dandekar, T., Schultz, J., Wolf, M., 2006. 4SALE–a tool for synchronous RNA sequence and secondary structure alignment and editing. BMC Bioinformatics 7(1), 498-504

Selander, E., Thor, P., Toth, G., Pavia, H., 2006. Copepods induce paralytic shellfish toxin production in marine dinoflagellates. Proceedings of the Royal Society of London B: Biological Sciences 273(1594), 1673-1680.

Selina, M. and Levchenko, E. 2011. Species composition and morphology of dinoflagellates (Dinophyta) of epiphytic assemblages of Peter the Great Bay in the Sea of Japan. Russian Journal of Marine Biology 37, 23-32.

Selina, M.S., Orlova, T.Y., 2010. First occurrence of the genus *Ostreopsis* (Dinophyceae) in the Sea of Japan. Botanica Marina 53(3), 243-9.

Selwood, A.I., van Ginkel, R., Harwood, D.T., McNabb, P.S., Rhodes, L.R., Holland, P.T., 2012. A sensitive assay for palytoxins, ovatoxins and ostreocins using LC-MS/MS analysis of cleavage fragments from micro-scale oxidation. Toxicon 60(5), 810-820.

Shazib, S.U.A., Vďačný, P., Kim, J.H., Jang, S.W., Shin, M.K., 2016. Molecular phylogeny and species delimitation within the ciliate genus *Spirostomum* (Ciliophora, Postciliodesmatophora, Heterotrichea), using the internal transcribed spacer region. Molecular Phylogenetics and Evolution.102, 128-144.

Shears, N. T. and Ross, P. M. 2009. Blooms of benthic dinoflagellates of the genus *Ostreopsis*; an increasing and ecologically important phenomenon on temperate reefs in New Zealand and worldwide. Harmful Algae 8, 916-25.

Shears, N.T., Ross, P.M., 2009. Blooms of benthic dinoflagellates of the genus *Ostreopsis*; an increasing and ecologically important phenomenon on temperate reefs in New Zealand and worldwide. Harmful Algae 8(6), 916-925.

Shen, B., 2003. Polyketide biosynthesis beyond the type I, II and III polyketide synthase paradigms. Current Opinion in Chemical Biology 7(2), 285-295.

Shimizu, Y., 1993. Microalgal metabolites. Chemical Reviews 93(5), 1685-1698.

Shimizu, Y., 1996. Microalgal metabolites: a new perspective. Annual Reviews in Microbiology 50(1), 431-465.

Shimizu, Y., 2003. Microalgal metabolites. Current Opinion in Microbiology 6(3), 236-243.

Shoguchi, E., Shinzato, C., Kawashima, T., Gyoja, F., Mungpakdee, S., Koyanagi, R., Takeuchi, T., Hisata, K., Tanaka, M., Fujiwara, M., 2013. Draft assembly of the

Symbiodinium minutum nuclear genome reveals dinoflagellate gene structure. Current Biology 23(15), 1399-1408.

Six, C., Finkel, Z.V., Rodriguez, F., Marie, D., Partensky, F., Campbell, D.A., 2008. Contrasting photoacclimation costs in ecotypes of the marine eukaryotic picoplankter *Ostreococcus*. Limnology and Oceanography 53(1), 255-265.

Sjöqvist, C., Godhe, A., Jonsson, P.R., Sundqvist, L., Kremp, A., 2015. Local adaptation and oceanographic connectivity patterns explain genetic differentiation of a marine diatom across the North Sea–Baltic Sea salinity gradient. Molecular Ecology 24(11), 2871-2885.

Slamovits, C.H., Keeling, P.J., 2008. Widespread recycling of processed cDNAs in dinoflagellates. Current Biology 18(13), R550-R552.

Smayda, T.J., 1990. Novel and nuisance phytoplankton blooms in the sea: evidence for a global epidemic. Toxic Marine Phytoplankton, 29-40.

Smayda, T.J., 1997. Harmful algal blooms: their ecophysiology and general relevance to phytoplankton blooms in the sea. Limnology and Oceanography 42(5part2), 1137-1153.

Smayda, T.J., Reynolds, C.S., 2003. Strategies of marine dinoflagellate survival and some rules of assembly. Journal of Sea Research 49(2), 95-106.

Smedsgaard, J., Nielsen, J., 2005. Metabolite profiling of fungi and yeast: from phenotype to metabolome by MS and informatics. Journal of Experimental Botany 56(410), 273-286.

Smith, S., 1994. The animal fatty acid synthase: one gene, one polypeptide, seven enzymes. The FASEB Journal 8(15), 1248-1259.

Snyder, R., Gibbs, P., Palacios, A., Abiy, L., Dickey, R., Lopez, J., Rein, K., 2003. Polyketide synthase genes from marine dinoflagellates. Marine Biotechnology 5(1), 1-12.

Snyder, R.V., Guerrero, M.A., Sinigalliano, C.D., Winshell, J., Perez, R., Lopez, J.V., Rein, K.S., 2005. Localization of polyketide synthase encoding genes to the toxic dinoflagellate *Karenia brevis*. Phytochemistry 66(15), 1767-1780.

Sonnenborn, U., Kunau, W.-H., 1982. Purification and properties of the fatty acid synthetase complex from the marine dinoflagellate, *Crypthecodinium cohnii*. Biochimica et Biophysica Acta (BBA)-Lipids and Lipid Metabolism 712(3), 523-534.

Stamatakis, A., 2006. RAxML-VI-HPC: maximum likelihood-based phylogenetic analyses with thousands of taxa and mixed models. Bioinformatics 22(21), 2688-2690.

Stat, M., Bird, C.E., Pochon, X., Chasqui, L., Chauka, L.J., Concepcion, G.T., Logan, D., Takabayashi, M., Toonen, R.J., Gates, R.D. 2011 Variation in *Symbiodinium* ITS2 Sequence Assemblages among Coral Colonies. PLoS ONE 6(1): e15854. doi: 10.1371/journal.pone.0015854

Stern, R.F., Horak, A., Andrew, R.L., Coffroth, M.-A., Andersen, R.A., Küpper, F.C., Jameson, I., Hoppenrath, M., Véron, B., Kasai, F., 2010. Environmental barcoding reveals massive dinoflagellate diversity in marine environments. PloS One 5(11), e13991.

Stüken, A., Orr, R.J., Kellmann, R., Murray, S.A., Neilan, B.A., Jakobsen, K.S., 2011. Discovery of nuclear-encoded genes for the neurotoxin saxitoxin in dinoflagellates. PloS One 6(5), e20096.

Suggett, D.J., Goyen, S., Evenhuis, C., Szabó, M., Pettay, D.T., Warner, M.E., Ralph, P.J., 2015. Functional diversity of photobiological traits within the genus *Symbiodinium* appears to be governed by the interaction of cell size with cladal designation. New Phytologist 208(2), 370-381.

Suggett, D.J., Moore, C.M., Hickman, A.E., Geider, R.J., 2009. Interpretation of fast repetition rate (FRR) fluorescence: signatures of phytoplankton community structure versus physiological state. Marine Ecology Progress Series 376, 1-19.

Sun, J., Liu, D., 2003. Geometric models for calculating cell biovolume and surface area for phytoplankton. Journal of Plankton Research 25(11), 1331-1346.

Suthers, I.M., Young, J.W., Baird, M.E., Roughan, M., Everett, J.D., Brassington, G.B., Byrne, M., Condie, S.A., Hartog, J.R., Hassler, C.S., 2011. The strengthening East Australian Current, its eddies and biological effects—an introduction and overview. Deep Sea Research Part II: Topical Studies in Oceanography 58(5), 538-546

Suthers, I.M., Young, J.W., Baird, M.E., Roughan, M., Everett, J.D., Brassington, G.B., Byrne, M., Condie, S.A., Hartog, J.R., Hassler, C.S., 2011. The strengthening East Australian Current, its eddies and biological effects—an introduction and overview. Elsevier.

Suzuki, T., Watanabe, R., Uchida, H., Matsushima, R., Nagai, H., Yasumoto, T., Yoshimatsu, T., Sato, S., Adachi, M., 2012. LC-MS/MS analysis of novel ovatoxin isomers in several *Ostreopsis* strains collected in Japan. Harmful Algae 20, 81-91.

Tahvanainen, P., Alpermann, T.J., Figueroa, R.I., John, U., Hakanen, P., Nagai, S., Blomster, J., Kremp, A., 2012. Patterns of post-glacial genetic differentiation in marginal populations of a marine microalga. PloS one 7(12), e53602.

Tamura, K., Stecher, G., Peterson, D., Filipski, A., Kumar, S., 2013. MEGA6: molecular evolutionary genetics analysis version 6.0. Molecular Biology and Evolution 30(12), 2725-2729.

Taniyama, S., Arakawa, O., Terada, M., Nishio, S., Takatani, T., Mahmud, Y. and Noguchi, T. 2003. *Ostreopsis* sp., a possible origin of palytoxin (PTX) in parrotfish *Scarus ovifrons*. *Toxicon* 42: 29-33.

Tartaglione, L., Mazzeo, A., Dell'Aversano, C., Forino, M., Giussani, V., Capellacci, S., Penna, A., Asnaghi, V., Faimali, M., Chiantore, M., Yasumoto, T., Ciminiello, P., 2016. Chemical, molecular, and eco-toxicological investigation of *Ostreopsis* sp. from Cyprus Island: structural insights into four new ovatoxins by LC-HRMS/MS. Analytical and Bioanalytical Chemistry 408(3), 915-932.

Tawong, W., Nishimura, T., Sakanari, H., Sato, S., Yamaguchi, H., Adachi, M., 2014. Distribution and molecular phylogeny of the dinoflagellate genus *Ostreopsis* in Thailand. Harmful Algae 37, 160-171.

Tawong, W., Yoshimatsu, T., Yamaguchi, H. and Adachi, M. 2015. Effects of temperature, salinity and their interaction on growth of benthic dinoflagellates *Ostreopsis* spp. from Thailand. *Harmful Algae* 44: 37-45.

Taylor, F., Hoppenrath, M., Saldarriaga, J.F., 2008. Dinoflagellate diversity and distribution. Biodiversity and Conservation 17(2), 407-418.

Taylor, F.J.R., 1987. The biology of dinoflagellates. Blackwell Scientific Publications.

Templeton, A.R., Crandall, K.A., Sing, C.F., 1992. A cladistic analysis of phenotypic associations with haplotypes inferred from restriction endonuclease mapping and DNA sequence data. III. Cladogram estimation. Genetics 132(2), 619-633.

Teng, S.T., Lim, P.T., Lim, H.C., Rivera-Vilarelle, M., Quijano-Scheggia, S., Takata, Y., Quilliam, M.A., Wolf, M., Bates, S.S., Leaw, C.P., 2015. A non-toxigenic but morphologically and phylogenetically distinct new species of *Pseudo-nitzschia*, *P. sabit* sp. nov. (Bacillariophyceae). Journal of Phycology 51(4), 706-725.

Thomas, M.K., Kremer, C.T., Litchman, E., 2016. Environment and evolutionary history determine the global biogeography of phytoplankton temperature traits. Global Ecology and Biogeography 25(1), 75-86.

Thompson, J.D., Gibson, T., Higgins, D.G., 2002. Multiple sequence alignment using ClustalW and ClustalX. Current Protocols in Bioinformatics, 2.3. 1-2.3. 22.

Thornhill, D.J., Lewis, A.M., Wham, D.C., LaJeunesse, T.C., 2014. Host-specialist lineages dominate the adaptive radiation of reef coral endosymbionts. Evolution 68(2), 352-367.

Thornton, D.C., 2002. Individuals, clones or groups? Phytoplankton behaviour and units of selection. Ethology Ecology & Evolution 14(2), 165-173.

Tichadou, L., Glaizal, M., Armengaud, A. et al. 2010. Health impact of unicellular algae of the *Ostreopsis* genus blooms in the Mediterranean Sea: experience of the French Mediterranean coast surveillance network from 2006 to 2009. *Clin. Toxicol.* 48: 839-44.

Tillmann, U., Alpermann, T.L., da Purificação, R.C., Krock, B., Cembella, A., 2009. Intra-population clonal variability in allelochemical potency of the toxigenic dinoflagellate *Alexandrium tamarense*. Harmful Algae 8(5), 759-769.

Tilman, D., 1999. The ecological consequences of changes in biodiversity: a search for general principles. Ecology 80(5), 1455-1474.

Tilman, D., Knops, J., Wedin, D., Reich, P., Ritchie, M., Siemann, E., 1997. The influence of functional diversity and composition on ecosystem processes. Science 277(5330), 1300-1302.

Tubaro, A., Durando, P., Del Favero, G., Ansaldi, F., Icardi, G., Deeds, J., Sosa, S., 2011. Case definitions for human poisonings postulated to palytoxins exposure. Toxicon 57(3), 478-495.

Uchida, H., Taira, Y., Yasumoto, T., 2013. Structural elucidation of palytoxin analogs produced by the dinoflagellate *Ostreopsis ovata* IK2 strain by complementary use of positive and negative ion liquid chromatography/quadrupole time-of-flight mass spectrometry. Rapid Communications in Mass Spectrometry 27(17), 1999-2008.

Uemura, D., Ueda, K., Hirata, Y., Naoki, H., Iwashita, T., 1981. Further studies on palytoxin. II. Structure of palytoxin. Tetrahedron letters 22(29), 2781-2784.

Ukena, T., Satake, M., Usami, M., Oshima, Y., Naoki, H., Fujita, T., Kan, Y., Yasumoto, T., 2001. Structure elucidation of ostreocin D, a palytoxin analog isolated from the dinoflagellate *Ostreopsis siamensis*. Bioscience, biotechnology, and biochemistry 65(11), 2585-2588.

Usami, M., Satake, M., Ishida, S., Inoue, A., Kan, Y., Yasumoto, T., 1995. Palytoxin analogs from the dinoflagellate *Ostreopsis siamensis*. Journal of the American chemical society 117(19), 5389-5390.

Usup, G., Hamid, S.Z., Chiet, P.K., Wah, C.K. and Ahmad, A., 2008. Marked differences in fatty acid profiles of some planktonic and benthic marine dinoflagellates from Malaysian waters. Phycologia 47(1), 105-111

Van Dolah, F.M., Zippay, M.L., Pezzolesi, L., Rein, K.S., Johnson, J.G., Morey, J.S., Wang, Z., Pistocchi, R., 2013. Subcellular localization of dinoflagellate polyketide synthases and fatty acid synthase activity. Journal of Phycology 49(6), 1118-1127.

Van Gremberghe, I., Vanormelingen, P., Vanelslander, B., Van der Gucht, K., D'hondt, S., De Meester, L., Vyverman, W., 2009. Genotype-dependent interactions among sympatric *Microcystis* strains mediated by Daphnia grazing. Oikos 118(11), 1647-1658.

Vanelslander, B., Creach, V., Vanormelingen, P., Ernst, A., Chepurnov, V.A., Sahan, E., Muyzer, G., Stal, L.J., Vyverman, W., Sabbe, K., 2009. Ecological differentiation between sympatric pseudocryptic species in the estuarine benthic diatom *Navicula Phyllepta* (Bacillariophyceae). Journal of Phycology 45(6), 1278-1289.

Vanucci, S., Pezzolesi, L., Pistocchi, R. et al. 2012. Nitrogen and phosphorus limitation effects on cell growth, biovolume, and toxin production in *Ostreopsis* cf. *ovata*. Harmful Algae 15: 78-90.

Verma, A., Hoppenrath, M., Dorantes-Aranda, J.J., Harwood, D.T., Murray, S.A., 2016a. Molecular and phylogenetic characterization of *Ostreopsis* (Dinophyceae) and the description of a new species, *Ostreopsis rhodesae* sp. nov., from a subtropical Australian lagoon. Harmful Algae 60, 116-130.

Verma, A., Hoppenrath, M., Harwood, T., Brett, S., Rhodes, L., Murray, S., 2016b. Molecular phylogeny, morphology and toxigenicity of *Ostreopsis* cf. *siamensis* (Dinophyceae) from temperate south-east Australia. Phycological Research 64(3), 146-159.

Wakeman, K.C., Yamaguchi, A., Roy, M.C., Jenke-Kodama, H., 2015. Morphology, phylogeny and novel chemical compounds from *Coolia malayensis* (Dinophyceae) from Okinawa, Japan. Harmful Algae 44, 8-19.

Wang, H., Fewer, D.P., Holm, L., Rouhiainen, L., Sivonen, K., 2014. Atlas of non-ribosomal peptide and polyketide biosynthetic pathways reveals common occurrence of non-modular enzymes. Proceedings of the National Academy of Sciences 111(25), 9259-9264.

Ward, B.A., Marañón, E., Sauterey, B., Rault, J., Claessen, D., 2017. The Size Dependence of Phytoplankton Growth Rates: A Trade-Off between Nutrient Uptake and Metabolism. The American Naturalist 189(2), 170-177.

Wayne Litaker, R., Vandersea, M.W., Kibler, S.R., Reece, K.S., Stokes, N.A., Lutzoni, F.M., Yonish, B.A., West, M.A., Black, M.N., Tester, P.A., 2007. Recognizing dinoflagellate species using ITS rDNA sequecnes. Journal of Phycology 43(2), 344-355.

Webb, G.E., Jell, J.S., Baker, J.C., 1999. Cryptic intertidal microbialites in beachrock, Heron Island, Great Barrier Reef: implications for the origin of microcrystalline beachrock cement. Sedimentary Geology 126(1–4), 317-334.

Weithoff, G., 2003. The concepts of 'plant functional types' and 'functional diversity'in lake phytoplankton–a new understanding of phytoplankton ecology? Freshwater Biology 48(9), 1669-1675.

West, R., Thorogood, C., Walford, T. and William, R. 1985. An Estuarine Inventory for New South Wales, Australia. Fisheries Bulletin 2, Department of Agriculture, New South Wales.

Whittaker, K.A., Rignanese, D.R., Olson, R.J., Rynearson, T.A., 2012. Molecular subdivision of the marine diatom *Thalassiosira rotula* in relation to geographic distribution, genome size, and physiology. BMC Evolutionary Biology 12(1), 209.

Williams, R. J., West, G., Morrison, D. and Creese, R. G. 2006. Estuarine Resources of New South Wales. Prepared for the Comprehensive Coastal Assessment, NSW Department of Primary Industries, Port Stephens, NSW.

Wood, A.M., Leatham, T., 1992. The species concept in phytoplankton ecology. Journal of Phycology 28(6), 723-729.

Wright, J.L. and Cembella, A.D., 1998. Ecophysiology and biosynthesis of polyether marine biotoxins. Nato ASI Series G Ecological Sciences, 41, 427-452.

Wu, C.H., 2009. Palytoxin: Membrane mechanisms of action. Toxicon 54(8), 1183-1189.

Wu, Y., Campbell, D.A., Irwin, A.J., Suggett, D.J., Finkel, Z.V., 2014. Ocean acidification enhances the growth rate of larger diatoms. Limnology and Oceanography 59(3), 1027-1034.

Yasumoto, T. and Murata, M., 1993. Marine toxins. Chemical reviews, 93(5), 1897-1909.

Zhang, H., Hou, Y., Miranda, L., Campbell, D.A., Sturm, N.R., Gaasterland, T., Lin, S., 2007. Spliced leader RNA trans-splicing in dinoflagellates. Proceedings of the National Academy of Sciences 104(11), 4618-4623.

Zhang, H., Lin, S., 2009. Retrieval of missing spliced leader in dinoflagellates. PLoS ONE 4(1), e4129.

Zhang, H., Zhuang, Y., Gill, J., Lin, S., 2013. Proof that dinoflagellate-spliced leader (DinoSL) is a useful hook for fishing dinoflagellate transcripts from mixed microbial samples: *Symbiodinium kawagutii* as a case study. Protist 164(4), 510-527.

Zhang, Y., Klapper, R., Lohbeck, K.T., Bach, L.T., Schulz, K.G., Reusch, T.B. and Riebesell, U., 2014. Between and within population variations in thermal reaction norms of the coccolithophore *Emiliania huxleyi*. Limnology and Oceanography, 59(5), 1570-1580.

Zhu, G., LaGier, M.J., Stejskal, F., Millership, J.J., Cai, X., Keithly, J.S., 2002. *Cryptosporidium parvum*: the first protist known to encode a putative polyketide synthase. Gene 298(1), 79-89.

Zingone, A., Oksfeldt Enevoldsen, H., 2000. The diversity of harmful algal blooms: a challenge for science and management. Ocean & Coastal Management 43(8–9), 725-748.

Supplementary Data

S1 Primers used for amplification and sequencing

Primer	Primer sequence	Target region	Direction	Ta
D1R[a]	5'-ACC CGC TGA ATT TAA GCA TA-3'	28S (D1-D3)	Forward	55 ºC
D2C[b]	5'-CCT TGG TCC GTG TTT CAA GA-3'	28S (D1-D2)	Reverse	55 ºC
D3B[c]	5'-TCG AGG GAA CCA GCT ACT A-3'	28S (D1-D3)	Reverse	55 ºC
FD8/D8[d]	5'-GGA TTG GCT CTG AGG GTT GGG-3'	28S (D8-D10)	Forward	62 ºC
RB/D10[d]	5'-GAT AGG AAG AGC CGA CAT CGA-3'	28S (D8-D10)	Reverse	62 ºC
GLD8_421F[e]	5'-ACA GCC AAG GGA ACG GGC TT-3'	28S (D8-D10)	Forward	62 ºC
GLD8_677R[e]	5'-TGT GCC GCC CCA GCC AAA CT-3'	28S (D8-D10)	Reverse	62 ºC
ITSA[f,g]	5'-GTA ACA AGG THT CCG TAG GT-3'	ITS1-5.8S-ITS2	Forward	55 ºC
ITSB[f,g]	5'-AKA TGC TTA ART TCA GCR GG-3'	ITS1-5.8S-ITS2	Reverse	55 ºC
SSU unif[h]	5'-CGA ATT CAA CCT GGT TGA TCC TGC CAG-3'	18S	Forward	62 ºC
SSU unir[h]	5'-CCG GAT CCT GAT CCT TCT GCA GGT TCA-3'	18S	Reverse	62 ºC

References

[a] Scholin, C.A., Herzog, M., Sogin, M., Anderson, D.M., 1994. Identification of group- and strain-specific genetic markers for globally distributed *Alexandrium* (Dinophyceae). II. Sequence analysis of a fragment of tyhe LSU rRNA gene. Journal of Phycology 30(6), 999-1011.

[b] Guillou, L., Nézan, E., Cueff, V., Erard-Le Denn, E., Cambon-Bonavita, M.A., Gentien, P. and Barbier, G., 2002. Genetic diversity and molecular detection of three toxic dinoflagellate genera (*Alexandrium*, *Dinophysis*, and *Karenia*) from French coasts. Protist 153(3), 223-238.

[c] Nunn, G., Theisen, B., Christensen, B., Arctander, P., 1996. Simplicity-correlated size growth of the nuclear 28S ribosomal RNA D3 expansion segment in the crustacean order *isopoda*. Jounal of Molecular Evolution 42(2), 211-223

[d] Chinain, M., Faust, M.A., Pauillac, S., 1999. Morphology and molecular analyses of three toxic species of *Gambierdiscus* (Dinophyceae): *G. pacificus*, sp. nov., *G. australes*, sp. nov., and *G. polynesiensis*, sp. nov. Journal of Phycology 35(6), 1282-1296.

[e] Nishimura, T., Sato, S., Tawong, W., Sakanari, H., Uehara, K., Shah, M. M. R, Suda, S., Yasumoto, T., Taira, Y., Yamaguchi, H., Adachi, M. 2013. Genetic diversity and distribution of the ciguatera-causing dinoflagellate *Gambierdiscus* spp. (Dinophyceae) in coastal areas of Japan. *PloS one*, 8(4), e60882.

[f] Sato, S., Nishimura, T., Uehara, K., Sakanari, H., Tawong, W., Hariganeya, N., smith, K., Rhodes, L., Yasumoto, T., Taira, Y., Suda, S., Yamaguchi, H., & Adachi, M. 2011. Phylogeography of *Ostreopsis* along west Pacific coast, with special reference to a novel clade from Japan. PloS one 6, e27983.

[g] LaJeunesse, T.C., 2001. Investigating the biodiversity, ecology, and phylogeny of endosymbiotic dinoflagellates in the genus *Symbiodinium* using the ITS region: in search of a "species" level marker. *Journal of Phycology*, 37(5), 866-880.

[h] Medlin, L., Elwood, H. J., Stickel, S., & Sogin, M. L. (1988). The characterization of enzymatically amplified eukaryotic 16S-like rRNA-coding regions. Gene 71(2), 491-499.

S2 List of *Ostreopsis* spp. clones used for phylogenetic reconstruction and for inferring *p*-distances

Species	Strain	D8-D10	ITS	D1-D3	18S
Ostreopsis **cf.** *siamensis*	CAWD173	AB674880	AB674915		
Ostreopsis **cf.** *siamensis*	CAWD 147	AB674879	AB674915		
Ostreopsis **cf.** *siamensis*	CAWD96	AB674878	AB674915		
Ostreopsis **sp. 4**	CAWD179	AB674881	AB674916		
Ostreopsis **sp. 3**	CAWD184	AB674877	AB674914		
Ostreopsis **sp. 2**	OdoOst6	AB674876	AB674913	AB605816	
Ostreopsis **sp. 7**	TA35OS	AB841370	AB841211		
Ostreopsis **sp. 7**	TB38OS	AB841380	AB841218	AB841258	
Ostreopsis **sp. 7**	TB17OS	AB841372			
Ostreopsis **sp. 1**	MB80614_2	AB674829			
Ostreopsis **sp. 1**	s0611	AB674824			
Ostreopsis **sp. 1**	s0605	AB674820			
Ostreopsis **sp. 6**	s0587	AB674897			
Ostreopsis **sp. 6**	s0595	AB674900			
Ostreopsis **sp. 6**	TF29OS	AB841410			
Ostreopsis **sp. 5**	IkeOst2	AB674885		AB605814	
Ostreopsis **sp. 5**	MB80828_4	AB674882	AB674917		
Ostreopsis **sp. 5**	O70421_1	AB674883			
Ostreopsis **cf.** *ovata*	KAC85	AB674788	AB674906		
Ostreopsis **cf.** *ovata*	s0705	AB674796			
Ostreopsis **cf.** *ovata*	KDo5	AB674777			
Ostreopsis **cf.** *ovata*	TF8OS	AB841387			
Ostreopsis **cf.** *ovata*	TG7OS	AB841408			
Ostreopsis **cf.** *ovata*	T152	AB841406			
Ostreopsis **cf.** *ovata*	OVPT2	AB674786	AB674905		
Ostreopsis **cf.** *ovata*	TD8OS	AB841402			
Ostreopsis **cf.** *ovata*	CAWD174	AB674785	AB674904		
Ostreopsis **cf.** *ovata*	HJ-2013 OVJJ1	HE793379	HE793379	HE793379	HE793379
Ostreopsis **cf.** *siamensis*	CNR-T5		FM244729		
Ostreopsis **cf.** *siamensis*	CNR-B4		AJ301643		
Ostreopsis **cf.** *siamensis*	CSIC-D5		AJ312944		
Ostreopsis **cf.** *siamensis*	IEO 1V		AJ319871		
Ostreopsis **cf.** *siamensis*	IEO-2V		AJ491313		
Ostreopsis **cf.** *siamensis*	IEO-3V		AJ491332		
Ostreopsis **cf.** *siamensis*	CSIC-D1		AJ491333		
Ostreopsis **cf.** *siamensis*	CNR-B5		AJ491335		
Ostreopsis **cf.** *siamensis*	CSIC-D7		AJ491334		
Ostreopsis **cf.** *siamensis*	Dn91EHU		JX987676		
Ostreopsis **cf.** *siamensis*	Dn201EHU		JX987699		
Ostreopsis **cf.** *siamensis*	Dn188EHU		JX987692		
Ostreopsis **cf.** *siamensis*	Dn86EHU		JX987675		
Ostreopsis **cf.** *siamensis*	Dn199EHU		JX987698		

Ostreopsis **cf.** *siamensis*	Dn144EHU	JX987683		
Ostreopsis **cf.** *siamensis*	Dn143EHU	JX987682		
Ostreopsis **cf.** *siamensis*	Dn142EHU	JX987681		
Ostreopsis **sp. 1**	T70828_5	AB674908		
Ostreopsis **sp.**	VGO881	FM244637		
Ostreopsis **sp. 1**	s0617	AB674910		
Ostreopsis **cf.** *ovata*	T60730_1	AB674902		
Ostreopsis **sp. 1**	MB61007_3	AB674909		
Ostreopsis **sp. 6**	VGO897	FM244728		
Ostreopsis **sp. 6**	OU11	AB674921		
Ostreopsis **sp. 6**		AF218465		
Ostreopsis **cf.** *ovata*	CBA_6	FM244725		
Ostreopsis **cf.** *ovata*	CBA_10	FM244727	FM997924	
Ostreopsis **cf.** *ovata*	OvPD07	AF218456		
Ostreopsis **cf.** *ovata*	OvPD06	AF218455		
Ostreopsis **cf.** *ovata*	T203	AB841247		
Ostreopsis **cf.** *ovata*	T194	AB841242		
Ostreopsis **cf.** *siamensis*	Dn20EHU		HQ414224	
Ostreopsis **cf.** *siamensis*	Dn19EHU		HQ414223	
Ostreopsis **cf.** *siamensis*	Dn18EHU		HQ414222	
Ostreopsis **cf.** *siamensis*	VGO-OS5V		FN256430	
Ostreopsis **cf.** *ovata*	OdoOst5		AB605825	
Ostreopsis **cf.** *ovata*	OS-10BR		FM997914	
Ostreopsis **cf.** *ovata*	OS-12BR		FN256432	
Ostreopsis **cf.** *ovata*	CBA_4		FM997921	
Ostreopsis **cf.** *siamensis*	CSIC-D		FN256431	
Ostreopsis **sp. 6**	OLPR01		AF244941	
Ostreopsis **cf.** *ovata*	OS-19BR		FM997920	
Ostreopsis **cf.** *ovata*	IshiOst61		AB605818	
Ostreopsis **cf.** *ovata*	OOAN0601		GQ380659	
Ostreopsis **cf.** *ovata*	OvPR04		AF244940	AF244939
Ostreopsis **cf.** *ovata*	KC69		FM946097	
Ostreopsis **cf.** *ovata*	VGO883		FM994930	
Ostreopsis **cf.** *siamensis*	CAWD206		KJ422860	
Ostreopsis **sp.**	VGO881		FM994895	
Ostreopsis **sp. 5**	UrGmb6		AB605815	
Ostreopsis **sp. 1**	s0716		AB841256	
Ostreopsis **sp.**	ORUS J1			KF360003
Ostreopsis **sp.**	ORUS O1			KF360001
Ostreopsis **sp.**	ORUS K2			KF360000
Ostreopsis **sp.**	ORUS H2			KF359999
Ostreopsis **sp.**	ORUS H1			KF359998
Ostreopsis **sp.**	ORUS A2			KF359997
Ostreopsis **sp.**	ORUS A1			KF359996

S3 Distance values (pairwise uncorrected *p*-distances) based on the SSU rDNA sequences (Clustal W alignment) between and within clades of *Ostreopsis*.

	Clade	1	2	3	4
1	Unclassified *Ostreopsis*	NA			
2	*Ostreopsis* sp. 1 (Korea)	0.017	NA		
3	*Ostreopsis* cf *ovata* (Malaysia)	0.06	0.054	NA	
4	*Ostreopsis* cf. *siamensis*	0.076	0.068	0.065	NA

S4 Comparison of acclimated growth rates of *Ostreopsis* spp. Growth rates were calculated from the exponential phase portion of the growth curve. Values are mean of three replicates.

Strain	Species	Growth rate	Media	Location	Temp (^{0}C)	Reference
s0662	*Ostreopsis* cf. *ovata*	0.866 0.802 0.608 0.181	F/2 IMK PES SWM3	Japan	25	Yamaguchi et al., 2012
OOAN0601	*Ostreopsis* cf. *ovata*	0.37	F/10	Adriatic Sea	25	Guerrini et al., 2010
OOTL0602	*Ostreopsis* cf. *ovata*	0.32	F/10	Tyrrhenian Sea	25	Guerrini et al., 2010
LCA-E7	*Ostreopsis* cf. *ovata*	0.15	L2/2	Brazil	24	Nascimento et al., 2012
LCA-B7	*Ostreopsis* cf. *ovata*	0.1	L2/2	Brazil	24	Nascimento et al., 2012
NA	*Ostreopsis lenticularis*	0.67	F/2	Puerto Rico	29	Tosteson et al., 1989
s0716	*Ostreopsis* sp. 1	0.608 0.629 0.384 0.431	F/2 IMK PES SWM3	Japan	25	Yamaguchi et al., 2012
O07421-2	*Ostreopsis* sp. 5	0.353 0.394 0.364 0.285	F/2 IMK PES SWM3	Japan	25	Yamaguchi et al., 2012
s0587	*Ostreopsis* sp. 6	0.918 1.09 0.468 0.347	F/2 IMK PES SWM3	Japan	25	Yamaguchi et al., 2012
-	*Ostreopsis siamensis*	0.3	GP	New Zealand	25	Rhodes et al., 2000
-	*Ostreopsis siamensis*	0.53	K	Tasmania, Australia	20	Pearce et al., 2001
T163	*Ostreopsis* cf. *ovata* (Thailand sub clade)	0.56	F/2	Thailand	25	Tawong et al., 2015
TF5OS	*Ostreopsis* cf. *ovata* (S China Sea sub clade)	0.53	F/2	Thailand	30	Tawong et al., 2015
TF29OS	*Ostreopsis* sp. 6	0.54	F/2	Thailand	25	Tawong et al., 2015
TB30OS	*Ostreopsis* sp. 7	0.47	F/2	Thailand	25	Tawong et al., 2015
CAWD203	*Ostreopsis* cf. *siamensis*	0.24 0.39	F/2 F/10	Merimbula, Australia	18	**This study**

S5 Palytoxin (PLTX)-equivalents quantification in *Ostreopsis siamensis* isolates from the Australian and New Zealand waters according to Selwood et al., 2012.

Strain code	PLTX equivalents (pg/cell)	Sampling location	Reference
CAWD203	0.17	Merimbula, Australia	Verma et al., 2016a
CAWD173	0.31	Rangaunu Harbour, Northland, New Zealand	Rhodes et al., 2010
CAWD96	0.74	Kerikeri, New Zealand	Rhodes et al., 2010
CAWD147	1.23	Mahinepua, New Zealand	Rhodes et al., 2010
CAWD206	0.72	Tapeka Point, Bay of Islands, New Zealand	Harwood, D.T., per comm.
CAWD208	0.46	Tapeka Point, Bay of Islands, New Zealand	Harwood, D.T., per comm.
NA	0.19	Oke bay, Northland, New Zealand	Harwood, D.T., per comm.
NA	0.1	Roberton Island lagoon Northland, New Zealand	Harwood, D.T., per comm.
NA	0.12	Roberton Island lagoon Northland, New Zealand	Harwood, D.T., per comm.

S6: ITS2 Secondary structures of *Ostreopsis* cf. *ovata* subclades. A: *Ostreopsis* cf. *ovata* Malacca Sea sub-clade; B: *Ostreopsis* cf. *ovata* Celebes Sea sub-clade; C: *Ostreopsis* cf. *ovata* South China Sea sub-clade; D: *Ostreopsis* cf. *ovata* Thailand sub-clade and; E: *Ostreopsis* cf. *ovata* Med/Pac clade. Full arrows represent the Hemi-CBCs between Celebes Sea and other sub-clades. Dashed arrows represent the Hemi-CBCs in Med/Pac sub-clade.

Ostreopsis cf. *ovata* Malacca Sea sub-clade
OvPD06- AF218455
OvPD07- AF218456
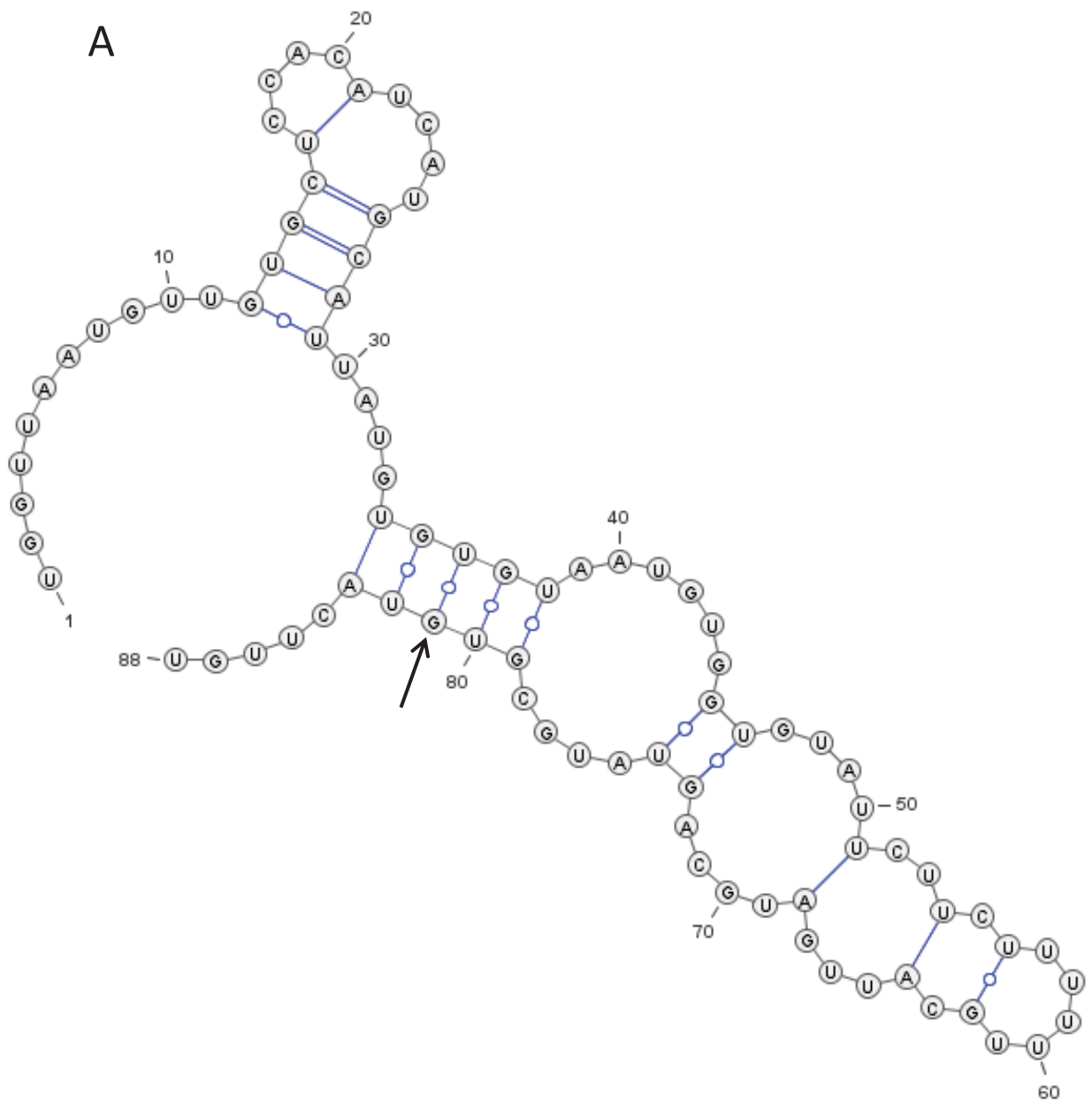
Ostreopsis cf. *ovata* Celebes Sea sub-clade
CBA 10 -FM244727
CBA 6- FM244725

B
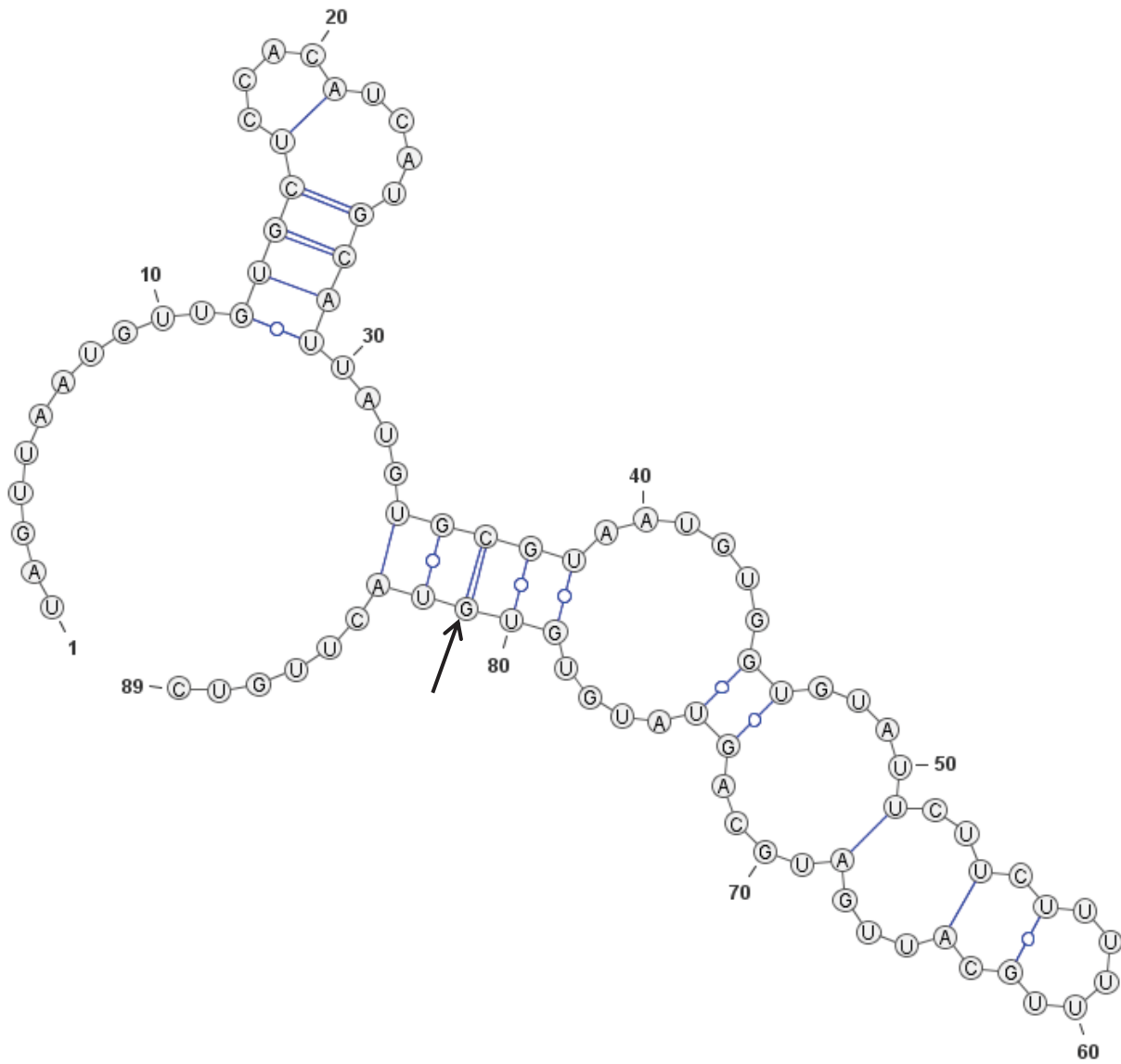
Ostreopsis cf. *ovata* South China Sea sub-clade
OVPT2- AB674905
CAWD174- AB674904
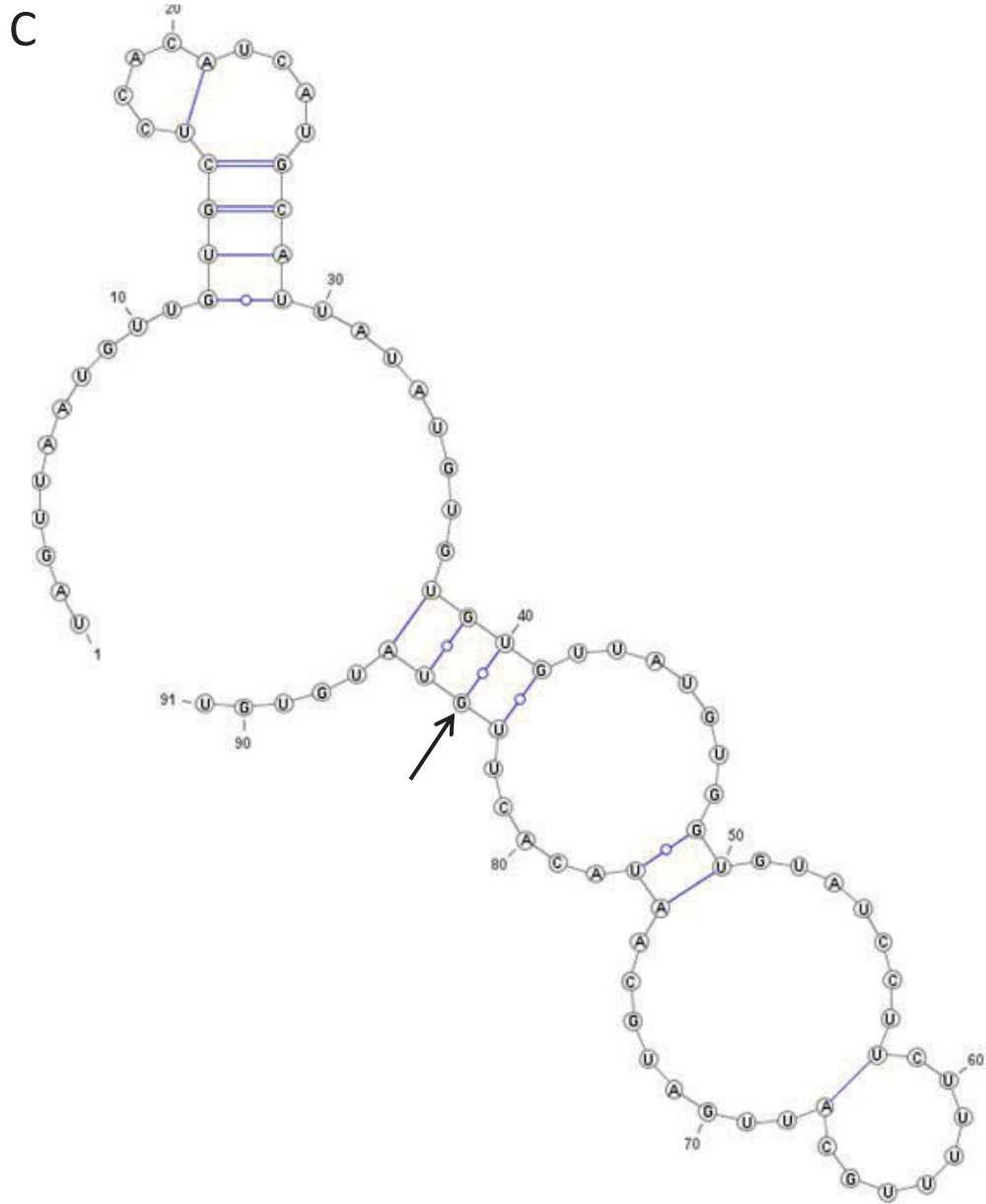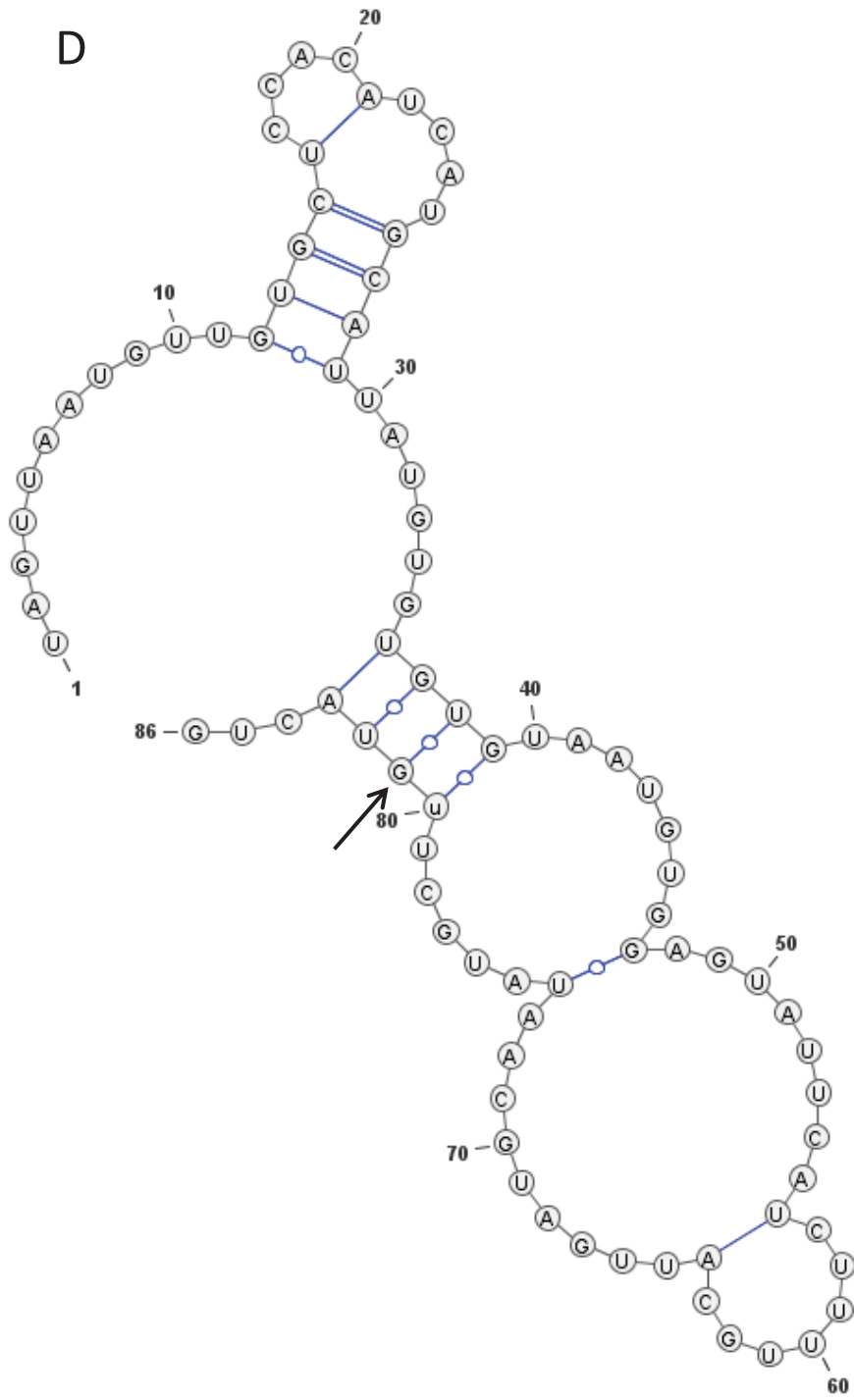
Ostreopsis cf. *ovata* **Med/Pac clade**
KAC85- AB674906
T674902_1- AB674902
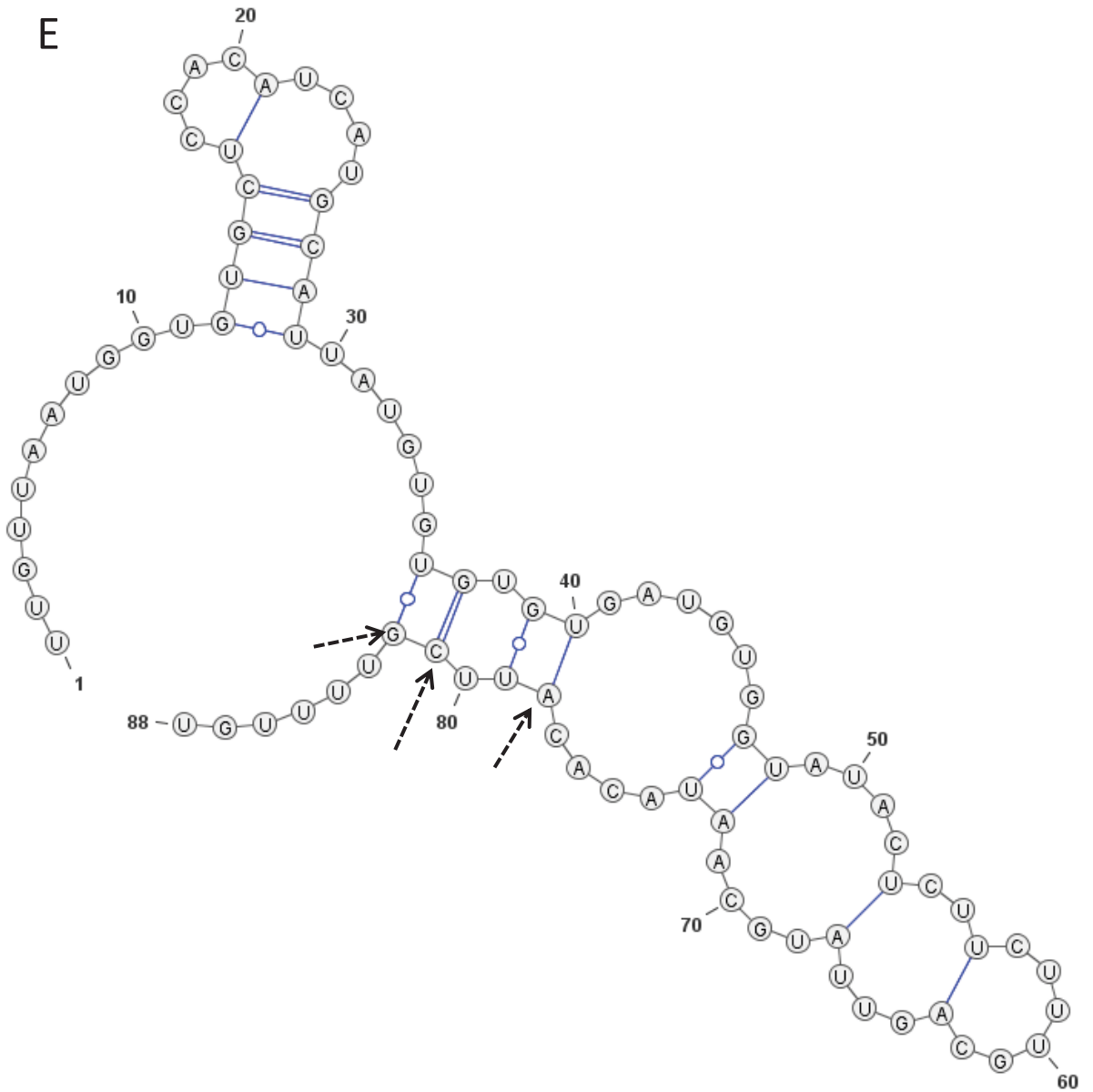
S7A Maximum Likelihood (ML) phylogenetic tree of various *Ostreopsis* cf. siamensis strains isolated along the New South Wales coastline using ITS1-5.8S-ITS2 primer set. Numbers at nodes represent posterior probabilities from Bayesian Inferences (BI) and bootstrap support values from ML based on 1000 pseudo-replicates. Only bootstrap values > 50% are shown. * represents 1, 100 support values for BI and ML respectively.

PC9
PC4
MW6
MW5
MW4
MER24
MER19
MER20
MER14
LM10
LM5
LM1
LM9
LM8
LM7
LM6
LM4
LM3
LM2
KM8
KM7
KM6
KM4
KM5
KM3
KM2
KM1
GB16
GB15
GB3
GB14
GB2
FR9
FR10
FR6
FR5
GB5
GB8
PC3
FR4
PC11
PC10
PC8
PC7
FR3
FR2
FR1
BH10
BH9
BH8
BH7
BH6
BH5
BH4
BH2
PC13
MW1
MW9 8
MW8
MW10 8
BH1
BH3
MW2
MW3
MW7
GB23
FR7
FR8
HER6
HER20
HER27

0.89, 63

1, 64

1, 98

0.05

202
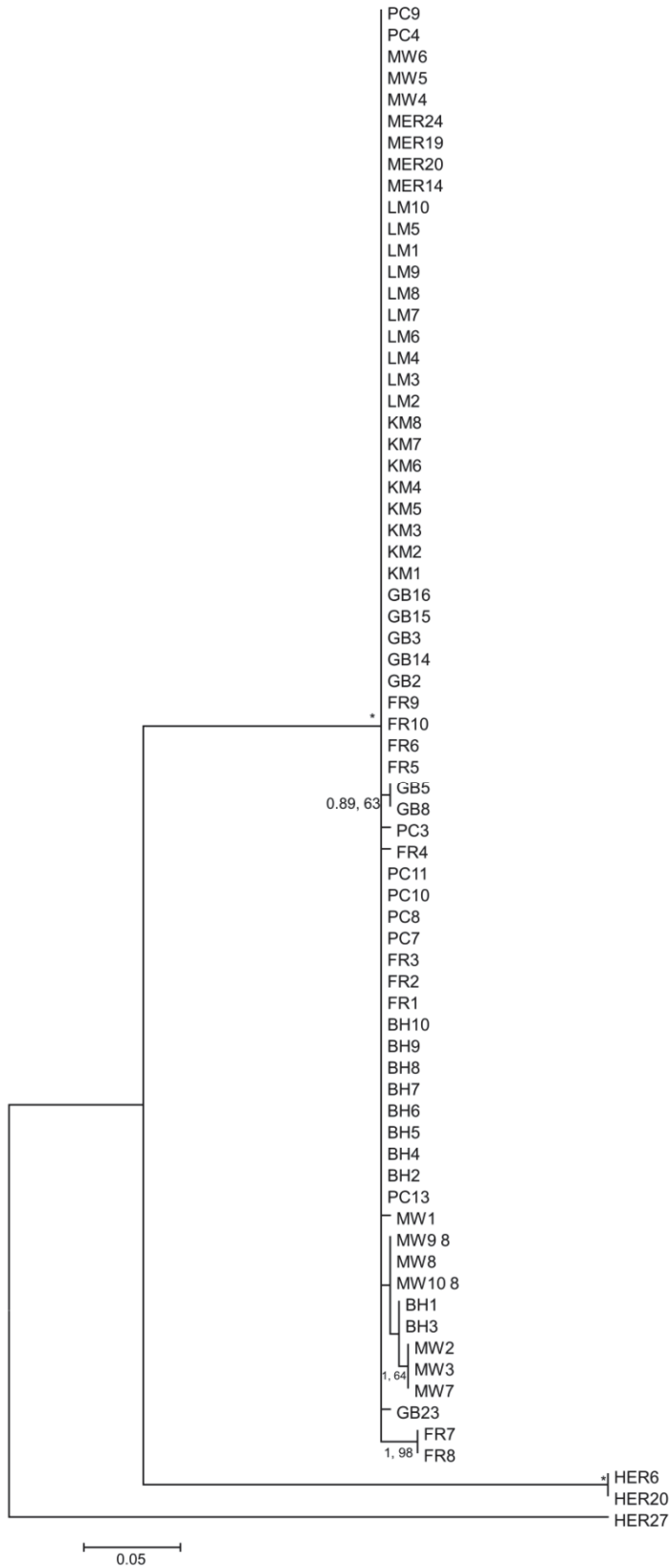
S7B Maximum Likelihood (ML) phylogenetic tree of various *Ostreopsis* cf. siamensis strains isolated along the New South Wales coastline using LSU D1-D3 rDNA region primer set. Numbers at nodes represent posterior probabilities from Bayesian Inferences (BI) and bootstrap support values from ML based on 1000 pseudo-replicates. Only bootstrap values > 50% are shown. * represents 1, 100 support values for BI and ML respectively.
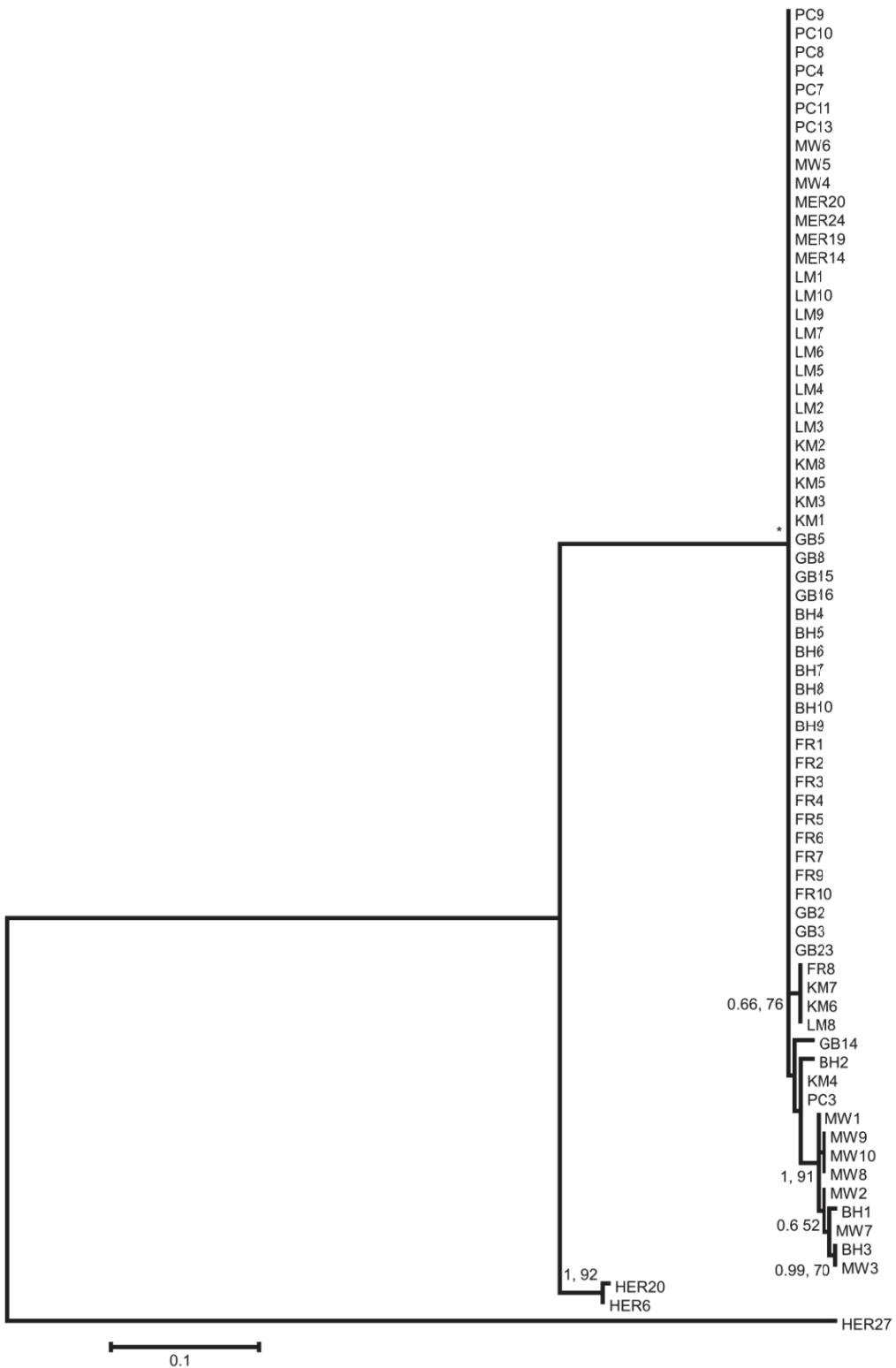
S7C Maximum Likelihood (ML) phylogenetic tree of various *Ostreopsis* cf. siamensis strains isolated along the New South Wales coastline using LSU D8-D10 rDNA region primer set. Numbers at nodes represent posterior probabilities from Bayesian Inferences (BI) and bootstrap support values from ML based on 1000 pseudo-replicates. Only bootstrap values > 50% are shown. * represents 1, 100 support values for BI and ML respectively.
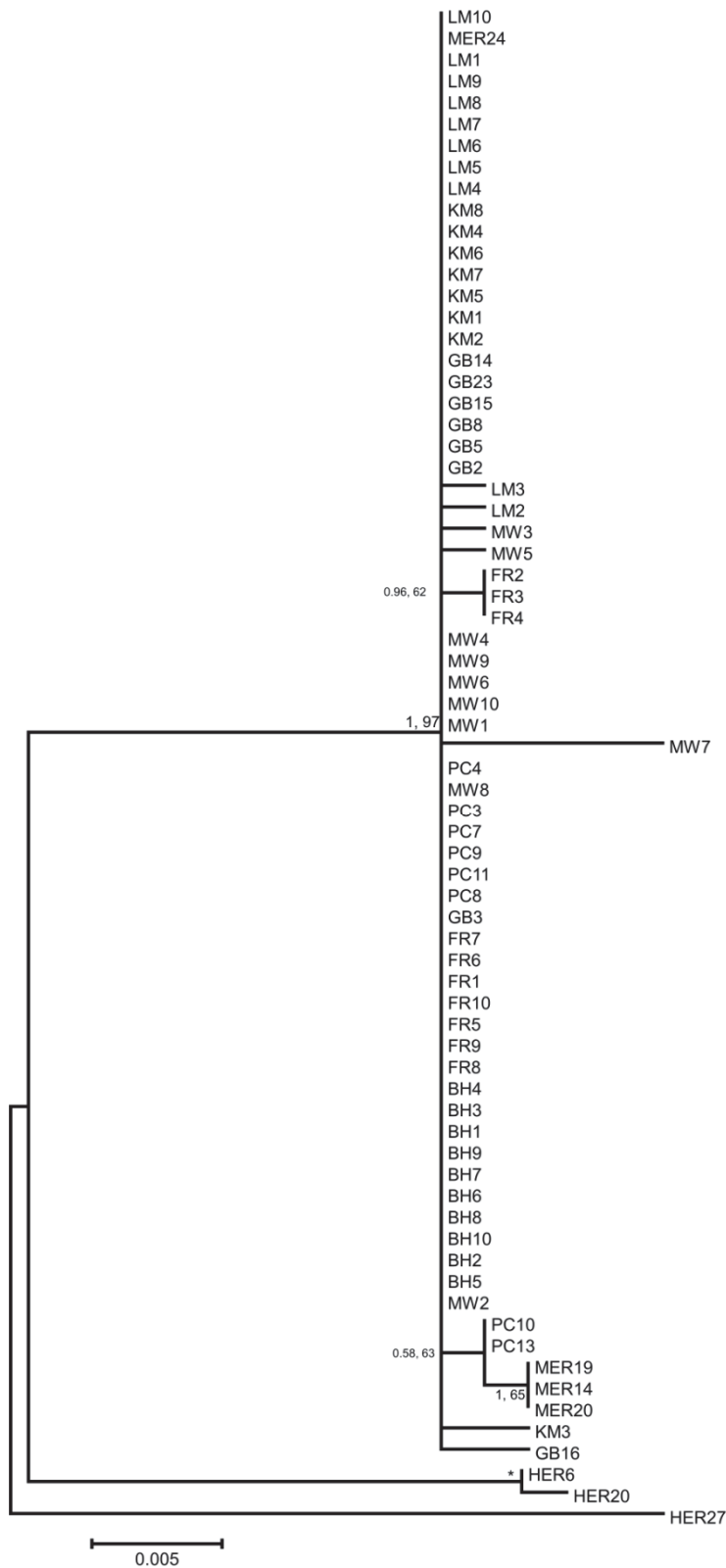
S8A List of all strains isolated, genotyped and used for physiological assessment from the New South Wales sampling sites.

Origin	Strain	Genotyped	Sub-Clade	Haplotype	Used for physiological data analysis
Minnie Waters	MW1	Yes	2	MW1	Yes
	MW2	Yes	2	MW2	Yes
	MW3	Yes	2	MW3	Yes
	MW4	Yes	1	Haplotype 1 (MW4)	Yes
	MW5	Yes	1	MW5	Yes
	MW6	Yes	1	Haplotype 1 (MW4)	Yes
	MW7	Yes	2	MW7	Yes
	MW8	Yes	2	MW8	No
	MW9	Yes	2	MW10	Yes
	MW10	Yes	2	MW10	Yes
Bonny Hills	BH1	Yes	2	BH1	Yes
	BH2	Yes	1	BH2	Yes
	BH3	Yes	2	BH3	Yes
	BH4	Yes	1	Haplotype 1 (BH10)	Yes
	BH5	Yes	1	Haplotype 1 (BH10)	Yes
	BH6	Yes	1	Haplotype 1 (BH10)	Yes
	BH7	Yes	1	Haplotype 1 (BH10)	Yes
	BH8	Yes	1	Haplotype 1 (BH10)	Yes
	BH9	Yes	1	Haplotype 1 (BH10)	Yes
	BH10	Yes	1	Haplotype 1 (BH10)	Yes
Wallis Lake, Forster	FR1	Yes	1	Haplotype 1 (FR1)	Yes
	FR2	Yes	1	FR2	Yes
	FR3	Yes	1	FR2	Yes
	FR4	Yes	1	FR4	Yes
	FR5	Yes	1	Haplotype 1 (FR1)	Yes
	FR6	Yes	1	Haplotype 1 (FR1)	Yes
	FR7	Yes	1	FR7	Yes
	FR8	Yes	1	FR7	No
	FR9	Yes	1	Haplotype 1 (FR1)	Yes
	FR10	Yes	1	Haplotype 1 (FR1)	Yes
Lake Macquarie	LM1	Yes	1	Haplotype 1 (LM5)	No
	LM2	Yes	1	LM2	Yes
	LM3	Yes	1	LM3	Yes
	LM4	Yes	1	Haplotype 1 (LM5)	Yes
	LM5	Yes	1	Haplotype 1 (LM5)	Yes
	LM6	Yes	1	Haplotype 1 (LM5)	Yes
	LM7	Yes	1	Haplotype 1 (LM5)	Yes
	LM8	Yes	1	Haplotype 1 (LM5)	Yes
	LM9	Yes	1	Haplotype 1 (LM5)	No
	LM10	Yes	1	Haplotype 1 (LM5)	No

Patonga Creek	PC3	Yes	1	PC3	Yes
	PC4	Yes	1	Haplotype 1 (PC7)	Yes
	PC7	Yes	1	Haplotype 1 (PC7)	No
	PC8	Yes	1	Haplotype 1 (PC7)	No
	PC9	Yes	1	Haplotype 1 (PC7)	Yes
	PC10	Yes	1	Haplotype 1 (PC7)	No
	PC11	Yes	1	Haplotype 1 (PC7)	Yes
	PC13	Yes	1	PC13	Yes
Gordons Bay	GB2	Yes	1	Haplotype 1 (GB2)	Yes
	GB3	Yes	1	Haplotype 1 (GB2)	Yes
	GB5	Yes	1	GB5	Yes
	GB8	Yes	1	GB5	Yes
	GB14	Yes	1	GB14	Yes
	GB15	Yes	1	Haplotype 1 (GB2)	Yes
	GB16	Yes	1	GB16	Yes
	GB23	Yes	1	Haplotype 1 (GB2)	No
Kiama	KM1	Yes	1	Haplotype 1 (KM8)	No
	KM2	Yes	1	Haplotype 1 (KM8)	Yes
	KM3	Yes	1	KM3	No
	KM4	Yes	1	Haplotype 1 (KM8)	No
	KM5	Yes	1	Haplotype 1 (KM8)	No
	KM6	Yes	1	Haplotype 1 (KM8)	Yes
	KM7	Yes	1	Haplotype 1 (KM8)	No
	KM8	Yes	1	Haplotype 1 (KM8)	Yes
Merimbula Lake Inlet	MER14	Yes	1	MER19	Yes
	MER19	Yes	1	MER19	No
	MER20	Yes	1	MER19	Yes
	MER24	Yes	1	Haplotype 1 (MER24)	Yes

S8B Mean growth rate (in div/day) (n=3), cell volume (in μM^3) (n=20) and PLTX-amine fragment equivalents (in pg cell^{-1}) for *Ostreopsis* cf. *siamensis* strains isolated along the New South Wales coastline. SE represents the standard error.

Origin	Strain	μ	SE	Cell Volume	SE	PLTX amine fragment equivalents
Minnie Water	MW1	0.13	0.02	14740.70	588.09	0
	MW2	0.15	0.04	12722.23	558.02	1.48
	MW3	0.18	0.02	11382.89	532.56	1.57
	MW4	0.17	0.03	12355.01	669.02	0
	MW5	0.16	0.04	12904.95	502.06	0.28
	MW6	0.19	0.02	24413.38	1042.62	0.58
	MW7	0.19	0.03	12169.33	621.14	0.41
	MW9	0.27	0.04	10893.99	569.46	0.58
	MW10	0.19	0.03	12383.38	588.00	0
Bonny Hills	BH1	0.22	0.02	17760.06	1166.21	0.71
	BH2	0.22	0.04	20030.39	951.36	0.90
	BH3	0.17	0.01	10267.63	601.53	0.40
	BH4	0.15	0.03	16036.31	947.76	0.57
	BH5	0.20	0.01	14737.50	755.19	1.01
	BH6	0.21	0.01	17243.66	898.88	0.55
	BH7	0.21	0.01	12139.21	551.45	0.47
	BH8	0.20	0.02	15272.47	1213.19	0.74
	BH9	0.17	0.02	11634.98	702.00	0.10
	BH10	0.22	0.04	19122.84	1118.70	0.37
Wallis Lake, Forster	FR1	0.24	0.00	14468.41	466.21	0.60
	FR2	0.20	0.01	13794.20	1053.38	0.43
	FR3	0.18	0.02	16245.73	778.52	0.02
	FR4	0.22	0.02	10204.12	663.17	0.35
	FR5	0.13	0.02	17698.50	1059.87	0.43
	FR6	0.13	0.02	18159.44	833.63	0.32
	FR7	0.19	0.05	13168.28	472.45	0
	FR9	0.16	0.03	12788.15	586.22	0.50
	FR10	0.20	0.04	27584.32	693.94	0.80
Lake Macquarie	LM2	0.19	0.02	15355.16	604.34	0.32
	LM3	0.18	0.01	12410.49	688.83	0.76
	LM4	0.20	0.02	12283.04	428.46	0.30
	LM5	0.24	0.02	21898.53	1246.08	0.04
	LM6	0.19	0.03	18272.80	990.73	1.35
	LM7	0.18	0.02	16391.50	829.17	0.47
	LM8	0.17	0.03	10394.60	902.07	0.50
Patonga Creek	PC3	0.20	0.03	16606.64	676.76	0.52
	PC4	0.19	0.03	9799.19	456.66	0.52
	PC9	0.16	0.01	10189.54	455.71	0.40

	PC11	0.13	0.00	9177.61	472.42	0.27
	PC13	0.17	0.04	9965.04	500.62	0.28
Gordons Bay	GB2	0.13	0.01	11682.04	510.14	0
	GB3	0.23	0.03	12190.54	523.04	1.56
	GB5	0.13	0.03	17099.91	898.99	0.25
	GB8	0.19	0.01	12300.75	697.93	0.46
	GB14	0.14	0.02	9458.88	562.24	0.30
	GB15	0.15	0.02	11973.05	560.99	0.27
	GB16	0.12	0.03	9924.78	532.63	0
Kiama	KM2	0.17	0.02	14260.66	573.81	0
	KM6	0.20	0.03	14949.94	1196.35	0
	KM8	0.18	0.02	13957.44	616.18	0.02
Merimbula Lake Inlet	MER14	0.14	0.01	13438.59	1021.95	0.03
	MER20	0.13	0.01	11268.47	575.52	0
	MER24	0.15	0.01	11418.06	559.63	0.20

S8C Steady-state growth and light-harvesting characteristics across *Ostreopsis* cf. *siamensis* isolates of photosystem II (PSII) maximum photochemical efficiency (Fv/Fm, dimensionless), PSII absorption cross-section (σ, nm^2), PSII reaction center content ([RCII], mol RCII m^{-3} x10 $^{-18}$ cell^{-1}), Chlorophyll –a content (in pg cell^{-1}) and PSU size (moles of chl/ moles of RCII). SE represents the standard error.

Origin	Strain	F_vF_m	SE	σ	SE	RCII	SE	Chl	SE	PSU size	SE
Minnie Water	MW1	0.44	0.01	3.33	0.01	338.77	33.31	65.2	1.7	1305.2	33.3
	MW2	0.42	0.01	3.38	0.03	230.54	23.35	43.9	0.9	1085.5	23.3
	MW3	0.45	0.00	3.53	0.04	421.66	13.50	80.6	1.0	1051.1	13.5
	MW4	0.46	0.00	3.49	0.03	290.36	24.66	59.7	1.4	1089.5	24.7
	MW5	0.50	0.01	3.97	0.17	289.65	53.99	105.1	3.2	1770.0	54.0
	MW6	0.48	0.01	3.49	0.07	360.11	15.21	77.6	1.2	977.3	15.2
	MW7	0.52	0.01	3.51	0.04	45.31	32.07	29.3	1.9	482.6	32.1
	MW9	0.46	0.01	3.60	0.07	147.81	12.06	48.6	0.7	791.1	12.1
	MW 10	0.46	0.00	3.51	0.08	265.65	14.08	68.2	0.8	1278.4	14.1
Bonny Hills	BH1	0.55	0.01	3.43	0.08	179.38	42.37	96.5	3.2	1268.1	42.4
	BH2	0.48	0.00	3.62	0.08	68.03	30.27	45.8	2.8	502.9	30.3
	BH3	0.45	0.01	3.50	0.05	100.89	3.49	65.0	0.2	1447.9	3.5
	BH4	0.47	0.01	3.59	0.02	123.01	33.65	59.4	2.0	1024.4	33.6
	BH5	0.53	0.00	3.65	0.04	299.58	19.68	62.4	1.2	1066.1	19.7
	BH6	0.51	0.01	3.56	0.05	90.04	21.55	65.3	2.6	540.9	21.6
	BH7	0.48	0.01	3.32	0.06	133.40	25.64	74.2	1.2	1580.4	25.6
	BH8	0.49	0.01	3.52	0.14	161.74	13.61	55.6	0.6	1173.4	13.6
	BH9	0.51	0.01	3.71	0.11	157.91	100.8	82.8	4.7	1779.6	100.8
	BH10	0.48	0.01	3.23	0.00	426.25	28.33	65.9	2.7	693.2	28.3
Wallis Lake, Forster	FR1	0.42	0.01	3.54	0.09	184.96	12.06	55.6	0.7	945.3	12.1
	FR2	0.48	0.01	3.51	0.08	203.98	6.80	65.3	0.5	846.9	6.8
	FR3	0.43	0.01	3.49	0.03	318.95	20.51	69.7	1.4	1054.6	20.5
	FR4	0.56	0.01	3.78	0.02	67.77	28.64	47.9	2.6	526.9	28.6
	FR5	0.55	0.01	3.59	0.11	323.59	176.3	100.9	11.1	1598.4	176.3
	FR6	0.57	0.01	3.63	0.03	45.74	61.92	53.8	3.8	877.8	61.9
	FR7	0.50	0.00	3.91	0.03	46.01	13.65	44.1	0.8	715.3	13.6
	FR9	0.52	0.01	3.53	0.15	215.31	288.2	65.5	18.1	1042.3	288.2
	FR10	0.54	0.00	3.60	0.01	57.67	17.40	69.0	1.3	892.1	17.4
Lake Macquarie	LM2	0.52	0.00	3.69	0.02	45.44	36.21	45.3	2.2	743.4	36.2
	LM3	0.47	0.01	3.08	0.05	315.11	96.13	100.9	8.3	1162.1	96.1
	LM4	0.58	0.00	3.48	0.01	39.19	36.75	74.7	1.9	1422.5	36.8
	LM5	0.53	0.01	3.45	0.04	51.54	99.17	55.2	6.8	799.7	99.2
	LM6	0.47	0.01	3.10	0.04	235.30	61.15	48.9	2.4	1266.0	61.2
	LM7	0.55	0.01	3.08	0.08	159.51	47.24	89.4	2.8	1497.2	47.2
	LM8	0.48	0.01	3.15	0.04	195.21	11.35	34.5	0.5	762.9	11.3
Patonga Creek	PC3	0.52	0.00	3.62	0.01	59.53	81.97	50.0	6.5	627.0	82.0
	PC4	0.53	0.02	3.36	0.09	221.70	58.03	61.5	2.1	1731.4	58.0

	PC9	0.52	0.01	3.46	0.06	104.29	66.10	35.8	3.6	661.9	66.1
	PC11	0.51	0.01	3.33	0.08	118.45	13.83	49.2	0.6	1118.1	13.8
	PC13	0.58	0.01	3.49	0.01	59.49	46.41	59.7	3.7	749.3	46.4
Gordons Bay	GB2	0.45	0.01	3.57	0.07	89.44	17.95	31.0	0.9	625.7	18.0
	GB3	0.59	0.01	3.72	0.04	30.57	24.49	35.0	1.0	854.0	24.5
	GB5	0.45	0.01	3.53	0.06	162.03	43.58	59.3	2.2	1194.4	43.6
	GB8	0.47	0.01	3.39	0.03	279.61	40.16	57.8	1.3	1851.9	40.2
	GB14	0.53	0.01	3.15	0.07	125.08	13.99	59.8	0.9	926.0	14.0
	GB15	0.49	0.01	3.85	0.06	57.51	48.44	50.9	3.7	661.0	48.4
	GB16	0.51	0.00	3.88	0.01	28.26	20.23	31.1	0.8	822.1	20.2
Kiama	KM2	0.52	0.00	3.51	0.00	66.03	36.52	50.6	3.0	618.5	36.5
	KM6	0.57	0.01	3.28	0.03	59.57	101.7	52.7	8.1	659.7	101.7
	KM8	0.53	0.00	3.57	0.04	73.74	32.04	59.9	1.1	1752.4	32.0
Merim-bula Lake inlet	MER 14	0.44	0.01	3.10	0.05	161.83	14.23	59.6	0.7	1223.7	14.2
	MER 20	0.47	0.01	3.53	0.08	91.95	76.78	46.4	2.6	1358.3	76.8
	MER 24	0.43	0.01	3.33	0.08	145.16	8.00	42.3	0.4	831.6	8.0

S8D Rapid light curve derived parameters for *Ostreopsis* cf. *siamensis* isolates representing maximum photosynthetic rate (ETRmax), the light saturation parameter (Ek), the light utilisation efficiency (α), photochemical (1-*C*) and non-photochemical quenching (1-*Q*). SE represents the standard error of n=3.

Origin	Strain	ETR max	SE	α	SE	Ek	SE	1-C	SE	1-Q	SE
Minnie Water	MW1	1168.62	74.48	6.72	0.22	173.81	13.97	0.43	0.03	0.97	0.01
	MW2	1303.39	203.04	8.69	1.40	149.92	0.65	0.38	0.02	0.83	0.01
	MW3	1912.71	130.77	9.54	0.55	200.49	9.13	0.52	0.02	1.00	0.02
	MW4	1536.75	122.79	8.10	0.56	189.80	11.67	0.46	0.01	1.00	0.02
	MW5	446.20	19.67	3.68	0.26	121.71	3.72	0.49	0.01	0.86	0.01
	MW6	1197.29	99.52	7.03	0.42	170.36	6.43	0.48	0.03	0.93	0.04
	MW7	959.85	172.48	7.63	1.08	124.70	6.13	0.50	0.04	0.85	0.02
	MW9	1211.28	108.35	8.56	0.54	141.57	14.57	0.46	0.02	0.91	0.04
	MW10	2451.22	122.07	10.15	0.30	241.44	4.86	0.56	0.02	0.97	0.03
Bonny Hills	BH1	834.39	228.59	4.01	0.58	208.26	34.36	0.47	0.05	0.94	0.05
	BH2	1302.66	334.03	9.22	2.08	138.54	6.24	0.50	0.06	0.75	0.04
	BH3	1396.49	152.23	10.15	0.60	137.59	7.90	0.44	0.03	0.82	0.02
	BH4	1255.84	48.97	8.78	0.11	143.00	4.59	0.49	0.01	0.76	0.03
	BH5	2270.49	322.70	10.08	1.15	225.31	7.29	0.54	0.00	0.95	0.03
	BH6	1285.01	82.25	9.28	0.65	138.78	5.57	0.52	0.03	0.83	0.03
	BH7	2031.21	352.67	13.88	2.43	146.32	3.31	0.47	0.01	0.86	0.02
	BH8	1242.82	233.89	7.91	1.26	157.08	5.81	0.61	0.10	0.71	0.09
	BH9	1560.81	404.75	7.41	1.60	210.60	9.90	0.56	0.06	0.87	0.09
	BH10	1495.95	143.69	8.45	0.43	176.94	7.88	0.47	0.01	1.00	0.01
Wallis Lake, Forster	FR1	1146.19	176.56	5.12	0.41	223.98	15.67	0.51	0.02	1.00	0.03
	FR2	2148.90	180.51	11.83	0.82	181.64	3.62	0.50	0.03	0.94	0.06
	FR3	1895.83	78.32	9.99	0.31	189.68	3.47	0.49	0.01	1.00	0.02
	FR4	334.66	56.33	3.06	0.56	109.99	1.80	0.44	0.02	0.93	0.01
	FR5	1687.66	317.04	9.92	1.55	170.12	8.54	0.46	0.04	0.78	0.20
	FR6	292.43	9.13	2.68	0.21	110.15	7.26	0.47	0.01	0.82	0.03

211

	FR7	739.16	27.16	7.73	0.13	95.68	3.94	0.39	0.01	0.81	0.01
	FR9	1260.31	441.51	7.71	2.46	163.48	5.89	0.49	0.06	0.84	0.08
	FR10	718.33	75.69	6.58	0.92	110.22	4.12	0.41	0.02	1.00	0.01
Lake Macquarie	LM2	769.93	67.95	6.75	0.78	114.77	2.89	0.44	0.01	0.97	0.01
	LM3	1631.32	14.58	8.91	0.57	183.01	13.69	0.48	0.02	1.00	0.02
	LM4	540.38	50.91	2.89	0.32	188.03	4.03	0.55	0.02	1.00	0.01
	LM5	628.17	121.30	5.12	1.04	123.62	6.00	0.44	0.03	0.96	0.02
	LM6	1501.78	374.68	7.60	1.61	197.63	7.53	0.46	0.03	1.00	0.07
	LM7	906.74	234.82	6.17	0.10	147.00	36.72	0.16	0.16	1.00	0.01
	LM8	1003.68	68.71	6.05	0.36	165.89	1.62	0.44	0.02	0.99	0.03
Patonga Creek	PC3	693.85	117.87	5.76	0.95	120.29	3.49	0.45	0.01	0.96	0.01
	PC4	698.78	82.44	5.46	0.57	127.96	31.31	0.31	0.04	0.95	0.04
	PC9	1206.73	119.61	6.68	0.63	180.56	2.62	0.51	0.03	0.86	0.04
	PC11	1408.91	121.22	8.44	0.51	166.97	4.66	0.48	0.03	0.86	0.05
	PC13	405.43	13.18	3.17	0.08	128.05	1.64	0.44	0.01	0.98	0.02
Gordons Bay	GB2	1859.42	97.07	10.40	0.41	178.78	2.39	0.45	0.03	0.92	0.08
	GB3	251.59	10.16	2.19	0.08	115.13	6.22	0.41	0.00	0.95	0.03
	GB5	500.05	29.17	3.41	0.13	146.38	5.87	0.40	0.02	0.71	0.05
	GB8	1706.62	15.06	9.27	0.50	184.03	8.56	0.44	0.01	1.00	0.03
	GB14	1325.84	131.94	6.71	0.81	197.69	8.90	0.45	0.03	0.96	0.03
	GB15	1025.90	56.56	11.67	0.92	88.48	5.09	0.34	0.01	0.85	0.01
	GB16	515.28	50.59	3.28	0.27	156.44	3.23	0.49	0.04	0.86	0.00
Kiama	KM2	924.66	94.10	8.23	0.50	112.12	7.94	0.44	0.02	0.91	0.01
	KM6	462.38	77.72	4.75	0.97	99.37	5.01	0.38	0.01	0.96	0.03
	KM8	404.39	75.34	3.88	0.36	102.68	10.35	0.34	0.04	0.85	0.01
Merimbula Lake inlet	MER14	1995.97	212.47	8.60	0.72	232.06	5.64	0.51	0.02	1.00	0.03
	MER20	1737.95	97.36	8.84	0.78	196.50	9.64	0.60	0.07	0.76	0.11
	MER24	2602.18	333.18	11.33	1.56	229.77	11.88	0.57	0.01	0.94	0.06

S9A Analysis of variance (one-way ANOVA) on growth rates, F*v*F*m*, σ, ETR$_{max}$, α, E$_k$ and cellular biovolume for strains isolated from Minnie Water

<div align="center">ANOVA</div>

		Sum of Squares	df	Mean Square	F	Sig.
Growth rates	Between Groups	.054	8	.007	4.093	.006
	Within Groups	.030	18	.002		
	Total	.084	26			
F*v*F*m*	Between Groups	.024	8	.003	23.064	.000
	Within Groups	.002	18	.000		
	Total	.026	26			
σ	Between Groups	.813	8	.102	9.820	.000
	Within Groups	.186	18	.010		
	Total	.999	26			
ETR$_{max}$	Between Groups	7832287.309	8	979035.914	20.168	.000
	Within Groups	873776.853	18	48543.158		
	Total	8706064.161	26			
α	Between Groups	86.266	8	10.783	7.347	.000
	Within Groups	26.420	18	1.468		
	Total	112.685	26			
E$_k$	Between Groups	35783.513	8	4472.939	18.037	.000
	Within Groups	4463.694	18	247.983		
	Total	40247.207	26			
Cell vol.	Between Groups	2730529322.633	8	341316165.329	40.597	.000
	Within Groups	1437679796.881	171	8407484.192		
	Total	4168209119.514	179			

S9B Analysis of variance (one-way ANOVA) on growth rates, FvFm, σ, ETR$_{max}$, α, E$_k$ and cellular biovolume for strains isolated from Bonny Hills

<div align="center">ANOVA</div>

		Sum of Squares	df	Mean Square	F	Sig.
Growth rates	Between Groups	.014	9	.002	1.087	.414
	Within Groups	.029	20	.001		
	Total	.043	29			
FvFm	Between Groups	.023	9	.003	18.194	.000
	Within Groups	.003	20	.000		
	Total	.026	29			
σ	Between Groups	.615	9	.068	4.000	.005
	Within Groups	.342	20	.017		
	Total	.956	29			
ETR$_{max}$	Between Groups	4601138.534	9	511237.615	2.567	.038
	Within Groups	3983103.861	20	199155.193		
	Total	8584242.395	29			
α	Between Groups	165.997	9	18.444	3.617	.008
	Within Groups	101.984	20	5.099		
	Total	267.980	29			
E$_k$	Between Groups	29873.804	9	3319.312	6.951	.000
	Within Groups	9550.359	20	477.518		
	Total	39424.163	29			
Cell vol.	Between Groups	1925446529.234	9	213938503.248	12.699	.000
	Within Groups	3200978266.838	190	16847254.036		
	Total	5126424796.071	199			

S9C Analysis of variance (one-way ANOVA) on growth rates, FvFm, σ, ETR$_{max}$, α, E$_k$ and cellular biovolume for strains isolated from Wallis Lake, Forster

<div align="center">ANOVA</div>

		Sum of Squares	df	Mean Square	F	Sig.
Growth rates	Between Groups	.033	8	.004	1.940	.116
	Within Groups	.038	18	.002		
	Total	.070	26			
FvFm	Between Groups	.072	8	.009	83.250	.000
	Within Groups	.002	18	.000		
	Total	.073	26			
σ	Between Groups	.465	8	.058	3.344	.016
	Within Groups	.313	18	.017		
	Total	.779	26			
ETR$_{max}$	Between Groups	10826669.161	8	1353333.645	10.825	.000
	Within Groups	2250333.317	18	125018.518		
	Total	13077002.477	26			
α	Between Groups	213.563	8	26.695	3.831	.009
	Within Groups	125.443	18	6.969		
	Total	339.007	26			
E$_k$	Between Groups	46335.799	8	5791.975	17.695	.000
	Within Groups	5891.808	18	327.323		
	Total	52227.607	26			
Cell vol.	Between Groups	4018831538.189	8	502353942.274	43.146	.000
	Within Groups	1990991976.986	171	11643227.936		
	Total	6009823515.175	179			

S9D Analysis of variance (one-way ANOVA) on growth rates, FvFm, σ, ETR$_{max}$, α, E$_k$ and cellular biovolume for strains isolated from Lake Macquarie

<div align="center">ANOVA</div>

		Sum of Squares	df	Mean Square	F	Sig.
Growth rates	Between Groups	.008	6	.001	.888	.529
	Within Groups	.020	14	.001		
	Total	.028	20			
FvFm	Between Groups	.033	6	.006	21.291	.000
	Within Groups	.004	14	.000		
	Total	.037	20			
σ	Between Groups	1.110	6	.185	29.502	.000
	Within Groups	.088	14	.006		
	Total	1.198	20			
ETR$_{max}$	Between Groups	3184342.443	6	530723.740	5.568	.004
	Within Groups	1334329.752	14	95309.268		
	Total	4518672.195	20			
α	Between Groups	65.424	6	10.904	5.252	.005
	Within Groups	29.068	14	2.076		
	Total	94.491	20			
E$_k$	Between Groups	18622.412	6	3103.735	4.375	.011
	Within Groups	9932.477	14	709.463		
	Total	28554.889	20			
Cell vol.	Between Groups	1901709348.127	6	316951558.021	21.929	.000
	Within Groups	1922309237.843	133	14453452.916		
	Total	3824018585.971	139			

S9E Analysis of variance (one-way ANOVA) on growth rates, FvFm, σ, ETR$_{max}$, α, E$_k$ and cellular biovolume for strains isolated from Patonga Creek

		Sum of Squares	df	Mean Square	F	Sig.
Growth rates	Between Groups	.010	4	.002	1.282	.340
	Within Groups	.019	10	.002		
	Total	.028	14			
FvFm	Between Groups	.009	4	.002	8.946	.002
	Within Groups	.002	10	.000		
	Total	.011	14			
σ	Between Groups	.151	4	.038	3.283	.058
	Within Groups	.115	10	.012		
	Total	.266	14			
ETR$_{max}$	Between Groups	2037498.483	4	509374.621	17.025	.000
	Within Groups	299192.264	10	29919.226		
	Total	2336690.747	14			
α	Between Groups	44.255	4	11.064	9.773	.002
	Within Groups	11.320	10	1.132		
	Total	55.576	14			
E$_k$	Between Groups	8164.959	4	2041.240	3.323	.056
	Within Groups	6143.239	10	614.324		
	Total	14308.198	14			
Cell vol.	Between Groups	756331342.012	4	189082835.503	35.067	.000
	Within Groups	512239328.278	95	5391992.929		
	Total	1268570670.290	99			

ANOVA

S9F Analysis of variance (one-way ANOVA) on growth rates, FvFm, σ, ETR$_{max}$, α, E$_k$ and cellular biovolume for strains isolated from Gordons Bay

<div align="center">ANOVA</div>

		Sum of Squares	df	Mean Square	F	Sig.
Growth rates	Between Groups	.026	6	.004	3.213	.034
	Within Groups	.019	14	.001		
	Total	.045	20			
FvFm	Between Groups	.043	6	.007	37.217	.000
	Within Groups	.003	14	.000		
	Total	.045	20			
σ	Between Groups	1.209	6	.201	23.606	.000
	Within Groups	.119	14	.009		
	Total	1.328	20			
ETR$_{max}$	Between Groups	7154734.806	6	1192455.801	82.390	.000
	Within Groups	202625.628	14	14473.259		
	Total	7357360.434	20			
α	Between Groups	263.550	6	43.925	50.890	.000
	Within Groups	12.084	14	.863		
	Total	275.634	20			
E$_k$	Between Groups	28288.021	6	4714.670	41.058	.000
	Within Groups	1607.597	14	114.828		
	Total	29895.618	20			
Cell vol.	Between Groups	738895717.056	6	123149286.176	15.710	.000
	Within Groups	1042560911.529	133	7838803.846		
	Total	1781456628.586	139			

218

S9G Analysis of variance (one-way ANOVA) on growth rates, FvFm, σ, ETR$_{max}$, α, E$_k$ and cellular biovolume for strains isolated from Kiama

<div align="center">ANOVA</div>

		Sum of Squares	df	Mean Square	F	Sig.
Growth rates	Between Groups	.002	2	.001	.706	.531
	Within Groups	.008	6	.001		
	Total	.010	8			
FvFm	Between Groups	.005	2	.003	8.233	.019
	Within Groups	.002	6	.000		
	Total	.007	8			
σ	Between Groups	.141	2	.070	25.410	.001
	Within Groups	.017	6	.003		
	Total	.157	8			
ETR$_{max}$	Between Groups	487754.222	2	243877.111	11.856	.008
	Within Groups	123423.921	6	20570.654		
	Total	611178.143	8			
α	Between Groups	31.790	2	15.895	12.037	.008
	Within Groups	7.923	6	1.321		
	Total	39.713	8			
E$_k$	Between Groups	262.673	2	131.337	.672	.545
	Within Groups	1172.253	6	195.376		
	Total	1434.926	8			
Cell vol.	Between Groups	10347306.699	2	5173653.350	.363	.697
	Within Groups	813261794.142	57	14267750.774		
	Total	823609100.842	59			

S9H Analysis of variance (one-way ANOVA) on growth rates, FvFm, σ, ETR$_{max}$, α, E$_k$ and cellular biovolume for strains isolated from Merimbula Lake inlet.

<div align="center">ANOVA</div>

		Sum of Squares	df	Mean Square	F	Sig.
Growth rates	Between Groups	.000	2	.000	.343	.723
	Within Groups	.002	6	.000		
	Total	.003	8			
FvFm	Between Groups	.002	2	.001	3.622	.093
	Within Groups	.002	6	.000		
	Total	.003	8			
σ	Between Groups	.287	2	.143	8.859	.016
	Within Groups	.097	6	.016		
	Total	.384	8			
ETR$_{max}$	Between Groups	1180962.531	2	590481.265	3.565	.095
	Within Groups	993789.392	6	165631.565		
	Total	2174751.923	8			
α	Between Groups	13.632	2	6.816	1.912	.228
	Within Groups	21.384	6	3.564		
	Total	35.016	8			
E$_k$	Between Groups	2218.349	2	1109.175	4.173	.073
	Within Groups	1594.961	6	265.827		
	Total	3813.310	8			
Cell vol.	Between Groups	58762086.306	2	29381043.153	2.610	.082
	Within Groups	641728095.121	57	11258387.634		
	Total	700490181.427	59			

S10 Functional groupings based on all factors regulating the ETR (σ, Fv/Fm, cellular RCII concentration ([RCII]), [1 − C] and [1 − Q) across all types. Cluster analysis and multidimensional scaling (MDS) were performed on the average of each variable per variant; similarity is shown at the 90 and 95% levels and vectors driving the clustering are shown in black.
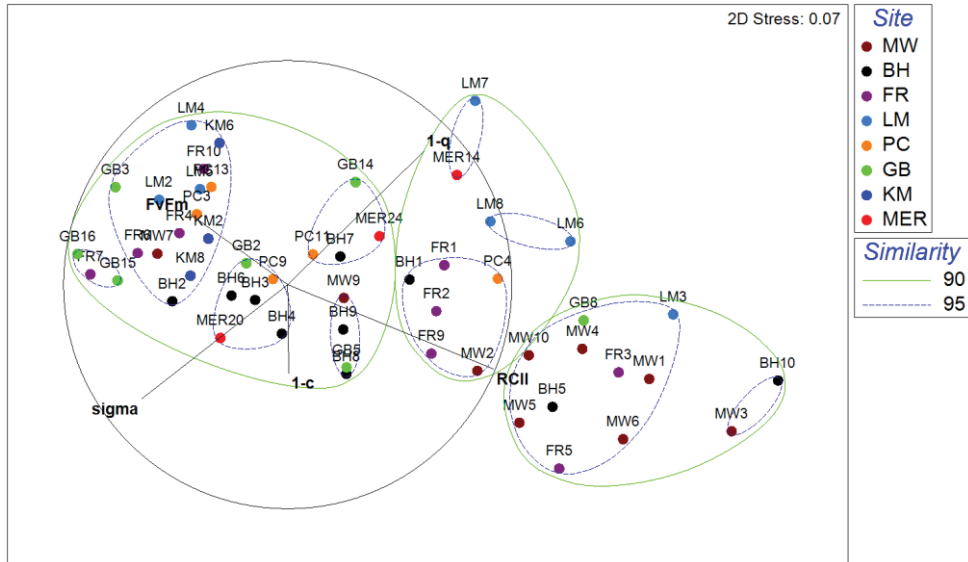
S11A Two-dimensional principal component analysis of phenotypic variables in *Ostreopsis* cf. *siamensis* clones. Light harvesting (Fv/Fm, σ, Cellular RCII concentration ([RCII])) and light utilization ([1-C] and [1-Q]) along with cell volume, toxin amounts and growth rates were normalised across all strains and indicated in black bars.
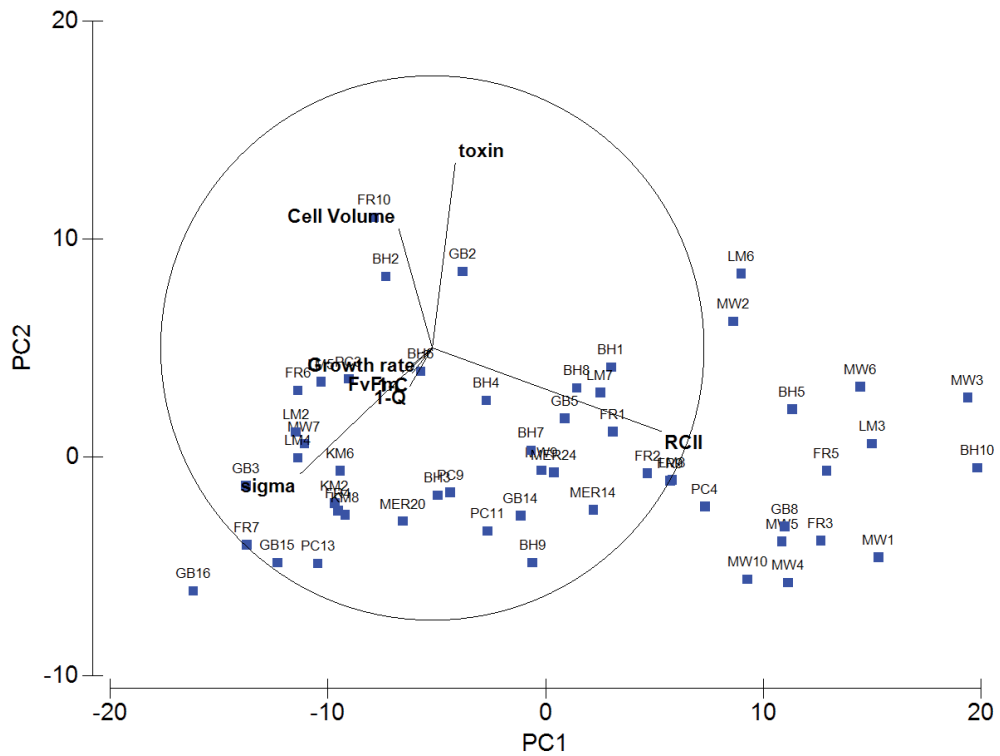
S11B Percentage variations in *Ostreopsis* cf. *siamensis* strains being explained by the factors making up the principal component axes.

PC	Eigenvalues	% Variation	Cum.% Variation
1	94.2	75.7	75.7
2	15.6	12.5	88.2
3	10	8.0	96.2
4	3.64	2.9	99.2
5	0.666	0.5	99.7

S11C Eigenvectors: Coefficient in the linear combination of variables making up the Principal component axes

Variable	PC1	PC2	PC3	PC4	PC5
1-C	-0.075	-0.094	0.075	-0.042	0.903
1-Q	-0.083	-0.140	-0.040	0.833	-0.191
FvFm	-0.110	-0.091	0.007	0.078	-0.037
σ	-0.488	-0.464	0.190	-0.454	-0.321
RCII	0.844	-0.307	-0.060	-0.192	-0.127
Growth Rate	-0.050	-0.021	-0.004	0.070	-0.001
Cell volume	-0.124	0.438	-0.769	-0.210	-0.084
Toxin	0.084	0.679	0.601	-0.083	-0.143

S12A Description of sequences from *Ostreopsis* cf. *ovata* HER27 encoding essential enzymes of various metabolic pathways. NA= enzymes not present in the transcriptome

Metabolic pathways	Enzymes	Contig name
Glycolysis	1.2.1.12/1.2.1.59: Glyceraldehyde 3-phosphate dehydrogenase /glyceraldehyde-3-phosphate dehydrogenase (NAD(P))	ost_ovt_her27_contig_48, ost_ovt_her27_contig_9631, ost_ovt_her27_contig_49, ost_ovt_her27_contig_2369, ost_ovt_her27_contig_10474, ost_ovt_her27_contig_313, ost_ovt_her27_contig_303, ost_ovt_her27_contig_1031, ost_ovt_her27_contig_314, ost_ovt_her27_contig_894, ost_ovt_her27_contig_7371, ost_ovt_her27_contig_2370, ost_ovt_her27_contig_1392,
	2.7.1.11: 6-phosphofructokinase	ost_ovt_her27_contig_26557, ost_ovt_her27_contig_9327, ost_ovt_her27_contig_3200, ost_ovt_her27_contig_9307, ost_ovt_her27_contig_38266
	2.7.1.2: Glucokinase	ost_ovt_her27_contig_37921, ost_ovt_her27_contig_16013
	2.7.1.40: Pyruvate kinase	ost_ovt_her27_contig_10971, ost_ovt_her27_contig_150, ost_ovt_her27_contig_149, ost_ovt_her27_contig_5396
	2.7.2.3: Phosphoglycerate kinase	ost_ovt_her27_contig_11223, ost_ovt_her27_contig_3439, ost_ovt_her27_contig_7564, ost_ovt_her27_contig_4977, ost_ovt_her27_contig_4932, ost_ovt_her27_contig_31683, ost_ovt_her27_contig_303, ost_ovt_her27_contig_11106, ost_ovt_her27_contig_31867, ost_ovt_her27_contig_3274
	4.1.2.13: Fructose-bisphosphate aldolase, class I	ost_ovt_her27_contig_848, ost_ovt_her27_contig_832, ost_ovt_her27_contig_7029, ost_ovt_her27_contig_26143, ost_ovt_her27_contig_10407, ost_ovt_her27_contig_11219, ost_ovt_her27_contig_380, ost_ovt_her27_contig_1157, ost_ovt_her27_contig_1156, ost_ovt_her27_contig_3689, ost_ovt_her27_contig_1159, ost_ovt_her27_contig_4511, ost_ovt_her27_contig_1158, ost_ovt_her27_contig_4698, ost_ovt_her27_contig_368, ost_ovt_her27_contig_17475, ost_ovt_her27_contig_367, ost_ovt_her27_contig_5232, ost_ovt_her27_contig_7030, ost_ovt_her27_contig_51020, ost_ovt_her27_contig_4393

	4.2.1.11: Enolase	ost_ovt_her27_contig_8255, ost_ovt_her27_contig_8256, ost_ovt_her27_contig_64531, ost_ovt_her27_contig_10017, ost_ovt_her27_contig_12208, ost_ovt_her27_contig_55284, ost_ovt_her27_contig_15128, ost_ovt_her27_contig_58852, ost_ovt_her27_contig_1863, ost_ovt_her27_contig_32378, ost_ovt_her27_contig_1031, ost_ovt_her27_contig_20566, ost_ovt_her27_contig_3273, ost_ovt_her27_contig_9042
	5.3.1.1: Triosephosphate isomerase (TIM)	ost_ovt_her27_contig_4408, ost_ovt_her27_contig_4407, ost_ovt_her27_contig_15128, ost_ovt_her27_contig_14523, ost_ovt_her27_contig_15931, ost_ovt_her27_contig_13156, ost_ovt_her27_contig_4315, ost_ovt_her27_contig_21236, ost_ovt_her27_contig_13047, ost_ovt_her27_contig_22318, ost_ovt_her27_contig_6965
	5.3.1.9: Glucose-6-phosphate isomerase	ost_ovt_her27_contig_1863, ost_ovt_her27_contig_13393
	5.4.2.1: Phosphoglycerate mutase	NA
TCA cycle	6.2.1.4/6.2.1.5: Succinyl-CoA synthetase alpha subunit	NA
	1.1.1.37: Malate dehydrogenase	ost_ovt_her27_contig_52108, ost_ovt_her27_contig_41061, ost_ovt_her27_contig_31959, ost_ovt_her27_contig_11742, ost_ovt_her27_contig_79285, ost_ovt_her27_contig_4236, ost_ovt_her27_contig_5611, ost_ovt_her27_contig_4697, ost_ovt_her27_contig_3264, ost_ovt_her27_contig_17255, ost_ovt_her27_contig_3881, ost_ovt_her27_contig_75030, ost_ovt_her27_contig_8670
	1.1.1.42: Isocitrate dehydrogenase	ost_ovt_her27_contig_48522, ost_ovt_her27_contig_5934, ost_ovt_her27_contig_5325, ost_ovt_her27_contig_8417, ost_ovt_her27_contig_13055, ost_ovt_her27_contig_1061, ost_ovt_her27_contig_11337, ost_ovt_her27_contig_12889, ost_ovt_her27_contig_31867, ost_ovt_her27_contig_20901
	1.2.4.1/2.3.1.12: Pyruvate dehydrogenase E1 component/ Pyruvate dehydrogenase E2 component (dihydrolipoamide acetyltransferase)	ost_ovt_her27_contig_7366

	1.2.4.2/2.3.1.61: 2-oxoglutarate dehydrogenase E1 component / 2-oxoglutarate dehydrogenase E2 component (dihydrolipoamide succinyltransferase)	ost_ovt_her27_contig_41540, ost_ovt_her27_contig_2419, ost_ovt_her27_contig_7366, ost_ovt_her27_contig_12880, ost_ovt_her27_contig_2097, ost_ovt_her27_contig_26581
	1.3.5.1/ 1.3.99.1: Succinate dehydrogenase (ubiquinone) flavoprotein subunit/ Succinate dehydrogenase flavoprotein subunit	ost_ovt_her27_contig_11245, ost_ovt_her27_contig_11246, ost_ovt_her27_contig_87, ost_ovt_her27_contig_17173, ost_ovt_her27_contig_9363
	2.3.3.1: Citrate synthase	NA
	4.2.1.2: Fumarate hydratase, class I	ost_ovt_her27_contig_24474, ost_ovt_her27_contig_11132, ost_ovt_her27_contig_3597, ost_ovt_her27_contig_2825
	4.2.1.3: Aconitate hydratase 1	ost_ovt_her27_contig_3404
Oxidative phosphorylation	1.6.5.3/1.6.99.3: NADH dehydrogenase/ NADH dehydrogenase (complex I)	ost_ovt_her27_contig_21786
	1.3.5.1/ 1.3.99.1: Succinate dehydrogenase (ubiquinone) flavoprotein subunit/ Succinate dehydrogenase flavoprotein subunit subunit (complex II)	ost_ovt_her27_contig_11245, ost_ovt_her27_contig_11246, ost_ovt_her27_contig_87, ost_ovt_her27_contig_17173, ost_ovt_her27_contig_9363
	1.10.2.2: Ubiquinol-cytochrome c reductase iron-sulfur subunit (complex III)	ost_ovt_her27_contig_16934, ost_ovt_her27_contig_16933, ost_ovt_her27_contig_24244, ost_ovt_her27_contig_22636
	1.9.3.1: Cb-type cytochrome c oxidase subunit I (complex IV)	ost_ovt_her27_contig_1875, ost_ovt_her27_contig_8433, ost_ovt_her27_contig_8432, ost_ovt_her27_contig_9, ost_ovt_her27_contig_56568, ost_ovt_her27_contig_19537, ost_ovt_her27_contig_15580, ost_ovt_her27_contig_2748
	3.6.3.6/3.6.3.14: H+ transporting ATPase/F-type H+-transporting ATPase subunit a (complex V)	NA
Carbon fixation (C3)	2.7.1.19: Phosphoribulokinase	ost_ovt_her27_contig_1754, ost_ovt_her27_contig_1753, ost_ovt_her27_contig_5000
	4.1.1.39: Ribulose-bisphosphate carboxylase large chain	ost_ovt_her27_contig_74578, ost_ovt_her27_contig_806, ost_ovt_her27_contig_25977, ost_ovt_her27_contig_43564, ost_ovt_her27_contig_28448, ost_ovt_her27_contig_1500, ost_ovt_her27_contig_4138, ost_ovt_her27_contig_64887, ost_ovt_her27_contig_38397, ost_ovt_her27_contig_34119, ost_ovt_her27_contig_60192, ost_ovt_her27_contig_9220
	2.7.2.3: Phosphoglycerate kinase	ost_ovt_her27_contig_11223, ost_ovt_her27_contig_3439,

225

	ost_ovt_her27_contig_7564, ost_ovt_her27_contig_4977, ost_ovt_her27_contig_4932, ost_ovt_her27_contig_31683, ost_ovt_her27_contig_303, ost_ovt_her27_contig_11106, ost_ovt_her27_contig_31867, ost_ovt_her27_contig_3274
1.2.1.13/1.2.1.59: Glyceraldehyde-3-phosphate dehydrogenase (NADP+) (phosphorylating)/ glyceraldehyde-3-phosphate dehydrogenase (NAD(P))	ost_ovt_her27_contig_48, ost_ovt_her27_contig_9631, ost_ovt_her27_contig_49, ost_ovt_her27_contig_2369, ost_ovt_her27_contig_10474, ost_ovt_her27_contig_313, ost_ovt_her27_contig_303, ost_ovt_her27_contig_1031, ost_ovt_her27_contig_314, ost_ovt_her27_contig_894, ost_ovt_her27_contig_7371, ost_ovt_her27_contig_2370, ost_ovt_her27_contig_1392
5.3.1.1: Triosephosphate isomerase (TIM)	ost_ovt_her27_contig_4408, ost_ovt_her27_contig_4407, ost_ovt_her27_contig_15128, ost_ovt_her27_contig_14523, ost_ovt_her27_contig_15931, ost_ovt_her27_contig_13156, ost_ovt_her27_contig_4315, ost_ovt_her27_contig_21236, ost_ovt_her27_contig_13047, ost_ovt_her27_contig_22318, ost_ovt_her27_contig_6965
4.1.2.13: Fructose-bisphosphate aldolase, class I	ost_ovt_her27_contig_848, ost_ovt_her27_contig_832, ost_ovt_her27_contig_7029, ost_ovt_her27_contig_26143, ost_ovt_her27_contig_10407, ost_ovt_her27_contig_11219, ost_ovt_her27_contig_380, ost_ovt_her27_contig_1157, ost_ovt_her27_contig_1156, ost_ovt_her27_contig_3689, ost_ovt_her27_contig_1159, ost_ovt_her27_contig_4511, ost_ovt_her27_contig_1158, ost_ovt_her27_contig_4698, ost_ovt_her27_contig_368, ost_ovt_her27_contig_17475, ost_ovt_her27_contig_367, ost_ovt_her27_contig_5232, ost_ovt_her27_contig_7030, ost_ovt_her27_contig_51020, ost_ovt_her27_contig_4393
3.1.3.11: Fructose-1,6-bisphosphatase I	ost_ovt_her27_contig_4924, ost_ovt_her27_contig_50437, ost_ovt_her27_contig_7662, ost_ovt_her27_contig_6157, ost_ovt_her27_contig_6850, ost_ovt_her27_contig_6851, ost_ovt_her27_contig_1940,

		ost_ovt_her27_contig_1939, ost_ovt_her27_contig_8548, ost_ovt_her27_contig_1938, ost_ovt_her27_contig_454
	2.2.1.1: Transketolase	ost_ovt_her27_contig_18275, ost_ovt_her27_contig_1416, ost_ovt_her27_contig_1421, ost_ovt_her27_contig_5741, ost_ovt_her27_contig_5740, ost_ovt_her27_contig_3240
	3.1.3.37: Sedoheptulose-1,7-bisphosphatase	ost_ovt_her27_contig_4924, ost_ovt_her27_contig_7662
	5.1.3.1: Ribulose-phosphate 3-epimerase	ost_ovt_her27_contig_3192, ost_ovt_her27_contig_3193, ost_ovt_her27_contig_3191, ost_ovt_her27_contig_56801, ost_ovt_her27_contig_12591
	5.3.1.6: Ribose 5-phosphate isomerase A	ost_ovt_her27_contig_4354, ost_ovt_her27_contig_4353, ost_ovt_her27_contig_32380
Pentose phosphate pathway	1.1.1.49 glucose-6-phosphate dehydrogenase	ost_ovt_her27_contig_39334, ost_ovt_her27_contig_85493, ost_ovt_her27_contig_43184
	3.1.1.31 6-phosphogluconolactonase	NA
	1.1.1.44 phosphogluconate dehydrogenase (NADP+-dependent, decarboxylating)	ost_ovt_her27_contig_64060, ost_ovt_her27_contig_19870, ost_ovt_her27_contig_25783
	5.3.1.6 ribose-5-phosphate isomerase	ost_ovt_her27_contig_4354, ost_ovt_her27_contig_4353, ost_ovt_her27_contig_32380
	5.1.3.1 ribulose-phosphate 3-epimerase	ost_ovt_her27_contig_3192, ost_ovt_her27_contig_3193, ost_ovt_her27_contig_3191, ost_ovt_her27_contig_56801, ost_ovt_her27_contig_12591
	2.2.1.1 transketolase	ost_ovt_her27_contig_18275, ost_ovt_her27_contig_1416, ost_ovt_her27_contig_1421, ost_ovt_her27_contig_5741, ost_ovt_her27_contig_5740, ost_ovt_her27_contig_3240
	2.2.1.2 transaldolase	ost_ovt_her27_contig_9097

Purine nucleotide synthesis

Inosine monophosphate synthesis (precursor)	2.7.6.1: Ribose-phosphate pyrophosphokinase	ost_ovt_her27_contig_18198, ost_ovt_her27_contig_51402, ost_ovt_her27_contig_17881
	2.1.2.2: GAR transformylase	ost_ovt_her27_contig_29588
	2.1.2.3: AICAR transformylase	ost_ovt_her27_contig_556
	2.4.2.14: Amidophosphoribosyltransferase	NA
	3.5.4.10: IMP cyclohydrolase	ost_ovt_her27_contig_556
	4.1.1.21: AIR carboxylase	
	4.3.2.2: Adenylosuccinate lyase	ost_ovt_her27_contig_23411
	6.3.2.6: SAICAR synthetase	

	6.3.3.1: AIR synthetase	ost_ovt_her27_contig_8507
	6.3.4.13: Phosphoribosylamine--glycine ligase	ost_ovt_her27_contig_84740, ost_ovt_her27_contig_556, ost_ovt_her27_contig_8507
	6.3.5.3: FGAM synthetase	ost_ovt_her27_contig_4284
Synthesis of AMP, ADP and ATP	6.3.4.4: Adenylosuccinate synthase	ost_ovt_her27_contig_4309
	4.3.2.2: Adenylosuccinate lyase	ost_ovt_her27_contig_23411
	2.7.4.3: Adenylate kinase	ost_ovt_her27_contig_12599, ost_ovt_her27_contig_15900, ost_ovt_her27_contig_20607, ost_ovt_her27_contig_4217, ost_ovt_her27_contig_66228, ost_ovt_her27_contig_4216, ost_ovt_her27_contig_68327, ost_ovt_her27_contig_5155, ost_ovt_her27_contig_24339, ost_ovt_her27_contig_30604
	2.7.4.6: Nucleoside-diphosphate kinase	ost_ovt_her27_contig_8710, ost_ovt_her27_contig_71721, ost_ovt_her27_contig_23976
Synthesis of dADP and dATP	1.17.4.1: Ribonucleotide reductase, class II	ost_ovt_her27_contig_1867, ost_ovt_her27_contig_6344, ost_ovt_her27_contig_636, ost_ovt_her27_contig_15551, ost_ovt_her27_contig_4366, ost_ovt_her27_contig_5131
	2.7.4.6: Nucleoside-diphosphate kinase	ost_ovt_her27_contig_8710, ost_ovt_her27_contig_71721, ost_ovt_her27_contig_23976
Synthesis of GMP, GDP and GTP	1.1.1.205: IMP dehydrogenase	ost_ovt_her27_contig_23952, ost_ovt_her27_contig_48516, ost_ovt_her27_contig_13762, ost_ovt_her27_contig_27453, ost_ovt_her27_contig_8591
	6.3.5.2: GMP synthase (glutamine-hydrolysing)	ost_ovt_her27_contig_4539
	2.7.4.8: Guanylate kinase	ost_ovt_her27_contig_1458, ost_ovt_her27_contig_23993, ost_ovt_her27_contig_55284, ost_ovt_her27_contig_65613
	2.7.4.6: Nucleoside-diphosphate kinase	ost_ovt_her27_contig_8710, ost_ovt_her27_contig_71721, ost_ovt_her27_contig_23976
Synthesis of dGDP and dGTP	1.17.4.1: Ribonucleotide reductase, class II	ost_ovt_her27_contig_1867, ost_ovt_her27_contig_6344, ost_ovt_her27_contig_636, ost_ovt_her27_contig_15551, ost_ovt_her27_contig_4366, ost_ovt_her27_contig_5131
	2.7.4.6: Nucleoside-diphosphate kinase	ost_ovt_her27_contig_8710, ost_ovt_her27_contig_71721, ost_ovt_her27_contig_23976

Pyrimidine nucleotide synthesis

Uridine monophosphate synthesis (precursor)	6.3.5.5: carbamoyl-phosphate synthase	ost_ovt_her27_contig_1266, ost_ovt_her27_contig_80671
	2.1.3.2: aspartate	ost_ovt_her27_contig_1191

	carbamoyltransferase	
	3.5.2.3: dihydroorotase	
	1.3.5.2: dihydroorotate dehydrogenase	ost_ovt_her27_contig_46159, ost_ovt_her27_contig_15162
	2.4.2.10: orotate phosphoribosyltransferase	ost_ovt_her27_contig_20203
	4.1.1.23: orotidine-5'-monophosphate decarboxylase	ost_ovt_her27_contig_20203
UDP, UTP, CTP and CDP synthesis	2.7.4.4: nucleoside phosphate kinase	NA
	2.7.4.6: nucleoside-diphosphate kinase	ost_ovt_her27_contig_8710, ost_ovt_her27_contig_71721, ost_ovt_her27_contig_23976
	6.3.4.2: CTP synthase	ost_ovt_her27_contig_2435
dCDP, dCTP, dUDP and dUTP synthesis	1.17.4.1: ribonucleotide reductase, class II	ost_ovt_her27_contig_1867, ost_ovt_her27_contig_6344, ost_ovt_her27_contig_636, ost_ovt_her27_contig_15551, ost_ovt_her27_contig_4366, ost_ovt_her27_contig_5131
	2.7.4.6: nucleoside-diphosphate kinase	ost_ovt_her27_contig_8710, ost_ovt_her27_contig_71721, ost_ovt_her27_contig_23976
dTMP, dTDP and dTTP synthesis	2.7.4.4 nucleoside phosphate kinase	NA
	2.1.1.45: thymidylate synthase	ost_ovt_her27_contig_13654
	2.7.4.9: dTMP kinase	ost_ovt_her27_contig_15224
	2.7.4.6: nucleoside-diphosphate kinase	ost_ovt_her27_contig_8710, ost_ovt_her27_contig_71721, ost_ovt_her27_contig_23976

Tyrosine (Y), Phenylalanine (F), Tryptopham (W) synthesis

Chorismate synthesis (precursor)	2.5.1.54: 3-deoxy-7-phosphoheptulonate synthase	ost_ovt_her27_contig_20034, ost_ovt_her27_contig_18957
	4.2.3.4: 3-dehydroquinate synthase	ost_ovt_her27_contig_4866, ost_ovt_her27_contig_35137
	4.2.1.10: 3-dehydroquinate dehydratase I	ost_ovt_her27_contig_48911, ost_ovt_her27_contig_48232
	1.1.1.25: Shikimate dehydrogenase	NA
	2.7.1.71: Shikimate kinase	NA
	2.5.1.19: 3-phosphoshikimate 1-carboxyvinyltransferase	ost_ovt_her27_contig_13818
	4.2.3.5: Chorismate synthase	ost_ovt_her27_contig_4628
Y synthesis	5.4.99.5: Chorismate mutase	ost_ovt_her27_contig_354
	1.3.1.13: Prephenate dehydrogenase (NADP+)	NA
	2.6.1.1: Aspartate aminotransferase, cytoplasmic	ost_ovt_her27_contig_72072
F synthesis	5.4.99.5: Chorismate mutase	ost_ovt_her27_contig_354
	4.2.1.51: Prephenate dehydratase	NA
	2.6.1.1: Aspartate aminotransferase, cytoplasmic	ost_ovt_her27_contig_72072
W synthesis	4.1.3.27: Anthranilate synthase	ost_ovt_her27_contig_9437
	2.4.2.18: Anthranilate phosphoribosyltransferase	ost_ovt_her27_contig_687

	5.3.1.24: Phosphoribosylanthranilate isomerase	NA
	4.1.1.48: Indole-3-glycerol phosphate synthase	NA
	4.2.1.20: Tryptophan synthase alpha chain	ost_ovt_her27_contig_4208, ost_ovt_her27_contig_31627

Serine (S), Glycine (G), Threonien (T) synthesis

S synthesis from 3-phosphoglycerate	1.1.1.95: D-3-phosphoglycerate dehydrogenase	NA
	2.6.1.52: Phosphoserine aminotransferase	ost_ovt_her27_contig_817, ost_ovt_her27_contig_14660
	3.1.3.3: Phosphoserine phosphatase	ost_ovt_her27_contig_17051, ost_ovt_her27_contig_40985, ost_ovt_her27_contig_12593
G synthesis from serine	2.1.2.1: Glycine hydroxymethyltransferase	ost_ovt_her27_contig_183, ost_ovt_her27_contig_8753, ost_ovt_her27_contig_4895, ost_ovt_her27_contig_4894, ost_ovt_her27_contig_4893, ost_ovt_her27_contig_41132
T synthesis from L-aspartate	2.7.2.4: Aspartate kinase	NA
	1.2.1.11: Aspartate-semialdehyde dehydrogenase	ost_ovt_her27_contig_4837, ost_ovt_her27_contig_73323, ost_ovt_her27_contig_12012
	1.1.1.3: Homoserine dehydrogenase	ost_ovt_her27_contig_22821, ost_ovt_her27_contig_76212
	2.7.1.39: Homoserine kinase	NA
	4.2.3.1: Threonine synthase	NA

Arginine (R), Proline (P) synthesis

R synthesis from glutamate	2.3.1.1: Amino-acid N-acetyltransferase	ost_ovt_her27_contig_33838
	2.7.2.8: Acetylglutamate kinase	NA
	1.2.1.38: N-acetyl-gamma-glutamyl-phosphate reductase	ost_ovt_her27_contig_4837, ost_ovt_her27_contig_73323, ost_ovt_her27_contig_12012, ost_ovt_her27_contig_1478
	2.6.1.11: Acetylornithine aminotransferase	NA
	3.5.1.16: Acetylornithine deacetylase	NA
	2.1.3.3: Ornithine carbamoyltransferase (urea cycle)	NA
	6.3.4.5: Argininosuccinate synthase (urea cycle)	NA
	4.3.2.1: Argininosuccinate lyase (urea cycle)	ost_ovt_her27_contig_11216
P synthesis from glutamate	2.7.2.11: Glutamate 5-kinase	NA
	1.2.1.41: Glutamate-5-semialdehyde dehydrogenase	NA
	1.5.1.2: Pyrroline-5-carboxylate reductase	ost_ovt_her27_contig_16178, ost_ovt_her27_contig_42222

Alanine (A), Aspartic acid (D), Asparginine (N), Glutamic acid (E), Glutamine (Q) synthesis

A synthesis from pyruvate	2.6.1.44: Alanine-glyoxylate transaminase (alanine-glyoxylate aminotransferase)	NA
D synthesis from oxaloacetate	2.6.1.1: Aspartate aminotransferase, cytoplasmic	ost_ovt_her27_contig_72072
N synthesis from aspartate	6.3.5.4: Asparagine synthase (glutamine-hydrolysing)	ost_ovt_her27_contig_7511, ost_ovt_her27_contig_62911, ost_ovt_her27_contig_34383
E synthesis from 2-oxoglutarate	1.4.1.13 /1.4.1.14: Glutamate synthase NADPH/ Glutamate synthase NADH	NA
Q synthesis from glutamate	6.3.1.2: Glutamine synthetase	ost_ovt_her27_contig_2060, ost_ovt_her27_contig_44217, ost_ovt_her27_contig_25660, ost_ovt_her27_contig_13241, ost_ovt_her27_contig_2260

Cysteine (C), Methionine (M) synthesis

C synthesis from serine	2.3.1.30: Serine O-acetyltransferase	NA
	2.5.1.47: Cysteine synthase A	ost_ovt_her27_contig_10027, ost_ovt_her27_contig_14242, ost_ovt_her27_contig_14241
M synthesis from aspartate	2.7.2.4: Aspartate kinase	NA
	1.2.1.11: Aspartate-semialdehyde dehydrogenase	ost_ovt_her27_contig_4837, ost_ovt_her27_contig_73323, ost_ovt_her27_contig_12012
	1.1.1.3: Homoserine dehydrogenase	ost_ovt_her27_contig_22821, ost_ovt_her27_contig_76212
	2.3.1.31: Homoserine O-acetyltransferase	ost_ovt_her27_contig_2762
	2.5.1.48: Cystathionine gamma-synthase	ost_ovt_her27_contig_29227
	4.4.1.8: Cystathionine beta-lyase	ost_ovt_her27_contig_21787
	2.1.1.5/2.1.1.10/2.1.1.13/2.1.1.14: Betaine-homocysteine S-methyltransferase /Homocysteine S-methyltransferase/5-methyltetrahydrofolate--homocysteine methyltransferase /5-methyltetrahydropteroyltriglutamate--homocysteine methyltransferase	ost_ovt_her27_contig_22083, ost_ovt_her27_contig_16641

Valine (V), Leucine (L), Isoleucine (I) synthesis

V synthesis from pyruvate	2.2.1.6: Acetolactate synthase I/II/III large subunit	NA
	1.1.1.86: Ketol-acid reductoisomerase	ost_ovt_her27_contig_12566
	4.2.1.9: Dihydroxy-acid dehydratase	ost_ovt_her27_contig_5814
	2.6.1.42: Branched-chain amino acid aminotransferase	ost_ovt_her27_contig_10586, ost_ovt_her27_contig_48963, ost_ovt_her27_contig_2852, ost_ovt_her27_contig_9007, ost_ovt_her27_contig_51234, ost_ovt_her27_contig_16366, ost_ovt_her27_contig_43634, ost_ovt_her27_contig_28361
L synthesis from pyruvate	2.2.1.6: Acetolactate synthase I/II/III	NA

	large subunit	
	1.1.1.86: Ketol-acid reductoisomerase	ost_ovt_her27_contig_12566
	4.2.1.9: Dihydroxy-acid dehydratase	ost_ovt_her27_contig_5814
	2.3.3.13: 2-isopropylmalate synthase	NA
	4.2.1.33: 3-isopropylmalate dehydratase	ost_ovt_her27_contig_5021
	1.1.1.85: 3-isopropylmalate dehydrogenase	ost_ovt_her27_contig_15035
	2.6.1.42: Branched-chain amino acid aminotransferase	ost_ovt_her27_contig_10586, ost_ovt_her27_contig_48963, ost_ovt_her27_contig_2852, ost_ovt_her27_contig_9007, ost_ovt_her27_contig_51234, ost_ovt_her27_contig_16366, ost_ovt_her27_contig_43634, ost_ovt_her27_contig_28361
I synthesis from 2-oxobutanoate	2.2.1.6: Acetolactate synthase I/II/III large subunit	NA
	1.1.1.86: Ketol-acid reductoisomerase	ost_ovt_her27_contig_12566
	4.2.1.9: Dihydroxy-acid dehydratase	ost_ovt_her27_contig_5814
	2.6.1.42: Branched-chain amino acid aminotransferase	ost_ovt_her27_contig_10586, ost_ovt_her27_contig_48963, ost_ovt_her27_contig_2852, ost_ovt_her27_contig_9007, ost_ovt_her27_contig_51234, ost_ovt_her27_contig_16366, ost_ovt_her27_contig_43634, ost_ovt_her27_contig_28361

Lysine (K) synthesis

K synthesis from aspartate	2.7.2.4: Aspartate kinase	NA
	1.2.1.11: Aspartate-semialdehyde dehydrogenase	ost_ovt_her27_contig_4837, ost_ovt_her27_contig_73323, ost_ovt_her27_contig_12012
	4.2.1.52: Dihydrodipicolinate synthase	NA
	1.3.1.26: Dihydrodipicolinate reductase	NA
	2.3.1.117: 2,3,4,5-tetrahydropyridine-2-carboxylate N-succinyltransferase	NA
	2.6.1.17: N-succinyldiaminopimelate aminotransferase	NA
	3.5.1.18: Succinyl-diaminopimelate desuccinylase	NA
	5.1.1.7: Diaminopimelate epimerase	NA
	4.1.1.20: Diaminopimelate decarboxylase	NA

Histidine (H) synthesis

H synthesis from PRPP	2.4.2.17: ATP phosphoribosyltransferase	ost_ovt_her27_contig_19943
	3.6.1.31: Phosphoribosyl-ATP	ost_ovt_her27_contig_25570

232

pyrophosphohydrolase

3.5.4.19: Phosphoribosyl-AMP cyclohydrolase	ost_ovt_her27_contig_29798
5.3.1.16: Phosphoribosylformimino-5-aminoimidazole carboxamide ribotide isomerase	ost_ovt_her27_contig_19155
2.6.1.16: Glutamine amidotransferase	ost_ovt_her27_contig_1822, ost_ovt_her27_contig_207, ost_ovt_her27_contig_27507, ost_ovt_her27_contig_14604
4.2.1.19: Imidazoleglycerol-phosphate dehydratase	ost_ovt_her27_contig_41785
2.6.1.9: Histidinol-phosphate aminotransferase	ost_ovt_her27_contig_72072, ost_ovt_her27_contig_32318
3.1.3.15: Histidinol-phosphatase	NA
1.1.1.23: histidinol dehydrogenase	ost_ovt_her27_contig_8036, ost_ovt_her27_contig_55013

S12B Description of sequences from *Ostreopsis* cf. *siamensis* BH1 encoding essential enzymes of various metabolic pathways. NA= enzymes not present in the transcriptome

Metabolic pathways	Enzymes	Contig name
Glycolysis	1.2.1.12/1.2.1.59: Glyceraldehyde 3-phosphate dehydrogenase /glyceraldehyde-3-phosphate dehydrogenase (NAD(P))	ost_siam_bh1_contig_12953, ost_siam_bh1_contig_1933, ost_siam_bh1_contig_1228, ost_siam_bh1_contig_486, ost_siam_bh1_contig_20, ost_siam_bh1_contig_4515, ost_siam_bh1_contig_4956, ost_siam_bh1_contig_21, ost_siam_bh1_contig_549, ost_siam_bh1_contig_4234, ost_siam_bh1_contig_6910, ost_siam_bh1_contig_4567, ost_siam_bh1_contig_33708, ost_siam_bh1_contig_1121, ost_siam_bh1_contig_1120
	2.7.1.11: 6-phosphofructokinase	ost_siam_bh1_contig_13384, ost_siam_bh1_contig_555, ost_siam_bh1_contig_22842
	2.7.1.2: Glucokinase	ost_siam_bh1_contig_20254, ost_siam_bh1_contig_25511
	2.7.1.40: Pyruvate kinase	ost_siam_bh1_contig_9205, ost_siam_bh1_contig_3537, ost_siam_bh1_contig_3536, ost_siam_bh1_contig_12651, ost_siam_bh1_contig_11794, ost_siam_bh1_contig_4958, ost_siam_bh1_contig_3903, ost_siam_bh1_contig_4959, ost_siam_bh1_contig_23677, ost_siam_bh1_contig_6010
	2.7.2.3: Phosphoglycerate kinase	ost_siam_bh1_contig_5587, ost_siam_bh1_contig_630, ost_siam_bh1_contig_631, ost_siam_bh1_contig_61373, ost_siam_bh1_contig_5988, ost_siam_bh1_contig_4954, ost_siam_bh1_contig_20, ost_siam_bh1_contig_12981, ost_siam_bh1_contig_7199
	4.1.2.13: Fructose-bisphosphate aldolase, class I	ost_siam_bh1_contig_10648, ost_siam_bh1_contig_3787, ost_siam_bh1_contig_107, ost_siam_bh1_contig_10296, ost_siam_bh1_contig_4549, ost_siam_bh1_contig_105, ost_siam_bh1_contig_7366, ost_siam_bh1_contig_7337, ost_siam_bh1_contig_13061, ost_siam_bh1_contig_42254, ost_siam_bh1_contig_1145, ost_siam_bh1_contig_1146, ost_siam_bh1_contig_3686, ost_siam_bh1_contig_1143, ost_siam_bh1_contig_1144, ost_siam_bh1_contig_9014

	4.2.1.11: Enolase	ost_siam_bh1_contig_12953, ost_siam_bh1_contig_13898, ost_siam_bh1_contig_64806, ost_siam_bh1_contig_499, ost_siam_bh1_contig_18739, ost_siam_bh1_contig_53165, ost_siam_bh1_contig_6219, ost_siam_bh1_contig_52431, ost_siam_bh1_contig_47095, ost_siam_bh1_contig_12102, ost_siam_bh1_contig_33227, ost_siam_bh1_contig_23751, ost_siam_bh1_contig_7942, ost_siam_bh1_contig_5587, ost_siam_bh1_contig_7634, ost_siam_bh1_contig_48409, ost_siam_bh1_contig_29966
	5.3.1.1: Triosephosphate isomerase (TIM)	ost_siam_bh1_contig_6909, ost_siam_bh1_contig_1702, ost_siam_bh1_contig_9659, ost_siam_bh1_contig_18739, ost_siam_bh1_contig_9658, ost_siam_bh1_contig_1066, ost_siam_bh1_contig_3967
	5.3.1.9: Glucose-6-phosphate isomerase	ost_siam_bh1_contig_32220, ost_siam_bh1_contig_33227
	5.4.2.1: Phosphoglycerate mutase	NA
TCA cycle	6.2.1.4/6.2.1.5: Succinyl-CoA synthetase alpha subunit	NA
	1.1.1.37: Malate dehydrogenase	ost_siam_bh1_contig_9535, ost_siam_bh1_contig_12028, ost_siam_bh1_contig_9774, ost_siam_bh1_contig_4387, ost_siam_bh1_contig_9775, ost_siam_bh1_contig_2436, ost_siam_bh1_contig_595, ost_siam_bh1_contig_5954, ost_siam_bh1_contig_1101, ost_siam_bh1_contig_28312, ost_siam_bh1_contig_22401
	1.1.1.42: Isocitrate dehydrogenase	ost_siam_bh1_contig_928, ost_siam_bh1_contig_16959, ost_siam_bh1_contig_4907, ost_siam_bh1_contig_15180, ost_siam_bh1_contig_5632, ost_siam_bh1_contig_10539, ost_siam_bh1_contig_5910
	1.2.4.1/2.3.1.12: Pyruvate dehydrogenase E1 component/ Pyruvate dehydrogenase E2 component (dihydrolipoamide acetyltransferase)	ost_siam_bh1_contig_18749, ost_siam_bh1_contig_75400
	1.2.4.2/2.3.1.61: 2-oxoglutarate dehydrogenase E1 component / 2-oxoglutarate dehydrogenase E2 component (dihydrolipoamide succinyltransferase)	ost_siam_bh1_contig_50508, ost_siam_bh1_contig_13006, ost_siam_bh1_contig_43699
	1.3.5.1/ 1.3.99.1: Succinate dehydrogenase (ubiquinone) flavoprotein subunit/	ost_siam_bh1_contig_709, ost_siam_bh1_contig_5420,

	Succinate dehydrogenase flavoprotein subunit	ost_siam_bh1_contig_12966, ost_siam_bh1_contig_6764, ost_siam_bh1_contig_710
	2.3.3.1: Citrate synthase	ost_siam_bh1_contig_14499
	4.2.1.2: Fumarate hydratase, class I	ost_siam_bh1_contig_29472, ost_siam_bh1_contig_26685, ost_siam_bh1_contig_32776
	4.2.1.3: Aconitate hydratase 1	ost_siam_bh1_contig_4096
Oxidative phosphorylation	1.6.5.3/1.6.99.3: NADH dehydrogenase/ NADH dehydrogenase (complex I)	NA
	1.3.5.1/ 1.3.99.1: Succinate dehydrogenase (ubiquinone) flavoprotein subunit/ Succinate dehydrogenase flavoprotein subunit subunit (complex II)	ost_siam_bh1_contig_709, ost_siam_bh1_contig_5420, ost_siam_bh1_contig_12966, ost_siam_bh1_contig_6764, ost_siam_bh1_contig_710
	1.10.2.2: Ubiquinol-cytochrome c reductase iron-sulfur subunit (complex III)	ost_siam_bh1_contig_31165, ost_siam_bh1_contig_7024, ost_siam_bh1_contig_4014, ost_siam_bh1_contig_4015, ost_siam_bh1_contig_4602, ost_siam_bh1_contig_129, ost_siam_bh1_contig_6618
	1.9.3.1: Cb-type cytochrome c oxidase subunit I (complex IV)	ost_siam_bh1_contig_9857, ost_siam_bh1_contig_12492, ost_siam_bh1_contig_1610, ost_siam_bh1_contig_4797, ost_siam_bh1_contig_2532, ost_siam_bh1_contig_11011, ost_siam_bh1_contig_79
	3.6.3.6/3.6.3.14: H+ transporting ATPase/F-type H+-transporting ATPase subunit a (complex V)	NA
Carbon fixation (C3)	2.7.1.19: Phosphoribulokinase	ost_siam_bh1_contig_5441, ost_siam_bh1_contig_93, ost_siam_bh1_contig_95, ost_siam_bh1_contig_94, ost_siam_bh1_contig_3035
	4.1.1.39: Ribulose-bisphosphate carboxylase large chain	ost_siam_bh1_contig_40889, ost_siam_bh1_contig_11855, ost_siam_bh1_contig_43958, ost_siam_bh1_contig_20728, ost_siam_bh1_contig_870, ost_siam_bh1_contig_34240, ost_siam_bh1_contig_22271, ost_siam_bh1_contig_49243, ost_siam_bh1_contig_55854, ost_siam_bh1_contig_17333, ost_siam_bh1_contig_32901, ost_siam_bh1_contig_19126, ost_siam_bh1_contig_5959, ost_siam_bh1_contig_98, ost_siam_bh1_contig_8204, ost_siam_bh1_contig_40021, ost_siam_bh1_contig_30219, ost_siam_bh1_contig_65287, ost_siam_bh1_contig_58690, ost_siam_bh1_contig_2233,

2.7.2.3: Phosphoglycerate kinase	ost_siam_bh1_contig_66602, ost_siam_bh1_contig_63303, ost_siam_bh1_contig_61756 ost_siam_bh1_contig_5587, ost_siam_bh1_contig_630, ost_siam_bh1_contig_631, ost_siam_bh1_contig_61373, ost_siam_bh1_contig_5988, ost_siam_bh1_contig_4954, ost_siam_bh1_contig_20, ost_siam_bh1_contig_12981, ost_siam_bh1_contig_7199
1.2.1.13/1.2.1.59: Glyceraldehyde-3-phosphate dehydrogenase (NADP+) (phosphorylating)/ glyceraldehyde-3-phosphate dehydrogenase (NAD(P))	ost_siam_bh1_contig_12953, ost_siam_bh1_contig_1933, ost_siam_bh1_contig_1228, ost_siam_bh1_contig_486, ost_siam_bh1_contig_20, ost_siam_bh1_contig_4515, ost_siam_bh1_contig_4956, ost_siam_bh1_contig_21, ost_siam_bh1_contig_549, ost_siam_bh1_contig_4234, ost_siam_bh1_contig_6910, ost_siam_bh1_contig_4567, ost_siam_bh1_contig_33708, ost_siam_bh1_contig_1121, ost_siam_bh1_contig_1120
5.3.1.1: Triosephosphate isomerase (TIM)	ost_siam_bh1_contig_6909, ost_siam_bh1_contig_1702, ost_siam_bh1_contig_9659, ost_siam_bh1_contig_18739, ost_siam_bh1_contig_9658, ost_siam_bh1_contig_1066, ost_siam_bh1_contig_3967
4.1.2.13: Fructose-bisphosphate aldolase, class I	ost_siam_bh1_contig_10648, ost_siam_bh1_contig_3787, ost_siam_bh1_contig_107, ost_siam_bh1_contig_10296, ost_siam_bh1_contig_4549, ost_siam_bh1_contig_105, ost_siam_bh1_contig_7366, ost_siam_bh1_contig_7337, ost_siam_bh1_contig_13061, ost_siam_bh1_contig_42254, ost_siam_bh1_contig_1145, ost_siam_bh1_contig_1146, ost_siam_bh1_contig_3686, ost_siam_bh1_contig_1143, ost_siam_bh1_contig_1144, ost_siam_bh1_contig_9014
3.1.3.11: Fructose-1,6-bisphosphatase I	ost_siam_bh1_contig_61029, ost_siam_bh1_contig_32883, ost_siam_bh1_contig_14312, ost_siam_bh1_contig_2739, ost_siam_bh1_contig_19573, ost_siam_bh1_contig_6795, ost_siam_bh1_contig_3970, ost_siam_bh1_contig_7713, ost_siam_bh1_contig_7712, ost_siam_bh1_contig_19572,

	2.2.1.1: Transketolase	ost_siam_bh1_contig_2740, ost_siam_bh1_contig_2047, ost_siam_bh1_contig_26586 ost_siam_bh1_contig_1313, ost_siam_bh1_contig_7646, ost_siam_bh1_contig_2762, ost_siam_bh1_contig_2761, ost_siam_bh1_contig_9903
	3.1.3.37: Sedoheptulose-1,7-bisphosphatase	ost_siam_bh1_contig_3970, ost_siam_bh1_contig_14312
	5.1.3.1: Ribulose-phosphate 3-epimerase	ost_siam_bh1_contig_30060, ost_siam_bh1_contig_4317, ost_siam_bh1_contig_4318, ost_siam_bh1_contig_13985
	5.3.1.6: Ribose 5-phosphate isomerase A	ost_siam_bh1_contig_14171, ost_siam_bh1_contig_15708, ost_siam_bh1_contig_28911
Pentose phosphate pathway	1.1.1.49 glucose-6-phosphate dehydrogenase	ost_siam_bh1_contig_35242
	3.1.1.31 6-phosphogluconolactonase	NA
	1.1.1.44 phosphogluconate dehydrogenase (NADP+-dependent, decarboxylating)	ost_siam_bh1_contig_23484, ost_siam_bh1_contig_66793, ost_siam_bh1_contig_23472
	5.3.1.6 ribose-5-phosphate isomerase	ost_siam_bh1_contig_14171, ost_siam_bh1_contig_15708, ost_siam_bh1_contig_28911
	5.1.3.1 ribulose-phosphate 3-epimerase	ost_siam_bh1_contig_30060, ost_siam_bh1_contig_4317, ost_siam_bh1_contig_4318, ost_siam_bh1_contig_13985
	2.2.1.1 transketolase	ost_siam_bh1_contig_1313, ost_siam_bh1_contig_7646, ost_siam_bh1_contig_2762, ost_siam_bh1_contig_2761, ost_siam_bh1_contig_9903
	2.2.1.2 transaldolase	NA

Purine nucleotide synthesis

Inosine monophosphate synthesis (precursor)	2.7.6.1: Ribose-phosphate pyrophosphokinase	ost_siam_bh1_contig_18273, ost_siam_bh1_contig_1190
	2.1.2.2: GAR transformylase	ost_siam_bh1_contig_31072
	2.1.2.3: AICAR transformylase	ost_siam_bh1_contig_8674, ost_siam_bh1_contig_13628
	2.4.2.14: Amidophosphoribosyltransferase	NA
	3.5.4.10: IMP cyclohydrolase	ost_siam_bh1_contig_8674, ost_siam_bh1_contig_13628
	4.1.1.21: AIR carboxylase	NA
	4.3.2.2: Adenylosuccinate lyase	ost_siam_bh1_contig_1115
	6.3.2.6: SAICAR synthetase	NA
	6.3.3.1: AIR synthetase	ost_siam_bh1_contig_6738, ost_siam_bh1_contig_7297, ost_siam_bh1_contig_17535
	6.3.4.13: Phosphoribosylamine--glycine	ost_siam_bh1_contig_13628,

	ligase	ost_siam_bh1_contig_7297, ost_siam_bh1_contig_17535
	6.3.5.3: FGAM synthetase	ost_siam_bh1_contig_2870
Synthesis of AMP, ADP and ATP	6.3.4.4: Adenylosuccinate synthase	ost_siam_bh1_contig_1369
	4.3.2.2: Adenylosuccinate lyase	ost_siam_bh1_contig_1115
	2.7.4.3: Adenylate kinase	ost_siam_bh1_contig_3260, ost_siam_bh1_contig_7820, ost_siam_bh1_contig_551, ost_siam_bh1_contig_27561, ost_siam_bh1_contig_19633
	2.7.4.6: Nucleoside-diphosphate kinase	ost_siam_bh1_contig_20551, ost_siam_bh1_contig_6397, ost_siam_bh1_contig_30351
Synthesis of dADP and dATP	1.17.4.1: Ribonucleotide reductase, class II	ost_siam_bh1_contig_2826, ost_siam_bh1_contig_2150, ost_siam_bh1_contig_27063, ost_siam_bh1_contig_8884, ost_siam_bh1_contig_2049, ost_siam_bh1_contig_1297
	2.7.4.6: Nucleoside-diphosphate kinase	ost_siam_bh1_contig_20551, ost_siam_bh1_contig_6397, ost_siam_bh1_contig_30351
Synthesis of GMP, GDP and GTP	1.1.1.205: IMP dehydrogenase	ost_siam_bh1_contig_19198, ost_siam_bh1_contig_7956, ost_siam_bh1_contig_11089
	6.3.5.2: GMP synthase (glutamine-hydrolysing)	NA
	2.7.4.8: Guanylate kinase	ost_siam_bh1_contig_25040, ost_siam_bh1_contig_21204
	2.7.4.6: Nucleoside-diphosphate kinase	ost_siam_bh1_contig_20551, ost_siam_bh1_contig_6397, ost_siam_bh1_contig_30351
Synthesis of dGDP and dGTP	1.17.4.1: Ribonucleotide reductase, class II	ost_siam_bh1_contig_2826, ost_siam_bh1_contig_2150, ost_siam_bh1_contig_27063, ost_siam_bh1_contig_8884, ost_siam_bh1_contig_2049, ost_siam_bh1_contig_1297
	2.7.4.6: Nucleoside-diphosphate kinase	ost_siam_bh1_contig_20551, ost_siam_bh1_contig_6397, ost_siam_bh1_contig_30351

Pyrimidine nucleotide synthesis

Uridine monophosphate synthesis (precursor)	6.3.5.5: carbamoyl-phosphate synthase	NA
	2.1.3.2: aspartate carbamoyltransferase	ost_siam_bh1_contig_22459
	3.5.2.3: dihydroorotase	NA
	1.3.5.2: dihydroorotate dehydrogenase	ost_siam_bh1_contig_66611, ost_siam_bh1_contig_29746
	2.4.2.10: orotate phosphoribosyltransferase	ost_siam_bh1_contig_29521
	4.1.1.23: orotidine-5'-monophosphate decarboxylase	ost_siam_bh1_contig_29521
UDP, UTP, CTP	2.7.4.4: nucleoside phosphate kinase	NA

and CDP synthesis		
	2.7.4.6: nucleoside-diphosphate kinase	ost_siam_bh1_contig_20551, ost_siam_bh1_contig_6397, ost_siam_bh1_contig_30351
	6.3.4.2: CTP synthase	NA
dCDP, dCTP, dUDP and dUTP synthesis	1.17.4.1: ribonucleotide reductase, class II	ost_siam_bh1_contig_2826, ost_siam_bh1_contig_2150, ost_siam_bh1_contig_27063, ost_siam_bh1_contig_8884, ost_siam_bh1_contig_2049, ost_siam_bh1_contig_1297
	2.7.4.6: nucleoside-diphosphate kinase	ost_siam_bh1_contig_20551, ost_siam_bh1_contig_6397, ost_siam_bh1_contig_30351
dTMP, dTDP and dTTP synthesis	2.7.4.4 nucleoside phosphate kinase	NA
	2.1.1.45: thymidylate synthase	NA
	2.7.4.9: dTMP kinase	NA
	2.7.4.6: nucleoside-diphosphate kinase	ost_siam_bh1_contig_20551, ost_siam_bh1_contig_6397, ost_siam_bh1_contig_30351

Tyrosine (Y), Phenylalanine (F), Tryptopham (W) synthesis

Chorismate synthesis (precursor)	2.5.1.54: 3-deoxy-7-phosphoheptulonate synthase	ost_siam_bh1_contig_15626, ost_siam_bh1_contig_14295, ost_siam_bh1_contig_18264
	4.2.3.4: 3-dehydroquinate synthase	ost_siam_bh1_contig_6421
	4.2.1.10: 3-dehydroquinate dehydratase I	ost_siam_bh1_contig_9752
	1.1.1.25: Shikimate dehydrogenase	NA
	2.7.1.71: Shikimate kinase	NA
	2.5.1.19: 3-phosphoshikimate 1-carboxyvinyltransferase	ost_siam_bh1_contig_36036
	4.2.3.5: Chorismate synthase	NA
Y synthesis	5.4.99.5: Chorismate mutase	ost_siam_bh1_contig_17294
	1.3.1.13: Prephenate dehydrogenase (NADP+)	NA
	2.6.1.1: Aspartate aminotransferase, cytoplasmic	ost_siam_bh1_contig_53022
F synthesis	5.4.99.5: Chorismate mutase	ost_siam_bh1_contig_17294
	4.2.1.51: Prephenate dehydratase	NA
	2.6.1.1: Aspartate aminotransferase, cytoplasmic	ost_siam_bh1_contig_53022
W synthesis	4.1.3.27: Anthranilate synthase	ost_siam_bh1_contig_2446
	2.4.2.18: Anthranilate phosphoribosyltransferase	NA
	5.3.1.24: Phosphoribosylanthranilate isomerase	NA
	4.1.1.48: Indole-3-glycerol phosphate synthase	NA
	4.2.1.20: Tryptophan synthase alpha chain	ost_siam_bh1_contig_2313, ost_siam_bh1_contig_30401

Serine (S), Glycine (G), Threonien (T) synthesis

S synthesis from 3-phosphoglycerate	1.1.1.95: D-3-phosphoglycerate dehydrogenase	NA
	2.6.1.52: Phosphoserine aminotransferase	ost_siam_bh1_contig_443
	3.1.3.3: Phosphoserine phosphatase	ost_siam_bh1_contig_8564, ost_siam_bh1_contig_7733
G synthesis from serine	2.1.2.1: Glycine hydroxymethyltransferase	ost_siam_bh1_contig_5304, ost_siam_bh1_contig_5305, ost_siam_bh1_contig_21503, ost_siam_bh1_contig_3244, ost_siam_bh1_contig_3243, ost_siam_bh1_contig_57619, ost_siam_bh1_contig_11223
T synthesis from L-aspartate	2.7.2.4: Aspartate kinase	NA
	1.2.1.11: Aspartate-semialdehyde dehydrogenase	ost_siam_bh1_contig_3305, ost_siam_bh1_contig_2056
	1.1.1.3: Homoserine dehydrogenase	ost_siam_bh1_contig_20837, ost_siam_bh1_contig_53942
	2.7.1.39: Homoserine kinase	NA
	4.2.3.1: Threonine synthase	NA

Arginine (R), Proline (P) synthesis

R synthesis from glutamate	2.3.1.1: Amino-acid N-acetyltransferase	ost_siam_bh1_contig_19391
	2.7.2.8: Acetylglutamate kinase	NA
	1.2.1.38: N-acetyl-gamma-glutamyl-phosphate reductase	ost_siam_bh1_contig_28031, ost_siam_bh1_contig_3305, ost_siam_bh1_contig_2056
	2.6.1.11: Acetylornithine aminotransferase	NA
	3.5.1.16: Acetylornithine deacetylase	NA
	2.1.3.3: Ornithine carbamoyltransferase (urea cycle)	NA
	6.3.4.5: Argininosuccinate synthase (urea cycle)	ost_siam_bh1_contig_9026
	4.3.2.1: Argininosuccinate lyase (urea cycle)	NA
P synthesis from glutamate	2.7.2.11: Glutamate 5-kinase	NA
	1.2.1.41: Glutamate-5-semialdehyde dehydrogenase	NA
	1.5.1.2: Pyrroline-5-carboxylate reductase	ost_siam_bh1_contig_8583

Alanine (A), Aspartic acid (D), Asparginine (N), Glutamic acid (E), Glutamine (Q) synthesis

A synthesis from pyruvate	2.6.1.44: Alanine-glyoxylate transaminase (alanine-glyoxylate aminotransferase)	NA
D synthesis from oxaloacetate	2.6.1.1: Aspartate aminotransferase, cytoplasmic	ost_siam_bh1_contig_53022
N synthesis from aspartate	6.3.5.4: Asparagine synthase (glutamine-hydrolysing)	ost_siam_bh1_contig_9700, ost_siam_bh1_contig_60325, ost_siam_bh1_contig_59387, ost_siam_bh1_contig_48023, ost_siam_bh1_contig_19297, ost_siam_bh1_contig_75196,

		ost_siam_bh1_contig_35526
E synthesis from 2-oxoglutarate	1.4.1.13 /1.4.1.14: Glutamate synthase NADPH/ Glutamate synthase NADH	ost_siam_bh1_contig_15730
Q synthesis from glutamate	6.3.1.2: Glutamine synthetase	ost_siam_bh1_contig_28719, ost_siam_bh1_contig_25135

Cysteine (C), Methionine (M) synthesis

C synthesis from serine	2.3.1.30: Serine O-acetyltransferase	NA
	2.5.1.47: Cysteine synthase A	ost_siam_bh1_contig_7496, ost_siam_bh1_contig_10641, ost_siam_bh1_contig_10982
M synthesis from aspartate	2.7.2.4: Aspartate kinase	NA
	1.2.1.11: Aspartate-semialdehyde dehydrogenase	ost_siam_bh1_contig_3305, ost_siam_bh1_contig_2056
	1.1.1.3: Homoserine dehydrogenase	ost_siam_bh1_contig_20837, ost_siam_bh1_contig_53942
	2.3.1.31: Homoserine O-acetyltransferase	ost_siam_bh1_contig_5245, ost_siam_bh1_contig_7181, ost_siam_bh1_contig_16413
	2.5.1.48: Cystathionine gamma-synthase	ost_siam_bh1_contig_5618
	4.4.1.8: Cystathionine beta-lyase	NA
	2.1.1.5/2.1.1.10/2.1.1.13/2.1.1.14: Betaine-homocysteine S-methyltransferase /Homocysteine S-methyltransferase/5-methyltetrahydrofolate--homocysteine methyltransferase /5-methyltetrahydropteroyltriglutamate--homocysteine methyltransferase	ost_siam_bh1_contig_39713

Valine (V), Leucine (L), Isoleucine (I) synthesis

V synthesis from pyruvate	2.2.1.6: Acetolactate synthase I/II/III large subunit	NA
	1.1.1.86: Ketol-acid reductoisomerase	ost_siam_bh1_contig_8195
	4.2.1.9: Dihydroxy-acid dehydratase	ost_siam_bh1_contig_9624
	2.6.1.42: Branched-chain amino acid aminotransferase	ost_siam_bh1_contig_33586, ost_siam_bh1_contig_22260, ost_siam_bh1_contig_2399, ost_siam_bh1_contig_25266, ost_siam_bh1_contig_38127, ost_siam_bh1_contig_8076, ost_siam_bh1_contig_34116
L synthesis from pyruvate	2.2.1.6: Acetolactate synthase I/II/III large subunit	NA
	1.1.1.86: Ketol-acid reductoisomerase	ost_siam_bh1_contig_8195
	4.2.1.9: Dihydroxy-acid dehydratase	ost_siam_bh1_contig_9624
	2.3.3.13: 2-isopropylmalate synthase	NA
	4.2.1.33: 3-isopropylmalate dehydratase	NA
	1.1.1.85: 3-isopropylmalate dehydrogenase	ost_siam_bh1_contig_22319
	2.6.1.42: Branched-chain amino acid aminotransferase	ost_siam_bh1_contig_33586, ost_siam_bh1_contig_22260, ost_siam_bh1_contig_2399, ost_siam_bh1_contig_25266, ost_siam_bh1_contig_38127,

I synthesis from 2-oxobutanoate	2.2.1.6: Acetolactate synthase I/II/III large subunit	ost_siam_bh1_contig_8076, ost_siam_bh1_contig_34116 NA
	1.1.1.86: Ketol-acid reductoisomerase	ost_siam_bh1_contig_8195
	4.2.1.9: Dihydroxy-acid dehydratase	ost_siam_bh1_contig_9624
	2.6.1.42: Branched-chain amino acid aminotransferase	ost_siam_bh1_contig_33586, ost_siam_bh1_contig_22260, ost_siam_bh1_contig_2399, ost_siam_bh1_contig_25266, ost_siam_bh1_contig_38127, ost_siam_bh1_contig_8076, ost_siam_bh1_contig_34116
Lysine (K) synthesis		
K synthesis from aspartate	2.7.2.4: Aspartate kinase	NA
	1.2.1.11: Aspartate-semialdehyde dehydrogenase	ost_siam_bh1_contig_3305, ost_siam_bh1_contig_2056
	4.2.1.52: Dihydrodipicolinate synthase	NA
	1.3.1.26: Dihydrodipicolinate reductase	NA
	2.3.1.117: 2,3,4,5-tetrahydropyridine-2-carboxylate N-succinyltransferase	NA
	2.6.1.17: N-succinyldiaminopimelate aminotransferase	NA
	3.5.1.18: Succinyl-diaminopimelate desuccinylase	NA
	5.1.1.7: Diaminopimelate epimerase	NA
	4.1.1.20: Diaminopimelate decarboxylase	NA
Histidine (H) synthesis		
H synthesis from PRPP	2.4.2.17: ATP phosphoribosyltransferase	ost_siam_bh1_contig_6949
	3.6.1.31: Phosphoribosyl-ATP pyrophosphohydrolase	ost_siam_bh1_contig_64011
	3.5.4.19: Phosphoribosyl-AMP cyclohydrolase	ost_siam_bh1_contig_2918
	5.3.1.16: Phosphoribosylformimino-5-aminoimidazole carboxamide ribotide isomerase	ost_siam_bh1_contig_5118
	2.6.1.16: Glutamine amidotransferase	ost_siam_bh1_contig_15896
	4.2.1.19: Imidazoleglycerol-phosphate dehydratase	ost_siam_bh1_contig_19716
	2.6.1.9: Histidinol-phosphate aminotransferase	ost_siam_bh1_contig_22780, ost_siam_bh1_contig_53022
	3.1.3.15: Histidinol-phosphatase	
	1.1.1.23: histidinol dehydrogenase	ost_siam_bh1_contig_75186, ost_siam_bh1_contig_20501

S12C Description of sequences from *Ostreopsis rhodesae* HER26 encoding essential enzymes of various metabolic pathways. NA= enzymes not present in the transcriptome

Metabolic pathways	Enzymes	Contig name
Glycolysis	1.2.1.12/1.2.1.59: Glyceraldehyde 3-phosphate dehydrogenase /glyceraldehyde-3-phosphate dehydrogenase (NAD(P))	ost_sp8_her26_contig_1771, ost_sp8_her26_contig_1661, ost_sp8_her26_contig_5973, ost_sp8_her26_contig_4189, ost_sp8_her26_contig_5950, ost_sp8_her26_contig_1770, ost_sp8_her26_contig_5609, ost_sp8_her26_contig_3927, ost_sp8_her26_contig_5163, ost_sp8_her26_contig_148, ost_sp8_her26_contig_325
	2.7.1.11: 6-phosphofructokinase	ost_sp8_her26_contig_5744, ost_sp8_her26_contig_29817, ost_sp8_her26_contig_21260, ost_sp8_her26_contig_24495, ost_sp8_her26_contig_3736
	2.7.1.2: Glucokinase	ost_sp8_her26_contig_25867, ost_sp8_her26_contig_34297, ost_sp8_her26_contig_35434
	2.7.1.40: Pyruvate kinase	ost_sp8_her26_contig_8857, ost_sp8_her26_contig_6469, ost_sp8_her26_contig_1245, ost_sp8_her26_contig_7335, ost_sp8_her26_contig_8343, ost_sp8_her26_contig_747, ost_sp8_her26_contig_9370
	2.7.2.3: Phosphoglycerate kinase	ost_sp8_her26_contig_48964, ost_sp8_her26_contig_1261, ost_sp8_her26_contig_1262, ost_sp8_her26_contig_16637, ost_sp8_her26_contig_148, ost_sp8_her26_contig_10473, ost_sp8_her26_contig_147, ost_sp8_her26_contig_20465, ost_sp8_her26_contig_3835
	4.1.2.13: Fructose-bisphosphate aldolase, class I	ost_sp8_her26_contig_31, ost_sp8_her26_contig_9020, ost_sp8_her26_contig_9021, ost_sp8_her26_contig_9022, ost_sp8_her26_contig_9023, ost_sp8_her26_contig_44670, ost_sp8_her26_contig_5561, ost_sp8_her26_contig_30313, ost_sp8_her26_contig_12196, ost_sp8_her26_contig_17487, ost_sp8_her26_contig_17026, ost_sp8_her26_contig_17027, ost_sp8_her26_contig_5227, ost_sp8_her26_contig_2698, ost_sp8_her26_contig_11895, ost_sp8_her26_contig_11433, ost_sp8_her26_contig_2571, ost_sp8_her26_contig_10238, ost_sp8_her26_contig_653, ost_sp8_her26_contig_2646

	4.2.1.11: Enolase	ost_sp8_her26_contig_21776, ost_sp8_her26_contig_21714, ost_sp8_her26_contig_14088, ost_sp8_her26_contig_30403, ost_sp8_her26_contig_7194, ost_sp8_her26_contig_12579, ost_sp8_her26_contig_5973, ost_sp8_her26_contig_6754, ost_sp8_her26_contig_2136, ost_sp8_her26_contig_11028, ost_sp8_her26_contig_10745, ost_sp8_her26_contig_42101, ost_sp8_her26_contig_25664, ost_sp8_her26_contig_600, ost_sp8_her26_contig_7748
	5.3.1.1: Triosephosphate isomerase (TIM)	ost_sp8_her26_contig_13121, ost_sp8_her26_contig_118, ost_sp8_her26_contig_10053, ost_sp8_her26_contig_22420
	5.3.1.9: Glucose-6-phosphate isomerase	ost_sp8_her26_contig_6754, ost_sp8_her26_contig_33447
	5.4.2.1: Phosphoglycerate mutase	NA
TCA cycle	6.2.1.4/6.2.1.5: Succinyl-CoA synthetase alpha subunit	NA
	1.1.1.37: Malate dehydrogenase	ost_sp8_her26_contig_5437, ost_sp8_her26_contig_19651, ost_sp8_her26_contig_8225, ost_sp8_her26_contig_57297, ost_sp8_her26_contig_9624, ost_sp8_her26_contig_1126, ost_sp8_her26_contig_3428, ost_sp8_her26_contig_15400, ost_sp8_her26_contig_55733
	1.1.1.42: Isocitrate dehydrogenase	ost_sp8_her26_contig_100, ost_sp8_her26_contig_4497, ost_sp8_her26_contig_10879, ost_sp8_her26_contig_38484, ost_sp8_her26_contig_74244, ost_sp8_her26_contig_4496, ost_sp8_her26_contig_4719, ost_sp8_her26_contig_23332, ost_sp8_her26_contig_23356, ost_sp8_her26_contig_23224
	1.2.4.1/2.3.1.12: Pyruvate dehydrogenase E1 component/ Pyruvate dehydrogenase E2 component (dihydrolipoamide acetyltransferase)	ost_sp8_her26_contig_4998
	1.2.4.2/2.3.1.61: 2-oxoglutarate dehydrogenase E1 component / 2-oxoglutarate dehydrogenase E2 component (dihydrolipoamide succinyltransferase)	ost_sp8_her26_contig_12184, ost_sp8_her26_contig_2469
	1.3.5.1/ 1.3.99.1: Succinate dehydrogenase (ubiquinone) flavoprotein subunit/ Succinate dehydrogenase flavoprotein subunit	ost_sp8_her26_contig_1993, ost_sp8_her26_contig_10787, ost_sp8_her26_contig_4134, ost_sp8_her26_contig_14367
	2.3.3.1: Citrate synthase	ost_sp8_her26_contig_8470
	4.2.1.2: Fumarate hydratase, class I	ost_sp8_her26_contig_7217, ost_sp8_her26_contig_29001
	4.2.1.3: Aconitate hydratase 1	ost_sp8_her26_contig_846

Oxidative phosphorylation	1.6.5.3/1.6.99.3: NADH dehydrogenase/ NADH dehydrogenase (complex I)	NA
	1.3.5.1/ 1.3.99.1: Succinate dehydrogenase (ubiquinone) flavoprotein subunit/ Succinate dehydrogenase flavoprotein subunit subunit (complex II)	ost_sp8_her26_contig_1993, ost_sp8_her26_contig_10787, ost_sp8_her26_contig_4134, ost_sp8_her26_contig_14367
	1.10.2.2: Ubiquinol-cytochrome c reductase iron-sulfur subunit (complex III)	ost_sp8_her26_contig_47666, ost_sp8_her26_contig_18200, ost_sp8_her26_contig_11720, ost_sp8_her26_contig_10438, ost_sp8_her26_contig_1912, ost_sp8_her26_contig_2250, ost_sp8_her26_contig_14028
	1.9.3.1: Cb-type cytochrome c oxidase subunit I (complex IV)	ost_sp8_her26_contig_25458, ost_sp8_her26_contig_5259, ost_sp8_her26_contig_19915, ost_sp8_her26_contig_12230, ost_sp8_her26_contig_30349, ost_sp8_her26_contig_29664, ost_sp8_her26_contig_6839, ost_sp8_her26_contig_17365, ost_sp8_her26_contig_1635
	3.6.3.6/3.6.3.14: H+ transporting ATPase/F-type H+-transporting ATPase subunit a (complex V)	NA
Carbon fixation (C3)	2.7.1.19: Phosphoribulokinase	ost_sp8_her26_contig_1310, ost_sp8_her26_contig_1591, ost_sp8_her26_contig_6642
	4.1.1.39: Ribulose-bisphosphate carboxylase large chain	ost_sp8_her26_contig_71453, ost_sp8_her26_contig_48760, ost_sp8_her26_contig_38076, ost_sp8_her26_contig_72839, ost_sp8_her26_contig_45150, ost_sp8_her26_contig_32722, ost_sp8_her26_contig_78536, ost_sp8_her26_contig_32721, ost_sp8_her26_contig_79715, ost_sp8_her26_contig_30151, ost_sp8_her26_contig_10984, ost_sp8_her26_contig_28221, ost_sp8_her26_contig_2581, ost_sp8_her26_contig_7477, ost_sp8_her26_contig_57682, ost_sp8_her26_contig_66774, ost_sp8_her26_contig_94
	2.7.2.3: Phosphoglycerate kinase	ost_sp8_her26_contig_48964, ost_sp8_her26_contig_1261, ost_sp8_her26_contig_1262, ost_sp8_her26_contig_16637, ost_sp8_her26_contig_148, ost_sp8_her26_contig_10473, ost_sp8_her26_contig_147, ost_sp8_her26_contig_20465, ost_sp8_her26_contig_3835
	1.2.1.13/1.2.1.59: Glyceraldehyde-3-phosphate dehydrogenase (NADP+) (phosphorylating)/ glyceraldehyde-3-phosphate dehydrogenase (NAD(P))	NA

5.3.1.1: Triosephosphate isomerase (TIM)	ost_sp8_her26_contig_13121, ost_sp8_her26_contig_118, ost_sp8_her26_contig_10053, ost_sp8_her26_contig_22420
4.1.2.13: Fructose-bisphosphate aldolase, class I	ost_sp8_her26_contig_31, ost_sp8_her26_contig_9020, ost_sp8_her26_contig_9021, ost_sp8_her26_contig_9022, ost_sp8_her26_contig_9023, ost_sp8_her26_contig_44670, ost_sp8_her26_contig_5561, ost_sp8_her26_contig_30313, ost_sp8_her26_contig_12196, ost_sp8_her26_contig_17487, ost_sp8_her26_contig_17026, ost_sp8_her26_contig_17027, ost_sp8_her26_contig_5227, ost_sp8_her26_contig_2698, ost_sp8_her26_contig_11895, ost_sp8_her26_contig_11433, ost_sp8_her26_contig_2571, ost_sp8_her26_contig_10238, ost_sp8_her26_contig_653, ost_sp8_her26_contig_2646
3.1.3.11: Fructose-1,6-bisphosphatase I	ost_sp8_her26_contig_44022, ost_sp8_her26_contig_14185, ost_sp8_her26_contig_4185, ost_sp8_her26_contig_7420, ost_sp8_her26_contig_4186, ost_sp8_her26_contig_8871, ost_sp8_her26_contig_16689, ost_sp8_her26_contig_3300, ost_sp8_her26_contig_7421, ost_sp8_her26_contig_5627, ost_sp8_her26_contig_5418, ost_sp8_her26_contig_5628, ost_sp8_her26_contig_1327
2.2.1.1: Transketolase	ost_sp8_her26_contig_1386, ost_sp8_her26_contig_132, ost_sp8_her26_contig_750, ost_sp8_her26_contig_7930, ost_sp8_her26_contig_1385, ost_sp8_her26_contig_11372, ost_sp8_her26_contig_1370, ost_sp8_her26_contig_28970, ost_sp8_her26_contig_35695, ost_sp8_her26_contig_48869
3.1.3.37: Sedoheptulose-1,7-bisphosphatase	ost_sp8_her26_contig_3300, ost_sp8_her26_contig_7421, ost_sp8_her26_contig_7420, ost_sp8_her26_contig_1327
5.1.3.1: Ribulose-phosphate 3-epimerase	ost_sp8_her26_contig_13866, ost_sp8_her26_contig_6787, ost_sp8_her26_contig_6786, ost_sp8_her26_contig_19272
5.3.1.6: Ribose 5-phosphate isomerase A	ost_sp8_her26_contig_27639, ost_sp8_her26_contig_9567, ost_sp8_her26_contig_23059

Pentose phosphate pathway	1.1.1.49 glucose-6-phosphate dehydrogenase	ost_sp8_her26_contig_27005
	3.1.1.31 6-phosphogluconolactonase	NA
	1.1.1.44 phosphogluconate dehydrogenase (NADP+-dependent, decarboxylating)	ost_sp8_her26_contig_28022, ost_sp8_her26_contig_7340, ost_sp8_her26_contig_39776
	5.3.1.6 ribose-5-phosphate isomerase	ost_sp8_her26_contig_27639, ost_sp8_her26_contig_9567, ost_sp8_her26_contig_23059
	5.1.3.1 ribulose-phosphate 3-epimerase	ost_sp8_her26_contig_13866, ost_sp8_her26_contig_6787, ost_sp8_her26_contig_6786, ost_sp8_her26_contig_19272
	2.2.1.1 transketolase	ost_sp8_her26_contig_1386, ost_sp8_her26_contig_132, ost_sp8_her26_contig_750, ost_sp8_her26_contig_7930, ost_sp8_her26_contig_1385, ost_sp8_her26_contig_11372, ost_sp8_her26_contig_1370, ost_sp8_her26_contig_28970, ost_sp8_her26_contig_35695, ost_sp8_her26_contig_48869
	2.2.1.2 transaldolase	ost_sp8_her26_contig_10071

Purine nucleotide synthesis

Inosine monophosphate synthesis (precursor)	2.7.6.1: Ribose-phosphate pyrophosphokinase	ost_sp8_her26_contig_14061, ost_sp8_her26_contig_37289, ost_sp8_her26_contig_4800, ost_sp8_her26_contig_15565
	2.1.2.2: GAR transformylase	NA
	2.1.2.3: AICAR transformylase	ost_sp8_her26_contig_1678
	2.4.2.14: Amidophosphoribosyltransferase	NA
	3.5.4.10: IMP cyclohydrolase	ost_sp8_her26_contig_1678
	4.1.1.21: AIR carboxylase	ost_sp8_her26_contig_20650
	4.3.2.2: Adenylosuccinate lyase	ost_sp8_her26_contig_11653
	6.3.2.6: SAICAR synthetase	NA
	6.3.3.1: AIR synthetase	ost_sp8_her26_contig_3565, ost_sp8_her26_contig_28231
	6.3.4.13: Phosphoribosylamine--glycine ligase	ost_sp8_her26_contig_28231, ost_sp8_her26_contig_1678
	6.3.5.3: FGAM synthetase	ost_sp8_her26_contig_10904
Synthesis of AMP, ADP and ATP	6.3.4.4: Adenylosuccinate synthase	ost_sp8_her26_contig_47265, ost_sp8_her26_contig_1705
	4.3.2.2: Adenylosuccinate lyase	ost_sp8_her26_contig_11653
	2.7.4.3: Adenylate kinase	ost_sp8_her26_contig_17806, ost_sp8_her26_contig_23369, ost_sp8_her26_contig_25517, ost_sp8_her26_contig_10948, ost_sp8_her26_contig_32489, ost_sp8_her26_contig_5590, ost_sp8_her26_contig_38984
	2.7.4.6: Nucleoside-diphosphate kinase	ost_sp8_her26_contig_12424, ost_sp8_her26_contig_13555, ost_sp8_her26_contig_53514,

		ost_sp8_her26_contig_50489
Synthesis of dADP and dATP	1.17.4.1: Ribonucleotide reductase, class II	ost_sp8_her26_contig_3895, ost_sp8_her26_contig_1387, ost_sp8_her26_contig_42, ost_sp8_her26_contig_8578, ost_sp8_her26_contig_3563, ost_sp8_her26_contig_17532
	2.7.4.6: Nucleoside-diphosphate kinase	ost_sp8_her26_contig_12424, ost_sp8_her26_contig_13555, ost_sp8_her26_contig_53514, ost_sp8_her26_contig_50489
Synthesis of GMP, GDP and GTP	1.1.1.205: IMP dehydrogenase	ost_sp8_her26_contig_32916, ost_sp8_her26_contig_4582, ost_sp8_her26_contig_13285
	6.3.5.2: GMP synthase (glutamine-hydrolysing)	ost_sp8_her26_contig_14802
	2.7.4.8: Guanylate kinase	ost_sp8_her26_contig_48386, ost_sp8_her26_contig_29609, ost_sp8_her26_contig_32307
	2.7.4.6: Nucleoside-diphosphate kinase	ost_sp8_her26_contig_12424, ost_sp8_her26_contig_13555, ost_sp8_her26_contig_53514, ost_sp8_her26_contig_50489
Synthesis of dGDP and dGTP	1.17.4.1: Ribonucleotide reductase, class II	ost_sp8_her26_contig_3895, ost_sp8_her26_contig_1387, ost_sp8_her26_contig_42, ost_sp8_her26_contig_8578, ost_sp8_her26_contig_3563, ost_sp8_her26_contig_17532
	2.7.4.6: Nucleoside-diphosphate kinase	ost_sp8_her26_contig_12424, ost_sp8_her26_contig_13555, ost_sp8_her26_contig_53514, ost_sp8_her26_contig_50489

Pyrimidine nucleotide synthesis

Uridine monophosphate synthesis (precursor)	6.3.5.5: carbamoyl-phosphate synthase	ost_sp8_her26_contig_19669, ost_sp8_her26_contig_7709
	2.1.3.2: aspartate carbamoyltransferase	ost_sp8_her26_contig_6182
	3.5.2.3: dihydroorotase	NA
	1.3.5.2: dihydroorotate dehydrogenase	ost_sp8_her26_contig_46287
	2.4.2.10: orotate phosphoribosyltransferase	ost_sp8_her26_contig_16565
	4.1.1.23: orotidine-5'-monophosphate decarboxylase	ost_sp8_her26_contig_16565
UDP, UTP, CTP and CDP synthesis	2.7.4.4: nucleoside phosphate kinase	NA
	2.7.4.6: nucleoside-diphosphate kinase	ost_sp8_her26_contig_12424, ost_sp8_her26_contig_13555, ost_sp8_her26_contig_53514, ost_sp8_her26_contig_50489
	6.3.4.2: CTP synthase	ost_sp8_her26_contig_9083
dCDP, dCTP, dUDP and dUTP synthesis	1.17.4.1: ribonucleotide reductase, class II	ost_sp8_her26_contig_3895, ost_sp8_her26_contig_1387, ost_sp8_her26_contig_42, ost_sp8_her26_contig_8578, ost_sp8_her26_contig_3563,

		ost_sp8_her26_contig_17532
	2.7.4.6: nucleoside-diphosphate kinase	ost_sp8_her26_contig_12424, ost_sp8_her26_contig_13555, ost_sp8_her26_contig_53514, ost_sp8_her26_contig_50489
dTMP, dTDP and dTTP synthesis	2.7.4.4 nucleoside phosphate kinase	NA
	2.1.1.45: thymidylate synthase	NA
	2.7.4.9: dTMP kinase	ost_sp8_her26_contig_28935
	2.7.4.6: nucleoside-diphosphate kinase	ost_sp8_her26_contig_12424, ost_sp8_her26_contig_13555, ost_sp8_her26_contig_53514, ost_sp8_her26_contig_50489

Tyrosine (Y), Phenylalanine (F), Tryptopham (W) synthesis

Chorismate synthesis (precursor)	2.5.1.54: 3-deoxy-7-phosphoheptulonate synthase	ost_sp8_her26_contig_10548, ost_sp8_her26_contig_57732
	4.2.3.4: 3-dehydroquinate synthase	ost_sp8_her26_contig_50984
	4.2.1.10: 3-dehydroquinate dehydratase I	ost_sp8_her26_contig_16655
	1.1.1.25: Shikimate dehydrogenase	NA
	2.7.1.71: Shikimate kinase	NA
	2.5.1.19: 3-phosphoshikimate 1-carboxyvinyltransferase	ost_sp8_her26_contig_4860
	4.2.3.5: Chorismate synthase	NA
Y synthesis	5.4.99.5: Chorismate mutase	ost_sp8_her26_contig_20068
	1.3.1.13: Prephenate dehydrogenase (NADP+)	ost_sp8_her26_contig_15639
	2.6.1.1: Aspartate aminotransferase, cytoplasmic	NA
F synthesis	5.4.99.5: Chorismate mutase	ost_sp8_her26_contig_20068
	4.2.1.51: Prephenate dehydratase	ost_sp8_her26_contig_15639
	2.6.1.1: Aspartate aminotransferase, cytoplasmic	NA
W synthesis	4.1.3.27: Anthranilate synthase	NA
	2.4.2.18: Anthranilate phosphoribosyltransferase	ost_sp8_her26_contig_25376
	5.3.1.24: Phosphoribosylanthranilate isomerase	NA
	4.1.1.48: Indole-3-glycerol phosphate synthase	NA
	4.2.1.20: Tryptophan synthase alpha chain	ost_sp8_her26_contig_9667, ost_sp8_her26_contig_15523

Serine (S), Glycine (G), Threonien (T) synthesis

S synthesis from 3-phosphoglycerate	1.1.1.95: D-3-phosphoglycerate dehydrogenase	NA
	2.6.1.52: Phosphoserine aminotransferase	ost_sp8_her26_contig_10536, ost_sp8_her26_contig_184
	3.1.3.3: Phosphoserine phosphatase	ost_sp8_her26_contig_4348, ost_sp8_her26_contig_2793, ost_sp8_her26_contig_4281, ost_sp8_her26_contig_56459
G synthesis from serine	2.1.2.1: Glycine hydroxymethyltransferase	ost_sp8_her26_contig_463, ost_sp8_her26_contig_462, ost_sp8_her26_contig_15263

T synthesis from L-aspartate	2.7.2.4: Aspartate kinase	NA
	1.2.1.11: Aspartate-semialdehyde dehydrogenase	ost_sp8_her26_contig_1731, ost_sp8_her26_contig_39768, ost_sp8_her26_contig_22651
	1.1.1.3: Homoserine dehydrogenase	ost_sp8_her26_contig_51275, ost_sp8_her26_contig_68507
	2.7.1.39: Homoserine kinase	NA
	4.2.3.1: Threonine synthase	NA

Arginine (R), Proline (P) synthesis

R synthesis from glutamate	2.3.1.1: Amino-acid N-acetyltransferase	ost_sp8_her26_contig_2883, ost_sp8_her26_contig_27435
	2.7.2.8: Acetylglutamate kinase	ost_sp8_her26_contig_28420
	1.2.1.38: N-acetyl-gamma-glutamyl-phosphate reductase	ost_sp8_her26_contig_7013, ost_sp8_her26_contig_1731, ost_sp8_her26_contig_39768, ost_sp8_her26_contig_22651
	2.6.1.11: Acetylornithine aminotransferase	NA
	3.5.1.16: Acetylornithine deacetylase	NA
	2.1.3.3: Ornithine carbamoyltransferase (urea cycle)	NA
	6.3.4.5: Argininosuccinate synthase (urea cycle)	ost_sp8_her26_contig_21453
	4.3.2.1: Argininosuccinate lyase (urea cycle)	NA
P synthesis from glutamate	2.7.2.11: Glutamate 5-kinase	ost_sp8_her26_contig_23921
	1.2.1.41: Glutamate-5-semialdehyde dehydrogenase	NA
	1.5.1.2: Pyrroline-5-carboxylate reductase	ost_sp8_her26_contig_28988

Alanine (A), Aspartic acid (D), Asparginine (N), Glutamic acid (E), Glutamine (Q) synthesis

A synthesis from pyruvate	2.6.1.44: Alanine-glyoxylate transaminase (alanine-glyoxylate aminotransferase)	ost_sp8_her26_contig_16293
D synthesis from oxaloacetate	2.6.1.1: Aspartate aminotransferase, cytoplasmic	
N synthesis from aspartate	6.3.5.4: Asparagine synthase (glutamine-hydrolysing)	ost_sp8_her26_contig_60548, ost_sp8_her26_contig_9660, ost_sp8_her26_contig_6128, ost_sp8_her26_contig_21926
E synthesis from 2-oxoglutarate	1.4.1.13 /1.4.1.14: Glutamate synthase NADPH/ Glutamate synthase NADH	NA
Q synthesis from glutamate	6.3.1.2: Glutamine synthetase	ost_sp8_her26_contig_808, ost_sp8_her26_contig_807, ost_sp8_her26_contig_7508, ost_sp8_her26_contig_8140

Cysteine (C), Methionine (M) synthesis

C synthesis from serine	2.3.1.30: Serine O-acetyltransferase	NA
	2.5.1.47: Cysteine synthase A	ost_sp8_her26_contig_11972, ost_sp8_her26_contig_24708, ost_sp8_her26_contig_11084, ost_sp8_her26_contig_11970
M synthesis from aspartate	2.7.2.4: Aspartate kinase	NA

1.2.1.11: Aspartate-semialdehyde dehydrogenase	ost_sp8_her26_contig_1731, ost_sp8_her26_contig_39768, ost_sp8_her26_contig_22651
1.1.1.3: Homoserine dehydrogenase	ost_sp8_her26_contig_51275, ost_sp8_her26_contig_68507
2.3.1.31: Homoserine O-acetyltransferase	ost_sp8_her26_contig_23698, ost_sp8_her26_contig_13241
2.5.1.48: Cystathionine gamma-synthase	ost_sp8_her26_contig_8157
4.4.1.8: Cystathionine beta-lyase	ost_sp8_her26_contig_6908, ost_sp8_her26_contig_15895
2.1.1.5/2.1.1.10/2.1.1.13/2.1.1.14: Betaine-homocysteine S-methyltransferase /Homocysteine S-methyltransferase/5-methyltetrahydrofolate--homocysteine methyltransferase /5-methyltetrahydropteroyltriglutamate--homocysteine methyltransferase	ost_sp8_her26_contig_10378

Valine (V), Leucine (L), Isoleucine (I) synthesis

V synthesis from pyruvate	2.2.1.6: Acetolactate synthase I/II/III large subunit	NA
	1.1.1.86: Ketol-acid reductoisomerase	ost_sp8_her26_contig_6453
	4.2.1.9: Dihydroxy-acid dehydratase	ost_sp8_her26_contig_1116
	2.6.1.42: Branched-chain amino acid aminotransferase	ost_sp8_her26_contig_5525, ost_sp8_her26_contig_19738, ost_sp8_her26_contig_7276, ost_sp8_her26_contig_13076, ost_sp8_her26_contig_37388, ost_sp8_her26_contig_5526, ost_sp8_her26_contig_14542
L synthesis from pyruvate	2.2.1.6: Acetolactate synthase I/II/III large subunit	NA
	1.1.1.86: Ketol-acid reductoisomerase	ost_sp8_her26_contig_6453
	4.2.1.9: Dihydroxy-acid dehydratase	ost_sp8_her26_contig_1116
	2.3.3.13: 2-isopropylmalate synthase	
	4.2.1.33: 3-isopropylmalate dehydratase	ost_sp8_her26_contig_5378
	1.1.1.85: 3-isopropylmalate dehydrogenase	ost_sp8_her26_contig_5464
	2.6.1.42: Branched-chain amino acid aminotransferase	ost_sp8_her26_contig_5525, ost_sp8_her26_contig_19738, ost_sp8_her26_contig_7276, ost_sp8_her26_contig_13076, ost_sp8_her26_contig_37388, ost_sp8_her26_contig_5526, ost_sp8_her26_contig_14542
I synthesis from 2-oxobutanoate	2.2.1.6: Acetolactate synthase I/II/III large subunit	NA
	1.1.1.86: Ketol-acid reductoisomerase	ost_sp8_her26_contig_6453
	4.2.1.9: Dihydroxy-acid dehydratase	ost_sp8_her26_contig_1116
	2.6.1.42: Branched-chain amino acid aminotransferase	ost_sp8_her26_contig_5525, ost_sp8_her26_contig_19738, ost_sp8_her26_contig_7276, ost_sp8_her26_contig_13076, ost_sp8_her26_contig_37388, ost_sp8_her26_contig_5526, ost_sp8_her26_contig_14542

Lysine (K) synthesis

K synthesis from aspartate	2.7.2.4: Aspartate kinase	NA
	1.2.1.11: Aspartate-semialdehyde dehydrogenase	ost_sp8_her26_contig_1731, ost_sp8_her26_contig_39768, ost_sp8_her26_contig_22651
	4.2.1.52: Dihydrodipicolinate synthase	NA
	1.3.1.26: Dihydrodipicolinate reductase	NA
	2.3.1.117: 2,3,4,5-tetrahydropyridine-2-carboxylate N-succinyltransferase	NA
	2.6.1.17: N-succinyldiaminopimelate aminotransferase	NA
	3.5.1.18: Succinyl-diaminopimelate desuccinylase	NA
	5.1.1.7: Diaminopimelate epimerase	NA
	4.1.1.20: Diaminopimelate decarboxylase	NA

Histidine (H) synthesis

H synthesis from PRPP	2.4.2.17: ATP phosphoribosyltransferase	ost_sp8_her26_contig_23659
	3.6.1.31: Phosphoribosyl-ATP pyrophosphohydrolase	ost_sp8_her26_contig_52579
	3.5.4.19: Phosphoribosyl-AMP cyclohydrolase	ost_sp8_her26_contig_38258
	5.3.1.16: Phosphoribosylformimino-5-aminoimidazole carboxamide ribotide isomerase	NA
	2.6.1.16: Glutamine amidotransferase	ost_sp8_her26_contig_1861, ost_sp8_her26_contig_19917
	4.2.1.19: Imidazoleglycerol-phosphate dehydratase	ost_sp8_her26_contig_2021
	2.6.1.9: Histidinol-phosphate aminotransferase	NA
	3.1.3.15: Histidinol-phosphatase	NA
	1.1.1.23: histidinol dehydrogenase	ost_sp8_her26_contig_14541

S12D Description of sequences from *Coolia malayensis* MAB encoding essential enzymes of various metabolic pathways. NA= enzymes not present in the transcriptome

Metabolic pathways	Enzymes	Contig name
Glycolysis	1.2.1.12/1.2.1.59: Glyceraldehyde 3-phosphate dehydrogenase /glyceraldehyde-3-phosphate dehydrogenase (NAD(P))	coolia_mab_contig_16584, coolia_mab_contig_8150, coolia_mab_contig_11230, coolia_mab_contig_641, coolia_mab_contig_5230, coolia_mab_contig_1095, coolia_mab_contig_1152, coolia_mab_contig_24327, coolia_mab_contig_5289, coolia_mab_contig_1131, coolia_mab_contig_257, coolia_mab_contig_4033, coolia_mab_contig_10339, coolia_mab_contig_1002, coolia_mab_contig_1001, coolia_mab_contig_1003, coolia_mab_contig_361, coolia_mab_contig_30396, coolia_mab_contig_360, coolia_mab_contig_4877, coolia_mab_contig_9913, coolia_mab_contig_13024, coolia_mab_contig_2709
	2.7.1.11: 6-phosphofructokinase	coolia_mab_contig_6858, coolia_mab_contig_5458, coolia_mab_contig_25172, coolia_mab_contig_12492
	2.7.1.2: Glucokinase	coolia_mab_contig_12959, coolia_mab_contig_27672, coolia_mab_contig_12039
	2.7.1.40: Pyruvate kinase	coolia_mab_contig_19875, coolia_mab_contig_16099, coolia_mab_contig_18022, coolia_mab_contig_14477, coolia_mab_contig_34898, coolia_mab_contig_14313, coolia_mab_contig_1087
	2.7.2.3: Phosphoglycerate kinase	coolia_mab_contig_15781, coolia_mab_contig_12191, coolia_mab_contig_1152, coolia_mab_contig_5289, coolia_mab_contig_1131, coolia_mab_contig_8123, coolia_mab_contig_7517, coolia_mab_contig_361, coolia_mab_contig_1104, coolia_mab_contig_4939, coolia_mab_contig_37744, coolia_mab_contig_18933, coolia_mab_contig_17876
	4.1.2.13: Fructose-bisphosphate aldolase, class I	coolia_mab_contig_448, coolia_mab_contig_2161, coolia_mab_contig_27238, coolia_mab_contig_2672, coolia_mab_contig_24469,

254

		coolia_mab_contig_24348, coolia_mab_contig_54179, coolia_mab_contig_1850, coolia_mab_contig_12935, coolia_mab_contig_49382, coolia_mab_contig_8911, coolia_mab_contig_7921, coolia_mab_contig_8910, coolia_mab_contig_27354, coolia_mab_contig_1852, coolia_mab_contig_2754, coolia_mab_contig_27353, coolia_mab_contig_48102, coolia_mab_contig_58400, coolia_mab_contig_11861, coolia_mab_contig_12873, coolia_mab_contig_13778, coolia_mab_contig_12998, coolia_mab_contig_13795
	4.2.1.11: Enolase	coolia_mab_contig_8529, coolia_mab_contig_20746, coolia_mab_contig_26260, coolia_mab_contig_2449, coolia_mab_contig_4877, coolia_mab_contig_2709, coolia_mab_contig_20530, coolia_mab_contig_7176, coolia_mab_contig_8341, coolia_mab_contig_4178, coolia_mab_contig_11742, coolia_mab_contig_17932
	5.3.1.1: Triosephosphate isomerase (TIM)	coolia_mab_contig_35429, coolia_mab_contig_8529, coolia_mab_contig_438, coolia_mab_contig_27785, coolia_mab_contig_13407, coolia_mab_contig_199, coolia_mab_contig_9668, coolia_mab_contig_642
	5.3.1.9: Glucose-6-phosphate isomerase	coolia_mab_contig_17932, coolia_mab_contig_2263
	5.4.2.1: Phosphoglycerate mutase	NA
TCA cycle	6.2.1.4/6.2.1.5: Succinyl-CoA synthetase alpha subunit	NA
	1.1.1.37: Malate dehydrogenase	coolia_mab_contig_19348, coolia_mab_contig_12889, coolia_mab_contig_1578, coolia_mab_contig_9439, coolia_mab_contig_9438, coolia_mab_contig_16648, coolia_mab_contig_12653, coolia_mab_contig_4826, coolia_mab_contig_24688, coolia_mab_contig_41436
	1.1.1.42: Isocitrate dehydrogenase	coolia_mab_contig_19039, coolia_mab_contig_4664, coolia_mab_contig_6699, coolia_mab_contig_9559,

		coolia_mab_contig_9045, coolia_mab_contig_9202, coolia_mab_contig_10466
	1.2.4.1/2.3.1.12: Pyruvate dehydrogenase E1 component/ Pyruvate dehydrogenase E2 component (dihydrolipoamide acetyltransferase)	NA
	1.2.4.2/2.3.1.61: 2-oxoglutarate dehydrogenase E1 component / 2-oxoglutarate dehydrogenase E2 component (dihydrolipoamide succinyltransferase)	coolia_mab_contig_25047
	1.3.5.1/ 1.3.99.1: Succinate dehydrogenase (ubiquinone) flavoprotein subunit/ Succinate dehydrogenase flavoprotein subunit	coolia_mab_contig_20941, coolia_mab_contig_208, coolia_mab_contig_2057, coolia_mab_contig_927, coolia_mab_contig_926, coolia_mab_contig_6046
	2.3.3.1: Citrate synthase	coolia_mab_contig_21060
	4.2.1.2: Fumarate hydratase, class I	coolia_mab_contig_28565, coolia_mab_contig_13545
	4.2.1.3: Aconitate hydratase 1	coolia_mab_contig_2316, coolia_mab_contig_141
Oxidative phosphorylation	1.6.5.3/1.6.99.3: NADH dehydrogenase/ NADH dehydrogenase (complex I)	coolia_mab_contig_20765
	1.3.5.1/ 1.3.99.1: Succinate dehydrogenase (ubiquinone) flavoprotein subunit/ Succinate dehydrogenase flavoprotein subunit subunit (complex II)	coolia_mab_contig_20941, coolia_mab_contig_208, coolia_mab_contig_2057, coolia_mab_contig_927, coolia_mab_contig_926, coolia_mab_contig_6046
	1.10.2.2: Ubiquinol-cytochrome c reductase iron-sulfur subunit (complex III)	coolia_mab_contig_14750, coolia_mab_contig_34293, coolia_mab_contig_19033, coolia_mab_contig_43838, coolia_mab_contig_27903, coolia_mab_contig_1320, coolia_mab_contig_27053, coolia_mab_contig_13899, coolia_mab_contig_17447, coolia_mab_contig_14851, coolia_mab_contig_17446, coolia_mab_contig_17449, coolia_mab_contig_17448
	1.9.3.1: Cb-type cytochrome c oxidase subunit I (complex IV)	coolia_mab_contig_11748, coolia_mab_contig_27919, coolia_mab_contig_8419, coolia_mab_contig_64540, coolia_mab_contig_22714, coolia_mab_contig_35123, coolia_mab_contig_3166, coolia_mab_contig_3165
	3.6.3.6/3.6.3.14: H+ transporting ATPase/F-type H+-transporting ATPase subunit a (complex V)	NA
Carbon fixation (C3)	2.7.1.19: Phosphoribulokinase	coolia_mab_contig_20512, coolia_mab_contig_1501, coolia_mab_contig_65014, coolia_mab_contig_30927, coolia_mab_contig_14876, coolia_mab_contig_37117

256

4.1.1.39: Ribulose-bisphosphate carboxylase large chain	coolia_mab_contig_18764, coolia_mab_contig_701, coolia_mab_contig_19742, coolia_mab_contig_4490, coolia_mab_contig_22023, coolia_mab_contig_64348, coolia_mab_contig_6065, coolia_mab_contig_65706, coolia_mab_contig_60548, coolia_mab_contig_62416, coolia_mab_contig_5899, coolia_mab_contig_1640, coolia_mab_contig_3278, coolia_mab_contig_34848, coolia_mab_contig_1105, coolia_mab_contig_59018, coolia_mab_contig_35465, coolia_mab_contig_13831, coolia_mab_contig_1768, coolia_mab_contig_10761, coolia_mab_contig_2715, coolia_mab_contig_36964
2.7.2.3: Phosphoglycerate kinase	coolia_mab_contig_15781, coolia_mab_contig_12191, coolia_mab_contig_1152, coolia_mab_contig_5289, coolia_mab_contig_1131, coolia_mab_contig_8123, coolia_mab_contig_7517, coolia_mab_contig_361, coolia_mab_contig_1104, coolia_mab_contig_4939, coolia_mab_contig_37744, coolia_mab_contig_18933, coolia_mab_contig_17876
1.2.1.13/1.2.1.59: Glyceraldehyde-3-phosphate dehydrogenase (NADP+) (phosphorylating)/ glyceraldehyde-3-phosphate dehydrogenase (NAD(P))	NA
5.3.1.1: Triosephosphate isomerase (TIM)	coolia_mab_contig_35429, coolia_mab_contig_8529, coolia_mab_contig_438, coolia_mab_contig_27785, coolia_mab_contig_13407, coolia_mab_contig_199, coolia_mab_contig_9668, coolia_mab_contig_642
4.1.2.13: Fructose-bisphosphate aldolase, class I	coolia_mab_contig_448, coolia_mab_contig_2161, coolia_mab_contig_27238, coolia_mab_contig_2672, coolia_mab_contig_24469, coolia_mab_contig_24348, coolia_mab_contig_54179, coolia_mab_contig_1850, coolia_mab_contig_12935, coolia_mab_contig_49382, coolia_mab_contig_8911, coolia_mab_contig_7921, coolia_mab_contig_8910,

		coolia_mab_contig_27354, coolia_mab_contig_1852, coolia_mab_contig_2754, coolia_mab_contig_27353, coolia_mab_contig_48102, coolia_mab_contig_58400, coolia_mab_contig_11861, coolia_mab_contig_12873, coolia_mab_contig_13778, coolia_mab_contig_12998, coolia_mab_contig_13795
	3.1.3.11: Fructose-1,6-bisphosphatase I	coolia_mab_contig_3534, coolia_mab_contig_15111, coolia_mab_contig_48581, coolia_mab_contig_22409, coolia_mab_contig_409, coolia_mab_contig_1080, coolia_mab_contig_26326, coolia_mab_contig_7743
	2.2.1.1: Transketolase	coolia_mab_contig_22328, coolia_mab_contig_11448, coolia_mab_contig_762, coolia_mab_contig_15988, coolia_mab_contig_15987, coolia_mab_contig_36289, coolia_mab_contig_15989, coolia_mab_contig_722, coolia_mab_contig_5465, coolia_mab_contig_12159, coolia_mab_contig_9388
	3.1.3.37: Sedoheptulose-1,7-bisphosphatase	coolia_mab_contig_1080
	5.1.3.1: Ribulose-phosphate 3-epimerase	coolia_mab_contig_14805, coolia_mab_contig_11575, coolia_mab_contig_39226
	5.3.1.6: Ribose 5-phosphate isomerase A	coolia_mab_contig_28919, coolia_mab_contig_15533
Pentose phosphate pathway	1.1.1.49 glucose-6-phosphate dehydrogenase	coolia_mab_contig_31012
	3.1.1.31 6-phosphogluconolactonase	NA
	1.1.1.44 phosphogluconate dehydrogenase (NADP+-dependent, decarboxylating)	coolia_mab_contig_39905, coolia_mab_contig_49134, coolia_mab_contig_19681, coolia_mab_contig_49307, coolia_mab_contig_20036, coolia_mab_contig_9364
	5.3.1.6 ribose-5-phosphate isomerase	coolia_mab_contig_28919, coolia_mab_contig_15533
	5.1.3.1 ribulose-phosphate 3-epimerase	coolia_mab_contig_14805, coolia_mab_contig_11575, coolia_mab_contig_39226
	2.2.1.1 transketolase	coolia_mab_contig_22328, coolia_mab_contig_11448, coolia_mab_contig_762, coolia_mab_contig_15988, coolia_mab_contig_15987, coolia_mab_contig_36289, coolia_mab_contig_15989, coolia_mab_contig_722,

258

		coolia_mab_contig_5465, coolia_mab_contig_12159, coolia_mab_contig_9388
	2.2.1.2 transaldolase	NA

Purine nucleotide synthesis

Inosine monophosphate synthesis (precursor)	2.7.6.1: Ribose-phosphate pyrophosphokinase	coolia_mab_contig_1203, coolia_mab_contig_30205
	2.1.2.2: GAR transformylase	coolia_mab_contig_20681
	2.1.2.3: AICAR transformylase	coolia_mab_contig_292, coolia_mab_contig_12746, coolia_mab_contig_2668
	2.4.2.14: Amidophosphoribosyltransferase	
	3.5.4.10: IMP cyclohydrolase	coolia_mab_contig_292, coolia_mab_contig_12746, coolia_mab_contig_2668
	4.1.1.21: AIR carboxylase	coolia_mab_contig_18184
	4.3.2.2: Adenylosuccinate lyase	coolia_mab_contig_13706
	6.3.2.6: SAICAR synthetase	NA
	6.3.3.1: AIR synthetase	coolia_mab_contig_7218, coolia_mab_contig_11126
	6.3.4.13: Phosphoribosylamine--glycine ligase	coolia_mab_contig_12746, coolia_mab_contig_7218, coolia_mab_contig_20681, coolia_mab_contig_11126
	6.3.5.3: FGAM synthetase	coolia_mab_contig_6745
Synthesis of AMP, ADP and ATP	6.3.4.4: Adenylosuccinate synthase	coolia_mab_contig_16580, coolia_mab_contig_7809
	4.3.2.2: Adenylosuccinate lyase	coolia_mab_contig_13706
	2.7.4.3: Adenylate kinase	coolia_mab_contig_13572, coolia_mab_contig_4604, coolia_mab_contig_12240, coolia_mab_contig_19749
	2.7.4.6: Nucleoside-diphosphate kinase	coolia_mab_contig_12716, coolia_mab_contig_3520, coolia_mab_contig_9462, coolia_mab_contig_7048, coolia_mab_contig_18826
Synthesis of dADP and dATP	1.17.4.1: Ribonucleotide reductase, class II	coolia_mab_contig_14693, coolia_mab_contig_827, coolia_mab_contig_826, coolia_mab_contig_7641, coolia_mab_contig_9375, coolia_mab_contig_6000
	2.7.4.6: Nucleoside-diphosphate kinase	coolia_mab_contig_12716, coolia_mab_contig_3520, coolia_mab_contig_9462, coolia_mab_contig_7048, coolia_mab_contig_18826
Synthesis of GMP, GDP and GTP	1.1.1.205: IMP dehydrogenase	coolia_mab_contig_14033, coolia_mab_contig_20898, coolia_mab_contig_14705, coolia_mab_contig_15525, coolia_mab_contig_17238,

		coolia_mab_contig_25139
	6.3.5.2: GMP synthase (glutamine-hydrolysing)	coolia_mab_contig_17302, coolia_mab_contig_26113, coolia_mab_contig_25012, coolia_mab_contig_33959, coolia_mab_contig_16727, coolia_mab_contig_16437
	2.7.4.8: Guanylate kinase	coolia_mab_contig_14594, coolia_mab_contig_40688, coolia_mab_contig_3440, coolia_mab_contig_4220
	2.7.4.6: Nucleoside-diphosphate kinase	coolia_mab_contig_12716, coolia_mab_contig_3520, coolia_mab_contig_9462, coolia_mab_contig_7048, coolia_mab_contig_18826
Synthesis of dGDP and dGTP	1.17.4.1: Ribonucleotide reductase, class II	coolia_mab_contig_14693, coolia_mab_contig_827, coolia_mab_contig_826, coolia_mab_contig_7641, coolia_mab_contig_9375, coolia_mab_contig_6000
	2.7.4.6: Nucleoside-diphosphate kinase	coolia_mab_contig_12716, coolia_mab_contig_3520, coolia_mab_contig_9462, coolia_mab_contig_7048, coolia_mab_contig_18826

Pyrimidine nucleotide synthesis

Uridine monophosphate synthesis (precursor)	6.3.5.5: carbamoyl-phosphate synthase	coolia_mab_contig_11142, coolia_mab_contig_6796, coolia_mab_contig_1340
	2.1.3.2: aspartate carbamoyltransferase	coolia_mab_contig_17733
	3.5.2.3: dihydroorotase	
	1.3.5.2: dihydroorotate dehydrogenase	coolia_mab_contig_45016, coolia_mab_contig_26771
	2.4.2.10: orotate phosphoribosyltransferase	coolia_mab_contig_25797
	4.1.1.23: orotidine-5'-monophosphate decarboxylase	coolia_mab_contig_25797
UDP, UTP, CTP and CDP synthesis	2.7.4.4: nucleoside phosphate kinase	NA
	2.7.4.6: nucleoside-diphosphate kinase	coolia_mab_contig_12716, coolia_mab_contig_3520, coolia_mab_contig_9462, coolia_mab_contig_7048, coolia_mab_contig_18826
	6.3.4.2: CTP synthase	coolia_mab_contig_706, coolia_mab_contig_9899
dCDP, dCTP, dUDP and dUTP synthesis	1.17.4.1: ribonucleotide reductase, class II	coolia_mab_contig_14693, coolia_mab_contig_827, coolia_mab_contig_826, coolia_mab_contig_7641, coolia_mab_contig_9375, coolia_mab_contig_6000
	2.7.4.6: nucleoside-diphosphate kinase	coolia_mab_contig_12716, coolia_mab_contig_3520,

		coolia_mab_contig_9462, coolia_mab_contig_7048, coolia_mab_contig_18826
dTMP, dTDP and dTTP synthesis	2.7.4.4 nucleoside phosphate kinase	NA
	2.1.1.45: thymidylate synthase	coolia_mab_contig_10602
	2.7.4.9: dTMP kinase	coolia_mab_contig_12065, coolia_mab_contig_10842
	2.7.4.6: nucleoside-diphosphate kinase	coolia_mab_contig_12716, coolia_mab_contig_3520, coolia_mab_contig_9462, coolia_mab_contig_7048, coolia_mab_contig_18826

Tyrosine (Y), Phenylalanine (F), Tryptopham (W) synthesis

Chorismate synthesis (precursor)	2.5.1.54: 3-deoxy-7-phosphoheptulonate synthase	coolia_mab_contig_3538, coolia_mab_contig_50692, coolia_mab_contig_12014, coolia_mab_contig_12831
	4.2.3.4: 3-dehydroquinate synthase	coolia_mab_contig_25803, coolia_mab_contig_3469
	4.2.1.10: 3-dehydroquinate dehydratase I	coolia_mab_contig_18894, coolia_mab_contig_32737
	1.1.1.25: Shikimate dehydrogenase	NA
	2.7.1.71: Shikimate kinase	NA
	2.5.1.19: 3-phosphoshikimate 1- carboxyvinyltransferase	coolia_mab_contig_29000
	4.2.3.5: Chorismate synthase	coolia_mab_contig_3981
Y synthesis	5.4.99.5: Chorismate mutase	coolia_mab_contig_22681
	1.3.1.13: Prephenate dehydrogenase (NADP+)	NA
	2.6.1.1: Aspartate aminotransferase, cytoplasmic	NA
F synthesis	5.4.99.5: Chorismate mutase	coolia_mab_contig_22681
	4.2.1.51: Prephenate dehydratase	coolia_mab_contig_20803
	2.6.1.1: Aspartate aminotransferase, cytoplasmic	coolia_mab_contig_36526
W synthesis	4.1.3.27: Anthranilate synthase	coolia_mab_contig_23388
	2.4.2.18: Anthranilate phosphoribosyltransferase	coolia_mab_contig_21949
	5.3.1.24: Phosphoribosylanthranilate isomerase	coolia_mab_contig_43299
	4.1.1.48: Indole-3-glycerol phosphate synthase	coolia_mab_contig_43299
	4.2.1.20: Tryptophan synthase alpha chain	coolia_mab_contig_4656, coolia_mab_contig_36972

Serine (S), Glycine (G), Threonien (T) synthesis

S synthesis from 3- phosphoglycerate	1.1.1.95: D-3-phosphoglycerate dehydrogenase	NA
	2.6.1.52: Phosphoserine aminotransferase	coolia_mab_contig_10841
	3.1.3.3: Phosphoserine phosphatase	coolia_mab_contig_5803, coolia_mab_contig_5280, coolia_mab_contig_20023, coolia_mab_contig_3010
G synthesis from serine	2.1.2.1: Glycine hydroxymethyltransferase	coolia_mab_contig_6181, coolia_mab_contig_15487,

		coolia_mab_contig_6180, coolia_mab_contig_11145, coolia_mab_contig_1491, coolia_mab_contig_1490, coolia_mab_contig_14675, coolia_mab_contig_32459
T synthesis from L-aspartate	2.7.2.4: Aspartate kinase	coolia_mab_contig_970
	1.2.1.11: Aspartate-semialdehyde dehydrogenase	coolia_mab_contig_17850, coolia_mab_contig_15072
	1.1.1.3: Homoserine dehydrogenase	coolia_mab_contig_25125
	2.7.1.39: Homoserine kinase	NA
	4.2.3.1: Threonine synthase	NA

Arginine (R), Proline (P) synthesis

R synthesis from glutamate	2.3.1.1: Amino-acid N-acetyltransferase	coolia_mab_contig_49653
	2.7.2.8: Acetylglutamate kinase	NA
	1.2.1.38: N-acetyl-gamma-glutamyl-phosphate reductase	coolia_mab_contig_17850, coolia_mab_contig_15072
	2.6.1.11: Acetylornithine aminotransferase	NA
	3.5.1.16: Acetylornithine deacetylase	NA
	2.1.3.3: Ornithine carbamoyltransferase (urea cycle)	NA
	6.3.4.5: Argininosuccinate synthase (urea cycle)	coolia_mab_contig_12276
	4.3.2.1: Argininosuccinate lyase (urea cycle)	coolia_mab_contig_28736
P synthesis from glutamate	2.7.2.11: Glutamate 5-kinase	coolia_mab_contig_27413
	1.2.1.41: Glutamate-5-semialdehyde dehydrogenase	NA
	1.5.1.2: Pyrroline-5-carboxylate reductase	coolia_mab_contig_8027, coolia_mab_contig_50312, coolia_mab_contig_25878, coolia_mab_contig_21641

Alanine (A), Aspartic acid (D), Asparginine (N), Glutamic acid (E), Glutamine (Q) synthesis

A synthesis from pyruvate	2.6.1.44: Alanine-glyoxylate transaminase (alanine-glyoxylate aminotransferase)	NA
D synthesis from oxaloacetate	2.6.1.1: Aspartate aminotransferase, cytoplasmic	NA
N synthesis from aspartate	6.3.5.4: Asparagine synthase (glutamine-hydrolysing)	coolia_mab_contig_29567, coolia_mab_contig_17749, coolia_mab_contig_13889, coolia_mab_contig_18406, coolia_mab_contig_158
E synthesis from 2-oxoglutarate	1.4.1.13 /1.4.1.14: Glutamate synthase NADPH/ Glutamate synthase NADH	NA
Q synthesis from glutamate	6.3.1.2: Glutamine synthetase	coolia_mab_contig_24591, coolia_mab_contig_2636, coolia_mab_contig_26144, coolia_mab_contig_2303, coolia_mab_contig_23690, coolia_mab_contig_14458, coolia_mab_contig_31162, coolia_mab_contig_14702, coolia_mab_contig_2582,

coolia_mab_contig_43778

Cysteine (C), Methionine (M) synthesis

C synthesis from serine	2.3.1.30: Serine O-acetyltransferase	NA
	2.5.1.47: Cysteine synthase A	coolia_mab_contig_5484, coolia_mab_contig_1627
M synthesis from aspartate	2.7.2.4: Aspartate kinase	coolia_mab_contig_970
	1.2.1.11: Aspartate-semialdehyde dehydrogenase	coolia_mab_contig_17850, coolia_mab_contig_15072
	1.1.1.3: Homoserine dehydrogenase	coolia_mab_contig_25125
	2.3.1.31: Homoserine O-acetyltransferase	coolia_mab_contig_38695, coolia_mab_contig_6840
	2.5.1.48: Cystathionine gamma-synthase	NA
	4.4.1.8: Cystathionine beta-lyase	coolia_mab_contig_39473, coolia_mab_contig_17423
	2.1.1.5/2.1.1.10/2.1.1.13/2.1.1.14: Betaine-homocysteine S-methyltransferase /Homocysteine S-methyltransferase/5-methyltetrahydrofolate--homocysteine methyltransferase /5-methyltetrahydropteroyltriglutamate--homocysteine methyltransferase	NA

Valine (V), Leucine (L), Isoleucine (I) synthesis

V synthesis from pyruvate	2.2.1.6: Acetolactate synthase I/II/III large subunit	coolia_mab_contig_25630
	1.1.1.86: Ketol-acid reductoisomerase	coolia_mab_contig_1507
	4.2.1.9: Dihydroxy-acid dehydratase	coolia_mab_contig_1507
	2.6.1.42: Branched-chain amino acid aminotransferase	coolia_mab_contig_19788, coolia_mab_contig_10646, coolia_mab_contig_5685, coolia_mab_contig_31325, coolia_mab_contig_38208
L synthesis from pyruvate	2.2.1.6: Acetolactate synthase I/II/III large subunit	coolia_mab_contig_25630
	1.1.1.86: Ketol-acid reductoisomerase	coolia_mab_contig_1507
	4.2.1.9: Dihydroxy-acid dehydratase	coolia_mab_contig_1507
	2.3.3.13: 2-isopropylmalate synthase	coolia_mab_contig_16746
	4.2.1.33: 3-isopropylmalate dehydratase	coolia_mab_contig_4459
	1.1.1.85: 3-isopropylmalate dehydrogenase	coolia_mab_contig_10762
	2.6.1.42: Branched-chain amino acid aminotransferase	coolia_mab_contig_19788, coolia_mab_contig_10646, coolia_mab_contig_5685, coolia_mab_contig_31325, coolia_mab_contig_38208
I synthesis from 2-oxobutanoate	2.2.1.6: Acetolactate synthase I/II/III large subunit	coolia_mab_contig_25630
	1.1.1.86: Ketol-acid reductoisomerase	coolia_mab_contig_1507
	4.2.1.9: Dihydroxy-acid dehydratase	coolia_mab_contig_1507
	2.6.1.42: Branched-chain amino acid aminotransferase	coolia_mab_contig_19788, coolia_mab_contig_10646, coolia_mab_contig_5685, coolia_mab_contig_31325,

coolia_mab_contig_38208

Lysine (K) synthesis

K synthesis from aspartate	2.7.2.4: Aspartate kinase	coolia_mab_contig_970
	1.2.1.11: Aspartate-semialdehyde dehydrogenase	coolia_mab_contig_17850, coolia_mab_contig_15072
	4.2.1.52: Dihydrodipicolinate synthase	NA
	1.3.1.26: Dihydrodipicolinate reductase	NA
	2.3.1.117: 2,3,4,5-tetrahydropyridine-2-carboxylate N-succinyltransferase	NA
	2.6.1.17: N-succinyldiaminopimelate aminotransferase	NA
	3.5.1.18: Succinyl-diaminopimelate desuccinylase	NA
	5.1.1.7: Diaminopimelate epimerase	NA
	4.1.1.20: Diaminopimelate decarboxylase	coolia_mab_contig_18616

Histidine (H) synthesis

H synthesis from PRPP	2.4.2.17: ATP phosphoribosyltransferase	NA
	3.6.1.31: Phosphoribosyl-ATP pyrophosphohydrolase	coolia_mab_contig_38340
	3.5.4.19: Phosphoribosyl-AMP cyclohydrolase	coolia_mab_contig_53177
	5.3.1.16: Phosphoribosylformimino-5-aminoimidazole carboxamide ribotide isomerase	coolia_mab_contig_30292
	2.6.1.16: Glutamine amidotransferase	coolia_mab_contig_570, coolia_mab_contig_9888
	4.2.1.19: Imidazoleglycerol-phosphate dehydratase	coolia_mab_contig_13855
	2.6.1.9: Histidinol-phosphate aminotransferase	coolia_mab_contig_33946
	3.1.3.15: Histidinol-phosphatase	NA
	1.1.1.23: histidinol dehydrogenase	coolia_mab_contig_11284

S13 Distributions of second level cellular component, biological processes and molecular function GO annotations in the annotated transcriptomes.

Level 2 Cellular Component GO annotations

Level 2 Biological Processes GO annotations

Level 2 Molecular Function GO annotations

■ *Ostreopsis cf. ovata HER27*   ■ *Ostreopsis rhodesae HER26*   ■ *Ostreopsis cf. siamensis BH1*   ■ *Coolia malayensis MAB*
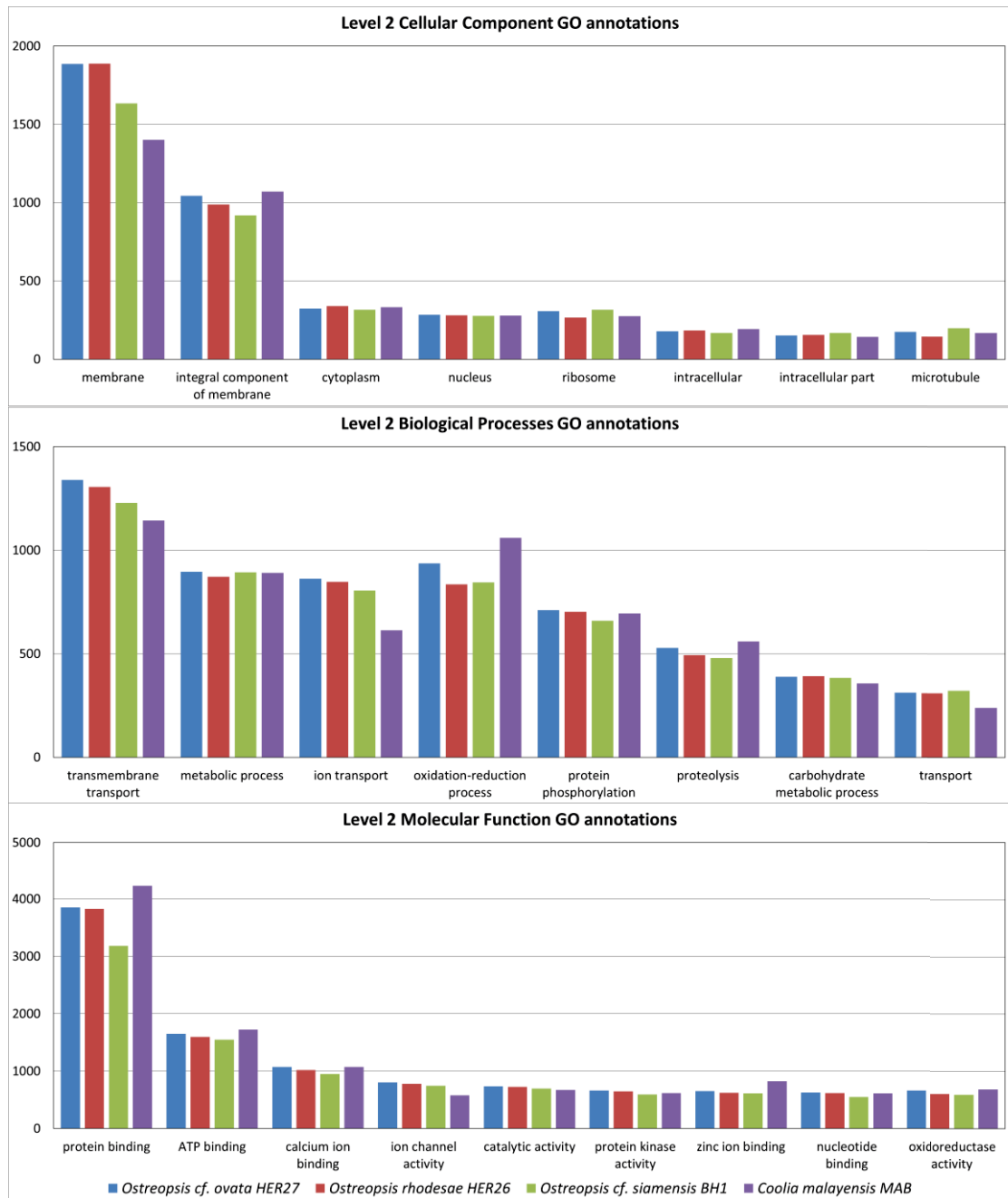
S14A List of transcripts encoding full ketoacyl synthase domain identified in *Coolia malayensis* MAB, *Ostreopsis* cf. *ovata* HER27, *Ostreopsis* cf. *siamensis* BH1 and *Ostreopsis rhodesae* HER26.

Species	S. no.	Contig name	Length (bp)
Coolia malayensis **MAB**	1	coolia_mab_contig_279	3375
	2	coolia_mab_contig_594	5071
	3	coolia_mab_contig_889	3055
	4	coolia_mab_contig_898	3958
	5	coolia_mab_contig_1540	3033
	6	coolia_mab_contig_1930	4011
	7	coolia_mab_contig_2508	3860
	8	coolia_mab_contig_2630	3972
	9	coolia_mab_contig_2832	3476
	10	coolia_mab_contig_2882	3946
	11	coolia_mab_contig_2956	3865
	12	coolia_mab_contig_2976	3670
	13	coolia_mab_contig_3397	3630
	14	coolia_mab_contig_3414	3208
	15	coolia_mab_contig_3799	3130
	16	coolia_mab_contig_3918	3575
	17	coolia_mab_contig_4218	3787
	18	coolia_mab_contig_4296	3543
	19	coolia_mab_contig_4580	4029
	20	coolia_mab_contig_5333	4109
	21	coolia_mab_contig_5355	3379
	22	coolia_mab_contig_5723	3092
	23	coolia_mab_contig_6003	4011
	24	coolia_mab_contig_6076	3693
	25	coolia_mab_contig_7073	4246
	26	coolia_mab_contig_7317	3251
	27	coolia_mab_contig_7604	3736
	28	coolia_mab_contig_7826	3071
	29	coolia_mab_contig_9002	3702
	30	coolia_mab_contig_9305	4125
	31	coolia_mab_contig_9515	2888
	32	coolia_mab_contig_9807	4167
	33	coolia_mab_contig_9908	3043
	34	coolia_mab_contig_10430	4415
	35	coolia_mab_contig_10790	3062
	36	coolia_mab_contig_10907	2686
	37	coolia_mab_contig_10970	3084
	38	coolia_mab_contig_12048	2886
	39	coolia_mab_contig_12068	3363

	40	coolia_mab_contig_12145	3939
	41	coolia_mab_contig_12704	4000
	42	coolia_mab_contig_12721	3853
	43	coolia_mab_contig_13995	2981
	44	coolia_mab_contig_14574	3089
	45	coolia_mab_contig_14951	2970
	46	coolia_mab_contig_15733	3363
	47	coolia_mab_contig_16164	3330
	48	coolia_mab_contig_16713	3802
	49	coolia_mab_contig_17768	3057
	50	coolia_mab_contig_18497	4003
	51	coolia_mab_contig_19232	4269
	52	coolia_mab_contig_19391	2977
	53	coolia_mab_contig_20348	4492
	54	coolia_mab_contig_21011	3874
	55	coolia_mab_contig_21740	3142
	56	coolia_mab_contig_21780	3793
	57	coolia_mab_contig_23605	3364
	58	coolia_mab_contig_23711	3135
	59	coolia_mab_contig_24272	4376
	60	coolia_mab_contig_24391	4147
	61	coolia_mab_contig_24551	3436
	62	coolia_mab_contig_25363	4705
	63	coolia_mab_contig_26386	3157
	64	coolia_mab_contig_30043	3820
	65	coolia_mab_contig_30720	2501
	66	coolia_mab_contig_31491	4128
	67	coolia_mab_contig_34285	4210
	68	coolia_mab_contig_35552	3818
	69	coolia_mab_contig_35760	3080
	70	coolia_mab_contig_35826	4084
	71	coolia_mab_contig_37298	3105
	72	coolia_mab_contig_37614	4207
	73	coolia_mab_contig_38539	3734
	74	coolia_mab_contig_40018	3760
	75	coolia_mab_contig_43031	3675
	76	coolia_mab_contig_45156	3643
Ostreopsis **cf.** *ovata* **HER27**	77	ost_ovt_her27_contig_350	3644
	78	ost_ovt_her27_contig_828	3080
	79	ost_ovt_her27_contig_1889	3708
	80	ost_ovt_her27_contig_2076	3868
	81	ost_ovt_her27_contig_2280	3624
	82	ost_ovt_her27_contig_2522	3956
	83	ost_ovt_her27_contig_2977	3294

84	ost_ovt_her27_contig_3457	4229
85	ost_ovt_her27_contig_3909	3349
86	ost_ovt_her27_contig_4540	3930
87	ost_ovt_her27_contig_4849	3857
88	ost_ovt_her27_contig_5132	3745
89	ost_ovt_her27_contig_5276	3109
90	ost_ovt_her27_contig_5289	4018
91	ost_ovt_her27_contig_5722	3112
92	ost_ovt_her27_contig_5787	3313
93	ost_ovt_her27_contig_6006	3320
94	ost_ovt_her27_contig_6116	4191
95	ost_ovt_her27_contig_6192	4178
96	ost_ovt_her27_contig_6223	4347
97	ost_ovt_her27_contig_6415	3982
98	ost_ovt_her27_contig_7045	2965
99	ost_ovt_her27_contig_7177	3517
100	ost_ovt_her27_contig_7368	3076
101	ost_ovt_her27_contig_7390	4272
102	ost_ovt_her27_contig_7391	3168
103	ost_ovt_her27_contig_7392	2521
104	ost_ovt_her27_contig_7885	3829
105	ost_ovt_her27_contig_8240	3170
106	ost_ovt_her27_contig_8323	4022
107	ost_ovt_her27_contig_8686	3859
108	ost_ovt_her27_contig_9281	2976
109	ost_ovt_her27_contig_10374	3145
110	ost_ovt_her27_contig_10425	3156
111	ost_ovt_her27_contig_10810	2991
112	ost_ovt_her27_contig_10898	3755
113	ost_ovt_her27_contig_11589	4348
114	ost_ovt_her27_contig_11635	3344
115	ost_ovt_her27_contig_11810	3908
116	ost_ovt_her27_contig_11861	3998
117	ost_ovt_her27_contig_12663	3498
118	ost_ovt_her27_contig_12798	3888
119	ost_ovt_her27_contig_13028	3980
120	ost_ovt_her27_contig_13615	3549
121	ost_ovt_her27_contig_13809	3767
122	ost_ovt_her27_contig_13820	4149
123	ost_ovt_her27_contig_14747	3411
124	ost_ovt_her27_contig_15103	3746
125	ost_ovt_her27_contig_15506	4178
126	ost_ovt_her27_contig_16412	2306
127	ost_ovt_her27_contig_17166	2976

	128	ost_ovt_her27_contig_17192	4032
	129	ost_ovt_her27_contig_17659	4030
	130	ost_ovt_her27_contig_17719	4540
	131	ost_ovt_her27_contig_18224	3930
	132	ost_ovt_her27_contig_18295	2867
	133	ost_ovt_her27_contig_19210	3263
	134	ost_ovt_her27_contig_19453	3957
	135	ost_ovt_her27_contig_21182	3591
	136	ost_ovt_her27_contig_21528	2884
	137	ost_ovt_her27_contig_21548	2731
	138	ost_ovt_her27_contig_21864	3007
	139	ost_ovt_her27_contig_21893	3358
	140	ost_ovt_her27_contig_22719	3812
	141	ost_ovt_her27_contig_23201	3233
	142	ost_ovt_her27_contig_25090	3923
	143	ost_ovt_her27_contig_28600	3470
	144	ost_ovt_her27_contig_29033	3135
	145	ost_ovt_her27_contig_34491	3177
	146	ost_ovt_her27_contig_36186	4017
	147	ost_ovt_her27_contig_38321	2709
	148	ost_ovt_her27_contig_39462	3883
	149	ost_ovt_her27_contig_42830	2567
	150	ost_ovt_her27_contig_47210	3972
	151	ost_ovt_her27_contig_49915	3073
	152	ost_ovt_her27_contig_49951	3518
	153	ost_ovt_her27_contig_72948	1362
***Ostreopsis* cf. *siamensis* BH1**	154	ost_siam_bh1_contig_87	3722
	155	ost_siam_bh1_contig_1173	4182
	156	ost_siam_bh1_contig_1174	3905
	157	ost_siam_bh1_contig_1574	3878
	158	ost_siam_bh1_contig_1971	4028
	159	ost_siam_bh1_contig_2125	4045
	160	ost_siam_bh1_contig_2727	2340
	161	ost_siam_bh1_contig_4112	3977
	162	ost_siam_bh1_contig_5046	3607
	163	ost_siam_bh1_contig_5279	2772
	164	ost_siam_bh1_contig_5416	4796
	165	ost_siam_bh1_contig_6056	3956
	166	ost_siam_bh1_contig_6690	3144
	167	ost_siam_bh1_contig_8817	3939
	168	ost_siam_bh1_contig_9619	3079
	169	ost_siam_bh1_contig_9942	3853
	170	ost_siam_bh1_contig_10458	3269
	171	ost_siam_bh1_contig_11643	3659

172	ost_siam_bh1_contig_12376	3016
173	ost_siam_bh1_contig_12527	3003
174	ost_siam_bh1_contig_12528	2316
175	ost_siam_bh1_contig_12851	3203
176	ost_siam_bh1_contig_13401	3178
177	ost_siam_bh1_contig_13634	3921
178	ost_siam_bh1_contig_13674	4105
179	ost_siam_bh1_contig_13994	4452
180	ost_siam_bh1_contig_14439	3890
181	ost_siam_bh1_contig_14644	3741
182	ost_siam_bh1_contig_15612	2179
183	ost_siam_bh1_contig_15652	3992
184	ost_siam_bh1_contig_16251	3259
185	ost_siam_bh1_contig_16929	3183
186	ost_siam_bh1_contig_16953	3827
187	ost_siam_bh1_contig_17150	2479
188	ost_siam_bh1_contig_17605	3211
189	ost_siam_bh1_contig_17654	2923
190	ost_siam_bh1_contig_17743	3795
191	ost_siam_bh1_contig_18167	3988
192	ost_siam_bh1_contig_18462	3501
193	ost_siam_bh1_contig_19528	3048
194	ost_siam_bh1_contig_20084	2983
195	ost_siam_bh1_contig_20215	3891
196	ost_siam_bh1_contig_20439	3497
197	ost_siam_bh1_contig_21247	4122
198	ost_siam_bh1_contig_21478	3304
199	ost_siam_bh1_contig_24242	3570
200	ost_siam_bh1_contig_24297	3201
201	ost_siam_bh1_contig_24332	3324
202	ost_siam_bh1_contig_24984	3562
203	ost_siam_bh1_contig_25485	4046
204	ost_siam_bh1_contig_25968	3990
205	ost_siam_bh1_contig_26495	3176
206	ost_siam_bh1_contig_27329	2623
207	ost_siam_bh1_contig_28440	3364
208	ost_siam_bh1_contig_28918	3711
209	ost_siam_bh1_contig_29624	3099
210	ost_siam_bh1_contig_30748	4286
211	ost_siam_bh1_contig_32332	4180
212	ost_siam_bh1_contig_32461	2733
213	ost_siam_bh1_contig_34490	3199
214	ost_siam_bh1_contig_34856	3128
215	ost_siam_bh1_contig_39839	3938

Ostreopsis rhodesae **HER26**	216	ost_sp8_her26_contig_253	4255
	217	ost_sp8_her26_contig_290	3037
	218	ost_sp8_her26_contig_346	3102
	219	ost_sp8_her26_contig_395	4810
	220	ost_sp8_her26_contig_946	3973
	221	ost_sp8_her26_contig_1612	2296
	222	ost_sp8_her26_contig_1673	4122
	223	ost_sp8_her26_contig_1924	3119
	224	ost_sp8_her26_contig_2383	4118
	225	ost_sp8_her26_contig_2502	3957
	226	ost_sp8_her26_contig_2980	3784
	227	ost_sp8_her26_contig_3271	3787
	228	ost_sp8_her26_contig_3419	3673
	229	ost_sp8_her26_contig_3556	2275
	230	ost_sp8_her26_contig_3926	3159
	231	ost_sp8_her26_contig_4011	4042
	232	ost_sp8_her26_contig_4150	3226
	233	ost_sp8_her26_contig_6004	4039
	234	ost_sp8_her26_contig_6028	3232
	235	ost_sp8_her26_contig_6197	3175
	236	ost_sp8_her26_contig_6198	3379
	237	ost_sp8_her26_contig_6270	3493
	238	ost_sp8_her26_contig_6664	3895
	239	ost_sp8_her26_contig_7389	4499
	240	ost_sp8_her26_contig_7561	3276
	241	ost_sp8_her26_contig_7589	2812
	242	ost_sp8_her26_contig_7852	4515
	243	ost_sp8_her26_contig_7971	2728
	244	ost_sp8_her26_contig_8228	3573
	245	ost_sp8_her26_contig_8539	3336
	246	ost_sp8_her26_contig_8682	3651
	247	ost_sp8_her26_contig_8803	4023
	248	ost_sp8_her26_contig_9177	3977
	249	ost_sp8_her26_contig_9581	4065
	250	ost_sp8_her26_contig_11742	3786
	251	ost_sp8_her26_contig_11756	3864
	252	ost_sp8_her26_contig_13156	3982
	253	ost_sp8_her26_contig_13191	3944
	254	ost_sp8_her26_contig_13273	3997
	255	ost_sp8_her26_contig_13420	4170
	256	ost_sp8_her26_contig_13525	3710
	257	ost_sp8_her26_contig_14479	3504
	258	ost_sp8_her26_contig_15269	3408
	259	ost_sp8_her26_contig_17042	3255

260	ost_sp8_her26_contig_17232	2998
261	ost_sp8_her26_contig_17732	4173
262	ost_sp8_her26_contig_18171	3851
263	ost_sp8_her26_contig_18903	3039
264	ost_sp8_her26_contig_20148	3162
265	ost_sp8_her26_contig_20264	3974
266	ost_sp8_her26_contig_20852	2771
267	ost_sp8_her26_contig_21145	3864
268	ost_sp8_her26_contig_21254	3587
269	ost_sp8_her26_contig_21735	3902
270	ost_sp8_her26_contig_22124	3808
271	ost_sp8_her26_contig_22418	3823
272	ost_sp8_her26_contig_23187	3870
273	ost_sp8_her26_contig_24650	3194
274	ost_sp8_her26_contig_25827	1756
275	ost_sp8_her26_contig_27497	3637
276	ost_sp8_her26_contig_30161	1596
277	ost_sp8_her26_contig_30746	3539
278	ost_sp8_her26_contig_31365	4058
279	ost_sp8_her26_contig_33540	2863
280	ost_sp8_her26_contig_35422	3360
281	ost_sp8_her26_contig_36893	3687
282	ost_sp8_her26_contig_37429	3831
283	ost_sp8_her26_contig_40922	4200

S14B List of transcripts encoding partial ketoacyl synthase domain identified in *Coolia malayensis* MAB, *Ostreopsis* cf. *ovata* HER27, *Ostreopsis* cf. *siamensis* BH1 and *Ostreopsis rhodesae* HER26.

Species	S.No.	Contig name	Length (bp)
	1	coolia_mab_contig_19150	258
	2	coolia_mab_contig_22126	2231
	3	coolia_mab_contig_43208	200
	4	coolia_mab_contig_52402	309
	5	coolia_mab_contig_52403	438
	6	coolia_mab_contig_52439	1420
	7	coolia_mab_contig_54618	562
	8	coolia_mab_contig_54869	623
Coolia malayensis **MAB**	9	coolia_mab_contig_56497	305
	10	coolia_mab_contig_57234	472
	11	coolia_mab_contig_57874	869
	12	coolia_mab_contig_58504	438
	13	coolia_mab_contig_60704	286
	14	coolia_mab_contig_61853	519
	15	coolia_mab_contig_62171	377
	16	coolia_mab_contig_62292	597
	17	coolia_mab_contig_66654	226
	18	ost_ovt_her27_contig_8665	333
	19	ost_ovt_her27_contig_11858	639
	20	ost_ovt_her27_contig_22680	1321
	21	ost_ovt_her27_contig_40631	1064
	22	ost_ovt_her27_contig_49871	556
	23	ost_ovt_her27_contig_54223	607
	24	ost_ovt_her27_contig_54265	809
	25	ost_ovt_her27_contig_58182	237
	26	ost_ovt_her27_contig_58202	250
Ostreopsis **cf.** *ovata* **HER27**	27	ost_ovt_her27_contig_58203	545
	28	ost_ovt_her27_contig_60404	212
	29	ost_ovt_her27_contig_62432	656
	30	ost_ovt_her27_contig_67167	297
	31	ost_ovt_her27_contig_67168	298
	32	ost_ovt_her27_contig_69011	909
	33	ost_ovt_her27_contig_71275	575
	34	ost_ovt_her27_contig_73326	504
	35	ost_ovt_her27_contig_73383	413
	36	ost_ovt_her27_contig_74056	404

37	ost_ovt_her27_contig_76382	830
38	ost_ovt_her27_contig_80789	305
39	ost_siam_bh1_contig_5282	1905
40	ost_siam_bh1_contig_9472	2068
41	ost_siam_bh1_contig_9473	1131
42	ost_siam_bh1_contig_12771	1873
43	ost_siam_bh1_contig_14757	2344
44	ost_siam_bh1_contig_15351	1815
45	ost_siam_bh1_contig_20664	315
46	ost_siam_bh1_contig_28362	1771
47	ost_siam_bh1_contig_31255	1803
48	ost_siam_bh1_contig_34621	1292
49	ost_siam_bh1_contig_40676	1105
50	ost_siam_bh1_contig_41385	242
51	ost_siam_bh1_contig_41617	2541
52	ost_siam_bh1_contig_43294	1002
53	ost_siam_bh1_contig_46025	793
54	ost_siam_bh1_contig_49498	453
55	ost_siam_bh1_contig_50705	430
56	ost_siam_bh1_contig_54434	369
57	ost_siam_bh1_contig_56224	505
58	ost_siam_bh1_contig_56665	1239
59	ost_siam_bh1_contig_60783	340
60	ost_siam_bh1_contig_61990	1095
61	ost_siam_bh1_contig_65058	1330
62	ost_siam_bh1_contig_65178	637
63	ost_siam_bh1_contig_65775	676
64	ost_siam_bh1_contig_67397	317
65	ost_siam_bh1_contig_68581	245
66	ost_siam_bh1_contig_69036	871
67	ost_siam_bh1_contig_70166	703
68	ost_siam_bh1_contig_70918	510
69	ost_siam_bh1_contig_71416	280
70	ost_siam_bh1_contig_71937	994
71	ost_siam_bh1_contig_74353	224
72	ost_siam_bh1_contig_74833	294
73	ost_siam_bh1_contig_75098	691
74	ost_siam_bh1_contig_75287	314
75	ost_siam_bh1_contig_75345	279
76	ost_siam_bh1_contig_75701	475

Ostreopsis **cf.** *siamensis* **BH1**

	77	ost_siam_bh1_contig_76408	590
	78	ost_siam_bh1_contig_76836	347
	79	ost_siam_bh1_contig_77065	389
	80	ost_siam_bh1_contig_77147	298
	81	ost_siam_bh1_contig_77932	682
	82	ost_siam_bh1_contig_80315	349
	83	ost_siam_bh1_contig_80498	321
	84	ost_siam_bh1_contig_80540	414
	85	ost_siam_bh1_contig_81045	214
	86	ost_siam_bh1_contig_82701	496
	87	ost_siam_bh1_contig_82790	203
	88	ost_siam_bh1_contig_84396	337
	89	ost_siam_bh1_contig_85898	261
	90	ost_siam_bh1_contig_87524	246
	91	ost_siam_bh1_contig_88163	234
	92	ost_sp8_her26_contig_4471	1725
	93	ost_sp8_her26_contig_18672	311
	94	ost_sp8_her26_contig_21619	2007
	95	ost_sp8_her26_contig_26036	1228
	96	ost_sp8_her26_contig_30392	918
	97	ost_sp8_her26_contig_41815	524
	98	ost_sp8_her26_contig_43551	1833
	99	ost_sp8_her26_contig_46194	1603
	100	ost_sp8_her26_contig_47154	818
	101	ost_sp8_her26_contig_48128	795
	102	ost_sp8_her26_contig_48384	1551
	103	ost_sp8_her26_contig_55524	593
Ostreopsis rhodesae **HER26**	104	ost_sp8_her26_contig_57448	1892
	105	ost_sp8_her26_contig_59405	519
	106	ost_sp8_her26_contig_60648	890
	107	ost_sp8_her26_contig_65725	355
	108	ost_sp8_her26_contig_65893	529
	109	ost_sp8_her26_contig_67109	303
	110	ost_sp8_her26_contig_70800	327
	111	ost_sp8_her26_contig_75870	693
	112	ost_sp8_her26_contig_76461	348
	113	ost_sp8_her26_contig_78178	438
	114	ost_sp8_her26_contig_84915	284
	115	ost_sp8_her26_contig_85320	1102
	116	ost_sp8_her26_contig_89026	320

S14C List of transcripts encoding full ketoacyl reductase domain identified in *Coolia malayensis* MAB, *Ostreopsis* cf. *ovata* HER27, *Ostreopsis* cf. *siamensis* BH1 and *Ostreopsis rhodesae* HER26.

Species	S. no.	Contig name	Length (bp)
	1	coolia_mab_contig_1244	2034
	2	coolia_mab_contig_3272	2102
	3	coolia_mab_contig_8802	1912
	4	coolia_mab_contig_10638	2109
	5	coolia_mab_contig_12696	3880
Coolia malayensis **MAB**	6	coolia_mab_contig_32461	1988
	7	ost_ovt_her27_contig_2304	2089
	8	ost_ovt_her27_contig_8673	3692
	9	ost_ovt_her27_contig_18868	1970
	10	ost_ovt_her27_contig_21745	713
	11	ost_ovt_her27_contig_63049	1193
	12	ost_ovt_her27_contig_64642	681
	13	ost_ovt_her27_contig_65897	490
Ostreopsis **cf.** *ovata* **HER27**	14	ost_ovt_her27_contig_72919	785
	15	ost_siam_bh1_contig_6512	3674
	16	ost_siam_bh1_contig_7569	1920
	17	ost_siam_bh1_contig_8116	2181
	18	ost_siam_bh1_contig_21563	1982
Ostreopsis **cf.** *siamensis* **BH1**	19	ost_siam_bh1_contig_28846	1518
	20	ost_sp8_her26_contig_7225	2102
	21	ost_sp8_her26_contig_20927	1986
	22	ost_sp8_her26_contig_28549	1981
	23	ost_sp8_her26_contig_35094	3691
	24	ost_sp8_her26_contig_41477	605
	25	ost_sp8_her26_contig_55850	716
Ostreopsis rhodesae **HER26**	26	ost_sp8_her26_contig_67665	1077

S14D List of transcripts encoding partial ketoacyl reductase domain identified in *Coolia malayensis* MAB, *Ostreopsis* cf. *ovata* HER27, *Ostreopsis* cf. *siamensis* BH1 and *Ostreopsis rhodesae* HER26.

Species	S. no.	Contig name	Length (bp)
	1	coolia_mab_contig_19150	258
	2	coolia_mab_contig_22126	2231
	3	coolia_mab_contig_43208	200
	4	coolia_mab_contig_52402	309
	5	coolia_mab_contig_52403	438
	6	coolia_mab_contig_52439	1420
	7	coolia_mab_contig_54618	562
	8	coolia_mab_contig_54869	623
Coolia malayensis MAB	9	coolia_mab_contig_56497	305
	10	coolia_mab_contig_57234	472
	11	coolia_mab_contig_57874	869
	12	coolia_mab_contig_58504	438
	13	coolia_mab_contig_60704	286
	14	coolia_mab_contig_61853	519
	15	coolia_mab_contig_62171	377
	16	coolia_mab_contig_62292	597
	17	coolia_mab_contig_66654	226
	18	ost_ovt_her27_contig_8665	333
	19	ost_ovt_her27_contig_11858	639
	20	ost_ovt_her27_contig_22680	1321
	21	ost_ovt_her27_contig_40631	1064
	22	ost_ovt_her27_contig_49871	556
	23	ost_ovt_her27_contig_54223	607
	24	ost_ovt_her27_contig_54265	809
	25	ost_ovt_her27_contig_58182	237
	26	ost_ovt_her27_contig_58202	250
Ostreopsis cf. *ovata* HER27	27	ost_ovt_her27_contig_58203	545
	28	ost_ovt_her27_contig_60404	212
	29	ost_ovt_her27_contig_62432	656
	30	ost_ovt_her27_contig_67167	297
	31	ost_ovt_her27_contig_67168	298
	32	ost_ovt_her27_contig_69011	909
	33	ost_ovt_her27_contig_71275	575
	34	ost_ovt_her27_contig_73326	504
	35	ost_ovt_her27_contig_73383	413
	36	ost_ovt_her27_contig_74056	404

37	ost_ovt_her27_contig_76382	830
38	ost_ovt_her27_contig_80789	305
39	ost_siam_bh1_contig_5282	1905
40	ost_siam_bh1_contig_9472	2068
41	ost_siam_bh1_contig_9473	1131
42	ost_siam_bh1_contig_12771	1873
43	ost_siam_bh1_contig_14757	2344
44	ost_siam_bh1_contig_15351	1815
45	ost_siam_bh1_contig_20664	315
46	ost_siam_bh1_contig_28362	1771
47	ost_siam_bh1_contig_31255	1803
48	ost_siam_bh1_contig_34621	1292
49	ost_siam_bh1_contig_40676	1105
50	ost_siam_bh1_contig_41385	242
51	ost_siam_bh1_contig_41617	2541
52	ost_siam_bh1_contig_43294	1002
53	ost_siam_bh1_contig_46025	793
54	ost_siam_bh1_contig_49498	453
55	ost_siam_bh1_contig_50705	430
56	ost_siam_bh1_contig_54434	369
Ostreopsis **cf.** *siamensis* **BH1**	57	ost_siam_bh1_contig_56224	505
	58	ost_siam_bh1_contig_56665	1239
	59	ost_siam_bh1_contig_60783	340
	60	ost_siam_bh1_contig_61990	1095
	61	ost_siam_bh1_contig_65058	1330
	62	ost_siam_bh1_contig_65178	637
	63	ost_siam_bh1_contig_65775	676
	64	ost_siam_bh1_contig_67397	317
	65	ost_siam_bh1_contig_68581	245
	66	ost_siam_bh1_contig_69036	871
	67	ost_siam_bh1_contig_70166	703
	68	ost_siam_bh1_contig_70918	510
	69	ost_siam_bh1_contig_71416	280
	70	ost_siam_bh1_contig_71937	994
	71	ost_siam_bh1_contig_74353	224
	72	ost_siam_bh1_contig_74833	294
	73	ost_siam_bh1_contig_75098	691
	74	ost_siam_bh1_contig_75287	314
	75	ost_siam_bh1_contig_75345	279
	76	ost_siam_bh1_contig_75701	475

	77	ost_siam_bh1_contig_76408	590
	78	ost_siam_bh1_contig_76836	347
	79	ost_siam_bh1_contig_77065	389
	80	ost_siam_bh1_contig_77147	298
	81	ost_siam_bh1_contig_77932	682
	82	ost_siam_bh1_contig_80315	349
	83	ost_siam_bh1_contig_80498	321
	84	ost_siam_bh1_contig_80540	414
	85	ost_siam_bh1_contig_81045	214
	86	ost_siam_bh1_contig_82701	496
	87	ost_siam_bh1_contig_82790	203
	88	ost_siam_bh1_contig_84396	337
	89	ost_siam_bh1_contig_85898	261
	90	ost_siam_bh1_contig_87524	246
	91	ost_siam_bh1_contig_88163	234
	92	ost_sp8_her26_contig_4471	1725
	93	ost_sp8_her26_contig_18672	311
	94	ost_sp8_her26_contig_21619	2007
	95	ost_sp8_her26_contig_26036	1228
	96	ost_sp8_her26_contig_30392	918
	97	ost_sp8_her26_contig_41815	524
	98	ost_sp8_her26_contig_43551	1833
	99	ost_sp8_her26_contig_46194	1693
	100	ost_sp8_her26_contig_47154	818
	101	ost_sp8_her26_contig_48128	795
	102	ost_sp8_her26_contig_48384	1551
	103	ost_sp8_her26_contig_55524	593
Ostreopsis rhodesae **HER26**	104	ost_sp8_her26_contig_57448	1892
	105	ost_sp8_her26_contig_59405	519
	106	ost_sp8_her26_contig_60648	890
	107	ost_sp8_her26_contig_65725	355
	108	ost_sp8_her26_contig_65893	529
	109	ost_sp8_her26_contig_67109	303
	110	ost_sp8_her26_contig_70800	327
	111	ost_sp8_her26_contig_75870	693
	112	ost_sp8_her26_contig_76461	348
	113	ost_sp8_her26_contig_78178	438
	114	ost_sp8_her26_contig_84915	284
	115	ost_sp8_her26_contig_85320	1102
	116	ost_sp8_her26_contig_89026	320

S15 List of multi-domain PKSs found in *Coolia malayensis* MAB, *Ostreopsis* cf. *ovata* HER27, *Ostreopsis* cf. *siamensis* BH1 and *Ostreopsis rhodesae* HER26

Organism	Contig name	Encoding sequence	Length	GC content (%)
***Coolia malayensis* MAB**	8406	KS-DH-KR-ACP-KS(p)	5705	59.3
	4512	ACP-KS-DH-KR-ACP-KS-KR-ACP-AT-DH-ER-ACP-TE	5182	59.1
	19331	DH-KR-ACP-KS-KR-ACP-AT-KS-DH-KR(p)-ER-KR-ACP-TE	4223	61.4
	37898	DH-KS-AT-KR	2667	61.4
	5624	KR(p)-ACP-KS-KR-ACP-TE-AT(p)	2443	61.6
	15214	ER(p)-KR-ACP-AT-KS-KR	2398	59.8
	35731	KS-AT-DH-KR	2350	65.7
	35361	MT(p)-KR	1975	62
	16242	MT(p)-KR	1948	59.6
	40291	ACP-AT-KS-DH	1238	63
	12048	KS-KR(p)	961	62
	51310	MT-KR(p)	942	61.4
	50259	KR(p)-ACP-ACP-KS	914	62.7
	50602	KR(p)-ACP-KS	886	60.6
	15328	KS-ACP	761	57.6
	16700	MT-KR	640	57.5
	54868	KS(p)-DH(p)	560	60.3
	54132	KS-DH(p)	420	60.9
	59879	ACP-KS(p)	243	60.8
	65773	ACP-KS(p)	196	63.5
***Ostreopsis* cf. *ovata* HER27**	20389	ACP-KS-DH-KR-ACP-KS(p)	2487	67.8
	6640	MT(p)-KR	1966	61.5
	31078	MT-KR	1911	66.6
	22085	MT-KR	1831	65.3
	40326	DH-ER-KR-ACP-TE	1469	65.6
	35650	ER-KR-ACP-TE	996	68.5
	35443	KS(p)-AT-DH-KR(p)	993	69.4
	8666	KS(p)-KR-ACP-KS(p)	980	70.5
	57828	ACP-KS-KR(p)	894	62.8
	36934	KS-ACP	757	64.1
	34366	KR-DH(p)	685	71.5
	9710	MT-KR	683	67.7
	36565	KS-DH(p)	666	66.7
	61462	ER-KR(p)	426	66.4
	61132	KR(p)-ACP-KS(p)	415	67.3
	64675	KR(p)-ACP	259	70.6
	46260	KS(p)-DH(p)	253	67.1
	54266	ACP-KS(p)	242	63.4

	58181	KS(p)-DH(p)	237	66.2
	74456	ACP-AT(p)	235	62.9
	65142	ER(p)-KR(p)	194	65.5
	81124	ACP-KS(p)	173	61.9
	79967	ACP-KS(p)	135	65.8
Ostreopsis cf. *siamensis* **BH1**	21404	MT(p)-KR	1963	61.3
	5989	MT(p)-KR	1012	65.7
	45353	MT(p)-KR	1004	66.5
	35697	ER(p)-KR-ACP-TE	898	68.6
	12688	KS-ACP	752	63.7
	63151	ACP-KS	637	67.7
	22082	MT-KR	635	67.5
	55722	KR(p)-ACP	472	66.1
	79614	ACP-KS(p)	228	69.8
	84315	ACP-KS(p)	109	67.8
Ostreopsis rhodesae **HER26**	7384	AT-KS-DH-ER-KR-ACP-TE	2649	69.4
	36504	AT-KS-DH-KR-ACP-TE	2224	53.9
	15997	AT-KS-KR	2095	58.9
	14885	AT-KS-DH-ER-KR-ACP-TE	2092	65.9
	9734	MT(p)-KR	1956	61.5
	9459	KS(p)-KR-ACP-KS-DH-ER(p)	1836	67.8
	11189	MT(p)-KR	1830	65.3
	34777	KR-ACP-KS-KR-ACP-KS(p)	1752	65.5
	26035	KS-DH-KR-ACP-KS(p)	1658	68.5
	11794	MT(p)-KR	1642	68.8
	33435	ACP-AT-KS	1627	63.3
	14440	KS-DH-KR(p)	1302	68.1
	41958	AT-KS-KR(p)	1264	67.5
	34778	ACP-ACP-KS-DH-KR(p)	1044	66.1
	47213	DH-ER-KR	1035	67.8
	50159	KR-ACP-KS	922	68.4
	14666	ER(p)-KR-ACP-KS(p)	796	68.9
	12913	KS-ACP	764	64.5
	53011	KS-KR(p)	755	63.5
	15922	KR-DH(p)	626	72.8
	72826	ACP-KS(p)	614	63.1
	41031	ER-KR	527	68.1
	72061	KR(p)-ACP	267	69.8
	67029	ACP-AT(p)	230	69.8
	76621	ACP-AT(p)	225	67.5
	74120	ACP-KS(p)	189	72

S16 Top BLAST hits of polyketide synthase genes found in *Coolia malayensis* MAB, *Ostreopsis* cf. *ovata* HER27, *Ostreopsis* cf. *siamensis* BH1 and *Ostreopsis rhodesae* HER26 transcriptomes (492 contigs out of 557)

S. no.	Sequence name	Seq. description	Seq. length	Hit description	Hit ACC	E-Val.
1	coolia_mab_contig_10430	polyketide partial	4415	gi|941355192|dbj|BAT21730.1|polyketide synthase, partial [Karenia mikimotoi]	BAT21730	2.97E-102
2	coolia_mab_contig_10638	6-methylsalicylic acid synthase	2109	gi|1129199127|gb|OLQ02654.1|6-methylsalicylic acid synthase [Symbiodinium microadriaticum]	OLQ02654	1.98E-143
3	coolia_mab_contig_10790	type i polyketide synthase-like protein kb1008	3062	gi|148536473|gb|ABQ85796.1|type I polyketide synthase-like protein KB1008 [Karenia brevis]	ABQ85796	4.67E-126
4	coolia_mab_contig_10907	type i polyketide synthase	2686	gi|414091051|gb|AFW98413.1|type I polyketide synthase [Alexandrium ostenfeldii]	AFW98413	0
5	coolia_mab_contig_10970	polyketide partial	3084	gi|148536473|gb|ABQ85796.1|type I polyketide synthase-like protein KB1008 [Karenia brevis]	ABQ85796	0
6	coolia_mab_contig_12048	type i fatty acid partial	2886	gi|818211084|gb|AKG25414.1|putative polyketide synthase [Hematodinium sp. SG-2015]	AKG25414	1.46E-85
7	coolia_mab_contig_12141	polyketide synthase	8362	gi|1059529246|emb|SCL25381.1|Acyl transferase domain-containing protein [Micromonospora nigra]	SCL25381	0
8	coolia_mab_contig_12145	phthiocerol synthesis polyketide synthase type i	3939	gi|1129192690|gb|OLP97452.1|Phthiocerol synthesis polyketide synthase type I PpsC [Symbiodinium microadriaticum]	OLP97452	0
9	coolia_mab_contig_1244	6-methylsalicylic acid synthase	2034	gi|1129199127|gb|OLQ02654.1|6-methylsalicylic acid synthase [Symbiodinium microadriaticum]	OLQ02654	2.09E-145
10	coolia_mab_contig_12696	calcium-dependent protein kinase 2	3880	gi|1129164416|gb|OLP76751.1|Calcium-dependent protein kinase 2 [Symbiodinium microadriaticum]	OLP76751	4.17E-170
11	coolia_mab_contig_12704	phthiocerol synthesis polyketide synthase type i	4000	gi|1129192690|gb|OLP97452.1|Phthiocerol synthesis polyketide synthase type I PpsC [Symbiodinium microadriaticum]	OLP97452	0
12	coolia_mab_contig_12721	type i polyketide synthase-like protein kb6736	3853	gi|148536485|gb|ABQ85802.1|type I polyketide synthase-like protein KB6736 [Karenia brevis]	ABQ85802	0
13	coolia_mab_contig_13995	type i polyketide synthase	2981	gi|414091049|gb|AFW98412.1|type I polyketide synthase [Alexandrium ostenfeldii]	AFW98412	0
14	coolia_mab_contig_14951	type i polyketide synthase-like protein kb1008	2970	gi|148536473|gb|ABQ85796.1|type I polyketide synthase-like protein KB1008 [Karenia brevis]	ABQ85796	1.18E-126
15	coolia_mab_contig_15214	short-chain dehydrogenase reductase related	7195	gi|1129204261|gb|OLQ06785.1|Oleandomycin polyketide synthase, modules 5 and 6 [Symbiodinium microadriaticum]	OLQ06785	0
16	coolia_mab_contig_15328	polyketide synthase	2285	gi|585112304|gb|EWM29724.1|polyketide synthase [Nannochloropsis gaditana]	EWM29724	9.70E-63

17	coolia_mab_contig_1540	type i polyketide synthase	3033	gi|414091049|gb|AFW98412.1|type I polyketide synthase [Alexandrium ostenfeldii]	AFW98412	0
18	coolia_mab_contig_16242	6-phosphofructokinase 7	5845	gi|1129173556|gb|OLP82883.1|6-phosphofructokinase 7 [Symbiodinium microadriaticum]	OLP82883	4.28E-49
19	coolia_mab_contig_16700	lovastatin nonaketide synthase	1920	gi|1129179982|gb|OLP87649.1|Lovastatin nonaketide synthase [Symbiodinium microadriaticum]	OLP87649	3.37E-87
20	coolia_mab_contig_16713	type i polyketide synthase-like protein kb1008	3802	gi|148536473|gb|ABQ85796.1|type I polyketide synthase-like protein KB1008 [Karenia brevis]	ABQ85796	6.55E-145
21	coolia_mab_contig_17768	type i polyketide synthase	3057	gi|414091049|gb|AFW98412.1|type I polyketide synthase [Alexandrium ostenfeldii]	AFW98412	0
22	coolia_mab_contig_18497	phthiocerol synthesis polyketide synthase type i	4003	gi|1129192690|gb|OLP97452.1|Phthiocerol synthesis polyketide synthase type I PpsC [Symbiodinium microadriaticum]	OLP97452	2.30E-121
23	coolia_mab_contig_19150	hybrid non-ribosomal peptide synthetase type i polyketide synthase	258	gi|917105572|ref|WP_051712284.1|hybrid non-ribosomal peptide synthetase/type I polyketide synthase [Spirillospora albida]	WP_051712284	2.18E-11
24	coolia_mab_contig_19232	phthiocerol synthesis polyketide synthase type i	4269	gi|1129206593|gb|OLQ08682.1|Phthiocerol synthesis polyketide synthase type I PpsD [Symbiodinium microadriaticum]	OLQ08682	3.14E-142
25	coolia_mab_contig_1930	phthiocerol synthesis polyketide synthase type i	4011	gi|1129192690|gb|OLP97452.1|Phthiocerol synthesis polyketide synthase type I PpsC [Symbiodinium microadriaticum]	OLP97452	0
26	coolia_mab_contig_19331	erythronolide modules 5 and 6	12670	gi|1129204260|gb|OLQ06784.1|Erythronolide synthase, modules 5 and 6 [Symbiodinium microadriaticum]	OLQ06784	0
27	coolia_mab_contig_19391	polyketide synthase as3d906	2977	gi|712037596|gb|AIW63289.1|polyketide synthase AS3D906 [Azadinium spinosum]	AIW63289	0
28	coolia_mab_contig_20348	phthiocerol synthesis polyketide synthase type i	4492	gi|1129179243|gb|OLP87030.1|Phthiocerol synthesis polyketide synthase type I PpsC [Symbiodinium microadriaticum]	OLP87030	2.73E-57
29	coolia_mab_contig_21011	phthiocerol synthesis polyketide synthase type i	3874	gi|1129192690|gb|OLP97452.1|Phthiocerol synthesis polyketide synthase type I PpsC [Symbiodinium microadriaticum]	OLP97452	0
30	coolia_mab_contig_21780	phthiocerol synthesis polyketide synthase type i	3793	gi|1129192690|gb|OLP97452.1|Phthiocerol synthesis polyketide synthase type I PpsC [Symbiodinium microadriaticum]	OLP97452	0
31	coolia_mab_contig_22126	type i polyketide synthase-like protein kb1008	2231	gi|148536473|gb|ABQ85796.1|type I polyketide synthase-like protein KB1008 [Karenia brevis]	ABQ85796	4.45E-88

32	coolia_mab_contig_2223	polyketide synthase	8223	gi|1129213410|gb|OLQ14315.1|Polyketide synthase PksN [Symbiodinium microadriaticum]	OLQ14315	0
33	coolia_mab_contig_22683	acyl transferase domain-containing protein	3531	gi|1095343304|emb|SEU29060.1|Acyl transferase domain-containing protein [Stigmatella erecta]	SEU29060	1.59E-75
34	coolia_mab_contig_24272	sodium calcium exchanger 3	4376	gi|1129171706|gb|OLP81580.1|Sodium/calcium exchanger 3 [Symbiodinium microadriaticum]	OLP81580	2.91E-168
35	coolia_mab_contig_24391	phthiocerol synthesis polyketide synthase type i	4147	gi|1129179243|gb|OLP87030.1|Phthiocerol synthesis polyketide synthase type I PpsC [Symbiodinium microadriaticum]	OLP87030	2.41E-53
36	coolia_mab_contig_24551	type i polyketide synthase-like protein kb1008	3436	gi|148536473|gb|ABQ85796.1|type I polyketide synthase-like protein KB1008 [Karenia brevis]	ABQ85796	1.51E-177
37	coolia_mab_contig_2508	type i polyketide synthase-like protein kb1008	3860	gi|148536473|gb|ABQ85796.1|type I polyketide synthase-like protein KB1008 [Karenia brevis]	ABQ85796	0
38	coolia_mab_contig_25363	phthiocerol synthesis polyketide synthase type i	4705	gi|1129192690|gb|OLP97452.1|Phthiocerol synthesis polyketide synthase type I PpsC [Symbiodinium microadriaticum]	OLP97452	0
39	coolia_mab_contig_2630	phthiocerol synthesis polyketide synthase type i	3972	gi|1129192690|gb|OLP97452.1|Phthiocerol synthesis polyketide synthase type I PpsC [Symbiodinium microadriaticum]	OLP97452	0
40	coolia_mab_contig_2832	polyketide partial	3476	gi|941355192|dbj|BAT21730.1|polyketide synthase, partial [Karenia mikimotoi]	BAT21730	1.39E-142
41	coolia_mab_contig_2882	type i polyketide synthase-like protein kb6736	3946	gi|148536485|gb|ABQ85802.1|type I polyketide synthase-like protein KB6736 [Karenia brevis]	ABQ85802	8.36E-179
42	coolia_mab_contig_2956	phthiocerol synthesis polyketide synthase type i	3865	gi|1129192690|gb|OLP97452.1|Phthiocerol synthesis polyketide synthase type I PpsC [Symbiodinium microadriaticum]	OLP97452	0
43	coolia_mab_contig_2976	type i polyketide synthase-like protein kb1008	3670	gi|148536473|gb|ABQ85796.1|type I polyketide synthase-like protein KB1008 [Karenia brevis]	ABQ85796	7.17E-167
44	coolia_mab_contig_30043	phthiocerol synthesis polyketide synthase type i	3820	gi|1129192690|gb|OLP97452.1|Phthiocerol synthesis polyketide synthase type I PpsC [Symbiodinium microadriaticum]	OLP97452	0
45	coolia_mab_contig_30720	phthiocerol synthesis polyketide synthase type i	2501	gi|1129186276|gb|OLP92465.1|Phthiocerol synthesis polyketide synthase type I PpsC [Symbiodinium microadriaticum]	OLP92465	0
46	coolia_mab_contig_31491	phthiocerol synthesis polyketide synthase type i	4128	gi|1129192690|gb|OLP97452.1|Phthiocerol synthesis polyketide synthase type I PpsC [Symbiodinium microadriaticum]	OLP97452	0

47	coolia_mab_contig_31948	6-phosphofructokinase 7	5826	gi|1129173556|gb|OLP82883.1|6-phosphofructokinase 7 [Symbiodinium microadriaticum]	OLP82883	2.27E-106
48	coolia_mab_contig_32461	6-methylsalicylic acid synthase	1988	gi|1129199127|gb|OLQ02654.1|6-methylsalicylic acid synthase [Symbiodinium microadriaticum]	OLQ02654	7.54E-126
49	coolia_mab_contig_3272	6-methylsalicylic acid synthase	2102	gi|1129199127|gb|OLQ02654.1|6-methylsalicylic acid synthase [Symbiodinium microadriaticum]	OLQ02654	0
50	coolia_mab_contig_3397	type i polyketide synthase-like protein kb1008	3630	gi|148536473|gb|ABQ85796.1|type I polyketide synthase-like protein KB1008 [Karenia brevis]	ABQ85796	2.97E-157
51	coolia_mab_contig_34285	phthiocerol synthesis polyketide synthase type i	4210	gi|1129192690|gb|OLP97452.1|Phthiocerol synthesis polyketide synthase type I PpsC [Symbiodinium microadriaticum]	OLP97452	0
52	coolia_mab_contig_35361	6-phosphofructokinase 7	5927	gi|1129173556|gb|OLP82883.1|6-phosphofructokinase 7 [Symbiodinium microadriaticum]	OLP82883	1.25E-45
53	coolia_mab_contig_35552	type i polyketide synthase-like protein kb6736	3818	gi|148536485|gb|ABQ85802.1|type I polyketide synthase-like protein KB6736 [Karenia brevis]	ABQ85802	0
54	coolia_mab_contig_35731	mycocerosic acid synthase-like	7050	gi|1110958791|ref|XP_003439205.2|PREDICTED: uncharacterized protein LOC100711629 [Oreochromis niloticus] >gi|1110958793|ref|XP_019218572.1| PREDICTED: uncharacterized protein LOC100711629 [Oreochromis niloticus]	XP_003439205	7.21E-69
55	coolia_mab_contig_35760	type i polyketide synthase	3080	gi|414091049|gb|AFW98412.1|type I polyketide synthase [Alexandrium ostenfeldii]	AFW98412	0
56	coolia_mab_contig_35826	type i polyketide synthase-like protein kb1008	4084	gi|148536473|gb|ABQ85796.1|type I polyketide synthase-like protein KB1008 [Karenia brevis]	ABQ85796	8.16E-108
57	coolia_mab_contig_35884	oleandomycin polyketide modules 5 and 6	530	gi|1129204261|gb|OLQ06785.1|Oleandomycin polyketide synthase, modules 5 and 6 [Symbiodinium microadriaticum]	OLQ06785	7.89E-14
58	coolia_mab_contig_37614	phthiocerol synthesis polyketide synthase type i	4207	gi|1129192690|gb|OLP97452.1|Phthiocerol synthesis polyketide synthase type I PpsC [Symbiodinium microadriaticum]	OLP97452	4.73E-130
59	coolia_mab_contig_37898	short-chain partial	8004	gi|873227372|emb|CEM18661.1|unnamed protein product, partial [Vitrella brassicaformis CCMP3155]	CEM18661	1.24E-62
60	coolia_mab_contig_38539	phthiocerol synthesis polyketide synthase type i	3734	gi|1129192690|gb|OLP97452.1|Phthiocerol synthesis polyketide synthase type I PpsC [Symbiodinium microadriaticum]	OLP97452	1.87E-163

61	coolia_mab_contig_3918	type i polyketide synthase-like protein kb1008	3575	gi|148536473|gb|ABQ85796.1|type I polyketide synthase-like protein KB1008 [Karenia brevis]	ABQ85796	0
62	coolia_mab_contig_40018	phthiocerol synthesis polyketide synthase type i	3760	gi|1129192690|gb|OLP97452.1|Phthiocerol synthesis polyketide synthase type I PpsC [Symbiodinium microadriaticum]	OLP97452	0
63	coolia_mab_contig_40291	type i fatty acid partial	3716	gi|675129852|ref|XP_008886813.1|type I fatty acid synthase, putative [Hammondia hammondi] >gi|661334462|gb|KEP62607.1| type I fatty acid synthase, putative [Hammondia hammondi]	XP_008886813	3.74E-154
64	coolia_mab_contig_4218	phthiocerol synthesis polyketide synthase type i	3787	gi|1129192690|gb|OLP97452.1|Phthiocerol synthesis polyketide synthase type I PpsC [Symbiodinium microadriaticum]	OLP97452	4.61E-153
65	coolia_mab_contig_4296	phthiocerol synthesis polyketide synthase type i	3543	gi|1129192690|gb|OLP97452.1|Phthiocerol synthesis polyketide synthase type I PpsC [Symbiodinium microadriaticum]	OLP97452	0
66	coolia_mab_contig_43031	polyketide partial	3675	gi|148536473|gb|ABQ85796.1|type I polyketide synthase-like protein KB1008 [Karenia brevis]	ABQ85796	1.54E-127
67	coolia_mab_contig_43208	polyketide synthase	200	gi|61198403|gb|AAX39746.1|type I polyketide synthase-like protein AS1-1L, partial [Karenia brevis]	AAX39746	4.34E-17
68	coolia_mab_contig_43946	hypothetical protein	2923	gi|1094115322|ref|WP_071104821.1|hypothetical protein [Moorea producens] >gi|1092223157|gb|AOY81499.1| hypothetical protein BJP36_17855 [Moorea producens JHB]	WP_071104821	4.14E-118
69	coolia_mab_contig_4512	erythronolide modules 5 and 6	15546	gi|1129176947|gb|OLP85322.1|Erythronolide synthase, modules 5 and 6 [Symbiodinium microadriaticum]	OLP85322	0
70	coolia_mab_contig_45156	type i polyketide synthase-like protein kb1008	3643	gi|148536473|gb|ABQ85796.1|type I polyketide synthase-like protein KB1008 [Karenia brevis]	ABQ85796	4.80E-129
71	coolia_mab_contig_4580	phthiocerol synthesis polyketide synthase type i	4029	gi|1129192690|gb|OLP97452.1|Phthiocerol synthesis polyketide synthase type I PpsC [Symbiodinium microadriaticum]	OLP97452	0
72	coolia_mab_contig_50259	erythronolide modules 5 and 6	2744	gi|1129204260|gb|OLQ06784.1|Erythronolide synthase, modules 5 and 6 [Symbiodinium microadriaticum]	OLQ06784	0
73	coolia_mab_contig_50602	type i polyketide synthase	2659	gi|836726653|ref|WP_047858716.1|type I polyketide synthase [Archangium gephyra] >gi|827425189|gb|AKJ05085.1| Malonyl CoA-acyl carrier protein transacylase [Archangium gephyra]	WP_047858716	8.56E-109
74	coolia_mab_contig_51310	6-phosphofructokinase	2829	gi|1129173556|gb|OLP82883.1|6-phosphofructokinase 7 [Symbiodinium	OLP82883	1.77E-35

		7		microadriaticum]		
75	coolia_mab_contig_52402	beta-ketoacyl partial	309	gi|209877909|ref|XP_002140396.1|polyketide synthase [Cryptosporidium muris RN66] >gi|209556002|gb|EEA06047.1| polyketide synthase, putative [Cryptosporidium muris RN66]	XP_002140396	2.59E-22
76	coolia_mab_contig_52403	type i polyketide synthase	438	gi|575541661|gb|ETX42096.1|hypothetical protein P805_02877, partial [Serratia marcescens BIDMC 44]	ETX42096	1.55E-19
77	coolia_mab_contig_52439	phthiocerol synthesis polyketide synthase type i	1420	gi|1129198474|gb|OLQ02136.1|Phthiocerol synthesis polyketide synthase type I PpsD [Symbiodinium microadriaticum]	OLQ02136	4.06E-103
78	coolia_mab_contig_5333	type i polyketide synthase-like protein kb6736	4109	gi|148536485|gb|ABQ85802.1|type I polyketide synthase-like protein KB6736 [Karenia brevis]	ABQ85802	6.02E-180
79	coolia_mab_contig_5355	polyketide partial	3379	gi|148536473|gb|ABQ85796.1|type I polyketide synthase-like protein KB1008 [Karenia brevis]	ABQ85796	5.47E-152
80	coolia_mab_contig_54132	erythronolide modules 5 and 6	1261	gi|1129204261|gb|OLQ06785.1|Oleandomycin polyketide synthase, modules 5 and 6 [Symbiodinium microadriaticum]	OLQ06785	0
81	coolia_mab_contig_54618	oleandomycin polyketide modules 5 and 6	562	gi|1129204261|gb|OLQ06785.1|Oleandomycin polyketide synthase, modules 5 and 6 [Symbiodinium microadriaticum]	OLQ06785	7.38E-45
82	coolia_mab_contig_54868	erythronolide modules 5 and 6	1684	gi|1129176947|gb|OLP85322.1|Erythronolide synthase, modules 5 and 6 [Symbiodinium microadriaticum]	OLP85322	1.30E-34
83	coolia_mab_contig_54869	polyketide synthase	623	gi|504958240|ref|WP_015145342.1|polyketide synthase [Pleurocapsa minor] >gi|427981444|gb|AFY79044.1| polyketide synthase family protein [Pleurocapsa sp. PCC 7327]	WP_015145342	3.65E-38
84	coolia_mab_contig_55302	oleandomycin polyketide modules 5 and 6	691	gi|1129204261|gb|OLQ06785.1|Oleandomycin polyketide synthase, modules 5 and 6 [Symbiodinium microadriaticum]	OLQ06785	2.09E-45
85	coolia_mab_contig_5624	polyketide partial	7331	gi|818211090|gb|AKG25417.1|putative polyketide synthase, partial [Hematodinium sp. SG-2015]	AKG25417	1.81E-104
86	coolia_mab_contig_56497	phthiocerol synthesis polyketide synthase type i	305	gi|1129198474|gb|OLQ02136.1|Phthiocerol synthesis polyketide synthase type I PpsD [Symbiodinium microadriaticum]	OLQ02136	5.24E-46
87	coolia_mab_contig_57234	type i fatty acid	472	gi|672294693|gb|KFG59574.1|putative type I fatty acid synthase, partial [Toxoplasma gondii RUB]	KFG59574	3.14E-14
88	coolia_mab_contig_58504	oleandomycin polyketide modules 5 and 6	438	gi|1129204261|gb|OLQ06785.1|Oleandomycin polyketide synthase, modules 5 and 6 [Symbiodinium microadriaticum]	OLQ06785	7.44E-48

89	coolia_mab_contig_594	phthiocerol synthesis polyketide synthase type i	5071	gi|1129192690|gb|OLP97452.1|Phthiocerol synthesis polyketide synthase type I PpsC [Symbiodinium microadriaticum]	OLP97452	6.91E-159
90	coolia_mab_contig_59879	soraphen polyketide synthase related	730	gi|820690505|tpe|CEL66250.1|TPA: Soraphen polyketide synthase A, related [Neospora caninum Liverpool]	CEL66250	2.88E-27
91	coolia_mab_contig_6003	phthiocerol synthesis polyketide synthase type i	4011	gi|1129192690|gb|OLP97452.1|Phthiocerol synthesis polyketide synthase type I PpsC [Symbiodinium microadriaticum]	OLP97452	0
92	coolia_mab_contig_60704	phthiocerol synthesis polyketide synthase type i	286	gi|1129198474|gb|OLQ02136.1|Phthiocerol synthesis polyketide synthase type I PpsD [Symbiodinium microadriaticum]	OLQ02136	3.07E-51
93	coolia_mab_contig_6076	erythronolide modules 3 and 4	3693	gi|1129199229|gb|OLQ02729.1|Erythronolide synthase, modules 3 and 4 [Symbiodinium microadriaticum]	OLQ02729	3.79E-138
94	coolia_mab_contig_61853	oleandomycin polyketide modules 5 and 6	519	gi|1129204261|gb|OLQ06785.1|Oleandomycin polyketide synthase, modules 5 and 6 [Symbiodinium microadriaticum]	OLQ06785	2.23E-76
95	coolia_mab_contig_62171	oleandomycin polyketide modules 5 and 6	377	gi|1129204261|gb|OLQ06785.1|Oleandomycin polyketide synthase, modules 5 and 6 [Symbiodinium microadriaticum]	OLQ06785	1.19E-42
96	coolia_mab_contig_62292	beta-ketoacyl synthase	597	gi|1121289167|ref|WP_073601769.1|beta-ketoacyl synthase [Hydrococcus rivularis] >gi|1115253188|gb|OKH17705.1| beta-ketoacyl synthase [Hydrococcus rivularis NIES-593]	WP_073601769	3.11E-24
97	coolia_mab_contig_64114	oleandomycin polyketide modules 5 and 6	321	gi|1129204261|gb|OLQ06785.1|Oleandomycin polyketide synthase, modules 5 and 6 [Symbiodinium microadriaticum]	OLQ06785	1.03E-23
98	coolia_mab_contig_64416	erythronolide modules 5 and 6	279	gi|1129204261|gb|OLQ06785.1|Oleandomycin polyketide synthase, modules 5 and 6 [Symbiodinium microadriaticum]	OLQ06785	1.92E-30
99	coolia_mab_contig_65471	oleandomycin polyketide modules 5 and 6	240	gi|1129204261|gb|OLQ06785.1|Oleandomycin polyketide synthase, modules 5 and 6 [Symbiodinium microadriaticum]	OLQ06785	1.04E-25
100	coolia_mab_contig_65773	oleandomycin polyketide modules 5 and 6	591	gi|1129204261|gb|OLQ06785.1|Oleandomycin polyketide synthase, modules 5 and 6 [Symbiodinium microadriaticum]	OLQ06785	4.92E-66
101	coolia_mab_contig_65875	unnamed protein product	222	gi|873238038|emb|CEL96742.1|unnamed protein product [Vitrella brassicaformis CCMP3155]	CEL96742	9.34E-15
102	coolia_mab_contig_66192	erythronolide modules 5 and 6	352	gi|1129204261|gb|OLQ06785.1|Oleandomycin polyketide synthase, modules 5 and 6 [Symbiodinium microadriaticum]	OLQ06785	1.20E-31

103	coolia_mab_contig_66654	oleandomycin polyketide modules 5 and 6	226	gi|1129204261|gb|OLQ06785.1|Oleandomycin polyketide synthase, modules 5 and 6 [Symbiodinium microadriaticum]	OLQ06785	7.57E-33
104	coolia_mab_contig_66931	type i polyketide synthase	310	gi|515877981|ref|WP_017308564.1|type I polyketide synthase [Fischerella sp. PCC 9339]	WP_017308564	6.34E-19
105	coolia_mab_contig_7073	phthiocerol synthesis polyketide synthase type i	4246	gi|1129192690|gb|OLP97452.1|Phthiocerol synthesis polyketide synthase type I PpsC [Symbiodinium microadriaticum]	OLP97452	0
106	coolia_mab_contig_7604	phthiocerol synthesis polyketide synthase type i	3736	gi|1129198474|gb|OLQ02136.1|Phthiocerol synthesis polyketide synthase type I PpsD [Symbiodinium microadriaticum]	OLQ02136	0
107	coolia_mab_contig_7826	polyketide synthase as3d906	3071	gi|712037596|gb|AIW63289.1|polyketide synthase AS3D906 [Azadinium spinosum]	AIW63289	0
108	coolia_mab_contig_8802	6-methylsalicylic acid synthase	1912	gi|1129199127|gb|OLQ02654.1|6-methylsalicylic acid synthase [Symbiodinium microadriaticum]	OLQ02654	8.84E-122
109	coolia_mab_contig_889	type i polyketide synthase	3055	gi|414091049|gb|AFW98412.1|type I polyketide synthase [Alexandrium ostenfeldii]	AFW98412	0
110	coolia_mab_contig_898	phthiocerol synthesis polyketide synthase type i	3958	gi|1129192690|gb|OLP97452.1|Phthiocerol synthesis polyketide synthase type I PpsC [Symbiodinium microadriaticum]	OLP97452	1.01E-155
111	coolia_mab_contig_9002	type i polyketide synthase-like protein kb1008	3702	gi|148536473|gb|ABQ85796.1|type I polyketide synthase-like protein KB1008 [Karenia brevis]	ABQ85796	4.35E-168
112	coolia_mab_contig_9305	polyketide synthase 1	4125	gi|595389390|gb|AHM27264.1|polyketide synthase 1 [Gambierdiscus polynesiensis] >gi|595389401|gb|AHM27265.1| polyketide synthase 2 [Gambierdiscus polynesiensis]	AHM27264	0
113	coolia_mab_contig_9515	type i polyketide synthase	2888	gi|414091047|gb|AFW98411.1|type I polyketide synthase [Alexandrium ostenfeldii]	AFW98411	0
114	coolia_mab_contig_9807	type i polyketide synthase-like protein kb6736	4167	gi|148536485|gb|ABQ85802.1|type I polyketide synthase-like protein KB6736 [Karenia brevis]	ABQ85802	1.48E-158
115	coolia_mab_contig_9908	type i polyketide synthase	3043	gi|414091047|gb|AFW98411.1|type I polyketide synthase [Alexandrium ostenfeldii]	AFW98411	0
116	ost_ovt_her27_contig_10200	polyketide synthase	8371	gi|1059529246|emb|SCL25381.1|Acyl transferase domain-containing protein [Micromonospora nigra]	SCL25381	0
117	ost_ovt_her27_contig_10810	polyketide synthase as3d906	2991	gi|712037596|gb|AIW63289.1|polyketide synthase AS3D906 [Azadinium spinosum]	AIW63289	0
118	ost_ovt_her27_contig_10898	type i polyketide synthase-like protein kb6736	3755	gi|148536485|gb|ABQ85802.1|type I polyketide synthase-like protein KB6736 [Karenia brevis]	ABQ85802	0
119	ost_ovt_her27_contig_11589	phthiocerol synthesis polyketide	4348	gi|1129192690|gb|OLP97452.1|Phthiocerol synthesis polyketide synthase type I PpsC	OLP97452	0

		synthase type i		[Symbiodinium microadriaticum]		
120	ost_ovt_her27_contig_11810	phthiocerol synthesis polyketide synthase type i	3908	gi|1129192690|gb|OLP97452.1|Phthiocerol synthesis polyketide synthase type I PpsC [Symbiodinium microadriaticum]	OLP97452	0
121	ost_ovt_her27_contig_11858	type i polyketide synthase	639	gi|983097016|ref|WP_060435779.1|type I polyketide synthase [Serratia marcescens]	WP_060435779	7.10E-33
122	ost_ovt_her27_contig_11861	phthiocerol synthesis polyketide synthase type i	3998	gi|1129198474|gb|OLQ02136.1|Phthiocerol synthesis polyketide synthase type I PpsD [Symbiodinium microadriaticum]	OLQ02136	0
123	ost_ovt_her27_contig_12663	type i polyketide synthase-like protein kb1008	3498	gi|148536473|gb|ABQ85796.1|type I polyketide synthase-like protein KB1008 [Karenia brevis]	ABQ85796	4.93E-118
124	ost_ovt_her27_contig_12798	type i polyketide synthase-like protein kb6736	3888	gi|148536485|gb|ABQ85802.1|type I polyketide synthase-like protein KB6736 [Karenia brevis]	ABQ85802	0
125	ost_ovt_her27_contig_13028	phthiocerol synthesis polyketide synthase type i	3980	gi|1129192690|gb|OLP97452.1|Phthiocerol synthesis polyketide synthase type I PpsC [Symbiodinium microadriaticum]	OLP97452	0
126	ost_ovt_her27_contig_13367	6-methylsalicylic acid synthase	1428	gi|1129199127|gb|OLQ02654.1|6-methylsalicylic acid synthase [Symbiodinium microadriaticum]	OLQ02654	4.04E-98
127	ost_ovt_her27_contig_13615	polyketide partial	3549	gi|148536473|gb|ABQ85796.1|type I polyketide synthase-like protein KB1008 [Karenia brevis]	ABQ85796	0
128	ost_ovt_her27_contig_13809	phthiocerol synthesis polyketide synthase type i	3767	gi|1129198474|gb|OLQ02136.1|Phthiocerol synthesis polyketide synthase type I PpsD [Symbiodinium microadriaticum]	OLQ02136	0
129	ost_ovt_her27_contig_13820	phthiocerol synthesis polyketide synthase type i	4149	gi|1129192690|gb|OLP97452.1|Phthiocerol synthesis polyketide synthase type I PpsC [Symbiodinium microadriaticum]	OLP97452	0
130	ost_ovt_her27_contig_14747	polyketide partial	3411	gi|941355192|dbj|BAT21730.1|polyketide synthase, partial [Karenia mikimotoi]	BAT21730	1.52E-169
131	ost_ovt_her27_contig_15103	phthiocerol synthesis polyketide synthase type i	3746	gi|1129192690|gb|OLP97452.1|Phthiocerol synthesis polyketide synthase type I PpsC [Symbiodinium microadriaticum]	OLP97452	1.02E-159
132	ost_ovt_her27_contig_15506	phthiocerol synthesis polyketide synthase type i	4178	gi|1129192690|gb|OLP97452.1|Phthiocerol synthesis polyketide synthase type I PpsC [Symbiodinium microadriaticum]	OLP97452	0
133	ost_ovt_her27_contig_16660	polyketide synthase	948	gi|505164431|ref|WP_015351533.1|polyketide synthase [Myxococcus stipitatus] >gi|441490583|gb|AGC47278.1| polyketide synthase [Myxococcus stipitatus DSM 14675]	WP_015351533	8.19E-04
134	ost_ovt_her27_contig_17054	polyketide synthase	3798	gi|1129213410|gb|OLQ14315.1|Polyketide synthase PksN [Symbiodinium microadriaticum]	OLQ14315	0

135	ost_ovt_her27_contig_17166	type i polyketide synthase	2976	gi|414091049|gb|AFW98412.1|type I polyketide synthase [Alexandrium ostenfeldii]	AFW98412	0
136	ost_ovt_her27_contig_17192	phthiocerol synthesis polyketide synthase type i	4032	gi|1129192690|gb|OLP97452.1|Phthiocerol synthesis polyketide synthase type I PpsC [Symbiodinium microadriaticum]	OLP97452	0
137	ost_ovt_her27_contig_176	6-methylsalicylic acid synthase	2143	gi|1129199127|gb|OLQ02654.1|6-methylsalicylic acid synthase [Symbiodinium microadriaticum]	OLQ02654	0
138	ost_ovt_her27_contig_17659	phthiocerol synthesis polyketide synthase type i	4030	gi|1129192690|gb|OLP97452.1|Phthiocerol synthesis polyketide synthase type I PpsC [Symbiodinium microadriaticum]	OLP97452	0
139	ost_ovt_her27_contig_17719	phthiocerol synthesis polyketide synthase type i	4540	gi|1129179243|gb|OLP87030.1|Phthiocerol synthesis polyketide synthase type I PpsC [Symbiodinium microadriaticum]	OLP87030	6.00E-61
140	ost_ovt_her27_contig_18224	phthiocerol synthesis polyketide synthase type i	3930	gi|1129192690|gb|OLP97452.1|Phthiocerol synthesis polyketide synthase type I PpsC [Symbiodinium microadriaticum]	OLP97452	0
141	ost_ovt_her27_contig_18295	polyketide partial	2867	gi|941355192|dbj|BAT21730.1|polyketide synthase, partial [Karenia mikimotoi]	BAT21730	6.11E-126
142	ost_ovt_her27_contig_18868	6-methylsalicylic acid synthase	1970	gi|1129199127|gb|OLQ02654.1|6-methylsalicylic acid synthase [Symbiodinium microadriaticum]	OLQ02654	7.71E-115
143	ost_ovt_her27_contig_1889	type i polyketide synthase-like protein kb1008	3708	gi|148536473|gb|ABQ85796.1|type I polyketide synthase-like protein KB1008 [Karenia brevis]	ABQ85796	1.37E-144
144	ost_ovt_her27_contig_19453	phthiocerol synthesis polyketide synthase type i	3957	gi|1129192690|gb|OLP97452.1|Phthiocerol synthesis polyketide synthase type I PpsC [Symbiodinium microadriaticum]	OLP97452	1.90E-148
145	ost_ovt_her27_contig_20389	erythronolide modules 5 and 6	7465	gi|1129204260|gb|OLQ06784.1|Erythronolide synthase, modules 5 and 6 [Symbiodinium microadriaticum]	OLQ06784	0
146	ost_ovt_her27_contig_2076	type i polyketide synthase-like protein kb1008	3868	gi|148536473|gb|ABQ85796.1|type I polyketide synthase-like protein KB1008 [Karenia brevis]	ABQ85796	5.62E-160
147	ost_ovt_her27_contig_21182	type i polyketide synthase-like protein kb1008	3591	gi|148536473|gb|ABQ85796.1|type I polyketide synthase-like protein KB1008 [Karenia brevis]	ABQ85796	4.98E-101
148	ost_ovt_her27_contig_21528	polyketide partial	2884	gi|941355192|dbj|BAT21730.1|polyketide synthase, partial [Karenia mikimotoi]	BAT21730	1.72E-119
149	ost_ovt_her27_contig_21548	type i polyketide synthase	2731	gi|414091051|gb|AFW98413.1|type I polyketide synthase [Alexandrium ostenfeldii]	AFW98413	0
150	ost_ovt_her27_contig_21745	erythronolide modules 5 and 6	713	gi|1129176947|gb|OLP85322.1|Erythronolide synthase, modules 5 and 6 [Symbiodinium microadriaticum]	OLP85322	4.61E-37

151	ost_ovt_her27_contig_21864	type i polyketide synthase	3007	gi|414091047|gb|AFW98411.1|type I polyketide synthase [Alexandrium ostenfeldii]	AFW98411	0
152	ost_ovt_her27_contig_22085	6-phosphofructokinase 7	5494	gi|1129173556|gb|OLP82883.1|6-phosphofructokinase 7 [Symbiodinium microadriaticum]	OLP82883	6.79E-110
153	ost_ovt_her27_contig_22680	polyketide synthase	1321	gi|383100620|emb|CCE88376.1|polyketide synthase [Sorangium cellulosum]	CCE88376	5.24E-34
154	ost_ovt_her27_contig_22719	phthiocerol synthesis polyketide synthase type i	3812	gi|1129192690|gb|OLP97452.1|Phthiocerol synthesis polyketide synthase type I PpsC [Symbiodinium microadriaticum]	OLP97452	0
155	ost_ovt_her27_contig_2280	polyketide partial	3624	gi|941355192|dbj|BAT21730.1|polyketide synthase, partial [Karenia mikimotoi]	BAT21730	4.15E-137
156	ost_ovt_her27_contig_2304	6-methylsalicylic acid synthase	2089	gi|1129199127|gb|OLQ02654.1|6-methylsalicylic acid synthase [Symbiodinium microadriaticum]	OLQ02654	2.39E-143
157	ost_ovt_her27_contig_25090	phthiocerol synthesis polyketide synthase type i	3923	gi|1129192690|gb|OLP97452.1|Phthiocerol synthesis polyketide synthase type I PpsC [Symbiodinium microadriaticum]	OLP97452	0
158	ost_ovt_her27_contig_2522	phthiocerol synthesis polyketide synthase type i	3956	gi|1129192690|gb|OLP97452.1|Phthiocerol synthesis polyketide synthase type I PpsC [Symbiodinium microadriaticum]	OLP97452	0
159	ost_ovt_her27_contig_28600	type i polyketide synthase-like protein kb1008	3470	gi|148536473|gb|ABQ85796.1|type I polyketide synthase-like protein KB1008 [Karenia brevis]	ABQ85796	4.92E-117
160	ost_ovt_her27_contig_31078	6-phosphofructokinase 7	5735	gi|1129173556|gb|OLP82883.1|6-phosphofructokinase 7 [Symbiodinium microadriaticum]	OLP82883	2.29E-51
161	ost_ovt_her27_contig_34366	polyketide synthase	2057	gi|1129213410|gb|OLQ14315.1|Polyketide synthase PksN [Symbiodinium microadriaticum]	OLQ14315	5.94E-70
162	ost_ovt_her27_contig_3457	phthiocerol synthesis polyketide synthase type i	4229	gi|1129192690|gb|OLP97452.1|Phthiocerol synthesis polyketide synthase type I PpsC [Symbiodinium microadriaticum]	OLP97452	0
163	ost_ovt_her27_contig_350	type i polyketide synthase-like protein kb1008	3644	gi|148536473|gb|ABQ85796.1|type I polyketide synthase-like protein KB1008 [Karenia brevis]	ABQ85796	1.58E-166
164	ost_ovt_her27_contig_35443	erythronolide modules 5 and 6	2982	gi|1129204260|gb|OLQ06784.1|Erythronolide synthase, modules 5 and 6 [Symbiodinium microadriaticum]	OLQ06784	0
165	ost_ovt_her27_contig_35650	erythronolide modules 5 and 6	2988	gi|1129204260|gb|OLQ06784.1|Erythronolide synthase, modules 5 and 6 [Symbiodinium microadriaticum]	OLQ06784	0
166	ost_ovt_her27_contig_36186	phthiocerol synthesis polyketide synthase type i	4017	gi|1129192690|gb|OLP97452.1|Phthiocerol synthesis polyketide synthase type I PpsC [Symbiodinium microadriaticum]	OLP97452	8.01E-132

167	ost_ovt_her27_contig_36565	oleandomycin polyketide modules 5 and 6	1999	gi|1129204261|gb|OLQ06785.1|Oleandomycin polyketide synthase, modules 5 and 6 [Symbiodinium microadriaticum]	OLQ06785	0
168	ost_ovt_her27_contig_36934	type i fatty acid	2275	gi|873227372|emb|CEM18661.1|unnamed protein product, partial [Vitrella brassicaformis CCMP3155]	CEM18661	6.11E-68
169	ost_ovt_her27_contig_38321	phthiocerol synthesis polyketide synthase type i	2709	gi|1129206593|gb|OLQ08682.1|Phthiocerol synthesis polyketide synthase type I PpsD [Symbiodinium microadriaticum]	OLQ08682	4.27E-106
170	ost_ovt_her27_contig_39462	phthiocerol synthesis polyketide synthase type i	3883	gi|1129206593|gb|OLQ08682.1|Phthiocerol synthesis polyketide synthase type I PpsD [Symbiodinium microadriaticum]	OLQ08682	3.08E-133
171	ost_ovt_her27_contig_40326	erythronolide modules 5 and 6	4408	gi|1129204260|gb|OLQ06784.1|Erythronolide synthase, modules 5 and 6 [Symbiodinium microadriaticum]	OLQ06784	0
172	ost_ovt_her27_contig_40631	polyketide synthase	1064	gi|1129179243|gb|OLP87030.1|Phthiocerol synthesis polyketide synthase type I PpsC [Symbiodinium microadriaticum]	OLP87030	3.50E-20
173	ost_ovt_her27_contig_42830	type i polyketide synthase-like protein kb1008	2567	gi|148536473|gb|ABQ85796.1|type I polyketide synthase-like protein KB1008 [Karenia brevis]	ABQ85796	3.90E-53
174	ost_ovt_her27_contig_4540	type i polyketide synthase-like protein kb6736	3930	gi|148536485|gb|ABQ85802.1|type I polyketide synthase-like protein KB6736 [Karenia brevis]	ABQ85802	0
175	ost_ovt_her27_contig_46260	erythronolide modules 5 and 6	760	gi|1129204261|gb|OLQ06785.1|Oleandomycin polyketide synthase, modules 5 and 6 [Symbiodinium microadriaticum]	OLQ06785	6.88E-92
176	ost_ovt_her27_contig_47210	phthiocerol synthesis polyketide synthase type i	3972	gi|1129192690|gb|OLP97452.1|Phthiocerol synthesis polyketide synthase type I PpsC [Symbiodinium microadriaticum]	OLP97452	8.46E-168
177	ost_ovt_her27_contig_4849	phthiocerol synthesis polyketide synthase type i	3857	gi|1129192690|gb|OLP97452.1|Phthiocerol synthesis polyketide synthase type I PpsC [Symbiodinium microadriaticum]	OLP97452	0
178	ost_ovt_her27_contig_49871	oleandomycin polyketide modules 5 and 6	556	gi|1129204261|gb|OLQ06785.1|Oleandomycin polyketide synthase, modules 5 and 6 [Symbiodinium microadriaticum]	OLQ06785	2.87E-90
179	ost_ovt_her27_contig_49910	oleandomycin polyketide modules 5 and 6	679	gi|1129204261|gb|OLQ06785.1|Oleandomycin polyketide synthase, modules 5 and 6 [Symbiodinium microadriaticum]	OLQ06785	2.44E-59
180	ost_ovt_her27_contig_49915	type i polyketide synthase-like protein kb1008	3073	gi|148536473|gb|ABQ85796.1|type I polyketide synthase-like protein KB1008 [Karenia brevis]	ABQ85796	8.26E-93

181	ost_ovt_her27_contig_49951	phthiocerol synthesis polyketide synthase type i	3518	gi|1129192690|gb|OLP97452.1|Phthiocerol synthesis polyketide synthase type I PpsC [Symbiodinium microadriaticum]	OLP97452	0
182	ost_ovt_her27_contig_5132	erythronolide modules 3 and 4	3745	gi|1129199229|gb|OLQ02729.1|Erythronolide synthase, modules 3 and 4 [Symbiodinium microadriaticum]	OLQ02729	3.58E-134
183	ost_ovt_her27_contig_51547	erythronolide modules 5 and 6	411	gi|1129204260|gb|OLQ06784.1|Erythronolide synthase, modules 5 and 6 [Symbiodinium microadriaticum]	OLQ06784	1.07E-55
184	ost_ovt_her27_contig_5289	phthiocerol synthesis polyketide synthase type i	4018	gi|1129192690|gb|OLP97452.1|Phthiocerol synthesis polyketide synthase type I PpsC [Symbiodinium microadriaticum]	OLP97452	0
185	ost_ovt_her27_contig_54223	oleandomycin polyketide modules 5 and 6	607	gi|1129204261|gb|OLQ06785.1|Oleandomycin polyketide synthase, modules 5 and 6 [Symbiodinium microadriaticum]	OLQ06785	9.77E-46
186	ost_ovt_her27_contig_54265	short-chain dehydrogenase reductase related	809	gi|401395940|ref|XP_003879716.1|short-chain dehydrogenase/reductase SDR, related [Neospora caninum Liverpool] >gi|325114123|emb|CBZ49681.1| short-chain dehydrogenase/reductase SDR, related [Neospora caninum Liverpool]	XP_003879716	3.96E-58
187	ost_ovt_her27_contig_54266	unnamed protein product	727	gi|873222028|emb|CEM32068.1|unnamed protein product [Vitrella brassicaformis CCMP3155]	CEM32068	1.09E-27
188	ost_ovt_her27_contig_57469	erythronolide modules 5 and 6	288	gi|1129204260|gb|OLQ06784.1|Erythronolide synthase, modules 5 and 6 [Symbiodinium microadriaticum]	OLQ06784	3.97E-08
189	ost_ovt_her27_contig_57828	erythronolide modules 5 and 6	2683	gi|1129204260|gb|OLQ06784.1|Erythronolide synthase, modules 5 and 6 [Symbiodinium microadriaticum]	OLQ06784	0
190	ost_ovt_her27_contig_58181	erythronolide modules 5 and 6	712	gi|1129176947|gb|OLP85322.1|Erythronolide synthase, modules 5 and 6 [Symbiodinium microadriaticum]	OLP85322	5.99E-68
191	ost_ovt_her27_contig_58182	erythronolide modules 5 and 6	237	gi|1129204260|gb|OLQ06784.1|Erythronolide synthase, modules 5 and 6 [Symbiodinium microadriaticum]	OLQ06784	5.03E-19
192	ost_ovt_her27_contig_58202	oleandomycin polyketide modules 5 and 6	250	gi|1129204261|gb|OLQ06785.1|Oleandomycin polyketide synthase, modules 5 and 6 [Symbiodinium microadriaticum]	OLQ06785	6.20E-22
193	ost_ovt_her27_contig_58203	beta-ketoacyl partial	545	gi|1129204261|gb|OLQ06785.1|Oleandomycin polyketide synthase, modules 5 and 6 [Symbiodinium microadriaticum]	OLQ06785	5.90E-88
194	ost_ovt_her27_contig_60404	polyketide partial	212	gi|1129167743|gb|OLP78851.1|Polyketide synthase PksN [Symbiodinium microadriaticum]	OLP78851	1.64E-13

195	ost_ovt_her27_contig_61132	oleandomycin polyketide modules 5 and 6	1248	gi|1129204261|gb|OLQ06785.1|Oleandomycin polyketide synthase, modules 5 and 6 [Symbiodinium microadriaticum]	OLQ06785	0
196	ost_ovt_her27_contig_6116	type i polyketide synthase-like protein kb6736	4191	gi|148536485|gb|ABQ85802.1|type I polyketide synthase-like protein KB6736 [Karenia brevis]	ABQ85802	1.09E-154
197	ost_ovt_her27_contig_61462	erythronolide modules 5 and 6	1278	gi|1129204260|gb|OLQ06784.1|Erythronolide synthase, modules 5 and 6 [Symbiodinium microadriaticum]	OLQ06784	0
198	ost_ovt_her27_contig_6192	type i polyketide synthase-like protein kb6736	4178	gi|148536485|gb|ABQ85802.1|type I polyketide synthase-like protein KB6736 [Karenia brevis]	ABQ85802	1.80E-149
199	ost_ovt_her27_contig_62105	oleandomycin polyketide modules 5 and 6	296	gi|1129204261|gb|OLQ06785.1|Oleandomycin polyketide synthase, modules 5 and 6 [Symbiodinium microadriaticum]	OLQ06785	6.00E-33
200	ost_ovt_her27_contig_6223	sodium calcium exchanger 3	4347	gi|1129171706|gb|OLP81580.1|Sodium/calcium exchanger 3 [Symbiodinium microadriaticum]	OLP81580	1.10E-155
201	ost_ovt_her27_contig_62432	equisetin related protein	656	gi|557242469|emb|CDJ53564.1|hypothetical protein EBH_0017680 [Eimeria brunetti]	CDJ53564	1.26E-49
202	ost_ovt_her27_contig_63049	6-methylsalicylic acid synthase	1193	gi|1129199127|gb|OLQ02654.1|6-methylsalicylic acid synthase [Symbiodinium microadriaticum]	OLQ02654	1.03E-101
203	ost_ovt_her27_contig_6415	polyketide synthase 1	3982	gi|595389390|gb|AHM27264.1|polyketide synthase 1 [Gambierdiscus polynesiensis] >gi|595389401|gb|AHM27265.1| polyketide synthase 2 [Gambierdiscus polynesiensis]	AHM27264	0
204	ost_ovt_her27_contig_64642	oleandomycin polyketide modules 5 and 6	681	gi|1129204261|gb|OLQ06785.1|Oleandomycin polyketide synthase, modules 5 and 6 [Symbiodinium microadriaticum]	OLQ06785	3.36E-64
205	ost_ovt_her27_contig_64675	erythronolide modules 5 and 6	779	gi|1129204261|gb|OLQ06785.1|Oleandomycin polyketide synthase, modules 5 and 6 [Symbiodinium microadriaticum]	OLQ06785	2.81E-79
206	ost_ovt_her27_contig_65142	oleandomycin polyketide modules 5 and 6	586	gi|1129204261|gb|OLQ06785.1|Oleandomycin polyketide synthase, modules 5 and 6 [Symbiodinium microadriaticum]	OLQ06785	3.57E-67
207	ost_ovt_her27_contig_65897	oleandomycin polyketide modules 5 and 6	490	gi|1129204261|gb|OLQ06785.1|Oleandomycin polyketide synthase, modules 5 and 6 [Symbiodinium microadriaticum]	OLQ06785	1.76E-31
208	ost_ovt_her27_contig_66124	erythronolide modules 3 and 4	532	gi|1129182889|gb|OLP89862.1|Erythronolide synthase, modules 3 and 4 [Symbiodinium microadriaticum]	OLP89862	2.57E-19
209	ost_ovt_her27_contig_6640	polyketide synthase	5900	gi|1129173556|gb|OLP82883.1|6-phosphofructokinase 7 [Symbiodinium microadriaticum]	OLP82883	1.20E-53

210	ost_ovt_her27_contig_67167	type i fatty acid	297	gi|1129204261|gb|OLQ06785.1|Oleandomycin polyketide synthase, modules 5 and 6 [Symbiodinium microadriaticum]	OLQ06785	3.52E-27
211	ost_ovt_her27_contig_67168	oleandomycin polyketide modules 5 and 6	298	gi|1129204261|gb|OLQ06785.1|Oleandomycin polyketide synthase, modules 5 and 6 [Symbiodinium microadriaticum]	OLQ06785	1.47E-35
212	ost_ovt_her27_contig_69011	beta-ketoacyl-acp synthase	909	gi|760325535|ref|WP_043858226.1|hypothetical protein [Bacillus subtilis]	WP_043858226	2.60E-50
213	ost_ovt_her27_contig_7045	phthiocerol synthesis polyketide synthase type i	2965	gi|1129180700|gb|OLP88203.1|Phthiocerol synthesis polyketide synthase type I PpsC [Symbiodinium microadriaticum]	OLP88203	0
214	ost_ovt_her27_contig_71275	erythronolide modules 5 and 6	575	gi|1129176947|gb|OLP85322.1|Erythronolide synthase, modules 5 and 6 [Symbiodinium microadriaticum]	OLP85322	2.34E-52
215	ost_ovt_her27_contig_7177	polyketide partial	3517	gi|941355192|dbj|BAT21730.1|polyketide synthase, partial [Karenia mikimotoi]	BAT21730	3.12E-149
216	ost_ovt_her27_contig_72919	erythronolide modules 5 and 6	785	gi|1129176947|gb|OLP85322.1|Erythronolide synthase, modules 5 and 6 [Symbiodinium microadriaticum]	OLP85322	7.57E-78
217	ost_ovt_her27_contig_72948	phthiocerol synthesis polyketide synthase type i	1362	gi|1129206593|gb|OLQ08682.1|Phthiocerol synthesis polyketide synthase type I PpsD [Symbiodinium microadriaticum]	OLQ08682	8.13E-104
218	ost_ovt_her27_contig_73045	type i polyketide synthase	394	gi|917248511|ref|WP_051855223.1|type I polyketide synthase [Streptomyces sp. NRRL B-1347]	WP_051855223	5.07E-07
219	ost_ovt_her27_contig_73147	erythronolide modules 5 and 6	245	gi|1129204261|gb|OLQ06785.1|Oleandomycin polyketide synthase, modules 5 and 6 [Symbiodinium microadriaticum]	OLQ06785	1.64E-19
220	ost_ovt_her27_contig_73326	oleandomycin polyketide modules 5 and 6	504	gi|1129204261|gb|OLQ06785.1|Oleandomycin polyketide synthase, modules 5 and 6 [Symbiodinium microadriaticum]	OLQ06785	2.85E-53
221	ost_ovt_her27_contig_73383	oleandomycin polyketide modules 5 and 6	413	gi|1129204261|gb|OLQ06785.1|Oleandomycin polyketide synthase, modules 5 and 6 [Symbiodinium microadriaticum]	OLQ06785	6.86E-33
222	ost_ovt_her27_contig_7368	polyketide synthase as3d906	3076	gi|712037596|gb|AIW63289.1|polyketide synthase AS3D906 [Azadinium spinosum]	AIW63289	0
223	ost_ovt_her27_contig_7390	phthiocerol synthesis polyketide synthase type i	4272	gi|1129192690|gb|OLP97452.1|Phthiocerol synthesis polyketide synthase type I PpsC [Symbiodinium microadriaticum]	OLP97452	4.65E-148
224	ost_ovt_her27_contig_7392	type i polyketide synthase	2521	gi|414091049|gb|AFW98412.1|type I polyketide synthase [Alexandrium ostenfeldii]	AFW98412	3.86E-164
225	ost_ovt_her27_contig_74056	type i fatty acid	404	gi|1129204261|gb|OLQ06785.1|Oleandomycin polyketide synthase, modules 5 and 6	OLQ06785	7.29E-23

				[Symbiodinium microadriaticum]		
226	ost_ovt_her27_contig_74456	erythronolide modules 5 and 6	707	gi|1129176947|gb|OLP85322.1|Erythronolide synthase, modules 5 and 6 [Symbiodinium microadriaticum]	OLP85322	1.39E-43
227	ost_ovt_her27_contig_76382	oleandomycin polyketide modules 5 and 6	830	gi|1129204261|gb|OLQ06785.1|Oleandomycin polyketide synthase, modules 5 and 6 [Symbiodinium microadriaticum]	OLQ06785	1.12E-81
228	ost_ovt_her27_contig_7885	polyketide partial	3829	gi|941355192|dbj|BAT21730.1|polyketide synthase, partial [Karenia mikimotoi]	BAT21730	0
229	ost_ovt_her27_contig_79967	oleandomycin polyketide modules 5 and 6	409	gi|1129204261|gb|OLQ06785.1|Oleandomycin polyketide synthase, modules 5 and 6 [Symbiodinium microadriaticum]	OLQ06785	5.71E-51
230	ost_ovt_her27_contig_80386	type i fatty acid	428	gi|1129204261|gb|OLQ06785.1|Oleandomycin polyketide synthase, modules 5 and 6 [Symbiodinium microadriaticum]	OLQ06785	4.05E-56
231	ost_ovt_her27_contig_80789	short-chain dehydrogenase reductase related	305	gi|1132233752|ref|WP_075901920.1|hypothetical protein [Moorea bouillonii] >gi|1130578861|gb|OLT61097.1| hypothetical protein BJP37_20840 [Moorea bouillonii PNG5-198]	WP_075901920	5.81E-19
232	ost_ovt_her27_contig_80972	type i polyketide synthase	443	gi|655097742|ref|WP_028545526.1|type I polyketide synthase [Paenibacillus taiwanensis]	WP_028545526	1.39E-07
233	ost_ovt_her27_contig_81124	non-ribosomal peptide synthetase	520	gi|1129158909|gb|OLP74521.1|Erythronolide synthase, modules 5 and 6, partial [Symbiodinium microadriaticum]	OLP74521	2.99E-64
234	ost_ovt_her27_contig_828	type i polyketide synthase	3080	gi|414091049|gb|AFW98412.1|type I polyketide synthase [Alexandrium ostenfeldii]	AFW98412	0
235	ost_ovt_her27_contig_8323	phthiocerol synthesis polyketide synthase type i	4022	gi|1129192690|gb|OLP97452.1|Phthiocerol synthesis polyketide synthase type I PpsC [Symbiodinium microadriaticum]	OLP97452	0
236	ost_ovt_her27_contig_85947	6-phosphofructokinase 7	322	gi|1129173556|gb|OLP82883.1|6-phosphofructokinase 7 [Symbiodinium microadriaticum]	OLP82883	1.92E-06
237	ost_ovt_her27_contig_8665	oleandomycin polyketide modules 5 and 6	333	gi|1129204261|gb|OLQ06785.1|Oleandomycin polyketide synthase, modules 5 and 6 [Symbiodinium microadriaticum]	OLQ06785	2.27E-44
238	ost_ovt_her27_contig_8666	erythronolide modules 5 and 6	2940	gi|1129204260|gb|OLQ06784.1|Erythronolide synthase, modules 5 and 6 [Symbiodinium microadriaticum]	OLQ06784	0
239	ost_ovt_her27_contig_8673	calcium-dependent protein kinase 2	3692	gi|1129164416|gb|OLP76751.1|Calcium-dependent protein kinase 2 [Symbiodinium microadriaticum]	OLP76751	8.71E-164
240	ost_ovt_her27_contig_8686	phthiocerol	3859	gi|1129192690|gb|OLP97452.1|Phthiocerol	OLP97452	0

		synthesis polyketide synthase type i		synthesis polyketide synthase type I PpsC [Symbiodinium microadriaticum]		
241	ost_ovt_her27_contig_9281	type i polyketide synthase	2976	gi|414091049|gb|AFW98412.1|type I polyketide synthase [Alexandrium ostenfeldii]	AFW98412	0
242	ost_ovt_her27_contig_9710	lovastatin nonaketide synthase	2051	gi|1129179982|gb|OLP87649.1|Lovastatin nonaketide synthase [Symbiodinium microadriaticum]	OLP87649	4.48E-88
243	ost_siam_bh1_contig_11643	type i polyketide synthase-like protein kb1008	3659	gi|148536473|gb|ABQ85796.1|type I polyketide synthase-like protein KB1008 [Karenia brevis]	ABQ85796	1.45E-166
244	ost_siam_bh1_contig_1173	type i polyketide synthase-like protein kb6736	4182	gi|148536485|gb|ABQ85802.1|type I polyketide synthase-like protein KB6736 [Karenia brevis]	ABQ85802	1.32E-152
245	ost_siam_bh1_contig_1174	type i polyketide synthase-like protein kb6736	3905	gi|148536485|gb|ABQ85802.1|type I polyketide synthase-like protein KB6736 [Karenia brevis]	ABQ85802	0
246	ost_siam_bh1_contig_12376	polyketide synthase as3d906	3016	gi|712037596|gb|AIW63289.1|polyketide synthase AS3D906 [Azadinium spinosum]	AIW63289	0
247	ost_siam_bh1_contig_12527	phthiocerol synthesis polyketide synthase type i	3003	gi|1129180700|gb|OLP88203.1|Phthiocerol synthesis polyketide synthase type I PpsC [Symbiodinium microadriaticum]	OLP88203	0
248	ost_siam_bh1_contig_12528	phthiocerol synthesis polyketide synthase type i	2316	gi|1129180700|gb|OLP88203.1|Phthiocerol synthesis polyketide synthase type I PpsC [Symbiodinium microadriaticum]	OLP88203	0
249	ost_siam_bh1_contig_12688	type i fatty acid	2259	gi|873227372|emb|CEM18661.1|unnamed protein product, partial [Vitrella brassicaformis CCMP3155]	CEM18661	6.67E-68
250	ost_siam_bh1_contig_12771	polyketide synthase	1873	gi|941355190|dbj|BAT21729.1|polyketide synthase [Karenia mikimotoi]	BAT21729	6.21E-73
251	ost_siam_bh1_contig_13158	type i polyketide synthase	10016	gi|1132232290|ref|WP_075900458.1|hypothetical protein [Moorea bouillonii] >gi|1130578090|gb|OLT60326.1| hypothetical protein BJP37_16130 [Moorea bouillonii PNG5-198]	WP_075900458	2.69E-127
252	ost_siam_bh1_contig_13634	phthiocerol synthesis polyketide synthase type i	3921	gi|1129192690|gb|OLP97452.1|Phthiocerol synthesis polyketide synthase type I PpsC [Symbiodinium microadriaticum]	OLP97452	0
253	ost_siam_bh1_contig_13674	phthiocerol synthesis polyketide synthase type i	4105	gi|1129192690|gb|OLP97452.1|Phthiocerol synthesis polyketide synthase type I PpsC [Symbiodinium microadriaticum]	OLP97452	0
254	ost_siam_bh1_contig_13994	phthiocerol synthesis polyketide synthase type i	4452	gi|1129192690|gb|OLP97452.1|Phthiocerol synthesis polyketide synthase type I PpsC [Symbiodinium microadriaticum]	OLP97452	0

255	ost_siam_bh1_contig_14439	phthiocerol synthesis polyketide synthase type i	3890	gi|1129192690|gb|OLP97452.1|Phthiocerol synthesis polyketide synthase type I PpsC [Symbiodinium microadriaticum]	OLP97452	0
256	ost_siam_bh1_contig_14644	erythronolide modules 3 and 4	3741	gi|1129199229|gb|OLQ02729.1|Erythronolide synthase, modules 3 and 4 [Symbiodinium microadriaticum]	OLQ02729	8.01E-134
257	ost_siam_bh1_contig_14757	phthiocerol synthesis polyketide synthase type i	2344	gi|1129192690|gb|OLP97452.1|Phthiocerol synthesis polyketide synthase type I PpsC [Symbiodinium microadriaticum]	OLP97452	2.16E-90
258	ost_siam_bh1_contig_15351	sodium calcium exchanger 3	1815	gi|1129171706|gb|OLP81580.1|Sodium/calcium exchanger 3 [Symbiodinium microadriaticum]	OLP81580	1.52E-88
259	ost_siam_bh1_contig_15612	type i polyketide synthase-like protein kb1008	2179	gi|148536473|gb|ABQ85796.1|type I polyketide synthase-like protein KB1008 [Karenia brevis]	ABQ85796	6.25E-129
260	ost_siam_bh1_contig_15652	phthiocerol synthesis polyketide synthase type i	3992	gi|1129192690|gb|OLP97452.1|Phthiocerol synthesis polyketide synthase type I PpsC [Symbiodinium microadriaticum]	OLP97452	0
261	ost_siam_bh1_contig_1574	phthiocerol synthesis polyketide synthase type i	3878	gi|1129198474|gb|OLQ02136.1|Phthiocerol synthesis polyketide synthase type I PpsD [Symbiodinium microadriaticum]	OLQ02136	0
262	ost_siam_bh1_contig_16953	phthiocerol synthesis polyketide synthase type i	3827	gi|1129198474|gb|OLQ02136.1|Phthiocerol synthesis polyketide synthase type I PpsD [Symbiodinium microadriaticum]	OLQ02136	0
263	ost_siam_bh1_contig_17150	phthiocerol synthesis polyketide synthase type i	2479	gi|1129206593|gb|OLQ08682.1|Phthiocerol synthesis polyketide synthase type I PpsD [Symbiodinium microadriaticum]	OLQ08682	1.28E-134
264	ost_siam_bh1_contig_17654	type i polyketide synthase	2923	gi|414091049|gb|AFW98412.1|type I polyketide synthase [Alexandrium ostenfeldii]	AFW98412	0
265	ost_siam_bh1_contig_17743	phthiocerol synthesis polyketide synthase type i	3795	gi|1129192690|gb|OLP97452.1|Phthiocerol synthesis polyketide synthase type I PpsC [Symbiodinium microadriaticum]	OLP97452	2.48E-171
266	ost_siam_bh1_contig_18167	phthiocerol synthesis polyketide synthase type i	3988	gi|1129192690|gb|OLP97452.1|Phthiocerol synthesis polyketide synthase type I PpsC [Symbiodinium microadriaticum]	OLP97452	0
267	ost_siam_bh1_contig_18462	polyketide partial	3501	gi|941355192|dbj|BAT21730.1|polyketide synthase, partial [Karenia mikimotoi]	BAT21730	5.32E-143
268	ost_siam_bh1_contig_19528	type i polyketide synthase	3048	gi|414091049|gb|AFW98412.1|type I polyketide synthase [Alexandrium ostenfeldii]	AFW98412	0
269	ost_siam_bh1_contig_1971	phthiocerol synthesis polyketide synthase type i	4028	gi|1129192690|gb|OLP97452.1|Phthiocerol synthesis polyketide synthase type I PpsC [Symbiodinium microadriaticum]	OLP97452	0
270	ost_siam_bh1_contig_20084	polyketide synthase as3d906	2983	gi|712037596|gb|AIW63289.1|polyketide synthase AS3D906 [Azadinium spinosum]	AIW63289	0

271	ost_siam_bh1_contig_20215	type i polyketide synthase-like protein kb6736	3891	gi|148536485|gb|ABQ85802.1|type I polyketide synthase-like protein KB6736 [Karenia brevis]	ABQ85802	0
272	ost_siam_bh1_contig_20439	type i polyketide synthase-like protein kb1008	3497	gi|148536473|gb|ABQ85796.1|type I polyketide synthase-like protein KB1008 [Karenia brevis]	ABQ85796	1.61E-122
273	ost_siam_bh1_contig_20664	polyketide partial	315	gi|354464931|gb|AER26679.1|putative polyketide synthase, partial [uncultured marine cyanobacterium]	AER26679	1.47E-14
274	ost_siam_bh1_contig_21247	phthiocerol synthesis polyketide synthase type i	4122	gi|1129192690|gb|OLP97452.1|Phthiocerol synthesis polyketide synthase type I PpsC [Symbiodinium microadriaticum]	OLP97452	0
275	ost_siam_bh1_contig_2125	phthiocerol synthesis polyketide synthase type i	4045	gi|1129192690|gb|OLP97452.1|Phthiocerol synthesis polyketide synthase type I PpsC [Symbiodinium microadriaticum]	OLP97452	0
276	ost_siam_bh1_contig_21404	6-phosphofructokinase 7	5892	gi|1129173556|gb|OLP82883.1|6-phosphofructokinase 7 [Symbiodinium microadriaticum]	OLP82883	2.14E-53
277	ost_siam_bh1_contig_21563	6-methylsalicylic acid synthase	1982	gi|1129199127|gb|OLQ02654.1|6-methylsalicylic acid synthase [Symbiodinium microadriaticum]	OLQ02654	5.70E-118
278	ost_siam_bh1_contig_22082	lovastatin nonaketide synthase	1909	gi|1129179982|gb|OLP87649.1|Lovastatin nonaketide synthase [Symbiodinium microadriaticum]	OLP87649	1.34E-88
279	ost_siam_bh1_contig_24242	polyketide partial	3570	gi|148536473|gb|ABQ85796.1|type I polyketide synthase-like protein KB1008 [Karenia brevis]	ABQ85796	0
280	ost_siam_bh1_contig_24984	polyketide partial	3562	gi|941355192|dbj|BAT21730.1|polyketide synthase, partial [Karenia mikimotoi]	BAT21730	0
281	ost_siam_bh1_contig_25485	phthiocerol synthesis polyketide synthase type i	4046	gi|1129192690|gb|OLP97452.1|Phthiocerol synthesis polyketide synthase type I PpsC [Symbiodinium microadriaticum]	OLP97452	0
282	ost_siam_bh1_contig_25968	phthiocerol synthesis polyketide synthase type i	3990	gi|1129192690|gb|OLP97452.1|Phthiocerol synthesis polyketide synthase type I PpsC [Symbiodinium microadriaticum]	OLP97452	4.96E-169
283	ost_siam_bh1_contig_2727	polyketide synthase as3d902	2340	gi|712037589|gb|AIW63286.1|polyketide synthase AS3D902 [Azadinium spinosum]	AIW63286	0
284	ost_siam_bh1_contig_27329	polyketide partial	2623	gi|941355192|dbj|BAT21730.1|polyketide synthase, partial [Karenia mikimotoi]	BAT21730	1.58E-112
285	ost_siam_bh1_contig_28362	type i polyketide synthase-like protein kb1008	1771	gi|148536473|gb|ABQ85796.1|type I polyketide synthase-like protein KB1008 [Karenia brevis]	ABQ85796	2.54E-61
286	ost_siam_bh1_contig_28846	6-methylsalicylic acid synthase	1518	gi|1129199127|gb|OLQ02654.1|6-methylsalicylic acid synthase [Symbiodinium microadriaticum]	OLQ02654	6.61E-116

287	ost_siam_bh1_contig_28918	phthiocerol synthesis polyketide synthase type i	3711	gi|1129192690|gb|OLP97452.1|Phthiocerol synthesis polyketide synthase type I PpsC [Symbiodinium microadriaticum]	OLP97452	2.51E-153
288	ost_siam_bh1_contig_30748	phthiocerol synthesis polyketide synthase type i	4286	gi|1129192690|gb|OLP97452.1|Phthiocerol synthesis polyketide synthase type I PpsC [Symbiodinium microadriaticum]	OLP97452	0
289	ost_siam_bh1_contig_31255	polyketide synthase as3d902	1803	gi|712037589|gb|AIW63286.1|polyketide synthase AS3D902 [Azadinium spinosum]	AIW63286	0
290	ost_siam_bh1_contig_31392	oleandomycin polyketide modules 5 and 6	329	gi|1129204261|gb|OLQ06785.1|Oleandomycin polyketide synthase, modules 5 and 6 [Symbiodinium microadriaticum]	OLQ06785	1.24E-29
291	ost_siam_bh1_contig_32332	type i polyketide synthase-like protein kb6736	4180	gi|148536485|gb|ABQ85802.1|type I polyketide synthase-like protein KB6736 [Karenia brevis]	ABQ85802	5.09E-148
292	ost_siam_bh1_contig_32461	type i polyketide synthase	2733	gi|414091049|gb|AFW98412.1|type I polyketide synthase [Alexandrium ostenfeldii]	AFW98412	0
293	ost_siam_bh1_contig_33569	6-methylsalicylic acid synthase	630	gi|1129199127|gb|OLQ02654.1|6-methylsalicylic acid synthase [Symbiodinium microadriaticum]	OLQ02654	4.83E-34
294	ost_siam_bh1_contig_34621	type i polyketide synthase	1292	gi|414091047|gb|AFW98411.1|type I polyketide synthase [Alexandrium ostenfeldii]	AFW98411	0
295	ost_siam_bh1_contig_35697	erythronolide modules 5 and 6	2697	gi|1129204260|gb|OLQ06784.1|Erythronolide synthase, modules 5 and 6 [Symbiodinium microadriaticum]	OLQ06784	0
296	ost_siam_bh1_contig_39839	phthiocerol synthesis polyketide synthase type i	3938	gi|1129192690|gb|OLP97452.1|Phthiocerol synthesis polyketide synthase type I PpsC [Symbiodinium microadriaticum]	OLP97452	0
297	ost_siam_bh1_contig_40676	phthiocerol synthesis polyketide synthase type i	1105	gi|1129206593|gb|OLQ08682.1|Phthiocerol synthesis polyketide synthase type I PpsD [Symbiodinium microadriaticum]	OLQ08682	1.19E-32
298	ost_siam_bh1_contig_4112	polyketide synthase 1	3977	gi|595389390|gb|AHM27264.1|polyketide synthase 1 [Gambierdiscus polynesiensis] >gi|595389401|gb|AHM27265.1| polyketide synthase 2 [Gambierdiscus polynesiensis]	AHM27264	0
299	ost_siam_bh1_contig_41385	oleandomycin polyketide modules 5 and 6	242	gi|1129204261|gb|OLQ06785.1|Oleandomycin polyketide synthase, modules 5 and 6 [Symbiodinium microadriaticum]	OLQ06785	5.91E-24
300	ost_siam_bh1_contig_41617	polyketide synthase	2541	gi|941355188|dbj|BAT21728.1|polyketide synthase [Karenia mikimotoi]	BAT21728	2.46E-56
301	ost_siam_bh1_contig_42957	erythronolide modules 5 and 6	376	gi|1129204260|gb|OLQ06784.1|Erythronolide synthase, modules 5 and 6 [Symbiodinium microadriaticum]	OLQ06784	4.78E-12
302	ost_siam_bh1_contig_43294	type i polyketide synthase	1002	gi|414091049|gb|AFW98412.1|type I polyketide synthase [Alexandrium ostenfeldii]	AFW98412	1.56E-74

303	ost_siam_bh1_contig_45353	6-phosphofructokinase 7	3013	gi|1129173556|gb|OLP82883.1|6-phosphofructokinase 7 [Symbiodinium microadriaticum]	OLP82883	1.33E-51
304	ost_siam_bh1_contig_46025	phthiocerol synthesis polyketide synthase type i	793	gi|1129206593|gb|OLQ08682.1|Phthiocerol synthesis polyketide synthase type I PpsD [Symbiodinium microadriaticum]	OLQ08682	2.14E-30
305	ost_siam_bh1_contig_46824	polyketide synthase	414	gi|1129213410|gb|OLQ14315.1|Polyketide synthase PksN [Symbiodinium microadriaticum]	OLQ14315	6.55E-30
306	ost_siam_bh1_contig_49417	6-phosphofructokinase 7	296	gi|1129173556|gb|OLP82883.1|6-phosphofructokinase 7 [Symbiodinium microadriaticum]	OLP82883	4.05E-05
307	ost_siam_bh1_contig_49498	phthiocerol synthesis polyketide synthase type i	453	gi|1129179243|gb|OLP87030.1|Phthiocerol synthesis polyketide synthase type I PpsC [Symbiodinium microadriaticum]	OLP87030	7.98E-14
308	ost_siam_bh1_contig_5046	type i polyketide synthase-like protein kb1008	3607	gi|148536473|gb|ABQ85796.1|type I polyketide synthase-like protein KB1008 [Karenia brevis]	ABQ85796	1.10E-163
309	ost_siam_bh1_contig_50705	erythronolide modules 5 and 6	430	gi|1129204260|gb|OLQ06784.1|Erythronolide synthase, modules 5 and 6 [Symbiodinium microadriaticum]	OLQ06784	1.60E-68
310	ost_siam_bh1_contig_5279	type i polyketide synthase	2772	gi|414091051|gb|AFW98413.1|type I polyketide synthase [Alexandrium ostenfeldii]	AFW98413	0
311	ost_siam_bh1_contig_5282	polyketide synthase 1	1905	gi|595389390|gb|AHM27264.1|polyketide synthase 1 [Gambierdiscus polynesiensis] >gi|595389401|gb|AHM27265.1| polyketide synthase 2 [Gambierdiscus polynesiensis]	AHM27264	5.76E-97
312	ost_siam_bh1_contig_5416	phthiocerol synthesis polyketide synthase type i	4796	gi|1129179243|gb|OLP87030.1|Phthiocerol synthesis polyketide synthase type I PpsC [Symbiodinium microadriaticum]	OLP87030	5.00E-60
313	ost_siam_bh1_contig_54434	polyketide synthase family partial	369	gi|545903977|ref|WP_021780892.1|type I polyketide synthase [Myxococcus hansupus] >gi|891160781|gb|AKQ65466.1| Malonyl CoA-acyl carrier protein transacylase [Myxococcus hansupus]	WP_021780892	1.03E-15
314	ost_siam_bh1_contig_55722	polyketide synthase	1418	gi|982040572|ref|WP_060214404.1|polyketide synthase [Burkholderia ubonensis] >gi|979912898|gb|KWB43999.1| polyketide synthase [Burkholderia ubonensis]	WP_060214404	2.35E-39
315	ost_siam_bh1_contig_56224	phthiocerol synthesis polyketide synthase type i	505	gi|1129200442|gb|OLQ03682.1|Phthiocerol synthesis polyketide synthase type I PpsA [Symbiodinium microadriaticum]	OLQ03682	3.05E-11
316	ost_siam_bh1_contig_56665	phthiocerol synthesis polyketide synthase type i	1239	gi|1129173060|gb|OLP82529.1|Phthiocerol synthesis polyketide synthase type I PpsD [Symbiodinium microadriaticum]	OLP82529	4.08E-25

317	ost_siam_bh1_contig_5989	6-phosphofructokinase 7	3038	gi|1129173556|gb|OLP82883.1|6-phosphofructokinase 7 [Symbiodinium microadriaticum]	OLP82883	1.53E-115
318	ost_siam_bh1_contig_6056	phthiocerol synthesis polyketide synthase type i	3956	gi|1129192690|gb|OLP97452.1|Phthiocerol synthesis polyketide synthase type I PpsC [Symbiodinium microadriaticum]	OLP97452	0
319	ost_siam_bh1_contig_60783	type i polyketide synthase- partial	340	gi|62549357|gb|AAX86997.1|type I polyketide synthase-like, partial [unidentified bacterium]	AAX86997	4.35E-21
320	ost_siam_bh1_contig_61990	phthiocerol synthesis polyketide synthase type i	1095	gi|1129173060|gb|OLP82529.1|Phthiocerol synthesis polyketide synthase type I PpsD [Symbiodinium microadriaticum]	OLP82529	4.26E-44
321	ost_siam_bh1_contig_63151	polyketide synthase	1912	gi|1129175031|gb|OLP83938.1|Polyketide synthase PksN [Symbiodinium microadriaticum]	OLP83938	0
322	ost_siam_bh1_contig_65058	phthiocerol synthesis polyketide synthase type i	1330	gi|1129206593|gb|OLQ08682.1|Phthiocerol synthesis polyketide synthase type I PpsD [Symbiodinium microadriaticum]	OLQ08682	4.21E-94
323	ost_siam_bh1_contig_6512	calcium-dependent protein kinase 2	3674	gi|1129164416|gb|OLP76751.1|Calcium-dependent protein kinase 2 [Symbiodinium microadriaticum]	OLP76751	5.00E-164
324	ost_siam_bh1_contig_65178	short-chain dehydrogenase	637	gi|1084329446|ref|WP_070393505.1|hypothetical protein [Moorea producens] >gi|1082411449|gb|AOX01054.1| hypothetical protein BJP34_17840 [Moorea producens PAL-8-15-08-1]	WP_070393505	1.63E-17
325	ost_siam_bh1_contig_65775	type i polyketide synthase-like protein partial	676	gi|148536487|gb|ABQ85803.1|type I polyketide synthase-like protein KB6842, partial [Karenia brevis]	ABQ85803	5.00E-36
326	ost_siam_bh1_contig_67397	oleandomycin polyketide modules 5 and 6	317	gi|1129204261|gb|OLQ06785.1|Oleandomycin polyketide synthase, modules 5 and 6 [Symbiodinium microadriaticum]	OLQ06785	3.73E-27
327	ost_siam_bh1_contig_68581	oleandomycin polyketide modules 5 and 6	245	gi|1129204261|gb|OLQ06785.1|Oleandomycin polyketide synthase, modules 5 and 6 [Symbiodinium microadriaticum]	OLQ06785	3.21E-22
328	ost_siam_bh1_contig_69036	phthiocerol synthesis polyketide synthase type i	871	gi|1129185842|gb|OLP92121.1|Phthiocerol synthesis polyketide synthase type I PpsA [Symbiodinium microadriaticum]	OLP92121	9.11E-32
329	ost_siam_bh1_contig_70166	erythronolide modules 5 and 6	703	gi|1129204260|gb|OLQ06784.1|Erythronolide synthase, modules 5 and 6 [Symbiodinium microadriaticum]	OLQ06784	1.07E-93
330	ost_siam_bh1_contig_70918	polyketide synthase	510	gi|1129213410|gb|OLQ14315.1|Polyketide synthase PksN [Symbiodinium microadriaticum]	OLQ14315	3.80E-33
331	ost_siam_bh1_contig_71416	oleandomycin polyketide modules 5 and 6	280	gi|1129204261|gb|OLQ06785.1|Oleandomycin polyketide synthase, modules 5 and 6 [Symbiodinium microadriaticum]	OLQ06785	1.43E-42

332	ost_siam_bh1_contig_71937	erythronolide modules 5 and 6	994	gi|1129204260|gb|OLQ06784.1|Erythronolide synthase, modules 5 and 6 [Symbiodinium microadriaticum]	OLQ06784	2.06E-136
333	ost_siam_bh1_contig_74353	oleandomycin polyketide modules 5 and 6	224	gi|1129204261|gb|OLQ06785.1|Oleandomycin polyketide synthase, modules 5 and 6 [Symbiodinium microadriaticum]	OLQ06785	5.30E-23
334	ost_siam_bh1_contig_74833	erythronolide modules 5 and 6	294	gi|1129204260|gb|OLQ06784.1|Erythronolide synthase, modules 5 and 6 [Symbiodinium microadriaticum]	OLQ06784	4.84E-31
335	ost_siam_bh1_contig_75049	erythronolide modules 5 and 6	383	gi|1129204260|gb|OLQ06784.1|Erythronolide synthase, modules 5 and 6 [Symbiodinium microadriaticum]	OLQ06784	1.67E-15
336	ost_siam_bh1_contig_75098	type i fatty acid partial	691	gi|672294693|gb|KFG59574.1|putative type I fatty acid synthase, partial [Toxoplasma gondii RUB]	KFG59574	5.52E-54
337	ost_siam_bh1_contig_75287	polyketide synthase	314	gi|917362857|ref|WP_051969569.1|polyketide synthase [Kitasatospora azatica]	WP_051969569	1.12E-11
338	ost_siam_bh1_contig_75345	oleandomycin polyketide modules 5 and 6	279	gi|1129204261|gb|OLQ06785.1|Oleandomycin polyketide synthase, modules 5 and 6 [Symbiodinium microadriaticum]	OLQ06785	1.51E-29
339	ost_siam_bh1_contig_7569	6-methylsalicylic acid synthase	1920	gi|1129199127|gb|OLQ02654.1|6-methylsalicylic acid synthase [Symbiodinium microadriaticum]	OLQ02654	5.14E-144
340	ost_siam_bh1_contig_75701	polyketide synthase	475	gi|1129213410|gb|OLQ14315.1|Polyketide synthase PksN [Symbiodinium microadriaticum]	OLQ14315	2.79E-53
341	ost_siam_bh1_contig_76408	erythronolide modules 5 and 6	590	gi|1129176947|gb|OLP85322.1|Erythronolide synthase, modules 5 and 6 [Symbiodinium microadriaticum]	OLP85322	7.26E-92
342	ost_siam_bh1_contig_76836	hybrid non-ribosomal peptide synthetase type i polyketide synthase	347	gi|928955487|ref|WP_053980166.1|hybrid non-ribosomal peptide synthetase/type I polyketide synthase [Marinagarivorans algicola]	WP_053980166	6.34E-10
343	ost_siam_bh1_contig_77065	type i fatty acid	389	gi|1129204261|gb|OLQ06785.1|Oleandomycin polyketide synthase, modules 5 and 6 [Symbiodinium microadriaticum]	OLQ06785	9.46E-27
344	ost_siam_bh1_contig_77147	erythronolide modules 5 and partial	298	gi|1129158909|gb|OLP74521.1|Erythronolide synthase, modules 5 and 6, partial [Symbiodinium microadriaticum]	OLP74521	4.88E-31
345	ost_siam_bh1_contig_77932	type i polyketide synthase	682	gi|414091049|gb|AFW98412.1|type I polyketide synthase [Alexandrium ostenfeldii]	AFW98412	4.96E-31
346	ost_siam_bh1_contig_79523	erythronolide modules 5 and 6	364	gi|1129204260|gb|OLQ06784.1|Erythronolide synthase, modules 5 and 6 [Symbiodinium microadriaticum]	OLQ06784	2.06E-20
347	ost_siam_bh1_contig_79614	erythronolide modules 5 and 6	688	gi|1129176947|gb|OLP85322.1|Erythronolide synthase, modules 5 and 6 [Symbiodinium	OLP85322	1.81E-47

348	ost_siam_bh1_contig_80315	phthiocerol synthesis polyketide synthase type i	349	gi|1129192690|gb|OLP97452.1|Phthiocerol synthesis polyketide synthase type I PpsC [Symbiodinium microadriaticum]	OLP97452	8.28E-17
349	ost_siam_bh1_contig_80498	hybrid non-ribosomal peptide synthetase type i polyketide synthase	321	gi|1129204261|gb|OLQ06785.1|Oleandomycin polyketide synthase, modules 5 and 6 [Symbiodinium microadriaticum]	OLQ06785	2.60E-28
350	ost_siam_bh1_contig_80540	oleandomycin polyketide modules 5 and 6	414	gi|1129204261|gb|OLQ06785.1|Oleandomycin polyketide synthase, modules 5 and 6 [Symbiodinium microadriaticum]	OLQ06785	2.99E-61
351	ost_siam_bh1_contig_81045	erythronolide modules 5 and partial	214	gi|1129158909|gb|OLP74521.1|Erythronolide synthase, modules 5 and 6, partial [Symbiodinium microadriaticum]	OLP74521	2.21E-21
352	ost_siam_bh1_contig_8116	6-methylsalicylic acid synthase	2181	gi|1129199127|gb|OLQ02654.1|6-methylsalicylic acid synthase [Symbiodinium microadriaticum]	OLQ02654	0
353	ost_siam_bh1_contig_81749	6-methylsalicylic acid synthase	475	gi|1129199127|gb|OLQ02654.1|6-methylsalicylic acid synthase [Symbiodinium microadriaticum]	OLQ02654	7.49E-44
354	ost_siam_bh1_contig_82701	polyketide synthase	496	gi|504914906|ref|WP_015102008.1|polyketide synthase [Saccharothrix espanaensis] >gi|407884253|emb|CCH31896.1| Polyketide synthase [Saccharothrix espanaensis DSM 44229]	WP_015102008	1.68E-19
355	ost_siam_bh1_contig_82790	erythronolide modules 5 and 6	203	gi|1129204260|gb|OLQ06784.1|Erythronolide synthase, modules 5 and 6 [Symbiodinium microadriaticum]	OLQ06784	1.84E-13
356	ost_siam_bh1_contig_82995	polyketide partial	257	gi|1129204260|gb|OLQ06784.1|Erythronolide synthase, modules 5 and 6 [Symbiodinium microadriaticum]	OLQ06784	7.61E-12
357	ost_siam_bh1_contig_84315	oleandomycin polyketide modules 5 and 6	329	gi|1129204261|gb|OLQ06785.1|Oleandomycin polyketide synthase, modules 5 and 6 [Symbiodinium microadriaticum]	OLQ06785	1.11E-33
358	ost_siam_bh1_contig_84396	erythronolide modules 5 and 6	337	gi|1129204260|gb|OLQ06784.1|Erythronolide synthase, modules 5 and 6 [Symbiodinium microadriaticum]	OLQ06784	1.94E-43
359	ost_siam_bh1_contig_85898	erythronolide modules 5 and 6	261	gi|1129204260|gb|OLQ06784.1|Erythronolide synthase, modules 5 and 6 [Symbiodinium microadriaticum]	OLQ06784	7.33E-26
360	ost_siam_bh1_contig_85949	erythronolide modules 5 and 6	204	gi|1129204260|gb|OLQ06784.1|Erythronolide synthase, modules 5 and 6 [Symbiodinium microadriaticum]	OLQ06784	1.17E-18
361	ost_siam_bh1_contig_87	phthiocerol synthesis polyketide	3722	gi|1129192690|gb|OLP97452.1|Phthiocerol synthesis polyketide synthase type I PpsC	OLP97452	0

		synthase type i		[Symbiodinium microadriaticum]		
362	ost_siam_bh1_contig_87200	erythronolide modules 5 and 6	344	gi|1129204261|gb|OLQ06785.1|Oleandomycin polyketide synthase, modules 5 and 6 [Symbiodinium microadriaticum]	OLQ06785	4.17E-34
363	ost_siam_bh1_contig_87524	oleandomycin polyketide modules 5 and 6	246	gi|1129204261|gb|OLQ06785.1|Oleandomycin polyketide synthase, modules 5 and 6 [Symbiodinium microadriaticum]	OLQ06785	8.65E-19
364	ost_siam_bh1_contig_88163	erythronolide modules 5 and 6	234	gi|1129204260|gb|OLQ06784.1|Erythronolide synthase, modules 5 and 6 [Symbiodinium microadriaticum]	OLQ06784	7.28E-22
365	ost_siam_bh1_contig_8817	type i polyketide synthase-like protein kb6736	3939	gi|148536485|gb|ABQ85802.1|type I polyketide synthase-like protein KB6736 [Karenia brevis]	ABQ85802	0
366	ost_siam_bh1_contig_9472	phthiocerol synthesis polyketide synthase type i	2068	gi|1129192690|gb|OLP97452.1|Phthiocerol synthesis polyketide synthase type I PpsC [Symbiodinium microadriaticum]	OLP97452	2.04E-173
367	ost_siam_bh1_contig_9473	phthiocerol synthesis polyketide synthase type i	1131	gi|595389390|gb|AHM27264.1|polyketide synthase 1 [Gambierdiscus polynesiensis] >gi|595389401|gb|AHM27265.1| polyketide synthase 2 [Gambierdiscus polynesiensis]	AHM27264	7.16E-69
368	ost_siam_bh1_contig_9619	type i polyketide synthase	3079	gi|414091049|gb|AFW98412.1|type I polyketide synthase [Alexandrium ostenfeldii]	AFW98412	0
369	ost_siam_bh1_contig_9942	type i polyketide synthase-like protein kb1008	3853	gi|148536473|gb|ABQ85796.1|type I polyketide synthase-like protein KB1008 [Karenia brevis]	ABQ85796	2.58E-137
370	ost_sp8_her26_contig_10364	polyketide partial	4815	gi|941355194|dbj|BAT21731.1|polyketide synthase, partial [Karenia mikimotoi]	BAT21731	1.40E-74
371	ost_sp8_her26_contig_11189	6-phosphofructokinase 7	5492	gi|1129173556|gb|OLP82883.1|6-phosphofructokinase 7 [Symbiodinium microadriaticum]	OLP82883	7.51E-111
372	ost_sp8_her26_contig_11742	erythronolide modules 3 and 4	3786	gi|1129199229|gb|OLQ02729.1|Erythronolide synthase, modules 3 and 4 [Symbiodinium microadriaticum]	OLQ02729	8.54E-133
373	ost_sp8_her26_contig_11756	type i polyketide synthase-like protein kb1008	3864	gi|148536473|gb|ABQ85796.1|type I polyketide synthase-like protein KB1008 [Karenia brevis]	ABQ85796	1.89E-135
374	ost_sp8_her26_contig_11794	6-phosphofructokinase 7	4928	gi|1129173556|gb|OLP82883.1|6-phosphofructokinase 7 [Symbiodinium microadriaticum]	OLP82883	8.72E-51
375	ost_sp8_her26_contig_12913	type i fatty acid	2292	gi|873227372|emb|CEM18661.1|unnamed protein product, partial [Vitrella brassicaformis CCMP3155]	CEM18661	2.45E-68

376	ost_sp8_her26_contig_13156	phthiocerol synthesis polyketide synthase type i	3982	gi|1129192690|gb|OLP97452.1|Phthiocerol synthesis polyketide synthase type I PpsC [Symbiodinium microadriaticum]	OLP97452	0
377	ost_sp8_her26_contig_13191	phthiocerol synthesis polyketide synthase type i	3944	gi|1129192690|gb|OLP97452.1|Phthiocerol synthesis polyketide synthase type I PpsC [Symbiodinium microadriaticum]	OLP97452	1.02E-151
378	ost_sp8_her26_contig_13273	phthiocerol synthesis polyketide synthase type i	3997	gi|1129192690|gb|OLP97452.1|Phthiocerol synthesis polyketide synthase type I PpsC [Symbiodinium microadriaticum]	OLP97452	6.21E-167
379	ost_sp8_her26_contig_13312	polyketide synthase	955	gi|505164431|ref|WP_015351533.1|polyketide synthase [Myxococcus stipitatus] >gi|441490583|gb|AGC47278.1| polyketide synthase [Myxococcus stipitatus DSM 14675]	WP_015351533	7.95E-04
380	ost_sp8_her26_contig_13420	phthiocerol synthesis polyketide synthase type i	4170	gi|1129192690|gb|OLP97452.1|Phthiocerol synthesis polyketide synthase type I PpsC [Symbiodinium microadriaticum]	OLP97452	0
381	ost_sp8_her26_contig_13525	polyketide partial	3710	gi|941355192|dbj|BAT21730.1|polyketide synthase, partial [Karenia mikimotoi]	BAT21730	0
382	ost_sp8_her26_contig_14440	oleandomycin polyketide modules 5 and 6	3907	gi|1129204261|gb|OLQ06785.1|Oleandomycin polyketide synthase, modules 5 and 6 [Symbiodinium microadriaticum]	OLQ06785	0
383	ost_sp8_her26_contig_14479	polyketide partial	3504	gi|941355192|dbj|BAT21730.1|polyketide synthase, partial [Karenia mikimotoi]	BAT21730	2.66E-143
384	ost_sp8_her26_contig_14666	oleandomycin polyketide modules 5 and 6	2390	gi|1129204261|gb|OLQ06785.1|Oleandomycin polyketide synthase, modules 5 and 6 [Symbiodinium microadriaticum]	OLQ06785	0
385	ost_sp8_her26_contig_14885	erythronolide modules 5 and 6	6277	gi|1129204260|gb|OLQ06784.1|Erythronolide synthase, modules 5 and 6 [Symbiodinium microadriaticum]	OLQ06784	0
386	ost_sp8_her26_contig_15922	type i polyketide synthase	1879	gi|1129213410|gb|OLQ14315.1|Polyketide synthase PksN [Symbiodinium microadriaticum]	OLQ14315	4.41E-60
387	ost_sp8_her26_contig_15997	mycocerosic acid synthase-like	6286	gi|1126186736|ref|XP_019626097.1|PREDICTED: uncharacterized protein LOC109471257 [Branchiostoma belcheri] >gi|1126186738|ref|XP_019626098.1| PREDICTED: uncharacterized protein LOC109471257 [Branchiostoma belcheri]	XP_019626097	1.96E-104
388	ost_sp8_her26_contig_1612	polyketide synthase as3d906	2296	gi|712037596|gb|AIW63289.1|polyketide synthase AS3D906 [Azadinium spinosum]	AIW63289	0
389	ost_sp8_her26_contig_1673	type i polyketide synthase-like protein kb6736	4122	gi|148536485|gb|ABQ85802.1|type I polyketide synthase-like protein KB6736 [Karenia brevis]	ABQ85802	2.75E-147

390	ost_sp8_her26_contig_17232	polyketide synthase as3d902	2998	gi|712037589|gb|AIW63286.1|polyketide synthase AS3D902 [Azadinium spinosum]	AIW63286	0
391	ost_sp8_her26_contig_17707	6-methylsalicylic acid synthase	566	gi|1129199127|gb|OLQ02654.1|6-methylsalicylic acid synthase [Symbiodinium microadriaticum]	OLQ02654	2.42E-59
392	ost_sp8_her26_contig_17732	type i polyketide synthase-like protein kb6736	4173	gi|148536485|gb|ABQ85802.1|type I polyketide synthase-like protein KB6736 [Karenia brevis]	ABQ85802	1.47E-171
393	ost_sp8_her26_contig_18171	phthiocerol synthesis polyketide synthase type i	3851	gi|1129192690|gb|OLP97452.1|Phthiocerol synthesis polyketide synthase type I PpsC [Symbiodinium microadriaticum]	OLP97452	3.77E-159
394	ost_sp8_her26_contig_18672	equisetin related	311	gi|1129204260|gb|OLQ06784.1|Erythronolide synthase, modules 5 and 6 [Symbiodinium microadriaticum]	OLQ06784	6.03E-25
395	ost_sp8_her26_contig_18903	type i polyketide synthase	3039	gi|414091049|gb|AFW98412.1|type I polyketide synthase [Alexandrium ostenfeldii]	AFW98412	0
396	ost_sp8_her26_contig_20264	phthiocerol synthesis polyketide synthase type i	3974	gi|1129192690|gb|OLP97452.1|Phthiocerol synthesis polyketide synthase type I PpsC [Symbiodinium microadriaticum]	OLP97452	0
397	ost_sp8_her26_contig_20852	type i polyketide synthase-like protein kb1008	2771	gi|148536473|gb|ABQ85796.1|type I polyketide synthase-like protein KB1008 [Karenia brevis]	ABQ85796	1.02E-133
398	ost_sp8_her26_contig_20927	6-methylsalicylic acid synthase	1986	gi|1129199127|gb|OLQ02654.1|6-methylsalicylic acid synthase [Symbiodinium microadriaticum]	OLQ02654	8.51E-139
399	ost_sp8_her26_contig_21145	phthiocerol synthesis polyketide synthase type i	3864	gi|1129206593|gb|OLQ08682.1|Phthiocerol synthesis polyketide synthase type I PpsD [Symbiodinium microadriaticum]	OLQ08682	9.41E-141
400	ost_sp8_her26_contig_21254	phthiocerol synthesis polyketide synthase type i	3587	gi|1129192690|gb|OLP97452.1|Phthiocerol synthesis polyketide synthase type I PpsC [Symbiodinium microadriaticum]	OLP97452	0
401	ost_sp8_her26_contig_21619	polyketide synthase 1	2007	gi|595389390|gb|AHM27264.1|polyketide synthase 1 [Gambierdiscus polynesiensis] >gi|595389401|gb|AHM27265.1| polyketide synthase 2 [Gambierdiscus polynesiensis]	AHM27264	8.53E-106
402	ost_sp8_her26_contig_21735	phthiocerol synthesis polyketide synthase type i	3902	gi|1129192690|gb|OLP97452.1|Phthiocerol synthesis polyketide synthase type I PpsC [Symbiodinium microadriaticum]	OLP97452	3.72E-175
403	ost_sp8_her26_contig_22124	phthiocerol synthesis polyketide synthase type i	3808	gi|1129192690|gb|OLP97452.1|Phthiocerol synthesis polyketide synthase type I PpsC [Symbiodinium microadriaticum]	OLP97452	9.18E-174
404	ost_sp8_her26_contig_22418	phthiocerol synthesis polyketide synthase type i	3823	gi|1129198474|gb|OLQ02136.1|Phthiocerol synthesis polyketide synthase type I PpsD [Symbiodinium microadriaticum]	OLQ02136	0

405	ost_sp8_her26_contig_23187	phthiocerol synthesis polyketide synthase type i	3870	gi|1129192690|gb|OLP97452.1|Phthiocerol synthesis polyketide synthase type I PpsC [Symbiodinium microadriaticum]	OLP97452	0
406	ost_sp8_her26_contig_2383	sodium calcium exchanger 3	4118	gi|1129171706|gb|OLP81580.1|Sodium/calcium exchanger 3 [Symbiodinium microadriaticum]	OLP81580	1.02E-153
407	ost_sp8_her26_contig_2502	phthiocerol synthesis polyketide synthase type i	3957	gi|1129192690|gb|OLP97452.1|Phthiocerol synthesis polyketide synthase type I PpsC [Symbiodinium microadriaticum]	OLP97452	0
408	ost_sp8_her26_contig_253	phthiocerol synthesis polyketide synthase type i	4255	gi|1129192690|gb|OLP97452.1|Phthiocerol synthesis polyketide synthase type I PpsC [Symbiodinium microadriaticum]	OLP97452	0
409	ost_sp8_her26_contig_25827	phthiocerol synthesis polyketide synthase type i	1756	gi|1129206593|gb|OLQ08682.1|Phthiocerol synthesis polyketide synthase type I PpsD [Symbiodinium microadriaticum]	OLQ08682	1.22E-123
410	ost_sp8_her26_contig_26035	erythronolide modules 5 and 6	4977	gi|1129204260|gb|OLQ06784.1|Erythronolide synthase, modules 5 and 6 [Symbiodinium microadriaticum]	OLQ06784	0
411	ost_sp8_her26_contig_26036	phthiocerol synthesis polyketide synthase type i	1228	gi|1129192690|gb|OLP97452.1|Phthiocerol synthesis polyketide synthase type I PpsC [Symbiodinium microadriaticum]	OLP97452	5.47E-43
412	ost_sp8_her26_contig_27497	phthiocerol synthesis polyketide synthase type i	3637	gi|1129192690|gb|OLP97452.1|Phthiocerol synthesis polyketide synthase type I PpsC [Symbiodinium microadriaticum]	OLP97452	0
413	ost_sp8_her26_contig_28549	6-methylsalicylic acid synthase	1981	gi|1129199127|gb|OLQ02654.1|6-methylsalicylic acid synthase [Symbiodinium microadriaticum]	OLQ02654	5.86E-115
414	ost_sp8_her26_contig_290	type i polyketide synthase	3037	gi|414091049|gb|AFW98412.1|type I polyketide synthase [Alexandrium ostenfeldii]	AFW98412	0
415	ost_sp8_her26_contig_2980	type i polyketide synthase-like protein kb1008	3784	gi|148536473|gb|ABQ85796.1|type I polyketide synthase-like protein KB1008 [Karenia brevis]	ABQ85796	3.93E-159
416	ost_sp8_her26_contig_30161	type i polyketide synthase	1596	gi|1120681711|gb|OKP26492.1|hypothetical protein BST62_23750, partial [Serratia marcescens subsp. marcescens]	OKP26492	4.12E-66
417	ost_sp8_her26_contig_30392	type i polyketide synthase	918	gi|414091049|gb|AFW98412.1|type I polyketide synthase [Alexandrium ostenfeldii]	AFW98412	1.03E-90
418	ost_sp8_her26_contig_30746	phthiocerol synthesis polyketide synthase type i	3539	gi|1129192690|gb|OLP97452.1|Phthiocerol synthesis polyketide synthase type I PpsC [Symbiodinium microadriaticum]	OLP97452	3.40E-180
419	ost_sp8_her26_contig_31365	phthiocerol synthesis polyketide synthase type i	4058	gi|1129192690|gb|OLP97452.1|Phthiocerol synthesis polyketide synthase type I PpsC [Symbiodinium microadriaticum]	OLP97452	0
420	ost_sp8_her26_contig_3271	phthiocerol synthesis polyketide	3787	gi|1129198474|gb|OLQ02136.1|Phthiocerol synthesis polyketide synthase type I PpsD	OLQ02136	0

		synthase type i		[Symbiodinium microadriaticum]		
421	ost_sp8_her26_contig_33435	type i fatty acid partial	4883	gi|1129204259|gb|OLQ06783.1|Delta(9)-fatty-acid desaturase fat-7 [Symbiodinium microadriaticum]	OLQ06783	0
422	ost_sp8_her26_contig_33540	polyketide partial	2863	gi|941355192|dbj|BAT21730.1|polyketide synthase, partial [Karenia mikimotoi]	BAT21730	1.39E-124
423	ost_sp8_her26_contig_3419	polyketide partial	3673	gi|941355192|dbj|BAT21730.1|polyketide synthase, partial [Karenia mikimotoi]	BAT21730	4.36E-144
424	ost_sp8_her26_contig_34777	erythronolide modules 5 and 6	5259	gi|1129204260|gb|OLQ06784.1|Erythronolide synthase, modules 5 and 6 [Symbiodinium microadriaticum]	OLQ06784	0
425	ost_sp8_her26_contig_35094	calcium-dependent protein kinase 2	3691	gi|1129164416|gb|OLP76751.1|Calcium-dependent protein kinase 2 [Symbiodinium microadriaticum]	OLP76751	5.77E-162
426	ost_sp8_her26_contig_3556	phthiocerol synthesis polyketide synthase type i	2275	gi|1129180700|gb|OLP88203.1|Phthiocerol synthesis polyketide synthase type I PpsC [Symbiodinium microadriaticum]	OLP88203	0
427	ost_sp8_her26_contig_36504	polyketide synthase	6673	gi|260807166|ref|XP_002598380.1|hypothetical protein BRAFLDRAFT_96863 [Branchiostoma floridae] >gi|229283652|gb|EEN54392.1| hypothetical protein BRAFLDRAFT_96863 [Branchiostoma floridae]	XP_002598380	1.22E-133
428	ost_sp8_her26_contig_36893	type i polyketide synthase-like protein kb1008	3687	gi|148536473|gb|ABQ85796.1|type I polyketide synthase-like protein KB1008 [Karenia brevis]	ABQ85796	2.46E-154
429	ost_sp8_her26_contig_37429	phthiocerol synthesis polyketide synthase type i	3831	gi|1129206593|gb|OLQ08682.1|Phthiocerol synthesis polyketide synthase type I PpsD [Symbiodinium microadriaticum]	OLQ08682	2.02E-131
430	ost_sp8_her26_contig_395	phthiocerol synthesis polyketide synthase type i	4810	gi|1129192690|gb|OLP97452.1|Phthiocerol synthesis polyketide synthase type I PpsC [Symbiodinium microadriaticum]	OLP97452	1.52E-130
431	ost_sp8_her26_contig_4011	polyketide synthase 1	4042	gi|595389390|gb|AHM27264.1|polyketide synthase 1 [Gambierdiscus polynesiensis] >gi|595389401|gb|AHM27265.1| polyketide synthase 2 [Gambierdiscus polynesiensis]	AHM27264	0
432	ost_sp8_her26_contig_40922	phthiocerol synthesis polyketide synthase type i	4200	gi|1129192690|gb|OLP97452.1|Phthiocerol synthesis polyketide synthase type I PpsC [Symbiodinium microadriaticum]	OLP97452	0
433	ost_sp8_her26_contig_41031	erythronolide modules 5 and 6	1581	gi|1129204260|gb|OLQ06784.1|Erythronolide synthase, modules 5 and 6 [Symbiodinium microadriaticum]	OLQ06784	0
434	ost_sp8_her26_contig_41477	type i polyketide synthase	605	gi|750915009|gb|KIJ74914.1|hypothetical protein SD81_24665 [Tolypothrix campylonemoides VB511288]	KIJ74914	1.34E-20

435	ost_sp8_her26_contig_41815	oleandomycin polyketide modules 5 and 6	524	gi|1129204261|gb|OLQ06785.1|Oleandomycin polyketide synthase, modules 5 and 6 [Symbiodinium microadriaticum]	OLQ06785	4.48E-84
436	ost_sp8_her26_contig_41958	type i fatty acid	3793	gi|1129204261|gb|OLQ06785.1|Oleandomycin polyketide synthase, modules 5 and 6 [Symbiodinium microadriaticum]	OLQ06785	0
437	ost_sp8_her26_contig_43551	phthiocerol synthesis polyketide synthase type i	1833	gi|1129173060|gb|OLP82529.1|Phthiocerol synthesis polyketide synthase type I PpsD [Symbiodinium microadriaticum]	OLP82529	6.70E-70
438	ost_sp8_her26_contig_4471	phthiocerol synthesis polyketide synthase type i	1725	gi|1129192690|gb|OLP97452.1|Phthiocerol synthesis polyketide synthase type I PpsC [Symbiodinium microadriaticum]	OLP97452	7.13E-109
439	ost_sp8_her26_contig_46194	type i polyketide synthase-like protein kb1008	1603	gi|148536473|gb|ABQ85796.1|type I polyketide synthase-like protein KB1008 [Karenia brevis]	ABQ85796	7.19E-64
440	ost_sp8_her26_contig_47154	phthiocerol synthesis polyketide synthase type i	818	gi|1129200442|gb|OLQ03682.1|Phthiocerol synthesis polyketide synthase type I PpsA [Symbiodinium microadriaticum]	OLQ03682	1.74E-49
441	ost_sp8_her26_contig_48128	polyketide synthase	795	gi|1129213410|gb|OLQ14315.1|Polyketide synthase PksN [Symbiodinium microadriaticum]	OLQ14315	2.83E-88
442	ost_sp8_her26_contig_48384	phthiocerol synthesis polyketide synthase type i	1551	gi|1129173060|gb|OLP82529.1|Phthiocerol synthesis polyketide synthase type I PpsD [Symbiodinium microadriaticum]	OLP82529	6.29E-26
443	ost_sp8_her26_contig_50159	oleandomycin polyketide modules 5 and 6	2768	gi|1129204261|gb|OLQ06785.1|Oleandomycin polyketide synthase, modules 5 and 6 [Symbiodinium microadriaticum]	OLQ06785	0
444	ost_sp8_her26_contig_50585	type i polyketide synthase	484	gi|917120614|ref|WP_051727326.1|type I polyketide synthase [Streptomyces griseus]	WP_051727326	2.07E-09
445	ost_sp8_her26_contig_53011	polyketide partial	2267	gi|873240533|emb|CEL93322.1|unnamed protein product, partial [Vitrella brassicaformis CCMP3155]	CEL93322	1.12E-75
446	ost_sp8_her26_contig_55524	amp-dependent synthetase and partial	593	gi|557242469|emb|CDJ53564.1|hypothetical protein EBH_0017680 [Eimeria brunetti]	CDJ53564	2.94E-14
447	ost_sp8_her26_contig_55850	oleandomycin polyketide modules 5 and 6	716	gi|1129204261|gb|OLQ06785.1|Oleandomycin polyketide synthase, modules 5 and 6 [Symbiodinium microadriaticum]	OLQ06785	4.09E-60
448	ost_sp8_her26_contig_57433	6-phosphofructokinase 7	423	gi|1129173556|gb|OLP82883.1|6-phosphofructokinase 7 [Symbiodinium microadriaticum]	OLP82883	3.73E-04
449	ost_sp8_her26_contig_57448	type i polyketide synthase-like protein kb1008	1892	gi|148536473|gb|ABQ85796.1|type I polyketide synthase-like protein KB1008 [Karenia brevis]	ABQ85796	7.70E-45

450	ost_sp8_her26_contig_59405	phthiocerol synthesis polyketide synthase type i	519	gi|1129173060|gb|OLP82529.1|Phthiocerol synthesis polyketide synthase type I PpsD [Symbiodinium microadriaticum]	OLP82529	5.17E-14
451	ost_sp8_her26_contig_6004	phthiocerol synthesis polyketide synthase type i	4039	gi|1129192690|gb|OLP97452.1|Phthiocerol synthesis polyketide synthase type I PpsC [Symbiodinium microadriaticum]	OLP97452	0
452	ost_sp8_her26_contig_60648	type i polyketide synthase	890	gi|501599639|ref|WP_012599249.1|type I polyketide synthase [Cyanothece sp. PCC 7424] >gi|218171573|gb|ACK70306.1| Beta-ketoacyl synthase [Cyanothece sp. PCC 7424]	WP_012599249	3.85E-51
453	ost_sp8_her26_contig_6198	polyketide partial	3379	gi|148536473|gb|ABQ85796.1|type I polyketide synthase-like protein KB1008 [Karenia brevis]	ABQ85796	0
454	ost_sp8_her26_contig_6270	type i polyketide synthase-like protein kb1008	3493	gi|148536473|gb|ABQ85796.1|type I polyketide synthase-like protein KB1008 [Karenia brevis]	ABQ85796	1.51E-123
455	ost_sp8_her26_contig_65725	type i polyketide synthase	355	gi|522173924|ref|WP_020682473.1|type I polyketide synthase [Marinobacterium rhizophilum]	WP_020682473	1.85E-15
456	ost_sp8_her26_contig_65893	phthiocerol synthesis polyketide synthase type i	529	gi|1129200879|gb|OLQ04015.1|hypothetical protein AK812_SmicGene12952 [Symbiodinium microadriaticum]	OLQ04015	6.28E-24
457	ost_sp8_her26_contig_6664	type i polyketide synthase-like protein kb6736	3895	gi|148536485|gb|ABQ85802.1|type I polyketide synthase-like protein KB6736 [Karenia brevis]	ABQ85802	0
458	ost_sp8_her26_contig_67029	erythronolide modules 5 and 6	691	gi|1129204260|gb|OLQ06784.1|Erythronolide synthase, modules 5 and 6 [Symbiodinium microadriaticum]	OLQ06784	2.39E-79
459	ost_sp8_her26_contig_67109	erythronolide modules 5 and 6	303	gi|1129204260|gb|OLQ06784.1|Erythronolide synthase, modules 5 and 6 [Symbiodinium microadriaticum]	OLQ06784	2.64E-42
460	ost_sp8_her26_contig_67665	erythronolide modules 5 and 6	1077	gi|1129204260|gb|OLQ06784.1|Erythronolide synthase, modules 5 and 6 [Symbiodinium microadriaticum]	OLQ06784	6.43E-57
461	ost_sp8_her26_contig_70800	erythronolide modules 5 and 6	327	gi|1129204260|gb|OLQ06784.1|Erythronolide synthase, modules 5 and 6 [Symbiodinium microadriaticum]	OLQ06784	1.19E-26
462	ost_sp8_her26_contig_72061	erythronolide modules 5 and 6	804	gi|1129204261|gb|OLQ06785.1|Oleandomycin polyketide synthase, modules 5 and 6 [Symbiodinium microadriaticum]	OLQ06785	8.49E-103
463	ost_sp8_her26_contig_7225	6-methylsalicylic acid synthase	2102	gi|1129199127|gb|OLQ02654.1|6-methylsalicylic acid synthase [Symbiodinium microadriaticum]	OLQ02654	4.43E-143
464	ost_sp8_her26_contig_72826	erythronolide modules 5 and 6	1846	gi|1129176947|gb|OLP85322.1|Erythronolide synthase, modules 5 and 6 [Symbiodinium microadriaticum]	OLP85322	3.19E-147

465	ost_sp8_her26_contig_73774	polyketide synthase	346	gi|746308868|ref|WP_039355760.1|polyketide synthase [Pectobacterium carotovorum] >gi|734565012|gb|KHN90690.1| cfa6 protein [Pectobacterium carotovorum subsp. actinidiae]	WP_039355760	6.17E-04
466	ost_sp8_her26_contig_7384	erythronolide modules 5 and 6	7947	gi|1129204260|gb|OLQ06784.1|Erythronolide synthase, modules 5 and 6 [Symbiodinium microadriaticum]	OLQ06784	0
467	ost_sp8_her26_contig_7389	phthiocerol synthesis polyketide synthase type i	4499	gi|1129192690|gb|OLP97452.1|Phthiocerol synthesis polyketide synthase type I PpsC [Symbiodinium microadriaticum]	OLP97452	0
468	ost_sp8_her26_contig_74120	polyketide synthase	571	gi|551577402|ref|XP_005774327.1|polyketide synthase [Emiliania huxleyi CCMP1516] >gi|485626133|gb|EOD21898.1| polyketide synthase [Emiliania huxleyi CCMP1516]	XP_005774327	7.59E-17
469	ost_sp8_her26_contig_74474	oleandomycin polyketide modules 5 and 6	249	gi|1129204261|gb|OLQ06785.1|Oleandomycin polyketide synthase, modules 5 and 6 [Symbiodinium microadriaticum]	OLQ06785	1.63E-05
470	ost_sp8_her26_contig_7529	6-methylsalicylic acid synthase	1497	gi|1129199127|gb|OLQ02654.1|6-methylsalicylic acid synthase [Symbiodinium microadriaticum]	OLQ02654	3.27E-151
471	ost_sp8_her26_contig_75870	phthiocerol synthesis polyketide synthase type i	693	gi|1129179242|gb|OLP87029.1|hypothetical protein AK812_SmicGene31792 [Symbiodinium microadriaticum]	OLP87029	7.71E-13
472	ost_sp8_her26_contig_7589	polyketide synthase as3d906	2812	gi|712037596|gb|AIW63289.1|polyketide synthase AS3D906 [Azadinium spinosum]	AIW63289	0
473	ost_sp8_her26_contig_76461	beta-ketoacyl synthase	348	gi|1111846760|gb|OJJ29662.1|hypothetical protein ASPWEDRAFT_294248 [Aspergillus wentii DTO 134E9]	OJJ29662	1.17E-05
474	ost_sp8_her26_contig_76621	oleandomycin polyketide modules 5 and 6	676	gi|1129204261|gb|OLQ06785.1|Oleandomycin polyketide synthase, modules 5 and 6 [Symbiodinium microadriaticum]	OLQ06785	1.18E-71
475	ost_sp8_her26_contig_78178	polyketide synthase family partial	438	gi|62768237|gb|AAY00025.1|SA1_PKSA [uncultured bacterial symbiont of Discodermia dissoluta]	AAY00025	2.06E-17
476	ost_sp8_her26_contig_7852	phthiocerol synthesis polyketide synthase type i	4515	gi|1129179243|gb|OLP87030.1|Phthiocerol synthesis polyketide synthase type I PpsC [Symbiodinium microadriaticum]	OLP87030	8.33E-61
477	ost_sp8_her26_contig_7971	type i polyketide synthase	2728	gi|414091051|gb|AFW98413.1|type I polyketide synthase [Alexandrium ostenfeldii]	AFW98413	0
478	ost_sp8_her26_contig_804	polyketide synthase	8397	gi|981434975|ref|WP_059644920.1|polyketide synthase [Burkholderia ubonensis] >gi|976380332|gb|KVC85624.1| polyketide synthase [Burkholderia ubonensis]	WP_059644920	0

479	ost_sp8_her26_contig_8228	polyketide partial	3573	gi|148536473|gb|ABQ85796.1|type I polyketide synthase-like protein KB1008 [Karenia brevis]	ABQ85796	0
480	ost_sp8_her26_contig_84676	oleandomycin polyketide modules 5 and 6	407	gi|1129204261|gb|OLQ06785.1|Oleandomycin polyketide synthase, modules 5 and 6 [Symbiodinium microadriaticum]	OLQ06785	1.17E-13
481	ost_sp8_her26_contig_84915	polyketide partial	284	gi|294992559|gb|ADF57406.1|polyketide synthase, partial [uncultured bacterium]	ADF57406	5.79E-14
482	ost_sp8_her26_contig_85320	phthiocerol synthesis polyketide synthase type i	1102	gi|1129179243|gb|OLP87030.1|Phthiocerol synthesis polyketide synthase type I PpsC [Symbiodinium microadriaticum]	OLP87030	1.57E-13
483	ost_sp8_her26_contig_8682	type i polyketide synthase-like protein kb1008	3651	gi|148536473|gb|ABQ85796.1|type I polyketide synthase-like protein KB1008 [Karenia brevis]	ABQ85796	1.28E-163
484	ost_sp8_her26_contig_87173	polyketide synthase	337	gi|1129167743|gb|OLP78851.1|Polyketide synthase PksN [Symbiodinium microadriaticum]	OLP78851	8.40E-15
485	ost_sp8_her26_contig_8803	phthiocerol synthesis polyketide synthase type i	4023	gi|1129192690|gb|OLP97452.1|Phthiocerol synthesis polyketide synthase type I PpsC [Symbiodinium microadriaticum]	OLP97452	0
486	ost_sp8_her26_contig_89026	polyketide partial	320	gi|818211090|gb|AKG25417.1|putative polyketide synthase, partial [Hematodinium sp. SG-2015]	AKG25417	5.99E-26
487	ost_sp8_her26_contig_90006	type i polyketide synthase	244	gi|916526511|ref|WP_051137607.1|type I polyketide synthase [Amycolatopsis alba]	WP_051137607	1.36E-05
488	ost_sp8_her26_contig_9177	type i polyketide synthase-like protein kb6736	3977	gi|148536485|gb|ABQ85802.1|type I polyketide synthase-like protein KB6736 [Karenia brevis]	ABQ85802	0
489	ost_sp8_her26_contig_9459	erythronolide modules 5 and 6	5508	gi|1129204261|gb|OLQ06785.1|Oleandomycin polyketide synthase, modules 5 and 6 [Symbiodinium microadriaticum]	OLQ06785	0
490	ost_sp8_her26_contig_946	type i polyketide synthase-like protein kb6736	3973	gi|148536485|gb|ABQ85802.1|type I polyketide synthase-like protein KB6736 [Karenia brevis]	ABQ85802	0
491	ost_sp8_her26_contig_9581	phthiocerol synthesis polyketide synthase type i	4065	gi|1129192690|gb|OLP97452.1|Phthiocerol synthesis polyketide synthase type I PpsC [Symbiodinium microadriaticum]	OLP97452	0
492	ost_sp8_her26_contig_9734	6-phosphofructokinase 7	5869	gi|1129173556|gb|OLP82883.1|6-phosphofructokinase 7 [Symbiodinium microadriaticum]	OLP82883	1.07E-53

S17 List of putatively annotated entities featured in the non-targeted metabolite analyses of *Ostreopsis* cf. *ovata* HER27, *Ostreopsis* cf. *siamensis* BH1, *Ostreopsis rhodesae* HER26 and *Coolia malayensis* MAB.

S. no.	m/z	Retention time (min)	Formula	Compound ID
1	401.3419287	16.65866667	$C_{27}H_{46}O_3$	CSID30797200
2	407.214948	14.91938333	$C_{22}H_{34}O_4$	CSID10475009
3	407.2767979	12.4207	$C_{24}H_{40}O_6$	CSID23327317
4	418.2230032	9.586983333	$C_{19}H_{30}O_6$	CSID28419942
5	419.1835157	11.1108	$C_{22}H_{30}O_5$	CSID10274700
6	423.1129992	10.44135	$C_{20}H_{13}N_3O_4$	CSID29215652
7	430.2463655	4.644666667	$C_{28}H_{35}NO_5$	CSID10276162
8	438.2619021	10.53393333	$C_{25}H_{37}NO_4$	CSID30797270
9	446.2307282	3.13935	$C_{28}H_{33}NO_5$	CSID30797268
10	450.2768099	14.15641667	$C_{24}H_{35}NO_5$	CSID30797274
11	453.2743339	15.76738333	$C_{27}H_{42}O_3$	CSID30797197
12	455.2149319	14.63988333	$C_{21}H_{29}NO_6$	CSID29214215
13	455.3124879	11.15643333	$C_{27}H_{44}O_4$	CSID30797199
14	471.3473882	16.0195	$C_{30}H_{48}O_5$	CSID30797325
15	492.3532892	10.13496667	$C_{28}H_{44}O_3$	CSID10398054
16	500.3958675	12.83018333	$C_{28}H_{50}O_6$	CSID29215563
17	504.3606881	16.79573333	$C_{28}H_{46}O_5$	CSID8157412
18	508.3271397	10.1014	$C_{26}H_{42}O_7$	CSID30797320
19	517.3871447	15.04476667	$C_{32}H_{54}O_6$	CSID30797323
20	518.3762596	16.7879	$C_{27}H_{48}O_8$	CSID30797293
21	524.3253661	6.380833333	$C_{26}H_{42}O_8$	CSID30771313
22	531.1934355	10.43391667	$C_{12}H_{14}N_4O_2$	CSID29215649
23	539.3533079	14.34253333	$C_{16}H_{26}O_2$	CSID30771302
24	553.2969728	14.2241	$C_{28}H_{42}N_4O_6$	CSID27023622
25	578.3690137	9.893166667	$C_{30}H_{48}O_8$	CSID30797321
26	583.1868485	10.56275	$C_{15}H_{16}N_2O_3$	CSID29215648
27	585.3741989	12.02176667	$C_{31}H_{52}O_{10}$	CSID8546530
28	587.2293305	15.65416667	$C_{15}H_{18}N_2O_3$	CSID30770806
29	590.3914703	12.57073333	$C_{36}H_{44}N_4O$	CSID5006904
30	611.2182071	12.03015	$C_{16}H_{18}N_2O_3$	CSID29215647
31	615.2451976	13.35085	$C_{30}H_{40}O_{12}$	CSID30771310
32	617.4196213	10.40866667	$C_{29}H_{53}N_5O_8$	CSID30797237
33	627.2094473	14.1488	$C_{32}H_{38}O_{15}$	CSID10476959
34	638.4202765	15.35511667	$C_{40}H_{52}O_4$	CSID4444636
35	649.3935929	14.47471667	$C_{28}H_{51}N_5O_8$	CSID30797239
36	651.2306882	14.36976667	$C_{31}H_{40}O_{16}$	CSID30797288
37	676.4210709	14.47471667	$C_{41}H_{61}NO_9$	CSID9654410

38	681.4129888	15.41723333	$C_{42}H_{58}O_6$	CSID21864745
39	683.3561836	15.07878333	$C_{33}H_{57}NaO_{12}S$	CSID30797295
40	687.4102051	7.683416667	$C_{35}H_{51}N_5O_8$	CSID30771155
41	793.4875092	16.67408333	$C_{47}H_{70}O_{11}$	CSID30797246
42	800.5299247	16.28903333	$C_{38}H_{74}NO_{12}P$	CSID30797251
43	832.486833	5.933233333	$C_{46}H_{65}N_5O_9$	CSID30797331
44	849.4302347	16.30425	$C_{44}H_{68}O_{13}$	CSID30797282
45	877.4612606	17.20193333	$C_{48}H_{68}N_2O_{15}$	CSID30797151
46	879.4551247	6.01145	$C_{24}H_{36}O_6$	CSID29215571
47	947.4749341	10.81105	$C_{51}H_{66}N_8O_{12}$	CSID30797183
48	958.5543274	10.28005	$C_{48}H_{75}N_7O_{13}$	CSID17214520
49	1044.558505	10.84091667	$C_{54}H_{78}N_2O_{17}$	CSID30797147
50	1131.555377	10.16011667	$C_{54}H_{73}N_{11}O_{12}$	CSID30797185

Original publications from thesis

Molecular phylogeny, morphology and toxigenicity of *Ostreopsis* cf. *siamensis* (Dinophyceae) from temperate south-east Australia

Arjun Verma,[1]* Mona Hoppenrath,[3] Tim Harwood,[4] Steve Brett,[2] Lesley Rhodes[4] and Shauna Murray[1]

[1]Plant Functional Biology and Climate Change Cluster, University of Technology Sydney, Sydney, New South Wales, [2]Microalgal Services, Ormond, Victoria, Australia, [3]Senckenberg am Meer, Senckenberg Research Institute, German Center for Marine Biodiversity Research (DZMB), Wilhelmshaven, Germany and [4]Cawthron Institute, Nelson, New Zealand

SUMMARY

Ostreopsis is a genus of dinoflagellates that includes species producing palytoxin and structurally related compounds. The distribution of *Ostreopsis* species in Australia is largely unknown, but they have been reported from north Queensland (18°S) to Tasmania (41–43°S). *Ostreopsis* spp. have been recurrently reported from estuaries around New South Wales, with persistent occurrences in Merimbula Lake inlet throughout the year. We isolated and characterized a strain of *Ostreopsis* cf. *siamensis* using light and scanning electron microscopy as well as molecular sequences of small subunit (SSU), large subunit (LSU) and ITS regions of ribosomal DNA. The strain grew significantly faster in low nutrient concentrations. Palytoxin-like compounds were produced by the strain, as determined by chemical analysis, and the LD_{50} of the cell extract by intraperitoneal injection in mice was 25.1 mg kg^{-1}. This is the first comprehensive molecular, morphological and toxicological study of an *Ostreopsis* species from Australian waters. Increasing reports of *Ostreopsis* from temperate waters suggest an empirical need to expand the knowledge of their diversity and distribution to aid aquaculture monitoring in Australian estuaries.

Key words: *Ostreopsis*, palytoxin, taxonomy, toxicity.

INTRODUCTION

Species of the marine epiphytic genus *Ostreopsis* Schmidt (1902) occur in tropical and sub-tropical waters attached to coral rubble, macroalgae, seagrass and sand. Nine *Ostreopsis* species have been described based on size and thecal plate patterns (Fukuyo 1981; Besada *et al.* 1982; Norris *et al.* 1985; Faust & Morton 1995; Faust *et al.* 1996; Faust 1999). *Ostreopsis* species have been recorded globally, and more frequently from temperate regions in recent years (Rhodes 2011). Many *Ostreopsis* species produce highly toxic, complex non-peptide marine compounds in the palytoxin (PLTX, $C_{129}H_{223}N_3O_{54}$) group of compounds and also PLTX analogues (including Ostreocin-D, ovatoxins a-g and isobaric palytoxin) (Usami *et al.* 1995; Ciminiello *et al.* 2008, 2012b; García-Altares *et al.* 2014).

PLTX and/or its analogues have been associated with human poisonings through the consumption of contaminated crabs (*Demania* sp. and *Lophozozymus* sp.), serranid fish (*Epinephelus* sp.), parrotfish (*Scarus ovifrons* Temminck & Schlegel) and smoked mackerel (*Decapterus macrosoma* Bleeker) (Alcala *et al.* 1988; Kodama *et al.* 1989; Taniyama *et al.* 2003; Tubaro *et al.* 2011). Clupeotoxism, caused by consuming tropical clupeoids such as sardines (*Herklotsichthys quadrimaculatus* Rüppell), has been suggested to be related to PLTX, however, this is not yet demonstrated (Onuma *et al.* 1999; Tubaro *et al.* 2011). In the Mediterranean Basin, blooms of *Ostreopsis ovata* Fukuyo have been associated with human skin and eye irritations and respiratory illnesses, due to exposure to toxic aerosols and lysed cells (Durando *et al.* 2007; Tichadou *et al.* 2010; Ciminiello *et al.* 2014). *Ostreopsis* blooms in Greece and France have caused shellfish contamination in the Mediterranean (Aligizaki *et al.* 2008; Malagoli *et al.* 2008; Amzil *et al.* 2012). Accumulation of low amounts of PLTX-like compounds has been demonstrated in mussels (*Perna canaliculus* Gmelin), scallops (*Pecten novaezealandia* Reeve) and pacific oysters (*Crassostrea gigas* Thunberg) in New Zealand (Rhodes *et al.* 2002). Blooms of *Ostreopsis siamensis* Schmidt in northern New Zealand have been reported to coincide with large scale sea urchin mortalities (Shears & Ross 2009) highlighting the detrimental ecological impact of such blooms on benthic communities and the marine food web.

Distinguishing *Ostreopsis* species from one another in field samples based upon morphological differences is very difficult, due to their similarity in size, shape and thecal plate patterns, and also their co-existence in the environment (Penna *et al.* 2005). Almost all described *Ostreopsis* species are distinctly flattened, with a broadly oval to ovate shape, tapering ventrally in apical view. They all have thecal patterns that broadly fit with the description of the type species, *O. siamensis*, with the exception of *O. heptagona* Norris, Bomber et Balech (David *et al.* 2013; Hoppenrath *et al.* 2014). Schmidt (1902) originally reported *O. siamensis* as possessing a rounded apical structure but having an elongated and ventrally pointed epitheca. The cells were reported as coarsely porous, with relatively large sized pores that were visible with light microscopy (Schmidt 1902). Fukuyo (1981) displayed an undulated cingulum, also presented by Schmidt (1902), and reported a single pore size scattered all over the

thecal plates for *O. siamensis*. Fukuyo (1981) also proposed a new species, *O. lenticularis* Fukuyo with two pore sizes and no undulation in lateral view. Faust *et al.* (1996) reported larger sized cells with two kinds of pores for *O. siamensis*. However, lack of information about the undulation of the cingulum, led to uncertainty about the identity of Faust's specimens as *O. siamensis*. Some more recent reports of *Ostreopsis* specimens have described cells of various sizes but these studies have lacked molecular genetic data (Table 1). The identities of the strains were therefore uncertain. Penna *et al.* (2005) described *Ostreopsis* cf. *siamensis* from the Italian coast and Catalan Sea with a single class of thecal pore sizes but no undulation in their morphology (Penna *et al.* 2005). David *et al.* (2013) reported *Ostreopsis* cf. *siamensis* from the Atlantic Iberian peninsula with two sizes of thecal pores with the smaller pore size class in the internal side of the theca as previously reported by Aligizaki and Nikolaidis (2006) from North Aegean Sea.

Identification of *Ostreopsis* species using molecular sequencing, in particular, ribosomal RNA (rDNA) genes and internal transcribed spacer regions (ITS), has enhanced the accuracy of detection and is increasingly being used with microscopy to resolve the cryptic variations amongst *Ostreopsis* species (Leaw *et al.* 2001; Penna *et al.* 2005, 2010; Sato *et al.* 2011; Tawong *et al.* 2014). Morphologically cryptic species have been reported within clades of *Ostreopsis* species as more isolates from Atlantic, Mediterranean Sea and the Pacific regions are being sequenced (Sato *et al.* 2011; David *et al.* 2013; Penna *et al.* 2014).

In Australia, *O. siamensis* was first reported from tropical waters of Queensland (Heron Island, Lady Elliot Island and Hoffmans Rocks) based on morphological characteristics and the extraction of water-soluble toxins from isolated cultures similar to *O. siamensis* from Okinawa, Japan (Holmes *et al.* 1988). An intensive survey of toxic dinoflagellates around the Great Barrier Reef (18–20°S) reported high concentrations of *O. ovata*, *O. siamensis*, *O. lenticularis* and *O. heptagona* using light microscopy at Townsville, Magnetic and Orpheus Islands (18–20°S) (Heimann *et al.* 2009). *Ostreopsis siamensis* has also been reported as far south as the temperate lagoons of Tasmania (41–43°S) where sea surface temperatures can reach 9°C (Pearce *et al.* 2001). Monitoring of the New South Wales coast (28–37°S) between 2005 and 2009 revealed the recurrent presence of *Ostreopsis* species in 26 of 31 estuaries. However, cells were not identified to species level during this programme (Ajani *et al.* 2013).

No comprehensive toxicological, morphological and molecular studies have been carried out on *Ostreopsis* species in Australia. The aim of this study was to morphologically and genetically identify an *Ostreopsis* sp. and characterize the growth and morphometric features of the cultured strain. The strain was tested for the presence of PLTX-like compounds using liquid chromatography-mass spectrometry (LC–MS/MS) analysis and the acute toxicity of the sample extract was determined *via* mouse-bioassay.

MATERIALS AND METHODS

Site description

Merimbula Lake (36°53′S, 149°55′E) (Fig. 1) is an open coastal lake with a permanently open entrance and an inlet channel forming a large marine delta that opens into the main basin with a deep center and deep navigational channels. Extensive seagrass meadows occupy over 50% of the lake bed, forming the fourth largest seagrass bed on the New South Wales South Coast. The beds consist mostly of strap weed (*Posidonia australis* Hooker), eel grass (*Zostera capricorni* Ascherson) and paddleweed (*Halophila* spp.) (West *et al.* 1985; Williams *et al.* 2006).

Merimbula Lake is the fourth most productive estuary for the cultivation and sales of Sydney rock oysters (*Saccostrea glomerata* Gould) since 2010, along the coast of New South Wales (NSW Department of Primary Industries, 2013 to 2014). Oyster farms are mainly in the southern part of the lake, which is shallower than the main basin. The inlet also provides for a wide variety of recreational fishing activities.

Table 1. Geographic, morphological and molecular reports of *Ostreopsis siamensis/Ostreopsis* cf. *siamensis*

Site	Length (DV)	Width (W)	DV: W ratio	Pores	Ribotype reported	References
Koh Chang, Gulf of Thailand	90 F	NA	NA	1 size	No	Schmidt (1902)
Ryukyu Islands, Japan	60–100 F	45–90 F	NA	1 size	No	Fukuyo (1981)
East China Sea, Mascareignes Archipelago, Caribbean Sea	108–123 F	76–86 F	1.42	0.5 and 0.1	No	Faust *et al.* (1996)
Northland, New Zealand	30–68 C 60–85 F	20–55 C 38–45 F	NA	0.08–0.1 and 0.18–0.38	No	Chang *et al.* (2000) and Rhodes *et al.* (2000)
North Aegean Sea, Greece	36–66 F	24–50 F	NA	0.23–0.29	No	Aligizaki & Nikolaidis (2006)
Tyrrhenian Sea, Italy	50–75 C 63–90 F	38–62 C 34–56 F	NA	0.11–0.56	Yes	Penna *et al.* (2005)
Peter the Great bay, Russia	63–78 F	36–54 F	1.3–1.9	0.14–0.32	No	Selina & Levchenko (2011)
Cantabrian Sea, Bay of Biscay	51–67 C	33–56 C	NA	NA	Yes	Laza-Martinez *et al.* (2011)
Galé, Portugal	55–75.5 F	27–56 F	1.1–2.1	0.07–0.13 and 0.15–0.39	Yes	David *et al.* (2013)
San Sebastian, Spain	52–72 F	36–57 F	1.1–1.8	0.07–0.13 and 0.15–0.39	Yes	David *et al.* (2013)
Heron Island, Australia	36–60 C 88–115 F	26–51 C 64–93 F	1–1.8 C 1.2–1.6 F	NA	No	Holmes *et al.* (1988)
Isolabella, Italy	50–70 C	35–55 C	1.35	NA	Yes	Ciminiello *et al.* (2013)
Merimbula Australia	34–47 C	24.5–42 C	1.1–1.7	2 sizes	Yes	This Study

C, Cultured isolates; F, Field samples; NA, Data not available.

Sample collection and culture establishment

In May 2012 seagrass samples (*Zostera* sp.) were collected from approximately 1 m depth. At the time of sample collection, sea surface temperature was 17°C. Salinities in Merimbula Lake inlet commonly range from 30 to 35. Samples were placed in plastic bags containing local seawater and shaken vigorously to detach the epiphytic microalgal cells. The epiphytic suspension was then passed through a 100 μm mesh filter to remove larger fauna and debris (Kohli *et al.* 2014). Using a glass micropipette, a single *Ostreopsis* cell was isolated from this suspension under an inverted microscope and transferred to a drop of clean filtered seawater. The transfer was repeated five times until no nano- and pico-planktonic cells were observed in the vicinity of the cell under the inverted microscope. A non-axenic monoclonal culture was established in f/2 medium (Guillard 1975).

The strain was grown in 50 mL sterile tissue culture flasks (Becton Dickinson, Sydney, Australia) in both f/2 and f/10 media at 18°C and salinity of 35 under the photo illumination of 60–100 μmol photons m^{-2} s^{-1} and 12 : 12 h light-dark cycle. It has now been deposited at the Cawthron Institute Culture Collection of Microalgae, New Zealand (CICCM: CAWD203).

Fortnightly water samples were collected from a depth of 50 cm and preserved with Lugol's iodine solution. Harmful phytoplankton cells were counted and identified using phase contrast light microscopy (Ajani *et al.* 2013). *Ostreopsis* cells were identified to genus level only for the monitoring program.

Light microscopy

Living cells of interest were picked using a Leica DMIL inverted microscope (Leica Microsystems GmbH, Wetzlar, Germany), placed on an object slide and observed with a Leica DMRB (Leica Microsystems GmbH) equipped with differential interference contrast and epifluorescence optics at 400 and 640 times magnification with oil immersion objectives. Digital photos were taken using a Leica DFC420C camera (Leica Microsystems GmbH).

Scanning electron microscopy (SEM)

For SEM, the culture was fixed with Lugol's solution for several weeks. Cells were treated with hydrogen peroxide (H_2O_2) for 1 day and then were placed on a 5 μm Millipore filter (Merck Millipore Darmstadt, Germany), rinsed in distilled water, and dehydrated in a series of increasing ethanol concentrations (30%, 50%, 70%, 85%, 90%, and 100%), followed by chemical drying with hexamethyldisilazane at room temperature. When completely dry, the sample was mounted on a stub and sputter coated with gold-palladium (Bal-Tec SCD 050; BAL-TEC Präparations-gerätevertrieb, Wallof, Germany). Cells were observed using a Tescan VEGA3 microscope (Elekronen-Optik-Service GmbH, Dortmund, Germany) at 15 kV.

DNA extraction, PCR amplification and sequencing

DNA was extracted using FastDNA Spin kit for Soil (MP Biomedicals, Solon, USA), according to the manufacturer's protocol. The extracted DNA was visualized on 1% agarose gel and quantified using a Nanodrop ND-1000 (NanoDrop Technologies, Wilmington, DE, USA). The near complete SSU rDNA, the D1/D3 and D8/D10 regions of the LSU rDNA, ITS and 5.8S rDNA gene regions (ITS1/5.8S/ITS2) were amplified and sequenced using primers as listed in Appendix S1 in the Supporting Information.

All PCR reactions were performed in 25 μL reaction volumes containing 12.5 μL 2 × x Immomix (Bioline, Sydney, Australia), 7.5 pmol of each primer, 1 μg $μL^{-1}$ of BSA (Biolabs, Arundel, Australia), 1 μL of template DNA and PCR grade water to give the final volume. Thermocycling conditions consisted of an initial denaturing step of 95°C for 10 min, followed by 30 cycles of 95°C for 20 s, 30 s annealing (see Appendix S1 in the Supporting Information), 72°C for 1 min and a final extension of 72°C for 7 min. PCR products were purified with DNA Clean and Concentrator (Zymo Research, Irvine, USA) according to the manufacturer's protocol. The PCR products were sequenced using a commercial service (Macrogen Inc., Seoul, Korea).

Sequence alignment and phylogenetic analysis

Analyses on SSU rDNA, ITS1/5.8S/ITS2, D1/D3 and D8/D10 region of LSU rDNA were conducted separately. The forward and reverse sequences were trimmed, aligned and visually refined using BioEdit v7.2.5 (Hall 1999). The obtained sequences were aligned with reference sequences retrieved from GenBank (see Appendix S2 in the Supporting Information). Multiple sequence alignments were performed using ClustalW v1.6 program as implemented in MEGA v6 (Tamura *et al.* 2013) and manual inspection. Phylogenetic analysis was performed using both a maximum likelihood (ML) and Bayesian inference (BI) approach.

ML trees were produced in MEGA v6 using Tamura 3 (T92) + G + I with five gamma categories substitution model for all sequence analyses. Substitution models were selected for each dataset based on lowest Bayesian Information criterion as a measure of the relative quality of the models. Nodal support of the ML tree was estimated *via* bootstrap algorithm with 1000 replications. Bayesian analysis was performed using MrBayes v3.2.2 (Ronquist & Huelsenbeck 2003) as implemented in Geneious v6 (Kearse *et al.* 2012) using general time reversible (GTR) + gamma model for all analyses. Four independent Markov Chain Monte Carlo simulations were run simultaneously for 2 000 000 generations. Trees were sampled every 1000 generations and 1000 trees were discarded as burn- in.

Growth rate and cell size

To compare the strain growth rates in f/2 and f/10 batch cultures, 500 mL Erlenmeyer flasks containing 300 mL media were placed in an 18°C incubator under the photo illumination of 60–100 μmol photons m^{-2} s^{-1} and 12 : 12 h light–dark cycle. Triplicates were inoculated with exponentially growing cells (starting cell amount 60 000 cells) from respective stock cultures. Flasks within the incubator were randomly positioned during the experiment. Every 2 days, the flasks

were gently shaken before collecting 3 mL of culture volume to determine cell abundance in triplicates using a Sedgwick-Rafter chamber. The extracted culture volume was treated with 4 mM hydrochloric acid to dissolve mucous aggregates without disrupting *Ostreopsis* cells (Guerrini *et al.* 2010). Specific growth rates (μ) were calculated using the slope of natural log of cell number against culture day during exponential growth phase. Differences in growth rates between different media were tested using one way analysis of variance (ANOVA) in SPSS v22.0 (IBM, Armonk, USA).

Cell dimensions were measured under 400 × magnifications and analyzed using a calibrated scale in the eyepiece of an inverted microscope Eclipse TS100 (Nikon, Hilton, Australia). Cells in exponential growth phase were fixed in 1% Lugols to measure the depth = dorsoventral diameter (DV) and transdiameter width (W) using ImageJ v1.48 (Rasband 1997–2013).

Toxin analysis *via* LC-MS/MS and bioassays

Ostreopsis culture grown in f/10 medium was harvested in late stationary phase (Day 20) *via* centrifugation (50 mL; 2300 g; 10 min; room temperature) and the cell pellet was freeze dried. Screening for PLTX-like compounds was conducted using a quantitative LC–MS/MS method at the Cawthron Institute, New Zealand as described in Selwood *et al.* (2012). This analytical approach monitors substructures generated by the oxidative cleavage, using periodic acid, of vicinal diol groups present in the intact toxins. Periodate oxidation of vicinal diols results in cleavage of carbon-carbon bonds *via* a cyclic transition state with formation of two aldehyde-containing fragments. It yields an amino aldehyde common to known palytoxins, ovatoxins and ostreocins, and an amide aldehyde that varies depending on the toxin type.

The cell pellet was resuspended in 4 mL of methanol-water (1 : 1 v/v) and then ultrasonicated for 20 min in a 59 kHz sonication bath (model 160HT, Soniclean Pty, Thebarton, Australia). The sample was centrifuged at 3000 g for 5 min and 2 mL of supernatant was loaded onto the solid phase extraction cartridges for on-column periodic acid oxidation. PLTX standards (5, 10, 20 and 50 ng mL^{-1}) were processed to generate a calibration curve. The limit of detection was determined to be 0.5 ng mL^{-1} for the PLTX amine fragment. The relative standard deviation of repeatability for LC-MS of oxidized PLTX standards were <10% and <8% for amino aldehyde and amide aldehyde, respectively, at 1 or 2 ng mL^{-1}, making this method suitable for monitoring trace levels of PLTX and/or its analogues (Selwood *et al.* 2012). Several additional multiple reaction monitoring transitions were also included to monitor oxidative cleavage fragments from other known PLTX-like compounds, such as bishomopalytoxin.

Mouse bioassays were conducted at AgResearch, Hamilton, New Zealand, using methanolic extract after removing all of the solvent from the cell pellet. The pellet was extracted using 5 mL methanol taken to dryness under nitrogen. This extract was then resuspended in 1% Tween 60 in saline and administered by intraperitoneal injection in Swiss albino mice (body weight 18–20 g) at various dose levels. LD$_{50}$ values were determined by the up and down method according to Organization for economic Cooperation and Development Guideline 425 (OECD 2006). All mouse experiments were approved by the Ruakura Animal Ethics Committee.

RESULTS

Morphology

The strongly anterio-posteriorly flattened cells of the cultured *Ostreopsis* were drop/tear-shaped to nearly round (extremely wide) and ventrally tapering (Fig. 2a,d,e). Smaller cells had a more symmetrical ovate shape (Fig. 2c). Cells are 34–47 µm (41 ± 3 (SE), $n = 49$) long (in DV) and 24.5–42 µm (33 ± 4, $n = 49$) wide (in W), and varied from 1.1 to 1.7 (1.3 ± 0.1, $n = 49$) in DV/W ratio. Cells are densely packed with golden-brown chloroplasts, except for the ventral area (Fig. 2a–e). The nucleus is located dorsally (Fig. 2a,d). Cells with one (Fig. 2c) or two pusules (Fig. 2d) are observed. The curved, long and narrow apical pore complex is located parallel to the left dorsal cell margin (Fig. 2e). The cingulum is narrow and straight (not shown).

The plate formula is APC, 3′, 7″, 6/7c, 6–7s, 5‴, 2⁗ (Figs 2f,g, 3–4). Thecal plates are smooth with scattered pores of two size classes. The larger 'pores' are shown to be depressions with few small pores inside, which are best visible on plate inside views (Fig. 3d). Small pores are recorded only in low numbers, not evenly distributed on the plates and not recognizable in all cells (Fig. 3d). The first apical plate (1′) is long, hexagonal and located nearly in the center of the epitheca (Figs 2f, 3a). The third precingular (3″) and third apical (3′) plates are in contact. The fifth precingular plate (5″) is hexagonal and not connected to the 1′ plate (Figs 2f, 3a). The slightly curved and narrow apical pore plate with slit-
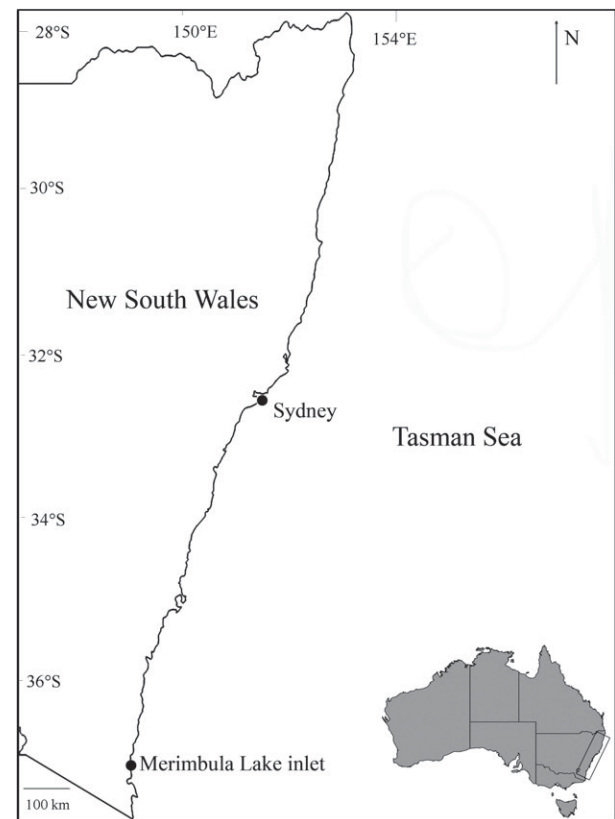

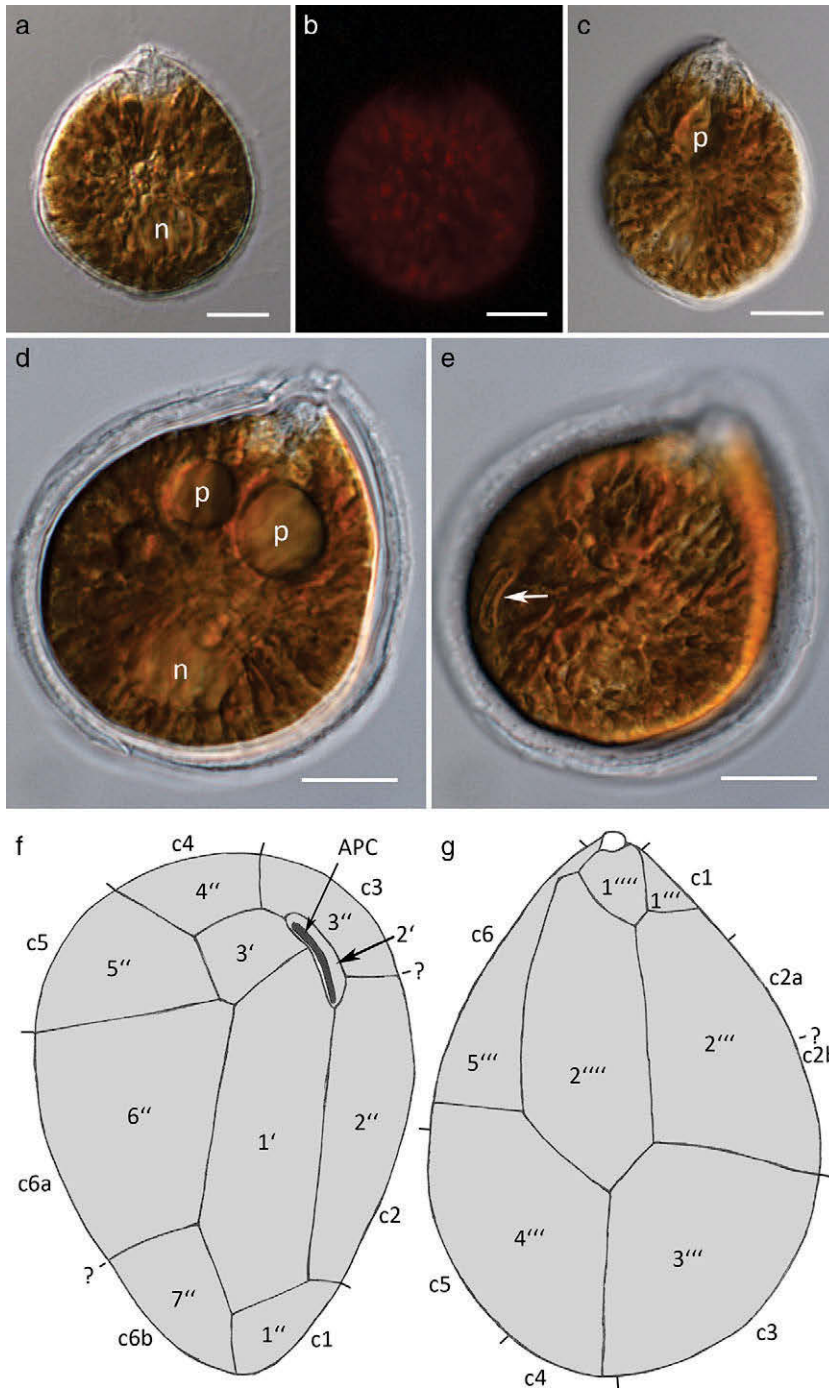**Fig. 1.** Map showing Merimbula lake inlet, south-east New South Wales, Australia.

Fig. 2. *Ostreopsis* cf. *siamensis* CAWD203 from Merimbula taken using light microscopy; (a, c–e) differential interference contrast showing the general morphology and (b) epifluorescence demonstrating the autofluorescence of the chloroplasts; (a) typical very wide cell, note the colourless ventral area and the dorsal nucleus (n); (b) chloroplast fluorescence of the cell shown in a; (c) smaller and narrower cell with one pusule (p) visible in the ventral cell half connected to the ventral area; (d, e) same cell in different focus; (d) note the nucleus (n) in the dorsal area and the two pusules (p); (e) The apical pore complex (arrow) in the dorsal area; (f, g) line drawings illustrate the thecal plate pattern of the epitheca (f) and hypotheca (g) including cingular plates. The scale bars represent 10 μm. '?' represent verification of cingular plate borders.

like pore is about 7.2–8.4 μm long (Fig. 3a,c). The plate margin connecting the third (3″) and fourth (4‴) postcingular plates is nearly equal to the dorsoventral axis (Figs 2g, 3b).

Both plates are relatively large and not markedly different in size. Cingular plates are difficult to determine; six or seven plates are recognized (Fig. 2f,g). In two cases it looked like the second and sixth plate respectively could split into two plates. More observations are needed for the cingular plates. Broken cells allowed the determination of the sulcal plates (Fig. 4). Six or seven sulcal plates were observed (Fig. 4), with seven plates including the split of the right anterior sulcal plate (sda) into two plates.

Phylogeny

Maximum likelihood and BI analyses conducted on SSU, LSU (D1/D3 and D8/D10) and ITS1/5.8S/ITS2 rDNA regions had the same topology and placed the Australian strain in a strongly supported clade with *Ostreopsis* cf. *siamensis* strains from Europe and New Zealand (only the ML trees are shown;
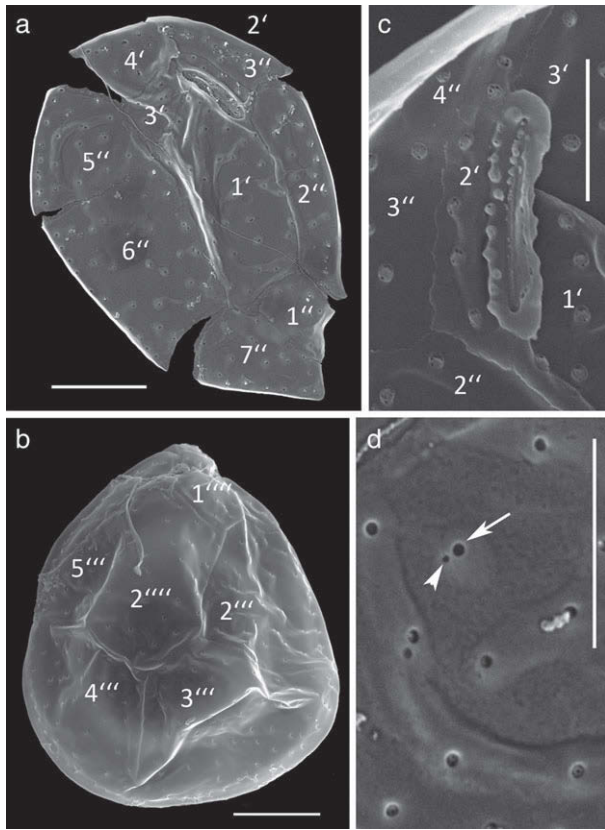
Fig. 3. Scanning electron micrographs (SEM) of *Ostreopsis* cf. *siamensis* CAWD203 from Merimbula; (a) epitheca; (b) hypotheca; (c) inside view of the apical pore complex and surrounding plates; (d) plate detail showing two size classes of pores, small (arrowhead) and large (arrow) ones. Scale bars represent 10 μm in a, b; 5 μm in c, d.

BI = 1.00, ML = 100 for LSU rDNA and BI = 0.76, ML = 99 for ITS) (Figs 5–6) (Accession numbers KT868526, KT868527 and KT868529). The ITS1/5.8S/ITS2 and D8/D10 LSU rDNA trees showed nine distinct clades and subsequent geographical sub-clades amongst the genus *Ostreopsis* as previously described in Sato *et al.* (2011) and Tawong *et al.* (2014) (Figs 5a, 6a).

The D1/D3 LSU rDNA sequences for *Ostreopsis* sp. four and *Ostreopsis* sp. three were not available in the GenBank but the topology of the phylogenetic tree was similar to that of the D8/D10 LSU rDNA analysis (Fig. 5). No *Ostreopsis* cf. *siamensis* SSU rDNA sequences were available in the database (Fig. 6b). When aligned with the other *Ostreopsis* SSU rDNA sequences, *Ostreopsis* cf. *siamensis* showed 6.8% differences to *Ostreopsis* cf. *ovata* (Korea) and 6.5% differences to *Ostreopsis* cf. *ovata* (Malaysia) (see Appendix S3 in the Supporting Information).

Culturing and growth rates

Ostreopsis cf. *siamensis* grew successfully in f/10 and f/2 and displayed a typical growth curve (Fig. 7). Aberrant cell shapes were observed in f/2 culture and the strain showed a growth rate of 0.24 ± 0.006 div day^{-1} (exponential phase between

days 7 and 16) and a maximum yield of 23 700 cells mL^{-1}. The cell density remained high and relatively constant during the whole stationary phase. Cultures maintained in f/10 media grew faster, with a growth rate of 0.39 ± 0.01 (ANOVA, $P < 0.001$) (exponential phase between days 5 and 11). The cell density declined rapidly after reaching a maximum yield of 28 100 cells mL^{-1}.

Distribution and abundance

Routine monitoring of plankton samples from New South Wales shellfish growing areas during 2005–2015 detected *Ostreopsis* bloom-like episodes (upto 750–1000 cells L^{-1}) at Merimbula Inlet, in October 2006, October 2010 and September and November 2013. High abundances consistently occurred in the warmer months (October to December), but sparse cells were persistent in April to August (austral winter) (Fig. 8).

Toxin analysis and toxicity

LC-MS/MS analysis of the oxidized cell extract showed presence of the amino aldehyde fragment, common to all known palytoxin, ovatoxin and ostreocin analogues. However, the PLTX amide fragment was not detected suggesting that another structurally related analogue gave rise to the amine fragment observed (Fig. 9). The total amount of PLTX-like compounds was determined as 4.62 ng (total 26 700 cells) resulting in an estimate of 0.17 pg. cell^{-1}.

The LD$_{50}$ of *Ostreopsis* cf. *siamensis* extract by intraperitoneal injection in mice was 25.1 mg kg^{-1} (95% confidence interval of 14.0–33.2 mg kg^{-1}). The mice became hunched and lethargic soon after dosing, and remained so during the day of dosing. Loss of appetite and significant amount of weight loss was reported over the next 3 days. By the fifth day since dosing, the condition and appetite had improved, and they recovered over the remainder of the 2 weeks observation period. The appearance and behavior of mice was normal during this time, however, adhesions between the liver and diaphragm and between the liver and stomach were noted at necropsy indicating an irritant effect, but no other macroscopic changes were recorded. At a higher dose, the hind legs became paralyzed and extended, and they died after 7.5 h without any reported abnormalities in necropsy.

DISCUSSION

This is the first study to characterize the morphology, molecular phylogeny, toxigenicity and growth characteristics of an *Ostreopsis* species from Australian waters. The *Ostreopsis* strain isolated from Merimbula was identical in ITS/5.8S regions to strains identified as *Ostreopsis* cf. *siamensis* from the Atlantic/Mediterranean region and New Zealand, which was further confirmed with D1/D3 and D8/D10 regions of LSU rDNA.

In this study, we documented the smallest cell size ranges yet reported for the species. In comparison to published records of *Ostreopsis* cf. *siamensis*, this population has a straight cingulum path in lateral view as described by David *et al.* (2013) and Penna *et al.* (2005), in contrast to the
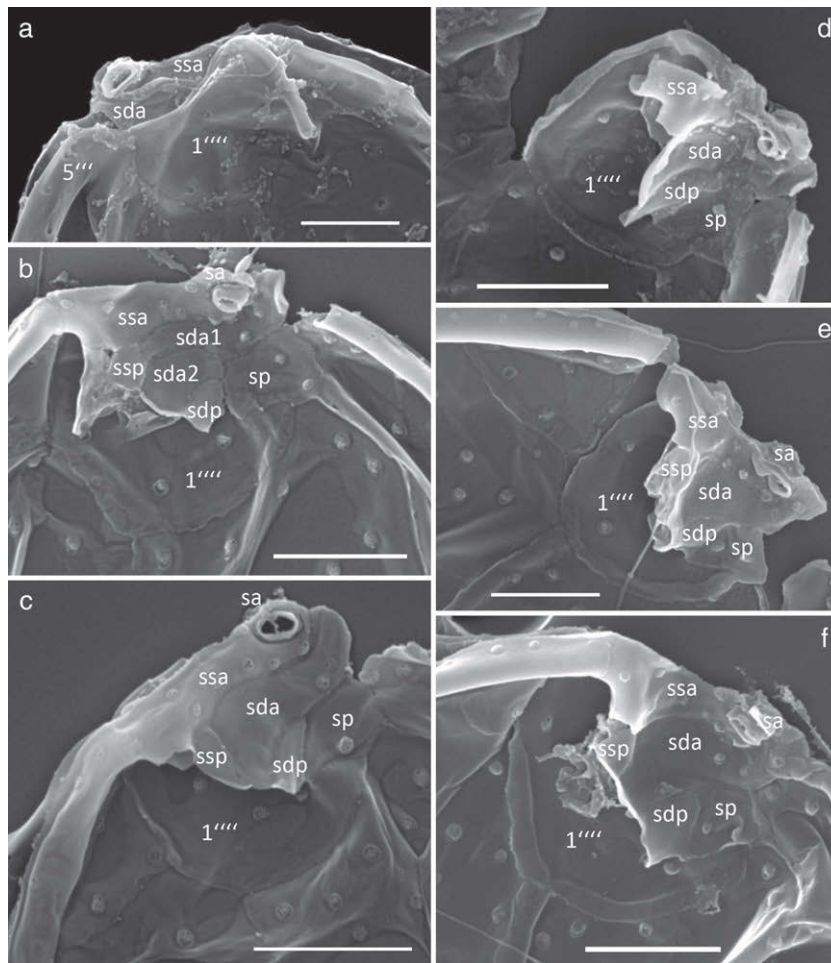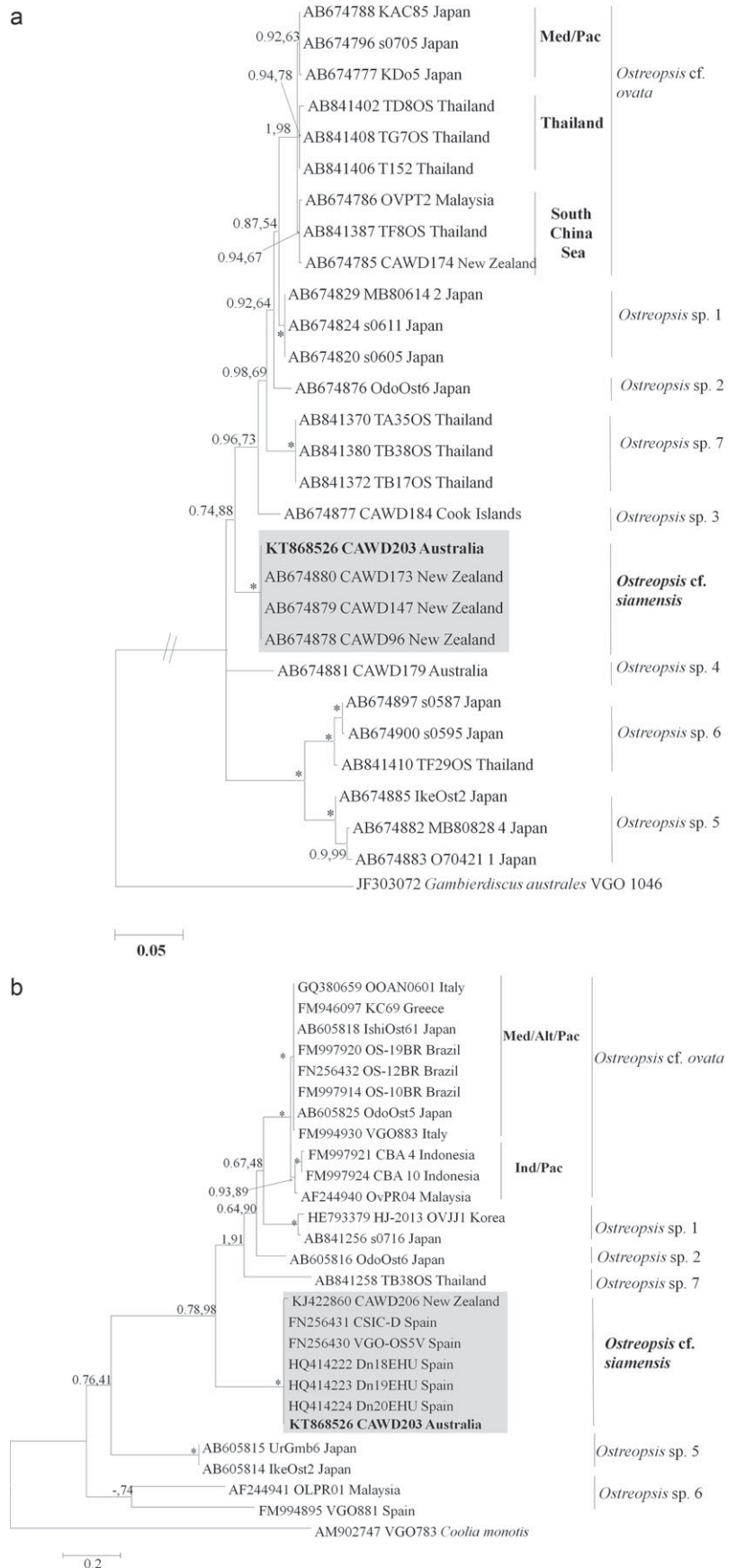
Fig. 4. SEM of *Ostreopsis* cf. *siamensis* CAWD203 from Merimbula. Details of the sulcal area; (a) hypothecal view of the ventral area; (b–f) inside views of broken cells. sa = anterior sulcal plate, ssa = anterior left sulcal plate, ssp = posterior left sulcal plate, sda = anterior right sulcal plate, sdp = posterior right sulcal plate, sp. = posterior sulcal plate, 1"" = first antapical plate. Scale bars represent 5 μm.

original description by Schmidt (1902) and observations by Fukuyo (1981) and Rhodes *et al.* (2000). Aligizaki and Niko-laidis (2006) stated that cingulum is sometimes undulated in side view. Thecal plates have small pores and large depressions that have been recorded as large pores in the literature (Faust *et al.* 1996; Aligizaki & Nikolaidis 2006; David *et al.* 2013). Fukuyo (1981), Rhodes *et al.* (2000), Penna *et al.* (2005) and Laza-Martinez *et al.* (2011) described only one pore size class (large). In the Merimbula population, small pores were not evenly distributed on the plates and rare. They were not recognizable in all cells. That is different from the evenly distributed small pores reported for *Ostreopsis* species so far (e.g. Fukuyo 1981; Faust *et al.* 1996). The apical pore plate (Po) was found to be 7.2–8.4 μm, smaller than that reported by David *et al.* (2013) (10.3–11.9 μm) and by Aligizaki and Nikolaidis (2006) (~11 μm), but similar to that reported by Laza-Martinez *et al.* (2011) (7–9 μm). The third precingular plate of *Ostreopsis* cf. *siamensis* shown by Laza-Martinez *et al.* (2011), fig. 21) is different in size and location compared to our and previous studies. From published observations, the species has no clearly distinguishable morphological characterization (Table 1). Such morphological plasticity and/or ambiguities within the genus *Ostreopsis*, especially for *O. siamensis*, *O. ovata* and *O. lenticularis*, has led to repeated statements of the need to re-investigate the type localities of

Ostreopsis species (Parsons *et al.* 2012; Hoppenrath *et al.* 2014).

Ostreopsis siamensis was initially described from the Gulf of Thailand (Schmidt 1902), however, no culture material from the type location was available until recently. Tawong *et al.* (2014) described the diversity and distribution of *Ostreopsis* spp. from the Gulf of Thailand and conducted sampling at Koh Chang, the type location for *O. siamensis*. Strains of *O. ovata* (Thailand sub-clade) were identified using molecular markers from this location that morphologically matched the description of *O. ovata* by Fukuyo (1981). This *O. ovata* sub-clade was most dominant in the Gulf of Thailand and present at all sampling sites, but no *Ostreopsis* cf. *siamensis* ribotype was reported (Tawong *et al.* 2014). Schmidt (1902) also reported the presence of large single sized pores for *O. siamensis* which was confirmed by Fukuyo (1981) from samples he obtained from Ryukyu Islands, Japan. Extensive sampling around the Japanese coast conducted in Sato *et al.* (2011) did not find any ribotype for *Ostreopsis* cf. *siamensis* from this region but described *O. ovata* complex with a cryptic new clade, *Ostreopsis* sp. 1. Conflicting descriptions of pore sizes and cingulum undulation have been reported for *Ostreopsis* species, and these reports have generally lacked genetic data (Fukuyo 1981; Faust & Morton 1995; Faust *et al.* 1996; Faust 1999; Chang *et al.* 2000; Rhodes *et al.* 2000;

Fig. 5. Maximum Likelihood (ML) phylogenetic trees of various *Ostreopsis* strains using LSU rDNA; (a) D8/D10 and; (b) D1/D3 regions. Merimbula strain CAWD203 shown in bold letters in *Ostreopsis* cf. *siamensis* clade shaded grey. External black vertical bars show each distinct *Ostreopsis* clade and internal vertical bars show each *Ostreopsis* sub-clade. Med; Atl; Pac; Ind represent Mediterranean Sea, Atlantic, Pacific and Indian Oceans sub-clades, respectively. South China Sea and Thailand are the *Ostreopsis* cf. *ovata* South China Sea and Gulf of Thailand sub-clades, respectively. Numbers at nodes represent posterior probabilities from Bayesian inference (BI) and bootstrap support values from ML based on 1000 pseudo-replicates. Robust branches (BI = 1.00 and ML = 100) are indicated by asterisks.
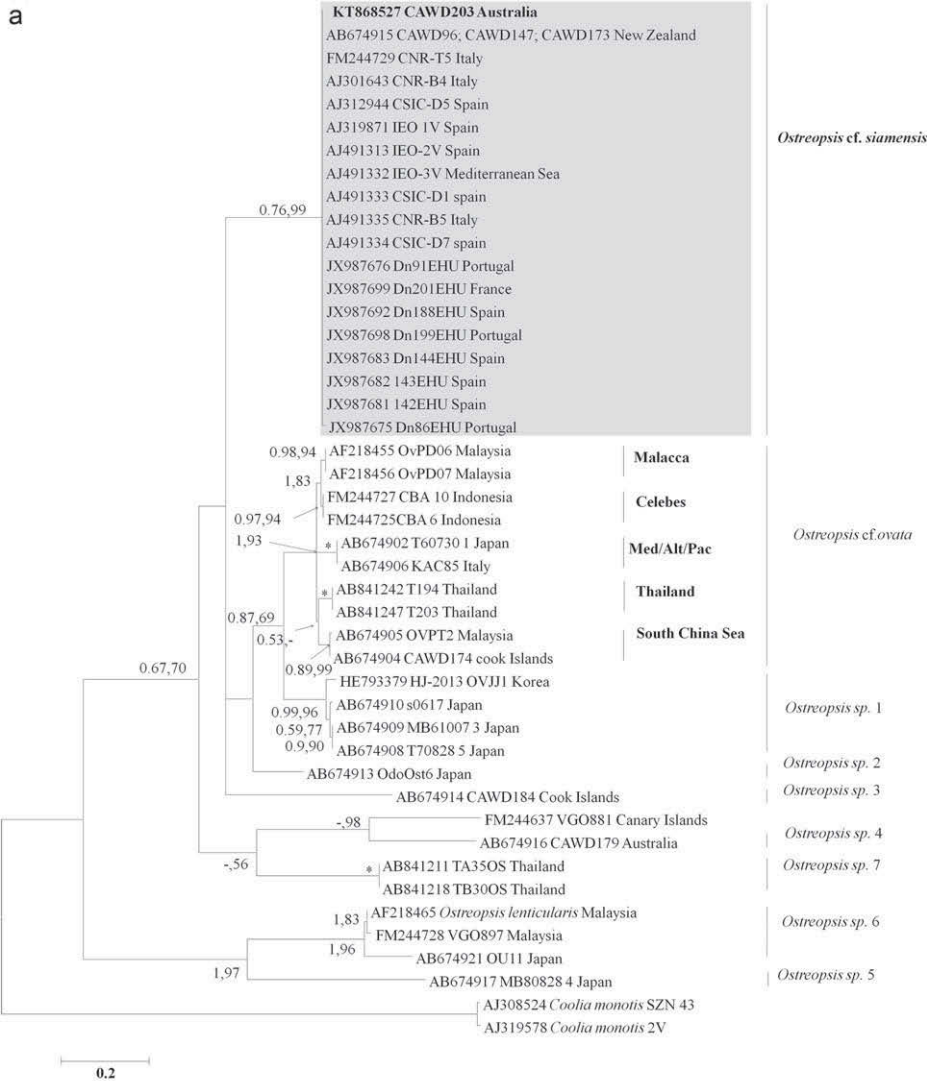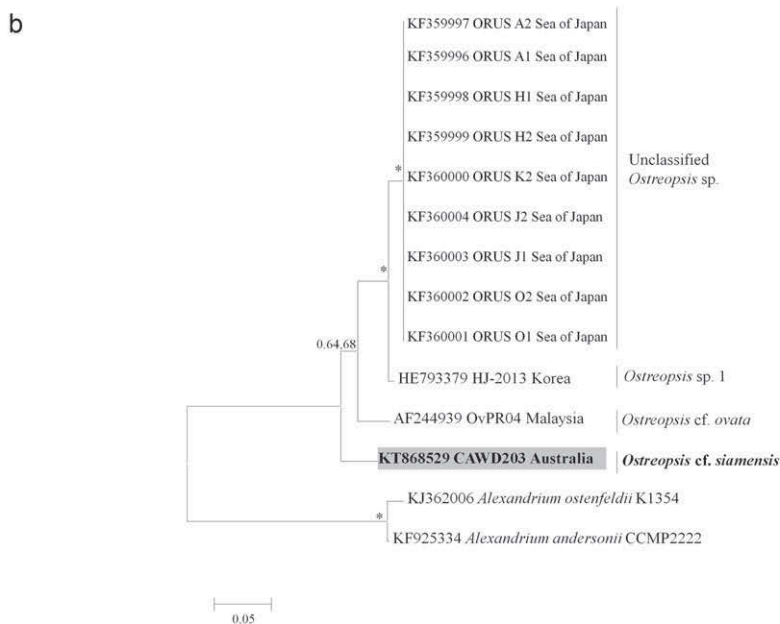
a

b

Fig. 7. Growth pattern of *Ostreopsis* cf. *siamensis* from Merimbula in f/2 and f/10 batch cultures. Each point represents the mean ± SE of three experiments of three replicates.

	Jan	Feb	Mar	Apr	May	Jun	Jul	Aug	Sept	Oct	Nov	Dec
2005										x		x
2006	x	x		x	x						x	
2007			x					x	x		x	x
2008				x	x						x	
2009					x	x	x	x	x		x	
2010		x			x		x	x				
2011		x				x						
2012					x	x	x	x	x	x	x	x
2013			x	x			x					
2014			x			x	x	x			x	x
2015			x									

< 100 cells L⁻¹ (light shade)   > 100 cells L⁻¹ (dark shade)   Absent (blank)   No sample X
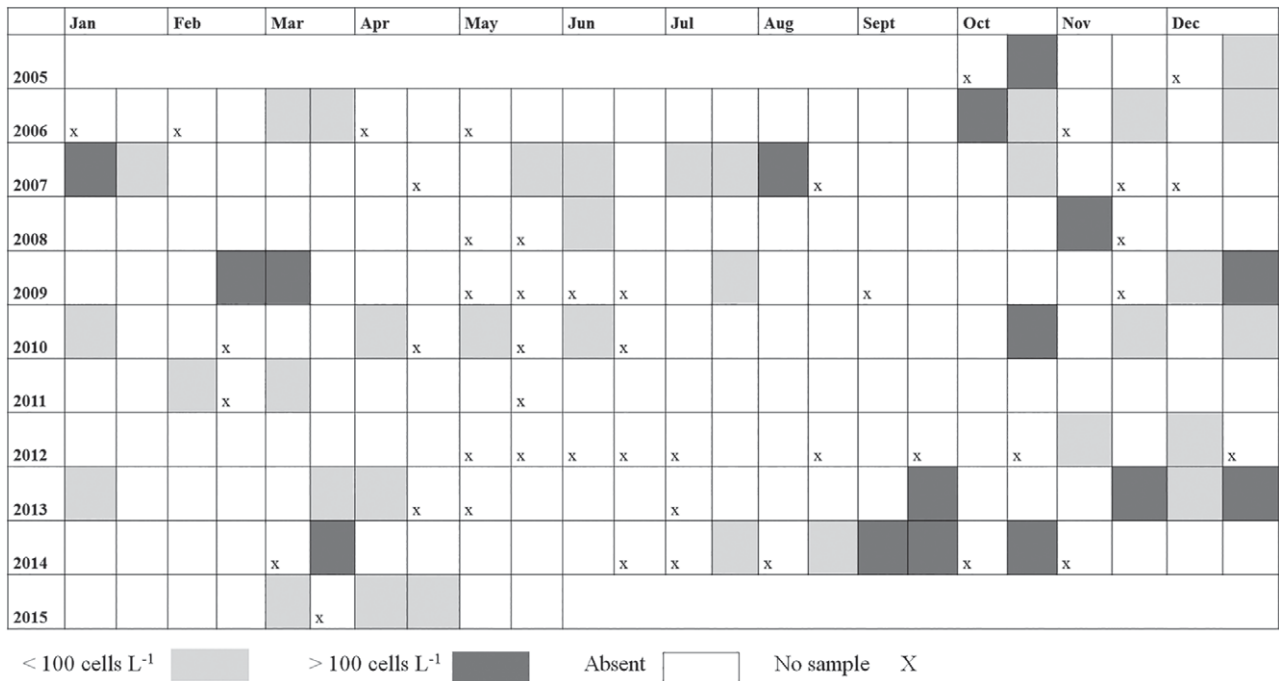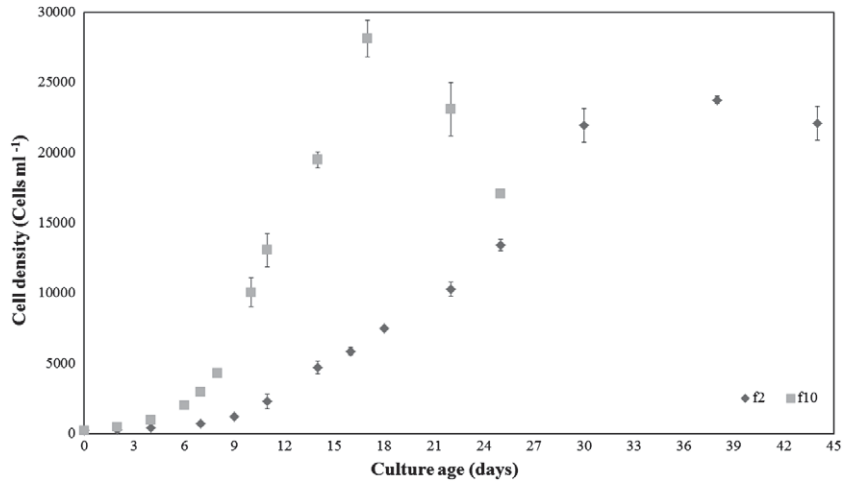
Fig. 8. Seasonal occurrence of *Ostreopsis* spp. in aquaculture plankton samples collected from Merimbula Lake Inlet (two sites within the inlet) between October 2005 and May 2015, indicating year around presence with higher abundance in austral spring-summer.

Aligizaki & Nikolaidis 2006). David *et al.* (2013) differentiated between *Ostreopsis* cf. *siamensis* and *Ostreopsis* cf. *ovata* by the presence of single sized pores for *Ostreopsis* cf. *ovata* in contrast to *Ostreopsis* cf. *siamensis* but did not observe any differences between both species based on thecal plate structures. Such historical and recent evidence suggests Schmidt's original description of *O. siamensis* may be closer to our present understanding of *Ostreopsis* cf. *ovata* and *Ostreopsis* cf. *siamensis*, possibly representing a different species than previously described (Penna *et al.* 2005, 2012; David *et al.* 2013).

Molecular and morphological characterization of *Ostreopsis* cf. *siamensis* has been reported from the Atlantic-Iberian peninsula, Mediterranean Sea, Aegean Sea and northern New Zealand with morphological reports from as north as

Peter the Great bay in Russia (Penna *et al.* 2005; Aligizaki & Nikolaidis 2006; Shears & Ross 2009; Selina & Orlova 2010; Rhodes 2011; David *et al.* 2013; Kang et al. 2013 Rhodes *et al.* 2014). This suggests the species are common in temperate waters (>30°N and 30°S) than other *Ostreopsis* species. Although phylogeographical studies using ITS and LSU rDNA regions have unraveled genetic diversity among geographically separated populations of *O. ovata* (Penna *et al.* 2005,2010), no significant differences in *Ostreopsis* cf. *siamensis* populations were observed using these molecular markers (Figs 5a,b, 6a). The significant genetic differences among the different *O. ovata* sub-clades indicate that these might be considered separate species in the future (Penna *et al.* 2014) which might also be the case for *Ostreopsis* cf. *siamensis* (Arjun Verma *et al.* 2016, unpubl. data).
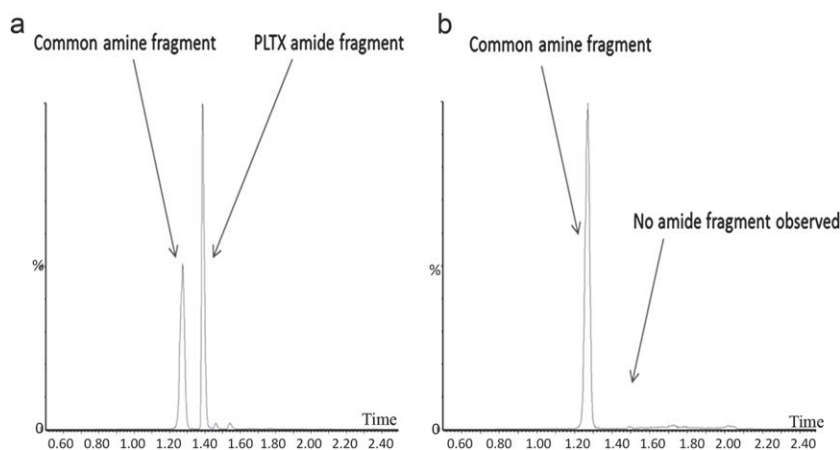
Fig. 9. Extracted ion chromatograms from the solid phase extraction and on-column oxidation of (a) Palytoxin (PLTX) standard (50 ng mL−1); (b) Ostreopsis cf. siamensis (CAWD203) from Merimbula, Australia.

At 18°C, which is close to the temperature at the site of isolation (17°C), *Ostreopsis* cf. *siamensis* grew more rapidly in lower nutrient conditions in our study (Fig. 7), similar to *Ostreopsis* sp. 7 and its growth in IMK/2 medium as opposed to IMK medium (Tawong *et al.* 2015). *Ostreopsis* cf. *siamensis* isolate from Northland, New Zealand grown in 20% GP media at 25°C exhibited a growth rate of 0.3 div day^{-1} (Rhodes *et al.* 2000). The growth rate for *Ostreopsis* cf. *siamensis* from Tasmania was reported to be higher (0.53 div day^{-1}) in low nitrogen and phosphate containing K media at 20°C compared to nutrient rich GSe and f/2 media (Pearce *et al.* 2001) (see Appendix S4 in the Supporting Information). *Ostreopsis* cf. *siamensis* may grow fastest in low nutrient conditions; however, strain-specific variability may occur, as documented in other dinoflagellate species (Doblin *et al.* 2000; Burkholder & Glibert 2006; Lartigue *et al.* 2009). Aberrant cell shapes were also reported from an *Ostreopsis* cf. *siamensis* culture from Tasmania grown in f/2 media (Pearce *et al.* 2001). Similar morphological irregularities were also reported from *Ostreopsis* cf. *ovata* when grown in L-2 medium as opposed to L-2/2 (Nascimento *et al.* 2012).

The consistent presence of *Ostreopsis* spp. in routine plankton surveys from Merimbula Lake inlet between 2005 and 2015 suggest that species from this genus may be well established in the region (Fig. 8), rather than being reintroduced every summer season from tropical Queensland *via* the East Australian Current (Hallegraeff 2010). However, there is a marked increase in the abundance of *Ostreopsis* spp. during warmer months (Fig. 8). Similar observations have also been reported from New Zealand, as *Ostreopsis* cf. *siamensis* has been found regularly throughout the austral summer season (Rhodes 2011, 2014). Previous studies have presented the role of temperature in regulating *Ostreopsis* blooms (Mangialajo *et al.* 2008; Shears & Ross 2009); however a positive correlation between temperature and *Ostreopsis* blooms has not yet been clearly shown (Accorroni *et al.* 2011). Sea surface temperature in Merimbula Inlet is 8–28°C highlighting a wide range of thermal tolerance for this species, similar to the reports from Peter the Great Bay in the Sea of Japan, in which *Ostreopsis* spp. cells have occurred on macrophytes at 7–22.2°C (Selina & Levchenko 2011; Kohli *et al.* 2014). The resting stages of *Ostreopsis* cf. *siamensis* were reported to survive at 10°C in culture conditions thereby suggesting a seeding mechanism for *Ostreopsis* cells to survive cooler

temperatures and reinitiate in the summer (Pearce *et al.* 2001). The mucilage matrix produced by *Ostreopsis* species has been reported to work as a protective coating which may enable cysts to survive in them for more than 6 months after their formation and help the population to survive cooler temperatures (Bravo *et al.* 2012).

PLTX is highly toxic upon i.p. administration in mice with reported LD$_{50}$ values ranging between 0.15 and 0.72 µg kg^{-1} (EFSA 2009; Munday 2011). The symptoms displayed by mice upon exposure to high dose of cell extract exhibited similar symptoms to PLTX exposure suggesting that the extract may have contained small amounts of very toxic substances or larger amounts of substances of relatively low toxicity as highlighted by the high LD$_{50}$ of 25 mg kg^{-1} i.p. in *Ostreopsis* cf. *siamensis* CAWD203 (Riobó *et al.* 2008; Munday 2011). Chemical analysis on CAWD203 exhibited only the common amine aldehyde fragment after periodate oxidation (Fig. 9), similar to *Ostreopsis* cf. *siamensis* CAWD173 from Selwood *et al.* (2012), but no amide aldehyde fragment was obtained suggesting that some structurally related PLTX analogues were detected in the cell extract but PLTX itself was not contained in the sample. The total amount of PLTX equivalents obtained from the cell extract was comparable and in some cases lower to other *Ostreopsis* cf. *siamensis* isolates from New Zealand (ranging 0.1–1.2 pg. cell^{-1}) but was much higher compared to *Ostreopsis* cf. *siamensis* strains from the Mediterranean and Atlantic regions that only produced PLTX-like compounds at levels in the range 0.4–0.8 fg cell^{-1} (Ciminiello *et al.* 2013; Rhodes *et al.* 2013) (see Appendix S5 in the supporting information). The cellular content of PLTX-like compounds in CAWD203 was also comparatively very low to that of some toxic *Ostreopsis* cf. *ovata* strains reported from previous studies (Guerrini *et al.* 2010; Suzuki *et al.* 2012).

Structural differences can have a great impact on the toxicity of the strain as highlighted by the mouse bioassay results where the LD$_{50}$ was a lot higher than LD$_{50}$ of palytoxin by i.p. in mice. Structural differences and varying amounts of PLTX-like compounds produced by *Ostreopsis* cf. *ovata* strains from Japan and Mediterranean regions have been identified by investigating the complete structures of such compounds, but have been relatively understudied amongst *Ostreopsis* cf. *siamensis* strains (Ciminiello *et al.* 2012a; Suzuki *et al.* 2012). Such distinctions may occur due to strain specific

variability, as documented in *Ostreopsis* cf. *ovata* and other dinoflagellate strains, as well as different culturing conditions that might alter toxin composition in *Ostreopsis* cultures (Tillmann *et al.* 2009; Pezzolesi *et al.* 2012; Vanucci *et al.* 2012). Since *Ostreopsis* cf. *siamensis* CAWD203 was cultured in 5× diluted f/2 media, the nitrogen and phosphorus limitation in the media may have induced lower toxin production. However, this may be species-specific trait since high toxin contents have been reported in *Ostreopsis* cf. *ovata* in the same nutrient conditions (Guerrini *et al.* 2010; Vanucci *et al.* 2012). So far, information on effects of nutrient conditions on *Ostreopsis* cf. *siamensis* growth and toxin production are lacking and need to be further investigated.

Non PLTX-like cytotoxic compounds such as Ostreol-A have also been reported from *Ostreopsis* species highlighting a broad spectrum of toxins synthesized by species of this genus (Hwang *et al.* 2013). There is an increasing need to investigate the macrostructures of such complex biomolecules and the molecular mechanism involved in their synthesis. The genus *Ostreopsis* has been little studied from Australian waters despite recurrent occurrences from temperate shellfish growing estuaries (Ajani *et al.* 2013). Nine clades and sub-clades of *Ostreopsis* have been identified using molecular methods (Sato *et al.* 2011; Tawong *et al.* 2014). Increasing knowledge of species identity, distribution and toxigenicity of *Ostreopsis* spp. will enable more effective monitoring of harmful algal taxa in Australian waters.

ACKNOWLEDGMENTS

REFERENCES

Accoroni, S., Romagnoli, T., Colombo, F. *et al.* 2011. *Ostreopsis* cf. *ovata* bloom in the northern Adriatic Sea during summer 2009: ecology, molecular characterization and toxin profile. *Mar. Pollut. Bull.* **62**: 2512–9.

Ajani, P., Brett, S., Krogh, M., Scanes, P., Webster, G. and Armand, L. 2013. The risk of harmful algal blooms (HABs) in the oyster-growing estuaries of New South Wales Australia. *Environ. Monit. Assess.* **185**: 5295–316.

Alcala, A. C., Alcala, L. C., Garth, J. S., Yasumura, D. and Yasumoto, T. 1988. Human fatality due to ingestion of the crab *Demania reynaudii* that contained a palytoxin-like toxin. *Toxicon* **26**: 105–7.

Aligizaki, K., Katikou, P., Nikolaidis, G. and Panou, A. 2008. First episode of shellfish contamination by palytoxin-like compounds from *Ostreopsis* species (Aegean Sea, Greece). *Toxicon* **51**: 418–27.

Aligizaki, K. and Nikolaidis, G. 2006. The presence of the potentially toxic genera *Ostreopsis* and *Coolia* (Dinophyceae) in the North Aegean Sea, Greece. *Harmful Algae* **5**: 717–30.

Amzil, Z., Sibat, M., Chomerat, N. *et al.* 2012. Ovatoxin-a and palytoxin accumulation in seafood in relation to *Ostreopsis* cf. *ovata* blooms on the French Mediterranean coast. *Mar. Drugs* **10**: 477–96.

Besada, E., Loeblich, L. and Loeblich, A. 1982. Observations on tropical, benthic dinoflagellates from ciguatera-endemic areas: *Coolia, Gambierdiscus*, and *Ostreopsis*. *Bull. Mar. Sci.* **32**: 723–35.

Bravo, I., Vila, M., Casabianca, S. *et al.* 2012. Life cycle stages of the benthic palytoxin-producing dinoflagellate *Ostreopsis* cf. *ovata* (Dinophyceae). *Harmful Algae* **18**: 24–34.

Burkholder, J. and Glibert, P. 2006. Intraspecific variability: an important consideration in forming generalisations about toxigenic algal species. *Afr. J. Mar. Sci.* **28**: 177–80.

Chang, F., Shimizu, Y., Hay, B., Stewart, R., Mackay, G. and Tasker, R. 2000. Three recently recorded *Ostreopsis* spp. (Dinophyceae) in New Zealand: temporal and regional distribution in the upper North Island from 1995 to 1997. *N. Z. J. Mar. Freshwater Res.* **34**: 29–39.

Ciminiello, P., Dell'aversano, C., Dello Iacovo, E. *et al.* 2012a. Isolation and structure elucidation of ovatoxin-a, the major toxin produced by *Ostreopsis ovata*. *J. Am. Chem. Soc.* **134**: 1869–75.

Ciminiello, P., Dell'aversano, C., Iacovo, E. D. *et al.* 2012b. Unique toxin profile of a Mediterranean *Ostreopsis* cf. *ovata* strain: HR LC–MS(n) characterization of ovatoxin-f, a new palytoxin congener. *Chem. Res. Toxicol.* **25**: 1243–52.

Ciminiello, P., Dell'aversano, C., Fattorusso, E. *et al.* 2008. Putative palytoxin and its new analogue, ovatoxin-a, in *Ostreopsis ovata* collected along the Ligurian coasts during the 2006 toxic outbreak. *J. Am. Soc. Mass Spectrom.* **19**: 111–20.

Ciminiello, P., Dell'aversano, C., Iacovo, E. D. *et al.* 2013. Investigation of toxin profile of Mediterranean and Atlantic strains of *Ostreopsis* cf. *siamensis* (Dinophyceae) by liquid chromatography–high resolution mass spectrometry. *Harmful Algae* **23**: 19–27.

Ciminiello, P., Dell'aversano, C., Iacovo, E. D. *et al.* 2014. First finding of *Ostreopsis* cf. *ovata* toxins in marine aerosols. *Environ. Sci. Technol.* **48**: 3532–40.

David, H., Laza-Martínez, A., Miguel, I. and Orive, E. 2013. *Ostreopsis* cf. *siamensis* and *Ostreopsis* cf. *ovata* from the Atlantic Iberian Peninsula: morphological and phylogenetic characterization. *Harmful Algae* **30**: 44–55.

Doblin, M. A., Blackburn, S. I. and Hallegraeff, G. M. 2000. Intraspecific variation in the selenium requirement of different geographic strains of the toxic dinoflagellate *Gymnodinium catenatum*. *J. Plankton Res.* **22**: 421–32.

Durando, P., Ansaldi, F., Oreste, P. *et al.* 2007. *Ostreopsis ovata* and human health: epidemiological and clinical features of respiratory syndrome outbreaks from a two-year syndromic surveillance, 2005–06, in north-west Italy. *Euro Surveill.* **12** (6): E070607.1.

EFSA 2009. The community summary report on trends and sources of zoonoses, zoonotic agents, antimicrobial resistance and foodborne outbreaks in the European Union in 2007. *EFSA J.* **223**: 14–38.

Faust, M. A. 1999. Three new *Ostreopsis* species (Dinophyceae): *O. marinus* sp. nov., *O. belizeanus* sp. nov., and *O. caribbeanus* sp. nov. *Phycologia* **38**: 92–9.

Faust, M. A. and Morton, S. L. 1995. Morphology and ecology of the marine dinoflagellate *Ostreopsis labens* sp. nov. (Dinophyceae). *J. Phycol.* **31**: 456–63.

Faust, M. A., Morton, S. L. and Quod, J. P. 1996. Further SEM study of marine dinoflagellates: the genus *Ostreopsis* (Dinophyceae). *J. Phycol.* **32**: 1053–65.

Fukuyo, Y. 1981. Taxonomical study on benthic dinoflagellates collected in coral reefs [French Polynesia, Japan]. *Bull. Jpn. Soc. Sci. Fish.* **47**: 967–78.

García-Altares, M., Tartaglione, L., Dell'aversano, C. *et al.* 2014. The novel ovatoxin-g and isobaric palytoxin (so far referred to as putative palytoxin) from *Ostreopsis* cf. *ovata* (NW Mediterranean Sea): structural insights by LC-high resolution MS^n. *Anal. Bioanal. Chem.* **407**: 1191–2014.

Guerrini, F., Pezzolesi, L., Feller, A. *et al.* 2010. Comparative growth and toxin profile of cultured *Ostreopsis ovata* from the Tyrrhenian and Adriatic Seas. *Toxicon* **55**: 211–20.

Guillard, R. R. 1975. Culture of phytoplankton for feeding marine invertebrates. *In* Smith, W. L. and Chanley, M. H. (Eds) *Culture of Marine Invertebrate Animals*. Springer. New York, USA, pp. 29–60.

Hall, T. A. 1999. BioEdit: a user-friendly biological sequence alignment editor and analysis program for Windows 95/98/NT. *Nucleic Acid Symp Ser.* **41**: 95–8.

Hallegraeff, G. M. 2010. Ocean climate change, phytoplankton community responses, and harmful algal blooms: a formidable predictive challenge. *J. Phycol.* **46**: 220–35.

Heimann, K., Sparrow, L. and Blair, D. 2009. Interim report on the continuing development of the toxic dinoflagellates atlas. *In* Marine and Tropical Sciences Research Facility (Ed.) *June Interim Report* (Part 1). Reef and Rainforest Research Center, Cairns, pp. 1–25.

Holmes, M., Gillespie, N. and Lewis, R. 1988. Toxicity and morphology of *Ostreopsis* cf. *siamensis* cultured from a ciguatera endemic region of Queensland, Australia. *In* Choat, J. H., Barnes, D., Borowitzka, M. A. *et al.* (Eds) *Proceedings 6th International Coral Reef Symposium*, 6th International Coral Reef Symposium Executive Committee, Coral Reef Ecology, Townsville, Australia, pp. 49–54.

Hoppenrath, M., Murray, S. A., Chomérat, N. and Horiguchi, T. 2014. *Marine Benthic Dinoflagellates-Unveiling their Worldwide Biodiversity*. Kleine Senckenberg-Reihe, Frankfurt Am Main, pp. 116–26.

Hwang, B. S., Yoon, E. Y., Kim, H. S. *et al.* 2013. Ostreol A: a new cytotoxic compound isolated from the epiphytic dinoflagellate Ostreopsis cf. ovata from the coastal waters of Jeju Island, Korea. *Bioorg. Med. Chem. Lett.* **23**: 3023–7.

Kang, N. S., Jeong, H. J., Lee, S. Y. *et al.* 2013. Morphology and molecular characterization of the epiphytic benthic dinoflagellate *Ostreopsis* cf. *ovata* in the temperate waters off Jeju Island, Korea. *Harmful Algae* **27**: 98–112.

Kearse, M., Moir, R., Wilson, A. *et al.* 2012. Geneious basic: an integrated and extendable desktop software platform for the organization and analysis of sequence data. *Bioinformatics* **28**: 1647–9.

Kodama, A. M., Hokama, Y., Yasumoto, T., Fukui, M., Jo Manea, S. and Sutherland, N. 1989. Clinical and laboratory findings implicating palytoxin as cause of ciguatera poisoning due to *Decapterus macrosoma* (mackerel). *Toxicon* **27**: 1051–3.

Kohli, G. S., Murray, S. A., Neilan, B. A. *et al.* 2014. High abundance of the potentially maitotoxic dinoflagellate *Gambierdiscus carpenteri* in temperate waters of new South Wales, Australia. *Harmful Algae* **39**: 134–45.

Lartigue, J., Jester, E. L. E., Dickey, R. W. and Villareal, T. A. 2009. Nitrogen source effects on the growth and toxicity of two strains of the ciguatera-causing dinoflagellate *Gambierdiscus toxicus*. *Harmful Algae* **8**: 781–91.

Laza-Martinez, A., Orive, E. and Miguel, I. 2011. Morphological and genetic characterization of benthic dinoflagellates of the genera Coolia, Ostreopsis and Prorocentrum from the South-Eastern Bay of Biscay. *Eur. J. Phycol.* **46**: 45–65.

Leaw, C. P., Lim, P. T., Ahmad, A. and Usup, G. 2001. Genetic diversity of *Ostreopsis ovata* (Dinophyceae) from Malaysia. *Marine Biotechnol.* **3**: 246–55.

Malagoli, D., Casarini, L. and Ottaviani, E. 2008. Effects of the marine toxins okadaic acid and palytoxin on mussel phagocytosis. *Fish Shellfish Immunol.* **24**: 180–6.

Mangialajo, L., Bertolotto, R., Cattaneo-Vietti, R. *et al.* 2008. The toxic benthic dinoflagellate *Ostreopsis ovata*: quantification of proliferation along the coastline of Genoa, Italy. *Mar. Pollut. Bull.* **56**: 1209–14.

Munday, R. 2011. Palytoxin toxicology: animal studies. *Toxicon* **57**: 470–7.

Nascimento, S. M., Corrêa, E. V., Menezes, M., Varela, D., Paredes, J. and Morris, S. 2012. Growth and toxin profile of *Ostreopsis* cf. *ovata* (Dinophyta) from Rio de Janeiro, Brazil. *Harmful Algae* **13**: 1–9.

Norris, D. R., Bomber, J. W. and Balech, E. 1985. Benthic dinoflagellates associated with ciguatera from Florida Keys I. *Ostreopsis heptagona* sp. nov. *In* Anderson, D. M., White, A. W. and Baden, D. G. (Eds) *Toxic Dinoflagellates.* Elsevier Scientific, New York, pp. 39–44.

OECD 2006. *OECD Guideline for Testing of Chemicals 425. Acute Oral Toxicity – Up-and-Down-Procedure (UDP)*. Organisation for Economic Co-operation and Development, Paris. Available from: http://213.253.134.43/oecd/pdfs/browseit/9742501e.pdf (accessed: 14 November 2015).

Onuma, Y., Satake, M., Ukena, T. *et al.* 1999. Identification of putative palytoxin as the cause of clupeotoxism. *Toxicon* **37**: 55–65.

Parsons, M. L., Aligizaki, K., Bottein, M. Y. D. *et al.* 2012. *Gambierdiscus* and *Ostreopsis*: reassessment of the state of knowledge of their taxonomy, geography, ecophysiology, and toxicology. *Harmful Algae* **14**: 107–29.

Pearce, I., Marshall, J. and Hallegraeff, G. 2001. Toxic epiphytic dinoflagellates from east coast Tasmania. *In* Hallegraeff, G., Blackburn, S., Bolch, C. and Lewis, R. (Eds) *Proceedings of the 9th International Conference on Harmful Algal Blooms.* International Society for the Study of Harmful Algae and Intergovernmental Oceanographic Commission of UNESCO, Paris, France, pp. 54–7.

Penna, A., Battocchi, C., Capellacci, S. *et al.* 2014. Mitochondrial, but not rDNA, genes fail to discriminate dinoflagellate species in the genus *Ostreopsis*. *Harmful Algae* **40**: 40–50.

Penna, A., Fraga, S., Battocchi, C. *et al.* 2010. A phylogeographical study of the toxic benthic dinoflagellate genus *Ostreopsis* Schmidt. *J. Biogeogr.* **37**: 830–41.

Penna, A., Fraga, S., Battocchi, C. *et al.* 2012. Genetic diversity of the genus *Ostreopsis* Schmidt: phylogeographical considerations and molecular methodology applications for field detection in the Mediterranean Sea. *Cryptogam. Algol.* **33**: 153–63.

Penna, A., Vila, M., Fraga, S. *et al.* 2005. Characterization of *Ostreopsis* and *Coolia* (Dinophyceae) isolates in the Western Mediterranean Sea based on morphology, toxicity and Internal transcribed spacer 5.8S rDNA sequences. *J. Phycol.* **41**: 212–5.

Pezzolesi, L., Guerrini, F., Ciminiello, P. *et al.* 2012. Influence of temperature and salinity on *Ostreopsis* cf. *ovata* growth and evaluation of toxin content through HR LC–MS and biological assays. *Water Res.* **46**: 82–92.

Rasband, W. S. 1997–2013. *Image J.* U.S. National Institutes of Health, Bethesda, MD . Available from: http://imagej.nih.gov/ij/.

Rhodes, L. 2011. World-wide occurrence of the toxic dinoflagellate genus *Ostreopsis* Schmidt. *Toxicon* **57**: 400–7.

Rhodes, L., Adamson, J., Suzuki, T., Briggs, L. and Garthwaite, I. 2000. Toxic marine epiphytic dinoflagellates, *Ostreopsis siamensis* and *Coolia monotis* (Dinophyceae), in New Zealand. *N. Z. J. Mar. Freshwater Res.* **34**: 371–83.

Rhodes, L., Smith, K., Munday, R. *et al.* 2013. *Ostreopsis* isolates from the Pacific region. *In* Pagou, P. and Hallegraeff, G. (Eds) *Proceedings of the 14th International Conference on Harmful Algae.* International Society for the Study of Harmful Algae and Intergovernmental Oceanographic Commission of UNESCO, Busan, Korea, pp. 36–8.

Rhodes, L., Smith, K., Papiol, G. G., Adamson, J., Harwood, T. and Munday, R. 2014. Epiphytic dinoflagellates in sub-tropical New Zealand, in particular the genus *Coolia* Meunier. *Harmful Algae* **34**: 36–41.

Rhodes, L., Towers, N., Briggs, L., Munday, R. and Adamson, J. 2002. Uptake of palytoxin-like compounds by shellfish fed *Ostreopsis siamensis* (Dinophyceae). *N. Z. J. Mar. Freshwater Res.* **36**: 631–6.

Riobó, P., Paz, B., Franco, J. M., Vázquez, J. A., Murado, M. A. and Cacho, E. 2008. Mouse bioassay for palytoxin. Specific symptoms and dose–response against dose–death time relationships. *Food Chem. Toxicol.* **46**: 2639–47.

Ronquist, F. and Huelsenbeck, J. P. 2003. MrBayes 3: Bayesian phylogenetic inference under mixed models. *Bioinformatics* **19**: 1572–4.

Sato, S., Nishimura, T., Uehara, K. *et al.* 2011. Phylogeography of *Ostreopsis* along West Pacific coast, with special reference to a novel clade from Japan. *PLoS One* **6**: e27983.

Schmidt, J. 1902. Contribution to the knowledge of the vegetation in the Gulf of Siam. Part IV. Peridiniales. *J. Botanique* **23**: 212–8.

Selina, M. S. and Levchenko, E. 2011. Species composition and morphology of dinoflagellates (Dinophyta) of epiphytic assemblages of Peter the Great Bay in the sea of Japan. *Russ. J. Mar. Biol.* **37**: 23–32.

Selina, M. S. and Orlova, T. Y. 2010. First occurrence of the genus *Ostreopsis* (Dinophyceae) in the Sea of Japan. *Bot. Mar.* **53**: 243–9.

Selwood, A. I., Van Ginkel, R., Harwood, D. T., Mcnabb, P. S., Rhodes, L. R. and Holland, P. T. 2012. A sensitive assay for palytoxins, ovatoxins and ostreocins using LC–MS/MS analysis of cleavage fragments from micro-scale oxidation. *Toxicon* **60**: 810–20.

Shears, N. T. and Ross, P. M. 2009. Blooms of benthic dinoflagellates of the genus *Ostreopsis*; an increasing and ecologically important phenomenon on temperate reefs in New Zealand and worldwide. *Harmful Algae* **8**: 916–25.

Suzuki, T., Watanabe, R., Uchida, H. *et al.* 2012. LC–MS/MS analysis of novel ovatoxin isomers in several *Ostreopsis* strains collected in Japan. *Harmful Algae* **20**: 81–91.

Tamura, K., Stecher, G., Peterson, D., Filipski, A. and Kumar, S. 2013. MEGA6: molecular evolutionary genetics analysis version 6.0. *Mol. Biol. Evol.* **30**: 2725–9.

Taniyama, S., Arakawa, O., Terada, M. *et al.* 2003. *Ostreopsis* sp., a possible origin of palytoxin (PTX) in parrotfish *Scarus ovifrons*. *Toxicon* **42**: 29–33.

Tawong, W., Nishimura, T., Sakanari, H., Sato, S., Yamaguchi, H. and Adachi, M. 2014. Distribution and molecular phylogeny of the dinoflagellate genus *Ostreopsis* in Thailand. *Harmful Algae* **37**: 160–71.

Tawong, W., Yoshimatsu, T., Yamaguchi, H. and Adachi, M. 2015. Effects of temperature, salinity and their interaction on growth of benthic dinoflagellates *Ostreopsis* spp. from Thailand. *Harmful Algae* **44**: 37–45.

Tichadou, L., Glaizal, M., Armengaud, A. *et al.* 2010. Health impact of unicellular algae of the *Ostreopsis* genus blooms in the Mediterranean Sea: experience of the French Mediterranean coast surveillance network from 2006 to 2009. *Clin. Toxicol.* **48**: 839–44.

Tillmann, U., Alpermann, T. L., da Purificação, R. C., Krock, B. and Cembella, A. 2009. Intra-population clonal variability in allelochemical potency of the toxigenic dinoflagellate *Alexandrium tamarense*. *Harmful Algae* **8**: 759–69.

Tubaro, A., Durando, P., Del Favero, G. *et al.* 2011. Case definitions for human poisonings postulated to palytoxins exposure. *Toxicon* **57**: 478–95.

Usami, M., Satake, M., Ishida, S., Inoue, A., Kan, Y. and Yasumoto, T. 1995. Palytoxin analogs from the dinoflagellate *Ostreopsis siamensis*. *J. Am. Chem. Soc.* **117**: 5389–90.

Vanucci, S., Pezzolesi, L., Pistocchi, R. *et al.* 2012. Nitrogen and phosphorus limitation effects on cell growth, biovolume, and toxin production in *Ostreopsis* cf. *ovata*. *Harmful Algae* **15**: 78–90.

West, R.J., Thorogood, C., Walford, T. and William, R. 1985. *An Estuarine Inventory for New South Wales, Australia*. Fisheries Bulletin 2, Department of Agriculture, NSW, Australia.

Williams, R. J., West, G., Morrison, D. and Creese, R. G. 2006. *Estuarine Resources of New South Wales. Prepared for the Comprehensive Coastal Assessment*. NSW Department of Primary Industries, Port Stephens.

SUPPORTING INFORMATION

Additional Supporting Information may be found in the online version of this article at the publisher's web-site:

Appendix S1. Primers used for amplification and sequencing.

Appendix S2. List of *Ostreopsis* spp. clones used for phylogenetic reconstruction.

Appendix S3. Distance values based on the Small ribosomal subunit (18S) sequences.

Appendix S4. Comparison of acclimated growth rates of *Ostreopsis* spp.

Appendix S5. Palytoxin (PLTX) equivalents quantification in *Ostreopsis cf. siamensis* isolates.
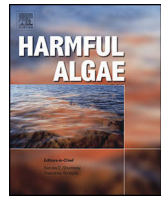
Molecular and phylogenetic characterization of *Ostreopsis* (Dinophyceae) and the description of a new species, *Ostreopsis rhodesae* sp. nov., from a subtropical Australian lagoon

Arjun Verma[a,*], Mona Hoppenrath[b], Juan José Dorantes-Aranda[c], D. Tim Harwood[d], Shauna A. Murray[a]

[a] Plant Functional Biology and Climate Change Cluster, University of Technology Sydney, PO Box 123, Broadway, New South Wales 2007, Australia
[b] Senckenberg Research Institute, Senckenberg am Meer, German Center for Marine Biodiversity Research (DZMB), Südstrand 44, D-26382 Wilhelmshaven, Germany
[c] Institute for Marine and Antarctic Studies, University of Tasmania, Private Bag 129, Hobart, Tasmania 7001, Australia
[d] Cawthron Institute, 98 Halifax Street East, Private Bag 2, Nelson 7010, New Zealand

ARTICLE INFO

ABSTRACT

Cryptic and pseudo-cryptic species are common amongst marine phytoplankton, and may cause misleading inferences of ecological and physiological data of plankton community studies. Deciphering the diversity and distribution of species of the benthic dinoflagellate *Ostreopsis* is one example, as there are many morphologically indistinct clades that differ greatly genetically and toxicologically from one another. In this study, a new species, *Ostreopsis rhodesae* from the southern Great Barrier Reef was described. While it initially appeared to be highly similar to several other *Ostreopsis* species, we found *O. rhodesae* can be distinguished based on the relative size of the second apical plate (2′), which is twice as long as the APC plate, and separates the third apical (3′) from the third precingular (3″) plate. Phylogenetic trees based on the SSU, ITS/5.8S and D1-D2 and D8-D10 regions of the LSU rRNA were well supported, and showed a clear difference to other *Ostreopsis* clades. Compensatory base changes (CBCs) were identified in helices of the ITS2 between *O. rhodesae* and *O.* cf. *ovata* and *O.* cf. *siamensis*, which were also present in the same habitat. Fish gill cell lines were toxic to *O. rhodesae*, cell extracts but no palytoxin-like analogues were found in them. The findings highlight a case of pseudo-cryptic speciation, found in sympatry with closely related and morphologically similar species, but biologically and functionally distinct.

© 2016 Elsevier B.V. All rights reserved.

1. Introduction

Studies of the diversity, evolution and ecology of dinoflagellates in marine ecosystems are challenging. Some of the reasons for this are a lack of field data, under sampling at large spatial and temporal scales, low abundance of certain species and difficulties in establishing cultures (Heger et al., 2014; Keeling et al., 2014; Murray et al., 2012b; Sampayo et al., 2009). 'Cryptic' species also appear to be common, and further complicate the identification of dinoflagellate species when techniques such as light and scanning microscopy are used (Amato et al., 2007; Montresor et al., 2003; Murray et al., 2012a; Richlen et al., 2008). Recently, large scale oceanic and coastal diversity surveys using 'meta-barcoding' and other culture-independent molecular methods have shown that a significantly larger number of operational taxonomic units (OTUs) for dinoflagellate lineages exists, than there are morphologically recognized taxa (de Vargas et al., 2015; Le Bescot et al., 2015; Massana et al., 2015). Environmental sequencing techniques are not error-proof and require an accurate and curated taxonomic validation before novel biological insights can be made from the sequence dataset (Del Campo et al., 2013, 2016). Largely growing sequencing platforms and rapidly generated molecular data raises significant discussions on the choice of genetic markers and the divergence between 'units' of diversity before classifying them as ecologically and evolutionary distinct species (Del Campo et al., 2016; LaJeunesse, 2001; Sampayo et al., 2009; Stat et al., 2011).

Cryptic and pseudo-cryptic species are being discovered in many different dinoflagellate taxa at an interesting rate and are

important for the precise representation of a phytoplankton community (Amato et al., 2007; Hoppenrath et al., 2014; Knowlton, 1993). Cryptic species are genetically different, but morphologically identical, whereas pseudo-cryptic species not only show genetic differences but also minor morphological variations after detailed examination (Lundholm et al., 2012). Such congeneric species can have different physiological responses despite similar morphologies (Hoppenrath et al., 2014; Orive et al., 2013). *Gambierdiscus toxicus* is an example of one such dinoflagellate taxon where detailed analyses suggested that it is not a single cosmopolitan species but a wide-ranging species complex with varying physiological traits which has aided in enhancing our knowledge of the tropical food borne disease ciguatera (Richlen et al., 2008). Intragenomic rDNA polymorphisms, the existence of high copy numbers of rDNA cistrons and the presence of pseudogenes can make species delimitation problematic amongst dinoflagellates even with the use of DNA sequencing techniques (Alverson, 2008; Orive et al., 2013; Stat et al., 2011).

The presence of compensatory base pair changes (CBCs) in the 3′ nuclear ribosomal transcribed spacer sequence region (second internal transcribed spacer region (ITS2)) has been extensively used for species delimitation purposes as their presence has been significantly correlated with mating incompatibility and reproductive isolation (Coleman, 2003, 2007, 2015; Coleman and Vacquier, 2002). DNA sequencing methods in combination with ITS2 secondary structure modelling have proven useful in resolving evolutionary relationships between diverse free living and symbiotic *Symbiodinium* lineages and also discovering novel clades (LaJeunesse, 2001; LaJeunesse et al., 2012; Pochon and Gates, 2010). It has also been used to delineate pseudo-cryptic species within toxin producing species complexes such as the *Alexandrium tamarense* species complex and the allopatric differentiation of *Coolia malayensis* and *C. monotis* (John et al., 2014; Leaw et al., 2010, 2016).

The genus *Ostreopsis* Schmidt comprises several species that are similar in shape, size and thecal plate patterns and co-exist in tropical and temperate coastal habitats worldwide (Fukuyo, 1981; Parsons et al., 2012; Penna et al., 2005; Rhodes, 2011; Schmidt, 1901). All *Ostreopsis* species are flattened with an oval-ovate shape that tapers ventrally in the apical view. The plate patterns are largely identical and broadly fit the description of the type species, *Ostreopsis siamensis* Schmidt, except for *Ostreopsis heptagona* Norris, Bomber et Balech (David et al., 2013; Hoppenrath et al., 2014; Penna et al., 2005). Some, but not all, *Ostreopsis* species are known to produce palytoxin (PLTX) and/or its analogues and form harmful blooms which have been associated with human poisonings and accumulation in seafood (Ciminiello et al., 2012a, 2006, 2012b; Rhodes et al., 2002; Tubaro et al., 2011; Usami et al., 1995). Based on analyses of 28S and ITS/5.8S rDNA sequences, several clades of *Ostreopsis ovata* Fukuyo exist that are morphologically indistinguishable, comprising the *O. ovata* species complex (Sato et al., 2011; Tawong et al., 2014). Additionally, isolates of *Ostreopsis*
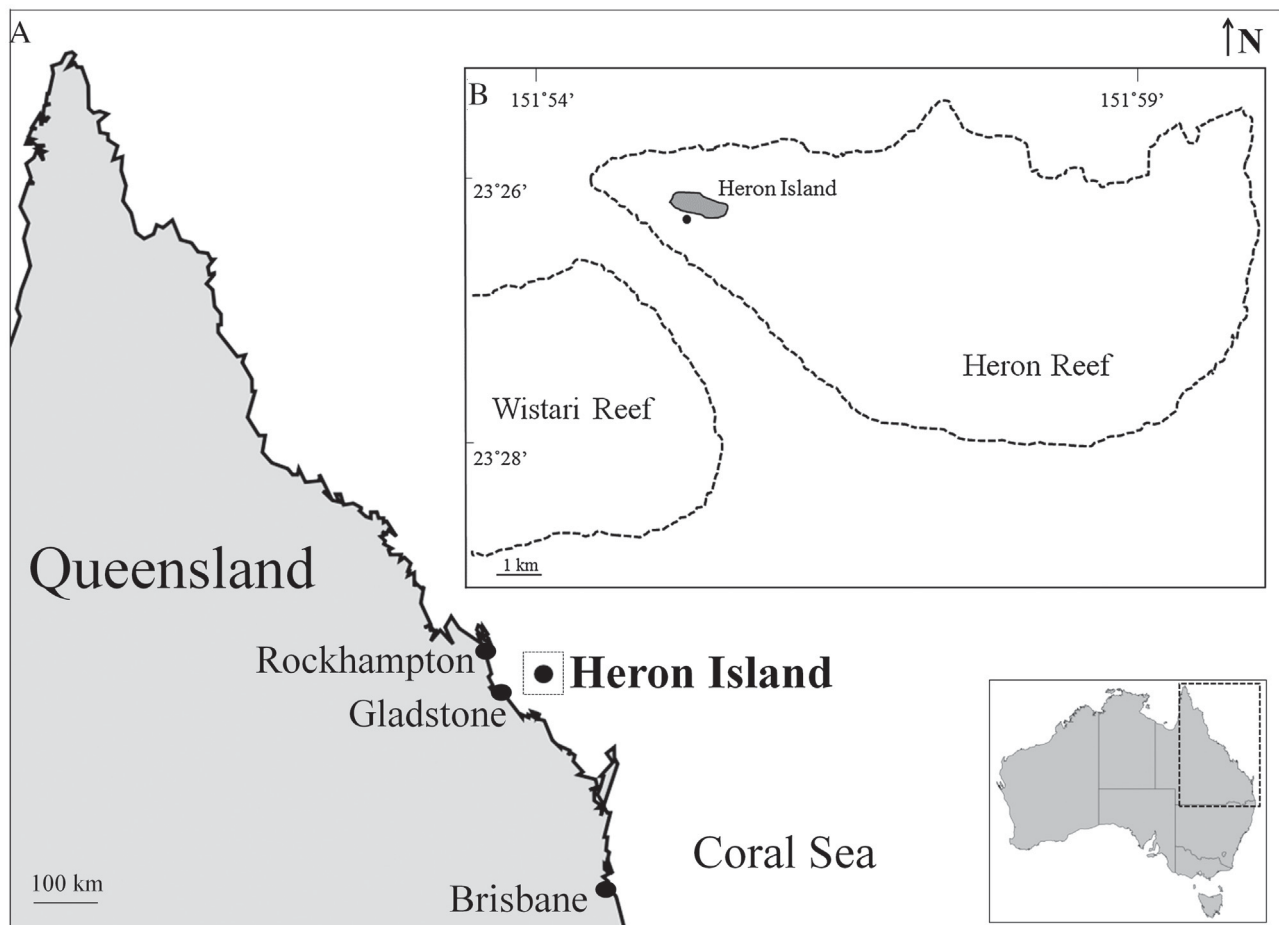

Fig. 1. A: Map of the north-eastern coastline of Australia, showing sampling location: Heron Island. B: Map of Heron reef lagoon, showing sampling site during June 2014 and February 2015 (shown as black dot).

cf. *ovata* from the Mediterranean, NE Atlantic and the Brazilian coasts have exhibited genetic differences compared to the Indo-Pacific isolates based on their 28S D1/D2 rDNA and ITS/5.8S rDNA sequences (Penna et al., 2014, 2010, 2005; Pin et al., 2001; Sato et al., 2011; Tawong et al., 2014). The widespread geographic distribution of *Ostreopsis* populations provides vast opportunities for speciation events to occur which are highlighted by the sequence data comparisons of faster evolving genes, however, in order to compare between published findings and to establish accurate and more recent historical phylogenetic reconstruction of this genus, reporting sequences from different genes and the use of different molecular techniques is essential (LaJeunesse, 2001; Sampayo et al., 2009).

In Australia, what little is known about the diversity and ecology of *Ostreopsis* species has been derived from microscopic and morphological studies (Ajani et al., 2013; Heimann et al., 2009; Holmes et al., 1988; Pearce et al., 2001). It was only recently that an *Ostreopsis* cf. *siamensis* strain producing PLTX-like analogues was isolated and characterized, despite its frequent presence (Verma et al., 2016). In this study, fourteen isolates were cultured from the lagoon of Heron Island, from the southern Great Barrier Reef (GBR), and report the morphological and molecular phylogenetic characterization from 18S (SSU), partial regions of 28S (LSU) and ITS/5.8S rDNA sequences. The strains were tested for the production of PLTX-like analogues using liquid chromatography-mass spectrometry (LC–MS/MS) analysis and the toxicity of the sample extracts was determined using a fish gill cell line bioassay.

2. Materials and methods

2.1. Sample collection and culture establishment

Heron Reef (23°27′S, 151°55′E) is located in the southern Great Barrier Reef, approximately 85 km northeast of Gladstone, Queensland (Fig. 1). This lagoonal platform reef is approximately 10 km in length and 4.5 km in width at its widest point, and the island itself, only 750 m by 240 m, is located at the western end of the reef (Rasheed et al., 2004; Webb et al., 1999). Seasonal water temperatures range from 19 to 26 °C, with occasional highs of 32 °C. At the time of sample collection, sea surface temperature was 20 °C.

Macroalgal samples (*Padina* and *Saragassum* spp.) were collected from a shallow area (less than 1.5 m) on the inner reef flat off Heron Island research station in June 2014 and February 2015. Samples were placed in plastic bags and bottles containing local seawater, and shaken vigorously to detach the epiphytic microalgal cells. The epiphytic suspension was passed through a 125 μm mesh filter to remove larger fauna and debris. Using a glass micropipette, single *Ostreopsis* cells were isolated using an inverted light microscope (Nikon Eclipse TS100) and transferred to a drop of clean filtered seawater. The transfer was repeated up to five times and fourteen non-axenic monoclonal cultures were established. The isolates were maintained in f/10 medium (Guillard, 1975), at 25 °C and salinity of 35 under the photo illumination of 80–100 μmol/m^{2}s^{-1} and 12:12 h light-dark cycle in 24 multi-well culture plate (Corning Inc. Durham, USA) with 1 mL medium. After 4–6 weeks, they were transferred to 50 mL sterile tissue culture flasks (Becton Dickinson, Sydney, Australia) and maintained in the same conditions. Cultures were subcultured in f/10 medium every 4 weeks thereafter.

2.2. Microscopy

Living cells of interest were picked using a Leica DMIL inverted microscope (Leica Microsystems GmbH, Wetzlar, Germany), placed on an object slide and observed with a Leica DMRB (Leica Microsystems GmbH, Wetzlar, Germany) equipped with differential interference contrast optics at 400 and 640 times magnification with oil immersion objectives. Digital photos were taken using a Leica DFC420C camera (Leica Microsystems GmbH, Wetzlar, Germany).

Cell dimensions of mid-log phase cultures were measured under 400 × using a calibrated eyepiece of Eclipse TS100 inverted microscope with bright field optics (Nikon, Hilton, Australia). Cells were harvested from the culture medium phase 8–10 days after subculturing and fixed in 4% Lugol solution to measure the depth = dorsoventral diameter (DV) and transdiameter width (W) using ImageJ v1.48 (Rasband 1997–2013). Thirty cells for each strain were measured. The variations in DV and W were assessed through one-way analysis of variance (ANOVA) in SPSS v11.5 (IBM, Armonk, USA).

For SEM, the culture was fixed with Lugol solution and stored in the dark. Cells were placed on a 5 μm Millipore filter, rinsed in distilled water, and dehydrated in a series of increasing ethanol concentrations (30, 50, 70, 85, 90, 100%), followed by chemical drying with hexamethyldisilazane at room temperature for 20 mins and finally at 50 °C in a drying oven for 5 mins. The sample/filter was mounted on a stub and sputter coated with gold-palladium (Bal-Tec SCD 050; BAL-TEC Präparations-gerätevertrieb, Wallof, Germany). Cells were observed using a Tescan VEGA3 microscope (Elekronen-Optik-Service GmbH, Dortmund, Germany) at 15 kV using the SE detector (Hoppenrath et al., 2014).The species description is based on light microscopic investigations of all 12 strains and a scanning electron microscopic study (theca description) of the type strain HER32.

2.3. DNA extraction and PCR amplification

DNA was extracted using a modified 3% CTAB buffer (100 mM Tris-HCl pH 8; 20 mM EDTA pH 8; 1.4 M NaCl; 0.5% beta-mercaptoethanol) (Hoppenrath et al., 2009). In summary, ten ml of dense culture was centrifuged at 2,300g for 10 mins at room temperature and the algal pellets were placed into 500 μL of buffer in the heat block at 68 °C for 2 h with several vigorous shakes during incubation. The aqueous layer was separated using 24:1 chloroform: isoamyl alcohol and precipitated in isopropanol and 3 M sodium acetate (pH 5.2). The DNA pellet was washed with 70% ethanol and vacuum dried to remove any traces of ethanol. Sterile Milli-Q water was added to DNA pellets and the samples were stored at −20 °C prior to PCR reactions (Lang and Burger, 2007). The extracted DNA was visualised on 1% agarose gel stained with GelRed (Gene Target Solutions, Dural, Australia) and quantified using a Nanodrop ND-1000 (NanoDrop Technologies, Wilmington, USA).

The partial nuclear SSU rRNA gene, the D1/D2 and D8/D10 regions of the LSU rRNA gene, the internal transcribed spacer regions and 5.8S rRNA gene (ITS1/5.8S/ITS 2) were amplified and sequenced as described in Verma et al. (2016) (see Supplementary data S1 for details). PCR products were purified with Sure Clean Plus (Bioline, Sydney, Australia), according to the supplied protocol from the manufacturer and sequenced using a commercial service (Macrogen Inc., Seoul, Korea).

2.4. Sequence analysis and phylogenetic reconstruction

Analyses on SSU, ITS1/5.8S/ITS2, D1-D2 and D8-D10 regions of LSU rDNA were conducted as described in Verma et al. (2016) (see Supplementary data S2 for reference sequences retrieved from GenBank). In summary, multiple sequence alignments, post manual inspection, were performed using ClustalW v1.6 as implemented in MEGA v6 (Tamura et al., 2013). Substitution models were selected for each dataset based on lowest Bayesian

information criterion (BiC). Phylogenetic analyses were performed using both maximum likelihood (ML) and Bayesian inference (BI) approaches. ML trees were produced in MEGA v6 using Tamura 3 (T92) +G +I with 5 gamma categories substitution model for all analyses with a bootstrap of 1000 replications. Bayesian analyses was performed using MrBayes v3.2.2 (Ronquist and Huelsenbeck, 2003) as implemented in Geneious v6 (Kearse et al., 2012) using general time reversible model (GTR) + gamma model for all analyses.

Genetic distance (pairwise uncorrected *p*-distance) were estimated from the ITS/5.8S, D1/D2 and D8/D10 LSU and SSU rDNA sequences using the *p*-distance model and bootstrap procedure (1000 replicates) in MEGA v6 (Tamura et al., 2013). All positions containing gaps and missing data were eliminated for the analyses.

2.5. Modelling ITS2 secondary structure

The second internal transcribed spacer (ITS2) region was identified and delimited based on alignment with *O.* cf. *ovata* strain OvPD04 (GenBank accession number AF076217) from Leaw et al. (2010) and *O.* cf. *siamensis* strain CNR-B4 (Genbank accession number AJ301643) from Penna et al. (2005). After removing the 3′ and 5′ termini of the ribosomal 5.8S and 28S rRNA respectively, the annotated ITS2 sequences were aligned using ClustalW in MEGA v6 and manually adjusted. For homologous modelling, *Coolia monotis* strain SZN 43 (GenBank accession number AJ308524) was used as template. A total of 37 ITS2 secondary structures were analysed of which, 23 ITS2 sequences were sampled from GenBank and 14 were newly obtained from this study (see Supplementary data S3). Incomplete ITS2 sequences were excluded from the analysis. RNA transcript folding of ITS2 for all *Ostreopsis* strains was predicted by the ITS2 Database V (http://its2.bioapps.biozentrum.uni-wuerz-burg.de/), with ITS2 PAM50 matrix chosen and the percentage of transfer helices at 75% similarity selected (Ankenbrand et al., 2015). Structures were visualised using VARNA (Darty et al., 2009). The compensatory base changes (CBCs) and hemi-CBCs in the predicted secondary structure models were identified manually and with the aid of the software 4SALE (Schultz and Wolf, 2009; Seibel et al., 2006).

2.6. Toxin analysis via LC–MS/MS

All *Ostreopsis* cultures were harvested in late stationary phase by centrifugation (50 mL; 2300*g*; 10 min; room temperature) and the cell pellets were freeze dried. PLTX and/or related structural analogues were screened using a quantitative LC–MS/MS method at the Cawthron Institute, New Zealand (Selwood et al., 2012). In summary, this analytical approach monitors substructures generated by the oxidative cleavage, using periodic acid, of vicinal diol groups present in the intact toxins. It yields an amino aldehyde common to known palytoxins, ovatoxins and ostreocins, used for quantification, and an amide aldehyde that varies depending on the toxin type (Selwood et al., 2012; Verma et al., 2016).

2.7. Fish gill cell line assay for toxicity

The fish gill cell line RTgill-W1 was obtained from the American Type Culture Collection (CRL-2523). Primary cells were originally initiated from gill filaments of rainbow trout *Oncorhynchus mykiss* (Bols et al., 1994). Fish gill cells were cultured in 75-cm^2 culture treated flasks with Leibovitz medium (L1518, Sigma, Sydney, Australia) supplemented with 10% fetal bovine serum (v/v) (12003C, Sigma, Sydney, Australia) and an antibiotic-antimycotic solution (A5955, Sigma, Sydney, Australia) at 20 °C in the dark. Confluent gill cells were detached with 0.25% trypsin-0.02% EDTA solution (59428C, Sigma, Sydney, Australia) for subculturing and seeding purposes (Dorantes-Aranda et al., 2011).

Pellets obtained from three *Ostreopsis* strains HER24 (*O.* cf. *siamensis*), HER27 (*O.* cf. *ovata*) and HER26 (*O. rhodesae*) at mid-exponential (day 8) and late stationary (day 21) growth phases were dissolved methanol (≥99.9%). Solvent volume was adjusted for each extract in order to achieve the same concentrations for all extracts. Pellets were resuspended in the solvents and sonicated for 5 mins to rupture the cells. Samples were centrifuged (3000 rpm; 10 mins) and the supernatant was transferred into new tubes and stored at −80 °C until analysis. Gill cells were detached, counted and seeded at a concentration of 1.5×10^5 cells mL^{-1} in quadruplicate in Greiner Bio-One 96-well microplates (655180, Interpath Services Pty Ltd, Heidelberg West, Australia) 48 h prior to the experiments (Dayeh et al., 2005; Dorantes-Aranda et al., 2011). Algal extracts were mixed with L-15/ex medium
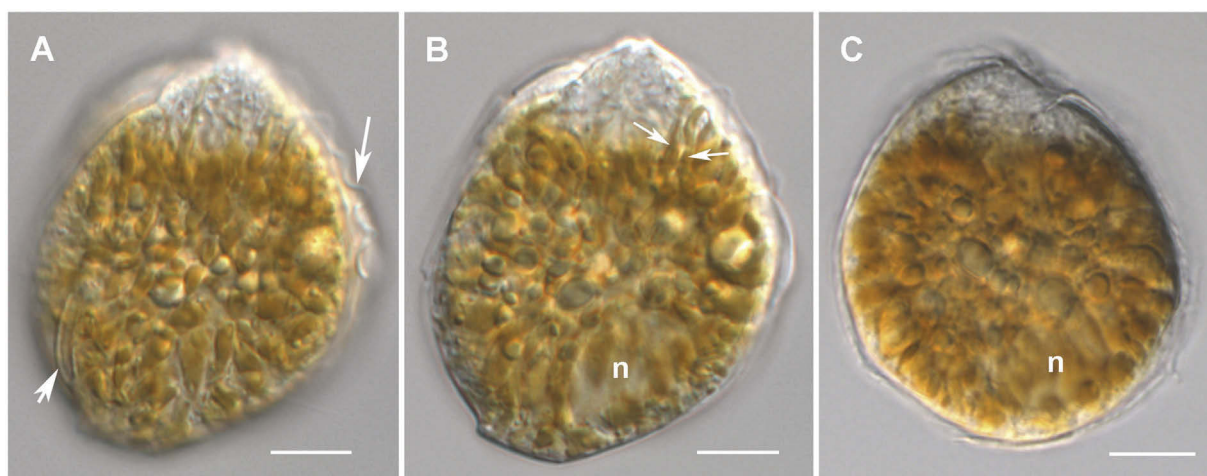
Fig. 2. Light micrographs of *Ostreopsis rhodesae* sp. nov. showing the cell shape and general features. A and B: Same cell in diffent focal planes. Ovate cell ventrally tapering and ventral area devoid of chloroplasts. A: Note the APC (short arrow) and the transverse flagellum (long arrow). B: The nucleus (n) is located in the right dorsal area. Chloroplasts are elongated (arrows). C: Cell with different shape confirming the nucleus (n) position. Scale bars = 10 μm.

(Schirmer et al., 1997) to achieve final concentrations of 0.2, 1, 2, 4 and 8% for the exposure (equivalent to 80, 400, 800, 1600 and 3200 cells mL^{-1}, respectively). The methanol solvent final concentration for all treatments, including the control groups, was methanol/mQ, 4%. This solvent concentration had no effect on gill cell viability. Gill cells were exposed to the algal extracts and control treatments (only L-15/ex with solvent) for 2 h. After completion of the 2 h exposure period, experimental solutions were discarded and gill cells were rinsed with phosphate buffer saline (PBS). Resazurin (Sigma, Sydney, Australia) in L-15-ex (5% v/v) was added to all wells and incubated for 2 h in the dark to measure viability of gill cells (Dorantes-Aranda et al., 2015). Fluorescence of metabolised resazurin was measured with a microplate reader (FLUOstar OPTIMA, BMG Labtech, 413-3350), using excitation and emission filters of 540 and 590 nm, respectively. Statistical analysis for the fish gill cell assays was performed using the software Statistica v13 (StatSoft, Dell, Australia). Data were subjected to one-way ANOVA and a posteriori analysis was performed using the Tukey test for multiple comparisons. A significance level of 95% ($\alpha = 0.05$) was considered for all analysis.

3. Results

3.1. Ostreopsis rhodesae Verma, Hoppenrath et Murray sp. nov

3.1.1. Morphological description

The strongly anterio-posteriorly flattened cells were ovate (drop/tear-shaped) and ventrally tapering (Fig. 2A–C). Cells of the type strain (HER32) were 32–56 μm deep (44.2 ± 6.3 S.E., n = 30; DV diameter) and 23–42 μm (32.4 ± 5.3 S.E., n = 30) wide (W) and varied from 1.2–1.9 (mean = 1.4) in DV/W ratio (Table 1). The maximal size ranges of all investigated strains were 28.3–57.8 μm deep and 16.7–44.2 μm wide (Table 1). Cells were densely packed with elongated golden-brown chloroplasts (Fig. 2B), except for the ventral area (Fig. 2A–C). The oval nucleus was located dorsally (Fig. 2B and C). Pusules were not recorded. No significant differences in DV diameter and width were identified between O. cf. ovata, O. cf. siamensis and O. rhodesae (Table 1).

The plate formula is APC 3′7″ 6c 8?s 5‴ 2⁗ (Figs. 3–6). The narrow, slightly curved and elongated apical pore complex (APC) was located parallel to the left mid-lateral to dorsal cell margin

(Figs. 3 A and D, 6 A). The Po plate was about 9–11 μm long. The first apical plate (1′) was long, hexagonal and most of it located left to the centre of the epitheca (Fig. 3A, B and D). Extremely few cells had a heptagonal 1′ plate contacting Plate 5″ (Fig. 3D, arrow). The characteristic second apical plate (2′) was narrow and elongated, about twice as long as the Po plate (Figs. 3 A and D, 4 and 6 A). Plate 2′ completely separates Plate 3′ from 3″ (Fig. 4A and B). Its extension was very difficult to observe in complete cells (Figs. 3 A and 4 C arrows). The third apical plate (3′) was pentagonal, had a suture with Plate 6″, and did not touch Plate 3″ (Figs. 3 A–C and 4 A). In the precingular series Plate 1″ was the smallest and 6″ the largest (Figs. 3 A–D and 6 A). All precingular plates were four-sided, except the second (2″) and sixth (6″) that were pentagonal (Figs. 3 A–D and 6 A). Plate 5″ was not in contact with Plate 1′, with a few exceptions (Fig. 3A–D). The cingulum was narrow, deep, and slightly undulated (Figs. 3 C and 5 A) and cingular plates were difficult to determine, nearly only in broken cells (not shown). Six cingular plates were observed (Fig. 6A and B). The postcingular plate series consisted of a very small first (1‴) plate, a medium sized fifth (5‴) plate and three large plates (2‴, 3‴, 4‴) with pentagonal 2‴ and four-sided 3‴ and 4‴ (Figs. 3 E and F and 6 B). The two antapical plates were of unequal size, 1⁗ relatively small and 2⁗ being asymmetrical pentagonal, and relatively wide with nearly parallel sides (sutures with 2‴ and 5‴) (Figs. 3 E and F and 6 B). The hidden sulcal construction was not completely visible (in broken cells) and it consisted of at least 8 plates (Fig. 5B–F, sa not visible). Thecal plates were smooth with scattered large pores with an internal sieve-like structure of small pores (Figs. 3 D and E and 5 G–J). Nearly all pores were of the same size class (Fig. 3D and E). Only in a very few cases, best recognizable in thecal plate inside views, single smaller and simple pores were observed (Fig. 5I and J).

3.1.2. Holotype

Fig. 3A was obtained from strain HER32. SEM-stub (designation CEDiT2016H56) deposited at Senckenberg am Meer, German Centre for Marine Biodiversity Research, Centre of Excellence for Dinophyte Taxonomy, Germany.

3.1.3. Isotype

Lugol-fixed subsample of strain HER32 (designation CEDiT2016I57) deposited at the Senckenberg am Meer, German

Table 1
Morphological characteristics (means and standard deviations, ranges) of *Ostreopsis* strains determined by light microscopy: dorso-ventral diameter (DV), trans-diameter (W) and DV/W ratio. All data were from cultured cells.

| S. No	Species	Strain	DV (μm)	DV range	W (μm)	W range	DV/W
1	*O.* cf. *ovata*	HER27	37.7 ± 4.3	30.2–48.3	28.7 ± 3.7	21.9–37.5	1.3 (1.1–1.8)
2	*O.* cf. *siamensis*	HER24	39.0 ± 4.0	32.3–46.9	30.1 ± 3.4	23.9–37.1	1.3 (1.2–1.4)
3	*O. rhodesae*	HER3	39.7 ± 3.1	32.7–46.3	30.3 ± 4.2	22.1–39.6	1.3 (1.1–1.8)
4		HER6	42.3 ± 3.5	37–52.8	30.3 ± 3.3	22.4–38.4	1.4 (1.1–1.9)
5		HER7	41.4 ± 4.3	33.7–48.8	30.4 ± 5.3	19.9–37.6	1.4 (1.1–2.1)
6		HER15	42.3 ± 4.3	36.6–54.4	30.7 ± 4.5	20.8–42.0	1.3 (1.1–1.9)
7		HER20	48 ± 3.8	40–57.8	36.8 ± 4.7	25.1–44.2	1.3 (1.1–1.9)
8		HER21	38.6 ± 3.1	32.1–45.7	28.7 ± 4.3	16.7–39.1	1.4 (1.1–2.1)
9		HER25	39.1 ± 3.7	32.1–45.7	27.9 ± 3.8	19.8–37.5	1.4 (1.2–1.9)
10		HER26	44.8 ± 4	37–52.8	32 ± 4.3	22.5–41.4	1.4 (1.2–1.8)
11		HER28	37.3 ± 3.3	28.9–43.1	28.2 ± 3.8	21.3–34.1	1.3 (1.1–1.7)
12		HER30	40.4 ± 6.2	32.7–55.4	27.7 ± 5.7	17.9–39.3	1.5 (1.2–1.9)
13		HER32[a]	44.2 ± 6.3	31.9–55.9	32.4 ± 5.3	22.9–42.3	1.4 (1.1–1.9)
14		HER301	37.1 ± 4.4	28.3–46	26.9 ± 4.6	19.5–36.8	1.4 (1.1–1.9)
		Mean	41.3 ± 5.3	28.3–57.8	30.2 ± 5.1	16.7–44.2	1.4 (1.1–2.1)

[a] Type strain.
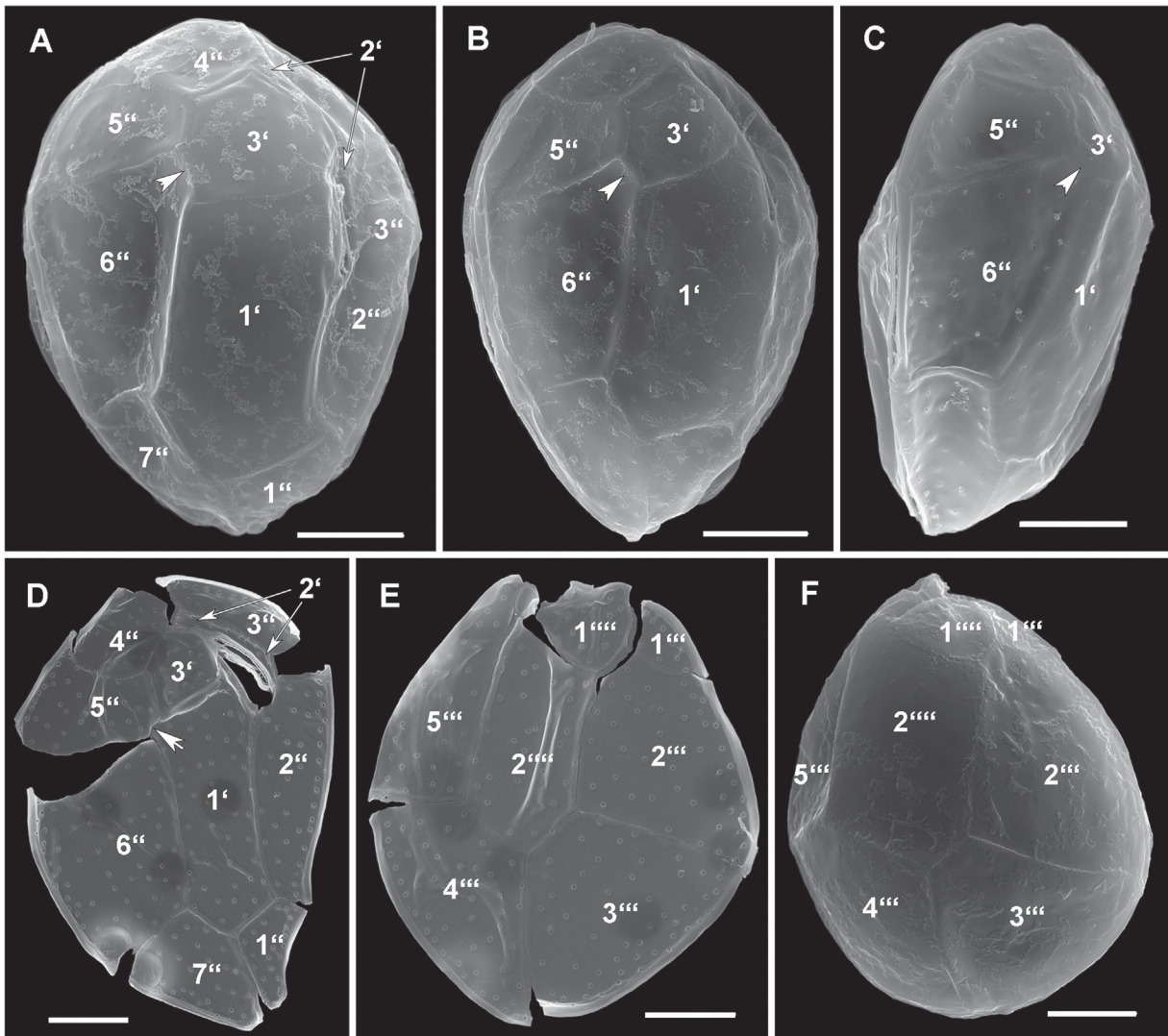
Fig. 3. Scanning electron micrographs of *Ostreopsis rhodesae* sp. nov. showing the general thecal tabulation. A, B: Epitheca in apical view. Note the suture between Plates 3′ and 6″ (arrowhead). C: Epitheca in right lateral view. Note the suture between Plates 3′ and 6″ (arrowhead). D: Epitheca in apical view with heptagonal 1′ plate, with suture between Plates 1′ and 5″ (arrow). E and F: Hypotheca in antapical view. Scale bars = 10 μm.

Centre for Marine Biodiversity Research, Centre of Excellence for Dinophyte Taxonomy, Germany.

3.1.4. Type locality

Heron Reef Lagoon, 23°27′ S, 151°55′ E, southern Great Barrier Reef, Coral Sea, Australia

3.1.5. Etymology

The species is named in honour of Dr. Lesley Rhodes, whose pioneering research has significantly contributed to the general understanding of the impact of toxic dinoflagellates and harmful algal blooms worldwide.

3.1.6. Accession numbers

ITS1/5.8S/ITS2 sequences (n = 12): KX0558769-80; SSU sequences (n = 12): KX055855-66; and LSU (D1-D2 and D8-D10) sequences (n = 12): KX055841-52.

3.2. Molecular analyses and phylogeny

ML and BI analyses performed on fourteen *Ostreopsis* strains with additional reference sequences from Genbank identified nine strongly supported clades (*O.* cf. *ovata*, *O.* cf. *siamensis* and *Ostreopsis* spp. 1–7). Twelve strains of *Ostreopsis rhodesae* clustered together and formed a novel fully supported monophyletic clade (BI = 1.00; ML = 100) shown by ITS/5.8S and D8/D10 LSU regions of rDNA (Accession numbers: KX0558769-80 and KX055841-52) (Fig. 7). This was further confirmed with D1/D2 LSU and partial 18S rDNA regions (Accession numbers: KX055841-52) (Fig. 8). This clade formed the sister clade to *O.*cf. *siamensis* with high nodal support in all phylogenetic analyses (Figs. 7 and 8).

The strain HER24 was placed in the *O.*cf. *siamensis* clade along with strains from the Mediterranean and South Pacific regions and showed identical sequences for all analysed rDNA regions (Accession numbers: KX055868, KX055882 and KX055854) (Figs. 7 and 8). The molecular phylogenetic trees revealed the separation of *O.* cf. *ovata* clade into various geographic sub-clades of which HER27 belonged with the South China Sea sub-clade (Accession numbers KX055867, KX055881 and KX055853) comprising strains isolated from Malaysia, Thailand and New Zealand (Figs. 7 and 8).

Uncorrected genetic distance values were calculated from the ITS/5.8S, D1/D2 and D8/D10 LSU rDNA and 18S rDNA datasets. The genetic distance values within *O. rhodesae* based on the LSU rDNA sequences were higher than ITS/5.8S and 18S sequences (Table 2).
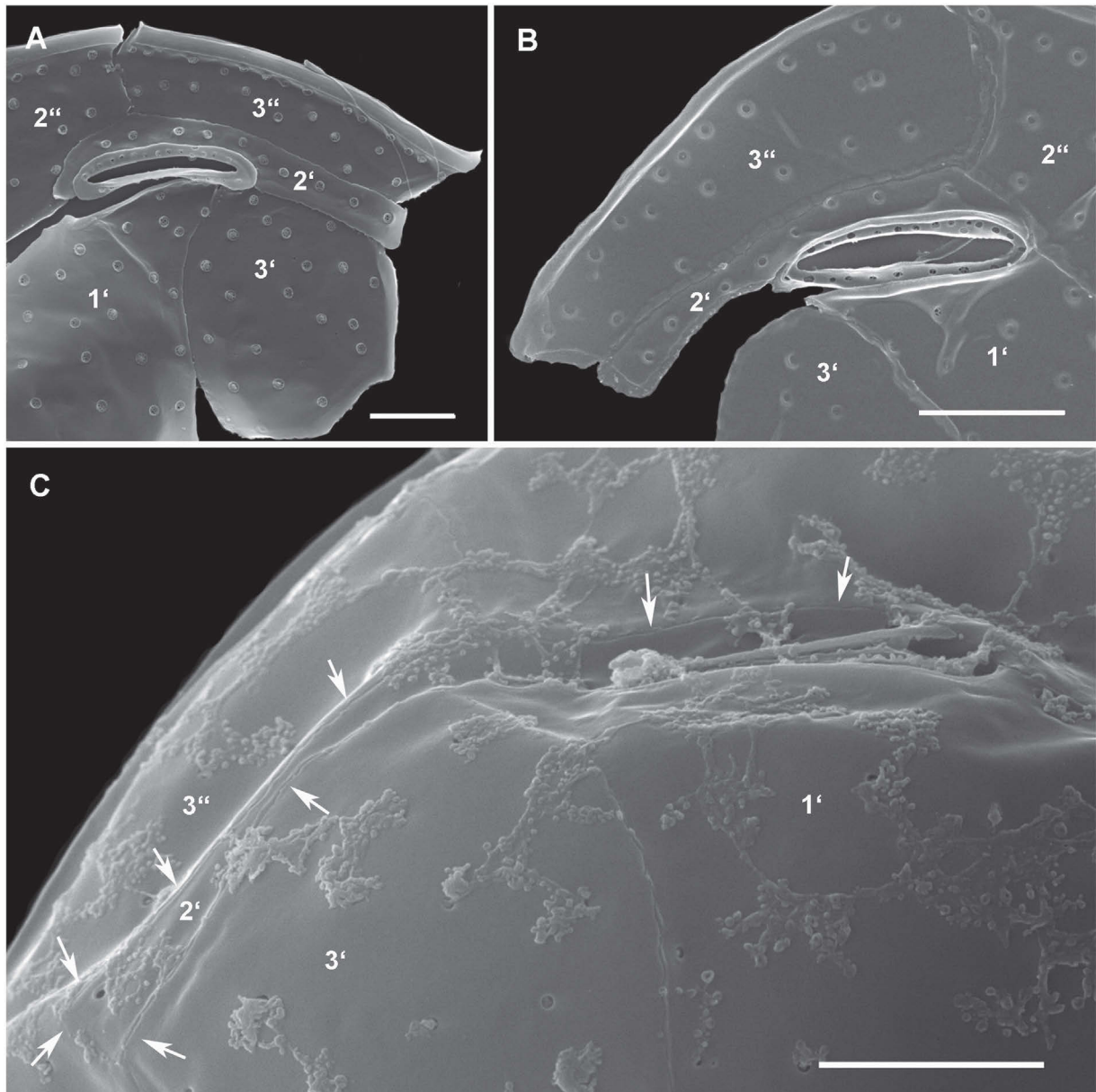
Fig. 4. Scanning electron micrographs of *Ostreopsis rhodesae* sp. nov. showing details of the second apical plate (2′). A: Inside view of a broken theca. B: Outside view of a broken theca. C: Outside view of an intact cell. Note the 2′ plate margins (arrows). Scale bars = 5 μm.

Furthermore, the genetic distance values based on the data from the rDNA regions between *O. rhodesae* and *O.* cf. *ovata* were larger than those between O. rhodesae and O. cf. siamensis and were comparable to the distance values between *O.* cf. *ovata* and *O.* cf. *siamensis* (Table 2).

3.3. ITS2 secondary structure

Only the *Ostreopsis* species discovered at Heron Island in this investigation were included in the molecular analyses. A total of 37 strains from *O.*cf. *siamensis*, *O.* cf. *ovata* and *O. rhodesae* were used for the analysis (14 sequences obtained from this study, 23 obtained from GenBank, see Supplementary data S3). The ITS2 region of the *Ostreopsis* species was 88–91 base pairs (bp): 90 bp for *O. rhodesae*, 91 bp for *O.* cf. *siamensis* and 88–91 bp for *O.* cf. *ovata*. The ITS2 transcripts for the analysed *Ostreopsis* species have two helices. Although there were exceptions, the structure of the

helices typically consisted of a base-paired stem capped by an apical loop of unpaired nucleotides (Fig. 9, see Supplementary data S3). The universal Helices III and IV are missing. No CBCs and Hemi-CBCs were detected within *O.* cf. *siamensis* strains from Med/Pac clade and the South Pacific (13 sequences). Also, the ITS2 transcripts for all *O. rhodesae* strains were identical and no CBCs were detected (12 sequences).

Helix I was conserved amongst all *O.* cf. *ovata* sub-clades but varied from *O.* cf. *siamensis* and *O. rhodesae* (Fig. 9). Sequence variability was observed within Helix II amongst *O.* cf. *ovata* strains (12 sequences) belonging to different sub-clades that led to different number of pairings in the branches, especially in South China Sea and Thailand sub-clades (see Supplementary data S3). Single Hemi-CBC was detected in Celebes Sea sub-clade (Helix II U-G ↔ C-G) whereas; three HCBCs were detected in *O.* cf. *ovata* Med/Pac subclade when compared with other *O.* cf. *ovata* sub clades (Helix II U-A ↔ U-G; G-U ↔ G-C; U-G ↔ U-A), including the motif of
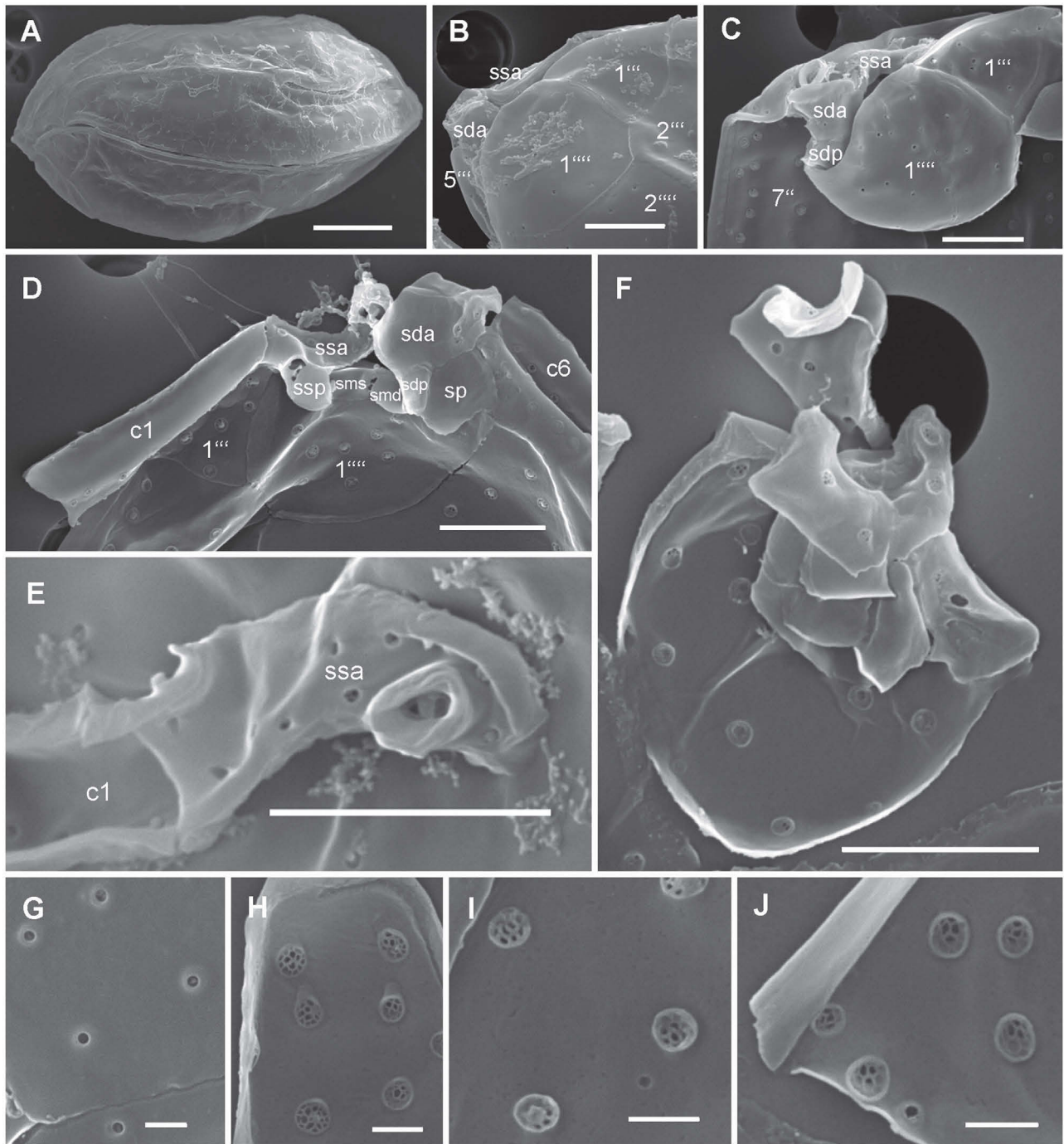
Fig. 5. Scanning electron micrographs of *Ostreopsis rhodesae* sp. nov. A: Cell in left lateral view showing the undulated cingulum path. B–F: Sulcal details. B: Ventral hypotheca, outside view. C: Ventral hypotheca, outside view of a broken cell. D: Ventral part of a broken cell. E: Isolated ssa plate in connection with the first cingular plate. F: Sulcal plates separated from the theca, inside view. G–J: Thecal pores. G: Thecal plate detail, outside view. H–J: Details of the inside of thecal pores showing the sieve-like structure. Note the simple small pores in I and J. Scale bars A: 10 μm, C–F: 5 μm, G–J: 1 μm.

pyrimidine–pyrimidine mismatch (U-G ↔ U-U) in helix II (see Supplementary data S3). CBCs and Hemi CBCs were detected between *O.* cf. *siamensis*, *O.* cf. *ovata* and *O. rhodesae* strains including the motif of pyrimidine–pyrimidine mismatch (U-G ↔ U-U) in helix I between *O.* cf. *ovata* and *O. rhodesae* (Table 3) (Fig. 9).

3.4. Toxin presence

LC–MS/MS analysis of the oxidized cell extract from *O.*cf. *ovata* HER27 showed the presence of both the amino aldehyde fragment,

common to all known PLTX, ovatoxin and ostreocin analogues, as well as the amide aldehyde fragment, thereby confirming the presence of PLTX-like analogues in the extract. The total amount of PLTX-like analogues found were 11.8 ng (total 6400 cells) resulting in an estimate of 1.8 pg cell^{-1}. No PLTX-like analogues were detected from cellular isolates of *O. rhodesae* strains and *O.* cf. *siamensis*.

3.5. Fish gill cell assays

Fish gill cells were sensitive to *Ostreopsis* extracts, especially those from *O. rhodesae* and *O.* cf. *ovata*, which caused ≥98.5%
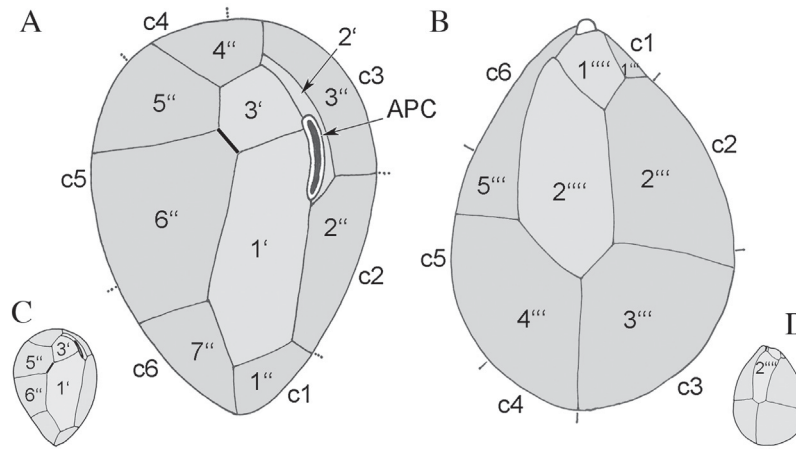
Fig. 6. Line drawings showing thecal plate patters. A and B: *Ostreopsis rhodesae* sp. nov. A: Epitheca. B: Hypotheca. C and D: *Ostreopsis heptagona* (from Hoppenrath et al., 2014). C: Epitheca. D: Hypotheca.

decrease of gill cell viability. Extracts from *O.* cf. *siamensis* decreased gill cell viability by no more than 69%; the extract prepared from the stationary growth phase was significantly less toxic than that from the exponential phase (p ≤ 0.009), particularly

at the two highest extract concentrations (4 and 8%). The same pattern was observed for the *O. rhodesae* extract, with the extract from the stationary growth phase being less toxic than the extract from exponential phase. This extract was the most toxic among all
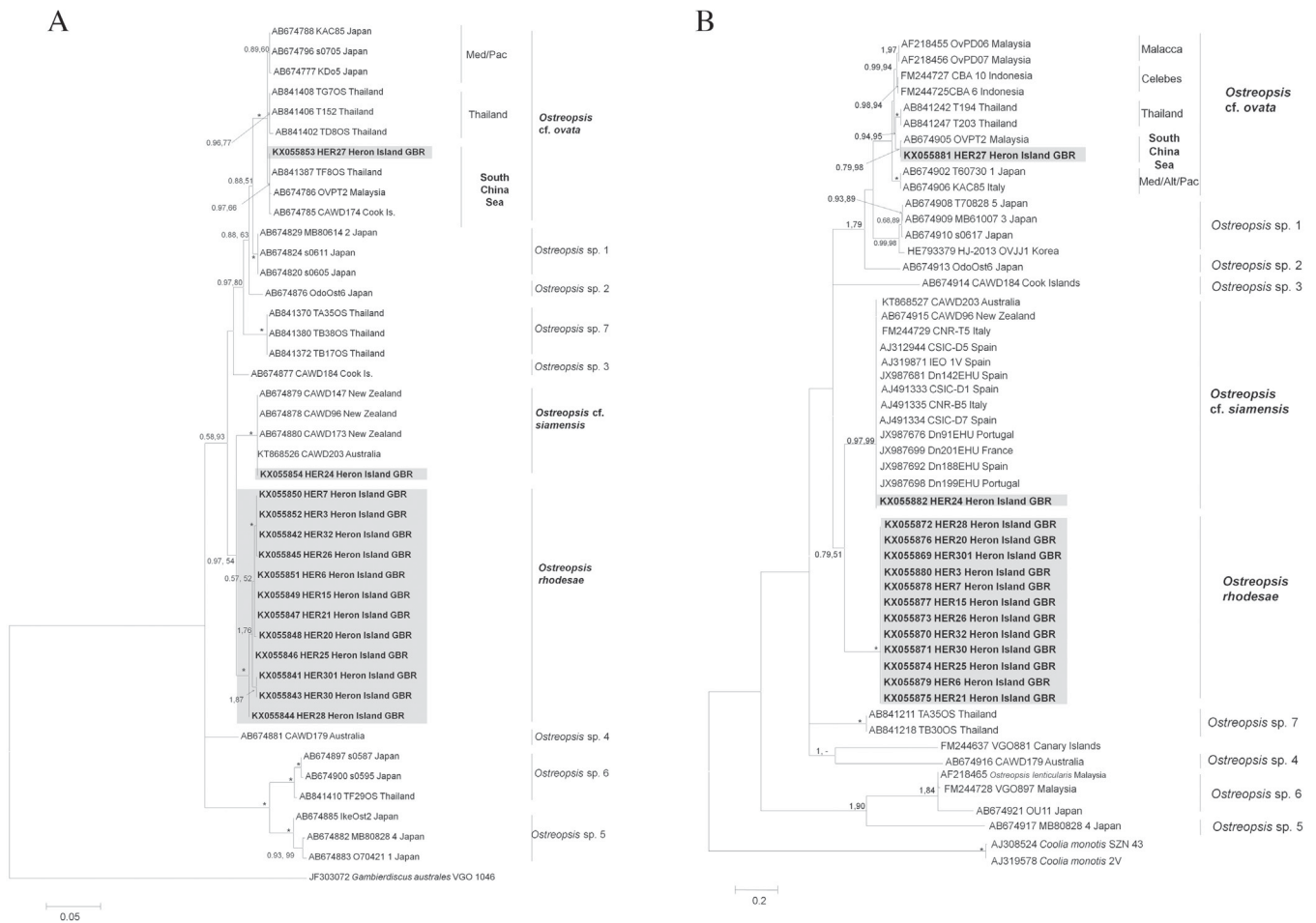
Fig. 7. Maximum Likelihood (ML) phylogenetic trees of various *Ostreopsis* strains using primer sets for A: ITS1-5.8S-ITS2 and B: D8-D10 LSU rDNA. External Black vertical bars show each distinct *Ostreopsis* clade and internal vertical bars show each *Ostreopsis* subclade. Med; Atl; Pac; Ind are the *Ostreopsis* cf. *ovata* Mediterranean Sea, Atlantic, Pacific and Indian Oceans subclades respectively. Malacca; Celebes; South China Sea; Thailand are the *Ostreopsis* cf. *ovata* Malacca strait, Celebes Sea, South China Sea and Gulf of Thailand sub clades respectively. Numbers at nodes represent posterior probabilities from Bayesian Inferences (BI) and bootstrap support values from Maximum Likelihood (ML) based on 1000 pseudo-replicates. * represents 1100 support values for BI and ML respectively.

A

B

Fig. 8. ML phylogenetic trees of various *Ostreopsis* strains using primer sets for A: D1-D3 LSU rDNA and; B: SSU rDNA. See the caption in Fig. 7 for the detailed information.

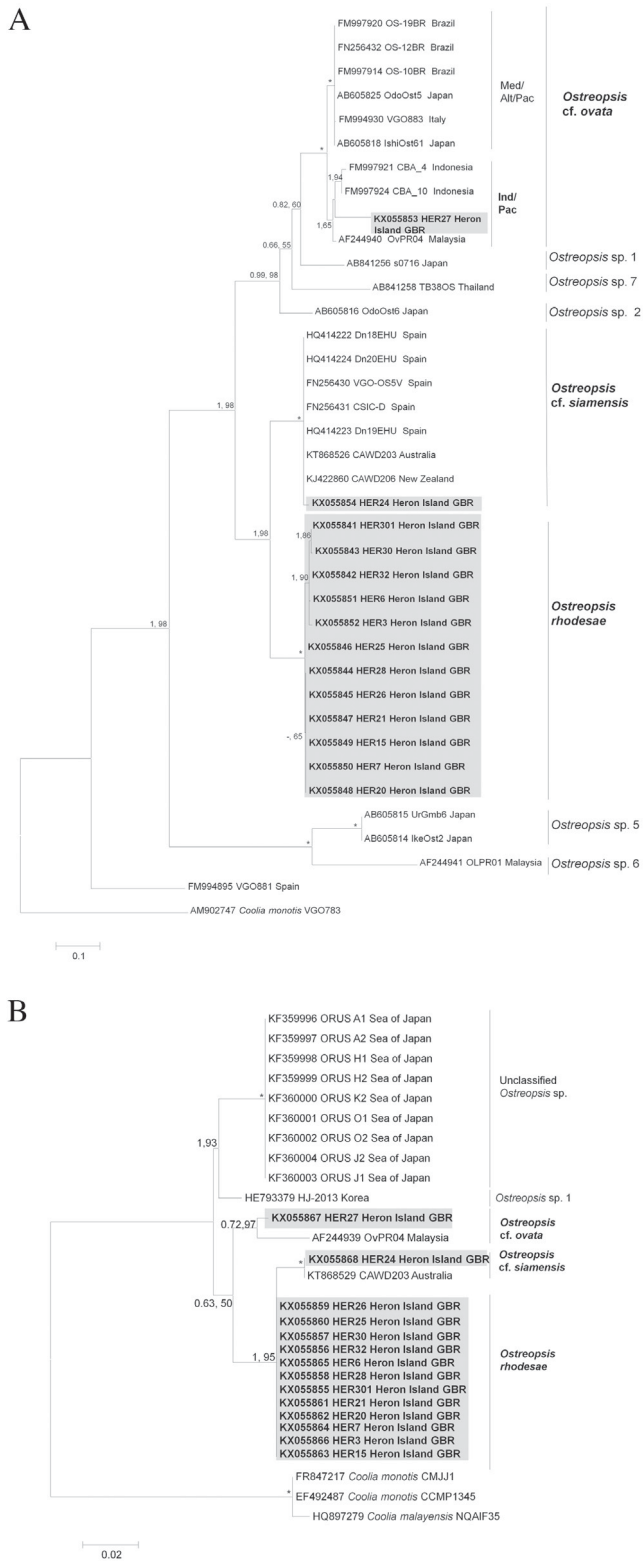extracts, causing a decrease of ≥97% in gill cell viability from concentrations of 4%, whereas the extract from the stationary growth phase caused ≤34% decrease in gill cell viability.

The opposite pattern was observed for the *O.* cf. *ovata* HER27 extract in which the stationary growth phase was significantly more toxic than the extract from the exponential growth phase at all concentrations (p ≤ 0.025). Gill cell viability decreased gradually with increasing extract concentration, decreasing by 26% and 99.6% in gill cell viability at 0.2% and 8% of the algal extract (stationary growth phase), respectively (Fig. 10).

4. Discussion

4.1. Morphological comparison among Ostreopsis species

Ostreopsis rhodesae sp. nov. has a tabulation pattern typical for the genus (Hoppenrath et al., 2014) and although it is genetically different from other *Ostreopsis* species, it appears highly similar to *O.* cf. *siamensis* and *O.* cf. *ovata* based on light microscopy (Table 1). The species distinction for *O. rhodesae* was determined through rDNA phylogenetic analyses, presence of CBCs in the ITS2 region and thorough SEM investigations.

The elongated second apical plate (2′) is twice as long as the APC plate and it separates the third apical (3′) from the third precingular (3″) plate (Fig. 6A). All *Ostreopsis* species have a 2′ plate about the length of the APC, and Plates 3′ and 3″ are in contact, except for *O. heptagona* Norris, Bomber et Balech (Faust et al., 1996; Hoppenrath et al., 2014; Norris et al., 1985). The 2′ plate is a characteristic feature for *O. rhodesae* and *O. heptagona* (Figs. 6A, C). The irregular heptagonal first apical plate (1′) having an additional suture with the fifth precingular plate (Fig. 6C) is special for *O. heptagona* (Faust et al., 1996; Norris et al., 1985). In contrast, *O. rhodesae* typically has a hexagonal 1′ plate that is not in contact with Plate 5″ (Fig. 6A) but Plates 3′ and 6″ touch each other in a suture (Fig. 3A–C arrowheads). Only extremely few cells were observed with a heptagonal Plate 1′ (Fig. 3D). Aberrant specimens with a heptagonal 1′ plate were also recorded in culture for *O. ovata* (Besada et al., 1982) and *O.* cf. *ovata* (Penna et al., 2010). In these rare cases, the shape of the 1′ plate is ambiguous for species identification. *Ostreopsis rhodesae* can additionally be clearly distinguished from *O. heptagona* by the shape of the second antapical plate (2″″) that has normal width as described for most *Ostreopsis* species and nearly parallel lateral plate sides (Fig. 6B), in contrast to a relatively narrow plate that widens ventrally (Fig. 6D) (1p plate in Norris et al., 1985). Many small protuberances, each with a pore, were described as thecal ornamentation in the original description of *O. heptagona* (Norris et al., 1985), but Faust et al. (1996) recorded a smooth surface. *O. heptagona* belongs to the largest species of the genus with a cell depth of 80–122 μm (Faust et al., 1996; Norris et al., 1985) in contrast to the small *O. rhodesae* with a depth range of 32–56 μm. The combination of morphological characters (hexagonal 1′ plate, elongated 2′ plate, shape of Plate 2″″, and cell size) distinguish *O. rhodesae* from all described *Ostreopsis* species and warrants its description as new species.

Interestingly, Parsons et al. (2012) provided an epithecal image of a species he identified as *O.* cf. *ovata* that shows an elongated 2′ plate disconnecting Plates 3′ and 3″ as in *O. rhodesae,* and additionally with a heptagonal 1′ plate as characteristic for *O. heptagona*. The size of the scale bar has not been provided. Hence, in the absence of further information no clear identification could be made. The corresponding specimen from the same strain in Penna et al. (2010) had a hexagonal 1′ plate and an elongated 2′ plate that was not twice the length of the APC, but also separated Plates 3′ from 3″ (not clearly visible). That makes it more similar to *O. rhodesae* and the cell was 57.5 μm deep, fitting into the species size range. Besada et al. (1982, Fig. 4) published an epitheca of *O. ovata* showing an elongated 2′ plate that seems to separate Plates 3′ and 3″ like the specimen in Penna et al. (2010).

Table 2
Distance values (pairwise uncorrected p-distances) based on the ITS/5.8S, D1/D2, D8/D10 LSU and 18S rDNA sequences respectively within *Ostroepsis rhodesae* strains and between *Ostreopsis* cf. *siamensis* HER24and *Ostreopsis* cf. *ovata* HER27 from Heron Island (based on Clustal W alignment). Standard error estimate(s) are shown in brackets and were obtained by a bootstrap procedure (1000 replicates).

	Ostreopsis rhodesae	*Ostreopsis* cf. *siamensis* HER 24	*Ostreopsis* cf. *ovata* HER27
Ostreopsis rhodesae	0		
	0.0126 (0.003)		
	0.0033 (0.001)		
	0		
Ostreopsis cf. *siamensis* HER 24	0.2783(0.0247)	n/a	
	0.1627 (0.162)	n/a	
	0.033 (0.006)	n/a	
	0.0795 (0.0068)	n/a	
Ostreopsis cf. *ovata* HER27	0.3172 (0.0256)	0.3398 (0.0264)	n/a
	0.5426 (0.0217)	0.5495 (0.022)	n/a
	0.0452 (0.0067)	0.0448 (0.0066)	n/a
	0.5493 (0.0176)	0.5912 (0.0194)	n/a

4.2. Phylogeny and biogeography of genus Ostreopsis

The phylogenetic analyses in our study revealed the discovery of a novel species *O. rhodesae* that diverged from other clades with full nodal support and was found to be sister group to *O.* cf. *siamensis*. *Ostreopsis* cf. *siamensis* and *O.* cf. *ovata* were also reported from the same environmental sample. Previously, Holmes et al. (1988) has reported *O. siamensis* from Heron Island, Lady Elliot Island and Hoffmans Rocks based on morphological characteristics. A survey of toxic dinoflagellates from Townsville, Magnetic and Orpheus Islands reported high concentrations of *O. ovata, O. siamensis, O. lenticularis* and *O. heptagona*, without accompanying data to verify their identities (Heimann et al., 2009). Here, the first molecular description of *Ostreopsis* species from the Australian GBR is reported.

O. cf. *siamensis* ribotype has previously been reported from temperate locations around the globe (Rhodes, 2011). This study has provided the first report of this ribotype from sub-tropical waters, suggestive of a more cosmopolitan distribution than previously described. Recently, *O.* cf. *siamensis* has been reported from a shellfish estuary in southern New South Wales and its seasonal occurrence in New Zealand suggests its transportation from tropical/sub-tropical waters via the East Australian current and the Tasman front (Murray et al., 2014; Rhodes, 2011). The genetic homogeneity of *O.* cf. *ovata* found in the Coral Sea with populations in Malaysia, Cook Islands and Japanese waters might be due to the connectivity of the Equatorial counter currents with the EAC in the southern hemisphere and the Kuroshio current in the north (Sato et al., 2011).

The genetic distances based on ITS regions between *O. rhodesae* and *O.* cf. *siamensis* were comparable to the distance between *O.* cf. *siamensis* and *O.* cf. *ovata*, which suggests that the genetic differentiation between O. *rhodesae* and other *Ostreopsis* species/clades are at the species level (Table 2) as suggested in Wayne Litaker et al. (2007). Low levels of intragenetic variations amongst *O. rhodesae* strains in the LSU rDNA regions were observed, however ITS regions in *O. rhodesae* were relatively homogenous (Table 2). Sato et al. (2011) suggested that the evolutionary divergence of the ITS region reflects the genomic heterogeneity in a cladal population and is reflective of its potential to adapt to changing environments, making O. cf. *ovata* clades to be more ecologically versatile compared to the genetically homogeneous *O. rhodesae* and *O.* cf. *siamensis*.

In this study, the ITS2 region of *Ostreopsis* species was found to be the shortest amongst dinoflagellates at 87–92 bp, as previously reported in Leaw et al. (2010) and Ramos et al. (2015). The ITS2 secondary structure does not conform to the conventional eukaryotic four domain structure, which has been observed in other genera of the order Gonyaulacales such as *Coolia, Alexandrium, Gambierdiscus* and *Fukuyoa* (John et al., 2014; Laza-Martínez et al., 2016; Leaw et al., 2016; Ramos et al., 2015; Schultz et al., 2005). ITS2 structure variants deviating from the eukaryote core structure are known in several organisms including alga, plant, fungi, and animals suggesting that several organisms, including *Ostreopsis*, may have species or organism specific solutions for ITS2 processing such as *Isopora/Acropora* scleractinian corals and the ciliate genus *Spirostomum* (Coleman, 2007, 2008; Shazib et al., 2016). Within dinoflagellate genera, non-coding internal transcribed spacers (i.e. ITS1 and ITS2) have a fast evolutionary rate, and the short ITS2 length of *Ostreopsis* may be a result of such rapid evolution as seen in the case of *Symbiodinium* clades and sub-clades (LaJeunesse et al., 2012; Ramos et al., 2015). Long periods of evolution or mutations may be responsible for such diversity in *Ostreopsis*. Three HCBCs were detected in the Mediterranean/Altantic *O.* cf. *ovata* sub clade as compared to other *O.* cf. *ovata* sub-clades from the Indian/Pacific Ocean regions. Although there is no rule about the presence of hemi-CBCs and species delineation, previous studies have separated biological species when two hemi-CBCs have been reported as in the case of *Pseudo-nitzschia* (Amato et al., 2007; Teng et al., 2015). Geographic isolation, phylogenetic divergence as reported in previous studies and the presence of HCBCs suggest that *O.* cf. *ovata* Med/Atl sub-clade represents a separate taxonomic unit and requires further investigation (Penna et al., 2014, 2010).

4.3. Toxicity

No PLTX-like analogues were detected from *O.* cf. *siamensis* HER24 and *O. rhodesae* strains, however the fish gill cells used in the bioassay were sensitive to their cellular extracts (Fig. 10A and B). Previously, non-PLTX derivatives produced by *Ostreopsis* species, such as Ostreol-A, have shown to be cytotoxic towards brime-shrimp (Hwang et al., 2013). Since the oxidative cleavage method does not identify these compounds, it is possible that the production of such non-PLTX-like compounds by *O. rhodesae* strains might be responsible for the toxic effect and were not detected (Selwood et al., 2012). Crude methanolic extracts from ichthyotoxic microalgae have shown to be highly toxic towards the fish gill cell line RTgill-W1. These effects have been associated with the production of fatty acids and reactive oxygen species (ROS) in microalgae, causing the release of free radicals that are toxic to the fish gill cells (Dorantes-Aranda et al., 2015). Usup et al. (2008) found *Ostreopsis* species to produce eicosapentaenoic (EPA, 20:5ω3) and docosahexaenoic (DHA, 22:6ω3) acids, which have

Fig. 9. Predicted ITS2 secondary structure of *Ostreopsis* strains A: *O.* cf. *ovata* HER27; B: *O.* cf. *siamensis* HER24 and C: *O. rhodesae* HER26.

been proven to be cytotoxic towards the fish gill cells RTgill-W1 (Mardones et al., 2015; Mooney et al., 2011). The toxic effect of *O. rhodesae* and *O.* cf. *siamensis* can be possibly explained by the production of such lipid molecules that were extracted in the methanol extracts of these species.

Using the oxidative cleavage method, both the amine and amide aldehyde fragments were detected in *O.* cf. *ovata* HER27 and the

Table 3
List of Compensatory base changes (CBCs) and hemi-CBCs between *Ostreopsis rhodesae*, *Ostreopsis* cf. *ovata* strain HER27 and *Ostreopsis* cf. *siamensis* strain HER24.

Species	Ostreopsis cf. ovata HER 27	Ostreopsis cf. siamensis HER24	Ostreopsis rhodesae HER26
Ostreopsis cf. *ovata* HER 27	X	1 CBC (Helix I G-C ↔ U-A) 1 HCBC (Helix II G-C ↔ G-U	
Ostreopsis cf. *siamensis* HER24	1 CBC (Helix II U-A ↔ G-C) 1 HCBC (Helix I G-U ↔ G-C)	X	
Ostreopsis rhodesae HER26	2 HCBCs (Helix I G-U ↔ A-U, Helix II G-U ↔ A-U); 2 CBCs (Helix I C-G ↔ U-A, Helix II G-U ↔ U-C)	3 HCBCs (Helix I G-U ↔ A-U, Helix II G-C ↔ U-C, Helix II G-U ↔ A-U); 1 CBC (Helix II G-C ↔ U-A)	X

Fig. 10. Effect of crude extracts from; A; *Ostreopsis cf. siamensis* HER24; B; *Ostreopsis rhodesae* HER26 and C; *Ostreopsis cf. ovata* HER27 on viability of fish gill cells RTgill-W1. Plots are average from quadruplicate wells and bars represent their standard deviation. Symbols (*) indicate significant differences (at $p \leq 0.05$) when comparing the effect of extracts from exponential and stationary growth phase at each extract concentration. Arrows and negative values show the decrease in gill cell viability.

peak area ratio was almost identical to the PLTX standard (Selwood et al., 2012). No intact PLTX molecules were detected, suggesting structural modifications in the central portion of the molecule which might yield different analogues in the cellular extract. The strain showed higher toxicity in the stationary phase compared to the exponential growth phase due to the accu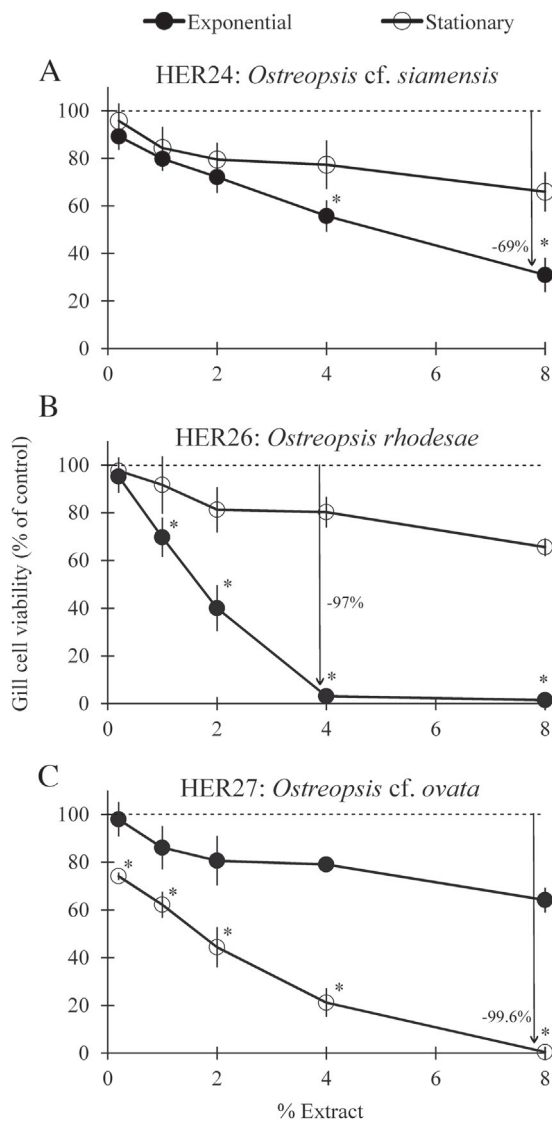mulation of PLTX-like compounds (Guerrini et al., 2010) (Fig. 10C). While the complete structure of these molecules remain to be elucidated, the cellular content of PLTX-like analogues was lower compared to the toxic *O.* cf. *ovata* strains reported in previous studies from Mediterranean and Japanese waters (Dell'Aversano et al., 2014; Guerrini et al., 2010; Suzuki et al., 2012).

5. Conclusion

A new pseudo-cryptic species, *Ostreopsis rhodesae*, is described based on a combination of morphological features and unique sequences of rRNA gene regions with the presence of CBCs present in the ITS2 secondary structure. This species was not found to produce PLTX-like analogues but showed toxicity towards fish gill cell lines. This species is morphologically similar to other toxic species of *Ostreopsis* which demonstrates that highly similar species of *Ostreopsis* with differing physiological or toxicological features may co-occur in a given habitat.

Author contributions

All authors contributed equally to the manuscript.

Appendix A. Supplementary data

Supplementary data associated with this article can be found, in the online version, at http://dx.doi.org/10.1016/j.hal.2016.11.004.

References

Ajani, P., Brett, S., Krogh, M., Scanes, P., Webster, G., Armand, L., 2013. The risk of harmful algal blooms (HABs) in the oyster-growing estuaries of New South Wales, Australia. Environ. Monit. Assess. 185 (6), 5295–5316.

Alverson, A.J., 2008. Molecular systematics and the diatom species. Protist 159 (3), 339–353.

Amato, A., Kooistra, W.H.C.F., Levialdi Ghiron, J.H., Mann, D.G., Pröschold, T., Montresor, M., 2007. Reproductive isolation among sympatric cryptic species in marine diatoms. Protist 158 (2), 193–207.

Ankenbrand, M.J., Keller, A., Wolf, M., Schultz, J., Förster, F., 2015. ITS2 database V: twice as much. Mol. Biol. Evol. 32 (11), 3030–3032. doi:http://dx.doi.org/10.1093/molbev/msv174.

Besada, E., Loeblich, L., Loeblich Iii, A., 1982. Observations on tropical, benthic dinoflagellates from ciguatera-endemic areas: *Coolia*, *Gambierdiscus*, and *Ostreopsis*. Bull. Mar. Sci. 32 (3), 723–735.

Bols, N., Barlian, A., Chirino-Trejo, M., Caldwell, S., Goegan, P., Lee, L., 1994. Development of a cell line from primary cultures of rainbow trout, *Oncorhynchus mykiss* (Walbaum), gills. J. Fish Dis. 17 (6), 601–611.

Ciminiello, P., Dell'Aversano, C., Fattorusso, E., Forino, M., Magno, G.S., Tartaglione, L., Grillo, C., Melchiorre, N., 2006. The genoa 2005 outbreak. determination of putative palytoxin in mediterranean *Ostreopsis ovata* by a new liquid chromatography tandem mass spectrometry method. Anal. Chem. 78 (17), 6153–6159.

Ciminiello, P., Dell'Aversano, C., Dello Iacovo, E., Fattorusso, E., Forino, M., Grauso, L., Tartaglione, L., Guerrini, F., Pezzolesi, L., Pistocchi, R., Vanucci, S., 2012a. Isolation and structure elucidation of ovatoxin-a, the major toxin produced by *Ostreopsis ovata*. J. Am. Chem. Soc. 134 (3), 1869–1875.

Ciminiello, P., Dell'Aversano, C., Iacovo, E.D., Fattorusso, E., Forino, M., Tartaglione, L., Battocchi, C., Crinelli, R., Carloni, E., Magnani, M., Penna, A., 2012b. Unique toxin profile of a Mediterranean *Ostreopsis* cf. *ovata* strain: HR LC-MS(n) characterization of ovatoxin-f, a new palytoxin congener. Chem. Res. Toxicol. 25 (6), 1243–1252.

Coleman, A.W., Vacquier, V.D., 2002. Exploring the phylogenetic utility of ITS sequences for animals: a test case for abalone (Haliotis). J. Mol. Evol. 54 (2), 246–257.

Coleman, A.W., 2003. ITS2 is a double-edged tool for eukaryote evolutionary comparisons. Trends Genet. 19 (7), 370–375.

Coleman, A.W., 2007. Pan-eukaryote ITS2 homologies revealed by RNA secondary structure. Nucleic Acids Res. 35 (10), 3322–3329.

Coleman, A.W., van Oppen, M.J., 2008. Secondary structure of the rRNA ITS2 region reveals key evolutionary patterns in acroporid corals. J. Mol. Evol. 67 (4), 389–396.

Coleman, A.W., 2015. Nuclear rRNA transcript processing versus internal transcribed spacer secondary structure. Trends Genet. 31 (3), 157–163.

Darty, K., Denise, A., Ponty, Y., 2009. VARNA: Interactive drawing and editing of the RNA secondary structure. Bioinformatics 25 (15), 1974–1975.

David, H., Laza-Martínez, A., Miguel, I., Orive, E., 2013. Ostreopsis cf. siamensis and Ostreopsis cf. ovata from the Atlantic Iberian Peninsula: morphological and phylogenetic characterization. Harmful Algae 30, 44–55.

Dayeh, S.A., Butler, D.P., Celik-Butler, Z., 2005. Micromachined infrared bolometers on flexible polyimide substrates. Sens. Actuators A Phys. 118 (1), 49–56.

Del Campo, J., Balagué, V., Forn, I., Lekunberri, I., Massana, R., 2013. Culturing bias in marine heterotrophic flagellates analyzed through seawater enrichment incubations. Microb. Ecol. 66 (3), 489–499.

Del Campo, J., Guillou, L., Hehenberger, E., Logares, R., López-García, P., Massana, R., 2016. Ecological and evolutionary significance of novel protist lineages. Eur. J. Protistol. 55, 4–11.

Dell'Aversano, C., Ciminiello, P., Iacovo, E.D., Tartaglione, L., Forino, M., Casabianca, S., Penna, A., 2014. Ostreopsis cf. ovata from the Mediterranean area. Variability in toxin profiles and structural elucidation of unknowns through LC-HRMSn. In: MacKenzie, A.L. (Ed.), 2015. Proceedings of the 16th International Conference on Harmful Algae. International Society for the Study of Harmful Algae and Intergovernmental Oceanographic Commission of UNESCO 40–40.

de Vargas, C., Audic, S., Henry, N., Decelle, J., Mahé, F., Logares, R., Lara, E., Berney, C., Le Bescot, N., Probert, I., 2015. Eukaryotic plankton diversity in the sunlit ocean. Science 348 (6237), 1261605.

Dorantes-Aranda, J.J., Waite, T.D., Godrant, A., Rose, A.L., Tovar, C.D., Woods, G.M., Hallegraeff, G.M., 2011. Novel application of a fish gill cell line assay to assess ichthyotoxicity of harmful marine microalgae. Harmful Algae 10 (4), 366–373.

Dorantes-Aranda, J.J., Seger, A., Mardones, J.I., Nichols, P.D., Hallegraeff, G.M., 2015. Progress in understanding algal bloom-mediated fish kills: the role of superoxide radicals, phycotoxins and fatty acids. PLoS One 10 (7), e0133549.

Faust, M.A., Morton, S.L., Quod, J.P., 1996. Further SEM study of marine dinoflagellates: the genus Ostreopsis (Dinophyceae). J. Phycol. 32 (6), 1053–1065.

Fukuyo, Y., 1981. Taxonomical study on benthic dinoflagellates collected in coral reefs [French Polynesia, Japan]. Bull. Japan. Soc. Sci. Fish. 47 (8), 967–978.

Guerrini, F., Pezzolesi, L., Feller, A., Riccardi, M., Ciminiello, P., Dell'Aversano, C., Tartaglione, L., Iacovo, E.D., Fattorusso, E., Forino, M., 2010. Comparative growth and toxin profile of cultured Ostreopsis ovata from the Tyrrhenian and Adriatic Seas. Toxicon Off. J. Int. Soc. Toxinol. 55 (2), 211–220.

Guillard, R.R., 1975. Culture of phytoplankton for feeding marine invertebrates. In: Smith, W.L., Chanley, M.H. (Eds.), Culture of Marine Invertebrate Animals. Springer, New York, USA, pp. 29–60.

Heger, T.J., Edgcomb, V.P., Kim, E., Lukeš, J., Leander, B.S., Yubuki, N., 2014. A resurgence in field research is essential to better understand the diversity, ecology, and evolution of microbial eukaryotes. J. Eukaryot. Microbiol. 61 (2), 214–223.

Heimann, K., Sparrow, L., Blair, D., 2009. Interim report on the continuing development of the toxic dinoflagellates atlas. Marine and Tropical Sciences Research Facility. Reef and Rainforest Research Center, Cairns, pp. 1–25 June Interim Report (Part 1).

Holmes, M., Gillespie, N., Lewis, R., et al., 1988. Toxicity and morphology of Ostreopsis cf. siamensis cultured from a ciguatera endemic region of Queensland, Australia. In: Choat, J.H., Barnes, D., Borowitzka, M.A. (Eds.), Proceedings 6th International Coral Reef Symposium, 6th International Coral Reef Symposium Executive Committee, Townsville, pp. 49–54.

Hoppenrath, M., Bachvaroff, T.R., Handy, S.M., Delwiche, C.F., Leander, B.S., 2009. Molecular phylogeny of ocelloid-bearing dinoflagellates (Warnowiaceae) as inferred from SSU and LSU rDNA sequences. BMC Evol. Biol. 9 (1), 116–130.

Hoppenrath, M., Murray, S.A., Chomérat, N., Horiguchi, T., 2014. Marine benthic dinoflagellates-unveiling their worldwide biodiversity, Kleine Senckenberg-Reihe. Frankfurt am Main 116–126.

Hwang, B.S., Yoon, E.Y., Kim, H.S., Yih, W., Park, J.Y., Jeong, H.J., Rho, J.R., 2013. Ostreol A: a new cytotoxic compound isolated from the epiphytic dinoflagellate Ostreopsis cf. ovata from the coastal waters of Jeju Island, Korea. Bioorg. Med. C=Chem. Lett. 23 (10), 3023–3027.

John, U., Litaker, R.W., Montresor, M., Murray, S., Brosnahan, M.L., Anderson, D.M., 2014. Formal revision of the Alexandrium tamarense species complex (Dinophyceae) taxonomy: the introduction of five species with emphasis on molecular-based (rDNA) classification. Protist 165 (6), 779–804.

Kearse, M., Moir, R., Wilson, A., Stones-Havas, S., Cheung, M., Sturrock, S., Buxton, S., Cooper, A., Markowitz, S., Duran, C., Thierer, T., 2012. Geneious Basic: an integrated and extendable desktop software platform for the organization and analysis of sequence data. Bioinformatics 28 (12), 1647–1649.

Keeling, P.J., Burki, F., Wilcox, H.M., Allam, B., Allen, E.E., Amaral-Zettler, L.A., Armbrust, E.V., Archibald, J.M., Bharti, A.K., Bell, C.J., Beszteri, B., Bidle, K.D., Cameron, C.T., Campbell, L., Caron, D.A., Cattolico, R.A., Collier, J.L., Coyne, K., Davy, S.K., Deschamps, P., Dyhrman, S.T., Edvardsen, B., Gates, R.D., Gobler, C.J., Greenwood, S.J., Guida, S.M., Jacobi, J.L., Jakobsen, K.S., James, E.R., Jenkins, B., John, U., Johnson, M.D., Juhl, A.R., Kamp, A., Katz, L.A., Kiene, R., Kudryavtsev, A., Leander, B.S., Lin, S., Lovejoy, C., Lynn, D., Marchetti, A., McManus, G., Nedelcu, A. M., Menden-Deuer, S., Miceli, C., Mock, T., Montresor, M., Moran, M.A., Murray, S., Nadathur, G., Nagai, S., Ngam, P.B., Palenik, B., Pawlowski, J., Petroni, G., Piganeau, G., Posewitz, M.C., Rengefors, K., Romano, G., Rumpho, M.E., Rynearson, T., Schilling, K.B., Schroeder, D.C., Simpson, A.G.B., Slamovits, C.H., Smith, D.R., Smith, G.J., Smith, S.R., Sosik, H.M., Stief, P., Theriot, E., Twary, S.N., Umale, P.E., Vaulot, D., Wawrik, B., Wheeler, G.L., Wilson, W.H., Xu, Y., Zingone, A., Worden, A.Z., 2014. The marine microbial eukaryote transcriptome sequencing project (MMETSP): illuminating the functional diversity of eukaryotic life in the oceans through transcriptome sequencing. PLoS Biol. 12 (6), e1001889.

Knowlton, N., 1993. Sibling species in the sea. Annu. Rev. Ecol. Syst. 24, 189–216.

LaJeunesse, T.C., Parkinson, J.E., Reimer, J.D., 2012. A genetics-based description of Symbiodinium minutum sp. nov. and S. psygmophilum sp. nov. (Dinophyceae), two dinoflagellates symbiotic with cnidaria. J. Phycol. 48 (6), 1380–1391.

LaJeunesse, T.C., 2001. Investigating the biodiversity, ecology, and phylogeny of endosymbiotic dinoflagellates in the genus Symbiodinium using the ITS region: in search of a species level marker. J. Phycol. 37 (5), 866–880.

Lang, B.F., Burger, G., 2007. Purification of mitochondrial and plastid DNA. Nat. Protoc. 2 (3), 652–660.

Laza-Martínez, A., David, H., Riobó, P., Miguel, I., Orive, E., 2016. Characterization of a strain of Fukuyoa paulensis (Dinophyceae) from the western mediterranean sea. J. Eukaryot. Microbiol. 63 (4), 481–497.

Le Bescot, N., Mahé, F., Audic, S., Dimier, C., Garet, M.J., Poulain, J., Wincker, P., Vargas, C., Siano, R., 2015. Global patterns of pelagic dinoflagellate diversity across protist size classes unveiled by metabarcoding. Environ. Microbiol. 18, 609–626.

Leaw, C.P., Lim, P.T., Cheng, K.W., Ng, B.K., Usup, G., 2010. Morphology and molecular characterization od a new species of thecate benthic dinoflagellate, Coolia malayensis sp. nov. (Dinophyceae). J. Phycol. 46 (1), 162–171.

Leaw, C.P., Tan, T.H., Lim, H.C., Teng, S.T., Yong, H.L., Smith, K.F., Rhodes, L., Wolf, M., Holland, W.C., Vandersea, M.W., 2016. New scenario for speciation in the benthic dinoflagellate genus Coolia (Dinophyceae). Harmful Algae 55, 137–149.

Lundholm, N., Bates, S.S., Baugh, K.A., Bill, B.D., Connell, L.B., Léger, C., Trainer, V.L., 2012. Crytpic and pseudo-cryptic diversity in diatoms- with descriptions of Pseudo-nitzschia hasleana sp. nov. and P. fryxelliana sp. nov. J. Phycol. 48 (2), 436–454.

Mardones, J.I., Dorantes-Aranda, J.J., Nichols, P.D., Hallegraeff, G.M., 2015. Fish gill damage by the dinoflagellate Alexandrium catenella from Chilean fjords: synergistic action of ROS and PUFA. Harmful Algae 49, 40–49.

Massana, R., Gobet, A., Audic, S., Bass, D., Bittner, L., Boutte, C., Chambouvet, A., Christen, R., Claverie, J.M., Decelle, J., 2015. Marine protist diversity in European coastal waters and sediments as revealed by high-throughput sequencing. Environ. Microbiol. 17 (10), 4035–4049.

Montresor, M., Sgrosso, S., Procaccini, G., Kooistra, W.H., 2003. Intraspecific diversity in Scrippsiella trochoidea (Dinophyceae): evidence for cryptic species. Phycologia 42 (1), 56–70.

Mooney, B.D., Dorantes-Aranda, J.J., Place, A.R., Hallegraeff, G.M., 2011. Ichthyotoxicity of gymnodinioid dinoflagellates: PUFA and superoxide effects in sheepshead minnow larvae and rainbow trout gill cells. Mar. Ecol. Prog. Ser. 426, 213–224.

Murray, S.A., Garby, T., Hoppenrath, M., Neilan, B.A., 2012a. Genetic diversity, morphological uniformity and polyketide production in dinoflagellates (Amphidinium, Dinoflagellata). PLoS One 7 (6), e38253.

Murray, S.A., Patterson, D.J., Thessen, A.E., 2012b. Transcriptomics and microbial eukaryote diversity: a way forward. Trends Ecol. Evol. 27 (12), 651–652.

Murray, S., Momigliano, P., Heimann, K., Blair, D., 2014. Molecular phylogenetics and morphology of Gambierdiscus yasumotoi from tropical eastern Australia. Harmful Algae 39, 242–252.

Norris, D., Bomber, J., Balech, E., 1985. Benthic dinoflagellates associated with ciguatera from the Florida Keys. I. Ostreopsis heptagona sp. nov. Toxic Dinoflagellates 39–44.

Orive, E., Pérez Aicua, L., David, H., García-Etxebarria, K., Laza-Martínez, A., Seoane, S., Miguel, I., 2013. The genus Pseudo-nitzschia (Bacillariophyceae) in a temperate estuary with description of two new species: Pseudo-nitzschia plurisecta sp. nov. and Pseudo-nitzschia abrensis sp. nov. J. Phycol. 49 (6), 1192–1206.

Parsons, M.L., Aligizaki, K., Bottein, M.-Y.D., Fraga, S., Morton, S.L., Penna, A., Rhodes, L., 2012. Gambierdiscus and Ostreopsis: reassessment of the state of knowledge of their taxonomy, geography, ecophysiology, and toxicology. Harmful Algae 14, 107–129.

Pearce, I., Marshall, J., Hallegraeff, G., 2001. Toxic epiphytic dinoflagellates from east coast Tasmania. In: Hallegraeff, G., Blackburn, S., Bolch, C., Lewis, R. (Eds.), Proceedings of the 9th International Conference on Harmful Algal Blooms. International Society for the Study of Harmful Algae and Intergovernmental Oceanographic Commission of UNESCO, pp. 54–57.

Penna, A., Vila, M., Fraga, S., Giacobbe, M.G., Andreoni, F., Riobó, P., Vernesi, C., 2005. Characterization os Ostreopsis and Coolia (Dinophyceae) isolates in the western Mediterranean Sea based on morphology, toxicity and Internal transcribed spacer 5.8S rDNA sequences. J. Phycol. 41 (1), 212–225.

Penna, A., Fraga, S., Battocchi, C., Casabianca, S., Giacobbe, M.G., Riobó, P., Vernesi, C., 2010. A phylogeographical study of the toxic benthic dinoflagellate genus Ostreopsis Schmidt. J. Biogeogr. 37 (5), 830–841.

Penna, A., Battocchi, C., Capellacci, S., Fraga, S., Aligizaki, K., Lemée, R., Vernesi, C., 2014. Mitochondrial, but not rDNA, genes fail to discriminate dinoflagellate species in the genus Ostreopsis. Harmful Algae 40, 40–50.

Pin, L.C., Teen, L.P., Ahmad, A., Usup, G., 2001. Genetic diversity of Ostreopsis ovata (Dinophyceae) from Malaysia. Mar. Biotechnol. 3 (3), 246–255.

Pochon, X., Gates, R.D., 2010. A new Symbiodinium clade (Dinophyceae) from soritid foraminifera in Hawai'i. Mol. Phylogenet. Evol. 56 (1), 492–497.

Ramos, V., Salvi, D., Machado, J.P., Vale, M., Azevedo, J., Vasconcelos, V., 2015. Culture-Independent study of the late-Stage of a bloom of the toxic dinoflagellate Ostreopsis cf. ovata: preliminary findings suggest genetic differences at the sub-Species level and allow ITS2 structure characterization. Toxins 7 (7), 2514–2533.

Rasheed, M., Wild, C., Franke, U., Huettel, M., 2004. Benthic photosynthesis and oxygen consumption in permeable carbonate sediments at Heron Island Great Barrier Reef, Australia. Estuar. Coast. Mar. Sci. 59 (1), 139–150.

Rhodes, L., Towers, N., Briggs, L., Munday, R., Adamson, J., 2002. Uptake of palytoxin-like compounds by shellfish fed Ostreopsis siamensis (Dinophyceae). N. Z. J. Mar. Freshwater Res. 36 (3), 631–636.

Rhodes, L., 2011. World-wide occurrence of the toxic dinoflagellate genus Ostreopsis Schmidt. Toxicon. Off. J. Int. Soc. Toxinol. 57 (3), 400–407.

Richlen, M.L., Morton, S.L., Barber, P.H., Lobel, P.S., 2008. Phylogeography, morphological variation and taxonomy of the toxic dinoflagellate Gambierdiscus toxicus (Dinophyceae). Harmful Algae 7 (5), 614–629.

Ronquist, F., Huelsenbeck, J.P., 2003. MrBayes 3: Bayesian phylogenetic inference under mixed models. Bioinformatics 19 (12), 1572–1574.

Sampayo, E.M., Dove, S., LaJeunesse, T.C., 2009. Cohesive molecular genetic data delineate species diversity in the dinoflagellate genus *Symbiodinium*. Mol. Ecol. 18 (3), 500–519.

Sato, S., Nishimura, T., Uehara, K., Sakanari, H., Tawong, W., Hariganeya, N., Smith, K., Rhodes, L., Yasumoto, T., Taira, Y., 2011. Phylogeography of *Ostreopsis* along west Pacific coast, with special reference to a novel clade from Japan. PLoS One 6, e27983.

Schirmer, K., Chan, A., Greenberg, B., Dixon, D., Bols, N., 1997. Methodology for demonstrating and measuring the photocytotoxicity of fluoranthene to fish cells in culture. Toxicol. In Vitro 11 (1), 107–119.

Schmidt, J., 1901. Preliminary report of the biological results of the Danish Expedition to Siam (1899–1900). Part IV. Peridiniales. 24. Flora of Koh Chang, Bot Tidss, pp. 212–221.

Schultz, J., Wolf, M., 2009. ITS2 sequence–structure analysis in phylogenetics: a how-to manual for molecular systematics. Mol. Phylogenet. Evol. 52 (2), 520–523.

Schultz, J., Maisel, S., Gerlach, D., Müller, T., Wolf, M., 2005. A common core of secondary structure of the internal transcribed spacer 2 (ITS2) throughout the Eukaryota. RNA 11 (4), 361–364.

Seibel, P.N., Müller, T., Dandekar, T., Schultz, J., Wolf, M., 2006. 4SALE?a tool for synchronous RNA sequence and secondary structure alignment and editing. BMC Bioinf. 7 (1), 498–504.

Selwood, A.I., van Ginkel, R., Harwood, D.T., McNabb, P.S., Rhodes, L.R., Holland, P.T., 2012. A sensitive assay for palytoxins, ovatoxins and ostreocins using LC-MS/MS analysis of cleavage fragments from micro-scale oxidation. Toxicon Off. J. Int. Soc. Toxinol. 60 (5), 810–820.

Shazib, S.U.A., Vďačný, P., Kim, J.H., Jang, S.W., Shin, M.K., 2016. Molecular phylogeny and species delimitation within the ciliate genus Spirostomum (Ciliophora, Postciliodesmatophora, Heterotrichea), using the internal transcribed spacer region. Mol. Phylogenet. Evol. 102, 128–144.

Stat, M., Bird, C.E., Pochon, X., Chasqui, L., Chauka, L.J., Concepcion, G.T., Logan, D., Takabayashi, M., Toonen, R.J., Gates, R.D., 2011. Variation in *Symbiodinium* ITS2 sequence assemblages among coral colonies. PLoS One 6 (1), e15854. doi:http://dx.doi.org/10.1371/journal.pone.0015854.

Suzuki, T., Watanabe, R., Uchida, H., Matsushima, R., Nagai, H., Yasumoto, T., Yoshimatsu, T., Sato, S., Adachi, M., 2012. LC-MS/MS analysis of novel ovatoxin isomers in several *Ostreopsis* strains collected in Japan. Harmful Algae 20, 81–91.

Tamura, K., Stecher, G., Peterson, D., Filipski, A., Kumar, S., 2013. MEGA6: molecular evolutionary genetics analysis version 6.0. Mol. Biol. Evol. 30, 2725–2729.

Tawong, W., Nishimura, T., Sakanari, H., Sato, S., Yamaguchi, H., Adachi, M., 2014. Distribution and molecular phylogeny of the dinoflagellate genus *Ostreopsis* in Thailand. Harmful Algae 37, 160–171.

Teng, S.T., Lim, P.T., Lim, H.C., Rivera-Vilarelle, M., Quijano-Scheggia, S., Takata, Y., Quilliam, M.A., Wolf, M., Bates, S.S., Leaw, C.P., 2015. A non-toxigenic but morphologically and phylogenetically distinct new species of *Pseudo-nitzschia*, *P. sabit* sp. nov. (Bacillariophyceae). J. Phycol. 51 (4), 706–725.

Tubaro, A., Durando, P., Del Favero, G., Ansaldi, F., Icardi, G., Deeds, J.R., Sosa, S., 2011. Case definitions for human poisonings postulated to palytoxins exposure. Toxicon Off. J. Int. Soc. Toxinol. 57 (3), 478–495.

Usami, M., Satake, M., Ishida, S., Inoue, A., Kan, Y., Yasumoto, T., 1995. Palytoxin analogs from the dinoflagellate *Ostreopsis siamensis*. J. Am. Chem. Soc. 117 (19), 5389–5390.

Verma, A., Hoppenrath, M., Harwood, T., Brett, S., Rhodes, L., Murray, S., 2016. Molecular phylogeny, morphology and toxigenicity of Ostreopsis cf. siamensis (Dinophyceae) from temperate south-east Australia. Phycol. Res. 64 (3), 146–159.

Wayne Litaker, R., Vandersea, M.W., Kibler, S.R., Reece, K.S., Stokes, N.A., Lutzoni, F. M., Yonish, B.A., West, M.A., Black, M.N., Tester, P.A., 2007. Recognizing dinoflagellate species using ITS rDNA sequecnes. J. Phycol. 43 (2), 344–355.

Webb, G.E., Jell, J.S., Baker, J.C., 1999. Cryptic intertidal microbialites in beachrock, Heron Island, Great Barrier Reef: implications for the origin of microcrystalline beachrock cement. Sediment. Geol. 126 (1–4), 317–334.

Systematics and diversity of genus *Ostreopsis* in the East Australian Current region

Arjun Verma[1*], Gurjeet S. Kohli[1,2], Mona Hoppenrath[3], D. Tim Harwood[4], Unnikrishnan Kuzhiumparambil[1], Peter J. Ralph[1] and Shauna Murray[1]

[1]Climate Change Cluster, University of Technology Sydney, Australia [*]arjun.verma-1@student.uts.edu.au
[2]Singapore Centre on Environmental Life Sciences Engineering, Nanyang Technological University, Singapore; [3] German Centre for Marine Biodiversity Research, Senckenberg am Meer, Wilhelmshaven, Germany; [4]Cawthron Institute, Nelson, New Zealand

Abstract

Specific *Ostreopsis* species/strains produce complex toxic polyketide molecules like palytoxin (PLTX, $C_{129}H_{223}N_3O_{54}$) and its analogues, which are associated with human illnesses through consumption of contaminated seafood and direct contact through aerosolic exposure during blooms. In this study, we analyzed the diversity, distribution and transcriptomic comparisons of *Ostreopsis* species from the East Australian current region. In sites along a ~2000 km coastline, we identified 3 species, including *O.* cf. *siamensis, O.* cf. *ovata* and a recently described species, *O. rhodesae*. LC-MS/MS was used to determine the PLTX-like analogues from the cellular extracts and the transcriptomes of representative strains of the three *Ostreopsis* species were analysed using high throughput sequencing technology. The results from this study present several candidate genes that can aid in bridging the gap between biodiversity and functional genetics through multigene phylogenies in marine phytoplankton, and are an important step forward in understanding the genetic basis of PLTX production.

Keywords: Ostreopsis, palytoxin, East Australian Current, phylogenetics, RNA-Seq

Introduction

Species of the genus *Ostreopsis* Schmidt (1902) are known to occur in tropical and temperate waters binding epiphytically to macroalgae, seagrass, rocks, coral rubble and sand (Rhodes, 2011). Certain *Ostreopsis* species produce highly toxic palytoxin (PLTX, $C_{129}H_{223}N_3O_{54}$) and/or its analogues, such as Ostreocin-D, ovatoxins a-g and isobaric palytoxin (Dell'Aversano et al., 2014; Usami et al., 1995). PLTX and/or its analogues have been associated with human poisonings through the consumption of contaminated fish and shellfish and have been linked to clupeotoxism incidents (Amzil et al., 2012; Tubaro et al., 2011). *O.* cf. *ovata* blooms in the Mediterranean Basin have been associated with skin and eye irritations as well as respiratory illnesses from exposure to toxic aerosols (Ciminiello et al., 2006; Ciminiello et al., 2014). Blooms of *O.* cf. *siamensis* in New Zealand have been linked with large scale sea urchin mortalities (Shears and Ross, 2009), thereby highlighting the global ecological and human health impact caused by these species and toxins.

Distinguishing *Ostreopsis* species from one another based upon morphological differences is difficult, due to their similarity in size, shape and thecal plate patterns, and also their co-existence in the environment (Hoppenrath et al., 2014; Penna et al., 2005). Along the East Australian coast, the increase of up to 2.0 °C in ocean temperature over the past few decades has been linked to the southern range extension of the East Australian Current (EAC) with an increase in harmful algal taxa reported along the south-eastern coastline (Ajani et al., 2013; Thompson et al., 2009). Little is known about the distribution and diversity of *Ostreopsis* species along the EAC despite recurrent occurrences in shellfish producing estuaries from the sub-tropical and temperate regions of the coast. To investigate the diversity of *Ostreopsis* species in the EAC region and to elucidate the unique biology of these PLTX producing dinoflagellates, we sampled various locations along the East Australian coast to establish *Ostreopsis* cultures and investigate the diversity using ribosomal rDNA genes, toxin profiles using LC-MS/MS and transcriptomes through high-throughput sequencing technology.

Material and Methods

Macroalgal and seagrass samples (*Padina, Saragassum, Hormosira* and *Zostera* spp.) were collected from nine sites as listed in Table 1 during April-June 2014. Eighty clonal strains were established in f/10 media as described in Verma et al. (2016b). DNA was extracted using modified CTAB- phenol-chloroform method and 5.8S-ITS region were sequences using previously described primers (Verma et al., 2016a). Maximum Likelihood tree was produced in MEGA v6 using Tamura 3+G+I with 1,000 bootstrap replications. Bayesian analysis was performed using MrBayes v3.2.2 using general time reversible + G model as described in Verma et al. (2016b).

Table 1: Geographic location of sampling sites in Australia, temperature and salinity measurements and number of *Ostreopsis* clones isolated during this study

S.no	Location	Latitude; Longitude	Temp. (^{0}C); Salinity (psu)	No. of clones
1	Heron Island	23°27′S, 151°55′E	20; 34	14
2	Minnie Water	29°77′S; 153°29′E	NA	10
3	Bonny Hills	31°58′S; 152°82′E	NA	10
4	Wallis Lake	32°23′S; 152°48′E	19; 34	10
5	Lake Macquarie	33°09′S; 151°88′ E	17; 34	10
6	Patonga Creek	33°51′S; 151°28′ E	18; 35	8
7	Gordons Bay	33°91′S; 151°26′ E	18;34	7
8	Kiama	34°67′S; 150°85′E	18; 34	7
9	Merimbula Lake inlet	36°53′S; 149°54′E	19; 28	4

All *Ostreopsis* cultures were harvested in late stationary phase by centrifugation (50 mL; 2,300 g; 10 mins; room temperature) and the cell pellets were freeze dried for PLTX screening using a quantitative LC-MS/MS method at the Cawthron Institute, New Zealand as described in Selwood et al., (2012). This approach monitors sub-structures generated by the oxidative cleavage of vicinal diol groups present in the intact toxins using periodic acid. It yields an amino-aldehyde, used for quantification, common to known palytoxins, ovatoxins and ostreocins, and an amide-aldehyde that varies depending on the toxin type (Selwood et al., 2012)

Triplicate 1 L cultures of representative isolates of each species; *O.* cf. *ovata* (HER27), *O.* cf. *siamensis* (BH1) and *O. rhodesae* (HER26) were sampled at mid-late exponential growth phase (days 11-14) for RNA extraction. RNA extraction was performed using Tri-reagent and purified using RNeasy Mini Kit. The libraries were prepared using TruSeq RNA Sample and sequencing was performed using NextSeq500 generating 75 base pair (bp) paired end reads. Raw reads were quality filtered and assembled as described in Kohli et al. (2015).

Results and Discussion

Light microscopy analyses on the isolated *Ostreopsis* strains did not reveal any significant differences between the strains/species. Phylogenetic analysis using ITS1-5.8S-ITS2 regions reported *Ostreopsis* cf. *siamensis* (HER24), *O.* cf. *ovata* (HER27) and the pseudo-cryptic *O. rhodesae* (12 strains) from Heron Island (Fig. 1). *O. rhodesae* diverged from other previously described *Ostreopsis* clades with full nodal support and was found to be sister group to *O.* cf. *siamensis* (Fig. 1) (Sato et al., 2011; Tawong et al., 2014). . This is the first molecular characterization of the *O. ovata* ribotype from Australian waters (Heimann et al., 2009). The remaining 66 isolates (identical ribotype to CAWD203) were all identified as *O.* cf. *siamensis* thereby highlighting a large cosmopolitan spatial distribution of this species along the EAC region (Fig. 1). Previously, *O. siamensis* blooms have been reported in New Zealand and its seasonal occurrence has been linked to the transportation from tropical/sub-tropical waters via the East Australian current and the Tasman front (Murray et al., 2014; Rhodes, 2011). This may highlight a potential source population that can possibly migrate to the southern temperate regions via ocean currents during warmer seasons.

LC-MS/MS analysis of the oxidized cell extract from *O.* cf. *ovata* showed the presence of PLTX-like analogues in the extract resulting in an estimate of 1.8 pg cell^{-1}. No PLTX-like analogues were detected from cellular isolates of *O. rhodesae* strains (Verma et al., 2016a). Variable amounts of PLTX-like analogues, ranging from 0-
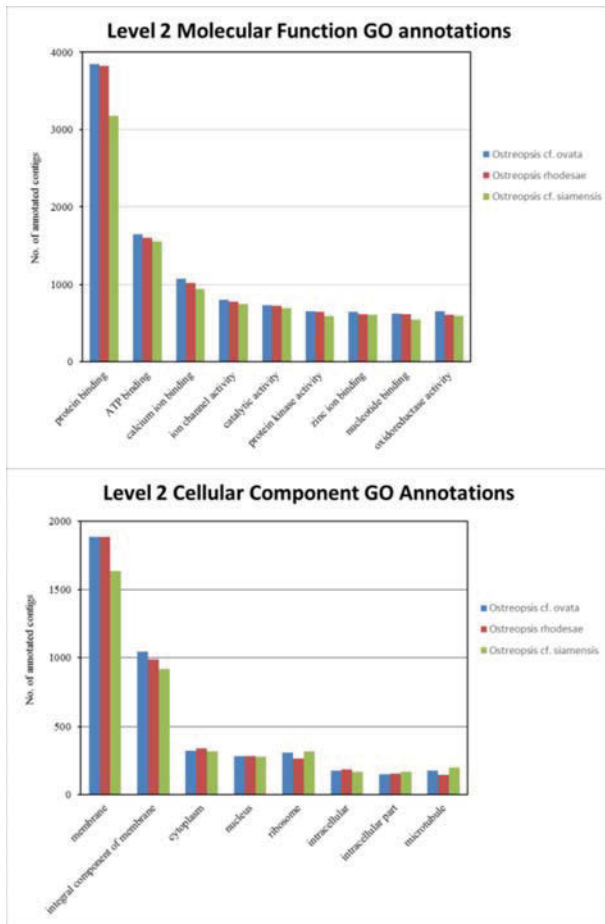
1.5 pg cell^{-1}, were determined from *O.* cf. *siamensis* extracts, highlighting a high amount of inter-strain variability in toxin production within this species (Verma et al., 2016b).

A total of 87.5, 87.6 and 75.8 million reads were extracted from *Ostreopsis* cf. *ovata*, *O. rhodesae* and *O.* cf. *siamensis* RNA-Seq libraries respectively. After removing redundancies, 87,382, 91,824 and 88,929 contigs were assembled of which, 68,759 (Mean length: 1002 bp), 71,151 (Mean length: 955 bp) and 67,786 (Mean length: 854 bp) contigs were greater than 300 bps amongst *O.* cf. *ovata*, *O. rhodesae* and *O.* cf. *siamensis* transcriptomes respectively.

Fig. 1: Maximum Likelihood and Bayesian Inference phylogenetic tree of various *Ostreopsis* species using 5.8S-ITS primer set. Numbers at nodes represent posterior probabilities from Bayesian Inferences and bootstrap support values from Maximum Likelihood based on 1000 bootstraps.

458 highly conserved proteins were identified in the transcriptomic data using the Core Eukaryotic Genes Mapping Approach (CEGMA). The transcriptomes of *O.* cf. *ovata*, *O. rhodesae* and *O.* cf. *siamensis* contained 392, 371 and 379 of these

proteins, respectively. This core of conserved annotated proteins is comparable to other dinoflagellate transcriptomes investigated to date (Kohli et al., 2017; Kohli et al., 2015; Meyer et al., 2015; Ryan et al., 2014).BLASTx analysis using BLAST2GO (e-value cut-off 10^{-3}) yielded 26.6% annotated and 25.3% non-annotated matches for *Ostreopsis* cf. *ovata*, and 25.4% annotated and 25.3% non-annotated matches for *O. rhodesae*. 25.2% and 25.1% annotated and non-annotated matches were found in *O.* cf. *siamensis* respectively. The remaining 48.1% (*O.* cf. *ovata*), 49.3% (*O. rhodesae*) and 49.5% (*O.* cf. *siamensis*) of the contigs lacked similarity to any sequence in the GenBank *nr* database. Such percentages have been observed in other protist studies, particularly amongst dinoflagellates, due to their complex and unknown genomic features (Keeling et al., 2014; Kohli et al., 2016; Murray et al., 2016). Of the transcripts with positive BLAST hits and annotations with Gene Ontology terms, similar distribution of transcripts involved in keystone molecular and metabolic functions were observed for the three *Ostreopsis* species (Fig. 2).

'Cryptic' species also appear to be common amongst dinoflagellate species and further complicate their identification when using techniques such as light and scanning microscopy. *Ostreopsis siamensis* was initially described from the Gulf of Thailand (Schmidt, 1902), however, no culture material from the type location is available to date. Since then, numerous microscopy based studies have reported conflicting descriptions of pore sizes and cingulum undulation for *Ostreopsis* species and have generally lacked genetic data (Hoppenrath et al., 2014). In order to compare between published findings and to establish accurate and more recent historical phylogenetic reconstruction of this genus, reporting sequences from different genes and the use of different molecular techniques is essential. In this study, we report three *Ostreopsis* species from the EAC region using ribosomal molecular markers and used a *de novo* transcriptomic approach to unravel several conserved genes that can be potential candidates for multigene phylogenies that can improve in deciphering the functional differences between these species and understand the genes involved in toxin biosynthesis.

Level 2 Molecular Function GO annotations

Level 2 Cellular Component GO Annotations

Fig. 2: Distribution of second-level cellular component and molecular function GO annotations in annotated *O.* cf. *ovata*, *O. rhodesae* and *O.* cf. *siamensis* transcripts.

References
Ajani, P., Brett, S., Krogh, M., et al. (2013) Environ. Monit. Assess. 185: 5295-5316.
Amzil, Z., Sibat, M., Chomerat, N., et al. (2012) Mar. Drugs 10: 477-496.
Ciminiello, P., Dell'Aversano, C., Fattorusso, E., et al. (2006). Anal. Chem. 78: 6153-6159.
Ciminiello, P., Dell'Aversano, C., Iacovo, E.D., et al. (2014). Environ. Sci. Technol. 48: 3532-3540.

Dell'Aversano, C., Ciminiello, P., Iacovo, E.D., et al. (2014) In: Proc. of the 16th International Conference on Harmful Algae, A. Lincoln MacKenzie (Ed.) Marine and Freshwater Harmful Algae 2014.The 16th International Conference on Harmful Algae, pp. 70-73.
Heimann, K., Sparrow, L. & Blair, D., (2009). In: Marine and Tropical Sciences Research facility (Ed.) June Interim Report (Part 1) to the Reef and Rainforest Centre, pp. 1-25.
Hoppenrath, M., Murray, S.A., Chomérat, N., et al. (2014). Kleine Senckenberg-Reihe, Frankfurt am Main, pp.116-126
Keeling, P.J., Burki, F., Wilcox, H.M., et al. (2014). PLoS Biol 12: e1001889.
Kohli, G.S., Campbell, K., John, U., et al. (2017). J. Eukaryot. Microbiol. doi:10.1111/jeu.12405
Kohli, G.S., John, U., Figueroa, R.I., et al. (2015). BMC Genomics 16: 410.
Kohli, G.S., John, U., Van Dolah, F.M., et al. (2016). ISME 10: 1877–1890.
Meyer, J.M., Rödelsperger, C., Eichholz, K., et al. 2015. BMC Genomics 16:27.
Murray, S., Momigliano, P., Heimann, K., et al. (2014). Harmful Algae 39: 242-252.
Murray, S.A., Suggett, D.J., Doblin, M.A., et al. (2016). Perspect. Phycol. 3: 37-52.
Penna, A., Vila, M., Fraga, S., et al. (2005). J. Phycol. 41: 212-225.
Rhodes, L. (2011). Toxicon 57: 400-407.
Ryan, D.E., Pepper, A.E. & Campbell, L. (2014). BMC Genomics 15: 888.
Sato, S., Nishimura, T., Uehara, K. et al. 2011. PLoS One 6: e27983.
Selwood, A. I., Van Ginkel, R., Harwood, D. T. et. al. 2012. Toxicon 60: 810-20,
Schmidt, J., (1902). J. Botanique 23: 212-218.
Shears, N.T. & Ross, P.M. (2009). Harmful Algae 8: 916-925.
Tawong, W., Nishimura, T., Sakanari, H. et al. (2014). Harmful Algae 37: 160-71.
Thompson, P., Baird, M.E., Ingleton, T. (2009) Mar. Ecol. Prog. Ser. 394: 1–19.
Tubaro, A., Durando, P., Del Favero, G. et al. 2011. Toxicon 57: 478-495.
Usami, M., Satake, M., Ishida, S. et al. (1995). J. Am. Chem. Soc. 117: 5389-90.
Verma, A., Hoppenrath, M., Dorantes-Aranda, J.J. et al. (2016a). Harmful Algae 60: 116-130.
Verma, A., Hoppenrath, M., Harwood, T. et al., (2016b). Phycol. Res. 64: 146-159.